

# Apprentissage de la causalité pour les données longitudinales

*Learning Causality for Longitudinal Data*

Thèse de doctorat de l'université Paris-Saclay

École doctorale n°573 Interfaces : matériaux, systèmes, usages (INTERFACES)

Spécialité de doctorat : Mathématiques appliquées

Graduate School : Sciences de l'ingénierie et des systèmes (SIS)

Composante référente : CentraleSupélec

Unité de recherche : Mathématiques et Informatique pour la Complexité et les Systèmes - EA 4037 (Université Paris-Saclay, CentraleSupélec)

Thèse préparée sous la direction de **Paul-Henry Cournède** (Directeur de recherche, Université Paris-Saclay, CentraleSupélec),

sous la co-supervision de **Myriam Tami** (Maître de conférences, Université Paris-Saclay, CentraleSupélec, MICS),

et sous la co-supervision de **Benoit Lepetit** (Chief Data and Analytics Officer, Saint-Gobain).

Thèse soutenue à Paris-Saclay, le 6 novembre 2025, par

**MOUAD EL BOUCHATTAOUI**

## Composition du jury :

Gilles Faÿ

Professor, Université Paris-Saclay, CentraleSupélec, MICS

Président du jury

Marianne Clausel

Professeure, Université de Lorraine, groupe SiMul, CRAN

Rapporteuse &  
examinatrice

Erwan Scornet

Professeur, Sorbonne Université, LPSM et SCAI

Rapporteur &  
examineur

Aurore Lomet

Ingénieure de recherche, CEA, centre de Saclay, laboratoire LIAD

Examinatrice

**Titre :** Apprentissage de la causalité pour les données longitudinales

**Mots clés :** Inférence Causale, Données Longitudinales, Apprentissage de Représentations Causales, Régression Contrefactuelle, Modélisation de Variables Latentes

**Résumé :**

Cette thèse porte sur l'inférence causale et l'apprentissage de représentations causales (CRL) pour des données de haute dimension évoluant dans le temps, avec des applications en médecine de précision, en marketing et en distribution. La première contribution introduit le modèle Causal Dynamic Variational Autoencoder (CDVAE), conçu pour estimer les effets individuels du traitement (ITE) en capturant l'hétérogénéité non observée dans la réponse au traitement, due à des facteurs de risque latents. Contrairement aux approches classiques supposant que tous les facteurs confondants sont observés, CDVAE se concentre sur les variables latentes influençant la séquence de réponses. Ce modèle repose sur des garanties théoriques relatives à la validité des variables d'ajustement latentes et aux bornes de généralisation de l'erreur d'estimation des ITE. Des évaluations extensives sur des jeux de données synthétiques et réels montrent que CDVAE surpasse les méthodes existantes. De plus, nous démontrons que les modèles à l'état de l'art améliorent significativement leurs estimations d'ITE lorsqu'ils sont enrichis par les substituts latents appris par CDVAE, atteignant des performances proches de l'oracle sans accès direct aux véritables variables d'ajustement.

La deuxième contribution traite le défi de l'estimation des effets de traitement à long terme à travers une nouvelle approche de régression contrefactuelle, axée sur l'efficacité computationnelle et la précision de la prévision. En s'appuyant sur des réseaux de neurones récurrents (RNN) enrichis par le codage prédictif contrastif (CPC) et la maximisation de l'information mutuelle (InfoMax), le modèle capture les dépendances temporelles à long terme en présence de facteurs confondants variant dans le temps, tout en évitant les coûts computationnels associés aux transform-

ers. Ce cadre établit de nouveaux standards en estimation contrefactuelle sur des jeux de données synthétiques et réels, et constitue la première intégration du CPC en inférence causale.

La troisième contribution aborde l'apprentissage de représentations causales (CRL), qui vise à découvrir des facteurs latents causaux influençant des observations de haute dimension. Si les progrès récents du CRL ont mis l'accent sur l'identifiabilité dans l'espace latent, l'interprétabilité de la manière dont ces causes latentes se manifestent dans les variables observées n'est pas encore suffisamment explorée – en particulier dans les données structurées comme les données tabulaires longitudinales. Nous introduisons un mécanisme d'interprétabilité agnostique à l'architecture du modèle utilisé, fondé sur la géométrie du Jacobien du décodeur. En imposant une contrainte de parcimonie auto-expressive sur les colonnes du Jacobien, nous induisons une structure modulaire où les variables observées sont regroupées selon leurs influences latentes partagées. Cette contrainte permet de retrouver des regroupements significatifs – potentiellement chevauchants – reflétant la structure causale sous-jacente. Nous établissons des conditions formelles garantissant l'identification cohérente de ces groupes : dans le cas disjoint, nous prouvons la détection de sous-espaces ; dans le cas chevauchant, nous établissons des bornes d'erreur de classification. Nos résultats montrent que la structure causale latente peut être récupérée à partir de la géométrie différentielle, sans recourir à des hypothèses restrictives telles que les variables ancrées ou les décodages mono-parentaux. Au-delà des apports théoriques, nous proposons une technique de régularisation basée sur le Jacobien, à la fois efficace et adaptée aux domaines à grande dimension.

**Title:** Learning Causality for Longitudinal Data

**Keywords:** Causal Inference, Longitudinal Data, Causal Representation Learning, Counterfactual Regression, Latent Variable Modeling

**Abstract:**

This thesis addresses causal inference and causal representation learning (CRL) for high-dimensional, time-varying data, with applications across fields such as precision medicine, marketing, and retail. The first contribution introduces the Causal Dynamic Variational Autoencoder (CDVAE), a model designed to estimate Individual Treatment Effects (ITEs) by capturing unobserved heterogeneity in treatment response due to latent risk factors. Unlike traditional approaches that assume some confounders are unobserved, CDVAE focuses on unobserved variables affecting only the outcome sequence. CDVAE is grounded in theoretical guarantees concerning the validity of latent adjustment variables and generalization bounds on ITE estimation error. Extensive evaluations on synthetic and real-world datasets show that CDVAE outperforms existing baselines. Moreover, we demonstrate that state-of-the-art models significantly improve their ITE estimates when augmented with the latent substitutes learned by CDVAE, approaching oracle-level performance without direct access to the true adjustment variables.

The second contribution expands on the challenge of long-term treatment effect estimation through a novel approach to counterfactual regression over time, prioritizing computational efficiency and long-term forecasting accuracy. By leveraging Recurrent Neural Networks (RNNs) enhanced with Contrastive Predictive Coding (CPC) and Information Maximization (InfoMax), the model captures long-term dependencies in the presence of time-varying confounders while avoiding the computational costs associated with transformers. This framework achieves state-of-the-art results

in counterfactual estimation across synthetic and real-world datasets and is the first to incorporate CPC into causal inference.

The third contribution tackles Causal Representation Learning (CRL), which seeks to uncover high-level latent factors that influence complex, high-dimensional observations. While recent advances in CRL have emphasized identifiability in the latent space, they often leave open the interpretability of how latent causes manifest in the observed variables—especially in structured data such as longitudinal tabular records. In this work, we introduce a model-agnostic interpretability layer grounded in the geometry of the decoder’s Jacobian. By enforcing a sparse self-expression prior on the Jacobian columns, we induce a modular structure wherein observed features are grouped according to shared latent influences. This constraint enables the recovery of meaningful, potentially overlapping clusters of observed variables, reflecting the underlying generative graph. We provide formal conditions under which these clusters can be consistently identified: in the disjoint setting, we prove subspace detection guarantees using tools from sparse subspace clustering; in the overlapping case, we derive misclassification bounds under a structured latent-feature model that combines sparsity, incoherence, and dominance conditions. Our results demonstrate that latent-to-observed causal structure can be recovered from gradient geometry without restrictive assumptions such as anchor features or single-parent decoding. Beyond the theoretical contributions, we propose efficient Jacobian-based regularization techniques that scale to high-dimensional domains.

*To my parents.*

*To my lovely sisters.*

*To the kid I was, to the man I am.*

*To the orchid once I watered but withered.*



# Acknowledgements

Un ouvrage est fini quand on ne peut plus  
l'améliorer, bien qu'on le sache insuffisant et  
incomplet. On en est tellement excédé, qu'on  
n'a plus le courage d'y ajouter une seule  
virgule, fût-elle indispensable. Ce qui décide  
du degré d'achèvement d'une œuvre, ce n'est  
nullement une exigence d'art ou de vérité,  
c'est la fatigue et, plus encore, le dégoût.

---

Emil Cioran

This thesis would not have been possible without the trust and support of Paul-Henry Cournède and Benoît Lepetit.

I am deeply grateful to Paul-Henry Cournède—my former teacher and my Ph.D. director—for welcoming the idea of a thesis on causality at CentraleSupélec. Your rigorous perspective on my research, your many interventions to ease administrative hurdles, and, above all, your trust in my work have been invaluable. I greatly admire both your intellectual clarity and your human warmth.

Benoît, I vividly remember our first meeting—as if it were yesterday. We had never met before, and our initial contact was simply through LinkedIn. Yet, within the first ten minutes, we were already discussing the framework of a Ph.D. program. Your openness and willingness to engage with a stranger aspiring to pursue a doctorate meant a great deal to me.

I must heartwarmingly acknowledge the support, kindness, and guidance of my Ph.D. supervisor, Myriam Tami. Without you, I would not be the researcher I am today. Working with you has been both a professional privilege and a profoundly human experience. I sincerely cherish your friendship.

This is also a moment to honor all the extraordinary teachers I have had—from primary school onward. I cannot name you all here, but I am profoundly indebted to you for the skills, knowledge, and way of seeing the world that you have instilled in me.

Finally, I must thank the people without whom I would not have seen the light of day or written this thesis: my parents. It is impossible to enumerate the debts I owe you. The sacrifices you have made are engraved in my soul. This thesis is for you.

# Contents

<b>Glossary</b>	<b>9</b>
<b>Acronyms</b>	<b>10</b>
<b>1 Introduction</b>	<b>13</b>
<b>2 Background</b>	<b>20</b>
2.1 Potential Outcome Framework: Static setting . . . . .	21
2.1.1 Definition . . . . .	21
2.1.2 Methods: An Overview . . . . .	26
2.2 Potential Outcome Framework for Longitudinal data: Main Setting of the Thesis . . . . .	29
2.2.1 Introduction: Dynamic vs. Time-Varying Treatment Regimes . . . . .	29
2.2.2 Causal Effects in Longitudinal Settings: Definitions and Identification . . . . .	32
2.2.3 Modeling Challenges . . . . .	36
2.2.4 Literature Overview: The Challenge of Missing Confounders . . . . .	38
2.2.5 Literature Overview: Methods verifying our Causal assumptions . . . . .	43
2.3 Causal graphs . . . . .	48
<b>3 Causal Dynamic Variational Autoencoder</b>	<b>55</b>
3.1 Introduction . . . . .	55
3.2 Related Work . . . . .	58
3.3 Problem Definition . . . . .	60
3.4 Mixed Effect Modeling and Heterogeneous Treatment Effect: A Unifying View . . . . .	62
3.5 Causal DVAE . . . . .	64
3.5.1 When does a Latent Representation Act as a Valid Substitute for Unobserved Adjustment Variables? . . . . .	64
3.5.2 Definition of the probabilistic model . . . . .	66
3.5.3 CDVAE in the near deterministic regime . . . . .	69
3.6 Generalization Bound over Treatment Effect Estimation and Derivation of Model Loss . . . . .	72
3.7 Experiments . . . . .	78
3.8 Algorithmic Details . . . . .	79

3.9	Models hyperparameters . . . . .	79
3.9.1	Adapting Baselines to Our Causal Settings . . . . .	81
3.9.2	Synthetic Data Sets . . . . .	81
3.9.3	Semi-Synthetic MIMIC-III Data . . . . .	84
3.10	Discussion . . . . .	86
<b>4</b>	<b>Causal Contrastive Predictive Coding</b>	<b>92</b>
4.1	Introduction . . . . .	92
4.2	Contributions . . . . .	93
4.3	Related Work . . . . .	94
4.4	Problem Formulation . . . . .	96
4.5	Causal CPC . . . . .	98
4.5.1	Representation Learning . . . . .	98
4.5.2	Balanced representation learning . . . . .	102
4.5.3	Causal CPC Training . . . . .	107
4.6	Experiments . . . . .	108
4.6.1	Experiments with Synthetic Data . . . . .	110
4.6.2	Experiments with semi-synthetic and real data . . . . .	112
4.7	Discussion . . . . .	115
<b>5</b>	<b>Toward a More Transparent Causal Representation Learning</b>	<b>119</b>
5.1	Introduction . . . . .	119
5.2	Preliminaries and Notations . . . . .	122
5.3	Intuitive Discussion of Jacobian Self-Expression . . . . .	129
5.4	Related Work . . . . .	133
5.4.1	CRL in a time-varying setting . . . . .	133
5.4.2	Understanding the Generation Mechanism in CRL . . . . .	134
5.4.3	Subspace Clustering . . . . .	136
5.5	Modeling . . . . .	137
5.5.1	Subspace Detection Under Self-Expression Property . . . . .	137
5.5.2	From Subspace Detection to Cluster Recovery . . . . .	146
5.5.3	Generalization and Stability of the Self-Expression Objective . . . . .	151
5.5.4	Computational efficiency: Calculating the Penalty $\bar{\ell}(C, f; \mathbf{x})$ . . . . .	154
5.5.5	Applying Static Self-Expression Theory in a CRL in Time-Series Setting . . . . .	155
5.6	Experiments . . . . .	156
5.6.1	Synthetic data . . . . .	156
5.6.2	Real data . . . . .	159
5.7	Discussion . . . . .	160



<b>6</b>	<b>Epilogue</b>	<b>162</b>
6.1	Towards a causal representation of confounders for causal inference . . . . .	162
6.2	Invariance of the generative maps and representation identifiability . . . . .	163
6.3	Uncertainty and Sensitivity in Causal Inference for Longitudinal Data . . . . .	164
6.4	Uncertainty in Causal Representation Learning . . . . .	166
<b>A</b>	<b>Appendix: Chapter 3</b>	<b>167</b>
A.1	Proofs . . . . .	167
A.1.1	Identifiability: Treatment Effects and Unobserved Adjustment Variables . . . . .	167
A.1.2	Derivation of CDVAE Loss . . . . .	169
A.1.3	Transfer of Ignorability under Invertible Maps . . . . .	171
A.1.4	CDVAE in the Near-Deterministic Regime . . . . .	172
A.1.5	Upper bound on weighted PEHE . . . . .	178
A.1.6	Proof of Proposition Prop3.2 . . . . .	180
A.2	Experiments on synthetic data: Details . . . . .	180
A.2.1	Additional results . . . . .	180
A.3	Experiments on MIMIC-III data . . . . .	181
A.3.1	Additional results . . . . .	181
A.4	Models hyperparameters Details . . . . .	181
A.5	The Neural Architecture of CDVAE . . . . .	181
<b>B</b>	<b>Appendix: Chapter 4</b>	<b>185</b>
B.1	Experiments on semi-synthetic data: Details . . . . .	185
B.1.1	Additional results . . . . .	185
B.2	Proofs of theoretical results . . . . .	185
B.2.1	Relation between InfoNCE loss and mutual information . . . . .	185
B.2.2	Relation between InfoMax and input reconstruction . . . . .	186
B.2.3	Proof of Theorem Thm4.1 . . . . .	187
B.2.4	On the relation between conditional entropy and reconstruction . . . . .	188
B.2.5	Proof of theorem Thm4.3 . . . . .	188
B.3	Causal CPC: Architecture details . . . . .	191
B.4	Models hyperparameters . . . . .	192
<b>C</b>	<b>Appendix: Chapter 5</b>	<b>194</b>
C.1	Proofs . . . . .	194
C.1.1	Background: Subspace detection in a deterministic model . . . . .	194
C.1.2	Proof of Theorem Thm5.1 . . . . .	196
C.1.3	High-Probability Guarantee for Subspace Detection . . . . .	198
C.1.4	Recovery of Feature Clusters via Spectral Clustering . . . . .	203

C.1.5	Guarantees of features grouping via clustering techniques . . . . .	204
C.1.6	Generalization and Stability Under the Self-Expression Problem . . . . .	211

# List of Figures

1.1	A compressed description of the data generation process behind the causal Question Q1.1.	16
1.2	A compressed description of the data generation process behind the causal Question Q1.2.	17
2.1	A general causal graph clarifying the causal links between outcome $Y$ , treatment $W$ , confounders $X$ , adjustment variables $U$ and instruments $I$ .	25
2.2	A causal graph is assumed to generate longitudinal data of 3-time steps ( $T = 3$ ). Edges are colored (pink, blue, and red) whenever the causal relation may contribute to confounding treatment and response at any time step $t$ .	34
3.1	A simplified representation of the Data-Generating Process (DGP) at time $t$ . Edges between $Y_{<t}$ , $W_{<t}$ , and $\mathbf{X}_{<t}$ are omitted for simplicity.	61
3.2	A causal graph describing panel data for the Vitamin D problem.	62
3.3	A simplified causal graph for the sketch of the proof for Theorem Thm3.2. We do not represent $W_{\leq t}$ , $\mathbf{X}_{\leq t}$ for simplicity.	65
3.4	Evolution of PEHE in estimating ACATE for synthetic data across increasing levels of heterogeneity induced by adjustment variables $\mathbf{U}$ .	84
3.5	Results on the Medical Information Mart for Intensive Care (MIMIC)-III data reported by Precision in Estimation of Heterogeneous Effects (PEHE) and organized following the three possible configurations. Smaller is better.	86
3.6	Evolution of variance parameter update during training for synthetic data (left) for each level of $\gamma_{(1)}^{YU}$ and MIMIC-III (right) averaged over 10 random initializations	87
3.7	Results of Causal Dynamic Variational Autoencoder (CDVAE) when varying the number of components $K$ of the prior for the synthetic data (left) and MIMIC-III (right) reported by PEHE. Smaller is better.	87
3.8	Evolution of CDVAE posterior predictive p-values for synthetic (left) and semi-synthetic MIMIC-III data (right). We report the average for 10 random initializations at each time step.	88
3.9	An example of an M-collider structure, where the variable $V$ influences both the treatment and the response, as indicated by the dashed arrows.	91

4.1	Causal graph over $\mathbf{H}_{t+1}$ . For simplicity, we represent past treatments as $W_{\leq t}$ such that each element in that sub-sequence confounds the next treatment and response $W_{t+1}$ and $Y_{t+1}$ . Idem for $Y_{\leq t}$ and $\mathbf{X}_{\leq t}$ . The static covariates $\mathbf{V}$ are assumed to affect all the time-varying variables. We omit the representation of exogenous noise for simplicity. Interactions between $W_{\leq t}$ , $\mathbf{X}_{\leq t}$ , and $Y_{\leq t}$ were also omitted for simplicity. . . . .	97
4.2	Causal Contrastive Predictive Coding (CPC) architecture: The left shows the encoder, which learns context $\mathbf{C}_t^{\text{enc}}$ from process history $\mathbf{H}_t$ , with CPC and Information Maximization (InfoMax) objectives used for pretraining. The right shows the decoder, which autoregressively predicts the future outcome sequence from $\mathbf{C}_t^{\text{enc}}$ . . . . .	104
4.3	Evolution of error Normalized Root Mean Squared Error (NRMSE) in estimating counterfactual responses for cancer simulation data. Top: training sequence length 60. Bottom: training sequence length 40. In both cases, $\rho = 10$ . MSM is excluded due to high prediction errors. . . . .	111
4.4	Models' performance for cancer simulation reported by NRMSE for $\gamma = 2$ and $\rho = 15$ . The training sequence length is 60. . . . .	112
4.5	Performance for MIMIC II semi-synthetic reported by RMSE over 10 forecasting horizons. The sequence training length is 60. . . . .	114
4.6	Factual estimation errors for baselines for Real MIMIC-III data reported by RMSE. The training sequence length is 100. . . . .	115
4.7	Ablation study of Causal CPC for MIMIC-III dataset. RMSE is reported for 10 forecasting horizons. Smaller is better. . . . .	116
5.1	Comparison of three structural assumptions over the generation process: single-parent decoding, anchor feature, and sparse self-expression assumption. Here, we assume $d_x = 12$ and $d_z = 5$ . . . . .	121
5.2	A geometric illustration of the assumption of subspaces union (Asm5.4) that underlies subspace clustering. Two planes are presented as subspaces of the Jacobian span $(\mathcal{S}_1, \mathcal{S}_2)$ , within which gradients are drawn. . . . .	139
5.3	An illustration of the two principal angles between two subspaces $\mathcal{S}_m, \mathcal{S}_{m'}$ . . . . .	143
5.4	Illustration of the modular latent structure from Proposition Prop5.1. Solving the sparse self-expression problem yields an adjacency matrix $A^*$ (cf. Equation5.4), whose nonzero entries define connected components in the feature graph $G_F$ . We recover these components via spectral clustering. . . . .	148
5.5	Hierarchical relationships in the Saint-Gobain transaction data. Subcategories form product categories, which in turn are grouped into broader product specialties. . . . .	159

# List of Tables

1	Summary of Main Mathematical Notations . . . . .	12
2.1	Comparison of Causal Inference Methods by Category . . . . .	29
2.2	Comprehensive Overview of Methods Addressing Missing Confounders in Longitudinal Data	42
3.1	Trainable parameters in thousands (k) for baselines in all configurations for the synthetic and semi-synthetic MIMIC-III data. . . . .	82
3.2	CDVAE ablation study conducted on the semi-synthetic MIMIC-III data reported by PEHE. Smaller is better. . . . .	86
3.3	Results on the synthetic data reported by PEHE. Smaller is better. . . . .	86
4.1	Summary of concurrent methods contrasted against Causal CPC across design aspects. . .	93
4.2	Results on the synthetic data set with training sequence length 60: mean±standard deviation of NRMSE. The best value for each metric is given in bold: smaller is better. . . . .	111
4.3	Results on the MIMIC-III semi-synthetic reported by mean±standard deviation of RMSEs. The training sequence length is 100. Smaller is better. . . . .	113
4.4	Models complexity and the running time averaged over five seeds. Results are reported for tumor growth simulation ( $\gamma = 1$ ). Hardware: GPU-1xNVIDIA Tesla M60. . . . .	114
4.5	The number of parameters to train for each model after hyper-parameters fine-tuning and the corresponding running time averaged over five seeds. Results are reported for semi-synthetic MIMIC-III data; the processing unit is GPU-1 x NVIDIA Tesla M60 . . . .	114
4.6	Ablation study with NRMSE averaged across ( $1 \leq \rho \leq 10$ ) for cancer simulation ( $\gamma = 1$ ) and MIMIC-III. . . . .	115
4.7	Results of the ablation study on the synthetic data set: mean±standard deviation of NRMSE. The best value for each metric is given in bold: smaller is better. . . . .	116
4.8	Results on MIMIC-III semi-synthetic data set: mean±standard deviation of NRMSE. The best value for each metric is given in bold: smaller is better. . . . .	116
4.9	Results of Nguyen, Wainwright, and Jordan (NWJ) and Mutual Information Neural Estimator (MINE) Mutual Information (MI) lower bounds when used for CPC and InfoMax for MIMIC-III semi-synthetic data set: mean±standard deviation of NRMSE. The best value for each metric is given in bold: smaller is better. . . . .	117

4.10	Results on the MIMIC-III when sequential ignorability is violated reported by RMSEs . .	118
5.1	Key differences between our analysis and prior SSC theory. . . . .	144
5.2	Clustering coherence on simulated data, true labels are simulated. . . . .	158
5.3	Performance metrics under overlapping features for synthetic data with varying overlap levels $\alpha$ . . . . .	159
5.4	Clustering coherence of Saint-Gobain data with different true label levels . . . . .	160
A.1	Results on the synthetic data reported by PEHE. Smaller is better. . . . .	180
A.2	Results of CDVAE when varying the number of components $K$ of the prior. The study is conducted on the synthetic data and is reported by PEHE. Smaller is better. . . . .	181
A.3	Results on the MIMIC III data reported by PEHE. Smaller is better. . . . .	181
A.4	Hyper-parameters search range for RMSN . . . . .	182
A.5	Hyper-parameters search range for CRN . . . . .	182
A.6	Hyper-parameters search range for G-Net . . . . .	182
A.7	Hyper-parameters search range for Causal Transformer . . . . .	183
A.8	Hyper-parameters search range for Causal CPC . . . . .	183
A.9	Hyper-parameters search range for CDVAE . . . . .	183
A.10	Architecture of the outcome model prediction, i.e., the decoder. . . . .	183
A.11	Architecture: representation learner $\phi$ of CDVAE . . . . .	184
A.12	Architecture: propensity network $e_{\theta_\omega}(\cdot)$ . . . . .	184
A.13	Inference network $q_\phi(\mathbf{z} \mid y_{\leq T}, \mathbf{x}_{\leq T}, \omega_{\leq T})$ . . . . .	184
B.1	Results over the MIMIC III semi-synthetic data set (same experimental protocol as in Melnichuk et al. (2022)): mean $\pm$ standard deviation of Rooted Mean Squared Errors (RMSEs). The best value for each metric is given in bold: smaller is better. . . . .	185
B.2	Architecture for learning local features $\mathbf{Z}_t$ . . . . .	191
B.3	Architecture for learning context representation $\mathbf{C}_t^{\text{enc}}$ . . . . .	191
B.4	Architecture for outcome prediction . . . . .	191
B.5	Architecture for treatment prediction . . . . .	191
B.6	Hyper-parameters search range for RMSN . . . . .	192
B.7	Hyper-parameters search range for CRN . . . . .	192
B.8	Hyper-parameters search range for G-Net . . . . .	192
B.9	Hyper-parameters search range for Causal Transformer . . . . .	193
B.10	Hyper-parameters search range for Causal CPC . . . . .	193

# Glossary

# Acronyms

<b>ACATE</b> Augmented Conditional Average Treatment Effect. 57, 61–65, 72, 75, 83, 85, 165	<b>H</b> Homogeneity. 160
<b>ATE</b> Average Treatment Effect. 18, 20, 22, 25–27, 35, 36, 77	<b>InfoMax</b> Information Maximization. 6, 7, 18, 93–96, 99–101, 104, 107, 115, 117
<b>CATE</b> Conditional Average Treatment Effect. 18, 20, 25–29, 35, 36, 41, 42, 57, 59–62, 71, 165	<b>InfoNCE</b> Information Noise Contrastive Estimation. 93, 99–101, 107, 111, 115, 117
<b>CDC</b> Counterfactual Domain Confusion. 45	<b>IPM</b> Integral Probability Metric. 75, 76, 78–80, 86
<b>CDVAE</b> Causal Dynamic Variational Autoencoder. 5, 7, 18, 20, 25, 56, 58, 69, 72, 75, 78–83, 85–88, 96	<b>IPTW</b> Inverse Probability of Treatment Weighting. 26, 43
<b>CLUB</b> Contrastive Log-ratio Upper Bound. 93, 94, 105	<b>ITE</b> Individualized Treatment Effect. 14, 18, 20, 22, 55–59, 70, 75, 81, 165
<b>CMM</b> Conditional Markov Model. 57, 65, 90	<b>KL</b> Kullback–Leibler. 68, 115, 116
<b>CPC</b> Contrastive Predictive Coding. 6, 7, 18, 20, 56, 59, 78, 81, 82, 86, 93, 94, 96, 98, 104, 107, 108, 110, 111, 113–118, 165	<b>LHS</b> left-hand side. 53
<b>CRL</b> Causal Representation Learning. 18, 19, 119–122, 126, 133–135, 144, 155, 156, 160–162, 164, 166	<b>LSTM</b> Long Short-Term Memory. 41, 44, 46, 93, 114
<b>CRN</b> Counterfactual Recurrent Network. 44, 56, 58, 78, 81, 82	<b>MI</b> Mutual Information. 7, 93–96, 99–101, 105, 106, 115–118
<b>CT</b> Causal Transformer. 56, 59, 78, 81	<b>MIMIC</b> Medical Information Mart for Intensive Care. 5–8, 57, 82, 84, 86–88, 94, 111–118
<b>CTE</b> Contemporaneous Treatment Effect. 37, 60, 61	<b>MINE</b> Mutual Information Neural Estimator. 7, 115–118
<b>DAG</b> Directed Acyclic Graph. 14, 49	<b>MSM</b> Marginal Structural Model. 38, 40, 42–44, 56, 58
<b>DGP</b> Data-Generating Process. 5, 15, 61, 101	<b>NMI</b> Normalized Mutual Information. 156, 158, 160, 161
<b>ELBO</b> Evidence Lower Bound. 66	<b>NRMSE</b> Normalized Root Mean Squared Error. 6, 7, 110–112, 115–117
<b>GLM</b> Generalized Linear Model. 27, 29	<b>NWJ</b> Nguyen, Wainwright, and Jordan. 7, 117, 118
<b>GMM</b> Gaussian Mixture Model. 57	<b>PEHE</b> Precision in Estimation of Heterogeneous Effects. 5, 7, 74, 75, 83, 85–87
<b>GNNs</b> Graph Neural Networks. 162	
<b>GRU</b> Gated Recurrent Unit. 78, 93, 94, 114	



**PO** Potential Outcomes. 14, 18, 20, 21, 27, 30, 38, 48, 60, 96, 165

**RCT** Randomized Controlled Trial. 13

**RMSM** Recurrent Marginal Structural Model. 43, 44, 56, 58, 78, 81, 82

**RNN** Recurrent Neural Network. 18, 41, 43–46, 92, 118, 162

**ROI** Return on Investment. 15

**SAAC** Spectral Algorithm with Additive Clustering. 122, 148, 150, 158, 159

**SCM** Structural Causal Model. 14, 18, 20, 48, 53, 54, 119, 120, 166

**SGDBF** Saint-Gobain Distribution Bâtiment France. 15

**SOTA** state-of-the-art. 19, 58, 59, 105, 108, 111–113, 115, 118

**SSC** Sparse Subspace Clustering. 121, 122, 137, 142, 144, 145, 194, 196, 203, 204

**SUTVA** Stable Unit Treatment Value Assumption. 20, 22

**SymNMF** Symmetric Nonnegative Matrix Factorization. 122, 148, 150, 158, 159

**TMLE** Targeted Maximum Likelihood Estimation. 26, 29

**w.h.p** with high probability. 122, 142–144, 148

**w.r.t.** with respect to. 32, 49

**XAI** Explainable Artificial Intelligence. 13

Table 1: Summary of Main Mathematical Notations

Notation	Description
$T$	Length of the longitudinal sequence (number of time steps)
$N$	Number of individuals
$t$	Time index, $t = 1, \dots, T$
$i$	Individual (subject) index
$\rho$	Forecasting horizon or number of lags in an autoregressive model
$\mathbf{X}_t$	Time-varying covariates at time $t$
$\mathbf{V}$	Static covariates
$W_t$	Treatment assignment at time $t$ (binary)
$Y_t$	Observed outcome at time $t$
$\mathbf{H}_t$	History/context up to $t$ : $(\mathbf{X}_{\leq t}, W_{< t}, Y_{< t})$
$\mathbf{F}_{t+j}$	Future components at time $t+j$ : $[\mathbf{V}, \mathbf{X}_{t+j}, W_{t+j-1}, Y_{t+j-1}]$
$\mathbf{C}_t^{\text{enc}}$	Encoded context representation (history)
$\mathbf{U}$	Unobserved static adjustment variables (risk factors)
$\mathbf{Z}$	Generic latent variable
$\tau_t(\cdot)$	Conditional average treatment effect (CATE) at time $t$
$\tau_t(\mathbf{h}_t, \mathbf{u})$	Augmented CATE (ACATE) at time $t$
$\Phi$	Representation function / encoder
$f$	Outcome model / decoder
$\theta, \phi$	Model parameters: generative ( $\theta$ ), inference ( $\phi$ )
$\sigma$	Variance (noise) parameter in generative model
$p(\cdot)$	Probability distribution or density
$q_\phi(\cdot)$	Variational (approximate) posterior distribution
$\mathcal{D}_T$	Observed data up to time $T$
ELBO	Evidence Lower Bound (variational objective)
$\mathcal{L}^{(\text{InfoNCE})}$	InfoNCE contrastive loss
$\mathcal{L}^{(\text{InfoMax})}$	InfoMax contrastive loss
$\mathcal{L}^{\text{CPC}}$	CPC loss (average InfoNCE)
$\mathcal{L}_Y$	Outcome prediction loss
$\mathcal{L}_W$	Treatment prediction loss
$\mathcal{B}$	Batch of samples
IPM	Integral Probability Metric (e.g., Wasserstein)
$I(\cdot, \cdot)$	Mutual information
$I_{\text{CLUB}}(\cdot, \cdot)$	CLUB upper bound on MI
$\alpha(\cdot)$	Importance sampling / weighting function
$\epsilon$	Generic error / noise parameter
$\mathbb{E}$	Expectation operator
$\mathbb{P}$	Probability operator
$\mathcal{N}$	Normal (Gaussian) distribution
$\mathcal{S}_m$	$m$ -th subspace in union-of-subspaces model
$n_m$	Number of observed features in subspace $\mathcal{S}_m$
$d_x$	Number of observed variables
$d_z$	Number of latent variables
$d_v$	Dimensionality of static covariates
$\text{aff}(\mathcal{S}_m, \mathcal{S}_{m'})$	Affinity between subspaces
$C \in \mathbb{R}^{d_x \times d_x}$	Self-expression coefficient matrix
$Df(\cdot)$	Jacobian of $f$ at $\mathbf{z}$ (shape $d_x \times d_z$ )
$\nabla_{\mathbf{z}} f(\cdot)$	Gradient of $f_j$ w.r.t. $\mathbf{z}$ (Jacobian column)
$Pa(i)$	Parent set of observed variable $i$
$Ch(j)$	Children set of latent variable $j$

# Chapter 1

## Introduction

As traditionally intended, machine learning models aim at recognizing patterns and identifying statistical dependencies for tasks like prediction, classification, and regression (Jordan & Mitchell, 2015). However, these models can *capture* spurious relationships by focusing primarily on correlations. When applied under different conditions, they may mislead, since a statistical association alone does not imply a causal link (Pearl, 2009b).

Causal inference provides a principled framework to capture cause-and-effect relationships (Spirtes, 2010b; Imbens & Rubin, 2015; Peters et al., 2017). In the context of Explainable Artificial Intelligence (XAI), there is growing recognition that purely correlation-based explanations can fail to generalize under interventions or distributional shifts (Linardatos et al., 2021; Carloni et al., 2025). Embedding causal assumptions into machine learning workflows strengthens the transparency and trustworthiness of model outputs and leverages scalable algorithms, such as deep neural networks, to handle high-dimensional and time-varying data more effectively (Berrevoets et al., 2024). At the same time, advances in machine learning have empowered causal inference methods to scale to large, complex datasets, including unstructured data like text and images, overcoming computational bottlenecks of traditional approaches (Deshpande et al., 2022; Deng et al., 2022). Together, this synergy between machine learning’s computational strengths and causal inference’s rigorous foundations paves the way for more robust, interpretable, and reliable data-driven decision making (Chernozhukov et al., 2018; Wang et al., 2021a;c; Sanchez et al., 2022).

Causal inference is dedicated to understanding cause-and-effect relationships and estimating causal effects between variables (Pearl, 2009b; Imbens & Rubin, 2015). For instance, we might ask: *Does a new drug (the “treatment”  $W$ ) lower blood pressure (the “outcome”  $Y$ )?* In a Randomized Controlled Trial (RCT), patients are randomly assigned to receive the drug or a placebo, ensuring that, on average, nothing else differs between the groups. In observational data, however, patients choose to receive the drug based on characteristics like age, health status, or socioeconomic factors, and the way such choice occurs is unknown, which we commonly refer to as the *unknown assignment mechanism*. These characteristics are called *confounders* ( $X$ ) when they influence  $W$  and  $Y$ . When confounders are present, comparing treated versus untreated individuals can give a misleading estimate of the treatment’s effect (Holland, 1986; Pearl, 2009b; Spirtes, 2010b). For example, if older patients are both more likely to receive the drug and have

higher blood pressure, an analysis that ignores age may wrongly conclude that the drug increases blood pressure.

Although machine learning models excel at capturing complex data dependencies and achieving high predictive performance (LeCun et al., 2015), predictive modeling alone is inadequate for causal inference from observational data. Observational data capture only factual outcomes and lack randomized treatment assignment, making it difficult to infer causation directly (Pearl, 2009b; Peters et al., 2017; Fernández-Loría & Provost, 2022). Hence, addressing these challenges requires a causal framework. There are two fundamental frameworks for learning causality, Structural Causal Model (SCM) (Pearl, 2009b) and Potential Outcomes (PO) (Rubin, 2005), which are equivalent in what they can express (Pearl, 2009a; Ibeling & Icard, 2023). A causal model is any model that explicitly encodes cause-and-effect relations between variables. An SCM consists of (cf. Chapter 2, Section 2.3): (1) A Directed Acyclic Graph (DAG) whose nodes represent random variables and whose arrows denote direct causal influence (e.g., "smoking  $\rightarrow$  lung disease"). (2) A corresponding set of structural mechanisms, each of which specifies how a variable is generated by its direct causes (its "parents" in the DAG), together with background noise. The graph and the mechanisms jointly define how variables would change under hypothetical interventions and support counterfactual reasoning (Pearl, 2009b). In contrast, the PO approach (cf. Chapter 2, Section 2.1.1) defines, for each unit, the outcome that would be observed under each treatment regime (e.g., "the blood-pressure reading if treated" vs. "if not treated") and defines causal effects as comparisons between these potential outcomes (Rubin, 2005).

In many applications where individuals may respond differently to the same intervention, such as healthcare, social sciences, and marketing, estimating an Individualized Treatment Effect (ITE) is instrumental. Understanding these heterogeneous treatment effects allows for more personalized and effective interventions. For instance, accurate treatment effect estimation in healthcare can enable clinicians to select optimal treatments tailored to individual patients (Shalit, 2020; Atan et al., 2018; Mueller & Pearl, 2023). In the social sciences, ITE estimation can inform targeted interventions that address the specific needs of different population groups (Morgan, 2013; Imbens & Rubin, 2015), while in marketing, it allows businesses to refine strategies tailored to particular groups of customers (Fang et al., 2023; Hair Jr & Sarstedt, 2021).

## **Handling Unobserved Heterogeneity in Treatment Effect Estimation for Longitudinal Data**

This thesis focuses on estimating treatment effects within longitudinal data settings, which present several challenges: complex temporal dependencies, time-dependent confounding, and unobserved heterogeneity. If the unobserved sources of heterogeneity are assumed to be confounders, then any naive estimation of the treatment from observed data will be biased. However, the thesis argues that other sets of unobserved features that are not confounders but only explain the response are also crucial if one aims to estimate ITE. These variables are called *adjustment variables* (Pearl, 2009b; Hassanpour & Greiner, 2019a; Qidong et al., 2020; Zhang et al., 2021a; Zheng et al., 2024), *risk factors* (Zhang et al., 2021a), or *effect modifiers* (VanderWeele & Robins, 2007; VanderWeele, 2012; Schouten, 2024). We therefore address this problem

as our first contribution in Chapter 3 while studying the immediate effect following the application of a treatment that is the *contemporaneous effects* (Assumption Asm2.8). We reframe our problem as follows:

**Question Q1.1**

In longitudinal data, when we are missing baseline covariates that affect only the series of responses, how can we estimate a time-varying treatment effect that is as individual as possible?

**Significance of the Question Q1.1 in Retail: Example of Saint-Gobain** *Saint-Gobain Distribution Bâtiment France (SGDBF)* is exploring solutions to enhance client satisfaction and operational sustainability. Causal inference is an attractive way to understand client behavior, leveraging transaction data that records customer interactions, preferences, and purchasing patterns over time. The sequential nature of this data provides an opportunity to infer the causality underlying customer decisions, thereby enabling SGDBF to better understand the effect of the continuing commercial action on the customer purchase behavior and, ultimately, the Return on Investment (ROI). An example of an application involves understanding the impact of commercial visits on client behavior. Here, clients are craftsmen or construction firms, and Saint-Gobain’s products are construction materials. Each client group is assigned to a sales representative who schedules in-person visits, sometimes following a phone call, and may visit multiple times within a week. The binary treatment variable (i.e., whether the client received a call or not) affects purchase behavior, which can be quantified in terms of purchase frequency or average purchase amount spent post-visit. Here, a client is considered *treated* if they received at least one visit at each time step, representing a week’s time window. As an illustration of Question Q1.1 and considering a time-varying setting where observable variables include client preferences  $\mathbf{X}_t$ , the intervention or treatment represented by an in-person visit  $W_t$ , and the subsequent outcome, or purchase amount  $Y_t$ . However, an unobserved variable,  $\mathbf{U}$ , representing the number of current construction projects of the client, introduces an additional challenge: If a client is managing multiple projects simultaneously, receiving a visit may increase their purchase frequency and amount. Conversely, if they have few or no active projects, even multiple commercial visits may fail to incentivize purchases due to a lack of projects to consume the materials.

We, therefore, aim to estimate the effect of treatment  $W_{t+1}$  on  $Y_{t+1}$  given a context history  $\mathbf{H}_t$  that includes all records as in Figure 1.1, while also accounting the possible heterogeneity in treatment effect that may be induced by the unobserved variable  $\mathbf{U}$ .

**Significance of the Question Q1.1 in Precision Medicine** Consider a scenario where we aim to estimate the effect of a medical intervention like chemotherapy  $W_t$  on the volume of a cancerous tumor  $Y_t$ . During a time window of medical treatment, one could gather all records on vital measures that were measured as  $\mathbf{X}_t$ . However, it is not infrequent in such a medical scenario to have missed essential baseline covariates  $\mathbf{U}$ , such as genetic predispositions, lifestyle factors, and pre-existing health conditions, that may influence patients’ responses to the treatment. Therefore, the underlying DGP could be described

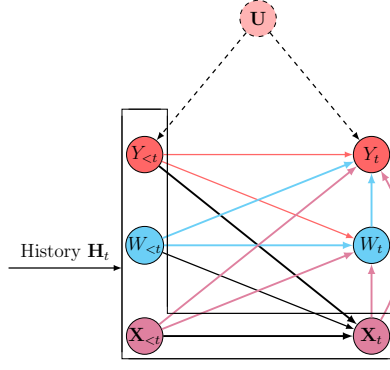


Figure 1.1: A compressed description of the data generation process behind the causal Question Q1.1.

compactly in Figure 1.1. As a result, individual response to treatment and, therefore, its efficacy may crucially depend on unobserved adjustment variables  $U$ .

### Related contributions to Question Q1.1

- *M El Bouchattaoui, M Tami, B Lepetit, PH Cournède. Causal dynamic variational autoencoder for counterfactual regression in longitudinal data.* Under review at TMLR 2025.
- *M El Bouchattaoui, M Tami, B Lepetit, PH Cournède. A non-linear mixed effect model for the estimation of causal effects through time.* The 54th Annual Meeting of the French Statistical Society, 2023, 10 pages.
- *M El Bouchattaoui, M Tami, B Lepetit, PH Cournède. CDVAE: Estimating causal effects over time under unobserved adjustment variables.* Colloquium Quarter causality (When Causal Inference meets Statistical Analysis, Paris 2023).
- Open source implementation: <https://github.com/moad-lihoconf/cdvae>.

**From Immediate to Long-Term Treatment Effects** Building on our initial focus on handling unobserved heterogeneity and estimating treatment effects for immediate responses, our second contribution broadens the causal question. Here, we aim to forecast the effect of a sequence of treatments across multiple future time points. We achieve this through careful temporal modeling and architectural design, ensuring a computationally efficient approach to infer long-term treatment effects across various horizons. To summarize, our second contribution answers the following causal question:

#### Question Q1.2

In longitudinal data, assuming no unobserved sources of heterogeneity (whether confounders or risk factors), how can we efficiently estimate the effect of any potential sequence of future treatments (Figure 1.2) on subsequent responses over extended forecasting horizons?

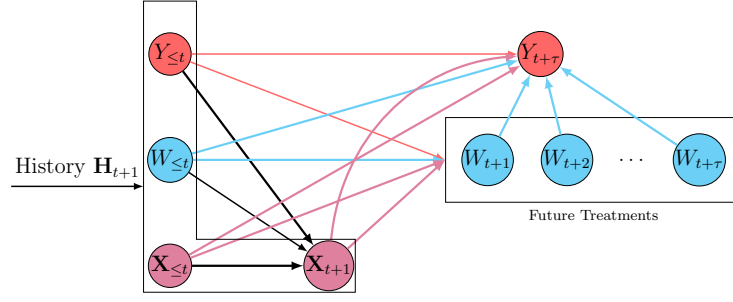


Figure 1.2: A compressed description of the data generation process behind the causal Question Q1.2.

**Significance of the Question Q1.2 in Retail: Example of Saint-Gobain** In retail, understanding the immediate effect of an intervention, like a promotional campaign or a commercial visit, and its influence over time is essential for long-term ROI and ensuring sustained customer engagement. Being able to assess the long-term effect of a treatment plan is strategic because it enables sales representatives to simulate, on an individual basis, all possible future treatment sequences counterfactually. They can then choose the sequence that maximizes a specific target, such as total or average purchase amount realized following those commercial actions. Using our current notation and following Figure 1.2, the QuestionQ1.2 amounts to assessing the treatment effect of the sequence  $(W_{t+1}, \dots, W_{t+\tau})$  on  $Y_{t+\tau}$  given the history of records  $\mathbf{H}_t$ .

**Significance of Question Q1.2 in Precision Medicine** Answering this question would allow clinicians to evaluate all possible counterfactual trajectories of patient responses following a treatment strategy  $(W_{t+1}, \dots, W_{t+\tau})$ , for example, administering chemotherapy this week, no treatment for the next eight weeks, then radiotherapy in the tenth week, and then choose the best possible treatment path based on the predicted outcome  $Y_{t+\tau}$  for a patient, given their historical records and characteristics  $\mathbf{H}_t$ . Such tailored interventions are data-driven and adaptive, meaning that the models could infer updated patient trajectories based on the updated vital signs.

#### Related contribution to Question Q1.2

- M El Bouchattaoui, M Tami, B Lepetit, PH Cournède. Causal Contrastive Learning for Counterfactual Regression Over Time. NeurIPS 2024.
- Open source implementation: <https://github.com/moad-lihoconf/causal-cpc>.

**From Treatment Effect Estimation to Discovering Causal Relationships** Building on our earlier contributions that focus on estimating treatment effects for specific outcomes, either immediately or over extended horizons, we now shift our attention to the relationships within the dimensions of covariates over time. This final contribution addresses the causal relationships embedded within the covariate dimensions themselves. Specifically, at Saint-Gobain, each time step’s covariates capture purchases by product, where each dimension corresponds to the number of purchases made for a particular item. In this context, understanding causal connections between these dimensions over time allows us to gain insight into

purchasing behaviors and the pathways that drive them. By studying these causal relationships within the covariate dimensions, we aim to uncover the underlying causal mechanisms that shape purchase patterns, shedding light on how various product purchases influence each other over time. This analysis provides a broader perspective on client behavior, enabling a deeper understanding of purchasing dynamics and effectively informing more targeted strategies for meeting client needs.

Our goal falls, therefore, under the theme of Causal Representation Learning (CRL) (Schölkopf et al., 2021), whose objective is to uncover high-level latent factors that give rise to complex data. While recent work has made progress in visual or linguistic domains, real-world applications such as retail analytics, healthcare, or behavioral science often involve structured, high-dimensional data evolving over time. In these settings, the high number of observed variables and their entangled dependencies pose a significant barrier to interpretability. Analysts are not only interested in identifying latent causes, but also in understanding how these causes manifest across familiar, fine-grained variables, such as products in retail or diagnoses in healthcare. Yet current CRL methods offer limited guidance for making these latent factors transparent and actionable. Once a model is trained, it is often unclear what the learned representations mean or how they relate to domain-specific concepts. This lack of interpretability hinders trust, downstream use, and scientific insight. To address this gap, we ask:

### Question Q1.3

How can we discover causal structure in high-dimensional, evolving data in an interpretable and grounded way, linking latent abstractions to meaningful groupings of observed variables?

### Related contribution to Question Q1.3

- *M El Bouchattaoui, M Tami, B Lepetit, PH Cournède. Toward a more transparent CRL, 9th Causal Inference Workshop at UAI 2024.*
- Open source implementation: [https://github.com/moad-lihoconf/crl\\_transparency](https://github.com/moad-lihoconf/crl_transparency).

## Thesis Roadmap

This thesis begins with a foundational exploration of the PO framework in Chapter 2, where we establish core concepts in causal inference, such as ITE, Conditional Average Treatment Effect (CATE) and Average Treatment Effect (ATE), using confounders and key identifiability assumptions to address causal inference questions. We then introduce SCM and causal graphs, setting the stage for CRL. In Chapter 3, we address estimating treatment effects in settings with unobserved risk factors that influence outcomes over time. Our model, CDVAE, estimates treatment effects by modeling this unobserved heterogeneity, achieving strong performance on synthetic and semi-synthetic datasets. Extending this approach, Chapter 4 presents a novel framework for long-term counterfactual regression using Recurrent Neural Network (RNN) with CPC and InfoMax. This efficient method captures long-term dependencies without transformers, delivering



state-of-the-art (SOTA) results. In Chapter 5, we address CRL for high-dimensional, time-varying data, introducing structural sparsity to enhance interpretability by linking latent variables, assumed causal, to observable data. Our method is applied to Saint-Gobain purchase data, showcasing its utility in real-world applications. Finally, Chapter 6 summarizes the contributions and discusses implications for advancing causal inference and representation learning in complex, time-varying datasets.

# Chapter 2

## Background

The PO framework is a cornerstone of causal inference, offering a structured approach to defining and estimating causal effects by considering hypothetical outcomes under varying treatment conditions. This chapter introduces the fundamental concepts of potential outcomes and treatments, emphasizing their importance through illustrative examples. The discussion includes the ITE and the fundamental challenge of causal inference, the inability to observe all potential outcomes for any given individual. Furthermore, we incorporate covariates and examine the role of confounders, introducing key metrics such as the CATE and ATE.

The chapter also covers identifiability issues, addressed through assumptions such as the *Stable Unit Treatment Value Assumption (SUTVA)*. We acknowledge complexities introduced by challenges like *spillover effects*, *carryover effects*, and *feedback mechanisms*, which can complicate causal estimation. We also discuss the role of instrumental and adjustment variables, using examples and a simple adjustment-based model to clarify these concepts. An overview of related work on identifiability, ATE, and CATE in static settings provides a foundation for subsequent discussions on more complex, dynamic environments.

In transitioning to *time-varying* settings, the chapter explores alternative definitions of potential outcomes, as highlighted in our key contributions, such as CDVAE (Bouchattaoui et al., 2023) and Causal CPC (Bouchattaoui et al., 2024). We address general definitions and the restrictive assumptions inherent to each model, underscoring the limitations of classical adjustment methods in time-varying contexts. This discussion leads into the identifiability assumptions required for *sequential ignorability* and emphasizes the challenges associated with time-varying treatment regimes.

Finally, the chapter introduces the concept of SCM and *causal graphs*, discussing principles such as d-separation and the do-operator. We clarify the distinct yet complementary roles of the PO framework and SCM in this thesis:

✎ *The PO framework is employed primarily for causal inference, SCM for causal representation learning, and causal graphs as tools applicable to both approaches.*

## 2.1 Potential Outcome Framework: Static setting

### 2.1.1 Definition

The PO framework, also known as the *Rubin Causal Model* or *Neyman-Rubin Causal Model* (Splawa-Neyman et al., 1990; Rubin, 1974), is one of the most widely adopted mathematical frameworks in causal inference. This framework provides a rigorous foundation for defining and estimating causal effects by considering hypothetical outcomes that could occur under different treatment conditions.

In causal inference, the main goal is to estimate the effect of an intervention on units such as individuals, organizations, or objects. We are usually interested in how different interventions can lead to different outcomes. For example, medical treatments like chemotherapy or radiotherapy can have distinct effects on the same patient's volume of their cancerous tumour; a commercial campaign with two different contents can have two different engagement/buying effects for the same customer. Moreover, the causal relationship depends not only on the nature and timing of the intervention but also on the specific context of the unit involved, for example, a patient's medical record.

#### Remark Rem2.1 [Treatment Range]

In this thesis, we will consider scenarios where the treatment variable, denoted by  $W$ , is *discrete* and takes *finite* values within a set  $\mathcal{W}$ . However, we relax this restriction in causal discovery tasks, allowing variables to originate from a continuous latent space. For discrete treatments, one regime typically corresponds to a passive state (i.e., no treatment or control group), while others correspond to active treatments, which may vary in type, intensity or dosage.

Let us assume we observe  $N$  units. Each pair of a unit and a treatment defines a potential outcome or response, denoted  $(i, \omega) \rightarrow Y_i(\omega)$ . A potential outcome  $Y_i(\omega)$  is said to be *observed* only if the unit  $i$  receives treatment  $\omega$ , i.e., under the event  $W_i = \omega$ . Importantly, the treatment must precede the observation of the corresponding potential outcome.

Consider the scenario where the treatment is binary, and we observe a finite sample of treatments and responses  $\{(W_i, Y_i)\}_{i=1}^N$ . The treatment assignment for each unit is defined as follows:

$$W_i = \begin{cases} 1, & \text{if unit } i \text{ receives the treatment,} \\ 0, & \text{if unit } i \text{ receives the control.} \end{cases}$$

Each unit  $i$  has two potential outcomes:

- $Y_i(1)$ , the outcome if the unit receives the treatment; and
- $Y_i(0)$ , the outcome if the unit receives the control.

The causal effect for unit  $i$  is the difference between these potential outcomes. This is formally captured

by the ITE:

$$\tau_i := Y_i(1) - Y_i(0).$$

By definition, for each unit  $i$  we observe only one potential outcome, namely the one corresponding to the observed treatment  $W_i$  which is  $Y_i(W_i)$ , and the counterfactual  $Y_i(1 - W_i)$  remains unobserved. This *fundamental problem of causal inference* (Holland, 1986) means that the individual treatment effect  $\tau_i$  is inherently a missing-data quantity. We must, therefore, establish connections between observed data and potential outcomes by comparing responses across different units. This necessitates consideration of the *treatment assignment mechanism*, which dictates how treatment is assigned across the population.

Since individual-level causal effects are unobservable, researchers often rely on aggregate measures, such as the ATE:

$$\tau := \mathbb{E}[Y_i(1) - Y_i(0)],$$

which captures the expected causal effect of treatment across the entire population. The expectation is taken over the population distribution of units (c.f. Remark Rem2.2).

Identifying the ATE depends on certain assumptions that allow for estimation based on observed data. Implicit in our formulation of potential outcomes is the assumption of *no spillover effect* (Imbens & Rubin, 2015), i.e., that the treatment of a unit is the sole determinant of its potential outcome, independent of the treatments assigned to other units. Moreover, the treatment for each unit has a consistent effect, with no variation in efficacy. These ideas are formalized by the *Stable Unit Treatment Value Assumption* (SUTVA) (Rubin, 1980), which consists of two key components:

**Assumption Asm2.1 [SUTVA]**

The SUTVA implies:

1. **No Interference/spillover effect:** The potential outcomes of any unit are unaffected by the treatments assigned to other units, meaning no interference exists between units.
2. **Consistency:** The observed outcome for a unit is the same as the potential outcome associated with the treatment it actually received. That is, if  $W_i = w$ , then  $Y_i = Y_i(w)$ .

The no-interference assumption is critical, though not universally applicable. In real-world scenarios like studying infectious diseases, one unit's potential outcome may be influenced by the treatment status of others, as in the case of immunization effects depending on herd immunity (Imbens & Rubin, 2015).

Additional assumptions are necessary to link observed data to potential outcomes to estimate the ATE. One fundamental assumption is *strong ignorability* (Rosenbaum & Rubin, 1983), which asserts that the treatment assignment,  $W$ , is independent of the potential outcomes, given a set of observed covariates,  $X$ . These covariates represent pre-treatment characteristics, i.e., they occur before the treatment and are therefore important for explaining the distribution of  $W$ .

☞ Throughout this thesis, covariates play a central role, mainly as we focus on estimating more individualized treatment effects that vary across subpopulations based on covariate values.

**Remark Rem2.2 [On the Use of Expectation]**

In causal inference studies, two main perspectives exist for addressing a set of units from a probabilistic standpoint (Imbens & Rubin, 2015; Ding & Li, 2018). The first considers a *fixed* set of observed units, where all potential outcomes are fixed but partially unknown. In this view, causal effects are defined only for specific units and may not generalize to other sets (Holland, 1986). The second, adopted in this thesis, assumes the set of units is randomly sampled from an infinite population, referred to as the *super-population* (Rubin, 1974). This perspective allows for the use of expectation, aligns with standard statistical theory, and offers mathematical convenience. Specifically, it facilitates reasoning about risks and generalization errors, central to machine learning (Vapnik, 1998; Shalev-Shwartz & Ben-David, 2014). By adopting this perspective, we apply principles from statistical learning theory, such as Empirical Risk Minimization, to assess model performance and ensure generalization to new data. While causal inference in fields like social sciences and epidemiology often refers to a finite set of observed units as the "population", we adhere to the statistical theory terminology, using *population* to denote an infinite set. For a finite set, we use the term *sample*.

In causal inference, we define probability distributions over the space  $\mathcal{Y}(0) \times \mathcal{Y}(1) \times \mathcal{W} \times \mathcal{X}$ , where  $\mathcal{Y}(0)$  and  $\mathcal{Y}(1)$  represent the domain ranges of the potential outcomes. For simplicity, we assume these domains are equal and denote the common outcome domain as  $\mathcal{Y}$ . Therefore, the probability distribution for causal inference is defined over  $\mathcal{Y}^2 \times \mathcal{W} \times \mathcal{X}$ , which allows us to sample  $(Y(0), Y(1), W, X)$  in an independent and identically distributed (i.i.d.) manner.

**Remark Rem2.3**

Since all relevant domains are either finite sets or subsets of Euclidean spaces, we assume all probability distributions are absolutely continuous w.r.t the Dirac or Lebesgue measure. As a result, a probability density function, denoted as  $p$ , exists by the Radon-Nikodym theorem (Billingsley, 2017).

Thus, individual data points  $(Y_i(0), Y_i(1), W_i, X_i)$  are sampled from the joint distribution:

$$p(Y_i(0), Y_i(1), W_i, X_i) = p(W_i \mid Y_i(0), Y_i(1), X_i) p(Y_i(0), Y_i(1) \mid X_i) p(X_i).$$

The treatment assignment mechanism is encapsulated in  $p(W_i \mid Y_i(0), Y_i(1), X_i)$ , which describes how treatment is assigned. Since much of this work assumes a binary treatment, it is often sufficient to study

the propensity score, defined as:

$$e(X_i, Y_i(0), Y_i(1)) := p(W_i = 1 \mid Y_i(0), Y_i(1), X_i).$$

However, because the general definition of the propensity score includes unobserved potential outcomes, we commonly assume the assignment mechanism to be *unconfounded* (also said ignorable). Formally,

**Assumption Asm2.2 [Ignorability/unconfoundedness]**

The treatment assignment does not depend on the potential outcomes:

$$\{Y_i(1), Y_i(0)\} \perp\!\!\!\perp W_i \mid X_i. \quad (2.1)$$

Under this assumption, the propensity score simplifies to:

$$e(X_i) = p(W_i = 1 \mid X_i). \quad (2.2)$$

The *ignorability assumption*, as stated in Equation 2.1, ensures that treated and untreated subpopulations are comparable within any homogeneous region of  $\mathcal{X}$ . To ensure this comparability, it is essential that both treated and control units are present at each level of  $X$ . This necessity leads to the "overlap" assumption:

**Assumption Asm2.3 [Overlap/Positivity]**

For any given context realization  $x \in \mathcal{X}$ , the probability of observing *any* treatment regime  $\omega \in \mathcal{W}$  is strictly positive:

$$p(x) \neq 0 \implies p(W = \omega \mid x) > 0. \quad (2.3)$$

These assumptions, namely consistency (Asm2.1), overlap (Asm2.3), and unconfoundedness (Asm2.2), provide the foundation for identifying causal effects that we summarize under the assumption of *strong ignorability*.

**Definition Def2.1 [Strong Ignorability]**

The treatment assignment is considered strongly ignorable if consistency, overlap, and unconfoundedness hold.

Given strong ignorability, we can relate the conditional expectations of potential outcomes to observable quantities (Imbens & Rubin, 2015):

$$\mathbb{E}[Y_i(\omega) \mid X_i = x] = \mathbb{E}[Y_i \mid W_i = \omega, X_i = x], \quad \omega \in \{0, 1\}.$$

This relationship enables estimation of the CATE for units with covariates  $X_i = x$ :

$$\tau(x) := \mathbb{E}[Y_i \mid W_i = 1, X_i = x] - \mathbb{E}[Y_i \mid W_i = 0, X_i = x].$$

The overlap assumption ensures that treated and control units exist at each value of  $x$ , allowing computation of  $\tau(x)$ . The ATE is then obtained by averaging  $\tau(x)$  over the distribution of  $X_i$ :

$$\tau = \mathbb{E}_X \left[ \mathbb{E}[Y_i(1) \mid X_i = x] - \mathbb{E}[Y_i(0) \mid X_i = x] \right].$$

#### Remark Rem2.4

In randomized experiments, the experimenter designs the assignment mechanism, specifying how individual treatments are assigned. However, this thesis focuses solely on observational studies, where the assignment mechanism is not controlled and must be inferred from data, even under strong ignorability, estimating propensity scores is crucial in this process.

**Taxonomy of variables for causal inference** In the field of causal inference, it is crucial to understand the taxonomy of variables to accurately estimate causal effects. This is depicted in Figure 2.1. The response variable,  $Y$ , represents the outcome we want to explain or predict. The treatment variable,  $W$ , is believed to influence  $Y$ , and we seek to estimate its causal effect. Confounders,  $X$ , are variables that affect both  $W$  and  $Y$ , which can potentially bias the causal effect if not properly controlled. In our modeling for CDVAE (Chapter 3), we also consider another important set of variables: adjustment variables,  $U$ . These variables affect the response but not the treatment, making them adjustment variables for outcome modeling to yield more precise individual response trajectories. Similarly, instruments,  $I$ , are variables that affect the treatment  $W$  but not  $Y$ , except indirectly through  $W$ . The study of causal inference in the presence of instruments is out of the scope of thesis.

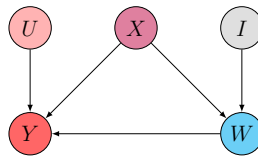


Figure 2.1: A general causal graph clarifying the causal links between outcome  $Y$ , treatment  $W$ , confounders  $X$ , adjustment variables  $U$  and instruments  $I$ .

#### Remark Rem2.5 [CATE vs ATE]

Understanding when to use the ATE versus the CATE is crucial in statistical causal inference because it influences the analytical approach and the interpretation of results. The ATE is used when the treatment effect is presumed to be consistent across an entire population or when making

policy decisions that affect everyone. This concept is particularly useful for generalizing findings, as highlighted in foundational works (Rubin, 1974; Holland, 1986).

On the other hand, the CATE is vital for examining how treatment effects differ among subpopulations defined by specific covariates like age, gender, or socioeconomic status. The CATE offers a deeper dive into the nuances of causal relationships, enabling a more tailored analysis in situations where treatment effects are not uniform across all individuals (Rosenbaum & Rubin, 1983). This approach is especially relevant in sectors such as personalized medicine, where understanding and leveraging the diversity in treatment responses can significantly enhance outcomes (Murphy, 2003).

Utilizing the CATE allows for the identification of subgroups that might benefit more from a treatment or, conversely, might be at risk of adverse effects. This strategic insight aids in decision-making and resource distribution, thereby elevating the effectiveness and precision of interventions.

### 2.1.2 Methods: An Overview

**Weighting Methods** Weighting methods are widely used in causal inference to adjust for confounding by reweighting the data. This creates a synthetic population where the treatment assignment is independent of covariates. This technique allows for the estimation of causal effects by weighting units inversely proportional to their probability of receiving the treatment or control. One of the key methods in this domain is *Inverse Probability of Treatment Weighting (IPTW)*, which employs the inverse of the propensity score (Equation 2.2) to weight observations (Rosenbaum & Rubin, 1983). IPTW adjusts the sample to create a pseudo-population where the covariates' distribution is balanced between treated and control units, facilitating an unbiased estimation of ATE. A refinement to IPTW, proposed by Hirano & Imbens (2001), involves *propensity score weighting with regression adjustment*, enhancing the estimator's efficiency. This method merges weighting with outcome regression, yielding consistent estimates even when the outcome model is inaccurately specified.

More recent developments have introduced machine learning-based methods to enhance the accuracy of weighting strategies. Athey & Imbens (2017) developed the *Generalized Propensity Score* approach, which allows for flexible, nonparametric modeling of the propensity score using random forests (Breiman, 2001). This is particularly useful for dealing with the limitations of parametric models, which may not perform well with high-dimensional covariates. Another method is the *Targeted Maximum Likelihood Estimation (TMLE)*, introduced by Van Der Laan & Rubin (2006). TMLE is a doubly robust estimator that incorporates propensity score weighting with a targeted regression adjustment for the outcome. It offers semiparametric efficiency and ensures valid inference even when the propensity score or outcome model is misspecified.

**Matching Methods** Matching methods are a prominent category of causal inference techniques designed to generate balanced treatment and control groups by pairing or grouping units with similar covariates. The objective is to emulate the randomization process, ensuring that treated and control units are



comparable on observed covariates. This reduces confounding and enhances the validity of causal effect estimates.

*Propensity Score Matching (PSM)* stands out as one of the most widely adopted matching techniques. Developed by Rosenbaum & Rubin (1983), PSM pairs treated and control units based on their propensity scores, which reflect the probability of receiving treatment given the covariates. Matching on the propensity score allows PSM to create groups that are balanced on covariates, facilitating unbiased estimation of treatment effects. Austin (2011b) offers an in-depth review of PSM's benefits and limitations, highlighting that while it significantly reduces bias, its efficacy is contingent on the quality of the propensity score model. *Nearest Neighbor Matching (NNM)* is another widely adopted method, pairing each treated unit with the control unit possessing the closest covariate values or propensity scores. Abadie & Imbens (2006) enhance NNM by introducing bias-corrected matching estimators that compensate for covariate discrepancies between treated and control units, thereby increasing the precision of treatment effect estimates. *Mahalanobis Distance Matching*, proposed by Rubin (1973a), employs the Mahalanobis distance for matching treated and control units based on the covariance structure of the covariates. This technique is especially effective when covariates are measured on differing scales, as the Mahalanobis distance accounts for correlations among covariates. Stuart (2010) extends the discussion to more sophisticated matching methods like *Optimal Matching* and *Genetic Matching*. Optimal Matching aims to minimize the total distance between treated and control units throughout the sample, whereas Genetic Matching leverages an evolutionary algorithm to optimize the balance between the groups. Recent developments have introduced matching methods based on machine learning to enhance flexibility and accuracy in high-dimensional settings. For example, Kallus (2018) suggests *Balanced Nearest Neighbor Matching*, which applies a machine learning approach to identify optimal matches that minimize covariate imbalance.

**Regression Adjustment** Including covariates in regression models allows for adjusting confounding, isolating the treatment's effect on the outcome. One of the earliest examples of regression adjustment can be found in the work of Cochran (1947), who proposed using linear regression models to adjust for covariates to estimate a treatment's causal effect. Rubin (1973b) expanded on this approach by formalizing regression adjustment within the PO framework, illustrating how regression can estimate both the ATE and the CATE. Generalized Linear Model (GLM) broadens the scope of linear regression to accommodate non-normal outcome distributions, such as binary or count data (McCullagh & Nelder, 1989). GLM are extensively utilized in causal inference studies, especially in epidemiology, where outcomes are often binary events (e.g., disease occurrence).

A significant advancement in regression adjustment methods is *Doubly Robust Estimation*. Introduced by Robins & Rotnitzky (1995), this method combines outcome regression with propensity score weighting to provide valid treatment effect estimates, even if one of the models (either the outcome model or the propensity score model) is incorrectly specified. Bang & Robins (2005) demonstrated that doubly robust estimators offer greater robustness to model misspecification than traditional regression methods. *Nonparametric Regression* techniques, such as *Kernel Regression* and *Spline Regression*, allow for flexible

modeling of the covariate-outcome relationship without assuming a specific functional form. Abadie (2005) introduced semiparametric regression models that mix parametric and nonparametric components for more flexible treatment effect modeling. In recent years, regression methods based on machine learning have become popular in causal inference. For example, Athey et al. (2019) proposed Generalized Random Forests (GRF), employing regression trees to estimate heterogeneous treatment effects.

**Non-parametric models** An important class of non-parametric models refers to the extension of random forests (Breiman, 2001) to perform causal inference. To this end, causal forests were introduced in Wager & Athey (2018); Athey et al. (2019) as a non-parametric approach to estimate treatment effects in complex settings. To do so, causal forests split the data into two groups based on the treatment assignment and then built separate trees for the treated and untreated groups. The prediction for an individual is then obtained by combining the predictions from the treated and untreated trees. The CATE is estimated as the difference between the predictions for the treated and untreated groups.

To develop more robust estimation methods, an emerging technique called *Double Machine Learning* (DML) (Chernozhukov et al., 2017; 2018; Foster & Syrgkanis, 2023) could provide an unbiased estimate of treatment effects on the condition that either the outcome model or the treatment model is well specified the general method consists of two stages of estimation. In the first step, we fit two predictive tasks, one on the outcome and one on the treatment, and then the two fitted models are combined to perform a second estimation targeting CATE.

**Neural Network-Based Approaches** Representation learning (Bengio et al., 2013) has emerged as a powerful strategy for causal inference, particularly useful when dealing with high-dimensional covariates and complex data structures. The goal is to transform the covariates into a lower-dimensional representation that facilitates the estimation of causal effects by reducing the bias due to confounding. This is typically achieved through creating representations where the distributions of treated and control groups are balanced. For instance, Shalit et al. (2017) proposed the concept of learning *balancing representations* by minimizing both the prediction error of the outcome and a discrepancy measure between the treated and control distributions in the representation space. They introduced an objective function that combines a supervised loss for outcome prediction with an unsupervised loss for distributional alignment. Building on this concept, Shalit et al. (2017) developed the *Counterfactual Regression* (CFR) model, which employs neural networks to learn representations that minimize the distance between the distributions of treated and control units using Integral Probability Metrics (IPMs) (Müller, 1997), such as the Wasserstein distance or Maximum Mean Discrepancy (MMD) (Gretton et al., 2012). By reducing this distance, the model aims to satisfy the unconfoundedness assumption in the representation space, effectively making the treatment assignment independent of the covariates after transformation. Further extending these ideas, Yoon et al. (2018) introduced *GANITE*, a Generative Adversarial Network (GAN)-based framework for estimating individualized treatment effects. *Dragonnet*, proposed by Shi et al. (2019), integrated propensity score estimation directly into the representation learning process and jointly learned the representation and the propensity score. Additionally, Hassanpour & Greiner (2019b)

presented *Counterfactual Networks*, which used domain adversarial training to learn representations invariant to treatment assignment while preserving outcome-predictive information. This approach helps mitigate biases due to observed confounding by ensuring that the learned representations do not carry treatment-specific information. Louizos et al. (2017) introduced the *Causal Effect Variational Autoencoder* (CEVAE), which used deep variational inference to model the joint distribution of covariates, treatments, and outcomes. Extension to multi-treatment settings was proposed by Schwab et al. (2018) where they combined representation learning with optimal transport to balance covariates across multiple treatment groups simultaneously.

As a summary, Table 2.1 presents a comparative overview of the main causal inference models discussed, grouped by category and highlighting key characteristics and references.

Table 2.1: Comparison of Causal Inference Methods by Category

Category	Method / Model	Key Characteristics	Reference(s)
Weighting Methods	IPTW	Uses inverse propensity score for weighting; creates pseudo-population	Rosenbaum & Rubin (1983)
	Propensity Score + Regression	Combines weighting and regression for robustness	Hirano & Imbens (2001)
	Generalized Propensity Score	Uses machine learning for flexible estimation	Athey & Imbens (2017); Breiman (2001)
	TMLE	Doubly robust; targeted estimation with ML enhancements	Van Der Laan & Rubin (2006)
Matching Methods	Propensity Score Matching (PSM)	Matches on estimated treatment probability	Rosenbaum & Rubin (1983)
	Nearest Neighbor Matching (NNM)	Pairs treated with nearest control units	Abadie & Imbens (2006)
	Mahalanobis Distance Matching	Accounts for covariate correlation in matching	Rubin (1973a)
	Optimal / Genetic Matching	Minimizes global imbalance; uses optimization algorithms	Stuart (2010)
	Balanced Nearest Neighbor Matching	ML-based flexible matching	Kallus (2018)
Regression Adjustment	Linear / GLM Regression	Adjusts for covariates using parametric models	Cochran (1947)
	Doubly Robust Estimation	Combines regression and weighting; robust to model misspecification	Robins & Rotnitzky (1995); Bang & Robins (2005)
	Semiparametric Regression	Blends linear and nonparametric terms	Abadie (2005)
	Generalized Random Forests (GRF)	Nonparametric, tree-based regression for heterogeneous treatment effects	Athey et al. (2019)
Non-Parametric Models	Causal Forests	Builds separate trees for treated and control; estimates CATE	Wager & Athey (2018); Athey et al. (2019)
	Double Machine Learning (DML)	Orthogonalizes outcome and treatment models using ML	Chernozhukov et al. (2017; 2018); Foster & Syrgkanis (2023)
Neural Network Approaches	Counterfactual Regression (CFR)	Balancing representations via neural networks	Shalit et al. (2017)
	GANITE	GAN-based model to estimate individual treatment effects	Yoon et al. (2018)
	Dragonnet	Integrates propensity score estimation within a deep net	Shi et al. (2019)
	Counterfactual Networks	Adversarial training to ensure balance and outcome prediction	Hassanpour & Greiner (2019b)
	CEVAE	Uses variational autoencoders to model unobserved confounders	Louizos et al. (2017)
	Perfect Match	Optimal transport-based method for multi-treatment settings	Schwab et al. (2018)

## 2.2 Potential Outcome Framework for Longitudinal data: Main Setting of the Thesis

### 2.2.1 Introduction: Dynamic vs. Time-Varying Treatment Regimes

**Motivation** In research across various fields, such as healthcare, the primary goal is the discovery of effective treatment regimes or intervention strategies. For instance, in clinical settings, a drug might be effective for one patient yet ineffective or even harmful for another (Collins & Varmus, 2015). Similarly, in business, what works for one customer may fail for another. This heterogeneity rules out a one-size-fits-all approach and motivates the use of *policies*, also known as *Dynamic Treatment Regimes (DTRs)*. Policies/DTRs provide a flexible and personalized approach by utilizing a series of decision rules that

facilitate adaptive interventions over time (Murphy, 2003; Robins, 2004). These rules map an individual’s historical data, such as medical records in healthcare or consumer attributes in retail, to specific treatments. For example, a company might develop a series of promotional actions or sales visits customized to a customer’s previous interactions with the brand. Decision rules could specify the timing and approach for in-person sales visits based on the customer’s past engagement and purchase history (Shin & Cho, 2006). In precision medicine, the type and dosage of treatments should be adjusted according to a patient’s medical records and vital statistics (Schulte et al., 2014). DTRs consist of decision rules aimed at selecting personalized treatments over time, adapting to individuals’ changing contexts and responses.

**Main challenges** Understanding cause and effect in complex, dynamic scenarios presents substantial challenges. Responses and evolving factors frequently influence time-varying treatments. For instance, a patient’s reaction to initial treatment can affect future treatment choices van der Laan & Petersen (2007). Other time-varying confounders, such as disease progression or changes in patient behavior, further complicate this situation. Similarly, in marketing, a customer’s response to an initial promotion might influence future marketing strategies and other dynamic covariates like customer preferences or external market conditions, which could also impact both treatment and response.

**Setup** Within the PO framework, as described by Robins & Hernán (2009b), we consider a cohort of individuals, also referred to as units, denoted by  $i \in \{1, 2, \dots, N\}$ , each observed over  $T$  sequential time steps. For each time step  $t \in \{1, 2, \dots, T\}$ , several key variables are tracked:

- **Treatment**  $W_{it} \in \mathcal{W} = \{0, \dots, K - 1\}$ : This represents the treatment administered to individual  $i$  at time  $t$  which takes  $K$  different values. For example, in a medical context,  $W_{it}$  might represent the administration of radiotherapy to treat a cancerous tumor.
- **Outcome**  $Y_{it} \in \mathcal{Y} \subset \mathbb{R}$ : This is the response or outcome of interest that we wish to evaluate as a result of the treatment in the case of a cancer patient,  $Y_{it}$  could represent the tumor volume at time  $t$ .
- **Context**  $\mathbf{X}_{it} \in \mathcal{X} \subset \mathbb{R}^{d_x}$ : This denotes the set of covariates or confounders that may influence both the treatment decision and the outcome. The context is represented as a  $d_x$ -dimensional vector that varies over time, for example, in a medical setting,  $\mathbf{X}_{it}$  could include a patient’s medical records, vital signs, or other health-related factors that change over time. Both static and dynamic confounders can be concatenated with dynamic variables at each time step and represented as  $\mathbf{X}_{it}$ .
- **Partially observed potential outcomes**  $\{Y_{it}(\omega_1, \dots, \omega_t) \mid (\omega_1, \dots, \omega_t) \in \mathcal{W}^t\} \subset \mathcal{Y} \subset \mathbb{R}$ : These represent the potential outcomes for an individual  $i$  at time  $t$ , conditional on the sequence of treatments  $(\omega_1, \dots, \omega_t)$  received up to that point.

We define the *history process*  $\mathbf{H}_{it} \in \mathcal{H}_t$  as the collection of all relevant information up to time  $t$  for an

individual  $i$ . Formally, this includes the covariates, past treatments, and past outcomes:

$$\mathbf{H}_{it} := [\mathbf{X}_{i,\leq t}, W_{i,<t}, Y_{i,<t}]. \quad (2.4)$$

This history encapsulates the context  $\mathbf{X}_{it}$ , past treatment assignments  $W_{i,<t}$ , and past outcomes  $Y_{i,<t}$ , which are critical in determining the treatment to be administered at a time  $t$ . We now define a dynamic treatment regime.

**Definition Def2.2 [Dynamic Treatment Regimes (DTRs)]**

A DTR  $\pi_{\leq T} := (\pi_1, \pi_2, \dots, \pi_T)$  is defined as a sequence of decision rules. Each decision rule  $\pi_t$  specifies the treatment to be assigned at a time  $t$  based on the available history up to that point. Formally, the treatment decision rule is expressed as:

$$\pi_t : \mathcal{H}_t \rightarrow \mathcal{W}.$$

This rule assigns a treatment  $W_{it}$  based on the individual's history  $\mathbf{H}_{it}$  at the time  $t$ . We can, therefore, define a particular set of potential outcomes under a treatment regime  $\pi_{\leq T}$ , where each element is represented as  $Y_t(\pi_{\leq t})$ . *Throughout the thesis, we use “dynamic treatment regime” and “policy” interchangeably.*

In this thesis, we focus on a type of treatment regime that we call *time-varying*, meaning that the potential treatment at a given time step  $t$  does not dynamically depend on the observed history, specifically:

**Assumption Asm2.4 [Time-Varying Treatment Regime]**

A treatment regime is considered time-varying when its values change over time but in a *non-dynamic* way, that is, for every time step  $t$ , and for every realization of the history process  $\mathbf{h}_t$ , the decision rule is a constant function, i.e.,  $\pi_t(\mathbf{h}_t) = \omega_t$ .

It is for this reason that through the thesis, the potential outcomes are denoted as  $Y_t(\omega_{\leq t})$ , where the potential treatment  $\omega_t$  is pre-specified and does not depend on the individual's observed history  $\mathbf{H}_t$ . Instead, each  $\omega_t$  is chosen exogenously from the treatment space  $\mathcal{W}$ , independently of the realized history process.

**Example Ex2.1 [Time-varying vs. Dynamic Treatments]**

For an individual, two treatment regimes could be : **Time-varying**: administer radiotherapy on days 1–5 of each 21-day cycle. **Dynamic**: increase dose if interim tumor volume has not fallen by 20% by day 10.

**Remark Rem2.6 [Intermediate Potential Outcomes]**

In our work, we are not only interested in estimating the treatment effect at the end/follow-up of a study, i.e., only defining causal effects with respect to (w.r.t.) the final potential outcomes  $Y_T(\omega_{\leq T})$ . The fact that we measure "intermediate" outcomes  $Y_1, \dots, Y_{T-1}$  motivates the definition of causal effects as functions of the remaining potential outcomes  $Y_t(\omega_{\leq t})$ . Virtually speaking, at each time step, we have a final outcome measured  $Y_t$ , for which we aim to estimate the causal effect, either conditional or averaged through  $\mathbb{E}(Y_t(\omega_{\leq t}) \mid \mathbf{X}_{\leq t}, Y_{<t})$  or  $\mathbb{E}(Y_t(\omega_{\leq t}))$ , respectively.

**2.2.2 Causal Effects in Longitudinal Settings: Definitions and Identification**

The missing data problem is exacerbated in longitudinal settings: at each time step  $t$ , we only observe one version of the outcome, while  $K^t - 1$  potential outcomes are missing because their corresponding treatment assignments were not chosen. This setting is more challenging than estimating causal effects at the end of a study, where only a total of  $K^T - 1$  missing potential outcomes exist. For our case (c.f. Remark Rem2.6), the total number of missing outcomes throughout the study is  $\sum_{t=1}^T (K^t - 1)$ .

For notational convenience, we denote the following vector form for a sequence of covariates:

$$\mathbf{X}_{<t}(\omega_{<t}) := (\mathbf{X}_1, \mathbf{X}_2(\omega_1), \mathbf{X}_3(\omega_1, \omega_2), \dots, \mathbf{X}_t(\omega_{<t})).$$

We have defined "potential covariates" due to the sequential nature of the data. This means that current covariates could potentially be affected by past treatments. Therefore, a rigorous definition of the potential outcome should consider both a potential sequence of treatments and a potential sequence of covariates (Robins, 2004; Vansteelandt & Joffe, 2014) :

$$Y_{\leq t}(\omega_{\leq t}, \mathbf{X}_{<t}(\omega_{<t})) := (Y_1(\omega_1), Y_2(\omega_{1,2}, \mathbf{X}_2(\omega_1)), \dots, Y_t(\omega_{\leq t}, \mathbf{X}_{<t}(\omega_{<t}))).$$

To draw causal inference in longitudinal data up to time  $t$ , we define a probability distribution over the product space consisting of:

- all treatments  $W_{\leq t}$  forming the space  $\mathcal{W}^t$ ,
- all potential outcomes

$$\{Y_s(\omega_{\leq s}) : \omega_{\leq s} \in \mathcal{W}^s\}_{1 \leq s \leq t},$$

forming the space

$$\prod_{s=1}^t \prod_{\omega_{\leq s} \in \mathcal{W}^s} \mathcal{Y} = \mathcal{Y}^{\sum_{s=1}^t |\mathcal{W}^s|},$$

- all potential covariates

$$\{\mathbf{X}_1\} \cup \{\mathbf{X}_s(\omega_{<s}) : \omega_{<s} \in \mathcal{W}^{s-1}\}_{2 \leq s \leq t},$$

forming the space

$$\mathcal{X} \times \prod_{s=2}^t \prod_{\omega_{<s} \in \mathcal{W}^{s-1}} \mathcal{X} = \mathcal{X}^{1 + \sum_{s=2}^t |\mathcal{W}^{s-1}|}.$$

In full generality, the assignment mechanism at time  $t$  takes the form:

$$p(W_t \mid \{Y_{\leq t}(\omega_{\leq t})\}_{\omega_{\leq t} \in \mathcal{W}^t}, \{\mathbf{X}_{\leq t}(\omega_{<t})\}_{\omega_{<t} \in \mathcal{W}^{t-1}}, W_{<t}),$$

which is highly complex due to its dependence on all sequences of potential outcomes and covariates defined up to time  $t$ . To simplify this assignment mechanism, we introduce a structural assumption similar to the concept of ignorability in static settings but adapted to longitudinal data. This is referred to as *sequential ignorability* (Robins & Hernán, 2009b), which assumes that at any time in the study, treatment is conditionally randomized given the history of observed variables:

**Assumption Asm2.5 [Sequential Ignorability]**

Sequential ignorability holds when, at each time step  $t$ , the treatment assignment is sequentially randomized given the observed history process up to time  $t$ , formally:

$$(\{Y_{\leq t}(\omega_{\leq t})\}_{\omega_{\leq t} \in \mathcal{W}^t}, \{\mathbf{X}_{\leq t}(\omega_{<t})\}_{\omega_{<t} \in \mathcal{W}^{t-1}}) \perp\!\!\!\perp W_t \mid \mathbf{H}_t.$$

Next, we present the consistency assumption to link the observed outcomes and covariates to the potential ones. Specifically, the observed outcome at time  $t$ ,  $Y_t$ , corresponds to the potential outcome  $Y_t(W_{\leq t})$ , and similarly for the covariates  $\mathbf{X}_t$ . Formally:

**Assumption Asm2.6 [Consistency]**

For every time step  $t$ , and for any sequence of treatments  $\omega_{\leq t}$ , the observed outcomes and covariates are equal to the potential outcomes and covariates under that treatment sequence, formally:

$$W_{\leq t} = \omega_{\leq t} \implies Y_t = Y_t(\omega_{\leq t}) \text{ and } \mathbf{X}_t = \mathbf{X}_t(\omega_{<t}).$$

The consistency assumption Asm2.6 states that one potential outcome is observed when a specific treatment is observed at any time step. This also implies that there is no interference *across* units, meaning that the treatments other units receive do not affect the potential outcome of other units (Assumption Asm2.1). However, it's important to note that without restrictive assumptions, we cannot assume that there is no interference *within* the observations of the same individual. This is why, in addition to the announced attributes  $\mathbf{X}_t$  being potential confounders, the past treatment trajectory  $W_{<t}$  also confounds both  $Y_t$  and  $W_t$ . This assumption applies to all past information  $\mathbf{H}_t$  up to the current time step  $t$  and assumes it to be confounding  $Y_{it}$  and  $W_{it}$  (Figure 2.2). Now, armed with the sequential ignorability

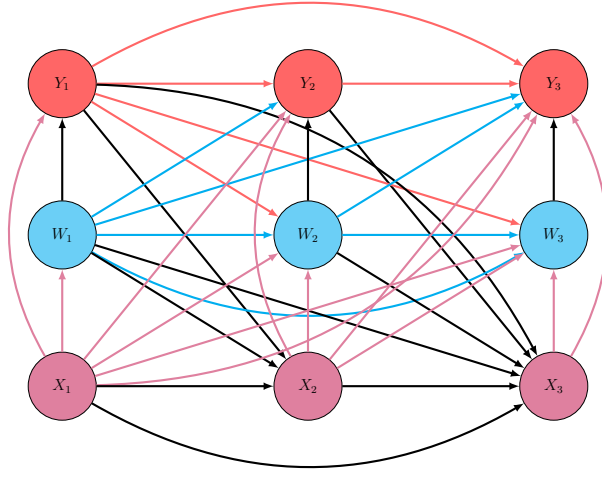


Figure 2.2: A causal graph is assumed to generate longitudinal data of 3-time steps ( $T = 3$ ). Edges are colored (pink, blue, and red) whenever the causal relation may contribute to confounding treatment and response at any time step  $t$ .

assumption and consistency, the assignment mechanism can be as

$$p(W_t \mid \{Y_{\leq t}(\omega_{\leq t})\}_{\omega_{\leq t} \in \mathcal{W}^t}, \{\mathbf{X}_{\leq t}(\omega_{\leq t})\}_{\omega_{\leq t} \in \mathcal{W}^{t-1}}, W_{<t}) = p(W_t \mid Y_{<t}, \mathbf{X}_{\leq t}, W_{<t}) = p(W_t \mid \mathbf{H}_t).$$

Similar to our discussion in the static setting (Section 2.1.1), the Assumption Asm2.5 guarantees that within a specific area of the space of  $\mathbf{H}_t$ , the groups of individuals who were treated and those who were not can be fairly compared. This kind of "local" comparability is ensured by having both treated and untreated individuals present at each level of  $\mathbf{H}_t$ :

**Assumption Asm2.7 [Overlap/Positivity]**

Given any time step  $t$ , and for any possible historical context  $\mathbf{h}_t$ , the probability of observing any of the two treatment regimes  $\omega_t$  is strictly positive:

$$p(\mathbf{h}_t) \neq 0 \implies p(W_t = \omega_t \mid \mathbf{h}_t) > 0.$$

👉 The causal quantity of interest in the longitudinal setting depends on the scientific objective of the study. In this thesis, we take the viewpoint that the primary causal quantity of interest is the mean of the potential outcomes given the observed covariates (Equation 2.5).

**Definition Def2.3 [Conditional Expected Potential Outcome]**

The expected potential outcome at time  $t$ , given the history of covariates  $\mathbf{X}_{\leq t} = \mathbf{x}_{\leq t}$  and responses



$Y_{<t} = y_{<t}$ , is formalized as:

$$m_t^{\omega_{\leq t}}(\mathbf{x}_{\leq t}, y_{<t}) := \mathbb{E}(Y_t(\omega_{\leq t}) \mid \mathbf{X}_{\leq t} = \mathbf{x}_{\leq t}, Y_{<t} = y_{<t}), \quad \omega_{\leq t} \in \mathcal{W}^t. \quad (2.5)$$

The conditional potential outcome allows us to evaluate the possible counterfactual trajectories of the responses given records for any given potential sequence of treatments. Furthermore, this causal quantity allows us to define another interesting causal quantity, the CATE in the time-varying setting.

**Definition Def2.4 [Time-varying CATE]**

Given two potential sequences of treatments  $\omega_{\leq t}$  and  $\omega'_{\leq t}$ , the time-varying CATE is defined as

$$\begin{aligned} \tau_t(\mathbf{x}_{\leq t}, y_{<t}; \omega_{\leq t}, \omega'_{\leq t}) &:= \mathbb{E}[Y_t(\omega_{\leq t}) - Y_t(\omega'_{\leq t}) \mid \mathbf{X}_{\leq t} = \mathbf{x}_{\leq t}, Y_{<t} = y_{<t}] \\ &= m_t^{\omega_{\leq t}}(\mathbf{x}_{\leq t}, y_{<t}) - m_t^{\omega'_{\leq t}}(\mathbf{x}_{\leq t}, y_{<t}). \end{aligned}$$

Based on this causal quantity, we can define the ATE for the longitudinal data up to time  $t$ .

**Definition Def2.5 [Time-varying ATE]**

Given two potential sequences of treatments  $\omega_{\leq t}$  and  $\omega'_{\leq t}$ , the time-varying ATE is defined as:

$$\tau_t(\omega_{\leq t}, \omega'_{\leq t}) := \mathbb{E}_{\mathbf{X}_{\leq t}, Y_{<t}}[\tau_t(\mathbf{x}_{\leq t}, y_{<t}; \omega_{\leq t}, \omega'_{\leq t})].$$

**Why do we focus on estimating conditional potential outcomes?** To estimate the CATE, it's necessary to calculate the difference in potential outcomes between a candidate treatment trajectory  $\omega_{\leq t}$  and a potential control trajectory  $\omega_{\leq t}^{(c)}$ . However, the control sequence need not be identical for all units (e.g.  $\omega_{\leq t}^{(c)} = (0, \dots, 0)$ ). Instead, it can be more informative to compare two counterfactual outcome trajectories corresponding to different treatment sequences  $\omega_{\leq t}$  and  $\omega'_{\leq t}$ , as in the general definition of the time-varying CATE. Therefore, we adopt an outcome-based approach, where the estimation of CATE (Definition Def2.4) can be performed in a later stage, tailored to the specific needs of the application. This approach also applies to the time-varying ATE, which similarly relies on comparing two treatment sequences. This later stage of estimation underscores the versatility of our method in applying CATE/ATE:

- Deciding which of the two potential treatments is favorable for a given individual by assessing  $\tau_t(\mathbf{x}_{\leq t}, y_{<t}; \omega_{\leq t}, \omega'_{\leq t})$ .
- Deciding on a population level whether it is more favorable to switch treatment from  $\omega'_{\leq t}$  to  $\omega_{\leq t}$ , depending on  $\tau_t(\omega_{\leq t}, \omega'_{\leq t})$ .

**Policy learning from counterfactuals** Additionally, framing our general causal inference task this way allows us to leverage the estimated counterfactual responses to learn a policy—that is, choosing the best possible treatment strategy for a given individual without explicitly estimating CATE or ATE. For instance, in the case of a cancer dataset, where the response of interest is tumor volume, one could choose the treatment sequence (e.g., chemotherapy, radiotherapy) that minimizes tumor volume. Formally, we learn such a DTR/policy by solving an optimisation problem over a prespecified class  $\Pi$  of admissible regimes (Murphy, 2003; Robins, 2004). For example, the *history-specific* optimal policy is

$$\pi_{\leq t}^*(\mathbf{h}_t) \in \arg \min_{\pi_{\leq t} \in \Pi} \mathbb{E}[Y_t(\pi_{\leq t}) \mid \mathbf{X}_{\leq t} = \mathbf{x}_{\leq t}, Y_{< t} = y_{< t}],$$

which reduces to the pointwise minimization  $\min_{\omega_{\leq t}} m_t^{\omega_{\leq t}}(\mathbf{x}_{\leq t}, y_{< t})$  when  $\Pi$  contains only fixed treatment sequences—that is, under the time-varying regime assumption (Asm2.4).

This approach demonstrates the flexibility and adaptability of our method to various research questions and practical applications, enhancing its potential impact and utility.

The three causal quantities defined so far are identified given the formulated assumptions of sequential ignorability, consistency, and positivity, collectively referred to as the *sequential ignorability assumptions*. We summarize the results in the following proposition.

**Proposition Prop2.1 [(Robins & Hernán, 2009a; Robins, 1999b)]**

Given the assumption of sequential ignorability, the conditional potential outcomes are identified as:

$$m_t^{\omega_{\leq t}}(\mathbf{x}_{\leq t}, y_{< t}) = \mathbb{E}_{Y_t | \mathbf{H}_t}(Y_t \mid \mathbf{H}_t = [\mathbf{x}_{\leq t}, y_{< t}, \omega_{< t}], W_t = \omega_t).$$

As a result, the time-varying CATE is identified as

$$\begin{aligned} \tau_t(\mathbf{x}_{\leq t}, y_{< t}; \omega_{\leq t}, \omega'_{\leq t}) &= \mathbb{E}_{Y_t | \mathbf{H}_t}(Y_t \mid \mathbf{H}_t = [\mathbf{x}_{\leq t}, y_{< t}, \omega_{< t}], W_t = \omega_t) \\ &\quad - \mathbb{E}_{Y_t | \mathbf{H}_t}(Y_t \mid \mathbf{H}_t = [\mathbf{x}_{\leq t}, y_{< t}, \omega'_{< t}], W_t = \omega'_t). \end{aligned}$$

The time-varying ATE is identified as:

$$\begin{aligned} \tau_t(\omega_{\leq t}, \omega'_{\leq t}) &= \mathbb{E}_{(\mathbf{X}_{\leq t}, Y_{< t})} [\mathbb{E}_{Y_t | \mathbf{H}_t}(Y_t \mid \mathbf{H}_t = [\mathbf{x}_{\leq t}, y_{< t}, \omega_{< t}], W_t = \omega_t)] \\ &\quad - \mathbb{E}_{(\mathbf{X}_{\leq t}, Y_{< t})} [\mathbb{E}_{Y_t | \mathbf{H}_t}(Y_t \mid \mathbf{H}_t = [\mathbf{x}_{\leq t}, y_{< t}, \omega'_{< t}], W_t = \omega'_t)]. \end{aligned}$$

### 2.2.3 Modeling Challenges

**Causal feedback** For longitudinal data, feedback refers to the idea that previous treatments may impact an intermediate variable, which in turn affects future treatments. In the literature, these intermediate variables are typically confounders, leading to what is often called *treatment-confounder feedback* (Robins,

1997; 1999a; Robins et al., 2000). However, in this thesis, we consider a more complex scenario where we also assume the existence of *treatment-response feedback*. Both types of causal feedback are depicted in Figure 2.2. To understand the importance of causal feedback in longitudinal data, let's consider a simple model of the time-varying outcome  $Y_t$ :

$$Y_t = \gamma Y_{t-1} + \beta W_t + \beta_1 W_{t-1} + \alpha^\top \mathbf{X}_t + \epsilon_t, \quad (2.6)$$

where  $\epsilon_t$  is an error term independent of  $Y_{<t}, W_{\leq t}, \mathbf{X}_{\leq t}$ . Assuming consistency, we can write the following model for the potential outcomes:

$$Y_t(\omega_{\leq t}) = \gamma Y_{t-1}(\omega_{<t}) + \beta \omega_t + \beta_1 \omega_{t-1} + \alpha^\top \mathbf{X}_t(\omega_{<t}) + \epsilon_t. \quad (2.7)$$

Since we consider the history process  $\mathbf{H}_t$  to confound the treatment  $W_t$  and outcome  $Y_t$ , we observe both *treatment-confounder feedback* through the term  $\mathbf{X}_t(\omega_{<t})$  and *treatment-response feedback* through the term  $Y_{t-1}(\omega_{<t})$ . These two types of feedback occur because we are considering the *carryover effect*:

**Definition Def2.6 [Carryover Effect]**

A *carryover effect* (or *lagged effect*) refers to any additional influence that treatments administered at one or more previous time points ( $W_{t-1}, W_{t-2}, \dots$ ) exert on the outcome  $Y_t$  *beyond* the direct, immediate effect of  $W_t$ .

Here, the carryover effect manifests because the past treatment  $W_{t-1}$  affects  $Y_t$  directly and also indirectly through the feedback paths

$$W_{t-1} \rightarrow Y_{t-1} \rightarrow Y_t \quad \text{and} \quad W_{t-1} \rightarrow \mathbf{X}_t \rightarrow Y_t.$$

When conditioning on  $Y_{t-1}$  and  $\mathbf{X}_t$ , we introduce *post-treatment bias* (Rosenbaum, 1984; Robins, 1997; Robins et al., 1999) because they are both affected by  $W_{t-1}$ . Consequently, we cannot consistently estimate the parameter  $\beta_1$ .

One might argue that removing conditioning on  $Y_{t-1}$  and  $\mathbf{X}_t$  could allow for consistent estimation of  $\beta_1$ . However, doing so would violate sequential ignorability (Asm2.5), and therefore the treatment effect  $\beta$ , associated with  $W_t$ , cannot be consistently estimated due to missing confounders—resulting in *omitted variable bias* (Angrist & Pischke, 2009; Cinelli & Hazlett, 2020) in the case of our linear regression model.

The simple model we presented is commonly called a *fixed effect model* (Blackwell & Glynn, 2018; Imbens, 2024), and it cannot handle causal feedback. However, if one is only interested in Contemporaneous Treatment Effect (CTE), that is we assume :

**Assumption Asm2.8 [Contemporaneous Treatment Effect (CTE)]**

We restrict ourselves to measuring only the CTE, i.e., the effect related to the current treatment

variable  $W_t$ . The potential trajectory of treatments up to  $t - 1$ ,  $\omega_{<t}$ , is assumed to be consistent with the **observed** history of treatments, i.e.,  $W_{<t} = \omega_{<t}$ . Therefore, the potential outcomes of interest at each time step  $t$  are  $\{Y_t(W_{<t}, \omega)\}_{\omega \in \mathcal{W}}$ .

The potential outcomes can then be written as

$$Y_t(W_{<t}, \omega_t) = \gamma Y_{t-1}(W_{<t}) + \beta \omega_t + \beta_1 W_{<t-1} + \alpha^\top \mathbf{X}_t(W_{<t}) + \epsilon_t. \quad (2.8)$$

which, by consistency assumption, is reduced to

$$Y_t(W_{<t}, \omega_t) = \gamma Y_{t-1} + \beta \omega_t + \beta_1 W_{<t-1} + \alpha^\top \mathbf{X}_t + \epsilon_t, \quad (2.9)$$

and the causal parameter  $\beta$  can be estimated consistently. It is therefore common and convenient in the case of Assumption Asm2.8 to denote the potential outcome  $Y_t(\omega_t)$  as it would be the case in Chapter 3.

**Controlling for Confounding Bias** Since conditioning for confounding variables in outcome models cannot fully address the estimation of causal effects in a sequence of variables, even standard methods discussed in static settings, such as matching Abadie et al. (2004); Austin (2011a), stratification (Frangakis & Rubin, 2002; Imbens & Rubin, 2015), or classical weighting methods (Rosenbaum & Rubin, 1983; D’Agostino, 1998), may fall short. To this end, *Marginal Structural Model (MSM)* (cf. Section 2.2.5) were introduced to estimate time-dependent causal effects in the presence of time-dependent confounders (Robins & Hernán, 2009a; Robins et al., 1999; 2000). MSM provides consistent estimates of causal effects for time-varying treatments through IPTW. This method accounts for time-dependent confounding by assigning each subject a weight based on the inverse probability of receiving the treatment, given their covariates. Intuitively, this creates a pseudo-population where each individual is duplicated as many times as the inverse of their weight. In this pseudo-population, weighted time-dependent confounders are balanced over time.

## 2.2.4 Literature Overview: The Challenge of Missing Confounders

**Unit Fixed Effects Regression Models** Unit fixed effects models are a widely used approach for addressing *time-invariant unobserved confounders* in longitudinal data, particularly in econometrics, political science, and social sciences (Beck, 2001; Wilson & Butler, 2007; Hsiao, 2007; Wooldridge, 2010; Bell & Jones, 2015; Clark & Linzer, 2015). These models adjust for individual-specific characteristics that do not change over time by including unit-specific intercepts, capturing the unobserved characteristics of each individual. This allows researchers to control for factors that affect the outcome but are not directly observed or measured. The general form of the PO model can be, for example, written as:

$$Y_t(W_{<t}, \omega_t) = \alpha_0 + \gamma Y_{t-1} + \beta \omega_t + \beta_1 W_{<t-1} + \alpha^\top \mathbf{X}_t + \epsilon_t,$$

where  $\alpha_0$  represents the *unit-specific effect* and is typically viewed as a function  $h$  of unobserved confounders,  $\mathbf{U}$ , that does not change over time,  $\alpha_0 = h(\mathbf{U})$ . This approach allows for the implicit control of these confounders through the unit-specific intercepts. However, as noted before, this method can introduce post-treatment bias when dynamic causal feedback paths are present, making it less suitable for models where past outcomes or covariates affect current treatments (Imai & Kim, 2019).

A natural extension of this model is the *two-way fixed effects model* (De Chaisemartin & d’Haultfoeuille, 2020; Callaway & Sant’Anna, 2021; Sant’Anna & Zhao, 2020; Goodman-Bacon, 2021; Arkhangelsky & Imbens, 2021; Athey & Imbens, 2017), which incorporates a time-specific effect,  $\lambda_t$ , to account for unobserved heterogeneity that varies across time but is constant across individuals:

$$Y_t(W_{<t}, \omega_t) = \alpha_0 + \lambda_t + \gamma Y_{t-1} + \beta \omega_t + \beta_1 W_{<t-1} + \alpha^\top \mathbf{X}_t + \epsilon_t.$$

Traditional two-way fixed effects models operate under the assumption of homogeneous treatment effects across individuals, which limits their applicability in scenarios where treatment effects may vary. To address this limitation, Callaway & Sant’Anna (2021) developed methodologies for estimating group-specific treatment effects, allowing for heterogeneity in treatment effects across different subpopulations. Building on this work, Arkhangelsky & Imbens (2021) proposed a doubly-robust linear estimator which maintains unbiasedness under two conditions: either when the two-way linear model holds in the presence of observed covariates, or when a set of assumption on treatment assignment are satisfied.

**Modeling Group-Based Unobserved Heterogeneity** As per unobserved heterogeneity that varies across groups, *group-based approaches* have been developed which cluster units into groups with shared characteristics, allowing researchers to control for unobserved heterogeneity across groups rather than individuals. Bonhomme & Manresa (2015) pioneered this method with their *grouped heterogeneity models*, which cluster units into latent groups based on both observed and unobserved characteristics. These models have been successfully applied in policy evaluation, where grouping units based on unobserved characteristics, such as economic conditions or regional factors, helps isolate the effects of an intervention (Bonhomme & Manresa, 2015). Su et al. (2016) extended this approach by developing methods to handle *latent group structures* in large datasets, making it possible to identify unobserved heterogeneity in panel data with high-dimensional covariates.

**Interactive Panel Models** Interactive fixed effects models extend two-way fixed effects models by allowing for interactions between units and time periods through latent factors. These models, introduced by (Bai, 2009), are particularly useful in addressing *time-varying unobserved confounders*, which are prevalent in longitudinal data settings such as macroeconomic studies or public health interventions. Interactive fixed effects models enhance the ability to capture more complex patterns in the data by incorporating unobserved factors that vary across units and over time (Bai, 2009). Interactive panel data is part of a broader class of general factor models for which synthetic control has been extensively studied (Abadie et al., 2010; Arkhangelsky et al., 2019; Chernozhukov et al., 2019; Ben-Michael et al., 2021).

**Instrumental variables for panel data** Despite the extensive focus on instrumental variables (IVs) for addressing unmeasured confounding in static settings (Hernán & Robins, 2006; Imbens, 2014; Imbens & Rubin, 2015; Hartford et al., 2017; Athey et al., 2019; Syrgkanis et al., 2019; Wang et al., 2022b; Cheng et al., 2023), their application in the context of time-varying data with missing confounders has been relatively underexplored in the literature. Early contributions by Angrist et al. (1996) introduced the potential outcomes framework in IV settings, demonstrating how IV estimands could be interpreted as local average treatment effects (LATE) for specific subpopulations. Building on this, Michael et al. (2024) proposed a weighted IV estimator for MSM, incorporating time-varying IVs to adjust for unobserved confounders dynamically. This estimator is particularly useful for complex longitudinal data as it generates stabilized weights that simultaneously account for treatment and confounders over time. Sun et al. (2018) tackled data missing not at random (MNAR) using IVs, providing a semiparametric framework capable of robust estimation, even when the missing data mechanism is non-ignorable.

**Proximal Causal Learning (PCI)** The PCI leverages proxy variables—measured covariates that serve as imperfect surrogates for unmeasured confounders, which allows for the identification of causal effects even when the standard *no unmeasured confounding* assumption fails (Miao et al., 2016; Tchetgen et al., 2020). These proxies facilitate the recovery of causal effects by solving inverse problems via bridge functions and the g-formula (Miao et al., 2016). Initially developed for point exposures, PCI has been extended to dynamic treatment regimes and time-varying treatments (Tchetgen et al., 2020; Zhang & Tchetgen, 2024).

**Proximal Causal Inference in Dynamic Treatment Settings** In dynamic treatment settings, PCI employs time-varying proxies to overcome hidden confounders across multiple time points. For example, Zhang & Tchetgen (2024) have shown that utilizing two independent proxy variables at each time point can identify the joint distribution of counterfactual outcomes. This approach aids in estimating optimal dynamic treatment regimes even with unmeasured confounding, extending the utility of the proximal g-formula. This formula generalizes Robins’ g-formula for time-varying treatments, as discussed in (Tchetgen et al., 2020). Moreover, the proximal inverse probability-weighted (PIPW) estimator, described in Ying et al. (2022), improves standard IPW methods by including proxy variables to adjust for hidden confounders. This allows for estimating survival curves and other longitudinal outcomes without assuming ignorability. Proximal doubly robust (PDR) estimators, which maintain consistency even when models for either confounders or outcomes are incorrectly specified, have also been proposed (Ying et al., 2023). Despite its advantages, PCI faces practical challenges in identifying suitable proxies that satisfy relevance and completeness conditions (Tchetgen et al., 2020; Zhang & Tchetgen, 2024). Estimating bridge functions and solving nested inverse problems can also be computationally intensive.

**The Deconfounding Approach** In genetic studies, latent, unobserved confounding factors; like population structure, complicate causal inference by inducing spurious associations between genotypes and phenotypes. To address this challenge, Tran & Blei (2018) propose a method based on *implicit causal*

*models* which incorporate implicit density functions, implemented via neural networks, allowing them to capture nonlinear relationships and gene-population interactions. Ranganath & Perotte (2018) formalize a general framework for causal inference in the presence of unmeasured confounding. They introduce two key assumptions (i) *shared confounding*: all treatments are influenced by a common set of latent variables. (ii) *independence given shared confounders*: conditioning on these latent variables renders the treatments conditionally independent. To estimate the unobserved confounders, they construct an *information-regularized estimator*, which balances two competing goals: preserving the shared confounding structure while ensuring that the independence condition is not violated. Expanding on this line of thought, Wang & Blei (2019a) articulate the *theory of the deconfounder*. Their central insight is that when many causes are observed jointly, the combined pattern of their assignments contains information about the latent confounders. They showed that it is possible to construct a latent variable, via a probabilistic factor model, that captures the influence of unobserved confounders. Conditioning on this variable permits unbiased estimation of treatment effects. The deconfounder framework has found practical applications beyond genetics. In recommendation systems, it enables more accurate predictions by adjusting for hidden user traits that simultaneously influence item exposure and preferences (Wang et al., 2018). In healthcare, Zhang et al. (2019) applied the deconfounder to observational studies using electronic health records to correct for unmeasured confounding in treatment effect estimation.

**Deconfounding in Temporal Settings** Researchers have extended the deconfounder approach to dynamic and time-series contexts, where treatments and confounders evolve over time. Bica et al. (2020b) introduce the *Time Series Deconfounder*, which uses a RNN with multitask outputs to build a temporal factor model. At each time step, the model infers latent variables that account for hidden confounders and ensures that assigned treatments are conditionally independent given these variables. This framework enables estimating treatment effects even in the presence of multiple time-varying confounders. Building on this idea, Kuzmanovic et al. (2021) propose the *Deconfounding Temporal Autoencoder* (DTA), designed for longitudinal data with noisy proxies of hidden variables. The DTA architecture combines a Long Short-Term Memory (LSTM) autoencoder with a causal regularization penalty, learning a latent representation that substitutes for unmeasured confounders. Once this embedding is learned, an outcome model is conditioned on it to estimate CATE.

**Deconfounding Continuous-Time Settings** In settings with continuous treatments and irregularly sampled data, Cao et al. (2023) adapt the deconfounding framework using neural differential equations. Their model constructs a latent factor process via a stochastic controlled differential equation, augmented by a Lipschitz-constrained convolutional operator. Hatt & Feuerriegel (2024) focus on sequential treatment settings where a single intervention is administered at each time step, and unobserved confounders remain stable. They model treatment assignment as a first-order Markov process, conditioned on observed covariates and latent variables. By inferring these latent variables, modeled via a Gaussian process, they restore conditional independence and enable CATE estimation.

**Substitute Adjustment and the Limits of Deconfounding** Recently, Adams & Hansen (2024) distinguished their work from the original deconfounder theory, particularly regarding causal interpretations and the methodology used for adjustments. While the deconfounder, as introduced by Wang & Blei (2019a), emphasizes adjusting for latent variables to estimate causal parameters under the assumption of unobserved confounding, Adams & Hansen (2024) argued for a broader approach termed "*Substitute Adjustment*." This method does not rely on strict causal assumptions but estimates adjusted regression parameters using inferred latent variables. This approach abstracts from causal interpretations, making the method applicable in a broader context where causal claims may not be strictly held.

As a summary, Table 2.2 presents a comparative overview of the main models discussed, grouped by category, main characteristics, and references.

Table 2.2: Comprehensive Overview of Methods Addressing Missing Confounders in Longitudinal Data

Category	Method / Model	Key Features	References
<b>Fixed Effects Models</b>	Unit Fixed Effects	Controls time-invariant unobserved confounders using unit intercepts. Prone to post-treatment bias.	(Hsiao, 2007; Wooldridge, 2010)
	Two-Way Fixed Effects	Time fixed effects; Treatment effects are homogeneous.	(Callaway & Sant'Anna, 2021; Arkhangelsky & Imbens, 2021)
	Grouped Heterogeneity Models	Units clustered into latent groups; shared unobserved factors across groups.	(Bonhomme & Manresa, 2015; Su et al., 2016)
<b>Interactive Panel Models</b>	Interactive Fixed Effects	Latent factors vary over units and time; captures time-varying confounding.	(Bai, 2009)
	Generalized Synthetic Control	Combines factor models and synthetic control; robust for high-dimensional confounding.	(Xu, 2017)
<b>Instrumental Variable Methods</b>	IV for MSM	Weighted IV estimator for marginal structural models with time-varying IVs.	(Michael et al., 2024)
	IVs for MNAR Data	Semi-parametric IV estimator.	(Sun et al., 2018)
<b>Proximal Causal Inference (PCI)</b>	Proximal G-Formula	Uses proxies and bridge functions to recover causal effects without ignorability.	(Tchetgen et al., 2020; Miao et al., 2016)
	PIPW Estimator	Proxy-based inverse probability weighting for survival analysis.	(Ying et al., 2022)
	Proximal DR Estimator	Doubly robust estimator under proxy-based confounding.	(Ying et al., 2023)
<b>Latent Variable / Deconfounder Models</b>	Implicit Causal Models	Neural density estimators for unobserved confounding in genetics.	(Tran & Blei, 2018)
	Shared Confounding Estimator	Assumes common latent confounders across multiple treatments.	(Ranganath & Perotte, 2018)
	The Deconfounder	Factor model for multiple causes; estimates substitute confounders.	(Wang & Blei, 2019a)
	Medical Deconfounder	EHR-based treatment effect estimation with latent confounder modeling.	(Zhang et al., 2019)
	Time Series Deconfounder	RNN-based factor model for time-varying unobserved confounders.	(Bica et al., 2020b)
	DTA	Proxy-driven autoencoder for CATE in time-series settings.	(Kuzmanovic et al., 2021)
<b>Alternative Adjustment</b>	Gaussian Process Factor Model	Uses GP over time to infer latent confounders in sequential treatments.	(Hatt & Feuerriegel, 2024)
	Neural Diff. Equation Model	Latent confounders in continuous-time data via stochastic diff. eqs.	(Cao et al., 2023)
	Substitute Adjustment	Does not assume causal structure; recovers latent variables to adjust regression.	(Adams & Hansen, 2024)



### 2.2.5 Literature Overview: Methods verifying our Causal assumptions

In this section, we review the models that follow the same assumptions as our work in Chapters 3 and 4, that is, they assume sequential ignorability (Asm2.5), work under binary or discrete treatments (Remark Rem2.1), and perform counterfactual regression, i.e, estimate the conditional counterfactual response (Definition Def2.3 and Proposition Prop2.1).

These models aim to estimate the effects of a given treatment sequence on the outcome over a prediction horizon  $\rho$ , given the patient's treatment history and covariates at time  $t$ . Formally, we model:

$$\mathbb{E}[Y_{t+\rho} \mid W_{t:t+\rho-1}, \mathbf{H}_t] = g(\rho, W_{t:t+\rho-1}, \mathbf{H}_t)$$

where  $g$  is a non-linear function. The goal is to predict the future outcome  $Y_{t+\rho}$  based on the patient's treatment sequence  $W_{t:t+\rho-1}$  and covariate history  $\mathbf{H}_t$ .

**MSM** To control for time-dependent confounding, MSM adjusts for the bias introduced by time-varying covariates through the use of *stabilized weights* (Robins et al., 2000):

$$SW(t, \rho) = \prod_{s=t}^{t+\rho-1} \frac{\prod_{k=0}^{K-1} p(W_s = k \mid W_{<s})}{\prod_{k=0}^{K-1} p(W_s = k \mid W_{<s}, \mathbf{X}_{\leq s})} \quad (2.10)$$

where  $p(\cdot)$  is the conditional probability mass function for discrete treatments, or the density function for continuous treatments, and  $K$  represents the number of treatment variables (e.g., chemotherapy, radiotherapy). The stabilized weights are computed by comparing the treatment probability given the patient's history  $\mathbf{H}_t$  with the treatment probability given only on past treatments  $W_{<t}$  (Numerator of Equation 2.10). We estimate the propensity weights using logistic regression:

$$\begin{aligned} p(W_t = k \mid W_{<t}) &= \sigma \left( \sum_{j=0}^{K-1} \alpha_{j,k} \left( \sum_{s=1}^{t-1} \mathbb{1}_{\{W_s=j\}} \right) \right), \\ p(W_t = k \mid \mathbf{H}_t) &= \sigma \left( \sum_{j=0}^{K-1} \phi_{j,k} \left( \sum_{s=1}^{t-1} \mathbb{1}_{\{W_s=j\}} \right) + \beta_1 \mathbf{X}_t + \beta_2 \mathbf{X}_{t-1} \right), \end{aligned}$$

where  $(\alpha_{j,k})_{0 \leq j, k \leq K-1}$ ,  $(\phi_{j,k})_{0 \leq j, k \leq K-1}$ ,  $(\beta_1, \beta_2)$  are regression coefficients and  $\sigma(\cdot)$  is the Sigmoid function. The model then uses the weighted regression to estimate the outcome at time  $t + \rho$ :

$$g(\rho, W_{t:t+\rho-1}, \mathbf{H}_t) = \sum_{k=0}^{K-1} \delta_k \left( \sum_{s=t}^{t+\rho-1} \mathbb{1}_{\{W_s=k\}} \right) + \boldsymbol{\eta}_1^\top \mathbf{X}_t + \boldsymbol{\eta}_2^\top \mathbf{X}_{t-1},$$

where  $(\delta_k)_{0 \leq k \leq K-1}$  and  $\boldsymbol{\eta}_1, \boldsymbol{\eta}_2$  are regression coefficients, representing the effects of the treatments and covariates, respectively.

**Recurrent Marginal Structural Model (RMSM)** The RMSM (Lim, 2018a) generalizes the standard MSM by enabling highly non-linear modeling of the dynamics between covariates and treatments using a RNN architecture. The model uses stabilized weights for the regression loss based on the IPTW, which

is generalized to handle multiple treatment assignments, censored data, and continuous dosages. Lim (2018a) suggested adding a second weighting term to the stabilized weight of MSM in Equation 2.10 to account for censoring:

$$SW^*(t, \rho) = \prod_{s=t}^{t+\rho} \frac{f(C_s = 0 \mid \mathcal{T} > s, W_{<s})}{f(C_s = 0 \mid \mathcal{T} > s, \mathbf{X}_{<s}, W_{<s})},$$

where  $C_n = 1$  represents censoring of the trajectory, and  $\mathcal{T}$  is the time of its occurrence. The stabilized weights are truncated at their 1st and 99th percentile values and normalized by their mean for each individual  $i$ :

$$\tilde{SW}_i^* = \frac{SW_i^*(t, \rho)}{\frac{1}{T_i} \sum_{t=1}^{T_i} \mathbb{E}(SW^*(t, \rho))},$$

where  $T_i$  is the number of observations per patient. These two stabilized weights are used to balance the individual regression loss over a time horizon  $\rho$  as follows:

$$\mathcal{L}_Y = SW_i(t, \rho) \times \tilde{SW}_i^*(t, \rho) \times \|Y_{t+\rho-1} - g(\rho, \omega_{t:\rho-1}, \mathbf{H}_t)\|^2.$$

**Model Architecture** The RMSM framework defines six neural networks:

- **Four propensity networks:** These RNN-based models compute the numerators and denominators of the two stabilized weights. Each network uses a Sigmoid output with binary cross-entropy loss for binary treatments, Softmax for categorical treatments, and a Variational RNN for continuous dosages.
- **Two prediction networks:** (1) **Encoder:** A LSTM processes the individual’s covariate and treatment history, learning a hidden representation at each time step. (2) **Decoder:** Given an intended treatment plan and hidden representation, the decoder predicts outcomes across future time steps.

**Counterfactual Recurrent Network (CRN)** In Bica et al. (2020a), the authors proposed CRN, a model that employs *domain adversarial training* (Li et al., 2018b; Schoenauer-Sebag et al., 2019; Ganin et al., 2016) to mitigate bias instead of weighting. Let  $q_{\theta_W}(\cdot \mid \Phi(\mathbf{H}_t))$  be the treatment classifier and  $G_Y(\Phi(\mathbf{H}_t; \theta_R); \theta_Y)$  be the outcome prediction network where  $\Phi(\cdot)$  is the representation function parameterized by  $\theta_R$ . The treatment loss  $\mathcal{L}_W(\theta_R, \theta_W)$  and outcome loss  $\mathcal{L}_Y(\theta_R, \theta_Y)$  are defined as:

$$\mathcal{L}_W(\theta_R, \theta_W) = -\log q_{\theta_W}(W_{t+1} \mid \Phi(\mathbf{H}_t; \theta_R)),$$

$$\mathcal{L}_Y(\theta_R, \theta_Y) = \|Y_{t+1} - G_Y(\Phi(\mathbf{H}_t; \theta_R), \theta_Y)\|^2.$$

The model aims to maximize the treatment loss and minimize the outcome regression loss to achieve a balanced representation, adversarially. The overall training loss is

$$\mathcal{L}(\theta_R, \theta_Y, \theta_W) = \mathcal{L}_Y(\theta_R, \theta_Y) - \lambda \mathcal{L}_W(\theta_R, \theta_W),$$

where  $\lambda$  is a hyperparameter that balances the contributions of the two loss functions. The adversarial training follows the approach of Ganin et al. (2016), using a gradient reversal layer on the discriminator network, allowing the model to minimize the overall loss using backpropagation while maintaining treatment invariance.

**Causal Transformer** Melnychuk et al. (2022) proposed a transformer-based architecture, the Causal Transformer, for estimating counterfactual outcomes over time. The model processes sequential data using three specialized transformer subnetworks that separately encode time-varying covariates  $\mathbf{X}_{\leq t}$ , past treatments  $W_{< t}$ , and past outcomes  $Y_{< t}$ . The model computes a representation  $\Phi_t = \Phi(\mathbf{H}_t; \theta_R)$  via an architecture that comprises the following three subnetworks: (1) **Covariate Network**: Encodes the sequence of observed covariates  $\mathbf{X}_{\leq t}$ . (2) **Treatment Network**: Encodes the sequence of prior treatments  $W_{< t}$ . (3) **Outcome Network**: Encodes the sequence of prior outcomes  $Y_{< t}$ .

Each of these networks uses: (1) **Masked Multi-head Self-Attention**: To ensure that no future information is seen during the encoding of past data. (2) **Shared Trainable Positional Encoding**: To retain temporal relationships.

**Training** The CT employs a custom end-to-end training procedure based on the Counterfactual Domain Confusion (CDC) loss, designed to reduce confounding bias: The loss consists of two components:

- Factual Outcome Loss:

$$\mathcal{L}_Y(\theta_Y, \theta_R) = \|Y_{t+1} - G_Y(\Phi_t, W_t; \theta_Y)\|^2.$$

- CDC Loss:

$$\mathcal{L}_{conf}(\theta_W, \theta_R) = - \sum_{j=1}^K 1[W_t = j] \log G_W(\Phi_t; \theta_W).$$

Here,  $G_W$  predicts treatment assignments, and the CDC loss encourages  $\Phi_t$  to remain non-predictive of the treatment  $W_t$ .

The overall objective function is:

$$\hat{\theta}_Y, \hat{\theta}_R = \arg \min_{\theta_Y, \theta_R} \{ \mathcal{L}_Y(\theta_Y, \theta_R) + \alpha \mathcal{L}_{conf}(\theta_W, \theta_R) \},$$

$$\hat{\theta}_W = \arg \min_{\theta_W} \mathcal{L}_W(\theta_R, \theta_W).$$

The CT is trained with an end-to-end learning approach, implementing techniques such as masked cross- and self-attention to ensure that the model learns from historical data while preventing look-ahead bias.

**G-Net** Unlike previous discussed models, which are designed for time-varying treatment regimes, G-Net (Li et al., 2021) is primarily designed for counterfactual prediction in dynamic treatment regimes (c.f. Definition Def2.2). It is a sequential, RNN-based model, which is built on the g-calculus, also called g-computation or g-formula (Robins, 1986; 1997; Vansteelandt & Joffe, 2014).

G-calculus is a general identification result introduced by Robins (1986) that expresses any conditional counterfactual responses (or full distribution) under dynamic treatment rules entirely in terms of observable conditional densities. In its general form, g-calculus can be presented as in the following proposition:

**Proposition Prop2.2 [G-calculus (Robins, 1986)]**

Assume the standard assumptions of consistency, positivity, and sequential ignorability (Assumptions Asm2.6, Asm2.7, Asm2.5). Fix a counterfactual forecasting horizon  $\rho > 0$  and let  $\pi_{t:t+\rho-1} := (\pi_t, \dots, \pi_{t+\rho-1})$  be the collection of decision rules that operate between time  $t$  and  $t + \rho - 1$  as in Definition Def2.2. The conditional counterfactual response at the horizon  $\rho$  can be expressed as

$$\begin{aligned} & \mathbb{E}[Y_{t+\rho}(\pi_{t:t+\rho-1}) \mid \mathbf{H}_t = \mathbf{h}_t] \\ &= \int_{\mathcal{X}^{\rho-1}} \int_{\mathcal{Y}^{\rho-1}} \mathbb{E}[Y_{t+\rho} \mid \mathbf{H}_t = \mathbf{h}_t, \mathbf{X}_{t+1:t+\rho-1} = \mathbf{x}, Y_{t+1:t+\rho-1} = y, \\ & \quad W_{t:t+\rho-1} = \pi_{t:t+\rho-1}(\mathbf{h}_t, \mathbf{x}, y)] \\ & \quad \times \prod_{j=t+1}^{t+\rho-1} p(\mathbf{x}_j, y_j \mid \mathbf{H}_t = \mathbf{h}_t, \mathbf{X}_{t+1:j-1} = \mathbf{x}_{t+1:j-1}, Y_{t+1:j-1} = y_{t+1:j-1}, \\ & \quad W_{t:j-1} = \pi_{t:j-1}(\mathbf{h}_t, \mathbf{x}_{t+1:j-1}, y_{t+1:j-1})) dy d\mathbf{x}. \end{aligned} \tag{2.11}$$

The utility of Proposition Prop2.2 is that it allows the conditional counterfactual response to be rewritten as a forward simulation that iteratively plugs in the conditional distributions of future covariates and outcomes  $\{\mathbf{X}_{t+j}, Y_{t+j}\}_{1 \leq j \leq \rho-1}$  given the entire past  $\mathbf{H}_t$ . After fitting the conditional distributions  $p_{\theta_W}(W_t \mid \mathbf{H}_t)$ ,  $p_{\theta_X}(\mathbf{X}_{t+1} \mid \mathbf{H}_t)$ ,  $p_{\theta_Y}(Y_{t+1} \mid \mathbf{H}_t, W_t)$  on the observed data, one can: first overwrite future treatments with a policy  $\pi$ , and second, roll the simulation forward to obtain Monte-Carlo draws of the conditional counterfactual response. An estimation with g-calculus  $\mathbb{E}[Y_{t+\rho}(\pi_{t:t+\rho-1}) \mid \mathbf{H}_t = \mathbf{h}_t]$  can therefore be described by the Algorithm 1.

G-Net is RNN-based realization of Algorithm 1 where similar to Causal transformers and CRN, a representation  $\Phi_t$  of the process history  $\mathbf{H}_t$  is learned through an LSTM which is used to learned conditional densities  $p_{\theta_W}(W_t \mid \Phi_t)$ ,  $p_{\theta_X}(\mathbf{X}_{t+1} \mid \Phi_t)$ ,  $p_{\theta_Y}(Y_{t+1} \mid \Phi_t, W_t)$ . Everything is trained end-to-end by the negative log-likelihood of the triples  $(W_t, \mathbf{X}_{t+1}, Y_{t+1})$ .

Since we only treat time-varying treatment regimes similar to RMSM, CRN, and Causal Transformers, the g-calculus could be adapted to this case by replacing a policy with a sequence of potential treatments:

**Corollary Cor2.1**

Assume we are operating under a time-varying treatment regime following Assumption Asm2.4. Given the same assumption as in the Proposition Prop2.2, the conditional counterfactual response at

---

**Algorithm 1** Monte Carlo g-computation

---

**Require:** Longitudinal data  $\{\{\mathbf{H}_t^{(i)}, W_t^{(i)}, Y_t^{(i)}\}_{t=1}^T, i = 1, \dots, n\}$

**Require:** Horizon  $\rho$

**Require:** Dynamic policy  $\pi = \{\pi_s\}_{s=t}^{t+\rho-1}$

**Require:** Number of (Monte-Carlo) simulation paths  $N_{MC}$

**Ensure:** Estimate  $\hat{\mu}_{t,\rho}^\pi(\mathbf{h}_t) = \mathbb{E}[Y_{t+\rho}(\pi) \mid \mathbf{H}_t = \mathbf{h}_t]$

1: **Stage 1: Model fitting**

2: Estimate conditional laws:

$$p_{\theta_W}(W_t \mid \mathbf{H}_t), p_{\theta_X}(\mathbf{X}_{t+1} \mid \mathbf{H}_t), p_{\theta_Y}(Y_{t+1} \mid \mathbf{H}_t, W_t)$$

by maximizing the joint log-likelihood on observed data.

3: **Stage 2: Forward simulation (g-calculate)**

4: **for**  $n \in \{1, \dots, N_{MC}\}$  **do**

5:   Initialize history:  $\mathbf{H}_t^{(n)} \leftarrow \mathbf{h}_t$

6:   **for**  $s \in \{t, \dots, t + \rho - 1\}$  **do**

7:     Set treatment by policy:  $W_s^{(n)} \leftarrow \pi_s(\mathbf{H}_s^{(n)})$

8:     Sample next covariates:  $\mathbf{X}_{s+1}^{(n)} \sim p_{\theta_X}(\cdot \mid \mathbf{H}_s^{(n)})$

9:     Sample next outcome:  $Y_{s+1}^{(n)} \sim p_{\theta_Y}(\cdot \mid \mathbf{H}_s^{(n)}, W_s^{(n)})$

10:    Update history:

$$\mathbf{H}_{s+1}^{(n)} \leftarrow \mathbf{H}_s^{(n)} \cup \{\mathbf{X}_{s+1}^{(n)}, W_s^{(n)}, Y_{s+1}^{(n)}\}$$

11:   **end for**

12: **end for**

13: **Stage 3: Causal estimand**

14: Compute:

$$\hat{\mu}_{t,\rho}^\pi(\mathbf{h}_t) = \frac{1}{N_{MC}} \sum_{n=1}^{N_{MC}} Y_{t+\rho}^{(n)}$$

15: **return**  $\hat{\mu}_{t,\rho}^\pi(\mathbf{h}_t)$ 

---

the horizon  $\rho$  for a fixed treatment plan  $\omega_{t:t+\rho-1} = (\omega_t, \dots, \omega_{t+\rho-1}) \in \mathcal{W}^\rho$  is expressed as

$$\begin{aligned}
& \mathbb{E}[Y_{t+\rho}(\omega_{t:t+\rho-1}) \mid \mathbf{H}_t = \mathbf{h}_t] \\
&= \int_{\mathcal{X}^{\rho-1}} \int_{\mathcal{Y}^{\rho-1}} \mathbb{E}[Y_{t+\rho} \mid \mathbf{H}_t = \mathbf{h}_t, \mathbf{X}_{t+1:t+\rho-1} = \mathbf{x}, Y_{t+1:t+\rho-1} = y, \\
&\quad W_{t:t+\rho-1} = \omega_{t:t+\rho-1}] \\
&\quad \times \prod_{j=t+1}^{t+\rho-1} p(\mathbf{x}_j, y_j \mid \mathbf{H}_t = \mathbf{h}_t, \mathbf{X}_{t+1:j-1} = \mathbf{x}_{t+1:j-1}, Y_{t+1:j-1} = y_{t+1:j-1}, \\
&\quad W_{t:j-1} = \omega_{t:j-1}) d\mathbf{x} dy.
\end{aligned} \tag{2.12}$$

## 2.3 Causal graphs

In this section, we define a causal graph mathematically. Establishing the formalism of such an object is crucial for this thesis because, although we adopt the PO framework in the first two contributions to reason about causal inference, having a graphical understanding of causal assumptions allows us to simplify conditional probabilities by leveraging the graphical structure between variables. On the other hand, the notion of a causal graph is fundamental in the third contribution, as we no longer reason about specific treatments and responses but instead focus on how the variables constituting the time-varying confounders  $\mathbf{X}_t$  interact with each other. Since these confounder variables are often high-dimensional and sparse, such as vectors representing baskets of purchased products (cf. Chapter 1, Section 5.1), the modern machine learning approach is to model them using neural network-based representations, as done in the first two contributions. This naturally raises the question of whether one can learn representations of confounders such that the latent variables are *causal*, meaning they exhibit causal relationships among themselves both instantaneously (within each time slice) and over time (across time slices). This field of study is commonly called *causal representation learning* (CRL) (Schölkopf et al., 2021).

It is worth mentioning that different causal modeling frameworks exist for reasoning about the causal learning problem. The two most common frameworks are causal graphical models (CGMs) and SCM. Causal Bayesian networks are another term used to refer to CGMs (Spirtes et al., 2001).

The first and necessary building block for defining a causal graphical model is to establish what we mean by a causal relationship between two arbitrary random variables.

### Definition Def2.7 [Causal Effect (Schölkopf & von Kügelgen, 2022)]

A random variable  $X_1$  is said to have a causal effect on a random variable  $X_2$  if there exist two values  $x_1 \neq x'_1$  such that the distribution of  $X_2$  after *intervening* on  $X_1$  and setting it to  $x_1$  differs from the distribution of  $X_2$  after setting  $X_1$  to  $x'_1$ .

A crucial component in defining a causal effect is the notion of *intervention*, which refers to an action

upon the cause  $X_1$ . This bears the same intuition as the nature of treatment in the potential outcome framework. However, one still needs to formally define what an intervention entails when dealing with causal graphs, which naturally leads to the discussion of the *do-operator*.

A causal graphical model is, first and foremost, a directed graphical model in the classical sense (Lauritzen, 1996; Koller, 2009) that is acyclic; i.e., every causal effect “propagates” from earlier to later variables, and no variable can (directly or indirectly) be its own ancestor, thereby enforcing the principle that causes precede their effects. However, unlike standard directed graphical models, the directed edges in a causal graphical model carry a *causal interpretation*: a directed edge signifies a causal effect, as stated in Definition Def2.7. Formally:

**Definition Def2.8 [CGM]**

A Causal Graphical Model (CGM)  $\mathcal{M} = (G, p)$  over  $n$  random variables  $X_1, \dots, X_n$  is a tuple consisting of:

- A directed acyclic graph (DAG)  $G$ , where directed edges  $(X_j \rightarrow X_i)$  represent a direct causal effect of  $X_j$  on  $X_i$ , as in Definition Def2.7.
- A probability distribution  $p(X_1, \dots, X_n)$  that is *Markovian* w.r.t.  $G$ , meaning it factorizes as:

$$p(X_1, \dots, X_n) = \prod_{i=1}^n p(X_i \mid Pa(X_i)) \quad (2.13)$$

where  $Pa(X_i) := \{X_j : (X_j \rightarrow X_i) \in G\}$  is the set of parents (i.e., direct causes) of  $X_i$  in the graph  $G$ .

Assuming  $p(X_1, \dots, X_n)$  admits a strictly positive density w.r.t. a product measure (e.g a product of Lebesgue and counting measures depending on whether  $X_i$  is continuous or discrete) so that the conditional probability distribution  $p(X_i \mid Pa(X_i))$  is well defined for every  $i \in \{1, \dots, n\}$  and for every possible choice of the set  $Pa(X_i)$  (Lauritzen et al., 1990), the Markov factorization is equivalent to what is known as the *local directed Markov condition* (Spirtes, 2010a), which is a purely probabilistic graphical property.

**Definition Def2.9 [Local Directed Markov Condition]**

A distribution  $p$  satisfies the local directed Markov condition w.r.t. a DAG  $G$  if every variable is conditionally independent of its non-descendants in  $G$ , given its parents in  $G$ .

For example, if we are given a probability distribution over three variables  $p(X_1, X_2, X_3)$  such that

$$p(X_1, X_3 \mid X_2) = p(X_1 \mid X_2) p(X_3 \mid X_2),$$

and we assume a DAG of the form

$$X_1 \leftarrow X_2 \rightarrow X_3,$$

then  $p$  satisfies the local directed Markov condition because  $X_1$ , given its parent  $X_2$ , is conditionally independent of its non-descendant  $X_3$ , i.e.,

$$X_1 \perp\!\!\!\perp X_3 \mid X_2.$$

The same property holds for  $X_3$  by symmetry.

Under the condition of strict positive density for  $p(X_1, \dots, X_n)$ , the Markov factorization is also equivalent to another important graphical criterion extensively used in causal inference: *d-separation*. To formally define d-separation, we first introduce the concept of a *path* being *blocked* in a graph.

**Definition Def2.10 [Path]**

A path  $\pi = (X_1, \dots, X_p)$  in a DAG  $G$  is a sequence of distinct nodes connected by edges, regardless of their orientation, that is, for  $i \neq j$ ,  $X_i \neq X_j$  and

$$X_j \rightarrow X_i \text{ or } X_i \rightarrow X_j.$$

**Definition Def2.11 [Blocking a Path]**

A path  $\pi = (X_1, \dots, X_p)$  is said to be blocked given a set of observed nodes  $\mathbf{O}$  if there exists a node  $X_i$  in the path such that:

- $X_i$  is a common parent, i.e.,  $X_{i-1} \leftarrow X_i \rightarrow X_{i+1}$ , and  $X_i \in \mathbf{O}$ .
- $X_i$  is part of a cascade structure, i.e.,  $X_{i-1} \rightarrow X_i \rightarrow X_{i+1}$  or  $X_{i-1} \leftarrow X_i \leftarrow X_{i+1}$ , and  $X_i \in \mathbf{O}$ .
- $X_i$  is a collider, i.e.,  $X_{i-1} \rightarrow X_i \leftarrow X_{i+1}$ , but  $X_i \notin \mathbf{O}$  and no descendant of  $X_i$  is in  $\mathbf{O}$ .

For example, let's consider the path  $X_1 \rightarrow X_2 \leftarrow X_3 \rightarrow X_4 \rightarrow X_5$  and let  $\mathbf{O} \subseteq \{X_2, X_3, X_4\}$ , then:

- At  $X_2$ : the structure  $X_1 \rightarrow X_2 \leftarrow X_3$  makes  $X_2$  a *collider*; it is blocked if  $X_2 \notin \mathbf{O}$ .
- At  $X_3$ : the structure  $X_2 \leftarrow X_3 \rightarrow X_4$  makes  $X_3$  a *fork*; it is blocked if  $X_3 \in \mathbf{O}$ .
- At  $X_4$ : the structure  $X_3 \rightarrow X_4 \rightarrow X_5$  makes  $X_4$  a *chain*; it is blocked if  $X_4 \in \mathbf{O}$ .

**All conditioning blocking sets:** the path is blocked by  $\mathbf{O}$  precisely when *at least one* of the following holds:

- *Collider at  $X_2$  is blocked:*  $X_2 \notin \mathbf{O}$ .
- *Fork at  $X_3$  is blocked:*  $X_3 \in \mathbf{O}$ .



- *Chain at  $X_4$  is blocked:*  $X_4 \in \mathbf{O}$ .

Equivalently, every subset  $\mathbf{O}$  except the one that contains  $X_2$  and contains neither  $X_3$  nor  $X_4$  will block the path. Thus, the seven blocking sets are:

Set $O$	Blocks via
$\emptyset$	$X_2$ (collider; $X_2 \notin \mathbf{O}$ )
$\{X_3\}$	$X_2$ or $X_3$
$\{X_4\}$	$X_2$ or $X_4$
$\{X_3, X_4\}$	$X_2$ , $X_3$ , or $X_4$
$\{X_2, X_3\}$	$X_3$
$\{X_2, X_4\}$	$X_4$
$\{X_2, X_3, X_4\}$	$X_3$ or $X_4$

**Non-blocking set:** The only subset that does *not* block is  $\mathbf{O} = \{X_2\}$ , since it “unblocks” the collider at  $X_2$  and contains neither  $X_3$  nor  $X_4$ .

#### Definition Def2.12 [D-separation]

Let  $A, B, C$  be non-overlapping sets of nodes in a graph  $G$ .  $A$  and  $B$  are *d-separated* given  $C$  if all paths connecting  $a \in A$  and  $b \in B$  are blocked by  $C$ , meaning the paths are inaccessible when conditioning on  $C$ .

One key application of d-separation is simplifying conditional probability dependencies based on the graphical relationships between variable sets  $A, B, C$ .

#### Proposition Prop2.3

If the sets of nodes  $A$  and  $B$  are d-separated given  $C$ , then:

$$p(A, B \mid C) = p(A \mid C)p(B \mid C).$$

#### Corollary Cor2.2

If the sets of nodes  $A$  and  $B$  are d-separated given  $C$ , then the conditional probability  $p(A \mid B, C)$  simplifies to  $p(A \mid C)$ , meaning it is sufficient to condition only on the set of nodes blocking the paths between  $A$  and  $B$ .

The global directed Markov condition is based on the d-separation property and is defined as follows:

**Definition Def2.13 [Global Directed Markov Condition]**

A probability distribution  $p$  is said to satisfy the global directed Markov condition if, for any disjoint sets of variables  $A, B, C$ , d-separation of  $A$  and  $B$  given  $C$  in  $G$  implies that  $A$  is conditionally independent of  $B$  given  $C$  in  $p$ .

When a graphical model is endowed with a causal interpretation, as in the case of CGM in Definition Def2.8, the local directed Markov condition becomes a key property that links causal relationships in a causal graph to conditional probabilities. This property is known as the *Causal Markov Condition* (Spirtes et al., 2001). To define it formally, we first introduce the notion of a causally sufficient set of variables in a graph.

**Definition Def2.14 [Causally Sufficient Set]**

A set of variables  $\mathbf{O}$  in a causal graph  $G$  is said to be causally sufficient if there is no variable  $X$  in  $\bar{\mathbf{O}}$  that is a common cause of at least two variables in  $\mathbf{O}$ .

In other words, a set of variables is causally sufficient if it includes all common causes of the variables within the set. For example, if a DAG has the form

$$X_1 \longrightarrow X_2 \longleftarrow X_3 \longrightarrow X_4 \longrightarrow X_5,$$

then the set  $\{X_1, X_2, X_4\}$  is not causally sufficient because it misses a common parent of two variables within the set,  $X_2$  and  $X_4$ , which is  $X_3$ . The set  $\{X_1, X_2, X_3, X_4\}$  is therefore causally sufficient.

We can now define the Causal Markov Condition.

**Definition Def2.15 [Causal Markov Condition]**

Let  $\mathcal{M} = (G, p)$  be a CGM over  $n$  random variables  $X_1, \dots, X_n$ . The causal graph is said to satisfy the Causal Markov Condition if the set of variables  $\{X_1, \dots, X_n\}$  is causally sufficient and the distribution  $p(X_1, \dots, X_n)$  satisfies the local directed Markov condition (cf. Definition Def2.9).

The utility of the Causal Markov Condition lies in its ability to express the joint probability distribution of the system variables  $X_1, \dots, X_n$ . If a variable, say  $X_j$ , is externally manipulated to follow a new mechanism  $p^*(X_j \mid Pa(X_j))$ , then one only needs to replace the original mechanism  $p(X_j \mid Pa(X_j))$  with its altered version  $p^*(X_j \mid Pa(X_j))$  in the Markov factorization according to the graph  $G$ :

$$p(X_1, \dots, X_n \mid do(X_j \sim p^*(X_j \mid Pa(X_j)))) := p^*(X_j \mid Pa(X_j)) \prod_{i=1, i \neq j}^n p(X_i \mid Pa(X_i)). \quad (2.14)$$

Here, we use the *do-notation* to emphasize that  $X_j$  has been actively intervened upon rather than

passively observed. As a result, the conditioning sign in the left-hand side (LHS) of Equation 2.14 does not represent classical probabilistic conditioning.

It is common for the variable  $X_j$  to be assigned a particular value, say  $x_j$ , typically denoted as  $do(X_j = x_j)$ . In this case, we replace  $p(X_j | Pa(X_j))$  with the Dirac distribution  $\delta(X_j = x_j)$ , and the interventional probability becomes:

$$p(X_1, \dots, X_n | do(X_j = x_j)) = \delta(X_j = x_j) \prod_{i=1, i \neq j}^n p(X_i | Pa(X_i)). \quad (2.15)$$

SCM represents another causal modeling framework that still relates to causal graphs but differs in its functional nature: direct causes (parents) influence their effects (children) through directed functional relationships:

**Definition Def2.16 [Structural Causal Model]**

An SCM is a causal model represented by a tuple  $M = \langle \Xi_n, \mathbb{X}_n, \mathbb{F}, p_{\Xi_n} \rangle$ , where:

1.  $\Xi_n := \{\xi_1, \dots, \xi_n\}$  is the set of exogenous noise variables that capture factors not explicitly represented in the model.
2.  $\mathbb{X}_n := \{X_1, \dots, X_n\}$  represents the set of observed variables in the model, also referred to as endogenous variables. These variables are determined by  $\Xi_n$  and  $\mathbb{X}_n$  itself through functional dependencies.
3.  $\mathbb{F} := \{f_1, f_2, \dots, f_n\}$  is the set of structural functions such that:

$$X_i := f_i(Pa(X_i), \xi_i), \quad i = 1, \dots, n$$

where  $Pa(X_i) \subset \mathbb{X}_n - \{X_i\}$ .

4.  $p_{\Xi_n}$  refers to the joint probability distribution over the noise terms  $p_{\Xi_n}(\xi_1, \dots, \xi_n)$ .

From the definition of an SCM, there is a strong connection with causal graphs. Given the structure of an SCM, we can define an associated causal graph as follows:

**Definition Def2.17 [Induced Causal Graph]**

The causal graph  $G$  induced by an SCM  $M = \langle \Xi_n, \mathbb{X}_n, \mathbb{F}, p_{\Xi_n} \rangle$  is the directed graph with nodes  $\mathbb{X}_n$  and a directed edge from each node in  $Pa(X_i)$  to  $X_i$  for all  $i \in \{1, \dots, n\}$ .

According to the induced causal graph, we must eliminate any possible cycles in the graph to ensure that the probability distribution over the observed variables  $\mathbb{X}_n$  is uniquely defined. We therefore assume the acyclicity of the induced causal graph:

**Assumption Asm2.9 [Acyclicity]**

The induced graph  $G$  of an SCM  $M$  is assumed to be a directed acyclic graph (DAG).

To ensure that the probability distribution over the observed variables  $\mathbb{X}_n$ , as induced by the SCM model, admits a Markov factorization according to its induced causal graph, we further assume that the exogenous noise variables are independent:

**Assumption Asm2.10 [Causal Sufficiency / No Hidden Confounders]**

The exogenous noise variables  $\Xi_n$  are jointly independent, i.e.,

$$p_{\Xi_n}(\xi_1, \dots, \xi_n) = p_{\xi_1}(\xi_1) \times \dots \times p_{\xi_n}(\xi_n).$$

The causal sufficiency assumption is equivalent to stating that the set of observed causal variables is causally sufficient according to Definition Def2.14. Moreover, this assumption is often referred to as the *no hidden confounders* assumption, since the presence of an unobserved common cause of variables within  $\mathbb{X}_n$  would violate causal sufficiency. Specifically, if a common cause of variables in  $\mathbb{X}_n$  is not itself part of  $\mathbb{X}_n$ , then  $\mathbb{X}_n$  would not be causally sufficient, leading to dependencies among the exogenous noise variables and violating the assumed independence of  $\Xi_n$ .

An important consequence of acyclicity and causal sufficiency is that the causal conditionals associated with the causal graph can now be defined as the push-forward of the noise distribution  $p_{\Xi_n}$  through the functional dependencies  $\mathbb{F}$ :

$$p(X_i \mid Pa(X_i)) := p_{\xi_i}(f_{Pa(X_i)}^{-1}(X_i)) \quad \text{for } i = 1, \dots, n,$$

where  $f_{Pa(X_i)}^{-1}(X_i)$  denotes the preimage of  $X_i$  under the mapping  $f_i$ , given the values of  $Pa(X_i)$ .

## Chapter 3

# Causal Dynamic Variational Autoencoder

### 3.1 Introduction

Estimating ITE helps us understand how individuals uniquely respond to the same treatment, enabling more personalized and effective decision-making. For example, in healthcare, two patients receiving the same drug might experience considerably different outcomes due to underlying genetic or lifestyle differences (Atan et al., 2018; Shalit, 2020; Mueller & Pearl, 2023). The exact curriculum might yield more remarkable improvement for one student than another in education, depending on background factors like socioeconomic status (Morgan, 2013; Imbens & Rubin, 2015). Likewise, in marketing, identical promotions might drive purchases in one customer segment but not another (Hair Jr & Sarstedt, 2021; Fang et al., 2023).

*Longitudinal data* arise naturally in these domains. Consider, for instance, a medical dataset recording blood pressure, treatments (e.g., vasopressors), and vitals for each patient at regular intervals. Or a retail dataset tracking weekly customer purchases following commercial campaigns. Each longitudinal data describe a sequence of treatments, covariates, and responses causally interacting through time. As discussed in Section 2.2.3 and 2.2.4, this setting brings unique challenges: (1) *Time-dependent confounding*: Confounders influenced by past treatment can impact subsequent treatments and responses (Platt et al., 2009); (2) *Selection bias*: Time-varying covariates exhibit imbalanced distributions across treatment regimes, which should be accounted for to estimate treatment effects accurately (Robins et al., 2000; Schisterman et al., 2009; Lim, 2018a); (3) *Long-term dependencies*: A treatment effect may unfold over extended periods, requiring models to capture complex long-range interactions between covariates, treatments, and responses (Choi et al., 2016; Pham et al., 2017); (4) *Missing covariates*: Some variables crucial for predicting outcomes—like genetic predispositions or environmental exposures—introduce bias and less personalized treatment effect estimation unless properly accounted for.

**Assumptions over Confounders and Existing Approaches** The existing literature primarily addresses the first three challenges under the assumption of *sequential ignorability* (Asm2.5), where all confounders, whether static or time-varying, are fully observed. Methods such as MSM (Robins & Hernán, 2009a), RMSM (Lim, 2018a), CRN (Bica et al., 2020a), G-Net (Li et al., 2021), Causal Transformer (CT) (Melnychuk et al., 2022), and our model Causal CPC (Bouchattaoui et al., 2024) have been developed based on this assumption (cf. Section 2.2.5, Chapter 2). When the fourth challenge—missing covariates—is addressed, it is often in the form of *missing confounders*, violating sequential ignorability. Existing approaches (cf. Section 2.2.4) either condition on *observed proxies* of confounders to infer a latent representation of the unobserved confounders (Kuroki & Pearl, 2014; Miao et al., 2016; Louizos et al., 2017; Cheng et al., 2021) or apply the *deconfounding technique*, which involves imposing a factor model over the treatment assignment to mitigate hidden confounding (Lopez & Gutman, 2017; Ranganath & Perotte, 2018; Wang & Blei, 2019a; Zhang et al., 2019; Bica et al., 2020b; Hatt & Feuerriegel, 2024).

**Our Focus** In contrast to missing confounders, we study for the first time the presence of *unobserved static adjustment variables*—factors that influence only the outcome sequence and remain *time-invariant*. In a medical context, these could include genetic factors, environmental conditions, or lifestyle attributes that impact treatment response but are not directly observed (Sadowski et al., 2024). The absence of such variables can lead to a loss of heterogeneity in the estimated treatment effect. This phenomenon can also be understood through the lens of *population structure*, which arises from distinct subgroups within a population that share characteristics such as geography, socioeconomic status, or cultural practices. Having knowledge of, or being able to infer accurately, population structure allows for a more precise estimation of ITE by capturing variations in treatment responses across subgroups. In genomics (Laird & Lange, 2011; Peter et al., 2020), for instance, such a structure arises due to evolutionary or migration histories. Moreover, population structure often acts as an *effect modifier* (Hernán & Robins, 2020), altering treatment effects across subgroups without directly influencing treatment assignment (Hyun et al., 2024). By accounting for such effect modifiers through stratified or interaction analyses, treatment effects can be estimated more accurately, even in randomized trials (Schochet, 2024).

In this work, we specifically address the challenge of missing covariates by focusing on estimating the contemporaneous treatment effect (Asm2.8)—the effect of the current treatment on the subsequent response. The potential trajectory of treatments up to  $t - 1$ ,  $\omega_{<t}$ , is assumed to be consistent with the observed history of treatments, i.e.,  $\omega_{<t} = W_{<t}$ . Therefore, the potential outcomes of interest at each time step  $t$  are  $\{Y_t(W_{<t}, \omega)\}_{\omega \in \mathcal{W}}$ .

**Remark Rem3.1 [Carryover Effect and CTE]**

Although we target the contemporaneous treatment effect in the CDVAE model, we do not formally assume the no carryover effect (Definition Def2.6), i.e., that past treatments do not affect current outcomes. This would imply that given any two potential treatment sequences  $\omega_{\leq t}$  and  $\omega'_{\leq t}$ , such that  $\omega_t = \omega'_t$ , then  $Y_t(\omega_{\leq t}) = Y_t(\omega'_{\leq t})$ , which is different from our Assumption Asm2.8.

We consider the ITE as an *Augmented Conditional Average Treatment Effect (ACATE)*, where the CATE depends not only on the confounding variables but also on adjustment variables. We aim to achieve *near-oracle performance* in treatment effect estimation by leveraging the learned representation of unobserved adjustment variables. Specifically, we prove that for all baselines satisfying sequential ignorability, treatment effect estimation is substantially improved when these models are augmented with the learned representation of unobserved adjustment variables produced by our model—ultimately delivering performance that approaches the oracle scenario, where the true unobserved adjustment variables are directly fed into the baselines. Extensive experiments on synthetic data and semi-synthetic data derived from real-world datasets such as MIMIC-III (Johnson et al., 2016) validate our approach.

**Our Approach** We treat the unobserved adjustment variables as latent variables and leverage a probabilistic modeling approach based on the *Dynamic Variational Autoencoder (DVAE)* framework (Girin et al., 2021) to estimate the ACATE, where we augment the CATE with the learned representation of unobserved adjustment variables, which we term *substitutes*. We address the covariate imbalance induced by selection bias in longitudinal data using a weighted empirical risk minimization strategy, where the weights are a function of the propensity scores. Additionally, we derive a generalization bound for the error in estimating ACATE and use its approximation as a loss function for our model, which we refer to as *Causal DVAE (CDVAE)*. To account for potential population structure induced by unobserved adjustment variables, we define a flexible prior over the latent variables using a learnable Gaussian Mixture Model (GMM). We ensure the causal validity of the learned substitutes by imposing a finite-order Conditional Markov Model (CMM) on the response series. The causal validity follows from our proof that, once the finite-order CMM holds, the learned substitutes account for all relevant adjustment variables (Theorem Thm3.2) and that the ACATE leveraging the substitutes is identifiable. To experimentally support the theoretical analysis, we discuss the relevance of all CDVAE components through an ablation study.

Furthermore, since we adopt a probabilistic approach, we represent the substitute for unobserved adjustment variables as a *stochastic* latent variable. Consequently, the choice of the substitute given individual longitudinal data is not unique. As a novel contribution, we study Causal DVAE in the *near-deterministic regime*, where we reduce the variance of the responses (outputs of the Causal DVAE) to near zero. This process indirectly pushes the covariance matrix of the substitutes toward zero, preventing their distribution from becoming overly diffuse. An intuitive consequence of this approach is that any sampled substitute of the adjustment variables yields the same treatment effect as the mean substitute. We demonstrate that as the response variance approaches zero, the treatment effect remains consistent regardless of the specific instance of the substitutes. The near-deterministic regime of VAEs has not been previously explored in the context of causal inference, making this a novel contribution. To draw an analogy, in the deconfounding literature (Lopez & Gutman, 2017; Ranganath & Perotte, 2018; Wang & Blei, 2019a; Zhang et al., 2019; Bica et al., 2020b; Hatt & Feuerriegel, 2024), substitutes—referring to learned representations of missing confounders—are theoretically assumed to follow a Dirac posterior. This enables deterministic selection and facilitates treatment effect identifiability. However, the training of

these models is based on a non-degenerate posterior, creating a disconnect between theoretical assumptions and practical implementation. Our approach bridges this gap by achieving near-deterministic behavior while maintaining a probabilistic framework.

We also examine the classical approach of mixed-effect modeling for treatment effect estimation, which uses *random effects* to capture individual-level variation and account for latent heterogeneity (Fitzmaurice et al., 2012; Demidenko, 2013). While these models address unobserved heterogeneity by incorporating random intercepts or slopes, our modeling goes further by learning representations of unobserved variables and seamlessly integrating them into the ITE estimation pipeline. This comparison highlights a shared objective: both approaches aim to mitigate unobserved heterogeneity to enhance the precision of treatment effect estimates.

Our *contributions* can be summarized as follows:

- We propose a principled approach to infer a latent representation of unobserved adjustment variables (Section 3.5).
- We prove the theoretical validity of the learned adjustment variables by modeling the response series as a finite-order conditional Markov process, ensuring that ITE conditioned on learned substitutes are identifiable (Section 3.5.1).
- We study for the first time the near-deterministic regime of VAEs for causal inference and show that reducing the variance of response predictions enforces consistency in treatment effect estimation, even under stochastic modeling of adjustment variables (Section 3.5.3).
- Numerical experiments confirm the effectiveness of CDVAE in estimating ITE, showing that our method consistently outperforms SOTA baselines (Section 3.7), as further analyzed through an ablation study.
- We show that for SOTA baselines, augmenting their input covariates with the inferred representation of adjustment variables given by CDVAE substantially enhances their accuracy in estimating ITE (Section 3.7) and even provide near-oracle performances.

## 3.2 Related Work

**Causal Inference in Time-Varying Settings.** In Section 2.2.5, we extensively covered MSM (Robins et al., 2000) and their role in addressing time-varying confounders in causal inference through IPTW (Robins & Hernán, 2009a). Despite their utility, MSM encounter challenges related to high-variance estimates and the need for a good specification of the treatment assignment mechanism, especially in complex scenarios. MSM are often integrated with g-computation (Vansteelandt & Joffe, 2014) and Structured Nested Mean Models (Robins, 1997), particularly in epidemiology. We also discussed recent advancements utilizing neural network-based models, such as the RMSM (Lim, 2018a), employing RNNs for enhanced modeling of propensity and outcomes, and the CRN (Bica et al., 2020a), which adopts adversarial domain training to mitigate bias in the presence of time-varying confounders. Additionally, we



examined the G-Net (Li et al., 2021) and the CT (Melnychuk et al., 2022), highlighting their contributions to multi-timestep counterfactual prediction through g-computation and adversarial training, respectively. Although the contribution of the next Chapter 4 (Causal CPC) targets the long-term counterfactual regression, we include it in this chapter’s experiments as a complementary baseline. Causal CPC leverages temporal dynamics through contrastive predictive coding and information maximization and learns a balanced representation using an adversarial training strategy (cf. Chapter 4 for a full description).

✎ While the aforementioned models have made significant strides in causal inference for time-varying settings, our approach laid by CDVAE enhances these methods by incorporating inferred adjustment variables into the modeling process. By augmenting the input covariates of these SOTA models with our inferred representations, we achieve a more accurate estimation of ITE and improve the overall robustness of causal inference in longitudinal data.

**Combining Weighting and Representation Learning** A key driver for developing representation learning in causal inference is to address covariate imbalance in high-dimensional settings. These methods aim to achieve balance in the learned feature space to mitigate covariates shift. Combining weighting methods, such as those proposed by Zubizarreta (2015); Li et al. (2018a); Johansson et al. (2018); Hassanpour & Greiner (2019b), with representation-based causal inference, offers a promising approach to address the challenges faced by representation learning in the context of causal inference. These methods demonstrate how properly designed weights can alleviate the difficulties associated with representation learning techniques. However, a trade-off exists between covariate balance and predictive performance: *overly strict balancing can lead to the loss of valuable features and exacerbate bias in estimating treatment effects* (Assaad et al., 2021; Zhang et al., 2020b). On the other hand, Zhang et al. (2020b) and Johansson et al. (2019) highlighted that such regularization might lead to a loss of ignorability in the representation and suggested learning representations in which context information remains preserved but where treatment groups overlap. To this end, Assaad et al. (2021) introduced the Balancing Weights Counterfactual Regression (BWCFR) method, which aims to achieve balance *within the reweighted covariate* representations instead of directly balancing the covariates representations. Assaad et al. (2021) argues that BWCFR provides bounds on the degree of imbalance as a function of the propensity model and offers theoretical guarantees for estimating the CATE using the overlapping weight. Johansson et al. (2022) built on the previous work on sampling weighting for counterfactual regression and representation learning (Johansson et al., 2016; Shalit et al., 2017; Kallus, 2020; Jung et al., 2020; Assaad et al., 2021), and provided a comprehensive theory for weighted risk minimization for CATE for a learned representation from the data.

#### Remark Rem3.2

In this work, we extend the weighted empirical risk minimization framework, which has been primarily developed for static settings, to the longitudinal context. Our approach focuses on contemporaneous treatments rather than sequences of interventions (see Assumption Asm2.8). This distinction allows

us to naturally adapt these methods to time-varying data without introducing unnecessary complexity. While these extensions are straightforward, they offer important practical insights by maintaining the balance between covariates across time points, even as treatment effects evolve.

**Probabilistic Modeling in Causal Inference** In scenarios where confounders are unobserved but proxy variables are available, probabilistic models were used to infer a representation for the unobserved confounding given the proxy variables (Kuroki & Pearl, 2014; Miao et al., 2016; Louizos et al., 2017; Cheng et al., 2021). While our work assumes the presence of observed confounding, it draws inspiration from the theory of deconfounding (Lopez & Gutman, 2017; Ranganath & Perotte, 2018; Wang & Blei, 2019a), and its recent extensions to time-varying settings. The idea behind the deconfounding is to impose a factor model over the treatment assignment, where each cause becomes conditionally independent given latent variables that serve as substitutes for the unobserved confounders. Bica et al. (2020b) extended the application of the deconfounding method to sequential settings with multiple treatments, aiming to infer time-varying confounders. They assumed that the joint distribution of treatments at each time step, conditioned on learned substitutes and observed confounders, could be decomposed into the product of the conditional distribution of each treatment. For the case of a single treatment per time step, Hatt & Feuerriegel (2024) assumed a conditional Markov model over the treatment sequences given the sequence of confounders and the latent variables to be inferred. However, extending the deconfounder theory to longitudinal settings does not guarantee the consistency assumption required for identifying the ATE. Wang & Blei (2019a) proposed a theory of identification that relies on the assumption that the operation on the latent variables follows a Dirac distribution, allowing for a certain construction of the substitute confounder. In contrast, Bica et al. (2020b) utilizes variational dropout to construct the substitute, and Hatt & Feuerriegel (2024) adopts variational inducing point-based inference for a Gaussian process latent variable model extended to the sequential setting.

✎ In this work, we aim to demonstrate that the core idea of the factor model can be applied to learn valid substitutes for unobserved adjustment variables in the time-varying domain. Unlike previous deconfounder works, we show that assuming a higher-order conditional Markov model for the series of responses is sufficient to infer a valid representation of static adjustment variables.

### 3.3 Problem Definition

This work adopts the PO framework for longitudinal data developed in Section 2.2.1. We consider a binary treatment variable and narrow the scope of PO to align with the CTE hypothesis, as outlined in Assumption Asm2.8. Consequently, we express the counterfactual outcomes as  $Y_t(W_{<t}, \omega)$ , simplified to  $Y_t(\omega)$  within this chapter for ease of notation.

Given the CTE assumption (Asm2.8) and the binary nature of treatments, the CATE  $\tau_t(\mathbf{x}_{\leq t}, y_{<t}; \omega_{\leq t}, \omega'_{\leq t})$

(Definition Def2.4) can be simplified to:

$$\tau_t(\mathbf{x}_{\leq t}, y_{< t}; \omega_{\leq t}, \omega'_{\leq t}) = \tau_t(\underbrace{\mathbf{x}_{\leq t}, y_{< t}, \omega_{< t}}_{\mathbf{h}_t}; \omega_t, \omega'_t) = \mathbb{E}(Y_t(\omega_t) - Y_t(\omega'_t) \mid \mathbf{H}_t = \mathbf{h}_t),$$

assuming that  $\omega_{< t} = \omega'_{< t}$  by CTE is consistent with the observed history process  $\mathbf{H}_t = \mathbf{h}_t$ , i.e.,  $W_{< t} = \omega_{< t}$  by the CTE assumption. Since the treatment is binary, we adopt the convention where the value 0 refers to control and 1 refers to applying the treatment of interest. This allows us to define the CATE as

$$\tau_t(\mathbf{h}_t; \omega_t, \omega'_t) = \tau_t(\mathbf{h}_t) = \mathbb{E}(Y_t(1) - Y_t(0) \mid \mathbf{H}_t = \mathbf{h}_t),$$

which represents the difference between the expected potential outcomes at a time  $t$ , given the context history  $\mathbf{H}_t = \mathbf{h}_t$ . The sequential ignorability assumption defined in Section Asm2.5 allows for the identification of CATE:

$$\tau_t(\mathbf{h}_t) = \mathbb{E}(Y_t \mid \mathbf{H}_t = \mathbf{h}_t, W_t = 1) - \mathbb{E}(Y_t \mid \mathbf{H}_t = \mathbf{h}_t, W_t = 0). \quad (3.1)$$

So far, we expressed the CATE as a function of the confounding history  $\mathbf{H}_t$ . Now, assuming we **observe adjustment variables**  $\mathbf{U}$  and aim to estimate a heterogeneous treatment effect depending on both  $\mathbf{H}_t$  and  $\mathbf{U}$ . We define the *Augmented CATE (ACATE)* as follows:

$$\tau_t(\mathbf{h}_t, \mathbf{u}) := \mathbb{E}(Y_t(1) - Y_t(0) \mid \mathbf{H}_t = \mathbf{h}_t, \mathbf{U} = \mathbf{u}). \quad (3.2)$$

The assumed risk factors  $\mathbf{U}$  affect the response series but not the treatment as in the diagram of Figure 3.1. The fact that the adjustment variables do not confound treatment and response at any time step makes the assumed ignorability of treatment given history context sufficient to identify the ACATE, i.e.,

$$\tau_t(\mathbf{h}_t, \mathbf{u}) = \mathbb{E}(Y_t \mid \mathbf{H}_t = \mathbf{h}_t, \mathbf{U} = \mathbf{u}, W_t = 1) - \mathbb{E}(Y_t \mid \mathbf{H}_t = \mathbf{h}_t, \mathbf{U} = \mathbf{u}, W_t = 0) \quad (3.3)$$

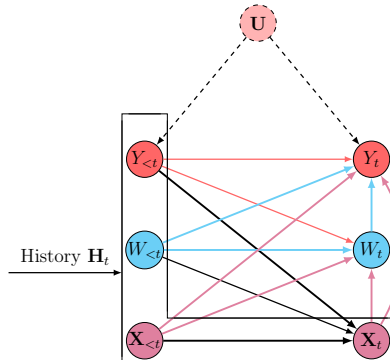


Figure 3.1: A simplified representation of the DGP at time  $t$ . Edges between  $Y_{< t}$ ,  $W_{< t}$ , and  $\mathbf{X}_{< t}$  are omitted for simplicity.

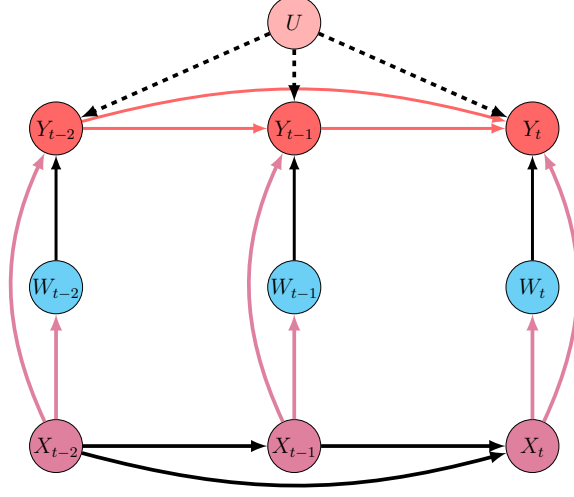


Figure 3.2: A causal graph describing panel data for the Vitamin D problem.

**Inference problem** Deriving the ACATE becomes straightforward when both confounding and adjustment variables are fully observed. However, when  $\mathbf{U}$  is missing, unobserved heterogeneity in the treatment effect arises, leading to incomplete or biased conclusions about treatment effects. This raises the following key inference question: *Under what conditions can a substitute  $\mathbf{Z}$  for the unobserved adjustment variables  $\mathbf{U}$  ensure the identifiability of the ACATE by replacing  $\mathbf{U}$  with  $\mathbf{Z}$ , specifically guaranteeing that the following equality (i) holds?*

$$\begin{aligned} \tau_t(\mathbf{h}_t, \mathbf{z}) &= \mathbb{E}(Y_t(1) - Y_t(0) \mid \mathbf{H}_t = \mathbf{h}_t, \mathbf{Z} = \mathbf{z}) \\ &\stackrel{(i)}{=} \mathbb{E}(Y_t \mid \mathbf{H}_t = \mathbf{h}_t, \mathbf{Z} = \mathbf{z}, W_t = 1) - \mathbb{E}(Y_t \mid \mathbf{H}_t = \mathbf{h}_t, \mathbf{Z} = \mathbf{z}, W_t = 0) \end{aligned} \quad (3.4)$$

### 3.4 Mixed Effect Modeling and Heterogeneous Treatment Effect: A Unifying View

To motivate our modeling approach, consider a study of vitamin D supplementation, represented by the treatment indicator  $W$ , on frailty  $Y$  (Bray et al., 2018; Cai et al., 2022), with financial resources  $\mathbf{X}$  as a confounder. For example, individuals with more economic resources may be more likely to afford and take vitamins. Observing data at multiple time points (e.g., monthly) allows us to use a causal graph to describe these relationships, as illustrated in Figure 3.2. The CATE can be defined, under the ignorability assumption of Asm2.2 as:

$$\tau(\mathbf{H}_t) := \mathbb{E}(Y_t \mid W_t = 1, \mathbf{H}_t) - \mathbb{E}(Y_t \mid W_t = 0, \mathbf{H}_t).$$

This equation shows that treatment effects can vary based on financial resources. However, consider the impact of vitamin D on frailty for younger versus older individuals. Age  $U$  can significantly affect the treatment response, as younger individuals may metabolize vitamin D more effectively. Therefore, we use

ACATE (similar to Equation 3.2) as a treatment effect estimation that includes the age variable:

$$\tau(\mathbf{H}_t, \mathbf{U}) := \mathbb{E}(Y_t \mid W_t = 1, \mathbf{H}_t, \mathbf{U}) - \mathbb{E}(Y_t \mid W_t = 0, \mathbf{H}_t, \mathbf{U}). \quad (3.5)$$

Including  $U$  improves prediction precision. When  $U$  is *unobserved*, mixed-effect models (Fitzmaurice et al., 2012; Demidenko, 2013) help address this by accounting for random effects, which can be seen as proxies for unobserved factors like age. For illustrative purposes, we specify a mixed-effect model for the outcome variable:

$$\mathbb{E}(Y_t \mid W_t, \mathbf{X}_{\leq t}, Y_{< t}, \alpha^{(1)}, \alpha^{(2)}) = \gamma_1 Y_{t-1} + \gamma_2 Y_{t-2} + \underbrace{(\beta_1 Y_{t-1} + (\beta_2 + \alpha^{(1)}) X_t + \alpha^{(2)})}_{\text{ACATE}} W_t + \beta_3 X_t.$$

Here,  $\alpha = (\alpha^{(1)}, \alpha^{(2)})$  are *random* effects, usually modeled with a Gaussian distribution  $\mathcal{N}(0, \Sigma)$ .  $\beta_1$  and  $\beta_2$  are unknown but *fixed* effects. Having the two types of effects is what makes such modeling a mixed-effect model (Demidenko, 2013).  $\gamma_1$  and  $\gamma_2$  are also fixed unknown parameters. An interesting observation from Equation 3.4 is that not all adjustment variables are necessarily present in the ACATE. The past response  $Y_{t-1}$  serves as an observed adjustment variable for  $Y_t$  and modifies ACATE when it changes through the parameter  $\beta_1$ . On the other hand,  $Y_{t-2}$  is still an adjustment variable but does not modify the effect ACATE when it changes. This behavior summarizes the concept of effect modification (Hernán MA, 2020; VanderWeele & Robins, 2007), where certain variables change the treatment effect when conditioned on them.

Random effects  $\alpha$  serve as a compact way to represent unobserved heterogeneity. This could be the case of factors such as age that are not directly recorded but nevertheless modify each subject’s response trajectory. For expositional clarity, let’s adopt the guiding viewpoint that these random effects are random variables, measurable with respect to the unobserved sources of heterogeneity. Consequently, we can express  $\alpha = \alpha(\mathbf{U}) := (\alpha^{(1)}(\mathbf{U}), \alpha^{(2)}(\mathbf{U}))$ , with  $\alpha^{(1)}, \alpha^{(2)} : \mathcal{U} \rightarrow \mathbb{R}$ , two arbitrary unknown mappings. By substituting random parameters with  $\mathbf{U}$  and incorporating mappings, we refine the model:

$$\mathbb{E}(Y_t \mid \text{Pa}(Y_t)) := \gamma_1 Y_{t-1} + \gamma_2 Y_{t-2} + \underbrace{(\beta_1 Y_{t-1} + (\beta_2 + \alpha^{(1)}(\mathbf{U})) X_t + \alpha^{(2)}(\mathbf{U}))}_{\text{ACATE}} W + \beta_3 \mathbf{X}_t.$$

Here,  $\text{Pa}(Y) = \{W_t, \mathbf{X}_{\leq t}, Y_{< t}, \mathbf{U}\}$  are the parent variables of  $Y_t$ . Our method of inferring unobserved risk variables parallels non-linear mixed-effects models (Demidenko, 2013). By viewing random effects as arising from unobserved risk factors, we may refer to these risk factors as random effects with slight terminology adjustments.

**Methodology** Our approach aligns with Bayesian network concepts (Peters et al., 2017) and mixed-effects modeling. Rather than directly learning random parameters, we propose learning a representation of unobserved  $\mathbf{U}$  and mapping  $\alpha(\cdot)$ . Using neural networks (Girin et al., 2021), we model complex non-linear dependencies and interactions among covariates, treatments, and inferred risk factors. Estimating the ACATE with unobserved variables involves the following methodology:

1. Learn a representation  $\mathbf{Z}$  of unobserved sources of variation.

2. Model the mapping  $\alpha(\cdot)$  using flexible neural networks to capture complex relationships.
3. Perform counterfactual regression, conditioning the treatment effect on representation  $\mathbf{Z}$  and the observed context history.

## 3.5 Causal DVAE

### 3.5.1 When does a Latent Representation Act as a Valid Substitute for Unobserved Adjustment Variables?

To address the issue of unobserved risk factors  $\mathbf{U}$  in our problem (as defined in Section 3.3), we treat  $\mathbf{Z}$  as a latent variable to be learned from the observed data distribution  $p(\mathbf{X}_{\leq T}, W_{\leq T}, Y_{\leq T})$  within a probabilistic model defined over the conditional responses as follows:

**Assumption Asm3.1 [CMM( $p$ ): Conditional Markov Model of order  $p$ ]**

We say that a latent variable  $\mathbf{Z}$  follows a Conditional Markov Model of order  $p$ , written  $\mathbf{Z} \sim CMM(p)$ , if there exists a fixed order  $p \in \mathbb{N}^*$  and a parameter vector  $\theta$  such that the response distribution factorizes as:

$$p_{\theta}(y_{\leq T}, \mathbf{z} \mid \mathbf{x}_{\leq T}, \omega_{\leq T}) = p(\mathbf{z}) \prod_{t=1}^T p_{\theta}(y_t \mid y_{t-1:t-p}, \mathbf{x}_{\leq t}, \omega_{\leq t}, \mathbf{z}).$$

For  $t < 1$ , we set  $y_t = \emptyset$  by convention.

The fact that  $\mathbf{Z}$  is set only with a prior in Assumption Asm3.1 mimics the role of  $\mathbf{U}$  because  $\mathbf{U}$  consists of static adjustment variables that are parentless, as illustrated in the causal graph (Figure 3.1). The bounded memory assumption over the sequence of responses, that is, the direct causal effect of past responses on future ones stops at an arbitrary order  $p$ , is a technical condition ensuring the causal validity of  $\mathbf{Z}$  as in the Theorem Thm3.1 where we demonstrate the sequential ignorability property when augmenting the history process with  $\mathbf{Z}$ , replicating the same result as if the true adjustment variables  $\mathbf{U}$  were available. All the proofs are deferred to Appendix A.1.

**Theorem Thm3.1 [Sequential Ignorability with Augmented History]**

Let  $\mathbf{Z}$  be a latent variable verifying CMM( $p$ ). Assume the response domain  $\mathcal{Y}$  is a Borel subset of a compact interval. Therefore, sequential ignorability holds when augmenting the history process with  $\mathbf{Z}$ :

$$Y_t(\omega) \perp\!\!\!\perp W_t \mid \mathbf{H}_t = \mathbf{h}_t, \mathbf{Z} = \mathbf{z} \quad \forall (\omega, \mathbf{h}_t, \mathbf{z}),$$

where  $\mathbf{H}_t$  represents the history process up to time  $t$ .

The ignorability result of Theorem Thm3.1 is the first step into answering the inference problem of 3.3 as it allows us to establish the identifiability of the ACATE when  $\mathbf{Z}$  replaces the true unobserved variable

$\mathbf{U}$  in Equation 3.3, summarized in the following corollary:

**Corollary Cor3.1 [Identifiability of ACATE with  $\mathbf{Z}$ ]**

Let  $\mathbf{Z}$  be a latent variable satisfying  $\text{CMM}(p)$ . The Augmented CATE, when augmented with  $\mathbf{Z}$  instead of  $\mathbf{U}$  as defined in (3.3), is identifiable. Specifically:

$$\tau_t(\mathbf{h}_t, \mathbf{z}) = \mathbb{E}(Y_t | \mathbf{H}_t = \mathbf{h}_t, \mathbf{Z} = \mathbf{z}, W_t = 1) - \mathbb{E}(Y_t | \mathbf{H}_t = \mathbf{h}_t, \mathbf{Z} = \mathbf{z}, W_t = 0) \quad (3.6)$$

As a result, Corollary Cor3.1 addresses the identifiability problem and its conditions as raised in Section 3.3: A CMM of arbitrary order over the conditional distribution of responses, along with a mild regularity condition on the response domain as stated in Theorem Thm3.1, constitutes a sufficient condition to ensure the identifiability of the ACATE. To further emphasize the relevance of  $\mathbf{Z} \sim \text{CMM}(p)$ , we show that any two substitutes satisfying  $\text{CMM}(p)$  must necessarily be related through a measurable map given the entire process history  $\mathbf{H}_T$ :

**Theorem Thm3.2**

Let  $\mathbf{Z}$  be a latent variable such that  $\mathbf{Z} \sim \text{CMM}(p)$ , and assume the domain  $\mathcal{Y}$  is a Borel subset of a compact interval. Then, any static adjustment variable that influences the entire series of responses in the panel must be measurable with respect to  $(\mathbf{Z}, \mathbf{H}_T)$ .

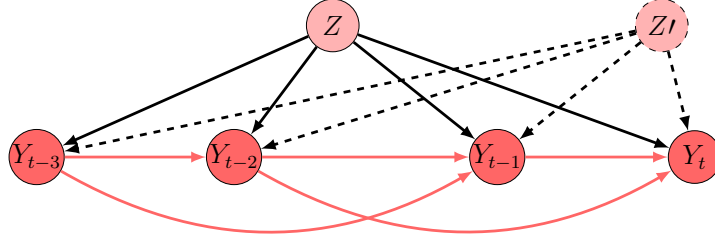


Figure 3.3: A simplified causal graph for the sketch of the proof for Theorem Thm3.2. We do not represent  $W_{\leq t}, \mathbf{X}_{\leq t}$  for simplicity.

**Intuition behind  $\text{CMM}(p)$ .** We provide an intuition behind the  $\text{CMM}(p)$  assumption by sketching a proof of Theorem Thm3.2 using d-separation properties, assuming the data generation process follows the graph depicted in Figure 3.3. Let  $\mathbf{Z}'$  be an unobserved risk variable independent of  $\mathbf{Z}$ , as illustrated in Figure 3.3. Given that  $\mathbf{Z} \sim \text{CMM}(p)$  and for  $m > p$ ,  $Y_t$  and  $Y_{t-m}$  are d-separated given

$$\{Y_{t-1:t-m+1}, \mathbf{Z}, W_{\leq t}, \mathbf{X}_{\leq t}\},$$

implying

$$Y_t \perp\!\!\!\perp Y_{t-m} \mid Y_{t-1:t-m+1}, \mathbf{Z}, W_{\leq t}, \mathbf{X}_{\leq t}.$$

Now, suppose  $\mathbf{Z}'$  influences the entire series of responses similarly to  $\mathbf{Z}$ . In this case,  $\mathbf{Z}'$  acts as a common

parent for both  $Y_t$  and  $Y_{t-m}$ , creating a path

$$Y_{t-m} \leftarrow \mathbf{Z}' \rightarrow Y_t$$

that cannot be blocked by conditioning on

$$\{Y_{t-1:t-m+1}, \mathbf{Z}, W_{\leq t}, \mathbf{X}_{\leq t}\}.$$

Consequently,

$$Y_t \not\perp\!\!\!\perp Y_{t-m} \mid Y_{t-1:t-m+1}, \mathbf{Z}, W_{\leq t}, \mathbf{X}_{\leq t},$$

which contradicts the implications of the conditional Markov assumption.

### 3.5.2 Definition of the probabilistic model

We define in the section the probabilistic model to learn a substitute  $\mathbf{Z}$ , building on the DVAE approach. We break down the approach into three steps, where we first deal with selection bias (Step 1), then we incorporate the inductive bias of population structure and define a GMM over the substitutes (Step 2). Finally, we define the suitable Evidence Lower Bound (ELBO) to be maximized (Step 3).

**Step 1: Handling Selection Bias** In a purely factual setting, modeling data with a DVAE involves maximizing:

$$\begin{aligned} \log p_\theta(y_{\leq T} \mid \mathbf{x}_{\leq T}, \omega_{\leq T}) &= \sum_{t=1}^T \log p_\theta(y_t \mid y_{<t}, \mathbf{x}_{\leq t}, \omega_{\leq t}) \\ &= \sum_{t=1}^T \log p_\theta(y_t \mid \mathbf{h}_t, \omega_t). \end{aligned}$$

based on the observed data distribution. However, this model cannot perform counterfactual regression—switching treatment assignment during inference to estimate counterfactual responses—nor does it allow for causal inference. This limitation arises in observational studies where treatment assignment is typically non-random and depends on observed covariates, resulting in a selection bias. We adopt the importance sampling strategy to reduce the selection bias by reweighing the likelihood of the factual model (Shimodaira, 2000). The key idea is to assign weights  $\{\alpha(\mathbf{h}_t, \omega_t)\}_{t=1}^T$  to units in the population such that the resulting distribution in a given treatment regime matches that of the entire population. Therefore, we seek to maximize the likelihood  $L$  defined as

$$L := \sum_{t=1}^T \mathbb{E}_{\mathbf{H}_t, W_t} \left[ \alpha(\mathbf{H}_t, W_t) \mathbb{E}_{Y_t \mid \mathbf{H}_t, W_t} (\log p_\theta(y_t \mid \mathbf{H}_t, W_t)) \right].$$

A more convenient formulation expresses  $L$  as an expectation over all individual-level panel series

$$\mathcal{D}_T := \{Y_{\leq T}, \mathbf{X}_{\leq T}, W_{\leq T}\} = \mathbf{H}_T \cup \{Y_T, W_T\} :$$



$$L = \sum_{t=1}^T \mathbb{E}_{\mathcal{D}_T} \left[ \alpha(\mathbf{H}_t, W_t) \log p_\theta(Y_t | \mathbf{H}_t, W_t) \right]. \quad (3.7)$$

We define a *conditional* DVAE model by specifying the conditional generative model  $p_\theta(y_{\leq T}, \mathbf{z} | \mathbf{x}_{\leq T}, \omega_{\leq T})$ , which is decomposed as follows:

$$p_\theta(y_{\leq T}, \mathbf{z} | \mathbf{x}_{\leq T}, \omega_{\leq T}) = \prod_{t=1}^T p_\theta(y_t | y_{<t}, \mathbf{x}_{\leq t}, \omega_{\leq t}, \mathbf{z}) p(\mathbf{z}).$$

**Step 2: Incorporating Population Structure** To account for an eventual population structure induced by unobserved adjustment variables, we place a Gaussian mixture prior over the latent variable  $\mathbf{Z}$ , with  $K$  components:

$$p(\mathbf{z}) = \sum_{c=1}^K \pi_c \mathcal{N}(\mathbf{z} | \mu_c, \Sigma_c). \quad (3.8)$$

This prior corresponds to first generating a cluster index  $C \sim \text{Cat}(\boldsymbol{\pi})$ , followed by  $\mathbf{Z} | C \sim \mathcal{N}(\mu_C, \Sigma_C)$ . Here,  $\boldsymbol{\pi}$  represents the probability distribution over cluster assignments, satisfying

$$\sum_{c=1}^K \pi_c = 1,$$

with  $\text{Cat}(\boldsymbol{\pi})$  denoting the categorical distribution parameterized by  $\boldsymbol{\pi}$ . Each cluster  $c$  is associated with a learnable Gaussian distribution of mean  $\mu_c$  and covariance  $\Sigma_c$ . The complete generative model becomes

$$p_\theta(y_{\leq T}, \mathbf{z}, c | \mathbf{x}_{\leq T}, \omega_{\leq T}) = \prod_{t=1}^T p_\theta(y_t | y_{<t}, \mathbf{x}_{\leq t}, \omega_{\leq t}, \mathbf{z}) p(\mathbf{z} | c) p(c). \quad (3.9)$$

We approximate the true posterior over  $(\mathbf{z}, c)$  using a factorized variational distribution

$$q_\phi(\mathbf{z}, c | \mathcal{D}_T) = q_{\phi_z}(\mathbf{z} | \mathcal{D}_T) q_{\phi_c}(c | \mathcal{D}_T), \quad (3.10)$$

where  $\phi = \phi_z \cup \phi_c$  collects the variational parameters. The following theorem characterizes the corresponding variational bound.

**Theorem Thm3.3 [Weighted ELBO Decomposition]**

Under the generative model defined by Equation 3.9 and the approximate posterior factorization of Equation 3.10, the weighted likelihood in Equation 3.7 can be decomposed as:

$$L = \mathbb{E}_{\mathcal{D}_T} [\text{ELBO}_0(\mathcal{D}_T; \theta, \phi)] + \mathbb{E}_{\mathcal{D}_T} [\Delta_0(\mathcal{D}_T; \theta, \phi)], \quad (3.11)$$

where the individual gap term  $\Delta_0$  is given by:

$$\Delta_0(\mathcal{D}_T; \theta, \phi) := \sum_{t=1}^T \alpha(\mathbf{h}_t, \omega_t) D_{KL}(q_\phi(\mathbf{z}, c | \mathcal{D}_T) \parallel p_\theta(\mathbf{z}, c | \mathcal{D}_T)), \quad (3.12)$$

and the individual ELBO termed  $\text{ELBO}_0$  is expressed as:

$$\begin{aligned} \text{ELBO}_0(\mathcal{D}_T; \theta, \phi) = & \sum_{t=1}^T \mathbb{E}_{\mathbf{z} \sim q_{\phi_z}(\cdot | \mathcal{D}_T)} [\alpha(\mathbf{h}_t, \omega_t) \log p_\theta(y_t | \mathbf{h}_t, \omega_t, \mathbf{Z})] \\ & - \left( \sum_{t=1}^T \alpha(\mathbf{h}_t, \omega_t) \right) \left\{ D_{KL}(q_{\phi_z}(\mathbf{z} | \mathcal{D}_T) \parallel p(\mathbf{z})) + \mathbb{E}_{\mathbf{z} \sim q_{\phi_z}(\cdot | \mathcal{D}_T)} D_{KL}(q_{\phi_c}(c | \mathcal{D}_T) \parallel p(c | \mathbf{Z})) \right\}. \end{aligned} \quad (3.13)$$

The individual gap  $\Delta_0$  is a positive term that quantifies the inaccuracy of the variational approximation of  $L$  using  $\text{ELBO}_0$  Equation 3.13. The ELBO term,  $\text{ELBO}_0$ , comprises three components: (1) A weighted sum of the conditional log-likelihoods of the responses (reconstruction term). (2) A Kullback–Leibler (KL) divergence between the approximate posterior of the continuous latent variables  $q_{\phi_z}(\cdot | \mathcal{D}_T)$ , which serve as substitutes for adjustment variables, and the prior  $p(\mathbf{z})$ . (3) A KL divergence between the approximate posterior of the discrete latent  $q_{\phi_c}(\cdot | \mathcal{D}_T)$  and the true conditional posterior  $p(\mathbf{C} | \mathbf{Z})$ , averaged over  $q_{\phi_z}(\cdot | \mathcal{D}_T)$ . The decoupling of these two approximate posteriors arises from the assumed factorization over the joint approximate posterior as in Equation 3.10.

### Remark Rem3.3

In a DVAE, the inference model  $q_\phi(\mathbf{z} | \mathcal{D}_T)$  approximates the true posterior  $p_\theta(\mathbf{z} | \mathcal{D}_T)$ . Although this structure is not always followed in applications (Bayer & Osendorfer, 2014; Krishnan et al., 2015; Li & Mandt, 2018; Han et al., 2021; Bai et al., 2021a), it is preferable that the approximate posterior mirrors the true one when simplified using d-separation. However, the true posterior cannot be simplified due to the data’s generation process and dynamics. For instance, omitting conditioning on the entire sequence of treatments and covariates is invalid since  $\{\mathbf{Z}\}$  and  $\{\mathbf{X}_{\leq T}, W_{\leq T}\}$  are not d-separated given  $\{Y_{\leq T}\}$ . For example, in the chain

$$W_{t-1} \rightarrow Y_t \leftarrow \mathbf{Z},$$

$Y_t$  acts as a collider and belongs to  $\{Y_{\leq T}\}$ .

**Step 3: Addressing the Discrete Latent Variable  $C$**  The approximate posterior  $q_\phi(\mathbf{z}, c | \mathcal{D}_T)$  involves both continuous and discrete latent variables,  $\mathbf{z}$  and  $c$ , respectively. Training deep generative models with discrete latent variables presents challenges due to difficulties in reparameterization and handling high cardinality, even when using classical approaches like Gumbel-Softmax (Jang et al., 2017; Tucker et al., 2017; Huijben et al., 2022). To avoid designing an additional inference network for  $q_{\phi_c}(c | \mathcal{D}_T)$  and the associated computational cost, we follow Jiang et al. (2017); Falck et al. (2021) and define a *Bayes-optimal posterior* for the discrete latent variable. Specifically, we leverage the decomposition of Equation 3.10 and choose  $q_{\phi_c}(c | \mathcal{D}_T)$  in such a way that the third term in the ELBO of Equation 3.13 is

minimized by definition:

$$\min_{q_{\phi_c}(\cdot | \mathcal{D}_T)} \mathbb{E}_{\mathbf{Z} \sim q_{\phi_z}(\cdot | \mathcal{D}_T)} D_{KL}(q_{\phi_c}(c | \mathcal{D}_T) \parallel p(c | \mathbf{Z})). \quad (3.14)$$

The minimal value of this optimization problem is

$$\min_{q_{\phi_c}(\cdot | \mathcal{D}_T)} \mathbb{E}_{\mathbf{Z} \sim q_{\phi_z}(\cdot | \mathcal{D}_T)} D_{KL}(q_{\phi_c}(\cdot | \mathcal{D}_T) \parallel p(\cdot | \mathbf{Z})) = -\log \text{Const}(q_{\phi_z}(\cdot | \mathcal{D}_T)), \quad (3.15)$$

where  $\text{Const}(q_{\phi_z}(\cdot | \mathcal{D}_T))$  is a constant that depends only on the approximate posterior over the continuous latents:

$$\text{Const}(q_{\phi_z}(\cdot | \mathcal{D}_T)) = \sum_{c=1}^K \exp(\mathbb{E}_{\mathbf{Z} \sim q_{\phi_z}(\cdot | \mathcal{D}_T)} \log p(c | \mathbf{Z})).$$

The minimizer is given by:

$$\pi(c | q_{\phi_z}(\cdot | \mathcal{D}_T)) = \frac{\exp(\mathbb{E}_{\mathbf{Z} \sim q_{\phi_z}(\cdot | \mathcal{D}_T)} \log p(c | \mathbf{Z}))}{\text{Const}(q_{\phi_z}(\cdot | \mathcal{D}_T))}. \quad (3.16)$$

Moreover, the minimal value is:

$$\min_{q_{\phi_c}(\cdot | \mathcal{D}_T)} \mathbb{E}_{\mathbf{Z} \sim q_{\phi_z}(\cdot | \mathcal{D}_T)} D_{KL}(q_{\phi_c}(\cdot | \mathcal{D}_T) \parallel p(c | \mathbf{Z})) = -\log Z(q_{\phi_z}(\cdot | \mathcal{D}_T)). \quad (3.17)$$

Thus, we update the original  $\text{ELBO}_0$  in Equation 3.13 to obtain a *modified* ELBO by replacing  $q_{\phi_c}(\cdot | \mathcal{D}_T)$  with the minimizer  $\pi(c | q_{\phi_z}(\cdot | \mathcal{D}_T))$  and plugging in the minimal value from Equation 3.17:

$$\begin{aligned} \text{ELBO}(\mathcal{D}_T; \theta, \phi) &= \sum_{t=1}^T \mathbb{E}_{\mathbf{Z} \sim q_{\phi_z}(\cdot | \mathcal{D}_T)} [\alpha(\mathbf{h}_t, \omega_t) \log p_\theta(y_t | \mathbf{H}_t, W_t, \mathbf{Z})] \\ &\quad - \left[ \sum_{t=1}^T \alpha(\mathbf{h}_t, \omega_t) \right] \{D_{KL}(q_{\phi_z}(\cdot | \mathcal{D}_T) \parallel p(\mathbf{z})) - \log Z(q_{\phi_z}(\cdot | \mathcal{D}_T))\}. \end{aligned} \quad (3.18)$$

As a result, the modified ELBO is computationally more efficient than the original one, as it bypasses the need for applying a reparameterization trick to discrete latent variables and eliminates the necessity of training over specific parameters  $\phi_c$ , all while remaining a valid lower bound for the weighted likelihood  $L$ . This validity holds since Theorem Thm3.3 applies to any arbitrary approximate posterior  $q_{\phi_c}(\cdot | \mathcal{D}_T)$ , and in particular, to  $\pi(c | q_{\phi_z}(\cdot | \mathcal{D}_T))$ , which is the minimizer of Equation 3.14. We henceforth use  $\phi$  to denote  $\phi_z$ .

### 3.5.3 CDVAE in the near deterministic regime

In this section, we explore the behavior of Causal DVAE in the *near-deterministic regime*, where the variance of the generative model approaches zero. We examine how this regime affects inference and causal identifiability, demonstrating that it leads to a non-diffuse posterior suitable for treatment effect estimation.

**Model Setup** For the remainder of our discussion, we define the DVAE model parameters as  $\mathcal{M}_{vae} = \{\theta, \phi\}$  and assume the approximate posterior to be Gaussian  $q_\phi(\mathbf{z} \mid \mathcal{D}_T) \sim \mathcal{N}(\mathbf{z} \mid \mu_{\mathbf{z}}, \Sigma_{\mathbf{z}})$ , where the mean is defined as  $\mu_{\mathbf{z}} = f_{\mu_{\mathbf{z}}}(\mathcal{D}_T; \phi)$ , and the covariance matrix is given by  $\Sigma_{\mathbf{z}} = S_{\mathbf{z}} S_{\mathbf{z}}^\top$ , with  $S_{\mathbf{z}} = f_{S_{\mathbf{z}}}(\mathcal{D}_T; \phi)$ . Moreover, we assume the conditional generative model to be Gaussian such that:

$$p_\theta(y_t \mid y_{<t}, \mathbf{x}_{\leq t}, \omega_{\leq t}, \mathbf{z}) = \mathcal{N}(f_t(\mathbf{h}_t, \omega_t, \mathbf{z}; \theta), \sigma^2), \quad (3.19)$$

with  $\sigma > 0$ , a spatially and temporally uniform scale parameter.

**Motivation** In probabilistic modeling, our inference model for the substitute adjustment variable is *stochastic*. However, to calculate ITE for each individual, we need to choose a unique instance of the latent variable representation. Otherwise, infinite ITE could be generated by sampling repeatedly from  $q_{\phi_z}(\cdot \mid \mathcal{D}_T)$ . A natural choice for this deterministic representation is the *mean* of the posterior. Yet, because we sample from the approximate posterior during training rather than using the mean, it is essential to prevent the posterior from becoming *overly diffuse* (i.e. it has high variance with no sharp peak)—ensuring that the mean remains valid during causal inference. Previous studies (Dai & Wipf, 2019; Takida et al., 2022) show that operating in the *near-deterministic regime* of the VAE decoder—where  $\sigma \rightarrow 0^+$ —leads the encoder’s covariance matrix toward zero, resulting in near-deterministic behavior. We, therefore, explore the near-deterministic regime in our Causal DVAE by controlling the decoder’s variance to induce a non-diffuse, stable posterior distribution suitable for causal inference in the latent space.

**Side Benefit: Preventing Posterior Collapse** A well-known challenge in training VAEs is *posterior collapse*, where the approximate posterior converges to the uninformative prior, making the latent space irrelevant (Bowman et al., 2015; Sønderby et al., 2016; Higgins et al., 2017; Dai & Wipf, 2019; Fu et al., 2019; Lucas et al., 2019; Wang et al., 2021b; Takida et al., 2022). A notable advantage of the near-deterministic regime is its ability to *avoid posterior collapse* within the latent space, a benefit demonstrated in *static VAEs* (Lucas et al., 2019; Takida et al., 2022). Specifically, Takida et al. (2022) showed that the decoder’s output variance and covariance could influence the latent space by causing over-smoothing by affecting the gradient regularization strength, which in turn leads to posterior collapse. By controlling variance in the near-deterministic regime, we mitigate this collapse and preserve meaningful latent representations.

We advance the study of *dynamic* VAE models by investigating their behavior in the near-deterministic regime within the context of causal inference. This work is the first to explore dynamic VAEs in this regime for causal applications, addressing a gap in the literature, as such behavior has yet to be thoroughly examined, even in non-causal, factual settings.

We prove that in our framework, replacing the original lower bound  $\text{ELBO}_0(\mathcal{D}_T; \theta, \phi)$  with the modified  $\text{ELBO}(\mathcal{D}_T; \theta, \phi)$  still ensures the existence of a parameterization under which the approximate likelihood of responses converges to the true likelihood. Specifically, Theorem Thm3.4 demonstrates that, for a sequence of inference and generative models parameterized by  $\sigma$ , the gap between the modified and true importance-weighted likelihoods asymptotically approaches zero.

**Theorem Thm3.4 [Asymptotic Likelihood Recovery]**

Suppose  $d_{\mathbf{z}} \leq T$ . There exists a family of autoencoders  $\{\phi_\sigma, \theta_\sigma\}_{\sigma>0}$  such that

$$\lim_{\sigma \rightarrow 0^+} p_{\theta_\sigma}(y_{\leq T} \mid \mathbf{x}_{\leq T}, \omega_{\leq T}) = p(y_{\leq T} \mid \mathbf{x}_{\leq T}, \omega_{\leq T}),$$

and when operating under the Bayes-optimal posterior over the discrete latent, i.e.,

$$q_\phi(c \mid \mathcal{D}_T) = \pi(c \mid q_\phi(\cdot \mid \mathcal{D}_T)),$$

the gap  $\Delta(\mathcal{D}_T; \theta_\sigma, \phi_\sigma)$  between the modified ELBO (Equation 3.18) and the true weighted likelihood  $L$  (Equation (3.7)) satisfies

$$\Delta(\mathcal{D}_T; \theta_\sigma, \phi_\sigma) = \text{ELBO}(\mathcal{D}_T; \theta_\sigma, \phi_\sigma) - L(\mathcal{D}_T; \theta_\sigma),$$

and converges to zero:

$$\lim_{\sigma \rightarrow 0^+} \Delta(\mathcal{D}_T; \theta_\sigma, \phi_\sigma) = 0.$$

This result generalizes prior findings for static VAEs (Dai & Wipf, 2019) to the more complex dynamic setting with GMM priors and weighted objectives. It also addresses an oversight in Dai & Wipf (2019) regarding the proof of gap convergence.

More importantly, we establish a critical property in our setting within the near-deterministic regime: the causal effect remains asymptotically consistent whether one uses an arbitrary realization of the latent variable  $\mathbf{z}$  or the posterior mean  $\mu_{\mathbf{z}}$ . Theorem Thm3.5 formalizes this insight as follows:

**Theorem Thm3.5 [Realization-Invariant Causal Consistency]**

For a fixed  $\sigma > 0$ , let a parametrization of Causal DVAE  $\mathcal{M}_{vae}^*(\sigma) = \{\theta_\sigma^*, \phi_\sigma^*\}$  be an optimal solution to the ELBO defined in Equation 3.18. Then, for any substitute realization  $\mathbf{z} \in \mathbb{R}^{d_z}$ , the conditional expected outcome satisfies the following consistency in the near-deterministic regime:

$$\lim_{\sigma \rightarrow 0^+} \mathbb{E}_{\mathcal{M}_{vae}^*(\sigma)} [Y_t \mid \mathbf{H}_t, W_t = \omega, \mathbf{Z} = \mathbf{z}] = \lim_{\sigma \rightarrow 0^+} \mathbb{E}_{\mathcal{M}_{vae}^*(\sigma)} [Y_t \mid \mathbf{H}_t, W_t = \omega, \mathbf{Z} = \mu_{\mathbf{z}}]. \quad (3.20)$$

As a result of Corollary Cor3.1, the Augmented CATE satisfies the same consistency in the near-deterministic regime:

$$\lim_{\sigma \rightarrow 0^+} \tau_{\mathcal{M}_{vae}^*(\sigma)}(\mathbf{H}_t, \mathbf{z}) = \lim_{\sigma \rightarrow 0^+} \tau_{\mathcal{M}_{vae}^*(\sigma)}(\mathbf{H}_t, \mu_{\mathbf{z}}). \quad (3.21)$$

Theorem Thm3.5 demonstrates that as the variance parameter  $\sigma$  of the generative model approaches zero, both the expected outcome and the estimated causal effect remain consistent, regardless of whether one relies on an arbitrary realization of the latent variable  $\mathbf{z}$  or its posterior mean  $\mu_{\mathbf{z}}$ . Such consistency

ensures that, in the near-deterministic regime, the causal effect is robust to the specific realization of the latent variable.

### 3.6 Generalization Bound over Treatment Effect Estimation and Derivation of Model Loss

We establish in this section a theoretical generalization bound for the error in estimating ACATE, which serves as a foundation for deriving the training loss of CDVAE. We begin by defining a suitable representation function to address the high dimensionality of the history  $\mathbf{H}_t$ . Next, we introduce a weighted risk minimization framework that ensures a covariates' balance between treatment groups. We then derive a generalization bound for treatment effect estimation, relating the error in estimating ACATE to the model's weighted risk. Finally, we construct the CDVAE training objective by integrating these theoretical insights into a structured loss function.

**Step 1: Representation Learning** In causal inference with high-dimensional covariates, increasing the number of covariates makes it challenging to satisfy the overlap assumption, as ensuring that all units have a non-zero probability of receiving each treatment becomes harder. This "curse of dimensionality" leads to greater imbalance between treated and control groups. While including more covariates can reduce bias from unobserved confounders, it may increase bias due to poor overlap, compromising the reliability of causal effect estimations. Additionally, high-dimensional models make causal effect estimation more prone to increased variance (Ning et al., 2020; D'Amour et al., 2021). To address these challenges and given the high-dimensional nature of the context history  $\mathbf{H}_t$ , we introduce a representation function  $\Phi$  that reduces dimensionality while retaining essential information in a latent space, allowing causal inference in a lower-dimensional setting, mitigating issues associated with high dimensionality.

We assume  $\Phi$  is invertible to prevent information loss in the latent space. In fact, if we formulate our sequential ignorability assumptions over the original space, then there is no guarantee the same assumptions should hold in the representation space for any general function  $\Phi$ . It is possible to lose information related to confounders after the transformation  $\Phi$ , so ignorability cannot hold anymore. As a result, the treatment effect becomes unidentifiable. To this end, we need to ensure identifiability assumptions over the latent space, namely sequential ignorability and overlap, i.e.:

$$Y_t(\omega) \perp\!\!\!\perp W_t | \Phi(\mathbf{H}_t), \quad p(W_t = \omega | \Phi(\mathbf{h}_t)) > 0, \quad \forall(\omega, \mathbf{h}_t).$$

#### Remark Rem3.4

Following Eq. (3.19), the generative model for the responses is defined as  $Y_t = f_t(\mathbf{H}_t, W_t, \mathbf{Z}) + \epsilon_t$ , where  $\epsilon_t \sim \mathcal{N}(0, \sigma^2)$  is the error term. A common modeling (Johansson et al., 2016; Shalit et al.,

2017; Shi et al., 2019; Johansson et al., 2022) approach for  $f_t$  is to assume

$$f_t(\mathbf{H}_t, W_t, \mathbf{Z}) := W_t f_{t,1}(\mathbf{H}_t, \mathbf{Z}) + (1 - W_t) f_{t,0}(\mathbf{H}_t, \mathbf{Z}),$$

where  $f_{t,0}$  and  $f_{t,1}$  denote the mappings to the response under each treatment regime  $W_t \in \{0, 1\}$ .

The representation function  $\Phi$  over  $\{\mathbf{H}_t\}_{t=1}^T$  produces lower-dimensional vectors  $\{\mathbf{r}_t\}_{t=1}^T$ , living in a space  $\mathcal{R} \subset \mathbb{R}^r$ . Instead of defining time-dependent generative functions  $f_t$ , we define a single hypothesis function

$$f : \mathcal{R} \times \mathcal{W} \times \mathbb{R}^{d_z} \rightarrow \mathcal{Y},$$

such that:

$$Y_t = f(\Phi(\mathbf{H}_t), W_t, \mathbf{Z}) + \epsilon_t = W_t f_1(\Phi(\mathbf{H}_t), \mathbf{Z}) + (1 - W_t) f_0(\Phi(\mathbf{H}_t), \mathbf{Z}) + \epsilon_t.$$

By assuming the invertibility of  $\Phi$ , we can show that such conditions hold in the latent space if they hold in the original space. We summarize the result in the following proposition:

**Proposition Prop3.1**

Let  $\Phi$  be a representation function according to Remark Rem3.4. then  $Y_t(\omega) \perp\!\!\!\perp W_t | \Phi(\mathbf{H}_t)$  holds if and only if  $Y_t(\omega) \perp\!\!\!\perp W_t | \mathbf{H}_t$ . Moreover,  $p(W_t = \omega | \Phi(\mathbf{h}_t)) > 0$  holds if and only if  $p(W_t = \omega | \mathbf{h}_t) > 0$ .

In practice and for the remainder of the work, the outcome and propensity models share the same representation  $\Phi(\mathbf{H}_t)$ , encouraging it to capture information predictive of both treatment and response. While invertibility is theoretically assumed to maintain identifiability, implementation does not enforce it. Instead, the focus is on ensuring that  $\Phi(\mathbf{H}_t)$  is predictive across treatment regimes, with regularization used to balance  $\Phi(\mathbf{H}_t)$  across the two treatment regimes  $W_t \in \{0, 1\}$  using the Wasserstein distance (Gretton et al., 2012), similar to Shalit et al. (2017); Lim (2018a); Bica et al. (2020a); Assaad et al. (2021); Melnychuk et al. (2022); Johansson et al. (2022).

**Step 2: Weighted Risk Minimization** To integrate causal inference into the DVAE framework, we employ weighted risk minimization techniques (Kallus, 2020; Johansson et al., 2022). First, we justify the choice of weights  $\alpha(\mathbf{H}_t, W_t)$  used in the definition of the weighted ELBO in Section 3.5.2. In general, these weights can be any arbitrary mapping

$$\alpha : \mathbf{H}_t \times \mathcal{W} \rightarrow \mathbb{R}^+$$

such that

$$\mathbb{E}_{\mathbf{H}_t | W_t = \omega} [\alpha(\mathbf{H}_t, \omega)] = 1 \quad \text{for all } \omega \in \mathcal{W},$$

meaning the weights  $\alpha(\mathbf{h}_t, \omega)$  induce a weighted probability *target distribution*  $g$  over the population such that

$$g(\mathbf{h}_t \mid W_t = \omega) := \alpha(\mathbf{h}_t, \omega) p(\mathbf{h}_t \mid W_t = \omega).$$

Intuitively, the weights either *stretch* or *shrink* each observed unit so that learning occurs on a *new synthetic population* whose covariates follow the distribution  $g$ . Choosing an appropriate weighting strategy  $\alpha(\mathbf{h}_t, \omega)$  is crucial for achieving covariate balance between treatment groups, i.e.,

$$g(\mathbf{h}_t \mid W_t = 1) = g(\mathbf{h}_t \mid W_t = 0).$$

We use *overlap weights* Li et al. (2018a); Assaad et al. (2021), defined as

$$\alpha(\mathbf{h}_t, \omega) \propto \frac{e(\Phi(\mathbf{h}_t)) (1 - e(\Phi(\mathbf{h}_t)))}{\omega e(\Phi(\mathbf{h}_t)) + (1 - \omega) (1 - e(\Phi(\mathbf{h}_t)))},$$

where  $e(\Phi(\mathbf{h}_t)) = p(W_t = 1 \mid \Phi(\mathbf{h}_t))$  is the propensity score in the representation space.

Overlap weights emphasize units with propensity scores near 0.5, focusing on regions where treated and control groups overlap most, which enhances comparability and improves covariate balance. This approach reduces variance by down-weighting units with extreme propensity scores, mitigating instability from excessively large weights, and leading to more reliable and efficient causal effect estimates (Li et al., 2018a).

We now define the *weighted population risk* for a given treatment regime  $W_t = \omega$ : we measure the expected risk for a given  $(f, \Phi)$  at time  $t$  over the weighted population distributed according to  $g$ , as:

$$R_{t,g}^\omega(f, \Phi) := \mathbb{E}_{\mathbf{H}_t \mid W_t} [\alpha(\mathbf{H}_t, W_t) \ell_{f,\Phi}(\mathbf{H}_t, W_t) \mid W_t = \omega],$$

where  $\ell_{f,\Phi}(\mathbf{h}_t, \omega)$  is the expected pointwise loss which averages prediction error over the encoder’s posterior and potential outcomes:

$$\ell_{f,\Phi}(\mathbf{h}_t, \omega) := \mathbb{E}_{\mathbf{Z} \sim q_\phi(\mathbf{Z} \mid \mathcal{D}_{\leq t-1})} \mathbb{E}_{Y_t(\omega) \mid \mathbf{H}_t, \mathbf{Z}} [L(Y_t(\omega), f(\Phi(\mathbf{H}_t), \mathbf{Z}, W_t)) \mid \mathbf{H}_t = \mathbf{h}_t, \mathbf{Z}]. \quad (3.22)$$

In the definition of the expected pointwise loss, we respect the temporal order by conditioning the approximate posterior of the continuous latents only on the longitudinal data up to time step  $t$ . In line with our probabilistic modeling in Section 3.5.2 and the distributional assumptions in Section 3.5.3, we define the loss as the negative log-likelihood:

$$L(Y_t(\omega), f(\Phi(\mathbf{H}_t), \mathbf{Z}, W_t)) = -\log \mathcal{N}(Y_t(\omega); f(\Phi(\mathbf{H}_t), \mathbf{Z}, W_t), \sigma^2).$$

**Step 3: Generalization Bound** Our aim during training is to minimize the factual quantities  $\{R_{t,g}^\omega(f, \Phi)\}_{t=1}^T$  to reduce the error in estimating treatment effects. To formalize and theoretically justify this objective, we establish a generalization bound for the PEHE (Hill, 2011), which accounts for our



weighted population risks  $\{R_{t,g}^\omega(f, \Phi)\}_{t=1}^T$ . PEHE measures the mean squared error (MSE) between the true and estimated ACATE at time  $t$  as <sup>1</sup>

$$\epsilon_{\text{PEHE}_t} = \mathbb{E}_{\mathbf{H}_t} \mathbb{E}_{\mathbf{Z} \sim q_\phi(\mathbf{Z} | \mathcal{D}_{\leq t-1})} \left[ (\tau(\mathbf{H}_t, \mathbf{Z}) - \hat{\tau}_{f, \Phi}(\mathbf{H}_t, \mathbf{Z}))^2 \right].$$

where  $\tau(\mathbf{H}_t, \mathbf{Z})$  is the true ITE and  $\hat{\tau}_{f, \Phi}(\mathbf{H}_t, \mathbf{Z})$  is the estimated ITE using hypothesis  $f$  and representation  $\Phi$ , as defined in the outcome model in Remark Rem3.4.

Similarly, we define the weighted PEHE with respect to the target distribution  $g$ :

$$\epsilon_{\text{PEHE}_{t,g}} = \mathbb{E}_{\mathbf{H}_t \sim g} \mathbb{E}_{\mathbf{Z} \sim q_\phi(\mathbf{Z} | \mathcal{D}_{\leq t-1})} \left[ (\tau(\mathbf{H}_t, \mathbf{Z}) - \hat{\tau}_{f, \Phi}(\mathbf{H}_t, \mathbf{Z}))^2 \right].$$

We provide an upper bound for the weighted PEHE for CDVAE similar to Assaad et al. (2021). This bound consists of three key components: the weighted factual prediction error, a term capturing the discrepancy between treatment and control distributions in the confounders representation space, and a term that accounts for the variance of the generative model over responses.

**Theorem Thm3.6 [Generalization Bound for Weighted PEHE]**

Let  $\mathcal{M}_{\text{VAE}}(\sigma) = \{\theta_\sigma, \phi_\sigma\}$  be the VAE model defined in Section 3.5.2. For a given class of functions  $G$ , assume there exists a constant  $B_\Phi$  such that  $\ell_{f, \Phi}/B_\Phi \in G$ . Assume the representation  $\Phi$  is invertible. Then, the error in estimating the treatment effect at time  $t$  for a weighted population is upper bounded by

$$\begin{aligned} \epsilon_{\text{PEHE}_{t,g}} \leq & 2\sigma^2 \left\{ R_{t,g}^{\omega=1}(f, \Phi) + R_{t,g}^{\omega=0}(f, \Phi) \right. \\ & \left. + B_\Phi \text{IPM}_G(g_\Phi(\cdot | W_t = 1), g_\Phi(\cdot | W_t = 0)) - \log(2\pi\sigma^2) \right\}, \end{aligned} \quad (3.23)$$

where  $g_\Phi(r)$  is the distribution induced by  $\Phi$  in the representation space  $\mathcal{R}$ . The Integral Probability Metric (IPM) (Müller, 1997; Sriperumbudur et al., 2009) measures the dissimilarity between distributions.

Assuming strict overlap in treatment assignment, where  $\delta \in (0, 0.5)$  such that  $\delta < e(\mathbf{h}_t) < 1 - \delta$ , then there exists constants  $A_{t,g}, B_{t,g}$  such that the unweighted PEHE  $\epsilon_{\text{PEHE}_t}$  is bounded:

$$A_{t,g} \cdot \epsilon_{\text{PEHE}_{t,g}}(\hat{\tau}) \leq \epsilon_{\text{PEHE}_t}(\hat{\tau}) \leq B_{t,g} \cdot \epsilon_{\text{PEHE}_{t,g}}(\hat{\tau}).$$

The representation discrepancy in 3.23 quantifies the distributional imbalance between treatment groups, measured using IPMs like the Wasserstein distance or Maximum Mean Discrepancy (Gretton et al., 2012). The connection between  $\epsilon_{\text{PEHE}_t}$  and  $\epsilon_{\text{PEHE}_{t,g}}$  indicates that minimizing the weighted PEHE can also minimize  $\epsilon_{\text{PEHE}_t}$ , thereby enhancing the reliability of ITE estimation across the original population.

To justify the pertinence of our probabilistic model defined in Section 3.5.2, we show in the following

<sup>1</sup>Note that  $p_\theta(\mathbf{H}_t, \mathbf{Z}) = p(\mathbf{Z} | \mathcal{D}_{\leq t-1}) p(\mathbf{H}_t)$  because  $\mathbf{X}_t$  is d-separated from  $\mathbf{Z}$  given  $\mathcal{D}_{\leq t-1} = [Y_{\leq t-1}, \mathbf{X}_{\leq t-1}, W_{\leq t-1}]$ .

how maximizing the likelihood term in the ELBO of Equation 3.18 implies minimization of the risks  $R_{t,g}^{\omega=1}(f, \Phi)$  and  $R_{t,g}^{\omega=0}(f, \Phi)$ .

**Proposition Prop3.2 [ELBO–Risk Connection]**

Assume stationarity of the approximated posterior of  $\mathbf{Z}$  given sub-longitudinal data; that is, there exists  $t_0$  such that for all  $t \geq t_0$ ,

$$q_\phi(\mathbf{Z} \mid \mathcal{D}_t) \approx q_\phi(\mathbf{Z} \mid \mathcal{D}_T).$$

Given a finite sample batch

$$\mathcal{B} = \{\mathcal{D}_{iT} = \{W_{it}, Y_{it}, \mathbf{X}_{it}\}_{t=1}^T : i = 1, \dots, |\mathcal{B}|\},$$

we have the following approximation:

$$\begin{aligned} & \sum_{t=t_0}^T \mathbb{E}_{\mathbf{Z} \sim q_\phi(\cdot \mid \mathcal{D}_T)} \left[ \alpha(\mathbf{H}_t, W_t) \log p_\theta(Y_t \mid \mathbf{H}_t, W_t, \mathbf{Z}) \right] \\ & \approx -\frac{1}{|\mathcal{B}|} \sum_{t=t_0}^T \left\{ n_1^{(t)} R_{t,g}^{\omega=1}(f, \Phi) + n_0^{(t)} R_{t,g}^{\omega=0}(f, \Phi) \right\}, \end{aligned} \tag{3.24}$$

with

$$R_{t,g}^\omega(f, \Phi) \approx -\frac{1}{n_\omega^{(t)}} \sum_{\substack{i \in \mathcal{B} \\ W_{it} = \omega}} \mathbb{E}_{\mathbf{Z} \sim q_\phi(\mathbf{Z} \mid \mathcal{D}_{iT})} \left[ \alpha(\mathbf{H}_{it}, \omega) \log p_\theta(Y_{it} \mid \mathbf{H}_{it}, \omega, \mathbf{Z}) \right],$$

where  $n_\omega^{(t)}$  represents the number of instances in the batch  $\mathcal{B}$  for which  $W_{it} = \omega$ .

As a result, maximizing the ELBO in Equation 3.18 not only maximizes the weighted conditional likelihood over responses (the "reconstruction term") but also, as shown in Equation 3.24, minimizes the weighted population risk. This, in turn, decreases the generalization bound in Theorem Thm3.6, reducing the error in treatment effect estimation. To further reduce this error, we include the IPM term from Theorem Thm3.6, regularizing the ELBO of Equation 3.18 with the IPM term at each time step:

$$\mathcal{L}_{\text{IPM}}(\theta_\omega, \Phi) := \sum_{t=1}^T \text{IPM}_G(g_{\theta_\omega, \Phi}(\cdot \mid W_t = 1), g_{\theta_\omega, \Phi}(\cdot \mid W_t = 0)).$$

where  $\theta_\omega$  are the parameters of the propensity score model  $e_{\theta_\omega}(\Phi(\cdot))$ .

**Intuition: Stationarity of the inferred latent variables** We further justify the core assumption made in Proposition Prop3.2. The representation learning for the adjustment variables is achieved by approximating the posterior  $p_\theta(\mathbf{z} \mid \mathcal{D}_T)$  with  $q_\phi(\mathbf{z} \mid \mathcal{D}_T)$ . Here, the missing baseline covariates are inferred by analyzing *all longitudinal data*  $\{y_{\leq T}, \mathbf{x}_{\leq T}, \omega_{\leq T}\}$ . However, since these covariates are *static* and *pre-response* variables, we should, ideally, be able to infer the exact substitute from a shorter longitudinal dataset  $\{y_{\leq T'}, \mathbf{x}_{\leq T'}, \omega_{\leq T'}\}$  where  $T' < T$ , or from any temporal slice  $\{y_{t_1:t_2}, \mathbf{x}_{t_1:t_2}, \omega_{t_1:t_2}\}$  with  $t_2 > t_1$ . Thus, ensuring a form of stationarity in our posterior approximation is crucial.

To understand the importance of this property, consider estimating the ATE for longitudinal data at time  $t$ :

$$\tau_t := \mathbb{E}(Y_t(1) - Y_t(0)) = \mathbb{E}_{\mathbf{Z}, \mathbf{H}_t} \left[ \mathbb{E}_{Y_t \mid \mathbf{Z}, \mathbf{H}_t, W_t} (Y_t \mid \mathbf{Z}, \mathbf{H}_t, W_t = 1) - \mathbb{E}_{Y_t \mid \mathbf{Z}, \mathbf{H}_t, W_t} (Y_t \mid \mathbf{Z}, \mathbf{H}_t, W_t = 0) \right].$$

To compute  $\tau_t$ , we need to marginalize the conditional response over the joint distribution of covariates and latent adjustment variables,  $p(\mathbf{h}_t, \mathbf{z}) = p(\mathbf{z} \mid \mathcal{D}_{\leq t}) p(\mathbf{h}_t)$ . Because we model  $p_\theta(\mathbf{z} \mid \mathcal{D}_T)$ , which depends on the *entire* history, there is, in general, no guarantee that

$$p(\mathbf{z} \mid \mathbf{h}_t) \approx p_\theta(\mathbf{z} \mid \mathcal{D}_T).$$

As a consequence of the stationarity assumption in Proposition Prop3.2, we introduce a penalty term in the form of the Wasserstein distance between consecutive posterior distributions  $q_\phi(\mathbf{z} \mid \mathcal{D}_t)$  and  $q_\phi(\mathbf{z} \mid \mathcal{D}_{t-1})$ , penalizing significant variations as the data history grows. To preserve the model’s capacity to capture time-varying dependencies, we begin regularization from  $t_0 \gg 0$ , typically  $t_0 = \frac{T}{2}$ :

$$\mathcal{L}_{\text{DistM}}(\phi) := \sum_{t=t_0}^T \mathbb{E}_{\mathcal{D}_t} W(q_\phi(\mathbf{z} \mid \mathcal{D}_t), q_\phi(\mathbf{z} \mid \mathcal{D}_{t-1})).$$

Assuming a Gaussian approximate posterior, the Wasserstein distance simplifies to

$$\mathcal{L}_{\text{DistM}}(\phi) = \sum_{t=t_0}^T \mathbb{E}_{\mathcal{D}_t} \|\mu_{\mathbf{z}}(\mathcal{D}_t) - \mu_{\mathbf{z}}(\mathcal{D}_{t-1})\|_2^2 + \mathbb{E}_{\mathcal{D}_t} \|S_{\mathbf{z}}(\mathcal{D}_t) - S_{\mathbf{z}}(\mathcal{D}_{t-1})\|_F^2,$$

where the penalty regularizes the first and second moments of the posterior distribution as the data history grows.

**Step 4: Total Loss Function and Training Strategy** The overall loss for the CDVAE model combines the ELBO from Equation 3.18 with two additional terms:  $\mathcal{L}_{\text{IPM}}$ , which reduces covariate imbalance at each time step and addresses residual imbalance not corrected by weighting, and  $\mathcal{L}_{\text{DistM}}$ , which captures the global, static nature of adjustment variables. To push the Causal DVAE toward a near-deterministic regime, we treat the variance parameter  $\sigma$  as learnable and fit it using the following loss function:

$$\mathcal{L}_{\text{tot}}(\theta, \theta_\omega, \phi, \Phi, \sigma) = -\text{ELBO}(\theta, \phi, \Phi, \sigma) + \lambda_{\text{IPM}} \mathcal{L}_{\text{IPM}}(\theta_\omega, \Phi) + \lambda_{\text{DistM}} \mathcal{L}_{\text{DistM}}(\phi). \quad (3.25)$$

Since the loss  $\mathcal{L}_{\text{tot}}$  depends on the treatment parameters  $\theta_\omega$ , as the weighted ELBO is also a function of the propensity scores, we introduce an additional loss function  $\mathcal{L}_W$ , a binary cross-entropy loss to predict treatment from confounders representation. To optimize CDVAE, we adopt an adversarial training strategy, simultaneously minimizing  $\mathcal{L}_{\text{tot}}$  with respect to  $\theta, \phi, \Phi$ , and  $\sigma$ , while minimizing  $\mathcal{L}_W$  with respect to  $\theta_\omega$  (c.f. Algorithm 4):

$$\begin{cases} \min_{\theta, \phi, \Phi, \sigma} \mathcal{L}_{\text{tot}}(\theta, \theta_\omega, \phi, \Phi, \sigma), \\ \min_{\theta_\omega} \mathcal{L}_W(\theta_\omega, \Phi). \end{cases}$$

The adversarial nature of the training arises because, in one optimization step, we learn the representation  $\Phi$  to predict the response while applying an IPM regularization to ensure balance between the weighted covariates. In the subsequent optimization step, for a fixed representation, we train the treatment classifier to predict the treatment. We use the Wasserstein distance as a specific case of IPM, with details on its computation provided in Algorithm 3.

**CDVAE: Model Specification and Architecture** We use a three-head neural network architecture for CDVAE to learn a shared representation between outcome and treatment models inspired by Shi et al. (2019). This architecture consists of two prediction heads for potential outcomes and one for treatment (Appendix A.5). We use a Gated Recurrent Unit (GRU) (Cho et al., 2014) to learn a representation  $\Phi(\mathbf{h}_{t+1})$  of the context history. The input of the outcome model  $f_{\theta_y}$  is the shared representation  $\Phi(\mathbf{h}_{t+1})$  and a sampled substitute  $\mathbf{z}$  from  $q_\phi(\mathbf{z} \mid \mathcal{D}_T)$ . The outcome model  $f_{\theta_y}$  is represented by two non-linear functions  $f_{\theta_y^1}$  and  $f_{\theta_y^0}$  for treatment assignments 1 and 0, respectively. The third head is a binary classifier  $f_{\theta_\omega}$  estimating the propensity score. The inference model (encoder)  $q_\phi(\mathbf{z} \mid y_{\leq T}, \mathbf{x}_{\leq T}, \omega_{\leq T})$  is modeled by an GRU, producing a hidden state that represents the sequence. Two non-linear mappings,  $\mu_{\phi_2}$  and  $\Sigma_{\phi_3}$ , learn the mean and diagonal covariance matrix in the latent space.

### 3.7 Experiments

**Baselines** In all our experiments, we compare CDVAE against the relevant baselines: RMSM, CRN, G-Net, CT, and Causal CPC. Each baseline is evaluated in three different configurations: 1. The "base approach," where models are trained using only static and time-varying confounders. 2. The "substitute approach," where models are augmented with substitutes for the unobserved adjustment variables, obtained from CDVAE and represented by the mean of the approximated posterior. 3. The "oracle approach," where models are trained with the true adjustment variables.

### 3.8 Algorithmic Details

In this section, we provide the algorithmic details for CDVAE. First, we describe the approximation of the IPM term used in Equation 3.25. The IPM term aims to reduce covariate imbalance between the treatment and control groups by quantifying the dissimilarity between their distributions. To calculate the IPM, we use the Sinkhorn-Knopp algorithm (Sinkhorn, 1967) and the Wasserstein distance computation algorithm (Algorithm 3 in Cuturi & Doucet (2014)). The Wasserstein distance computation (Algorithm 3) calculates the pairwise distances between data points and constructs a kernel matrix using a regularization parameter. It then computes the row and column marginals based on the weights assigned to each data point. The Sinkhorn-Knopp algorithm (Algorithm 2), integrated within the Wasserstein distance computation, is used to compute the optimal transport matrix. Finally, the Wasserstein distance is obtained by summing the products of the optimal transport matrix and the pairwise distances. Computing the Wasserstein distance at each time step and for every batch is computationally expensive. To accelerate training, we compute it for a subsample of the time indices, sampled randomly at each batch. Empirically, this approach is sufficient for maintaining model performance. Specifically, we sample 10% of the time indices at each batch, corresponding to  $m = \lfloor \frac{T}{10} \rfloor$  time steps, as shown in Algorithm 4.

---

#### Algorithm 2 Sinkhorn-Knopp Algorithm

---

**Require:** Kernel matrix  $K \in \mathbb{R}^{n_t \times n_c}$

**Require:** Row marginal vector  $a \in \mathbb{R}^{n_t}$ , Column marginal vector  $b \in \mathbb{R}^{n_c}$

**Ensure:** Optimal transport matrix  $T \in \mathbb{R}^{n_t \times n_c}$

- 1: Initialize transport matrix  $T^{(0)}$  with all entries set to 1
  - 2: Set iteration counter  $k \leftarrow 0$
  - 3: **while** not converged **do**
  - 4:   Update row scaling vector  $u \in \mathbb{R}^{n_t}$
  - 5:    $u_i \leftarrow \frac{a_i}{\sum_{j=1}^{n_c} K_{ij} T_{ij}^{(k)}}$
  - 6:   Update column scaling vector  $v \in \mathbb{R}^{n_c}$
  - 7:    $v_j \leftarrow \frac{b_j}{\sum_{i=1}^{n_t} K_{ij} T_{ij}^{(k)}}$
  - 8:   Update transport matrix  $T^{(k+1)}$
  - 9:    $T_{ij}^{(k+1)} \leftarrow \frac{u_i K_{ij} v_j}{\sum_{i'=1}^{n_t} \sum_{j'=1}^{n_c} u_{i'} K_{i'j'} v_{j'}}$
  - 10:   Increment iteration counter  $k \leftarrow k + 1$
  - 11:   **if** convergence criterion met **then**
  - 12:     **Return**  $T^{(k+1)}$
  - 13:   **end if**
  - 14: **end while**
- 

### 3.9 Models hyperparameters

**Hyperparameter Selection** All models are fine-tuned using a grid search over hyperparameters, including architecture and optimizer settings. Model selection is based on the mean squared error (MSE) of factual outcomes on a validation set, which is also used as the criterion for early stopping. More details are in Appendix A.4. We use PyTorch (Paszke et al., 2019) and PyTorch Lightning (Falcon & team, 2019) to implement CDVAE and all baselines. For hyperparameter selection, we fine-tune models using a random grid search. CDVAE is optimized using the weighted reconstruction error as the selection

---

**Algorithm 3** Weighted Wasserstein Distance Computation

---

**Require:** Batch  $\mathcal{B} = \{\{\omega_{it}, y_{it}, \mathbf{x}_{it}\}_{t=1}^T, i = 1, \dots, |\mathcal{B}|\}$

**Require:** Representation learner  $\Phi$

**Require:** Weights vectors  $\alpha_\Phi(\mathbf{h}_t, \omega)$

**Require:** Regularization parameter  $\lambda$

```
1: for  $t \in \{1, 2, \dots, T\}$  do
2:   Compute  $n_t^{(t)} \leftarrow \sum_{i \in \mathcal{B}} W_{it}$ ,  $n_c^{(t)} \leftarrow \sum_{i \in \mathcal{B}} (1 - W_{it})$ 
3:   Compute pairwise distances matrix  $M \in \mathbb{R}^{n_t^{(t)} \times n_c^{(t)}}$   $\{M_{ij}^{(t)} = \|\mathbf{H}_{it} - \mathbf{H}_{jt}\|_{L_2}, \forall i, j \in \mathcal{B}; W_{it} = 1 \text{ and } W_{jt} = 0\}$ 
4:   Initialize kernel matrix  $K \in \mathbb{R}^{n_t^{(t)} \times n_c^{(t)}}$  such that  $K_{ij}^{(t)} \leftarrow e^{-\lambda M_{ij}^{(t)}}$ 
5:   Compute row marginal vector  $a^{(t)} \in \mathbb{R}^{n_t}$  such that  $a_i^{(t)} \leftarrow \frac{\alpha_\Phi(\mathbf{h}_{it}, 1)}{\sum_{k=1, W_{kt}=1} \alpha_\Phi(\mathbf{h}_{it}, 1)}$ 
6:   Compute column marginal vector  $b^{(t)} \in \mathbb{R}^{n_c}$  such that  $b_j^{(t)} \leftarrow \frac{\alpha_\Phi(\mathbf{h}_{it}, 0)}{\sum_{k=1, W_{kt}=0} \alpha_\Phi(\mathbf{h}_{it}, 0)}$ 
7:   Compute optimal transport matrix  $T^{(t)} \in \mathbb{R}^{n_t^{(t)} \times n_c^{(t)}}$ :
8:      $T^{(t)} \leftarrow \text{Sinkhorn-Knopp}(K^{(t)}, a^{(t)}, b^{(t)})$ 
9:   Compute Wasserstein distance  $D_t \leftarrow \sum_{i=1}^{n_t} \sum_{j=1}^{n_c} T_{ij}^{(t)} M_{ij}^{(t)}$ 
10: end for
11: Return  $\sum_{t=1}^T D_t$ 
```

---

---

**Algorithm 4** Pseudo-code for training CDVAE

---

**Require:** Training Data  $\mathcal{D}_T = \{\{w_{it}, y_{it}, \mathbf{x}_{it}\}_{t=1}^T, i = 1, \dots, n\}$

**Require:** CDVAE parameters  $\phi, \theta_y, \theta_\omega, \Phi, \sigma$ , Optimizer parameters

```
1: for  $p \in \{1, \dots, \text{epoch}_{\max}\}$  do
2:   for batch  $\mathcal{B} = \{\{w_{it}, y_{it}, \mathbf{x}_{it}\}_{t=1}^T, i = 1, \dots, |\mathcal{B}|\}$  do
3:     Compute approximate posterior  $q_\phi(z \mid y_{\leq T}, \mathbf{x}_{\leq T}, \omega_{\leq T})$ 
4:     Sample latent variables  $z$  from  $q_\phi(z \mid y_{\leq T}, \mathbf{x}_{\leq T}, \omega_{\leq T})$ 
5:     Compute representation  $\Phi(\mathbf{H}_t)$  for  $t = 1, \dots, T$ .
6:     Compute ELBO( $\theta, \phi, \Phi, \sigma$ ).
7:     Compute  $\mathcal{L}_{\text{DistM}}(\phi)$ .
8:     Choose  $t_1, \dots, t_m \sim \mathcal{U}([1, T])$  compute IPM term as :
```

$$\mathcal{L}_{\text{IPM}} = \sum_{i=1}^m \text{IPM}_G(g_{\theta_\omega, \Phi}(\cdot \mid W_{t_i} = 1), g_{\theta_\omega, \Phi}(\cdot \mid W_{t_i} = 0))$$

```
9:   Compute total loss  $\mathcal{L}_{\text{tot}} = \text{ELBO}(\theta, \phi, \Phi, \sigma) + \lambda_{\text{IPM}} \mathcal{L}_{\text{IPM}}(\theta_\omega, \Phi) + \lambda_{\text{DistM}} \mathcal{L}_{\text{DistM}}(\phi)$ .
10:   Update parameters related to the total loss
```

$$[\theta, \phi, \Phi, \sigma] \leftarrow [\theta, \phi, \Phi, \sigma] - \mu \left( \frac{\partial \mathcal{L}_{\text{tot}}(\theta, \theta_\omega, \phi, \Phi, \sigma)}{\partial [\theta, \phi, \Phi, \sigma]} \right)$$

```
11:   Compute binary cross-entropy loss for the propensity network  $\mathcal{L}_W(\theta_\omega, \Phi)$ . and update parameters
```

$$\theta_\omega \leftarrow \theta_\omega - \mu_W \left( \frac{\partial \mathcal{L}_W(\theta_\omega, \Phi)}{\partial \theta_\omega} \right)$$

```
12:   end for
```

```
13: end for
```

```
14: Return Trained CDVAE model
```

---

criterion. We do not use a metric related to the quality of estimating ITE, as this would not be applicable in real-world scenarios where ITE are unavailable. Designing a suitable criterion for causal cross-validation or hyperparameter tuning in causal models remains an open problem. Various proxies are used in the literature, including loss over factual outcomes (Lim, 2018a; Hassanpour & Greiner, 2019a; Bica et al., 2020a;b), one nearest-neighbor imputation for counterfactual outcomes (Shalit et al., 2017; Johansson et al., 2022), influence functions (Alaa & Van Der Schaar, 2019), rank-preserving causal cross-validation (Schuler et al., 2018), and Robinson residual decomposition (Nie & Wager, 2021; Lu et al., 2020). Since we aim to select the best regularization parameters ( $\lambda_{IPM}$ ,  $\lambda_{MM}$ ) along with other CDVAE-related parameters, we avoid using total loss as it may bias ( $\lambda_{IPM}$ ,  $\lambda_{MM}$ ) toward small values. Instead, we use the weighted reconstruction error for fine-tuning. Similarly, Causal CPC, CT, CRN, and RMSM are fine-tuned using loss over the factual response. We report in Appendix A.4 the search space of hyperparameters for all baselines.

### 3.9.1 Adapting Baselines to Our Causal Settings

All the considered baselines do not assume the observation of adjustment variables; however, they only consider time-varying and static confounders. It is not straightforward to incorporate adjustment variables into these models when observed. Naively augmenting their input with adjustment variables and treating them as static confounders often results in suboptimal performance or even worse outcomes compared to excluding the adjustment variables altogether. This is primarily due to two reasons: 1. Most baselines concatenate static confounders with time-varying ones at each time step. When high-dimensional adjustment variables are included, this dramatically increases the number of parameters, leading to overfitting. 2. When comparing different versions of the same baseline, it is important to ensure comparable complexity represented by the number of learnable parameters (Table 3.1). 3. Models such as CRN, CT, and Causal CPC learn a balanced representation. Including adjustment variables naively as input may bias the learned representation towards these variables, as they are inherently balanced.

To ensure fair experimentation, we adapt the baselines as follows:

- **CRN, CT, and Causal CPC:** Instead of solely feeding the balanced representation to the outcome network, we augment it with static adjustment variables, similar to the CDVAE design, where the representation  $\Phi(\mathbf{H}_t)$  is augmented with substitutes  $\mathbf{Z}$ .
- **G-Net:** Adjustment variables are only used to augment the representation fed to the outcome model, not the representation used to reconstruct the current covariates  $\mathbf{X}_t$ .
- **RMSM:** Stabilized weights are learned solely as a function of  $\mathbf{H}_t$ , while the adjustment variables are concatenated with the representation of  $\mathbf{H}_t$ .

### 3.9.2 Synthetic Data Sets

**Generation** We simulate a longitudinal dataset of time-length  $T = 75$  by generating the time-varying variables autoregressively. Specifically, the confounders  $\mathbf{X}_t$  at each time step  $t$  are generated in  $\mathbb{R}^{d_x}$  with

Table 3.1: Trainable parameters in thousands (k) for baselines in all configurations for the synthetic and semi-synthetic MIMIC-III data.

Model	Params (k), synthetic data	Params (k), MIMIC-III data
CDVAE	11.5	5.7
Causal CPC (base)	6.7	5.3
Causal CPC (with substitute)	7.1	5.7
Causal CPC (oracle)	14.3	7.5
CT (base)	18.7	16.3
CT (with substitute)	18.9	16.7
CT (oracle)	26	18.7
G-Net (base)	21.2	4.1
G-Net (with substitute)	21.5	4.3
G-Net (oracle)	28.5	5.7
CRN (base)	8.3	3.5
CRN (with substitute)	8.5	3.7
CRN (oracle)	14.2	4.9
RMSM (base)	14	6.7
RMSM (with substitute)	15.3	6.9
RMSM (oracle)	20.9	8.0

$d_x = 100$ , and the dynamics are specified through an autoregression of order  $p = 8$  plus a regression over the past treatment trajectory. Each dimension  $j \in \{1, \dots, d_x\}$  of  $\mathbf{X}_t$  is defined as

$$\mathbf{X}_t^{(j)} = \frac{1}{p} \sum_{k=1}^p \gamma_k^{X,(t,j)} \mathbf{X}_{t-k}^{(j)} + \frac{1}{p} \sum_{k=1}^p \gamma_k^{XW,(t,j)} W_{t-k} + \epsilon_{t,j}^X,$$

with

$$\gamma_k^{X,(t,j)} \sim \mathcal{N}(0, 1), \quad \gamma_k^{XW,(t,j)} \sim \mathcal{N}(0, 1), \quad \epsilon_t^X := [\epsilon_{t,1}^X, \dots, \epsilon_{t,d_x}^X]^\top \sim \mathcal{N}(0, \Sigma_x).$$

To ensure dependence between confounders, the vector error  $\epsilon_t^X$  is generated by a Gaussian distribution with a non-diagonal covariance matrix

$$\Sigma_x = \rho \mathbf{1}_{d_x} \mathbf{1}_{d_x}^\top + (1 - \rho) \sigma^2 I_{d_x},$$

where  $\rho = 0.5$  and  $\sigma^2 = 0.3$ .

The treatment  $\omega_t$  is generated using a Bernoulli distribution with probability  $\sigma(\pi_t)$  defined by a logistic model to simulate the assignment mechanism. Here,  $\sigma(\cdot)$  denotes the sigmoid function:

$$\pi_t = \frac{1}{p} \sum_{k=1}^p \gamma_k^{W,t} W_{t-k} + \frac{1}{d_x p} \sum_{k=1}^p \langle \gamma_k^{WX,t}, \mathbf{X}_{t-k} \rangle + \frac{1}{p} \sum_{k=1}^p \gamma_k^{WY,t} Y_{t-k} + \epsilon_W.$$

To ensure the variation of imbalance between treatment and control groups through time, we simulate the regression parameters as follows:

$$\begin{aligned} \gamma_k^{W,t}, \gamma_k^{WY,t} &\sim \mathcal{N}(\sin(t/\pi), 0.01^2), \\ \gamma_k^{WX,t} &\sim \mathcal{N}(\sin(t/\pi), 0.01^2)^{\otimes d_x}, \\ \epsilon_W &\sim \mathcal{N}(0, 0.01^2). \end{aligned}$$



We generate treatment assignment as

$$W_t \sim \text{Bernoulli}(\sigma(\pi_t)).$$

To specify the outcome model, we first generate the unobserved adjustment variables  $\mathbf{U} \in \mathbb{R}^{d_u}$  with  $d_u = 100$  using a Gaussian mixture of three distributions:

$$\mathbf{U} \sim \frac{1}{K} \sum_{i=1}^K \mathcal{N}(\mu_i, \Sigma_u),$$

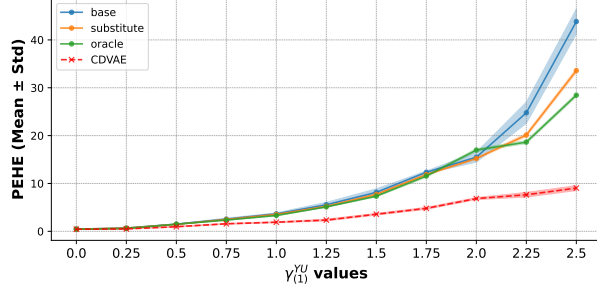
where  $\mu_1, \dots, \mu_K \sim \mathcal{U}([-10, 10])^{\otimes d_u}$ ,  $\Sigma_u = 0.2 \text{diag}(\mathbf{1}_{d_u})$ , and  $K = 8$ . Finally, we write the expression of the two potential outcomes as a function of the context history. The chosen specification is motivated by the classic mixed-effect approach. We introduce the random effects to have an individual reaction to the change in a covariate  $\mathbf{X}_{t,j}$ , and we model it by the Hadamard product between the covariate vector and the unobserved adjustment vector. The observed response is defined following the consistency assumption Asm2.6:

$$\begin{aligned} Y_t &= Y_t(1)W_t + Y_t(0)(1 - W_t) \\ Y_t(\omega) &= \frac{1}{d_U} \langle \gamma_\omega^{YU}, \mathbf{U} \rangle \sum_{k=1}^p W_{t-k} + \frac{1}{d_X p} \sum_{k=1}^p \langle \gamma_{k,\omega}^{YX,t}, \mathbf{X}_{t-k} \rangle + \frac{1}{p} \sum_{k=1}^p \gamma_{k,\omega}^{Y,t} Y_{t-k} + \epsilon_Y \\ \gamma_{k,\omega}^{YX,t} &\sim \mathcal{N}(\gamma_\omega^{YX}, 0.01^2), \quad \gamma_\omega^{YU} \sim \mathcal{N}(\gamma_\omega^{YU}, 0.01^2), \\ \gamma_{k,\omega}^{Y,t} &\sim \mathcal{N}(\gamma_\omega^Y, 0.1^2), \quad \epsilon_Y \sim \mathcal{N}(0, 0.01^2). \end{aligned}$$

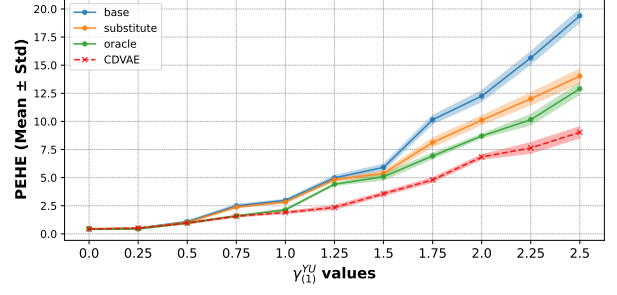
With  $\gamma_1^{YX}, \gamma_1^Y = 0.0, 0.2$  and  $\gamma_0^{YX}, \gamma_0^Y = 0.2, 0.1$  and  $\gamma_0^{YU} = 0.1$  while  $\gamma_1^{YU}$  is varied generate multiple datasets with different modifications levels of treatment effect induced by  $\mathbf{U}$ . The experiment is conducted with 5000 samples for training, 500 for validation, and 1000 for testing.

**Controlling the Effect of Unobserved Adjustment Variables** To assess the impact of unobserved variables  $\mathbf{U}$ , we vary the parameter  $\gamma_{(1)}^{YU}$  which determines the contribution of  $\mathbf{U}$  in generating  $Y_t(1)$ . By design,  $Y_t(1)$  increases with  $\gamma_{(1)}^{YU}$ , and the parameter  $\gamma_{(1)}^{YX}$  is varied within the range  $[0, 2.5]$  with a step size of 0.25, and we generate a longitudinal dataset at each level of  $\gamma_{(1)}^{YX}$ . We report the mean and standard deviation over 10 different seeds of PEHE in estimating the one-step-ahead ACATE, i.e.,  $\epsilon_{\text{PEHE}_{T+1}}$ , over the test individuals (smaller is better).

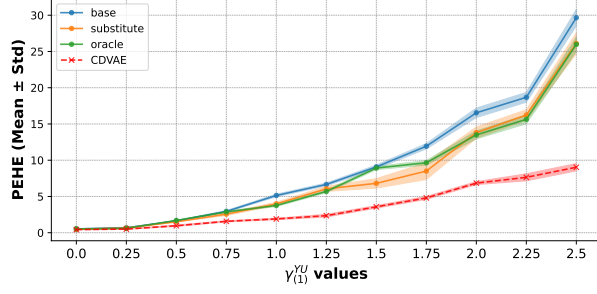
**Results** The Figure 3.4 shows the performances of all models given the three possible configurations (base, substitute and oracle). First, the error in estimating the ACATE increases substantially as the coefficient  $\gamma_{(1)}^{YU}$  increases because the contribution of the unobserved static variables becomes considerably more important in the writing of the potential outcomes. However, CDVAE notably displays a slower increase in error and superior performance in all data configurations. Second, the errors decrease across all levels of unobserved heterogeneity when the baselines are provided with the substitutes learned features by CDVAE, highlighting the superiority of the substitute approach assisted by CDVAE over the base one.



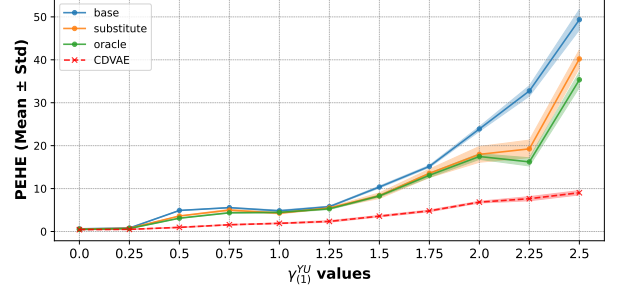
(a) Performance of Causal Transformer with CDVAE Comparison



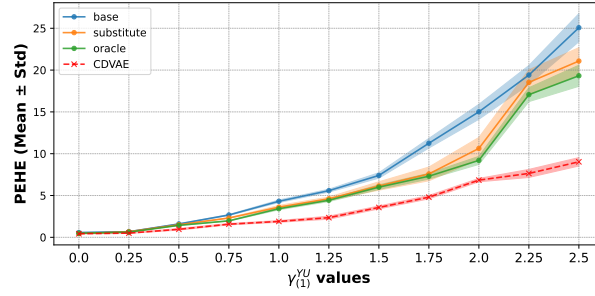
(b) Performance of Causal CPC with CDVAE Comparison



(c) Performance of CRN with CDVAE Comparison



(d) Performance of G-Net with CDVAE Comparison



(e) Performance of RMSN with CDVAE Comparison

Figure 3.4: Evolution of PEHE in estimating ACATE for synthetic data across increasing levels of heterogeneity induced by adjustment variables  $\mathbf{U}$ .

As expected, a baseline in the oracle approach generally performs better than with substitutes, especially at higher values of  $\gamma_{(1)}^{YU}$ , while the substitute approach provides near-oracle performance. Extended results are provided in Appendix A.2.1.

### 3.9.3 Semi-Synthetic MIMIC-III Data

We adapt to our setting a semi-synthetic dataset constructed by Melnychuk et al. (2022) based on the MIMIC-III dataset (Johnson et al., 2016). The covariates are high-dimensional and include several vital measurements recorded in intensive care units. We investigate the effect of vasopressor treatments on blood pressure in patients. The static covariates in the dataset (gender, ethnicity, and age) are included in the data construction as adjustment variables for the response (blood pressure). We conduct our experiments with 1400 patients for training, 200 patients for validation, and 400 patients for testing.

A cohort of 2,000 patients is extracted from the MIMIC-III dataset, with the simulation setup proposed by Melnychuk et al. (2022) extending the model introduced in Schulam & Saria (2017). Let  $d_y$  denote

the dimension of the outcome variable. For multiple outcomes, untreated outcomes, denoted as  $\mathbf{Z}_t^{j,(i)}$  for  $j = 1, \dots, d_y$ , are generated for each patient  $i$  in the cohort. The generation process is defined as:

$$\mathbf{Z}_t^{j,(i)} = \underbrace{\alpha_S^j \mathbf{B}\text{-spline}(t)}_{\text{endogenous}} + \underbrace{\alpha_g^j g^{j,(i)}(t)}_{\text{exogenous}} + \underbrace{\alpha_f^j f_Z^j(\mathbf{X}_t^{(i)})}_{\text{exogenous}} + \underbrace{\varepsilon_t}_{\text{noise}}, \quad (3.26)$$

where the B-spline  $\mathbf{B}\text{-spline}(t)$  models the endogenous component,  $g^{j,(i)}(\cdot)$  is sampled independently for each patient from a Gaussian process with a Matérn kernel, and  $f_Z^j(\cdot)$  is sampled from a Random Fourier Features (RFF) approximation of a Gaussian process.

To introduce confounding into the assignment mechanism, current time-varying covariates are incorporated via a random function  $f_Y^l(\mathbf{X}_t)$  and the average of a subset of the previous  $T_l$  treated outcomes,  $\bar{A}_{T_l}(\bar{\mathbf{Y}}_{t-1})$ . For  $d_a$  binary treatments  $\mathbf{A}_t^l$ , where  $l = 1, \dots, d_a$ , the treatment assignment mechanism is modeled as:

$$p_{\mathbf{A}_t^l} = \sigma(\gamma_A^l \bar{A}_{T_l}(\bar{\mathbf{Y}}_{t-1}) + \gamma_X^l f_Y^l(\mathbf{X}_t) + b_l),$$

$$\mathbf{A}_t^l \sim \text{Bernoulli}(p_{\mathbf{A}_t^l}),$$

where  $\sigma(\cdot)$  denotes the sigmoid function.

Static features  $\mathbf{U}$ , such as gender and ethnicity, which are categorical, are one-hot encoded. A random Singular Value Decomposition (SVD) transformation  $f_E(\cdot)$  is then applied to  $\mathbf{U}$ , retaining all singular components. Subsequently, treatments are applied to the untreated outcomes using the following expression:

$$E^j(t) = \sum_{i=t-w^l}^t \frac{\min_{l=1,\dots,d_a} \mathbb{I}[\mathbf{A}_i^l=1] p_{\mathbf{A}_i^l} \beta_{lj} + \left| \sum_{k=1}^{d_U} f_E(U)_k \right|}{(w^l - i)^2}, \quad (3.27)$$

where  $w^l$  is the treatment window.

The final outcome combines the treatment effect and the untreated simulated outcome:

$$Y_t^j = Z_t^j + E^j(t). \quad (3.28)$$

Similar to the synthetic data experiment, we evaluate all baselines using three approaches (base, with substitutes, and oracle), and report the PEHE in estimating the one-step-ahead ACATE for a patient trajectory.

**Results** Figure 3.5 reports the mean and standard deviation of PEHE for CDVAE and all baselines across all configurations. Similar to the synthetic data results, the base approach always performs worse than the substitute and oracle approaches. However, the substitute approach substantially enhances performance compared to the base approach, highlighting the relevance of the substitutes learned by CDVAE. Across all configurations, CDVAE achieves the best performance compared to all baselines. Extended results are provided in Appendix A.3.1.

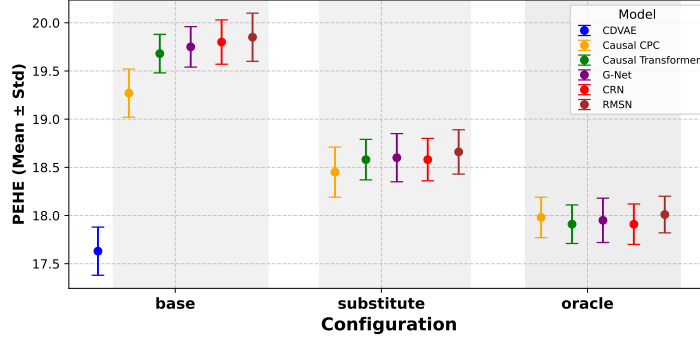


Figure 3.5: Results on the MIMIC-III data reported by PEHE and organized following the three possible configurations. Smaller is better.

Table 3.2: CDVAE ablation study conducted on the semi-synthetic MIMIC-III data reported by PEHE. Smaller is better.

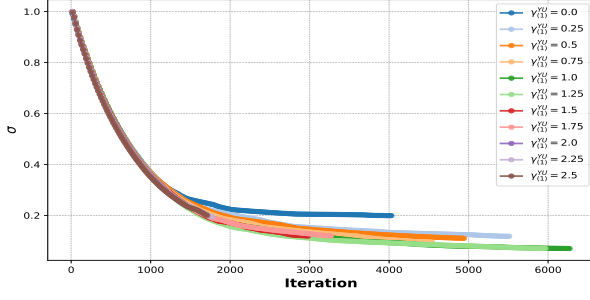
Model	PEHE
<b>CDVAE (ours)</b>	<b>17.63±0.25</b>
CDVAE ( $\lambda_{\text{IPM}} = 0$ )	18.38±0.26
CDVAE ( $\lambda_{\text{DistM}} = 0$ )	18.21±0.26
CDVAE ( $\sigma = 1$ )	20.50±1.04
CDVAE ( $\lambda_{\text{IPM}} = 0, \lambda_{\text{DistM}} = 0$ )	18.45±0.23
CDVAE ( $\lambda_{\text{IPM}} = 0$ , w/o weighting)	18.97±0.28
CDVAE ( $\lambda_{\text{IPM}} = 0, \lambda_{\text{DistM}} = 0$ , w/o weighting)	19.23±0.28

### 3.10 Discussion

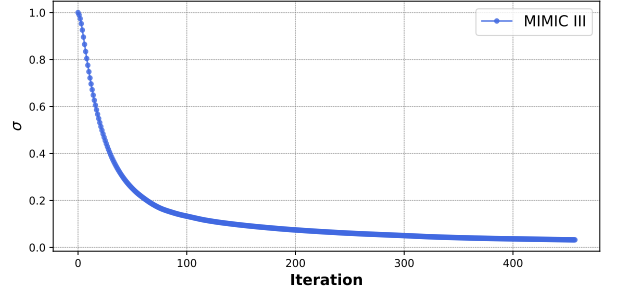
**Ablation Study** To experimentally validate the design of CDVAE, we perform an ablation study by exploring several model configurations: the full CDVAE model with all components; CDVAE without the IPM term ( $\lambda_{\text{IPM}} = 0$ ); CDVAE without the distribution matching term ( $\lambda_{\text{DistM}} = 0$ ); CDVAE without both the IPM term and distribution matching term ( $\lambda_{\text{IPM}} = 0, \lambda_{\text{DistM}} = 0$ ); CDVAE without the IPM term and weighting ( $\lambda_{\text{IPM}} = 0$ , w/o weighting); CDVAE ( $\lambda_{\text{IPM}} = 0, \lambda_{\text{DistM}} = 0$ , w/o weighting); and CDVAE with a fixed variance parameter ( $\sigma = 1$ ). We follow the same experimental protocol as in prior experiments, conducting the ablation for the synthetic dataset across all heterogeneity levels induced by  $\gamma_{(1)}^{YU}$  and for the semi-synthetic MIMIC-III dataset. Across all configurations, the full CDVAE consistently outperforms the other models. Furthermore, removing individual components results in progressively higher errors, as shown in Tables 3.3 and 3.2. Interestingly, the configurations ( $\lambda_{\text{IPM}} = 0, \lambda_{\text{DistM}} = 0$ , without weighting) and ( $\sigma = 1$ ) either perform comparably to or worse than the second-best model, Causal CPC, on both the synthetic dataset and the MIMIC-III dataset.

Table 3.3: Results on the synthetic data reported by PEHE. Smaller is better.

Model	$\gamma_{(1)}^{YU} = 0$	$\gamma_{(1)}^{YU} = 0.25$	$\gamma_{(1)}^{YU} = 0.5$	$\gamma_{(1)}^{YU} = 0.75$	$\gamma_{(1)}^{YU} = 1$	$\gamma_{(1)}^{YU} = 1.25$	$\gamma_{(1)}^{YU} = 1.5$	$\gamma_{(1)}^{YU} = 1.75$	$\gamma_{(1)}^{YU} = 2$	$\gamma_{(1)}^{YU} = 2.25$	$\gamma_{(1)}^{YU} = 2.5$
<b>CDVAE (ours)</b>	<b>0.43±0.02</b>	<b>0.50±0.03</b>	<b>0.96±0.09</b>	<b>1.57±0.08</b>	<b>1.90±0.10</b>	<b>2.35±0.18</b>	<b>3.57±0.17</b>	<b>4.80±0.20</b>	<b>6.84±0.20</b>	<b>7.64±0.48</b>	<b>9.03±0.50</b>
CDVAE ( $\lambda_{\text{IPM}} = 0$ )	0.48±0.02	0.57±0.03	1.12±0.01	1.80±0.15	2.23±0.12	2.53±0.15	3.88±0.13	5.23±0.11	7.37±0.21	7.95±0.12	9.32±0.36
CDVAE ( $\lambda_{\text{DistM}} = 0$ )	0.46±0.02	0.57±0.03	1.10±0.02	1.78±0.13	2.18±0.13	2.64±0.18	3.95±0.15	5.20±0.12	7.14±0.13	8.08±0.14	9.25±0.19
CDVAE ( $\sigma = 1$ )	0.81±0.40	0.66±0.07	2.17±0.53	5.73±1.51	9.27±3.27	10.67±2.02	12.66±2.16	14.28±4.23	15.63±4.04	18.23±5.71	17.19±5.71
CDVAE ( $\lambda_{\text{IPM}} = 0, \lambda_{\text{DistM}} = 0$ )	0.48±0.02	0.57±0.03	1.16±0.07	1.84±0.17	2.33±0.12	2.66±0.14	4.05±0.10	5.36±0.13	7.48±0.12	8.20±0.13	9.40±0.24
CDVAE ( $\lambda_{\text{IPM}} = 0$ , w/o weighting)	0.50±0.01	0.60±0.01	1.20±0.03	1.90±0.11	2.31±0.10	2.66±0.13	3.99±0.16	5.30±0.19	7.51±0.12	8.21±0.15	9.41±0.23
CDVAE ( $\lambda_{\text{IPM}} = 0, \lambda_{\text{DistM}} = 0$ , w/o weighting)	0.50±0.02	0.62±0.02	1.27±0.03	1.98±0.10	2.39±0.09	2.85±0.14	4.19±0.13	5.59±0.13	7.61±0.15	8.41±0.14	9.78±0.21



(a) Synthetic data.

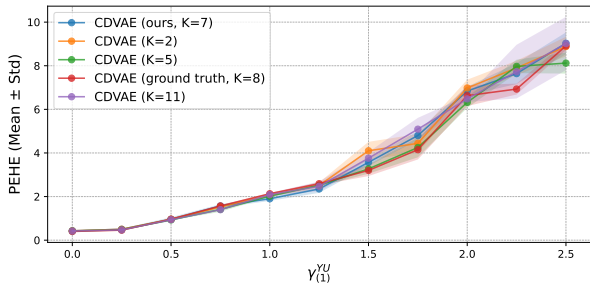


(b) MIMIC-III.

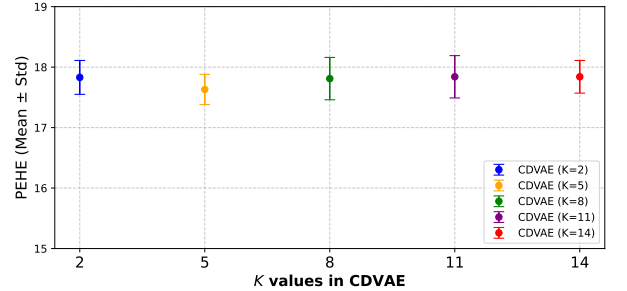
Figure 3.6: Evolution of variance parameter update during training for synthetic data (left) for each level of  $\gamma_{(1)}^{YU}$  and MIMIC-III (right) averaged over 10 random initializations

**On the Near-Deterministic Behavior of CDVAE** For the theoretical results in Section 3.5.3 to hold, it is necessary to verify whether the variance parameter  $\sigma$ , as a learnable parameter, indeed decreases toward zero during training. In all experiments,  $\sigma$  is initialized at one, and we show in Figure 3.6a its behavior during training on the synthetic dataset across all levels of  $\gamma_{(1)}^{YU}$ , as well as on the MIMIC-III dataset in Figure 3.6b. In all cases, the variance parameter stably decreases toward zero, validating the near-deterministic regime at the end of training. This supports the consistency result related to the treatment effect established in Theorem Thm3.5.

**CDVAE Robustness to the Number of Components in the Prior** We demonstrate that the number of components  $K$  in the Gaussian mixture prior does not substantially affect the PEHE. The chosen value, selected via random search, is  $K = 7$ , while the ground truth is  $K = 8$ . To test robustness, we evaluate CDVAE with values below and above this baseline, namely  $K = 2, 5, 8, 11$ . For the semi-synthetic MIMIC-III dataset, the true number of components is unknown, and the value selected via grid search is  $K = 5$ . To test robustness, we also evaluate  $K = 2, 8, 11, 14$ . Figure 3.7a shows the evolution of errors for the synthetic data across levels of  $\gamma_{(1)}^{YU}$  for different values of  $K$ . While there are slight differences in performance means for CDVAE with varying  $K$ , almost all error bars overlap across all levels of  $\gamma_{(1)}^{YU}$ . The same observations hold for MIMIC-III, as depicted in Figure 3.7b. This highlights the robustness of CDVAE to the choice of  $K$  for the prior and its low sensitivity compared to the components analyzed in the ablation study.



(a) Synthetic data.



(b) MIMIC data.

Figure 3.7: Results of CDVAE when varying the number of components  $K$  of the prior for the synthetic data (left) and MIMIC-III (right) reported by PEHE. Smaller is better.

**Bayesian Model Assessment of CDVAE** We assess the quality of the conditional response fitting in our variational framework through a posterior predictive check (Rubin, 1984; Meng, 1994; Gelman et al., 1995) and similar to Bica et al. (2020b); Hatt & Feuerriegel (2024). For each time step  $t$ , let  $\mathbf{y}_t^{\text{obs}} := \{y_{i,t}\}_{i=1}^{N_{\text{val}}}$  represent the observed responses in the validation dataset. We generate  $S$  replicated datasets of responses  $\mathbf{y}_t^{\text{rep}}(s) := \{y_{i,t}^{\text{rep}}(s)\}_{i=1}^{N_{\text{val}}}$  for  $s = 1, \dots, S$ , such that for each individual  $i$  in the validation dataset, we draw  $S$  samples of latent substitutes  $\mathbf{z}_i(1), \dots, \mathbf{z}_i(S) \sim q_\phi(\cdot \mid \mathcal{D})$ . The approximate posterior serves as a proxy for the true (inaccessible) posterior  $p(\mathbf{z} \mid \mathcal{D})$ . Replicated responses are then generated from the fitted conditional distribution:  $Y_t^{\text{rep}}(s) \sim Y_t \mid y_{<t}, \mathbf{x}_{\leq t}, \omega_{\leq t}, \mathbf{z}_i(s)$ .

To compare the observed and replicated data, we define a statistic  $\mathbb{T}$  based on the conditional log-likelihood:

$$\mathbb{T}(\mathbf{y}_t^{\text{obs}}) := \frac{1}{N_{\text{val}}} \sum_{i=1}^{N_{\text{val}}} \log p_\theta(y_{i,t} \mid \mathbf{h}_{i,t}, \omega_{i,t}, \mathbf{z}_i(s)),$$

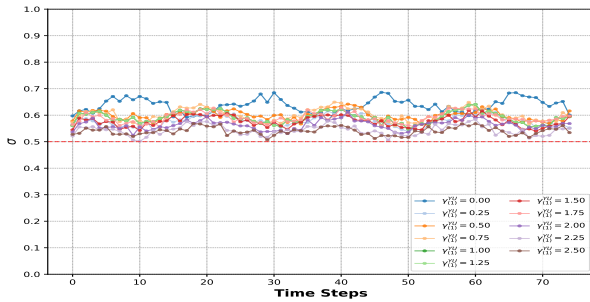
and for replicated responses:  $\mathbb{T}(\mathbf{y}_t^{\text{rep}}(s)) := \frac{1}{N_{\text{val}}} \sum_{i=1}^{N_{\text{val}}} \log p_\theta(y_{i,t}^{\text{rep}}(s) \mid \mathbf{h}_{i,t}, \omega_{i,t}, \mathbf{z}_i(s))$ . We then define a posterior predictive p-value as:

$$p = \Pr(\mathbb{T}(\mathbf{y}_t^{\text{rep}}(s)) > \mathbb{T}(\mathbf{y}_t^{\text{obs}})),$$

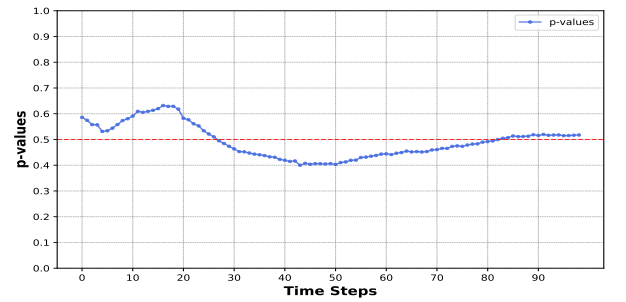
which is approximated as:

$$p \approx \frac{1}{S} \sum_{s=1}^S \mathbb{1}\{\mathbb{T}(\mathbf{y}_t^{\text{rep}}(s)) > \mathbb{T}(\mathbf{y}_t^{\text{obs}})\}.$$

We compare these p-values over time to assess how closely the distribution of the conditional responses matches the distribution of the replicated responses. If the model accurately captures the conditional response distribution given the substitutes, the test statistics for the replicated data should be close to those for the observed data, ideally resulting in a p-value equal to 0.5. Figures 3.8a and 3.8b show the temporal evolution of the p-values for both the synthetic data and semi-synthetic MIMIC-III. In general, all the p-values fluctuate inside the interval  $[0.41, 0.59]$  except for the synthetic dataset with  $\gamma_{(1)}^{YU} = 0.0$  because  $\mathbf{U}$  no longer modifies the potential outcomes  $(Y_t(1))_{t \geq 1}$ . Interestingly, the bias in the p-values (Figure 3.8a) decreases as  $\gamma_{(1)}^{YU}$  increases because CDVAE is designed to capture substantial heterogeneity in the responses due to the unobserved adjustment variables.



(a) Synthetic data



(b) MIMIC-III

Figure 3.8: Evolution of CDVAE posterior predictive p-values for synthetic (left) and semi-synthetic MIMIC-III data (right). We report the average for 10 random initializations at each time step.

**Connection to the Deconfounder Theory** Our approach can also provide a remedy for a key inconsistency in the deconfounder theory (Lopez & Gutman, 2017; Ranganath & Perotte, 2018; Wang & Blei, 2019a;b). Crucially, while the inference model for the latent confounder is probabilistic, leading to a distribution over the substitute confounder, the theory assumes that the posterior distribution collapses into a Dirac delta distribution, implying certainty in the confounders’ estimation. This assumption simplifies the theoretical framework but introduces a fundamental incoherence between the stochastic nature of the inference models and the deterministic assumption in the theory (D’Amour, 2019b; Imai & Jiang, 2019; D’Amour, 2019a). There is a significant theoretical-application gap: In theory, the deconfounder assumes that the substitute confounder is estimated with certainty, while in practice, inference models are *stochastic* (Zhang et al., 2019; Bica et al., 2020b; Hatt & Feuerriegel, 2024), and the latent confounder is described by a distribution, introducing uncertainty. Our use of near-deterministic VAEs indirectly controls the posterior variance, finding a compromise where the posterior remains less diffuse yet not fully deterministic. This approach enables a more precise estimation of the substitute confounder without assuming perfect certainty, addressing an inherent inconsistency. Applying this method within deconfounder theory holds independent interest beyond this work’s scope. Future research could explore integrating these improvements into the deconfounder framework, with near-deterministic VAEs for substitute confounders inference to bridge theory and practice.

**Comparing our approach to the deconfounder** Unlike the deconfounder, our method does not require the consistency assumption for identifying treatment effects. Whereas the deconfounder framework models unobserved covariates as confounders affecting both treatment and outcome, we treat these unobserved covariates as adjustment variables, thus bypassing the need for the consistency assumption.

**Estimating  $p(Y_t(\omega))$**  In causal inference, when unobserved confounders are present, the conditional distribution of potential outcomes plays a critical role. If the adjustment variables  $\mathbf{U}$  are observed, the potential outcome can be represented as:

$$p(Y_t(\omega)) = p(Y_t \mid \mathbf{h}_t, W_t = \omega) = \int p(y_t \mid \mathbf{h}_t, W_t = \omega, \mathbf{U} = \mathbf{u})p(\mathbf{u} \mid \mathbf{h}_t, W_t = \omega)d\mathbf{u}.$$

Due to the structural assumptions over the causal graph, the treatments  $W_t$  and covariates  $\mathbf{X}_t$  are d-separated from  $\mathbf{U}$  given  $\mathbf{H}_t$ , implying:

$$p(\mathbf{u} \mid \mathbf{h}_t, W_t = \omega) = p(\mathbf{u} \mid \mathcal{D}_{t-1}),$$

where the conditional potential outcome is identifiable, but estimating it requires sampling from the posterior distribution of the adjustment variables,  $p(\mathbf{u} \mid \mathcal{D}_{t-1})$ .

When  $\mathbf{U}$  is not observed, let  $\mathbf{Z}$  be a latent variable satisfying the CMM(p). Under what conditions

does the following equality hold?

$$\begin{aligned} \int p(y_t | \mathbf{h}_t, W_t = \omega, \mathbf{Z} = \mathbf{z}) p(\mathbf{z} | \mathcal{D}_{t-1}) d\mathbf{z} &\stackrel{(*)}{=} \int p(y_t | \mathbf{h}_t, W_t = \omega, \mathbf{U} = \mathbf{u}) p(\mathbf{u} | \mathcal{D}_{t-1}) d\mathbf{u} \\ &= p(Y_t(\omega) | \mathbf{h}_t). \end{aligned} \quad (3.29)$$

This equation addresses the potential risk of non-uniqueness in the CMM assumption, which could lead to varying values on the left-hand side (LHS) of Equation 3.29. However, our framework differs from the traditional deconfounder framework. Here, the identification of the conditional potential outcome  $p(Y_t | \mathbf{h}_t)$  occurs *independently* of the latent variables, as sequential ignorability holds without requiring conditioning on them. The CMM assumption, under the condition  $\mathbf{Z} \perp\!\!\!\perp \mathbf{X}_{\leq T}, W_{\leq T}$ , ensures that no confounding backdoor paths are introduced by conditioning on  $\mathbf{Z}$ . Thus, using  $\mathbf{Z}$  as a substitute for  $\mathbf{U}$  presents no identifiability or consistency issues. This conclusion also extends to the marginal distribution of potential outcomes, formally shown through a copula argument, as in D'Amour (2019a).

$$\begin{aligned} p(Y_t(\omega)) &= \int p(Y_t(\omega) | \mathbf{H}_t = \mathbf{h}_t) p(\mathbf{h}_t) d\mathbf{h}_t, \\ p(Y_t(\omega)) &= \int p(Y_t | \mathbf{H}_t = \mathbf{h}_t, W_t = \omega) p(\mathbf{h}_t) d\mathbf{h}_t, \\ p(Y_t(\omega)) &= \int p(y_{\leq t}, \mathbf{x}_{\leq t}, \omega_{\leq t}) \frac{p(\mathbf{h}_t)}{p(\mathbf{h}_t, \omega_t)} d\mathbf{h}_t, \\ p(Y_t(\omega)) &= \int \int p(y_{\leq t}, \mathbf{z} | \mathbf{x}_{\leq t}, \omega_{\leq t}) p(\mathbf{x}_{\leq t}, \omega_{\leq t}) \frac{p(\mathbf{h}_t)}{p(\mathbf{h}_t, \omega_t)} d\mathbf{h}_t d\mathbf{z}, \\ &= \int \int c(y_{\leq t}, \mathbf{z} | \mathbf{x}_{\leq t}, \omega_{\leq t}) p(y_t | \mathbf{h}_t, \omega_t) p(\mathbf{z} | \mathbf{x}_{\leq t}, \omega_{\leq t}) p(\mathbf{h}_t) d\mathbf{h}_t d\mathbf{z}. \end{aligned} \quad (3.30)$$

The copula  $c(y_{\leq t}, \mathbf{z} | \mathbf{x}_{\leq t}, \omega_{\leq t})$  is restricted by the CMM(p) assumption. This constraint differs significantly from the deconfounder theory, where factor models often separate multiple treatments or treatment sequences and impose no such restrictions on the outcome model. Therefore, identifying potential outcomes in the deconfounder framework requires additional assumptions, as discussed in Wang & Blei (2019a;b). However, our framework enforces conditional separation of responses given past sequences of treatments and covariates, implying independence between the latent variables and treatment sequences.

Finally, in practice, how can we estimate  $p(Y_t(\omega))$ ? We express this as:

$$\begin{aligned} p(Y_t(\omega)) &= \int p(y_t | \mathbf{H}_t = \mathbf{h}_t, W_t = \omega) p(\mathbf{h}_t) d\mathbf{h}_t, \\ &= \int \int p(y_t | \mathbf{h}_t, \omega, \mathbf{z}) p(\mathbf{z} | \mathbf{h}_t, \omega) p(\mathbf{h}_t) d\mathbf{h}_t d\mathbf{z}, \\ &= \int \int p(y_t | \mathbf{h}_t, \omega, \mathbf{z}) p(\mathbf{z} | \mathcal{D}_{t-1}) p(\mathbf{h}_t) d\mathbf{h}_t d\mathbf{z}, \\ &\approx \int \int p_\theta(y_t | \mathbf{h}_t, \omega, \mathbf{z}) q_\phi(\mathbf{z} | \mathcal{D}_T) p(\mathbf{h}_t) d\mathbf{h}_t d\mathbf{z}. \end{aligned} \quad (3.31)$$

Here,  $p_\theta(y_t | \mathbf{h}_t, \omega, \mathbf{z})$  is modeled by the outcome model (decoder), while  $q_\phi(\mathbf{z} | \mathcal{D}_T)$  is the approximate posterior distribution of the latent variables, estimated using the observed sequence of data.

**Capturing "bad variables"** We examine whether the substitute adjustment variables  $\mathbf{Z}$  can inadvertently capture "bad variables," that is, variables that may introduce bias into the estimation of causal



effects. One potential source of bias arises from M-colliders (Figure 3.9). If the substitute adjustment variables  $\mathbf{Z}$  capture information not only about the true adjustment variables  $\mathbf{U}$ , but also about a collider variable  $\mathbf{M}$ , this could result in  $\mathbf{Z} \not\perp W_{\leq T}$ .

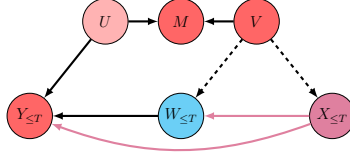


Figure 3.9: An example of an M-collider structure, where the variable  $V$  influences both the treatment and the response, as indicated by the dashed arrows.

The key concern is whether  $\mathbf{Z}$  could “blindly” capture information from the sequence of responses or treatments. Such cases may lead to open collider paths like

$$\mathbf{U} \rightarrow Y_t \leftarrow W_{\leq t} \quad \text{or} \quad \mathbf{U} \rightarrow Y_t \leftarrow \mathbf{X}_{\leq t}.$$

These scenarios would violate the assumption that  $\mathbf{Z} \perp W_{\leq t}$  and  $\mathbf{Z} \perp \mathbf{X}_{\leq t}$ . In essence, including colliders in the substitute adjustment variables can open “backdoor” paths, leading to biased treatment effect estimates. To prevent this, it is essential to ensure that the substitute variables  $\mathbf{Z}$  do not inadvertently encode information about colliders that affect both the treatments and the responses.

**Conclusion** In this work, we proposed CDVAE, a novel framework for estimating treatment effects in high-dimensional, time-varying settings. By leveraging variational inference with robust regularization techniques, we introduced a principled approach to infer latent adjustment variables while ensuring identifiability and mitigating covariate imbalance. Our framework demonstrated theoretical guarantees for generalization and treatment effect consistency in the near-deterministic regime of VAEs—an overlooked property in the causal inference literature. Extensive empirical evaluations support the effectiveness of CDVAE on both synthetic and semi-synthetic datasets. Future work could focus on extending this framework to: 1. dynamic treatment regimes (Definition Def2.2, Chapter 2), for example, by incorporating the g-calculus (Proposition Prop2.2); 2. providing generalization bounds for treatment effects when they depend on a sequence of treatments (Lewis & Syrgkanis, 2021; Vankadara et al., 2022; Oh et al., 2022; Csillag et al., 2024); 3. exploring theoretically the bias-variance trade-off in the estimation of treatment effects in the near-deterministic regime.

## Chapter 4

# Causal Contrastive Predictive Coding

### 4.1 Introduction

It is vital in real-world applications to estimate potential responses, i.e., responses under hypothetical treatment strategies. Individuals show diverse responses to the same treatment, emphasizing the need to quantify individual response trajectories. This enables personalized interventions, enhancing decision-making efficacy. In medical contexts, precise response estimation enables tailored treatments for patients (Atan et al., 2018; Shalit, 2020; Mueller & Pearl, 2023). This chapter focuses on *counterfactual regression over time*, estimating responses under hypothetical treatment plans based on individual records, including past covariates, responses, and treatment sequences up to the current prediction time (Robins et al., 2000; Robins & Hernán, 2009a). We have seen some of the challenges (Chapter 2 and 3) we need to address in the time-varying setting, which are *time-dependent confounding*, *selection bias*, and *long-term dependencies*. As mentioned in Sections 2.2.5 and 3.1, RMSNs (Lim, 2018b), CRN (Bica et al., 2020a), and G-Net Li et al. (2021), have tackled these causal inference challenges. However, their reliance on RNN limits their ability to capture long-term dependencies. Recent studies like Causal Transformer (Melnychuk et al., 2022) propose better integrating transformers to represent temporal dynamics. Rather than viewing this as a limitation of RNN, we see it as an opportunity to emphasize their strengths. We design specific architectures for counterfactual regression over large horizons, avoiding complex, hard-to-interpret models like transformers. Our approach leverages the computational efficiency of RNN, incorporating *Contrastive Predictive Coding (CPC)* (Oord et al., 2018; Henaff, 2020) for learning data history representations. This enhances model performance while maintaining efficiency, offering a compelling alternative to transformer-based approaches. Furthermore, we usually formulate identification assumptions of counterfactual responses over the original process history space, namely sequential ignorability, overlap, and consistency for longitudinal data (Assumptions Asm2.5, Asm2.7, Asm2.6). However, these assumptions may not hold in the representation space for arbitrary functions. Since identification often involves conditional independence, it applies when using an invertible representation function. Current models for time-varying settings (Lim, 2018b; Bica et al., 2020a; Melnychuk et al., 2022) do not enforce representation invertibility. To address this, instead of adding complexity with a decoder, we *implicitly* push the history process to be "reconstructable" from

the encoded representation by maximizing Mutual Information (MI) between representation and input, following the *Information Maximization (InfoMax)* principle Linsker (1988), akin to Deep InfoMax Hjelm et al. (2019). We summarize these main design differences between the baselines and Causal CPC in Table 4.1.

Table 4.1: Summary of concurrent methods contrasted against Causal CPC across design aspects.

Model	Backbone	Tailored to long-term forecast?	Learning of long-term dependencies	Use of contrastive learning	Prediction of counterfactuals	Handling selection bias	Invertibility of representation
<b>Causal CPC (ours)</b>	GRU	Yes	CPC	Yes	Autoregressive	Balanced representation	Yes, contrasts representation with input
<b>Causal Transformer</b>	3 Transformers	Yes	Transformers	N/A	Autoregressive	Balanced representation	N/A
<b>G-Net</b>	LSTM	No	N/A	N/A	Autoregressive	G-Computation	Current co-variables $\mathbf{X}_t$
<b>CRN</b>	LSTM	No	N/A	N/A	Autoregressive	Balanced representation	N/A
<b>RMSN</b>	LSTM	No	N/A	N/A	Autoregressive	Weighting	N/A
<b>MSM</b>	Logistic+linear model	No	N/A	N/A	Autoregressive	Weighting	N/A

## 4.2 Contributions

Our approach is inspired by *self-supervised learning* using MI objectives (Hjelm et al., 2019). We aim to maximize MI between different views of the same input, introducing counterfactual regression over time through CPC to capture long-term dependencies. Additionally, we propose a tractable lower bound to the original InfoMax objectives for more efficient representations. This is challenging due to the sequential nature and high dimensionality, marking a novelty. We demonstrate the importance of regularization terms via an ablation study. Previous work leveraging contrastive learning for causal inference applies only to the static setting with no theoretical grounding (Chu et al., 2022). To our knowledge, we frame for the first time the representation balancing problem from an information-theoretic perspective and show that the suggested adversarial game (Theorem Thm4.3) yields theoretically balanced representations using the Contrastive Log-ratio Upper Bound (CLUB) of MI (Cheng et al., 2020), computed efficiently. Key innovations of our Causal CPC model include:

- We showcase the capability of leveraging CPC to capture long-term dependencies in the process history using Information Noise Contrastive Estimation (InfoNCE) (Gutmann & Hyvärinen, 2010; 2012; Oord et al., 2018), an unexplored area in counterfactual regression over time where its integration into process history modeling is not straightforward in causality (Table 4.1).
- We enforce input reconstruction from representation by contrasting the representation with its input. Current baselines generally overlook such quality (c.f. Table 4.1), yet it ensures retaining confounding information which prevents biased counterfactual estimation.

- Applying InfoMax to process history while respecting its dynamic nature is challenging. We provide a tractable lower bound to the original InfoMax problem, bringing theoretical insights into the tightness.
- We suggest minimizing an upper bound on MI between representation and treatment to make the representation non-predictive of the treatment, using the CLUB of MI (Cheng et al., 2020). This novel information-theoretic perspective results in a theoretically balanced representation across all treatment regimes.
- By using a simple GRU layer (Cho et al., 2014) as the model backbone, we demonstrate that well-designed regularizations can outperform more complex models like transformers.

Finally, our experiments on synthetic data (cancer simulation (Geng et al., 2017)) and semi-synthetic data based on real-world datasets (MIMIC-III (Johnson et al., 2016)) show the superiority of Causal CPC at accurately estimating counterfactual responses.

## 4.3 Related Work

**Counterfactual Regression Over Time** We compare Causal CPC primarily to MSMs, RMSNs, CRN, G-Net, and CT. These models, like ours, assume *sequential ignorability* (Robins & Hernán, 2009a). Several alternative models operate under different assumptions, often addressing the presence of unobserved confounders. Some of these models build on deconfounding theory (Lopez & Gutman, 2017; Ranganath & Perotte, 2018; Wang & Blei, 2019a), which recent works have extended to time-varying settings. Deconfounding involves imposing a factor model on treatment assignment, where each treatment becomes conditionally independent, given latent variables that act as proxies for unobserved confounders. Examples of this approach include Bica et al. (2020b); Hatt & Feuerriegel (2021); Cao et al. (2023). Other models assume the presence of proxy variables, inferring a representation of unobserved confounders through probabilistic models based on these proxies (Veitch et al., 2020; Cheng et al., 2021; Kuzmanovic et al., 2021). Unlike our setting, which follows the sequential ignorability assumption, many models adopt a data-generating process similar to that in (Soleimani et al., 2017b;a; Qian et al., 2021). These methods, often non- or semi-parametric, tend to either ignore static covariates or handle them linearly, leading to computational inefficiencies and scalability issues. Nevertheless, some non- or semi-parametric approaches—such as Schulam & Saria (2017); Seedat et al. (2022); De Brouwer et al. (2022); H4zl4 et al. (2023)—align with our causal assumptions but extend them to continuous time, treating sequential ignorability in a continuous setting. Additionally, models like Jiang et al. (2023) incorporate continuous-time and assume interactions between units, where an individual’s outcome depends on both their treatment and the treatments of others. Berrevoets et al. (2021), focusing on binary treatment sequences, requires a stronger version of sequential ignorability—conditional on current covariates—. In contrast, our model assumes a weaker version, conditioning on the entire history of covariates to account for long-lasting confounding effects. Furthermore, Chen et al. (2023) focuses solely on binary treatments and targets estimating the average

treatment effect on the treated. The authors assume a specific treatment regime where individuals enter a post-treatment state after a defined time period. This assumption is restrictive compared to our framework, which allows for complex, individualized treatment assignment mechanisms and non-binary treatments, where treatment values fluctuate over time. As a result, Chen et al. (2023) is incompatible with our causal assumptions. Other methods, like Wu et al. (2023), address high-dimensional counterfactual generation based on time-varying treatment plans under the same sequential ignorability assumption. However, they are not designed for causal forecasting over multiple time steps, as required in our setting. Similarly, Frauen et al. (2023) focuses on estimating the average causal effect and is not suited for predicting individual treatment effects or conditional counterfactual responses, as it targets marginal counterfactual expectations via g-computation.

In contrast, we introduce a contrastive learning approach to capture long-term dependencies while maintaining a simple model and ensuring high computational efficiency in training and prediction. We demonstrate that simple models with well-designed regularization terms can still achieve high prediction quality. Additionally, previous works (Robins & Hernán, 2009a; Robins et al., 2000; Lim, 2018a; Li et al., 2021; Melnychuk et al., 2022) did not consider the role of invertible representation in improving counterfactual regression. Here, we introduce an InfoMax regularization term to make our encoder easier to invert.

**InfoMax Principle** The InfoMax principle aims to learn a representation that maximizes MI with its input (Linsker, 1988; Bell & Sejnowski, 1995). Estimating MI for high-dimensional data is challenging and is often addressed by maximizing a simple and tractable lower bound on MI (Hjelm et al., 2019; Poole et al., 2019a; Liang et al., 2023). Another approach involves maximizing MI between two lower-dimensional representations of different views of the same input (Bachman et al., 2019; Henaff, 2020; Tian et al., 2020; Tschannen et al., 2020), offering a more practical solution. We adopt this strategy by dividing our process history into two views, past and future (c.f. Figure 4.2), and maximizing a tractable lower bound on MI between them, encouraging a "reconstructable" representation of the process history. To our knowledge, the only work applying an InfoMax approach to counterfactual regression, albeit in static settings, is Chu et al. (2022). They propose maximizing MI between an individual’s representation and a global representation, aggregating information from all individuals into a single vector. However, the global representation lacks clarity and interpretability, raising uncertainties about its theoretical underpinnings in capturing confounders. Furthermore, there’s a lack of theoretical analysis on how minimizing MI between individual and treatment-predictive representations could yield a treatment-invariant representation. As a novelty, we extend the InfoMax principle to longitudinal data, providing a theoretical guarantee of learning balanced representations.

**Self-Supervised Learning and Mutual Information** In the self-supervised learning paradigm, Deep InfoMax (Hjelm et al., 2019) employs MI computation between input images and representations, emphasizing its maximization to enhance reconstruction quality. Additionally, local MI calculations between the representation and local features contribute to encoding more intricate patterns shared across

data patches. The strategy of maximizing average MI between the representation and local regions, such as patches, significantly improves downstream task performance. Notably, global MI assumes a more prominent role in reconstructing the complete input given the representation.

CPC aligns with the MI-based approach seen in Deep InfoMax, emphasizing the maximization of MI between global and local representation pairs. Distinct from Deep InfoMax, CPC processes local features sequentially, constructing partial "summary features" to predict specific local features in the future. Classical self-supervised paradigms often focus on tasks like classification or reconstruction-based objectives, leading to distinct preferences for maximizing MI in either local or global information. However, integrating both procedures becomes imperative in scenarios involving downstream tasks like counterfactual regression over time. Our proposed Causal CPC is strategically designed to align with these intuitions.

Several other methods share similarities with CPC, such as Contrastive Multiview Coding (Tian et al., 2020), which emphasizes maximizing MI between representations of different views of the same observation. Augmented Multiscale Deep InfoMax (Bachman et al., 2019), akin to CPC, makes predictions across space but differs by predicting representations across layers in the model. Instance Discrimination Zhao et al. (2020) also encourages learning representations capable of discriminating between individual examples in the dataset. Still, our preference for CPC arises from its adaptability in processing sequential features in an ordered and autoregressive manner. This aligns seamlessly with the requirements of our specific context, especially when dealing with counterfactual regression over time.

## 4.4 Problem Formulation

**Setup** In the PO framework (Rubin, 2005), and following Robins & Hernán (2009b), we extend the treatment variable to be discrete (unlike the binary treatment in CDVAE) and broaden the PO scope compared to CDVAE (Chapter 3) to consider the lagged treatment effect:

### Assumption Asm4.1 [Lagged Treatment Effect]

We focus our causal framework on examining causal quantities defined with respect to potential outcomes given a lag of  $\rho$  time steps, rather than the entire sequence of treatments. In mathematical terms, this can be represented as  $\{Y_t(W_{\leq t-\rho}, \omega_{t-\rho+1:t})\}_{\omega_{t-\rho+1:t} \in \mathcal{W}^\rho}$ . This approach relaxes the contemporaneous treatment effect assumption in the CDVAE model (Chapter 3), as it defines counterfactual trajectories of responses over sequences of potential outcomes rather than a single one. On the other hand, the lagged treatment effect assumption enables us to establish a framework for **causal forecasting**, i.e., estimating causal quantities over time beyond the scope of the observed longitudinal study. Specifically, we can consider the longitudinal study as observed data up to time  $t' = t - \rho$ , and then investigate future causal quantities defined as a function of  $\{Y_{t'+\rho}(W_{\leq t'}, \omega_{t'+1:t'+\rho})\}_{\omega_{t'+1:t'+\rho} \in \mathcal{W}^\rho}$ . **This is the main setting of our second contribution (Causal CPC).**

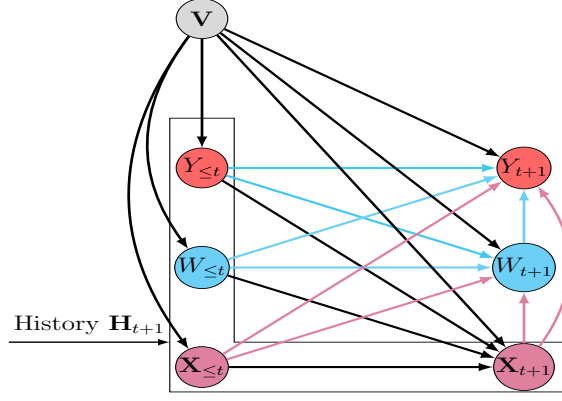


Figure 4.1: Causal graph over  $\mathbf{H}_{t+1}$ . For simplicity, we represent past treatments as  $W_{\leq t}$  such that each element in that sub-sequence confounds the next treatment and response  $W_{t+1}$  and  $Y_{t+1}$ . Idem for  $Y_{\leq t}$  and  $\mathbf{X}_{\leq t}$ . The static covariates  $\mathbf{V}$  are assumed to affect all the time-varying variables. We omit the representation of exogenous noise for simplicity. Interactions between  $W_{\leq t}$ ,  $\mathbf{X}_{\leq t}$ , and  $Y_{\leq t}$  were also omitted for simplicity.

As a result of Assumption Asm4.1 and for any time step  $t + \rho$ , we treat the longitudinal study as observed data up to time  $t$  and investigate future causal quantities defined by

$$\{Y_{t+\rho}(W_{\leq t}, \omega_{t+1:t+\rho})\}_{\omega_{t+1:t+\rho} \in \mathcal{W}^\rho}.$$

As described in Section 2.2.1, we track a cohort of individuals (units)  $i \in \{1, 2, \dots, N\}$  over  $t_{max}$  time steps. At each time  $t \in \{1, 2, \dots, t_{max}\}$ , we observe: (1) *Discrete treatment*  $W_{it} \in \mathcal{W} = \{0, 1, \dots, K - 1\}$ , (2) *Outcome of interest*  $Y_{it} \in \mathcal{Y} \subset \mathbb{R}$ , (3) *Time-varying context*  $\mathbf{X}_{it} \in \mathcal{X} \subset \mathbb{R}^{d_x}$ , a  $d_x$ -dimensional vector of confounders, and (4) *Static confounders*  $\mathbf{V} \in \mathcal{V} \subset \mathbb{R}^{d_v}$ . We define the history up to time  $t + 1$  as  $\mathbf{H}_{t+1} = [\mathbf{V}, \mathbf{X}_{\leq t+1}, W_{\leq t}, Y_{\leq t}]$ , capturing all information before assigning treatment  $W_{t+1}$ . This process is illustrated in the causal graph in Figure 4.1 where all of the past observed data encompassed in  $\mathbf{H}_{t+1}$  confounds future treatments and responses,  $W_{t+1}, W_{t+2}, \dots, W_{t_{max}}$  and  $Y_{t+1}, Y_{t+2}, \dots, Y_{t_{max}}$ , which create long-term dependencies. The fact that the covariates  $\mathbf{X}_{\leq t+1}$  are affected by the treatments  $W_{\leq t}$  creates time-dependent confounding. The static covariates  $\mathbf{V}$  are assumed to be affecting all of the time-varying variables. Since we suppose sequential ignorability, no possible exogenous noises are affecting both treatments and responses.

**Goal** Given a training dataset  $\{\mathbf{H}_{i,t+1}, i = 1, \dots, N\}$  sampled from the empirical distribution  $\mathbb{P}_{\mathbf{H}_{t+1}}$ , we address the causal inference problem:

*How can we efficiently estimate counterfactual responses up to time  $t + \rho$ , where  $\rho \geq 1$  is the prediction horizon for a potential treatment sequence  $\omega_{t+1:t+\rho} = (\omega_{t+1}, \dots, \omega_{t+\rho})$ , given history  $\mathbf{H}_{t+1}$ ?*

The goal is to estimate the causal quantity  $m_t^{W_{\leq t}, \omega_{t+1:t+\rho}}(\mathbf{x}_{\leq t}, y_{< t})$  (Equation 2.5). By Assumption Asm4.1 of the lagged treatment effect and sequential ignorability (Assumption Asm2.5), we obtain the

following identification result (Proposition Prop2.1):

$$\begin{aligned} m_t^{W_{\leq t}, \omega_{t+1:t+\rho}}(\mathbf{x}_{\leq t}, y_{< t}) &= \mathbb{E}(Y_{t+\rho}(\omega_{t+1:t+\rho}) \mid \mathbf{H}_{t+1}) \\ &= \mathbb{E}(Y_{t+\rho} \mid \mathbf{H}_{t+1}, W_{t+1:t+\rho} = \omega_{t+1:t+\rho}), \end{aligned}$$

where  $\mathbb{E}(Y_{t+\rho}(\omega_{t+1:t+\rho}) \mid \mathbf{H}_{t+1})$  is the expected outcome at time  $t + \rho$ , conditioned on the history  $\mathbf{H}_{t+1}$  and treatment sequence  $\omega_{t+1:t+\rho}$ .

## 4.5 Causal CPC

### 4.5.1 Representation Learning

**Contrastive Predictive Coding** Using contrastive learning, we illustrate how to efficiently learn a representation of the process history  $\mathbf{H}_t$ . Causal forecasting across multiple horizons requires representations with high variability predictability within  $\mathbf{H}_t$ . In short-term prediction, we aim to capture low-level information and exploit local signal smoothness. For long-term prediction, shared information between history and future points decreases over time, necessitating a more global structure. Capturing long-term dependencies and slow-varying features is crucial in our setting.

To achieve this, we learn a representation of  $\mathbf{H}_t$  that predicts future frames over multiple time steps. For each prediction horizon  $j \in \{1, \dots, \rho\}$  we define the future frames as

$$\mathbf{F}_{t+j} := [\mathbf{V}, \mathbf{X}_{t+j}, W_{t+j-1}, Y_{t+j-1}] \in \mathcal{U} \subset \mathbb{R}^{d_v+d_x+K+1}.$$

**Step 1: local encoding.** First, local features are extracted by encoding the frames  $(\mathbf{F}_t)_{1 \leq t \leq T-\rho}$ . Let

$$\Phi_{\theta_1} : \mathbb{R}^{d_v+d_x+K+1} \longrightarrow \mathbb{R}^{d_z}$$

be a component-level encoder. At a time  $t$  we obtain the local feature vector

$$\mathbf{Z}_t := \Phi_{\theta_1}(\mathbf{F}_t) = \Phi_{\theta_1}([\mathbf{V}, \mathbf{X}_t, W_{t-1}, Y_{t-1}]).$$

**Step 2: autoregressive summarisation.** Collect the sequence  $\mathbf{Z}_{1:t} = (\mathbf{Z}_1, \dots, \mathbf{Z}_t)$ . A GRU-based autoregressive map

$$\Phi_{\theta_2}^{\text{AR}} : (\mathbb{R}^{d_z})^t \longrightarrow \mathbb{R}^{d_c}$$

produces the *context representation*

$$\mathbf{C}_t^{\text{enc}} := \Phi_{\theta_2}^{\text{AR}}(\mathbf{Z}_{1:t}).$$

**Composite representation function.** The overall representation of the process history is therefore the composition

$$\Phi_{\theta_1, \theta_2} := \Phi_{\theta_2}^{\text{AR}} \circ \Phi_{\theta_1}, \quad \Phi_{\theta_1, \theta_2}(\mathbf{H}_t) = \mathbf{C}_t^{\text{enc}},$$



where  $\Psi_{\theta_1}(\mathbf{H}_t) := (\psi_{\theta_1}(\mathbf{V}, \mathbf{X}_s, W_{s-1}, Y_{s-1}))_{s=1}^t$  applies the frame encoder to each step (c.f. left side of Figure 4.2).

To train the model, we use a contrastive loss that encourages the context  $\mathbf{C}_t^{\text{enc}}$  to predict future local features  $\mathbf{Z}_{t+1}, \dots, \mathbf{Z}_{t+\rho}$  while distinguishing them from the features of other individuals within the same training batch. This is done by minimizing the InfoNCE loss  $\mathcal{L}_j^{(\text{InfoNCE})}$  for each horizon  $j$ :

$$\mathcal{L}_j^{(\text{InfoNCE})}(\theta_1, \theta_2, \Gamma_j) := -\mathbb{E}_{\mathcal{B}} \left[ \log \frac{\exp(T_j(\mathbf{F}_{t+j}, \mathbf{C}_t^{\text{enc}}))}{\sum_{l=1}^{|\mathcal{B}|} \exp(T_j(\mathbf{F}_{l,t+j}, \mathbf{C}_t^{\text{enc}}))} \right], \quad (4.1)$$

where  $\mathcal{B}$  is a batch containing individual histories, and  $\Gamma_j$  is a weight matrix. The discriminator  $T_j(\cdot, \cdot)$  classifies the correct future feature among negative samples from other individuals:

$$\begin{aligned} T_j(\mathbf{F}_{t+j}, \Phi_{\theta_1, \theta_2}(\mathbf{H}_t)) &:= \Phi_{\theta_1}(\mathbf{F}_{t+j})^\top \Gamma_j \mathbf{C}_t^{\text{enc}} \\ &= \mathbf{Z}_{t+j}^\top \Gamma_j \mathbf{C}_t^{\text{enc}} \\ &= \mathbf{Z}_{t+j}^\top \hat{\mathbf{Z}}_{t+j}. \end{aligned} \quad (4.2)$$

In practice, the projection of  $\mathbf{C}_t^{\text{enc}}$  on the matrix  $\Gamma_j$  yields a prediction  $\hat{\mathbf{Z}}_{t+j}$  whose quality is measured by the dot product with the true future local feature  $\mathbf{Z}_{t+j}^\top \hat{\mathbf{Z}}_{t+j}$ . Minimizing the InfoNCE loss  $\mathcal{L}_j^{(\text{InfoNCE})}$  provides a lower bound on the MI between the context and future features  $I(\mathbf{F}_{t+j}, \mathbf{C}_t)$  (Oord et al., 2018):

$$\log(|\mathcal{B}|) - \mathcal{L}_j^{(\text{InfoNCE})} \leq I(\mathbf{F}_{t+j}, \mathbf{C}_t). \quad (4.3)$$

For multiple forecasting horizons  $j = 1, 2, \dots, \rho$ , we learn long-term dependencies by minimizing the InfoNCE loss across all horizons:

$$\mathcal{L}^{CPC}(\theta_1, \theta_2, \{\Gamma_j\}_{j=1}^\rho) := \frac{1}{\rho} \sum_{j=1}^\rho \mathcal{L}_j^{(\text{InfoNCE})}(\theta_1, \theta_2, \Gamma_j). \quad (4.4)$$

Thus, minimizing  $\mathcal{L}^{CPC}$  maximizes the *shared information* between the context and future components as shown in Equation (4.5), pushing the model to capture the global structure of the process over large horizons—crucial for counterfactual regression across multiple time steps:

$$\log(|\mathcal{B}|) - \mathcal{L}^{CPC} \leq \frac{1}{\rho} \sum_{j=1}^\rho I(\mathbf{F}_{t+j}, \mathbf{C}_t). \quad (4.5)$$

**InfoMax Principle** We introduce a regularization term to make the context representation of the process history  $\mathbf{H}_t$  "reconstructable." We leverage the InfoMax principle to maximize the MI between  $\mathbf{H}_t$  and the context  $\mathbf{C}_t^{\text{enc}}$ . However, we avoid computing the contrastive loss between  $\mathbf{C}_t^{\text{enc}}$  and  $\mathbf{H}_t$  for two main reasons. First,  $\mathbf{H}_t$  is a high-dimensional sequence, making the loss computation very demanding. Secondly, we are still interested in incorporating inductive bias toward capturing global dependencies, this time by pushing any subsequence to be predictive of any future subsequence within  $\mathbf{H}_t$ . Hence, we divide the process history into two non-overlapping views,  $\mathbf{H}_t^h := \mathbf{F}_{1:t_0}$ ,  $\mathbf{H}_t^f := \mathbf{F}_{t_0+1:t}$  representing a *historical*

*subsequence* and a *future subsequence* of frames within the process history  $\mathbf{H}_t$ , with  $t_0$  randomly chosen per batch. We then maximize the MI between the representations of these views,  $\mathbf{C}_t^{\text{enc},h}$  and  $\mathbf{C}_t^{\text{enc},f}$ , resulting in a lower bound to the InfoMax objective as formulated below:

**Proposition Prop4.1**

Let  $\mathbf{C}_t^{\text{enc},h} = \Phi_{\theta_1,\theta_2}(\mathbf{H}_t^h)$  and  $\mathbf{C}_t^{\text{enc},f} = \Phi_{\theta_1,\theta_2}(\mathbf{H}_t^f)$  be the encodings of the two non-overlapping subsequences described above. Then

$$I(\mathbf{C}_t^{\text{enc},h}, \mathbf{C}_t^{\text{enc},f}) \leq I(\mathbf{H}_t, (\mathbf{C}_t^{\text{enc},h}, \mathbf{C}_t^{\text{enc},f})).$$

We provide an intuitive discussion of the inequality by providing an exact writing of the gap in Proposition Prop4.1:

**Theorem Thm4.1**

$$\begin{aligned} I(\mathbf{H}_t; (\mathbf{C}_t^{\text{enc},h}, \mathbf{C}_t^{\text{enc},f})) - I(\mathbf{C}_t^{\text{enc},h}, \mathbf{C}_t^{\text{enc},f}) &= I(\mathbf{H}_t; \mathbf{C}_t^{\text{enc},f} \mid \mathbf{C}_t^{\text{enc},h}) \\ &+ \mathbb{E}_{\mathbf{h}_t \sim P_{\mathbf{H}_t}} \mathbb{E}_{\mathbf{c}_t^f \sim P_{\mathbf{C}_t^f | \mathbf{h}_t}} \left[ D_{\text{KL}}(P_{\mathbf{C}_t^h | \mathbf{h}_t} \parallel P_{\mathbf{C}_t^h | \mathbf{c}_t^f}) \right]. \end{aligned} \quad (4.6)$$

Both terms on the RHS of Equation (4.6) are positive, providing an alternative proof to Proposition Prop4.1. When equality holds, it implies  $I(\mathbf{H}_t; \mathbf{C}_t^{\text{enc},f} \mid \mathbf{C}_t^{\text{enc},h}) = 0$ , indicating that  $\mathbf{H}_t$  is independent of  $\mathbf{C}_t^{\text{enc},f}$  given  $\mathbf{C}_t^{\text{enc},h}$ . This suggests that  $\mathbf{C}_t^{\text{enc},h}$  retains sufficient information from  $\mathbf{H}_t$  that is predictive of  $\mathbf{C}_t^{\text{enc},f}$ . The symmetry of MI also leads to the occurrence of the second term on the RHS when conditioning on  $\mathbf{C}_t^{\text{enc},f}$ . The equality in Proposition Prop4.1 implies  $\mathbb{P}_{\mathbf{C}_t^h | \mathbf{h}_t} = \mathbb{P}_{\mathbf{C}_t^h | \mathbf{c}_t^f}$ , suggesting that  $\mathbf{C}_t^{\text{enc},f}$  efficiently encodes its subsequence while sharing maximum information with  $\mathbf{C}_t^{\text{enc},h}$ .

By considering the proposed variant of the InfoMax principle, we can compute a contrastive bound to  $I(\mathbf{C}_t^{\text{enc},h}, \mathbf{C}_t^{\text{enc},f})$  more efficiently, as the random vectors reside in a low-dimensional space thanks to the encoding. We define a contrastive loss using InfoNCE similar to Equation (4.1):

$$\mathcal{L}^{(\text{InfoMax})}(\theta_1, \theta_2, \eta) := -\mathbb{E}_{\mathcal{B}} \left[ \log \frac{\exp(T_\eta(\mathbf{C}_t^f, \mathbf{C}_t^h))}{\sum_{l=1}^{|\mathcal{B}|} \exp(T_\eta(\mathbf{C}_{l,t}^f, \mathbf{C}_t^h))} \right]. \quad (4.7)$$

We use a non-linear discriminator  $T_\eta$  parametrized by  $\eta$  (detailed in Appendix B.3). The representation of the past subsequence  $\mathbf{C}_t^h$  is mapped to a prediction of the future subsequence  $\hat{\mathbf{C}}_t^f := F_\eta(\mathbf{C}_t^h)$  and  $T_\eta = \mathbf{C}_t^{f^\top} \hat{\mathbf{C}}_t^f$ .

Theorem Thm4.1 and Proposition Prop4.1 justify using the loss in Equation (4.7) by showing that our InfoMax simplification provides a valid lower bound; this is because the contrastive loss in Equation (4.7) verifies

$$\log(|\mathcal{B}|) - \mathcal{L}^{(\text{InfoMax})} \leq I(\mathbf{C}_t^h, \mathbf{C}_t^f) \leq I(\mathbf{H}_t, (\mathbf{C}_t^h, \mathbf{C}_t^f)). \quad (4.8)$$

The “mental model” behind our regularization term comes from the MI

$$I(\mathbf{H}_t; (\mathbf{C}_t^h, \mathbf{C}_t^f)) = H(\mathbf{H}_t) - H(\mathbf{H}_t \mid (\mathbf{C}_t^h, \mathbf{C}_t^f)),$$

which can be written using entropy.

Since the entropy term  $H(\mathbf{H}_t)$  is constant and parameter-free, minimizing the conditional entropy

$$H(\mathbf{H}_t \mid (\mathbf{C}_t^h, \mathbf{C}_t^f)) \geq 0$$

ensures that  $\mathbf{H}_t$  is almost surely a function of  $(\mathbf{C}_t^h, \mathbf{C}_t^f)$  (Appendix B.2.4, Proposition PropB.2). When MI is maximized, the theoretical existence of such a function suggests that the learned context  $\mathbf{C}_t^{\text{enc}}$  can decode and reconstruct  $\mathbf{H}_t$ .

**InfoNCE and DGP inversion** Beyond the idea of reconstruction, it was shown that the InfoNCE objective implicitly learns to invert the data’s generative model under mild assumptions (Zimmermann et al., 2021). Recent works (Daunhawer et al., 2023; Liu et al., 2024) extend this insight to multi-modal settings, which can reframe our InfoMax problem:  $\mathbf{H}_t^h$  and  $\mathbf{H}_t^f$  can be seen as two coupled modalities, allowing us to identify latent generative factors up to some mild indeterminacies (e.g., rotations, affine mappings). We anticipate that multi-modal causal representation learning could be extended to our longitudinal setting, where minimizing our InfoMax objective, in the limit of infinite data, will effectively invert the data generation process up to a class of indeterminacies that we conjecture to be broader and under weaker assumptions than those in current causal representation learning literature, given our focus is on causal inference rather than the identification of causal latent variables.

To initiate a formal basis for this claim, suppose the true data-generating process is given by  $\mathbf{H}_t = g(\mathbf{Z}_t)$ , where  $\mathbf{Z}_t$  represents the true latent factors. In the sequential context, we assume that the same function  $g$  generates the two historical subsequences:

$$\mathbf{H}_t^f = g(\mathbf{z}_t^f), \quad \mathbf{H}_t^h = g(\mathbf{z}_t^h)$$

We assume a general dependency of the form:

$$p(\mathbf{z}_t^f \mid \mathbf{z}_t^h) = \frac{Q(\mathbf{z}_t^f)}{Z(\mathbf{z}_t^h)} \exp(-d(\mathbf{z}_t^f, \mathbf{z}_t^h))$$

With  $d(.,.)$  is a metric as in Matthes et al. (2023). With  $\Phi$  being an encoder, we use the InfoMax regularization term as follows:

$$\mathcal{L}^{(InfoMax)}(\Phi, d, \mathcal{B}) := -\mathbb{E}_{\mathcal{B}} \left[ \log \frac{\exp(-d(\Phi(\mathbf{H}_t^f), \Phi(\mathbf{H}_t^h)))}{\sum_{l=1}^{|\mathcal{B}|} \exp(-d(\Phi(\mathbf{H}_{l,t}^f), \Phi(\mathbf{H}_t^h)))} \right]$$

According to Matthes et al. (2023), under mild regularity conditions, if the encoder  $f$  minimizes  $\mathcal{L}^{(InfoMax)}$ , then  $h = g \circ f$  is a scaled permutation matrix. This result suggests that when the encoder achieves a

minimizer for  $\mathcal{L}^{(InfoMax)}$ , the encoder function  $f$  closely approximates an invertible transformation of  $g$ . From a causal inference perspective, if  $Y_{it}(\omega_{it}) \perp\!\!\!\perp W_{it} \mid \mathbf{H}_{it}$  and  $\mathbf{H}_{it} = g(\mathbf{Z}_{it})$ , then an invertible function  $g \circ f$  ensures that:

$$Y_{it}(\omega_{it}) \perp\!\!\!\perp W_{it} \mid g \circ f(\mathbf{H}_{it})$$

Thus,  $Y_{it}(\omega_{it}) \perp\!\!\!\perp W_{it} \mid g(\mathbf{C}_{it}^{\text{enc}})$  and since  $g$  is invertible, we have:

$$Y_{it}(\omega_{it}) \perp\!\!\!\perp W_{it} \mid \mathbf{C}_{it}^{\text{enc}}$$

This demonstrates that the representation  $\mathbf{C}_{it}^{\text{enc}}$  retains the essential independence structure, facilitating accurate counterfactual inference.

## 4.5.2 Balanced representation learning

**Motivation** Our goal is counterfactual regression, specifically estimating

$$\mathbb{E}(Y_{t+\rho}(\omega_{t+1:t+\rho}) \mid \mathbf{H}_{t+1}).$$

For simplicity, with  $\rho = 1$ , we estimate the potential outcome for a given treatment  $W_{t+1} = \omega_{t+1}$ , where  $W_{t+1} \in \{0, 1, \dots, K-1\}$ , expressed as

$$\mathbb{E}(Y_{t+1}(\omega_{t+1}) \mid \mathbf{H}_{t+1}),$$

which, under standard assumptions, is identified as

$$\mathbb{E}(Y_{t+1}(\omega_{t+1}) \mid \mathbf{H}_{t+1}) = \mathbb{E}(Y_{t+1} \mid \mathbf{H}_{t+1}, W_{t+1} = \omega_{t+1}).$$

The RHS can be estimated from data as

$$\mathbb{E}(Y_{t+1} \mid \mathbf{H}_{t+1}, W_{t+1}) = f(\mathbf{H}_{t+1}, W_{t+1}).$$

Since only one treatment is observed per individual at each time step,  $W_{i,t+1} = \omega_{i,t+1}$ , a fitted model  $\hat{f}$  generates counterfactual responses by switching treatments

$$\hat{f}(\mathbf{h}_{i,t+1}, \omega'_{t+1}), \quad \text{where } \omega'_{t+1} \neq \omega_{t+1}$$

(e.g., chemotherapy vs. radiotherapy).

The challenge is that  $\mathbf{H}_{t+1}$  and  $W_{t+1}$  are not independent, introducing potential bias in counterfactual estimation (Robins, 1999b), leading to covariate shift or selection bias. To address this, we learn a representation  $\Phi(\mathbf{H}_{t+1})$  that enforces distributional balance during decoding.

**Setup** To mitigate selection bias, we leverage the context representation  $\mathbf{C}_t^{\text{enc}}$  of  $\mathbf{H}_t$  and introduce two sub-networks: one for response prediction and one for treatment prediction, both using a mapping of the context representation:

$$\Phi_t = \text{SELU}(\text{Linear}(\mathbf{C}_t^{\text{enc}})) = \Phi_{\theta_R}(\mathbf{H}_t),$$

where SELU represents the Scaled Exponential Linear Unit (Klambauer et al., 2017), and  $\theta_R$  denotes all parameters of the representation learner, i.e.,  $\theta_R = [\theta_1, \theta_2]$ . Following (Bica et al., 2020a; Melnychuk et al., 2022), our objective is to learn a representation that accurately predicts outcomes while remaining *distributionally balanced* across all possible treatment choices  $W_t = 0, 1, \dots, K - 1$ . To achieve this, we frame the problem as an adversarial game: one network learns to predict the next treatment from the representation, while a regularization term ensures that the representation is non-predictive of the treatment.

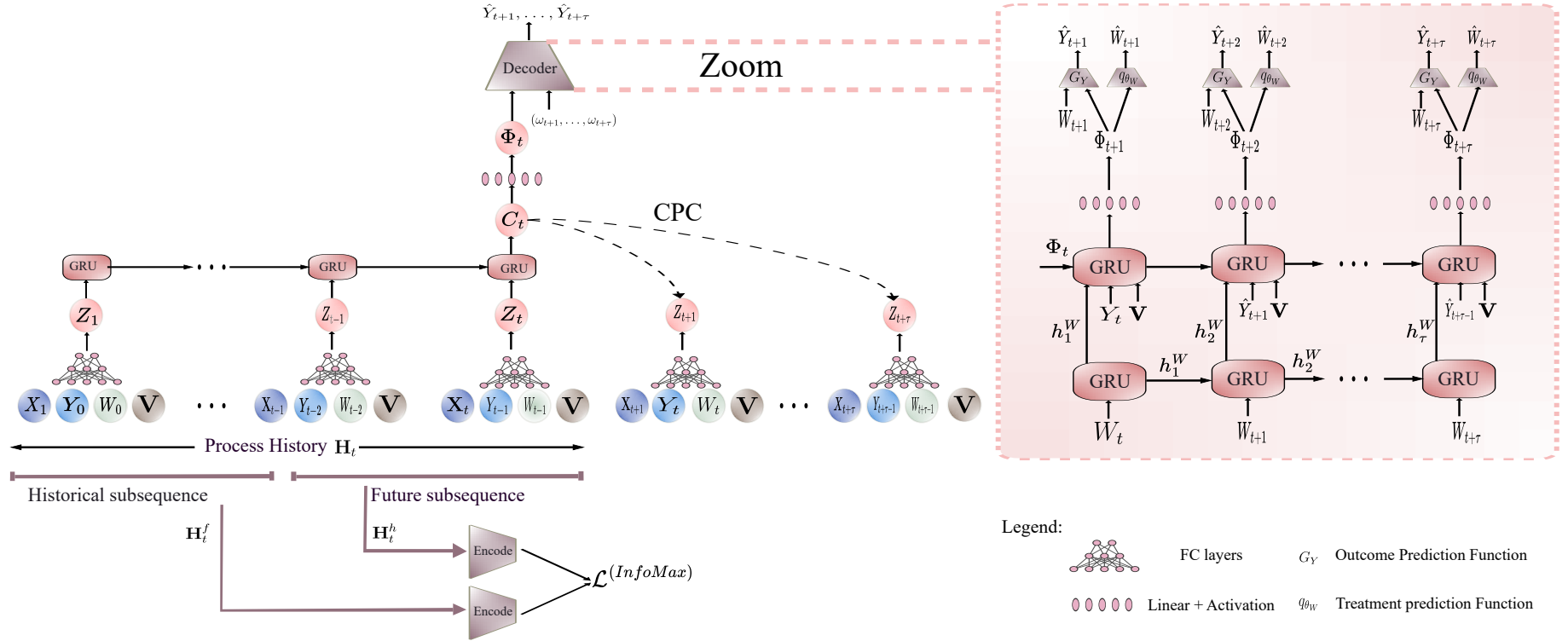


Figure 4.2: Causal CPC architecture: The left shows the encoder, which learns context  $\mathbf{C}_t^{\text{enc}}$  from process history  $\mathbf{H}_t$ , with CPC and InfoMax objectives used for pretraining. The right shows the decoder, which autoregressively predicts the future outcome sequence from  $\mathbf{C}_t^{\text{enc}}$ .

**Factual response prediction** Since we intend to predict counterfactual responses for  $\rho$  steps ahead in time, we train a decoder to predict the factual responses  $Y_{t+1}, \dots, Y_{t+\rho}$  given the sequence of treatments  $(W_{t+1}, \dots, W_{t+\rho})$ . We minimize the negative conditional likelihood

$$\begin{aligned}\mathcal{L}_Y(\theta_R, \theta_Y) &= -\log p_{\theta_Y}(y_{t+1:t+\rho} \mid \Phi_t, \omega_{t+1:t+\rho}) \\ &= -\sum_{j=1}^{\rho} \log p_{\theta_Y}(y_{t+j} \mid y_{t+1:t+j-1}, \Phi_t, \omega_{t+1:t+j}).\end{aligned}$$

We denote  $\mathcal{I}_t^j := [Y_{t+1:t+j-1}, \Phi_t, W_{t+1:t+j}]$  and assume a Gaussian distribution for the conditional responses

$$Y_{t+j} \mid \mathcal{I}_t^j \sim \mathcal{N}(G_Y(\mathcal{I}_t^j), \sigma^2),$$

where  $G_Y$  models the mean of the conditional response (see right side of Figure 4.2). The response sequence is estimated autoregressively using a GRU-based decoder without teacher forcing (Williams & Zipser, 1989) to ensure model training’s consistency with testing in real-world scenarios (Figure 4.2 and Algorithm 6).

**Treatment prediction** We learn a treatment prediction sub-network parameterized by  $\theta_W$  that takes as input the representation  $\Phi_{t+1}$  and predicts a distribution  $q_{\theta_W}(\omega_{t+1} \mid \Phi_{t+1})$  over the treatment  $W_{t+1}$  by minimizing the negative log-likelihood,

$$\mathcal{L}_W = -\log q_{\theta_W}(\omega_{t+1} \mid \Phi_{t+1}).$$

To assess the quality of the representation in predicting the treatment, the gradient from  $\mathcal{L}_W$  only updates the treatment network parameters  $\theta_W$  and is not backpropagated through the response of the parameters for the representation  $\Phi_{t+1}$  (Algorithm 6).

**Adversarial learning** To create an adversarial game, we update the representation learning parameters, and in the next step, the treatment network  $q_{\theta_W}(\cdot \mid \Phi_{t+1})$  with adverse losses such that the representation  $\Phi_{t+1}$  becomes invariant with respect to the assignment of  $W_{t+1}$ . Different from SOTA models (as highlighted in related work) and in line with our information guidelines principles, learning a balanced representation  $\Phi_{t+1}$  amounts to ensuring  $\Phi_{t+1} \perp\!\!\!\perp W_{t+1}$ , which is equivalent to  $I(\Phi_{t+1}, W_{t+1}) = 0$ . Hence, we minimize the MI as a way to confuse the treatment classifier. Specifically, we minimize an upper bound on  $I(\Phi_{t+1}, W_{t+1})$ , namely the CLUB of MI (Cheng et al., 2020).

$$\begin{aligned}I_{\text{CLUB}}(\Phi(\mathbf{H}_t), W_{t+1}; q_{\theta_W}) &:= \mathbb{E}_{\mathbb{P}_{(\Phi(\mathbf{H}_t), W_{t+1})}} [\log q_{\theta_W}(W_{t+1} \mid \Phi(\mathbf{H}_{t+1}))] \\ &\quad - \mathbb{E}_{\mathbb{P}_{\Phi(\mathbf{H}_t)}} \mathbb{E}_{\mathbb{P}_{W_{t+1}}} [\log q_{\theta_W}(W_{t+1} \mid \Phi(\mathbf{H}_{t+1}))].\end{aligned}\tag{4.9}$$

We use the objective in Equation (4.9) to update the representation learner  $\Phi(\cdot)$  (Brakel & Bengio, 2017; Hjelm et al., 2019). This update aims to minimize the discrepancy between the conditional likelihood of treatments for units sampled from  $\mathbb{P}_{(\mathbf{H}_t, W_{t+1})}$  and the conditional likelihood of treatments under the

assumption of independent sampling from the product of marginals  $\mathbb{P}_{\mathbf{H}_{t+1}} \otimes \mathbb{P}_{W_{t+1}}$ . In practice, we generate samples from the product of marginals by shuffling the treatment  $W_{t+1}$  across the batch dimension similar to Brakel & Bengio (2017); Hjelm et al. (2019).

When minimizing  $\mathcal{L}_W$ ,  $q_{\theta_W}(\omega_{t+1} \mid \Phi_{t+1})$  gets closer to the true conditional distribution  $p(\omega_{t+1} \mid \Phi_{t+1})$ , and, in this case, the objective in Equation (4.9) provides an upper bound of the MI between representation and treatment. We formalize the intuition by adapting the result of Cheng et al. (2020):

**Theorem Thm4.2**

(Cheng et al., 2020) Let  $q_{\theta_W}(\Phi_{t+1}, \omega_{t+1}) := q_{\theta_W}(\omega_{t+1} \mid \Phi_{t+1})p(\Phi_{t+1})$  be the joint distribution induced by  $q_{\theta_W}(\omega_{t+1} \mid \Phi_{t+1})$  over the representation space of  $\Phi_{t+1}$ . If:

$$D_{KL}(p(\Phi_{t+1}, \omega_{t+1}) \parallel q_{\theta_W}(\Phi_{t+1}, \omega_{t+1})) \leq D_{KL}(p(\Phi_{t+1})p(\omega_{t+1}) \parallel q_{\theta_W}(\Phi_{t+1}, \omega_{t+1})),$$

then  $I(\Phi_{t+1}, W_{t+1}) \leq I_{CLUB}(\Phi_{t+1}, W_{t+1}; q)$ .

Based on Theorem Thm4.2, our adversarial training is interpretable and can be explained as follows: the treatment classifier seeks to minimize  $\mathbb{E}_{\mathbb{P}_{(\mathbf{H}_t, W_{t+1})}} [\mathcal{L}_W]$ , which is equivalent to minimizing Kullback-Leibler divergence

$$D_{KL}(p(\Phi_{t+1}, \omega_{t+1}) \parallel q_{\theta_W}(\Phi_{t+1}, \omega_{t+1})).$$

Therefore,  $q_{\theta_W}(\Phi_{t+1}, \omega_{t+1})$  could get closer to  $p(\Phi_{t+1}, \omega_{t+1})$  than, ultimately, to  $p(\Phi_{t+1})p(\omega_{t+1})$ , as we train the network to predict  $W_{t+1}$  from  $\Phi_{t+1}$ . In this case, and by Theorem Thm4.2,  $I_{CLUB}$  provides an upper bound on the MI. Hence, in a subsequent step, we minimize  $I_{CLUB}$  w.r.t the representation parameters, minimizing the MI  $I(\Phi_{t+1}, W_{t+1})$  and achieving balance. We theoretically formulate such behavior by proving in the following theorem that, at the Nash equilibrium of this adversarial game, the representation is exactly balanced across the different treatment regimes provided by  $W_{t+1}$ .

**Theorem Thm4.3**

Let  $t \in \{1, 2, \dots, t_{\max}\}$ ,  $\Phi = \Phi_{\theta_R}$ , and  $q = q_{\theta_W}$  be, respectively, any representation and treatment network. Let  $\mathbb{P}_{\Phi(\mathbf{H}_t)}$  denote the probability distribution over the representation space, and  $\mathbb{P}_{\Phi(\mathbf{H}_t) \mid W_{t+1}}$  its conditional counterpart. Then, there exist  $\Phi^*$  and  $q^*$  such that

$$\Phi^* = \arg \min_{\Phi} I_{CLUB}(\Phi(\mathbf{H}_t), W_{t+1}; q^*),$$

$$q^* = \arg \max_q \mathbb{E}_{\mathbb{P}_{\Phi^*(\mathbf{H}_t)}} [\log q(W_{t+1} \mid \Phi^*(\mathbf{H}_t))].$$

Such an equilibrium holds if and only if

$$\mathbb{P}_{\Phi(\mathbf{H}_t) \mid W_{t+1}=0} = \mathbb{P}_{\Phi(\mathbf{H}_t) \mid W_{t+1}=1} = \dots = \mathbb{P}_{\Phi(\mathbf{H}_t) \mid W_{t+1}=k-1},$$



almost surely.

Since we target multi-timestep forecasting, covariate balancing in the representation space extends beyond  $t + 1$ . For simplicity, we presented it for  $t + 1$ , but in practice, the adversarial game applies the balancing across all forecasting horizons (Algorithm 6). The theorem also holds for other horizons by replacing  $\Phi(\mathbf{H}_t)$  with  $\Phi(\mathbf{H}_{t+j-1})$  and  $W_{t+1}$  with  $W_{t+j}$ , for  $2 \leq j \leq \rho$ .

### 4.5.3 Causal CPC Training

The Causal CPC model is trained in two stages:

**Encoder pretraining:** We first learn an efficient representation of the process history  $\mathbf{C}_t^{\text{enc}}$  by minimizing loss:

$$\mathcal{L}_{\text{enc}} = \mathcal{L}^{\text{CPC}}(\theta_1, \theta_2, \{\Gamma_j\}_{j=1}^\rho) + \mathcal{L}^{(\text{InfoMax})}(\theta_1, \theta_2, \gamma).$$

We train the encoder using only the contrastive terms, as outlined in Algorithm 5. Our primary objective is to ensure that, for each time step  $t$ , the process history  $\mathbf{H}_t$  is predictive of future local features  $\mathbf{Z}_t$ . However, calculating the InfoNCE loss for a batch across all possible time steps  $t = 0, \dots, t_{\max}$  can be computationally demanding.

To address this, we adopt a more efficient approach by uniformly sampling a single time step  $t$  per batch. Subsequently, the corresponding process history  $\mathbf{H}_t$  is contrasted. The sampled  $\mathbf{H}_t$  is then employed as input for the InfoMax objective and randomly partitioned into future  $\mathbf{H}_t^f$  and past  $\mathbf{H}_t^h$  sub-processes.

---

#### Algorithm 5 Pretraining of the encoder

---

**Require:** Encoder parameters  $\theta_{1,2,3}$ , learning rate  $\mu$

- 1: **Input:** data  $\{\mathbf{H}_{i,t_{\max}}, i = 1, \dots, N\}$
- 2: **for**  $p \in \{1, \dots, \text{epoch}_{\max}\}$  **do**
- 3:   **for**  $\mathcal{B} = \{\mathbf{H}_{i,t_{\max}}, i = 1, \dots, |\mathcal{B}|\}$  **do**
- 4:      $\mathbf{Z}_t = \Phi_{\theta_1}([\mathbf{X}_t, W_{t-1}, Y_{t-1}])$  for  $t = 0, \dots, t_{\max}$ .  
      {Contrastive Predictive Coding (CPC) Objective}
- 5:     Choose  $t \sim \mathcal{U}([1, t_{\max} - 1])$ .
- 6:     Compute  $\mathbf{C}_t^{\text{enc}} = \Phi_{\theta_1, \theta_2}(\mathbf{H}_t)$ .
- 7:     Compute  $\mathcal{L}^{\text{CPC}}(\theta_1, \theta_2, \{\Gamma_j\}_{j=1}^\rho)$ .  
      {Information Maximization (InfoMax) Objective}
- 8:     Choose  $t_0 \sim \mathcal{U}([1, t])$ .
- 9:     Compute  $\mathbf{C}_t^{\text{enc}, h} = \Phi_{\theta_1, \theta_2}(\mathbf{H}_t^h)$ ,  $\mathbf{C}_t^{\text{enc}, f} = \Phi_{\theta_1, \theta_2}(\mathbf{H}_t^f)$ .
- 10:    Compute  $\mathcal{L}^{(\text{InfoMax})}(\theta_1, \theta_2, \gamma)$ .  
      {Update Parameters}
- 11:    Update parameters:

$$\theta_{1,2,3} \leftarrow \theta_{1,2,3} - \mu \left( \frac{\partial \mathcal{L}^{\text{CPC}}}{\partial \theta_{1,2,3}} + \frac{\partial \mathcal{L}^{(\text{InfoMax})}}{\partial \theta_{1,2,3}} \right)$$

- 12:   **end for**
  - 13: **end for**
  - 14: **Return:** Trained encoder.
-

**Decoder training:** After pretraining, we fine-tune the encoder by optimizing the factual outcome and treatment networks in the adversarial game from Theorem Thm4.3. Formally:

$$\min_{\theta_R, \theta_Y} \mathcal{L}_{\text{dec}}(\theta_R, \theta_Y, \theta_W) = \mathcal{L}_Y(\theta_R, \theta_Y) + I_{\text{CLUB}}(\Phi_{\theta_R}(\mathbf{H}_t), W_{t+1}; q_{\theta_W}),$$

$$\min_{\theta_W} \mathcal{L}_W(\theta_W, \theta_R) = -\mathbb{E}_{\Phi_{\theta_R}(\mathbf{H}_t)} [\log q_{\theta_W}(W_{t+1} | \Phi_{\theta_R}(\mathbf{H}_t))].$$

The decoder is trained autoregressively without teacher forcing, using the encoder’s output as input (Algorithm 6). We apply a lower learning rate to the encoder than the decoder’s untrained components. This implies that for each time step  $t$ , our GRU-based decoder should predict the future sequence of treatments’ responses  $\hat{Y}_{t+1:t+\rho}$  with its hidden state initialized to the representation  $\Phi_t$  of the historical process up to time  $t$ .

To enhance training efficiency, instead of predicting  $\hat{Y}_{i,t+1:t+\rho}$  for all individuals  $i$  in a batch and for all possible time steps  $t$ , we randomly select  $m$  time indices  $t_{i,1}, \dots, t_{i,m}$  for each individual  $i$ . From these indices, we compute future treatment response sequences  $\hat{Y}_{i,t_{i,1}+1:t_{i,1}+\rho}, \dots, \hat{Y}_{i,t_{i,m}+1:t_{i,m}+\rho}$ . We found that it is enough to train while selecting randomly 10% of the time steps.

## 4.6 Experiments

We compare Causal CPC with SOTA baselines: MSMs Robins et al. (2000), RMSN Lim (2018a), CRN Bica et al. (2020a), G-Net Li et al. (2021), and CT Melnychuk et al. (2022). All models are fine-tuned via a grid search over hyperparameters, including architecture and optimizers. Model selection is based on mean squared error (MSE) on factual outcomes from a validation set, and the same criterion is used for early stopping.

All models were implemented using PyTorch (Paszke et al., 2019) and PyTorch Lightning (Falcon & team, 2019). In contrast to the approach in Melnychuk et al. (2022), we employed early stopping for all models. The stopping criterion was the Mean Squared Error over factual outcomes for a dedicated validation dataset. Specifically, for the Causal CPC encoder, the stopping criterion was determined by the encoder’s validation loss. While all models in the benchmark were trained using the Adam optimizer (Kingma & Ba, 2014), we opted for training Causal CPC (encoder plus decoder without the treatment subnetwork) with AdamW (Loshchilov & Hutter, 2017) due to its observed stability during training. Similar to the common practice in training GAN discriminators, the treatment subnetwork was optimized using SGD with momentum (Sutskever et al., 2013). The CT employed the Exponential Moving Average (EMA) (Yaz4c4 et al., 2019) of parameters to enhance training stability. However, this technique was not applied to Causal CPC, as experimental evidence suggested only marginal improvements. Weight decay was set to zero for all models. Details on hyperparameters selection per model are provided in Appendix B.4. We set  $\sigma = 0.05$  throughout our experiments.

---

**Algorithm 6** Training of the decoder
 

---

1. **Input:** data  $\{\mathbf{H}_{i,t_{\max}}\}_{i=1}^N$ ; pretrained encoder parameters  $\theta_{1,2,3}$  (including  $\theta_R$ ); decoder parameters  $\theta_4, \theta_Y, \theta_W$ ; learning rates  $\mu_{\text{enc}}, \mu_W, \mu_Y$ ; prediction horizon  $\rho$ ; number of random time indices  $m$ .

2. **For**  $p = 1$  to  $\text{epoch}_{\max}$  **do**:

(a) Sample a mini-batch  $\mathcal{B} \subset \{\mathbf{H}_{i,t_{\max}}\}_{i=1}^N$ .

(b) **Encoding phase (forward pass):**

i. For all  $i \in \{1, \dots, |\mathcal{B}|\}$  and  $t = 0, \dots, t_{\max}$ , compute

$$\mathbf{C}_{i,t} = \text{encoder}(\mathbf{H}_{i,t}), \quad \Phi_{i,t} = \Phi_{\theta_R}(\mathbf{H}_{i,t}).$$

(c) **Decoding and prediction phase:**

i. For each  $i = 1, \dots, |\mathcal{B}|$ :

A. Sample  $t_{i,1}, \dots, t_{i,m} \sim \mathcal{U}(\{1, \dots, t_{\max} - \rho\})$ .

B. For each  $t \in \{t_{i,1}, \dots, t_{i,m}\}$ , compute

$$\hat{Y}_{i,t+1:t+\rho}, \hat{W}_{i,t+1:t+\rho}, \Phi_{i,t+1:t+\rho-1} = \text{decoder}(\Phi_{i,t}, \mathbf{V}_i, W_{i,t}, Y_{i,t}, W_{i,t+1:t+\rho}).$$

(d) **Loss calculation:** compute

$$\mathcal{L}_{\text{dec}}(\theta_R, \theta_Y, \theta_W), \quad \mathcal{L}_W(\theta_W, \theta_R).$$

(e) **Parameter updates (sequential optimization):**

i. Update encoder parameters  $\theta_{1,2,3}$  (via  $\theta_R$ ):

$$\theta_{1,2,3} \leftarrow \theta_{1,2,3} - \mu_{\text{enc}} \frac{\partial \mathcal{L}_{\text{dec}}(\theta_R, \theta_Y, \theta_W)}{\partial \theta_{1,2,3}}.$$

ii. Update decoder and outcome parameters  $\theta_4, \theta_Y$ :

$$\theta_4 \leftarrow \theta_4 - \mu_Y \frac{\partial \mathcal{L}_{\text{dec}}(\theta_R, \theta_Y, \theta_W)}{\partial \theta_4}, \quad \theta_Y \leftarrow \theta_Y - \mu_Y \frac{\partial \mathcal{L}_{\text{dec}}(\theta_R, \theta_Y, \theta_W)}{\partial \theta_Y}.$$

iii. Update treatment parameters  $\theta_W$ :

$$\theta_W \leftarrow \theta_W - \mu_W \frac{\partial \mathcal{L}_W(\theta_W, \theta_R)}{\partial \theta_W}.$$

3. **Return** the trained decoder (and updated encoder).

---

### 4.6.1 Experiments with Synthetic Data

**Tumor Growth** We use the Pharmacokinetic-Pharmacodynamic (PK-PD) model Geng et al. (2017) to simulate responses of non-small cell lung cancer patients, following previous works (Lim, 2018a; Bica et al., 2020a; Melnychuk et al., 2022). In this simulation, we model the evolution of tumor volume, denoted as  $V(t)$ , in discrete time, with  $t$  representing the number of days since diagnosis:

$$V(t) = \left( 1 + \underbrace{\Lambda \log \left( \frac{K}{V(t-1)} \right)}_{\text{Tumor Growth}} - \underbrace{\kappa_c C(t)}_{\text{Chemotherapy}} - \underbrace{(\kappa_{rd} Rd(t) + v Rd(t)^2)}_{\text{Radiation}} + \underbrace{e_t}_{\text{Noise}} \right) V(t-1)$$

Here, the model parameters  $\Lambda, K, \kappa_c, \kappa_{rd}, v$  are sampled for each patient based on prior distributions from Geng et al. (2017). Additionally,  $Rd(t)$  represents the radiation dose applied at time  $t$ , and  $C(t)$  denotes the drug concentration.

We introduce confounding into the radiotherapy/chemotherapy treatment assignment by making it dependent on the evolution of the tumor volume. Treatment is simulated using a Bernoulli distribution with probability  $\sigma(\pi_t)$ , where:

$$\pi_t = \frac{\gamma}{D_{\max}} (\bar{D}(t) - \delta)$$

Here,  $\bar{D}(t)$  represents the average tumor diameter over the last 15 days, and  $D_{\max} = 13$  cm is the maximum tumor diameter. The parameter  $\delta$  is set to  $\delta = D_{\max}/2$ . The parameter  $\gamma$  controls the level of time-dependent confounding; a higher value of  $\gamma$  gives more weight to the history of tumor diameter in treatment assignment.

We evaluate our approach on simulated counterfactual trajectories, varying the confounding level via the parameter  $\gamma$ . Unlike Melnychuk et al. (2022), who used larger datasets (10,000 for training, 100 for validation, 1,000 for testing), we use a smaller, more challenging dataset (1,000 for training, 100 for validation, 500 for testing) to reflect real-world data limitations. Similar to Bica et al. (2020a); Melnychuk et al. (2022), counterfactual trajectories are generated with a single treatment per trajectory while the treatment slides over the forecasting range to generate multiple trajectories. We set the prediction horizon to 10 and evaluate two training sequence lengths, 60 and 40, with covariates of dimension 4.

**Results** We tested all models on the cancer simulation data across three confounding levels,  $\gamma = 1, 2, 3$ . Figures 4.3a, 4.3b and 4.3c show the evolution of NRMSE over counterfactual tumor volume as the prediction horizon increases. Causal CPC consistently outperforms all baselines at larger horizons, demonstrating its effectiveness in long-term predictions. This confirms the quality of  $\mathbf{C}_t$  in predicting future components across multiple time steps, capturing the global structure of the process as discussed in Equation (4.5). We report in Table 4.2 the detailed counterfactual errors for Causal CPC and baselines over the cancer simulation dataset, which are responsible for Figure 4.3.

In the more challenging case where the maximum sequence length is 40 (Figures 4.3d, 4.3e and 4.3f), the error evolution remains similar to Figure 4.3a, 4.3b and 4.3c. Our model maintains its advantage,

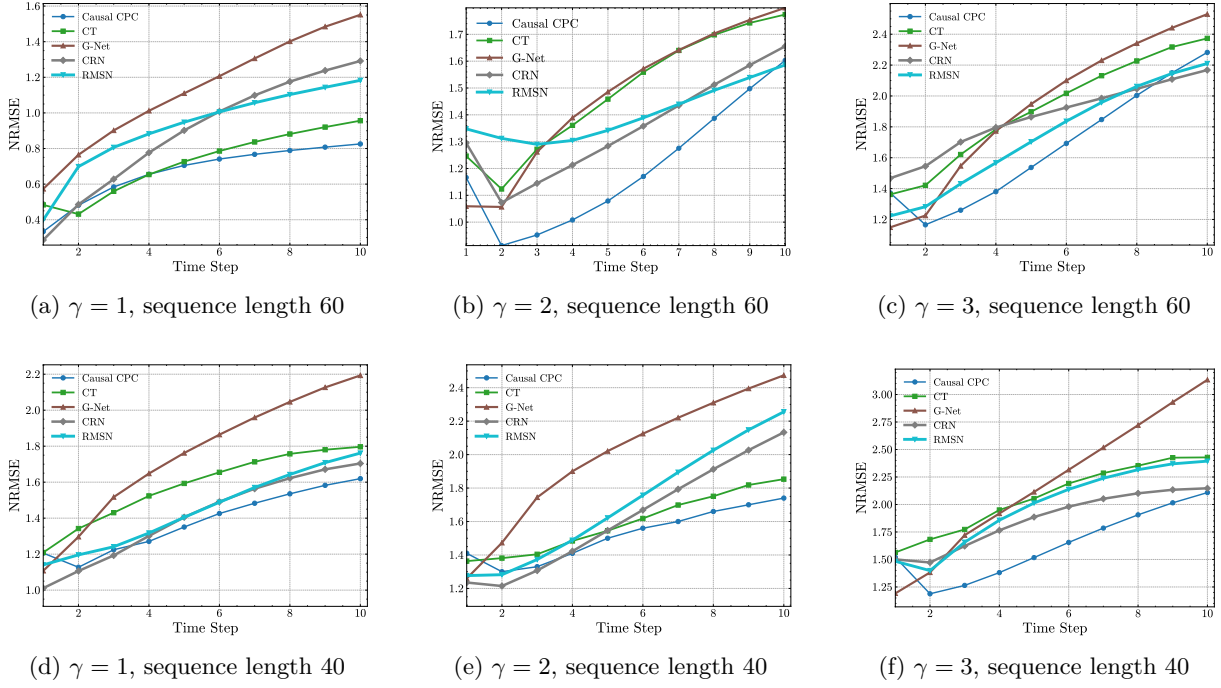


Figure 4.3: Evolution of error NRMSE in estimating counterfactual responses for cancer simulation data. Top: training sequence length 60. Bottom: training sequence length 40. In both cases,  $\rho = 10$ . MSM is excluded due to high prediction errors.

Table 4.2: Results on the synthetic data set with training sequence length 60: mean $\pm$ standard deviation of NRMSE. The best value for each metric is given in bold: smaller is better.

Model	$\gamma = 1$									
	$\rho = 1$	$\rho = 2$	$\rho = 3$	$\rho = 4$	$\rho = 5$	$\rho = 6$	$\rho = 7$	$\rho = 8$	$\rho = 9$	$\rho = 10$
Causal CPC (ours)	<b>0.83<math>\pm</math>0.06</b>	<b>0.86<math>\pm</math>0.09</b>	<b>0.94<math>\pm</math>0.09</b>	<b>0.97<math>\pm</math>0.08</b>	<b>1.03<math>\pm</math>0.10</b>	<b>1.07<math>\pm</math>0.10</b>	<b>1.12<math>\pm</math>0.10</b>	<b>1.17<math>\pm</math>0.09</b>	<b>1.22<math>\pm</math>0.08</b>	<b>1.26<math>\pm</math>0.08</b>
Causal Transformer	0.99 $\pm$ 0.13	0.92 $\pm$ 0.14	0.98 $\pm$ 0.14	1.05 $\pm$ 0.15	1.11 $\pm$ 0.18	1.11 $\pm$ 0.11	1.21 $\pm$ 0.17	1.26 $\pm$ 0.16	1.31 $\pm$ 0.005	1.35 $\pm$ 0.16
G-Net	0.91 $\pm$ 0.15	1.1 $\pm$ 0.16	1.24 $\pm$ 0.16	1.33 $\pm$ 0.17	1.40 $\pm$ 0.18	1.47 $\pm$ 0.19	1.52 $\pm$ 0.18	1.57 $\pm$ 0.22	1.63 $\pm$ 0.22	1.7 $\pm$ 0.25
CRN	0.84 $\pm$ 0.10	0.83 $\pm$ 0.09	0.92 $\pm$ 0.10	1.00 $\pm$ 0.11	1.09 $\pm$ 0.12	1.17 $\pm$ 0.14	1.25 $\pm$ 0.16	1.32 $\pm$ 0.18	1.37 $\pm$ 0.23	1.43 $\pm$ 0.26
RMSN	0.99 $\pm$ 0.13	0.91 $\pm$ 0.04	1.30 $\pm$ 0.65	1.43 $\pm$ 0.76	1.56 $\pm$ 0.83	1.66 $\pm$ 0.88	1.73 $\pm$ 0.91	1.77 $\pm$ 0.89	1.81 $\pm$ 0.88	1.84 $\pm$ 0.86
MSM	1.20 $\pm$ 0.10	1.83 $\pm$ 0.26	2.07 $\pm$ 0.44	2.38 $\pm$ 0.44	2.54 $\pm$ 0.45	2.90 $\pm$ 0.37	3.01 $\pm$ 0.38	3.06 $\pm$ 0.36	3.08 $\pm$ 0.36	3.08 $\pm$ 0.36
Model	$\gamma = 2$									
	$\rho = 1$	$\rho = 2$	$\rho = 3$	$\rho = 4$	$\rho = 5$	$\rho = 6$	$\rho = 7$	$\rho = 8$	$\rho = 9$	$\rho = 10$
Causal CPC (ours)	1.16 $\pm$ 0.22	<b>0.91<math>\pm</math>0.10</b>	<b>0.95<math>\pm</math>0.13</b>	<b>1.00<math>\pm</math>0.15</b>	<b>1.07<math>\pm</math>0.19</b>	<b>1.17<math>\pm</math>0.24</b>	<b>1.27<math>\pm</math>0.25</b>	<b>1.38<math>\pm</math>0.28</b>	<b>1.49<math>\pm</math>0.30</b>	<b>1.60<math>\pm</math>0.34</b>
Causal Transformer	1.24 $\pm$ 0.20	1.13 $\pm$ 0.15	1.27 $\pm$ 0.21	1.36 $\pm$ 0.28	1.44 $\pm$ 0.29	1.55 $\pm$ 0.27	1.64 $\pm$ 0.28	1.69 $\pm$ 0.20	1.74 $\pm$ 0.28	1.77 $\pm$ 0.29
G-Net	<b>1.05<math>\pm</math>0.21</b>	1.05 $\pm$ 0.08	1.26 $\pm$ 0.16	1.38 $\pm$ 0.23	1.48 $\pm$ 0.27	1.57 $\pm$ 0.31	1.64 $\pm$ 0.33	1.70 $\pm$ 0.36	1.75 $\pm$ 0.39	1.8 $\pm$ 0.42
CRN	1.25 $\pm$ 0.25	1.08 $\pm$ 0.06	1.14 $\pm$ 0.12	1.21 $\pm$ 0.17	1.30 $\pm$ 0.21	1.41 $\pm$ 0.25	1.54 $\pm$ 0.32	1.67 $\pm$ 0.41	1.8 $\pm$ 0.51	1.92 $\pm$ 0.63
RMSN	1.47 $\pm$ 0.27	1.33 $\pm$ 0.25	1.30 $\pm$ 0.23	1.33 $\pm$ 0.24	1.38 $\pm$ 0.26	1.45 $\pm$ 0.28	1.52 $\pm$ 0.31	1.60 $\pm$ 0.25	1.67 $\pm$ 0.38	1.75 $\pm$ 0.42
MSM	1.43 $\pm$ 0.27	2.22 $\pm$ 0.53	2.67 $\pm$ 0.63	2.98 $\pm$ 0.70	3.19 $\pm$ 0.74	3.33 $\pm$ 0.77	3.41 $\pm$ 0.79	3.44 $\pm$ 0.25	3.45 $\pm$ 0.78	3.34 $\pm$ 0.77
Model	$\gamma = 3$									
	$\rho = 1$	$\rho = 2$	$\rho = 3$	$\rho = 4$	$\rho = 5$	$\rho = 6$	$\rho = 7$	$\rho = 8$	$\rho = 9$	$\rho = 10$
Causal CPC (ours)	1.37 $\pm$ 0.31	<b>1.16<math>\pm</math>0.27</b>	<b>1.26<math>\pm</math>0.30</b>	<b>1.38<math>\pm</math>0.35</b>	<b>1.53<math>\pm</math>0.40</b>	<b>1.69<math>\pm</math>0.47</b>	<b>1.84<math>\pm</math>0.52</b>	<b>2.00<math>\pm</math>0.51</b>	2.14 $\pm$ 0.61	2.28 $\pm$ 0.66
Causal Transformer	1.36 $\pm$ 0.32	1.42 $\pm$ 0.36	1.62 $\pm$ 0.46	1.78 $\pm$ 0.53	1.89 $\pm$ 0.58	2.01 $\pm$ 0.63	2.13 $\pm$ 0.66	2.22 $\pm$ 0.69	2.31 $\pm$ 0.69	2.37 $\pm$ 0.73
G-Net	<b>1.14<math>\pm</math>0.24</b>	1.22 $\pm$ 0.15	1.54 $\pm$ 0.26	1.77 $\pm$ 0.33	1.94 $\pm$ 0.36	2.09 $\pm$ 0.40	2.23 $\pm$ 0.43	2.34 $\pm$ 0.47	2.44 $\pm$ 0.52	2.52 $\pm$ 0.56
CRN	1.46 $\pm$ 0.29	1.54 $\pm$ 0.38	1.70 $\pm$ 0.48	1.79 $\pm$ 0.53	1.86 $\pm$ 0.92	1.92 $\pm$ 0.58	1.98 $\pm$ 0.59	2.04 $\pm$ 0.61	<b>2.10<math>\pm</math>0.63</b>	<b>2.16<math>\pm</math>0.64</b>
RMSN	1.22 $\pm$ 0.26	1.28 $\pm$ 0.29	1.43 $\pm$ 0.40	1.56 $\pm$ 0.48	1.70 $\pm$ 0.53	1.83 $\pm$ 0.57	1.95 $\pm$ 0.59	2.06 $\pm$ 0.61	2.14 $\pm$ 0.61	2.21 $\pm$ 0.61
MSM	1.70 $\pm$ 0.35	2.73 $\pm$ 0.88	3.22 $\pm$ 1.03	3.25 $\pm$ 1.12	3.71 $\pm$ 1.18	3.85 $\pm$ 1.22	3.91 $\pm$ 1.23	3.95 $\pm$ 1.24	3.96 $\pm$ 1.24	3.94 $\pm$ 1.23

outperforming most baselines in long-term forecasting. However, Causal CPC does not outperform other models in short-term forecasting, a consistent limitation across experiments. Still, the model’s superior long-term performance highlights its potential in applications requiring long-term accuracy. At higher confounding levels, the model does not always outperform SOTA models at certain time steps. This may be due to the low dimensionality of the time-varying components and static covariates,  $\mathbf{F}_t = [\mathbf{V}, \mathbf{X}_t, W_{t-1}, Y_{t-1}]$ , which have only four dimensions. Our model leverages contrastive learning-based regularization to excel on datasets with higher confounding dimensions, as demonstrated on MIMIC-III where  $\mathbf{F}_t$  has 72 dimensions. In this setting, our model consistently outperforms baselines at longer prediction horizons. The occasional underperformance of Causal CPC at the final horizon is due to  $\rho = 10$  being the last contrasted horizon, not an issue specific to  $\rho = 10$ . To support this, we reran all models with a sequence length 60,  $\rho = 15$ , and  $\gamma = 2$ . As shown in Figure 4.4, Causal CPC still outperforms SOTA for horizons beyond  $\rho = 10$  due to the encoder’s retraining, where the InfoNCE loss is computed

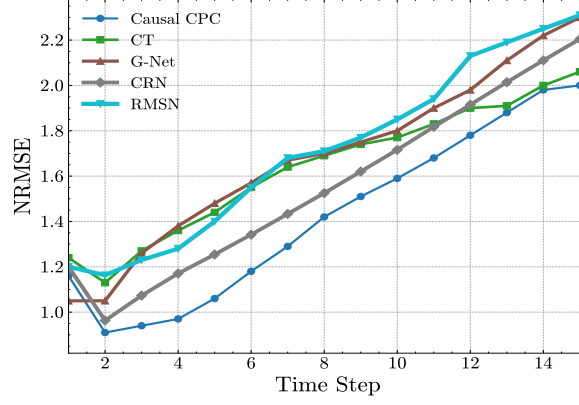


Figure 4.4: Models’ performance for cancer simulation reported by NRMSE for  $\gamma = 2$  and  $\rho = 15$ . The training sequence length is 60.

over all 15 time steps. The last prediction error remains close to SOTA, suggesting that training over larger horizons than initially intended may be beneficial.

#### 4.6.2 Experiments with semi-synthetic and real data

**Semi-synthetic MIMIC-III** We used a semi-synthetic dataset constructed by Melnychuk et al. (2022) based on the MIMIC-III dataset (Johnson et al., 2016), incorporating both endogenous temporal dependencies and exogenous dependencies from observational patient trajectories. Initially, a cohort of 1,000 patients is extracted from the MIMIC-III data, and the simulation proposed by Melnychuk et al. (2022) extends that of Schulam & Saria (2017).

**Step 1: untreated trajectories** Let  $d_y$  be the dimension of the outcome variable, in the case of multiple outcomes, then untreated outcomes, denoted as  $Y_t^{j,(i)}(0), j = 1, \dots, d_y$  are generated for each patient  $i$  within the cohort as

$$Y_t^{j,(i)}(0) = \alpha_{\text{spl}}^j B(t) + \alpha_{\text{gp}}^j g^{j,(i)}(t) + \alpha_{\text{exo}}^j f_{\text{RFF}}^j(\mathbf{X}_t^{(i)}) + \varepsilon_t, \quad \varepsilon_t \sim \mathcal{N}(0, \sigma_\varepsilon^2) \quad (4.10)$$

where the B-spline  $B(t)$  is an endogenous component,  $g^{j,(i)}$  is sampled independently for each patient from a Gaussian process with a Matérn kernel i.e.  $g^{j,(i)} \sim \mathcal{GP}(0, k_{\text{Matérn}})$ , and  $f_{\text{RFF}}^j$  is a Random-Fourier-Features (RFF) draw.

**Step 2: treatment assignment.** To introduce confounding in the treatment assignment, we incorporate current time-varying covariates through a random function  $f_Y^l(\mathbf{X}_t)$  and the average of the subset of the previous  $T_l$  treated outcomes. For  $K$  binary treatments  $\mathbf{W}_t^l, l = 0, \dots, K - 1$ , the assignment mechanism is modeled as follows: let  $\pi_{t,\omega}^{(i)} := \Pr(\mathbf{W}_t^{(i)} = \omega)$  for  $\omega = 0, \dots, K - 1$ . We use a soft-max with confounding

Table 4.3: Results on the MIMIC-III semi-synthetic reported by mean $\pm$ standard deviation of RMSEs. The training sequence length is 100. Smaller is better.

Model	$\rho = 1$	$\rho = 2$	$\rho = 3$	$\rho = 4$	$\rho = 5$	$\rho = 6$	$\rho = 7$	$\rho = 8$	$\rho = 9$	$\rho = 10$
<b>Causal CPC (ours)</b>	0.32 $\pm$ 0.04	0.45 $\pm$ 0.08	0.54 $\pm$ 0.06	0.61 $\pm$ 0.10	<b>0.66<math>\pm</math> 0.10</b>	<b>0.69<math>\pm</math>0.11</b>	<b>0.71<math>\pm</math> 0.11</b>	<b>0.73<math>\pm</math> 0.06</b>	<b>0.75<math>\pm</math> 0.05</b>	<b>0.77<math>\pm</math> 0.10</b>
<b>CT</b>	0.42 $\pm$ 0.38	<b>0.40<math>\pm</math> 0.06</b>	<b>0.52<math>\pm</math> 0.08</b>	<b>0.60<math>\pm</math> 0.005</b>	0.67 $\pm$ 0.10	0.72 $\pm$ 0.12	0.77 $\pm$ 0.13	0.81 $\pm$ 0.14	0.85 $\pm$ 0.16	0.88 $\pm$ 0.17
<b>G-Net</b>	0.54 $\pm$ 0.13	0.72 $\pm$ 0.14	0.85 $\pm$ 0.16	0.96 $\pm$ 0.17	1.05 $\pm$ 0.18	1.14 $\pm$ 0.18	1.24 $\pm$ 0.17	1.33 $\pm$ 0.16	1.41 $\pm$ 0.16	1.49 $\pm$ 0.16
<b>CRN</b>	<b>0.27<math>\pm</math>0.03</b>	0.45 $\pm$ 0.08	0.58 $\pm$ 0.09	0.72 $\pm$ 0.11	0.82 $\pm$ 0.15	0.92 $\pm$ 0.20	1.00 $\pm$ 0.25	1.06 $\pm$ 0.28	1.12 $\pm$ 0.32	1.17 $\pm$ 0.35
<b>RMSN</b>	0.40 $\pm$ 0.16	0.70 $\pm$ 0.21	0.80 $\pm$ 0.19	0.88 $\pm$ 0.17	0.94 $\pm$ 0.16	1.00 $\pm$ 0.15	1.05 $\pm$ 0.14	1.10 $\pm$ 0.14	1.14 $\pm$ 0.13	1.18 $\pm$ 0.13

via outcomes and covariates:

$$\tilde{\eta}_{t,\omega}^{(i)} = \gamma_W^\omega \bar{Y}_{t-1}^{(i)} + \gamma_X^\omega f_Y^\omega(\mathbf{X}_t^{(i)}) + b_\omega, \quad \omega = 0, \dots, K-1, \quad (4.11)$$

$$\eta_{t,0}^{(i)} := 0, \quad \pi_{t,\omega}^{(i)} = \frac{\exp(\eta_{t,\omega}^{(i)})}{\sum_{b=0}^{K-1} \exp(\eta_{t,b}^{(i)})}, \quad (4.12)$$

$$W_t^{(i)} \sim \text{Categorical}(\pi_{t,0}^{(i)}, \dots, \pi_{t,K-1}^{(i)}), \quad (4.13)$$

where  $\bar{Y}_{t-1}^{(i)} = \frac{1}{T_0} \sum_{s=t-T_0}^{t-1} Y_s^{j^*,(i)}$ .

**Step 3: cumulative treatment effect.** With window length  $w$  and per-label effect sizes  $\beta_{\omega j}$ , we define treatment effects as

$$\tau_{t,\omega}^{j,(i)} = \sum_{s=t-w}^t \frac{\mathbf{1}_{\{W_s^{(i)}=\omega\}} \pi_{s,\omega}^{(i)} \beta_{\omega j}}{(w-s)^2}, \quad \omega = 0, \dots, K-1. \quad (4.14)$$

**Step 4: observed outcomes (consistency).**

$$Y_t^{j,(i)} = Y_t^{j,(i)}(0) + \sum_{\omega=0}^{K-1} \mathbf{1}_{\{W_t^{(i)}=\omega\}} \tau_{t,\omega}^{j,(i)}. \quad (4.15)$$

Similar to the cancer simulation, the training data consisted of relatively few sequences (500 for training, 100 for validation, and 400 for testing). Table 4.3 presents counterfactual predictions' mean and standard deviation across multiple horizons ( $\rho = 10$ ). Counterfactual trajectories are generated so that treatment is generated randomly at each time step. As in the tumor growth experiments, we tested two maximum sequence lengths, 100 and 60, to assess the models' robustness for long-horizon forecasting.

**Results** Causal CPC consistently outperformed the baselines, especially at larger horizons, both with a sequence length of 100 and a reduced length of 60 (Figures 4.3, 4.5). Its superior performance at longer horizons is likely due to the high number of covariates, making it well-suited to contrastive-based training. We also tested the models with 800/200/200 individuals for training/validation/testing, as in Melnychuk et al. (2022) (Appendix B.1.1), where Causal CPC achieved SOTA results comparable to CT but with much shorter training and prediction times.

**Computational Efficiency and Model Complexity** Efficient execution is crucial for practical deployment, especially with periodic retraining. Beyond training, challenges arise in evaluating multiple counterfactual trajectories per individual, which grow exponentially with the forecasting horizon as  $K^\rho$ , where  $K$  is the number of possible treatments. This is particularly relevant when generating multiple treatment plans, such as minimizing tumor volume. Tables 4.4 and 4.5 show the models' complexity

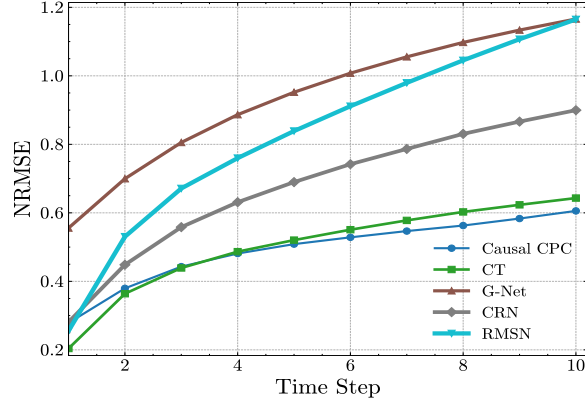


Figure 4.5: Performance for MIMIC II semi-synthetic reported by RMSE over 10 forecasting horizons. The sequence training length is 60.

(number of parameters) and running time, split between model fitting and prediction for cancer simulation data and MIMIC-III. Causal CPC is highly efficient during prediction due to its simple 1-layer GRU, similar to CRN (1-layer LSTM), while also outperforming it. In contrast, CT is less efficient due to its transformer architecture and teacher forcing, which requires recursive data loading during inference. G-Net also has longer prediction times due to Monte Carlo sampling. Overall, Causal CPC strikes a strong balance between accuracy and efficiency, making it well-suited under constrained resources.

Table 4.4: Models complexity and the running time averaged over five seeds. Results are reported for tumor growth simulation ( $\gamma = 1$ ). Hardware: GPU-1xNVIDIA Tesla M60.

Model	Trainable parameters (k)	Training time (min)	Prediction time (min)
Causal CPC (encoder + decoder)	8.2	16± 3	4 ± 1
CT	11	12± 2	30± 3
G-Net	1.2	2 ± 0.5	35 ± 3
CRN	5.2	13± 2	4± 1
RMSN	1.6	22± 2	4± 1
MSM	<0.1	1±0.5	1±0.5

Table 4.5: The number of parameters to train for each model after hyper-parameters fine-tuning and the corresponding running time averaged over five seeds. Results are reported for semi-synthetic MIMIC-III data; the processing unit is GPU-1 x NVIDIA Tesla M60 .

MODEL	TRAINABLE PARAMETERS (K)	TRAINING TIME (MIN)	PREDICTION TIME (MIN)
Causal CPC (ours)	<b>9.8</b>	12±2	<b>4±1</b>
Causal Transformer	12	14±1	38±2
G-Net	14.7	<b>7±1</b>	40±3
CRN	15.1	21±2	5±1
RMSN	20	48±4	5±1

**Real MIMIC-III Data** We evaluated our model on real MIMIC-III data, where counterfactual trajectories cannot be assessed due to the absence of observed counterfactual responses. However, performance can still be measured by forecasting factual (observed) responses over time. Our model estimates responses for each individual based on their observed treatment trajectory. As shown in Figure 4.6, Causal CPC consistently outperforms all baselines, especially at larger horizons, demonstrating its robustness and effectiveness in real-world settings.



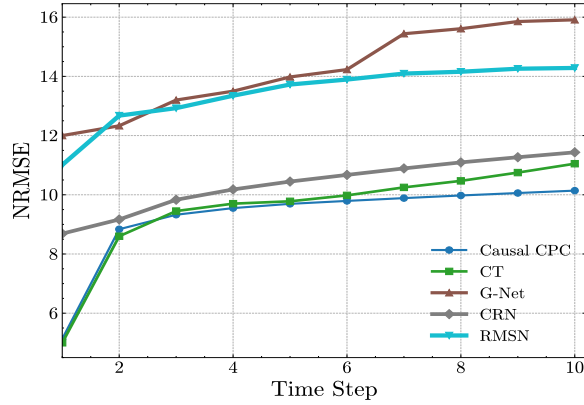


Figure 4.6: Factual estimation errors for baselines for Real MIMIC-III data reported by RMSE. The training sequence length is 100.

## 4.7 Discussion

**Why does Causal CPC outperform SOTA at large horizons?** Our context  $\mathbf{C}_t^{\text{enc}}$  is designed to capture shared information across future representations, particularly covariates, by minimizing the InfoNCE loss over multiple time steps (Equation 4.1). As shown in Equation (4.5), minimizing  $\mathcal{L}^{\text{CPC}}$  maximizes shared information between the context and future components, helping capture the *global structure* of the process. This is especially beneficial for counterfactual regression over long horizons, explaining the model’s superior performance. However, it may not consistently outperform SOTA in shorter-term predictions due to its focus on long-term dependencies.

**Short-term Counterfactual Regression** While our model is designed for long-term predictions, it may not consistently outperform SOTA for short-horizon tasks. However, the use of contrastive loss, particularly InfoNCE (Equation 4.4), suggests potential adaptability to balance both short- and long-term predictions without retraining. A trade-off could be achieved by adjusting the contrastive term weights across time steps in Equation (4.4), which we leave for future work.

**Ablation study** We examined the model’s performance in various configurations—full model, without CPC, and without InfoMax. Table 4.6 shows that removing either term reduces counterfactual accuracy across all horizons, underscoring their significance. Additionally, replacing our ICLUB objective with CDC loss (Melnychuk et al., 2022) or removing balancing increases errors. We report the detailed experimental results over MIMIC-III in Table 4.8 and for cancer simulation in Table 4.6.

Table 4.6: Ablation study with NRMSE averaged across ( $1 \leq \rho \leq 10$ ) for cancer simulation ( $\gamma = 1$ ) and MIMIC-III.

Model	Cancer_Sim	MIMIC-III
Causal CPC (Full)	<b>1.05</b>	<b>0.62</b>
Causal CPC (w/o $\mathcal{L}^{\text{InfoNCE}}$ )	1.07	0.68
Causal CPC (w/o $\mathcal{L}^{\text{InfoMax}}$ )	1.13	0.74
Causal CPC (w CDC loss)	1.07	0.73
Causal CPC (w/o balancing)	1.08	0.69

**What About Using Other MI Lower Bounds?** Other than InfoNCE, the MINE (Belghazi et al., 2018) leverages the relationship between MI and the KL divergence. MI can be expressed as the KL

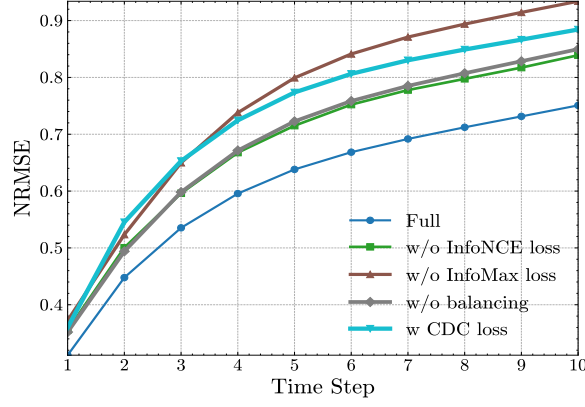


Figure 4.7: Ablation study of Causal CPC for MIMIC-III dataset. RMSE is reported for 10 forecasting horizons. Smaller is better.

Table 4.7: Results of the ablation study on the synthetic data set: mean $\pm$ standard deviation of NRMSE. The best value for each metric is given in bold: smaller is better.

Model	$\rho = 1$	$\rho = 2$	$\rho = 3$	$\rho = 4$	$\rho = 5$	$\rho = 6$	$\rho = 7$	$\rho = 8$	$\rho = 9$	$\rho = 10$
<b>CAUSAL CPC (FULL)</b>	<b>0.83 <math>\pm</math> 0.06</b>	<b>0.86 <math>\pm</math> 0.06</b>	0.94 $\pm$ 0.09	<b>0.97 <math>\pm</math> 0.08</b>	<b>1.03 <math>\pm</math> 0.10</b>	<b>1.07 <math>\pm</math> 0.10</b>	<b>1.12 <math>\pm</math> 0.10</b>	<b>1.17 <math>\pm</math> 0.06</b>	<b>1.22 <math>\pm</math> 0.08</b>	<b>1.26 <math>\pm</math> 0.08</b>
Causal CPC (w/o $\mathcal{L}^{(InfoNCE)}$ )	0.84 $\pm$ 0.04	0.91 $\pm$ 0.07	0.95 $\pm$ 0.07	0.99 $\pm$ 0.09	<b>1.03 <math>\pm</math> 0.10</b>	1.10 $\pm$ 0.07	1.15 $\pm$ 0.14	1.20 $\pm$ 0.14	1.23 $\pm$ 0.14	1.28 $\pm$ 0.15
Causal CPC (w/o $\mathcal{L}^{(InfoMax)}$ )	0.84 $\pm$ 0.04	0.86 $\pm$ 0.09	<b>0.91 <math>\pm</math> 0.08</b>	0.99 $\pm$ 0.10	1.07 $\pm$ 0.08	1.16 $\pm$ 0.08	1.24 $\pm$ 0.10	1.31 $\pm$ 0.12	1.38 $\pm$ 0.08	1.46 $\pm$ 0.10
Causal CPC (w CDC loss)	<b>0.83 <math>\pm</math> 0.02</b>	0.89 $\pm$ 0.07	0.96 $\pm$ 0.07	1.03 $\pm$ 0.07	1.07 $\pm$ 0.08	1.10 $\pm$ 0.07	1.13 $\pm$ 0.10	1.18 $\pm$ 0.09	1.24 $\pm$ 0.11	1.28 $\pm$ 0.11
Causal CPC (w Balancing)	0.84 $\pm$ 0.04	0.88 $\pm$ 0.05	0.97 $\pm$ 0.05	1.04 $\pm$ 0.07	1.08 $\pm$ 0.10	1.13 $\pm$ 0.08	1.15 $\pm$ 0.14	1.20 $\pm$ 0.10	1.25 $\pm$ 0.08	1.29 $\pm$ 0.12

Table 4.8: Results on MIMIC-III semi-synthetic data set: mean $\pm$ standard deviation of NRMSE. The best value for each metric is given in bold: smaller is better.

Model	$\rho = 1$	$\rho = 2$	$\rho = 3$	$\rho = 4$	$\rho = 5$	$\rho = 6$	$\rho = 7$	$\rho = 8$	$\rho = 9$	$\rho = 10$
<b>Causal CPC (FULL)</b>	<b>0.32 <math>\pm</math> 0.04</b>	<b>0.45 <math>\pm</math> 0.08</b>	<b>0.54 <math>\pm</math> 0.06</b>	<b>0.61 <math>\pm</math> 0.10</b>	<b>0.66 <math>\pm</math> 0.10</b>	<b>0.69 <math>\pm</math> 0.11</b>	<b>0.71 <math>\pm</math> 0.11</b>	<b>0.73 <math>\pm</math> 0.06</b>	<b>0.75 <math>\pm</math> 0.05</b>	<b>0.77 <math>\pm</math> 0.10</b>
Causal CPC (w/o $\mathcal{L}^{(InfoNCE)}$ )	0.35 $\pm$ 0.04	0.50 $\pm$ 0.05	0.59 $\pm$ 0.06	0.66 $\pm$ 0.06	0.71 $\pm$ 0.08	0.75 $\pm$ 0.06	0.77 $\pm$ 0.07	0.79 $\pm$ 0.08	0.81 $\pm$ 0.07	0.83 $\pm$ 0.07
Causal CPC (w/o $\mathcal{L}^{(InfoMax)}$ )	0.36 $\pm$ 0.02	0.53 $\pm$ 0.03	0.64 $\pm$ 0.04	0.71 $\pm$ 0.05	0.77 $\pm$ 0.05	0.77 $\pm$ 0.05	0.83 $\pm$ 0.05	0.86 $\pm$ 0.05	0.88 $\pm$ 0.08	0.90 $\pm$ 0.05
Causal CPC (CDC loss)	0.36 $\pm$ 0.02	0.54 $\pm$ 0.03	0.65 $\pm$ 0.05	0.72 $\pm$ 0.05	0.77 $\pm$ 0.05	0.70 $\pm$ 0.04	0.83 $\pm$ 0.04	0.85 $\pm$ 0.03	0.86 $\pm$ 0.03	0.88 $\pm$ 0.08
Causal CPC (w/o balancing)	0.35 $\pm$ 0.03	0.50 $\pm$ 0.05	0.60 $\pm$ 0.06	0.67 $\pm$ 0.06	0.72 $\pm$ 0.06	0.76 $\pm$ 0.06	0.78 $\pm$ 0.06	0.80 $\pm$ 0.06	0.83 $\pm$ 0.06	0.85 $\pm$ 0.06

divergence between the joint distribution and the product of marginals:

$$I(X; Z) := D_{KL}(\mathbb{P}_{(X,Z)} || \mathbb{P}_X \otimes \mathbb{P}_Z)$$

MINE employs the Donsker-Varadhan representation (Donsker & Varadhan, 1983) of the KL divergence:

$$D_{KL}(\mathbb{P} || \mathbb{Q}) = \sup_{T: \Omega \rightarrow \mathbb{R}} E_{\mathbb{P}}[T] - \log(E_{\mathbb{Q}}[e^T]) \quad (4.16)$$

Here, the supremum is over all functions  $T$  where the expectations exist. For a specific class of functions  $\mathcal{F}$ , potentially represented by a class of neural networks, we obtain the lower bound:

$$D_{KL}(\mathbb{P} || \mathbb{Q}) \geq \sup_{T \in \mathcal{F}} E_{\mathbb{P}}[T] - \log(E_{\mathbb{Q}}[e^T]) \quad (4.17)$$

In practice, we maximize

$$\hat{f}_{\gamma}^{\text{MINE}}(\mathbb{P} || \mathbb{Q}) = E_{\mathbb{P}}[T_{\gamma}] - \log(E_{\mathbb{Q}}[e^{T_{\gamma}}]),$$

where  $T_{\gamma}$  is a discriminator parameterized by  $\gamma$ , representing neural network parameters. The MINE estimator is a strongly consistent estimator of the true MI (Theorem 2 Belghazi et al. (2018)).

Alternatively, the  $f$ -divergence representation of  $D_{KL}$  Nowozin et al. (2016) allows us to derive another

lower bound on MI known as NWJ (Nguyen et al., 2010):

$$D_{\text{KL}}(\mathbb{P} \parallel \mathbb{Q}) \geq \sup_{T \in \mathcal{F}} \mathbb{E}_{\mathbb{P}}[T] - \log(\mathbb{E}_{\mathbb{Q}}[e^{T-1}]).$$

This results in the estimator

$$\hat{I}_{\gamma}^{\text{NWJ}}(\mathbb{P}, \mathbb{Q}) = \mathbb{E}_{\mathbb{P}}[T_{\gamma}] - \log(\mathbb{E}_{\mathbb{Q}}[e^{T_{\gamma}-1}]).$$

We benchmarked three variational lower-bound objectives—InfoNCE (Oord et al., 2018), NWJ (Nguyen et al., 2010), and MINE (Belghazi et al., 2018)— for both CPC and InfoMax on MIMIC-III data, finding that InfoNCE yielded the best results (Table 4.9). The InfoNCE objective performs better with notable error reduction at large horizons in all cases. The superiority of InfoNCE can be understood through the following qualities:

- (i) **Lower gradient variance.** NWJ and MINE rely on estimating an unnormalised density ratio whose variance explodes in high dimension (Poole et al., 2019b); InfoNCE’s soft-max normaliser acts as an implicit variance reducer, producing stabler gradients in long recurrent chains (Poole et al., 2019b; Song & Ermon, 2020).
- (ii) **Tighter bound with many negatives.** The InfoNCE bound tightens logarithmically with the number of samples (Oord et al., 2018; Wu et al., 2022); a single mini-batch of time-series data already supplies dozens of negatives (other patients, other timesteps), giving InfoNCE an automatic advantage.
- (iii) **Objective alignment with forecasting.** InfoNCE originates from CPC, whose loss is designed to keep exactly those latent features that maximise predictability of the future sequence (Oord et al., 2018). This alignment transfers directly to long-horizon prediction and aids in counterfactual regression.

Table 4.9: Results of NWJ and MINE MI lower bounds when used for CPC and InfoMax for MIMIC-III semi-synthetic data set: mean±standard deviation of NRMSE. The best value for each metric is given in bold: smaller is better.

Model	$\rho = 1$	$\rho = 2$	$\rho = 3$	$\rho = 4$	$\rho = 5$	$\rho = 6$	$\rho = 7$	$\rho = 8$	$\rho = 9$	$\rho = 10$
<b>Original Model</b>	<b>0.34± 0.04</b>	<b>0.45± 0.08</b>	<b>0.54±0.06</b>	<b>0.61 ± 0.10</b>	<b>0.66± 0.10</b>	<b>0.69±0.11</b>	<b>0.71± 0.11</b>	<b>0.73± 0.06</b>	<b>0.75 ± 0.05</b>	<b>0.77± 0.10</b>
<b>CPC with NWJ</b>	<b>0.34± 0.04</b>	0.48± 0.05	0.58± 0.06	0.66± 0.07	0.71± 0.08	0.75± 0.07	0.78± 0.07	0.81± 0.06	0.84± 0.06	0.87± 0.06
<b>CPC with MINE</b>	0.35± 0.03	0.50± 0.05	0.61± 0.04	0.69± 0.04	0.75± 0.04	0.79± 0.03	0.82± 0.03	0.85± 0.02	0.88± 0.02	0.91± 0.02
<b>InfoMax with NWJ</b>	0.42± 0.08	0.56± 0.04	0.69± 0.07	0.77± 0.08	0.83± 0.09	0.87± 0.09	0.90± 0.09	0.92± 0.09	0.94± 0.08	0.96± 0.08
<b>InfoMax with MINE</b>	0.37± 0.05	0.52± 0.03	0.65± 0.06	0.73± 0.8	0.80± 0.10	0.84± 0.11	0.87± 0.11	0.89± 0.10	0.91± 0.10	0.93± 0.09

**Falsifiability Test** This study assumes sequential ignorability, common in causal inference Lim (2018a); Bica et al. (2020a); Li et al. (2021); Melnychuk et al. (2022). To assess robustness, we performed a falsifiability test by omitting certain confounders during training while they remained in MIMIC-III data construction: we mask two confounders from the inputs of the benchmark models, namely sodium and glucose measurements. As seen in Table 4.10, violating sequential ignorability (i.e. results of Table 4.3) increased prediction errors for Causal CPC, CT, and CRN, though RMSN was less affected but underperformed at  $\rho \geq 2$ . Despite this, Causal CPC maintained its lead at larger horizons, demonstrating

strong encoding of long-term dependencies.

Table 4.10: Results on the MIMIC-III when sequential ignorability is violated reported by RMSEs

Model	$\rho = 1$	$\rho = 2$	$\rho = 3$	$\rho = 4$	$\rho = 5$	$\rho = 6$	$\rho = 7$	$\rho = 8$	$\rho = 9$	$\rho = 10$
Causal CPC	0.44± 0.04	0.56± 0.07	0.66±0.07	0.73 ± 0.08	0.78± 0.08	0.83±0.06	0.86± 0.10	0.88± 0.08	0.91 ± 0.08	0.95± 0.07
Causal Transformer	0.34±0.07	0.48±0.07	0.60±0.07	0.68±0.06	0.75± 0.06	0.80±0.07	0.86± 0.09	0.91±0.11	0.95 ±0.13	1.00 ±0.15
CRN	0.40± 0.07	0.54± 0.09	0.70± 0.09	0.84± 0.09	0.97± 0.09	1.08± 0.13	1.18± 0.16	1.26± 0.19	1.33± 0.21	1.39± 0.23
RMSN	0.38± 0.08	0.67± 0.21	0.78± 0.16	0.84± 0.14	0.91± 0.14	0.98± 0.15	1.04± 0.16	1.09± 0.18	1.15± 0.19	1.20± 0.23

**Tightness of Mutual Information (MI) Upper Bounds** Estimating MI bounds for high-dimensional variables is challenging and expensive (Rainforth et al., 2018; Poole et al., 2019b), often limited to low-dimensional inputs or Gaussian assumptions. In MI-constrained models, batch size is crucial. As shown in Equation (4.3), increasing the batch size  $\mathcal{B}$  tightens the lower bound via  $\log(|\mathcal{B}|)$ . To balance memory and performance, we chose batch sizes of 256 for the encoder and 128 for the decoder. While these bounds may not be perfectly tight, mutual information and self-supervision biases significantly enhance performance, as ablation studies confirm. Other MI estimators like NWJ and MINE (Nguyen et al., 2010; Belghazi et al., 2018) did not improve performance; our initial setup consistently performed better (Table 4.9).

**Extending Causal CPC to Continuous Treatment** Our approach could be extended to continuous treatments by replacing the treatment classifier with a regressor. Since the method maximizes likelihood, the equilibrium in Theorem Thm4.3 remains valid. However, in practice, continuous treatments will be represented by a single dimension, unlike discrete treatments with  $K$ -dimensional one-hot encoding. This risks losing important treatment information in counterfactual predictions. A more straightforward adaptation to our model could involve discretizing continuous treatments.

**Conclusion** We have introduced a novel approach to long-term counterfactual regression that combines RNN with CPC, achieving SOTA results without the need for complex transformer models. By prioritizing computational efficiency, we incorporate regularization techniques based on contrastive losses and guided by mutual information principles. Our method consistently outperforms existing models in counterfactual estimation on both synthetic and real-world datasets, marking the first application of CPC in the domain of causal inference.

Future research directions could explore improving the interpretability of counterfactual predictions by integrating Shapley values into temporal regression models. Given our reliance on causal graphs, investigating *Causal Shapley Values* (Heskes et al., 2020) may provide deeper insights into the influence of confounders over time. Additionally, there is a growing need for uncertainty-aware models (De Brouwer et al., 2022; Jesson et al., 2020; Yin et al., 2024), particularly tailored for longitudinal data, to enhance the reliability and transparency of predictions within our causal framework.

## Chapter 5

# Toward a More Transparent Causal Representation Learning

### 5.1 Introduction

High-dimensional data is ubiquitous across real-world domains, motivating interest in learning high-level *causal* latent factors that influence low-level observable variables, a pursuit known as causal representation learning (CRL) (Schölkopf et al., 2021). In CRL, latent factors are endowed with a causal structure, typically an SCM (Section 2.3). Recent advances in CRL have focused on disentangling latent variables, either independently or conditionally upon auxiliary variables, such as temporal indices or categorical labels (Yao et al., 2022; Komanduri et al., 2023; Song et al., 2023). Most successful examples to date occur in perceptual domains like images, videos, and text, where researchers investigate how abstract causal factors influence low-level data through: (1) *unsupervised factor disentanglement* (Chen et al., 2016; Higgins et al., 2017); (2) *concept-driven interpretability approaches* (Adebayo et al., 2018; Alvarez Melis & Jaakkola, 2018; Ghorbani et al., 2019; Koh et al., 2020; Do & Tran, 2020); (3) *temporal and video-specific latent variable analysis* (Dong et al., 2017; Kumar et al., 2018; Wang et al., 2024; Longa & Henriques, 2024). In contrast, discovering causal structures in high-dimensional, temporally evolving *tabular* data remains notably challenging (Hasan et al., 2023; Somvanshi et al., 2024).

Consider, for instance, retail transaction data, where each customer’s purchasing behavior is represented by a high-dimensional vector  $\mathbf{X}_t := [\mathbf{X}_t^1, \dots, \mathbf{X}_t^{d_x}] \in \mathbb{R}^{d_x}$  capturing thousands of product states at a given time  $t$ : each dimension  $j \in \llbracket 1, d_x \rrbracket$ ,  $\mathbf{X}_t^j$  may represent the number of purchases of product  $j$  at time  $t$ . Extracting causal relationships at this granular scale is computationally prohibitive and often leads to complex, uninterpretable results, limiting real-world applicability. A more promising approach is to abstract causal structures to a coarser level  $\mathbf{Z}_t \in \mathbb{R}^{d_z}$  with  $d_z \ll d_x$  (Beckers & Halpern, 2019; Beckers et al., 2020; Xia & Bareinboim, 2024). Typically, the causal structure governs the temporal process over

$(\mathbf{Z}_t)_{t \geq 1}$  through an SCM (Definition Def2.16):

$$\begin{aligned} \mathbf{X}_t &= f(\mathbf{Z}_t), \\ \mathbf{Z}_t^j &= g_j\left(\{\mathbf{Z}_{t-s}^k \mid \mathbf{Z}_{t-s}^k \in Pa(\mathbf{Z}_t^j), s = 1, \dots, \rho\}, \epsilon_t^j\right), \quad j \in \llbracket 1, d_z \rrbracket. \end{aligned} \tag{5.1}$$

where  $\mathbb{G} := \{g_1, \dots, g_{d_z}\}$  is the set of stationary structural functions ( $\mathbb{G}$  is fixed over time),  $\epsilon_t^j$  is the noise term,  $\rho$  is the maximum lag, and the function  $f$ , often called the generative, mixing, or decoding function, maps latent representations back to observed features. Because causal structure now resides at the abstract latent level, the challenge of interpretability becomes acute: it remains unclear precisely how each latent temporal factor  $\mathbf{Z}_t^j$  corresponds to particular subsets of the observed variables  $\mathbf{X}_t$ . Clarifying these latent-to-observed relationships is thus essential to ensuring transparency, facilitating a shift of CRL from academic benchmarks to trusted and practically useful tools for real-world decision-making.

**Limitations of Existing Structural Assumptions** To put our proposal in context, we now review two common structural assumptions used in the literature of both causal and non-causal models:

**1. Single-parent decoding** Boussard et al. (2023); Brouillard et al. (2024) used such an assumption in CRL models for time-series climate data to enforce that each observed variable coordinate  $\mathbf{X}_t^j$  is generated by only a single latent parent  $\mathbf{Z}_t^{k(j)}$  (Figure 5.1a). However, the single-parent assumption is highly restrictive, as it forbids any observed variable from being generated by a mixture of latent factors. This is problematic in settings where causal dependencies among observed features arise from *multiple* latent influences.

**2. Anchor/Pure features** In a non-causal and static VAE frameworks, Arora et al. (2013a); Bing et al. (2020); Chen et al. (2020); Moran et al. (2021); Bing et al. (2022) used a sparsity constraint and require that each latent variable  $\mathbf{Z}_t^k$  has at least a predefined number of *anchor features*, i.e., observed features that depend exclusively on  $\mathbf{Z}_t^k$  (e.g., two in Moran et al. (2021) as in Figure 5.1b).

Unlike single-parent decoding, this assumption is weaker: it allows the remaining children of  $\mathbf{Z}_t^k$  to be generated by multiple latent factors, or not at all. While the anchor/pure variable assumption facilitates provable identifiability in latent variable models, including topic models (Arora et al., 2013b; 2018), nonnegative matrix factorizations (Gillis, 2020), it imposes stringent structural constraints that are rarely satisfied in complex, high-dimensional data. In practice, anchor factorizations often do not exist, and even when the data exhibits low-rank structure, the required separability condition may be violated. Empirical studies have shown that statistical tests frequently reject anchor compatibility in real-world corpora, such as FOMC2 (Freyaldenhoven et al., 2025). Furthermore, small amounts of measurement noise, sampling variability, or preprocessing (e.g., normalization) can break the purity condition, leading to misidentification of anchors (Huang et al., 2016; Chen et al., 2022).

**Modular Influence with Soft Jacobian Constraints** The limitations of rigid structural assumptions call for a new approach that preserves interpretability and identifiability without restricting the generative

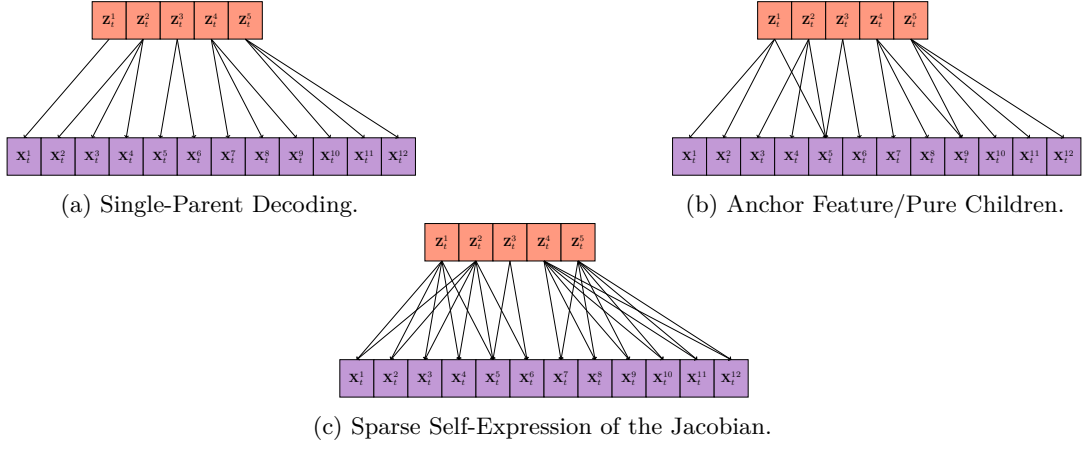


Figure 5.1: Comparison of three structural assumptions over the generation process: single-parent decoding, anchor feature, and sparse self-expression assumption. Here, we assume  $d_x = 12$  and  $d_z = 5$ .

model. Rather than enforcing hard constraints like single-parent decoding (Boussard et al., 2023; Brouillard et al., 2024) or anchor features (Moran et al., 2021), we impose a *soft sparsity constraint* directly on the Jacobian of the decoder. Our key idea is to regularize the Jacobian using a *self-expressiveness condition* following *Sparse Subspace Clustering (SSC)* (Elhamifar & Vidal, 2013): each gradient vector (column of the Jacobian) is encouraged to lie in the span of a small number of others through a sparsity constraint. Hence, the column space of the Jacobian decomposes into a union of low-dimensional subspaces, where each subspace reflects a group of observed variables jointly governed by a subset of latent causes. The result is a modular, interpretable mapping from latent to observed space, recovering overlapping causal groups from gradient structure without relying on exclusivity or hard-coded sparsity.

This work does not introduce a new CRL model per se, but instead addresses the "*so what?*" question that arises once a CRL model has been defined. Specifically, we ask how to effectively communicate the results of causal representation learning on complex high-dimensional data and how to build confidence in the learned causal concepts by transparently linking them back to the original high-dimensional feature space. To this end, we propose a regularization technique that is *model-agnostic* and can be seamlessly integrated into any CRL model backbone. Our approach is twofold:

- We impose a structural sparsity constraint on the decoding function, that is, the mixing function that maps latent causal variables to low-level observed variables.
- A key consequence of this sparsity is that many observed features become associated with only one or a few latent factors. This induces a clustering of the observed variables, which we exploit to enhance model transparency. By analyzing the content and coherence of these clusters, we can relate them to semantically meaningful labels not used during training. For example, in purchase data, products and, therefore, dimensions of  $\mathbf{X}_t$  may be grouped into categories of products. It is also common in retail to have products clustered in multiple hierarchical groups, for e.g., categories may contain subcategories of products.

While prior work has established identifiability of latent representations under statistical or structural assumptions (Hyvärinen & Pajunen, 1999; Locatello et al., 2019; Khemakhem et al., 2020), the identifiability

of induced structure over observed variables has received far less attention. Our framework addresses this gap. Via a Jacobian-based structural sparsity, we establish a provable recovery of disjoint and overlapping groupings of observed features that are consistent with explicit graphical clustering rules defined by the latent-to-observed generative map.

**Main Contributions** We provide formal guarantees characterizing when this modular structure can be recovered. Specifically, we establish conditions under which one can recover with high probability (w.h.p) disjoint clusters of observed variables via SSC (Theorem Thm5.2 and Proposition Prop5.1). Furthermore, we extend the analysis to the overlapping case by showing that methods such as *Spectral Algorithm with Additive Clustering (SAAC)* (Panov et al., 2017; Kaufmann et al., 2018) and *Symmetric Nonnegative Matrix Factorization (SymNMF)* (Kuang et al., 2012; 2015; Zhang & Liu, 2022) can recover overlapping groupings of observed variables with bounded misclassification error (Theorem Thm5.3). These groupings are interpretable: they arise directly from the latent-to-observed map and reflect the underlying graphical structure of the generative process. To the best of our knowledge, no prior work in CRL provides formal identifiability results for the modular organization of observed variables. This approach connects identifiability in the latent space with interpretability at the observational level, offering a complementary perspective on structure discovery in CRL. We also provide robustness guarantees for our framework by proving that the self-expression loss generalizes under finite samples and remains stable under Jacobian perturbations. These results (Theorem Thm5.4, Proposition Prop5.3) ensure that the learned clusters are reliable in the presence limited data and noisy access to the Jacobian. Finally, we demonstrate the practical effectiveness of our method through simulations where it substantially outperforms random baselines and on a large-scale retail transaction dataset, where it recovers semantically coherent product groupings.

## 5.2 Preliminaries and Notations

### Notations

Throughout this chapter, we use the following matrix and vector norms:

$$\|A\|_F := \left( \sum_{i,j} a_{ij}^2 \right)^{1/2} \quad (\text{Frobenius norm}),$$

$$\|A\|_{\text{op}} := \sup_{\|\mathbf{x}\|_2=1} \|A\mathbf{x}\|_2 \quad (\text{spectral/operator norm}),$$

$$\|A\|_{1 \rightarrow 1} := \max_j \sum_i |a_{ij}| \quad (\text{induced 1-1 norm}).$$

**Basic spaces and derivatives** The unit sphere in the Euclidean space  $\mathbb{R}^d$  is denoted as

$$\mathbb{S}^{d-1} := \{\mathbf{x} \in \mathbb{R}^d : \|\mathbf{x}\|_2 = 1\}.$$



$\mathcal{C}^p(\mathbb{R}^d; \mathbb{R}^k)$  is the space of  $p$ -times continuously differentiable maps  $\mathbb{R}^d \rightarrow \mathbb{R}^k$ .

For  $f : \mathbb{R}^{d_z} \rightarrow \mathbb{R}^{d_x}$ , typically representing a map from latent variables  $\mathbf{Z}_t$  to observed ones  $\mathbf{X}_t$ , we write it with its output coordinates as

$$f = (f_1, f_2, \dots, f_{d_x}) \quad \text{with} \quad f_j : \mathbb{R}^{d_z} \rightarrow \mathbb{R}.$$

For a coordinate function  $f_j$ ,  $\nabla_{\mathbf{z}} f_j$  denotes the gradient and  $D^2 f_j(\mathbf{z})$  the Hessian. The Jacobian of  $f$  will be denoted as

$$Df := [\nabla_{\mathbf{z}} f_1, \nabla_{\mathbf{z}} f_2, \dots, \nabla_{\mathbf{z}} f_{d_x}].$$

Here, it is important to note that we adopt the convention that gradients are the Jacobian columns, not the rows.

**Asymptotic notation** For non-negative functions  $h$  and  $g$ , asymptotic behaviors will be denoted as

$$h \lesssim g \quad \Longleftrightarrow \quad \exists C > 0 : h(x) \leq C g(x) \quad \text{for all admissible } x,$$

$$h = \Omega(g) \quad \Longleftrightarrow \quad \exists c > 0, x_0 : h(x) \geq c g(x) \quad \text{for all } x \geq x_0,$$

$$h = \Theta(g) \quad \Longleftrightarrow \quad h \lesssim g \quad \text{and} \quad h \gtrsim B, \quad \text{i.e. } c_1 g(x) \leq h(x) \leq c_2 g(x) \quad \text{for all admissible } x.$$

$$h \gg g \quad \Longleftrightarrow \quad \lim_{x \rightarrow \infty} \frac{h(x)}{g(x)} = \infty.$$

## Preliminary Definitions

We next gather some fundamental notions that will be used throughout the chapter: we will be studying a decoder  $f$  and, particularly, the image of the latent random variable  $\mathbf{Z}$ .  $f(\mathbf{Z})$  will be interpreted as an input reconstruction of data, and will study its behavior via its coordinates' gradients and Hessians. We will also assume that  $\mathbf{Z}$  is sub-Gaussian. We therefore provide the following definitions.

**Geometry of the Decoder Image** To describe how  $f$  can "stretch" or "compress" directions in  $\mathbb{R}^{d_x}$ , we recall isotropy and subspace notions:

### Definition Def5.1 [Isotropic vector]

A random vector  $\mathbf{X} \in \mathbb{R}^{d_x}$  is *isotropic* if

$$\mathbb{E}[\mathbf{X}] = \mathbf{0}, \quad \mathbb{E}[\mathbf{X} \mathbf{X}^\top] = I_{d_x}.$$

Equivalently,  $\text{Var}(\langle \mathbf{u}, \mathbf{X} \rangle) = 1$  for all  $\mathbf{u} \in \mathbb{S}^{d_x-1}$ .

**Definition Def5.2 [Column-isotropic matrix]**

A random matrix  $G = [\mathbf{X}_1, \dots, \mathbf{X}_m] \in \mathbb{R}^{d_x \times m}$  is *column-isotropic* if its columns are i.i.d. isotropic vectors. For the remainder, we will be referring to a matrix being *anisotropic* when it is not column-isotropic.

We will usually use anisotropy to describe the Jacobian of  $f$  being a random matrix  $Df(\mathbf{Z})$ . We will also study the linear subspaces spanned by Jacobian Columns. For this, we need the following definition:

**Definition Def5.3 [Grassmannian manifold (Bendokat et al., 2024)]**

A *Grassmannian* manifold is the set of fixed-dimensional linear subspaces of a Euclidean space. For integers  $0 \leq d \leq n$ , the Grassmannian manifold of  $d$ -dimensional subspaces of  $\mathbb{R}^n$  will be denoted as  $\text{Gr}(d, n)$ .

**Function-Space Norms and Sub-Gaussianity** We measure smoothness and tail decay via Orlicz norms, particularly via the  $\psi_2$  norm to define sub-Gaussian distributions.

**Definition Def5.4 [Orlicz function]**

A function  $\psi : [0, \infty) \rightarrow [0, \infty)$  is called an *Orlicz function* if  $\psi$  is convex, non-decreasing,  $\psi(0) = 0$ , and  $\lim_{x \rightarrow \infty} \psi(x) = \infty$ .

**Definition Def5.5 [Orlicz space and Orlicz norm (Vershynin, 2018)]**

Let  $(\Omega, \mathcal{F}, \mathbb{P})$  be a probability space and  $\psi$  an Orlicz function. The *Orlicz space*  $L_\psi(\Omega, \mathcal{F}, \mathbb{P})$  consists of all measurable random variables  $X$  for which the  $\|X\|_\psi$  is finite:

$$L_\psi(\Omega, \mathcal{F}, \mathbb{P}) := \{ X : (\Omega, \mathcal{F}) \rightarrow \mathbb{R} ; \|X\|_\psi < \infty \}.$$

In the space  $L_\psi(\Omega, \mathcal{F}, \mathbb{P})$ ,  $\|X\|_\psi$  is a norm.

**Definition Def5.6 [ $\psi_2$ -Orlicz norm]**

Define

$$\psi_2(x) := e^{x^2} - 1.$$

$\psi_2$  is an Orlicz function, and for a scalar random variable  $X$ , define

$$\|X\|_{\psi_2} := \inf \{ c > 0 : \mathbb{E}[\psi_2(|X|/c)] \leq 1 \},$$

which is a norm in the space  $L_{\psi_2}(\Omega, \mathcal{F}, \mathbb{P})$ .

#### Definition Def5.7 [Sub-Gaussian Random Variable]

A real random variable  $Z \in \mathbb{R}$  is *sub-Gaussian* if any (hence all) of the following equivalent conditions hold (Wainwright, 2019):

1. **Tail bound:** There exists  $K > 0$  such that for all  $t \geq 0$ ,

$$\mathbb{P}(|Z| \geq t) \leq 2 \exp\left(-\frac{t^2}{K^2}\right).$$

The inequality means the tails of  $Z$  decay at least as fast as a Gaussian with variance equal to  $K^2$ .

2.  **$\psi_2$ -Orlicz norm:** The  $\psi_2$ -norm of  $Z$  is finite, defined by

$$\|Z\|_{\psi_2} = \inf \left\{ s > 0 : \mathbb{E} \left[ e^{Z^2/s^2} \right] \leq 2 \right\}.$$

#### Definition Def5.8 [Sub-Gaussian vector with parameter $K > 0$ ]

A random vector  $\mathbf{Z} \in \mathbb{R}^{d_z}$  is said to be *sub-Gaussian with parameter  $K$* , written  $\mathbf{Z} \sim \text{subG}_{d_z}(K)$  if for every  $\mathbf{u} \in \mathbb{S}^{d_z-1}$ , the scalar random variable  $\langle \mathbf{u}, \mathbf{Z} \rangle$  is sub-Gaussian. The vector Orlicz norm is defined as

$$\|\mathbf{Z}\|_{\psi_2} := \sup_{\mathbf{u} \in \mathbb{S}^{d_z-1}} \|\langle \mathbf{u}, \mathbf{Z} \rangle\|_{\psi_2}.$$

**For the graphical view of latent-to-observed variables** Given that we will discuss how structurally Latent variables  $\mathbf{Z}_t$  connect to the observed ones  $\mathbf{X}_t$  and how coordinates of  $\mathbf{X}_t$  cluster together, we will need the following definitions.

#### Definition Def5.9 [Directed Bipartite Graph (Diestel, 2025)]

Let  $\mathbf{Z}$  and  $\mathbf{X}$  be two disjoint sets of vertices. A *directed bipartite graph* is a triple  $(\mathbf{Z}, \mathbf{X}, E)$ , where

$$E \subseteq \mathbf{Z} \times \mathbf{X}$$

is the set of *directed* edges, each of which is an ordered pair  $(z, x)$  with  $z \in \mathbf{Z}$  and  $x \in \mathbf{X}$ . No edges are allowed from  $\mathbf{X}$  to  $\mathbf{Z}$  or within  $\mathbf{Z}$ , or  $\mathbf{X}$  themselves. For simplicity, we will write  $\mathbf{Z} \rightarrow \mathbf{X}$  to indicate a directed bipartite graph.

**Definition Def5.10 [Transitive closure (Grami, 2023)]**

Let  $\mathbf{X}$  be an arbitrary set of vertices. For any binary relation  $\sim \subseteq \mathbf{X} \times \mathbf{X}$ , its *transitive closure*  $\sim^*$  is defined as

$$\sim^* := \bigcap \left\{ T \subseteq \mathbf{X} \times \mathbf{X} \mid \sim \subseteq T \text{ and } T \text{ is transitive} \right\}.$$

That is,  $\sim^*$  is the *smallest transitive relation containing*  $\sim$  with respect to set inclusion. Equivalently,

$$x \sim^* y \iff \exists m \in \mathbb{N}, \exists v_0, \dots, v_m \in \mathbf{X} : \begin{cases} v_0 = x, v_m = y, \\ v_{t-1} \sim v_t \quad \forall t = 1, \dots, m. \end{cases}$$

## Decoder Structure and Clustering of Observed Variables

In this work, we explicitly assume that the association between latent factors and observed variables remains stationary over time. This assumption simplifies the understanding of causal structures, but it is natural in domains where the causal abstraction remains stable: if  $\mathbf{Z}_t^j$  is associated with a subset of products  $\mathbf{X}_t$  which happens to be a known product category, then the product category remains the same through time. It is common for product taxonomies to remain fixed for a long period of time in retail. An important direction for future work is to extend the framework to accommodate regime shifts, seasonal effects, or evolving causal structures (cf. Discussion in Section 5.7).

**Assumption Asm5.1 [Stationarity]**

In this work, we address CRL as defined in the Equation 5.1 given temporally stationary environments, that is, the set of structural functions  $\mathbb{G}$  is *static*.

A key benefit of imposing structural sparsity on the generative model is the emergence of organization among the observed variables. The generative mechanism  $\mathbf{Z}_t \rightarrow \mathbf{X}_t$  can be represented as a stationary bipartite graph, where latent variables influence observed features through directed edges, and the edges remain the same through time. For that reason, we omit time dependence unless necessary and describe  $\mathbf{Z} \rightarrow \mathbf{X}$ .

**Definition Def5.11 [Bipartite View of Decoder Structure]**

We represent the generative process as a bipartite graph (Def5.9)  $G = (\mathbf{Z}, \mathbf{X}, E)$ , where: (1)  $\mathbf{Z} = \{\mathbf{z}^1, \dots, \mathbf{z}^{d_z}\}$  denotes the set of latent variables, (2)  $\mathbf{X} = \{\mathbf{x}^1, \dots, \mathbf{x}^{d_x}\}$  denotes the set of observed features, and (3) an edge  $(\mathbf{z}^j, \mathbf{x}^i) \in E$  exists if and only if  $\partial f_i / \partial \mathbf{z}^j \neq 0$ .

We exploit this influence pattern to perform *variable clustering* (McCulloch & Searle, 2004; Thalamuthu et al., 2006; Jacob et al., 2009; Bach et al., 2012; Aydore et al., 2019; Chavent et al., 2021), by grouping features according to well-defined rules derived from the underlying latent structure. We define the two main rules in this work: *shared-parent clustering*, which provides disjoint groups, and *overlapping-parent clustering*, which provides overlapping groups.

**Definition Def5.12 [Shared-Parent Clustering Rule]**

We define an undirected relation  $\sim$  on  $\mathbf{X}$  as follows:

$$\mathbf{x}^i \sim \mathbf{x}^j \iff \exists \mathbf{z}^k \in \mathbf{Z} \text{ such that } (\mathbf{z}^k, \mathbf{x}^i), (\mathbf{z}^k, \mathbf{x}^j) \in E.$$

Let  $\sim^*$  denote the transitive closure of  $\sim$  (cf. Def5.10). Then:

The shared-parent clustering of the observed variables is the partition of  $\mathbf{X}$  into equivalence classes under the relation  $\sim^*$ . That is, each cluster is a maximal subset  $\mathcal{C} \subseteq \mathbf{X}$  such that:

$$\forall \mathbf{x}^i, \mathbf{x}^j \in \mathcal{C}, \mathbf{x}^i \sim^* \mathbf{x}^j, \quad \text{and} \quad \forall \mathbf{x} \in \mathbf{X} \setminus \mathcal{C}, \mathbf{x} \not\sim^* \mathbf{x}^j \text{ for any } \mathbf{x}^j \in \mathcal{C}.$$

Each cluster corresponds to a connected component in the undirected graph over  $\mathbf{X}$ , where an edge exists between  $\mathbf{x}^i$  and  $\mathbf{x}^j$  if they share a latent parent.

Intuitively, Definition Def5.12 implies that two observed variables belong to the same group if there exists a path of features  $\mathbf{x}^{i_1}, \dots, \mathbf{x}^{i_k}$  such that each consecutive pair shares at least one latent parent, and both variables lie in the same connected component under the relation  $\sim$ . As an illustration, consider the graph in Figure 5.1b: applying the shared-parent clustering rule yields the following partition of the observed variables:

$$\mathcal{C}_{\text{disjoint}} = \{\mathcal{C}_1 = \{\mathbf{x}_t^1, \dots, \mathbf{x}_t^6\}, \quad \mathcal{C}_2 = \{\mathbf{x}_t^7, \dots, \mathbf{x}_t^{12}\}\}.$$

Here in the cluster  $\mathcal{C}_1$ , the path  $\mathbf{x}_t^1, \dots, \mathbf{x}_t^6$  is maximal because there is no other observed feature in  $\mathbf{X} \setminus \mathcal{C}_1$  that could be added, given no shared latent cause exists according to the graph in 5.1b.

**Definition Def5.13 [Overlapping-Parent Clustering Rule]**

The overlapping-parent clustering of the observed variables is the collection of clusters

$$\mathcal{C}_{\text{overlap}} := \{\text{Ch}(\mathbf{z}^1), \dots, \text{Ch}(\mathbf{z}^{d_z})\},$$

where

$$\text{Ch}(\mathbf{z}^k) := \{\mathbf{x}^j \in \mathbf{X} \mid (\mathbf{z}^k, \mathbf{x}^j) \in G\}.$$

Each cluster  $\text{Ch}(\mathbf{z}^k)$  is the children set: it contains all observed variables that are directly influenced by the latent variable  $\mathbf{z}^k$ .

In contrast, using the *overlapping-parent clustering rule* (Definition Def5.13), which groups features based on sharing at least one latent parent, results in a finer, overlapping structure:

$$\mathcal{C}_{\text{overlap}} = \left\{ \underbrace{\{\mathbf{x}_t^1, \mathbf{x}_t^2, \mathbf{x}_t^3\}}_{\text{Ch}(\mathbf{z}_t^1)}, \underbrace{\{\mathbf{x}_t^3, \mathbf{x}_t^4, \mathbf{x}_t^5\}}_{\text{Ch}(\mathbf{z}_t^2)}, \underbrace{\{\mathbf{x}_t^5, \mathbf{x}_t^6\}}_{\text{Ch}(\mathbf{z}_t^3)}, \underbrace{\{\mathbf{x}_t^7, \mathbf{x}_t^8, \mathbf{x}_t^9\}}_{\text{Ch}(\mathbf{z}_t^4)}, \underbrace{\{\mathbf{x}_t^9, \mathbf{x}_t^{10}, \mathbf{x}_t^{11}, \mathbf{x}_t^{12}\}}_{\text{Ch}(\mathbf{z}_t^5)} \right\}.$$

This overlapping clustering  $\mathcal{C}_{\text{overlap}}$  provides a more fine-grained abstraction than  $\mathcal{C}_{\text{disjoint}}$ . Notably, each cluster  $\text{Ch}(\mathbf{z}_t^j)$  is a subset of one of the disjoint clusters of  $\mathcal{C}_{\text{disjoint}}$ , illustrating the hierarchical relation between the two grouping strategies. Notably, the anchor feature assumption, as represented in Figure 5.1b, yields the same non-overlapping clustering as the sparse self-expression constraint. However, the latter permits far more complex latent-to-observed influence patterns. Specifically, only the subset  $\{\mathbf{z}_t^1, \mathbf{z}_t^2, \mathbf{z}_t^3\}$  is responsible for generating the features  $\{\mathbf{x}_t^1, \dots, \mathbf{x}_t^6\}$ , while  $\{\mathbf{z}_t^4, \mathbf{z}_t^5\}$  governs  $\{\mathbf{x}_t^7, \dots, \mathbf{x}_t^{12}\}$ . Thus, *modularity* is maintained, but without requiring the strict exclusivity assumptions imposed by anchor-based models.

The two clustering rules defined by Def5.12 and Def5.13 yield different, yet meaningful groupings of observed features, each consistent with distinct structural assumptions. The key insight is that *clustering is not unique*: it depends on the specific clustering rule, which in turn reflects a modeling choice.

To further formally clarify the dependence of variable clustering on the rule defined, we give a formalization of what a "clustering rule" is, and then show how clusters can be defined as a consequence. We will use the term *modularity* whenever we want to communicate that a subset of latent variables shares a common influence pattern with some subset of observed ones and not with the rest.

Intuitively, the two clustering rules defined above happen to reason both on how the parent set of observed variables, which are subsets of latent ones, interact with each other. We formalize this as the following

**Definition Def5.14 [Affinity predicate]**

Let  $G$  be a directed bipartite graph (Def5.9).

An *affinity predicate*  $P : \mathbf{X} \times \mathbf{X} \longrightarrow \{0, 1\}$  is any symmetric Boolean function

$$P(\mathbf{x}^i, \mathbf{x}^j \mid G) = \pi(\text{Pa}(\mathbf{x}^i), \text{Pa}(\mathbf{x}^j)),$$

with  $\pi : 2^{\mathbf{Z}} \times 2^{\mathbf{Z}} \rightarrow \{0, 1\}$  is a symmetric Boolean function of two subsets of  $\mathbf{Z}$ .

The shared parent clustering rule corresponds to the affinity predicate

$$P_{\text{SP}}(\mathbf{x}^i, \mathbf{x}^j \mid G) = \begin{cases} 1, & \text{Pa}(\mathbf{x}^i) \cap \text{Pa}(\mathbf{x}^j) \neq \emptyset, \\ 0, & \text{otherwise.} \end{cases}$$

and if one writes the binary relation

$$\mathbf{x}^i \sim_{SP} \mathbf{x}^j \iff P_{\text{SP}}(\mathbf{x}^i, \mathbf{x}^j \mid G) = 1,$$

then  $\sim_{SP}$  is symmetric and reflexive but not transitive and is identical to that of Definition Def5.12. For the overlapping-parent clustering, if for each  $\mathbf{z} \in \mathbf{Z}$ , one considers the predicate  $P_{\mathbf{z}}$  as the restriction of  $P_{\text{SP}}$  on  $\text{Ch}(\mathbf{z})$ , then  $\sim_{SP}$  defines trivially an equivalent relation when restricted to  $\text{Ch}(\mathbf{z}) \times \text{Ch}(\mathbf{z})$ . It has only one non-empty equivalence class, which is  $\text{Ch}(\mathbf{z})$  itself. Thus, by varying  $\mathbf{z}$ , we collect  $\{\text{Ch}(\mathbf{z})\}_{\mathbf{z} \in \mathbf{Z}}$  which coincides with the Definition Def5.13.

### 5.3 Intuitive Discussion of Jacobian Self-Expression

**Generalizing Anchor Features through Gradient Subspaces** We can naturally generalize the classical anchor feature assumption by shifting from exact functional separability to linear relationships between decoder gradients. Rather than defining the decoder as a fixed matrix as in Boussard et al. (2023) (c.f Related Work, Section 5.4), we allow it to be any smooth function  $f : \mathbb{R}^{d_z} \rightarrow \mathbb{R}^{d_x}$ , and impose structural sparsity through its Jacobian:

$$\mathbf{X}_t^j \sim \mathcal{N}(f_j(\mathbf{Z}_t), \sigma_j^2), \quad f(\mathbf{Z}_t) = [f_1(\mathbf{Z}_t), \dots, f_{d_x}(\mathbf{Z}_t)]^T.$$

We recall the standard anchor feature condition used in identifiable sparse VAE models in the *static* setting: Moran et al. (2021) defined the anchor feature assumption as: For each latent factor  $\mathbf{Z}^k$ , there exist at least two observed features  $\mathbf{X}^j$  and  $\mathbf{X}^{j_0}$  such that

$$\mathbb{E}[\mathbf{X}^j | \mathbf{Z}] = f_j(\mathbf{Z}^k) \quad \text{and} \quad \mathbb{E}[\mathbf{X}^{j_0} | \mathbf{Z}] = f_{j_0}(\mathbf{Z}^k). \quad (5.2)$$

To generalize this, denote the partial derivative as

$$\phi_{ij} := \frac{\partial f_j}{\partial \mathbf{z}^i}.$$

For example, from the graphical structure in Figure 5.1b, we have

$$\nabla_{\mathbf{z}} f_7(\mathbf{z}) = [0, 0, 0, \phi_{47}(\mathbf{z}), 0]^\top, \quad \nabla_{\mathbf{z}} f_8(\mathbf{z}) = [0, 0, 0, \phi_{48}(\mathbf{z}), 0]^\top.$$

Now, suppose the gradients of two decoding functions are collinear almost everywhere. Then there exist constants  $a, b$  such that

$$f_7(\mathbf{Z}) = a f_8(\mathbf{Z}) + b \quad \text{almost surely,}$$

and hence

$$\mathbb{E}[\mathbf{X}^7 \mid \mathbf{Z}] = a \mathbb{E}[\mathbf{X}^8 \mid \mathbf{Z}] + b.$$

This weakens the anchor feature assumption in Equation 5.2: rather than requiring that two observed features depend identically on one latent factor, we can only require their conditional expectations to be linearly related. Thus, the classical anchor condition becomes a special case of a broader gradient-based linear structure.

To uncover latent-induced modularity in the observed space, we examine the Jacobian matrix  $Df$  of the decoder  $f$

$$Df := [\nabla_{\mathbf{z}} f_1, \nabla_{\mathbf{z}} f_2, \dots, \nabla_{\mathbf{z}} f_{d_x}]$$

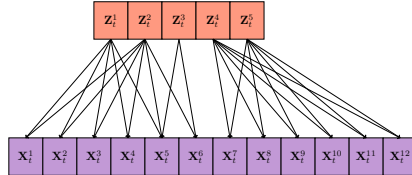
and encode its structural geometry via a self-expression matrix  $C \in \mathbb{R}^{d_x \times d_x}$ . Each column of  $Df$  is represented as a sparse linear combination of the others:

$$\nabla_{\mathbf{z}} f_j = \sum_{k \neq j} C_{kj} \nabla_{\mathbf{z}} f_k.$$

We must satisfy  $C_{jj} = 0$  for all  $j = 1, \dots, d_x$  to eliminate the trivial identity solution, i.e., a gradient should not be self-expressed by itself.

The Jacobian  $Df$  reflecting the sparse structure in Figure 5.1c which we restate below, has the form:

$$Df = \begin{bmatrix} \phi_{1,1} & \phi_{1,2} & \phi_{1,3} & \phi_{1,4} & \phi_{1,5} & 0 & 0 & 0 & 0 & 0 & 0 & 0 \\ \phi_{2,1} & \phi_{2,2} & \phi_{2,3} & \phi_{2,4} & \phi_{2,5} & \phi_{2,6} & 0 & 0 & 0 & 0 & 0 & 0 \\ 0 & 0 & 0 & 0 & \phi_{3,5} & \phi_{3,6} & 0 & 0 & 0 & 0 & 0 & 0 \\ 0 & 0 & 0 & 0 & 0 & 0 & \phi_{4,7} & \phi_{4,8} & \phi_{4,9} & \phi_{4,10} & \phi_{4,11} & \phi_{4,12} \\ 0 & 0 & 0 & 0 & 0 & 0 & \phi_{5,7} & \phi_{5,8} & \phi_{5,9} & \phi_{5,10} & \phi_{5,11} & \phi_{5,12} \end{bmatrix} \quad (5.3)$$



An example of a structure corresponding to the sparse self-expression of the Jacobian. A restatement of Figure 5.1c

$$C = \begin{pmatrix} C_1 & 0 \\ 0 & C_2 \end{pmatrix}, \quad C_1, C_2 \in \mathbb{R}^{6 \times 6}, \quad (5.4)$$



$$C_1 = \begin{pmatrix} 0 & C_{1,2} & C_{1,3} & C_{1,4} & C_{1,5} & C_{1,6} \\ C_{2,1} & 0 & C_{2,3} & C_{2,4} & C_{2,5} & C_{2,6} \\ C_{3,1} & C_{3,2} & 0 & C_{3,4} & C_{3,5} & C_{3,6} \\ C_{4,1} & C_{4,2} & C_{4,3} & 0 & C_{4,5} & C_{4,6} \\ 0 & 0 & 0 & 0 & 0 & C_{5,6} \\ 0 & 0 & 0 & 0 & C_{6,5} & 0 \end{pmatrix}, \quad C_2 = \begin{pmatrix} 0 & C_{7,8} & C_{7,9} & C_{7,10} & C_{7,11} & C_{7,12} \\ C_{8,7} & 0 & C_{8,9} & C_{8,10} & C_{8,11} & C_{8,12} \\ C_{9,7} & C_{9,8} & 0 & C_{9,10} & C_{9,11} & C_{9,12} \\ C_{10,7} & C_{10,8} & C_{10,9} & 0 & C_{10,11} & C_{10,12} \\ C_{11,7} & C_{11,8} & C_{11,9} & C_{11,10} & 0 & C_{11,12} \\ C_{12,7} & C_{12,8} & C_{12,9} & C_{12,10} & C_{12,11} & 0 \end{pmatrix}. \quad (5.5)$$

**Clustering via Shared Gradient Support** Our formulation recovers feature clusters by identifying subspaces of mutually expressible gradients, that is, observed features whose Jacobians span the same low-dimensional subspace. For instance, from Figure 5.1c, we identify the groupings:

$$\{\{\mathbf{x}_t^1, \dots, \mathbf{x}_t^6\}, \{\mathbf{x}_t^7, \dots, \mathbf{x}_t^{12}\}\}.$$

where the gradients  $\{\nabla_{\mathbf{z}} f_1, \dots, \nabla_{\mathbf{z}} f_6\}$  are expressible in terms of each other. A valid self-expression would be:

$$\nabla_{\mathbf{z}} f_1 = \sum_{i=2}^6 C_{i,1} \nabla_{\mathbf{z}} f_i.$$

In contrast, an invalid expression such as:

$$\nabla_{\mathbf{z}} f_1 = \sum_{i=2}^6 C_{i,1} \nabla_{\mathbf{z}} f_i + C_{7,1} \nabla_{\mathbf{z}} f_7, \quad C_{7,1} \neq 0 \quad (5.6)$$

is precluded, since  $\nabla_{\mathbf{z}} f_7$  has disjoint support with  $\nabla_{\mathbf{z}} f_1$  and including it would imply that  $\phi_{4,7} \equiv \phi_{5,7} \equiv 0$  which is not possible by maximum sparsity of Jacobian in Equation 5.3. As a remedy, one might also include other gradients with the same support as  $\nabla_{\mathbf{z}} f_7$  (e.g.  $\nabla_{\mathbf{z}} f_8$ ). However, adding such terms would violate sparsity, as we aim to discourage unnecessary inclusion of uninformative features.

**Support Overlap and Subspace Consistency** This yields a principled clustering criterion: two observed features  $i$  and  $j$  belong to the same cluster if and only if

1.  $C_{i,j} \neq 0$  or  $C_{j,i} \neq 0$ , and
2.  $\text{supp}(\nabla_{\mathbf{z}} f_i) \cap \text{supp}(\nabla_{\mathbf{z}} f_j) \neq \emptyset$ .

Under these conditions, the optimal self-expression matrix  $C^*$  is block-diagonal (up to permutation), with each block identifying a latent-induced subspace. Consequently, the clustering is non-overlapping, and each cluster comprises exactly those gradients sharing the same support in the latent space.

We propose to achieve so through sparse subspace clustering over the Jacobian Dictionary. Informally, let there be  $n$  linear subspaces  $(\mathcal{S}_l)_{l=1}^n$  in  $\mathbb{R}^{d_z}$  such that  $\nabla_{\mathbf{z}} f_j$  lies within their union. The Jacobian can

be rewritten as

$$Df = [\nabla_{\mathbf{z}} f_1, \dots, \nabla_{\mathbf{z}} f_{d_x}] = [J_1, \dots, J_n] P,$$

where  $P \in \mathbb{R}^{d_x \times d_x}$  is a permutation matrix. Each  $J_l$  is a matrix of gradient vectors whose column span defines the corresponding subspace  $\mathcal{S}_l$ , i.e.

$$\text{span}(\text{cols}(J_l)) = \mathcal{S}_l.$$

This leads to a matrix formulation of the self-expressiveness assumption:

**Assumption Asm5.2 [Matrix Formulation of Self-Expressiveness]**

We assume the existence of self-expressiveness in the Jacobian columns, that is, there exists  $C \in \mathbb{R}^{d_x \times d_x}$  with  $\text{diag}(C) = \mathbf{0}$  such that each gradient can be written as

$$\nabla_{\mathbf{z}} f_j = Df C_{:,j}, \quad j \in \{1, 2, \dots, d_x\}.$$

Equivalently, in a matrix form

$$Df C = Df, \quad \text{diag}(C) = \mathbf{0}.$$

Since this expression is generally non-unique, we aim to enforce sparsity in the matrix  $C$ . To achieve this, we can optimize  $C$  by solving:

$$\begin{aligned} \min_{C_{:,j} \in \mathbb{R}^{d_x}} \quad & \|C_{:,j}\|_1 \\ \text{subject to} \quad & \nabla_{\mathbf{z}} f_j(\mathbf{Z}) = Df(\mathbf{Z}) C_{:,j} \text{ a.s.,} \\ & C_{j,j} = 0. \end{aligned}$$

The optimization problem establishes the link between latent factors  $\mathbf{Z}$  and observed features  $\mathbf{X}$  using the solution  $C^*$ . The underlying rationale is that variables that cluster together should have gradients of the decoding function with respect to  $\mathbf{z}$  lying in the same linear subspace of the Jacobian. Specifically, the nonzero entries in  $C_{:,j}$  should correspond to gradients from the same subspace  $\mathcal{S}_l$  when  $\nabla_{\mathbf{z}} f_j$  belongs to  $\mathcal{S}_l$ . In other terms, the first objective is to define geometric and probabilistic conditions under which this subspace preservation property holds (cf. Definition Def5.16).

Once we ensure that the self-expression matrix  $C^*$  preserves subspaces, it can then be leveraged to perform clustering of the observed variables. For example, let  $\mathcal{V}$  be the set of vertices corresponding to the gradients <sup>1</sup>

$$\nabla_{\mathbf{z}} f_1, \dots, \nabla_{\mathbf{z}} f_{d_x}.$$

Denote by  $\Gamma \subseteq \mathcal{V} \times \mathcal{V}$  the set of edges between nodes, and let  $A \in \mathbb{R}_+^{d_x \times d_x}$  be the (symmetric) edge-weight

<sup>1</sup>Here, the set of gradients is equivalent to considering the set of observed features  $\{\mathbf{X}^1, \dots, \mathbf{X}^{d_x}\}$ . The rationale here is: to perform variable clustering, we give a "vectorial representation" to each scalar dimension  $\mathbf{X}^j$  through its gradient w.r.t. the latent factors  $\nabla_{\mathbf{z}} f_j$  and thus reason on (subspace) clustering of gradients.

matrix defined by

$$A = \frac{1}{2}(|C^*| + |C^*|^\top).$$

Clusters are then obtained by applying spectral clustering (Von Luxburg, 2007) to the weighted graph  $(\mathcal{V}, \Gamma, A)$ .

We show in Proposition Prop5.1 under which conditions such a pipeline recovers clusters that are consistent with those obtained by the shared parent clustering rule (Definition Def5.12). The same reasoning is followed in the case of the recovery of overlapping clusters, where spectral clustering is replaced by overlapping-aware clustering methods such as Synmf (Kuang et al., 2015) and SAAC (Panov et al., 2017), and we show in Theorem Thm5.3 under which conditions the resulting clusters are consistent with those obtained by the overlapping clustering rule (Definition Def5.13).

## 5.4 Related Work

### 5.4.1 CRL in a time-varying setting

Yao et al. (2022) were the first to introduce CRL over time-varying data while providing theoretical guarantees for the identifiability of the true latent causal variables. In their model, each latent variable  $\mathbf{Z}_t^j$  obeyed time-delayed causal relations as in Equation 5.1, except that the noise  $\epsilon_t^j$  follows a non-stationary distribution

$$\epsilon_t^j \sim p_{\epsilon^j|\mathbf{a}},$$

with  $\mathbf{a}$  an observed auxiliary variable that can take various forms: (i) a *time index* to account for sequential dependencies, (ii) a *domain index* to capture distributional shifts across domains, (iii) or a *class label* in supervised learning contexts (Hyvarinen & Morioka, 2016; Hyvarinen et al., 2019b; Locatello et al., 2019; Khemakhem et al., 2020; Morioka et al., 2021). The inductive bias introduced by the auxiliary variable facilitates the identifiability of the latent factors up to mild transformations such as permutations and component-wise invertible mappings.

Song et al. (2023) considered the case where the side information  $\mathbf{a}$  is unobserved, and similar to Hälvä & Hyvärinen (2020), they treated the domain index variables as latent and modeled them via a Markov chain. The resulting generative model is

$$a_1, a_2, \dots, a_T \sim \text{MC}(A),$$

$$\epsilon_t^j \sim p_{\epsilon^j}, \quad j = 1, \dots, d_z,$$

$$\mathbf{Z}_t^j = g_j\left(\{\mathbf{Z}_{t-s}^k \mid \mathbf{Z}_{t-s}^k \in Pa(\mathbf{Z}_t^j), s = 1, \dots, \rho\}, a_t, \epsilon_t^j\right),$$

$$\mathbf{X}_t = f(\mathbf{Z}_t),$$

where  $a_t \in \{1, \dots, d_a\}$  is a discrete domain index and  $A$  is the  $d_a \times d_a$  transition matrix of the Markov chain  $(a_t)_{t \geq 1}$ . Here, the structural functions, unlike those of Equation 5.1, are non-stationary because

they are modulated by  $(a_t)_{t \geq 1}$ . The identifiability of the latent process stems first from identifying the non-stationarity represented by  $(a_t)_{t \geq 1}$ , similar to Gassiat et al. (2016); Hälvä & Hyvärinen (2020); Morioka et al. (2021), and then establishing the identifiability of the causal latent variables  $(\mathbf{Z}_t)_{t \geq 1}$ , as in Yao et al. (2022).

Chen et al. (2024) challenged the longstanding assumption of invertibility in the generative process  $f$  and proposed leveraging temporal context for both generation and identification. Specifically, they used the historical latent process to generate the observed data and the historical observed process to identify the latent causal factors:

$$\begin{aligned}\mathbf{X}_t &= f(\mathbf{Z}_{t:t-r}), \\ \mathbf{Z}_t &= m(\mathbf{X}_{t:t-\mu}), \\ \epsilon_t^j &\sim p_{\epsilon^j}, \quad j = 1, \dots, d_z, \\ \mathbf{Z}_t^j &= g_j(\{\mathbf{Z}_{t-s}^k \mid \mathbf{Z}_{t-s}^k \in Pa(\mathbf{Z}_t^j), s = 1, \dots, \rho\}, \epsilon_t^j).\end{aligned}$$

Here,  $r$  and  $\mu$  are predefined lags and  $m$  is a nonlinear mapping that reconstructs the current causal latent factor  $\mathbf{Z}_t$  from a slice of the observed process  $\mathbf{X}_{t:t-\mu}$ . The bijectivity of  $f$  is thus replaced in Chen et al. (2024) by a temporal context mechanism, where the observed data are generated, and the latent factors are inferred via two distinct and generally unrelated mappings:  $f$  and  $m$ .

#### Remark Rem5.1

While several models have been proposed before Yao et al. (2022) in the time-varying setting to learn identifiable representations, these models do not treat the latent variables as causal, nor do they attempt to learn a causal process within the latent space. Notable examples include *Time-Contrastive Learning (TCL)* (Hyvärinen & Morioka, 2016), *Permutation-based Contrastive Learning (PCL)* (Hyvärinen et al., 2019a), and *SlowVAE* (Klindt et al., 2021), as well as methods designed for noisy data with structured nonlinear ICA (Hälvä et al., 2021). Additional approaches include nonlinear ICA with a hidden Markov model to capture non-stationarity (Hälvä & Hyvärinen, 2020), error estimation in nonlinear vector autoregressive models (Morioka et al., 2021), and generalized nonlinear ICA frameworks for temporal data (Hyvärinen & Morioka, 2017). Finally, recent contributions also explore identifiability in multi-view time series (Huang et al., 2023).

### 5.4.2 Understanding the Generation Mechanism in CRL

Most CRL work focuses on recovering latent factors but pays little attention to how those factors generate observations. Exploring this generative mapping matters because it validates and interprets the resulting causal representations. Lachapelle et al. (2022b); Boussard et al. (2023) did impose structural constraints in CRL but did not explicitly focus on uncovering the underlying generative process. A contribution in

this direction is the Sparse VAE introduced by Moran et al. (2021), which enforces a sparsity constraint on the decoder. Their model applies a binary mask  $\Gamma \in \{0, 1\}^{d_z \times d_x}$  to the latent variables before decoding them into the observed space. This formulation rests on the assumption of pure children (Equation 5.2), and the generative process follows

$$\mathbf{X}^j \sim \mathcal{N}(f_\theta(\Gamma_{:,j} \odot \mathbf{Z}), \sigma_j^2), \quad j = 1, \dots, d_x,$$

where  $\odot$  denotes the Hadamard product,  $f_\theta$  is the decoder, and  $\sigma_1^2, \dots, \sigma_{d_x}^2$  are fixed variance parameters. For inference, Moran et al. (2021) adopted a Bayesian framework, placing a Spike-and-Slab Lasso prior (Bai et al., 2021b) on  $\Gamma$  and estimating its posterior via maximum a posteriori (MAP) optimization. While elegant, this framework is restricted to *static data* and does not infer any *causal structure* among the latent variables. Moreover, it remains unclear whether the employed sparsity prior adequately encodes the assumed structural constraints of Equation 5.2, as the theoretical assumptions are not explicitly embedded in the inference mechanism. Related efforts by Zheng et al. (2022); Zheng & Zhang (2023) likewise imposed sparsity constraints in static, nonlinear ICA settings, leveraging either  $\ell_1$  regularization or hybrid penalties combining  $\ell_0$  and  $\ell_1$  norms, but similarly stop short of modeling causal structure in the latent space.

Two important papers integrating CRL and sparsity are worth mentioning. First, Lachapelle et al. (2022b) proposed learning a causal representation  $\mathbf{Z}_t$  over time-varying data  $\mathbf{X}_t$  with a *sparse mechanism shift*, meaning that only a few edges relate past latent representations to future ones. The transition mechanism in the latent space is expressed as:

$$p(\mathbf{z}_t^j | \mathbf{z}_{<t}) = h_j(\mathbf{z}_{<t}) \exp\left(T_j(\mathbf{z}_t^j)^\top \lambda_j(\Gamma \odot \mathbf{z}_{<t}) - \Psi(\mathbf{z}_{<t})\right), \quad j = 1, \dots, d_z,$$

where (i)  $h_j(\cdot)$  is the base measure, (ii)  $T_j(\cdot)$  is the vector of sufficient statistics for the coordinate  $j$ , (iii)  $\lambda_j(\cdot)$  is the natural-parameter map returning the canonical parameters of the exponential family, (iv)  $\Psi(\cdot)$  is the log-partition function ensuring normalization (Wainwright et al., 2008), (v) and  $\Gamma$  is a binary mask enforcing sparsity on the past-latent vector  $\mathbf{Z}_{<t}$ . The inference is performed using variational inference, with the ELBO regularized by an  $\ell_0$  or  $\ell_1$  penalty over  $\Gamma$ .

It is important to note that, as in Moran et al. (2021), the inference strategy in Lachapelle et al. (2022b) is not fully aligned with the theoretical structural assumptions supporting their identifiability results. Specifically, identifiability in their model relies on a graphical criterion requiring the existence of latent subsets whose parental and child sets uniquely identify each latent factor. However, it remains unclear how standard  $\ell_1$  regularization during inference could enforce such a structural constraint in practice. More importantly, no form of sparsity is imposed on the mapping between latent and observed variables, which is what our approach instantiates.

The second most similar work to ours is Boussard et al. (2023); Brouillard et al. (2024), which enforces a sparsity constraint on the decoding function while performing CRL for time-series climate data. However, their approach assumes a single-parent decoding constraint (Figure 5.1a). To achieve this, the edge weights

relating the latent factors  $\mathbf{Z}_t$  to the observed features  $\mathbf{X}_t$  are modeled with a non-negative and orthogonal matrix  $\Gamma$ , ensuring that at most one entry per row is nonzero. Formally, the generative model assumes:

$$\mathbf{X}_t^j \mid \mathbf{Z}_t \sim \mathcal{N}(\Gamma_{:,j} \mathbf{Z}_t, \sigma_j^2). \quad (5.7)$$

To enforce structural single-parent decoding, Boussard et al. (2023) defined the orthogonality constraint  $h(\Gamma) = \Gamma^\top \Gamma - I_{d_x}$  during training, which is consistent with the structural constraint of single-parent decoding. However, this single-parent assumption is highly restrictive, as explained in Section 5.1, since it does not allow a mixture of latent factors to generate observed variables. Such a scenario arises where causal relationships among observed features lead to multiple latent parents. Our work generalizes this approach by allowing multiple latent factors as parents, making it a more flexible and realistic assumption for a broader range of applications.

### 5.4.3 Subspace Clustering

Subspace clustering segments data that lie near a union of low-dimensional linear subspaces. In contrast, Principal Component Analysis (PCA) (Hastie et al., 2009) fits all data with a single subspace. Hence, subspace clustering can be intuitively understood as a generalization of PCA by fitting multiple subspaces, these subspaces may intersect when different clusters share overlapping dimensions, so that the heterogeneous structure in high-dimensional data is better captured. Our method adopts the self-expression property from subspace clustering, but applies it to the gradients of observed features with respect to latent variables. A general definition of subspace clustering is as follows (Abdolali & Gillis, 2021; Qu et al., 2023):

**Definition Def5.15 [Subspace Clustering]**

Let  $X \in \mathbb{R}^{d \times n}$  be a high-dimensional dataset, where each column represents a data point in  $\mathbb{R}^d$ . Suppose the data lie in a union of  $c$  unknown linear subspaces  $\mathcal{S}_1, \mathcal{S}_2, \dots, \mathcal{S}_c \subset \mathbb{R}^d$ , with corresponding intrinsic dimensions  $d_1, d_2, \dots, d_c$ , where  $d_i \ll d$  for all  $i \in \{1, \dots, c\}$ .

The goal of *subspace clustering* is twofold: (1) to assign each data point to its generating subspace, and (2) to estimate the parameters (e.g., bases or projection matrices) that define each subspace.

Definition Def5.15 highlights that similarity between data points is assessed through their compatibility with low-dimensional subspaces. Consequently, points within the same cluster exhibit strong linear dependencies and lie close to a shared subspace.

**Sparse Subspace Clustering (SSC)** Most classical subspace clustering methods struggle to handle both noise and outliers simultaneously (Costeira & Kanade, 1998; Tipping & Bishop, 1999; Tseng, 2000; Kanatani, 2001; Zhang et al., 2009; Yan & Pollefeys, 2006; Goh & Vidal, 2007), and they typically rely on prior knowledge of the dimensions of the underlying subspaces. To address these limitations, a major line

of work introduces *sparsity* into subspace clustering algorithms (Vidal et al., 2009; Elhamifar & Vidal, 2010; Soltanolkotabi & Candés, 2012b; Elhamifar & Vidal, 2013). Sparsity helps to mitigate noise and alleviates the need for explicit knowledge of subspace dimensions. A foundational idea underpinning many SSC approaches is the self-expression property. Imposing sparsity on the coefficients of this linear combination leads to models that encourage locality and robustness. The seminal work of Vidal et al. (2009) employed  $\ell_1$ -regularization for this purpose. Subsequent developments have explored a variety of regularization schemes, including  $\ell_0$ -based formulations (Yang et al., 2016; 2018), nuclear norm minimization (Liu et al., 2012), Frobenius norm penalties (Lu et al., 2012), and elastic net regularization (You et al., 2016).

**Deep SSC** Given the high ambient dimensionality of many real-world datasets, recent efforts have focused on learning lower-dimensional representations in which subspace structure is more amenable to analysis. The motivation is that the raw input space may not satisfy the assumptions required for linear self-expression, and thus, a learned representation could better reveal the latent subspace geometry. Early work projected data into linear latent spaces (Patel et al., 2013), while more recent approaches employ neural networks for joint representation learning and subspace clustering (Ji et al., 2017; Abavisani & Patel, 2018; Zhou et al., 2019; Peng et al., 2020; Xie et al., 2020; Yang et al., 2020). Unlike these approaches, our framework does not seek to learn representations in which standard SSC can be applied, but rather induces a modular structure directly in the observation space via an SSC over decoder gradients.

## 5.5 Modeling

### 5.5.1 Subspace Detection Under Self-Expression Property

#### Main modeling assumptions

To analyze the recoverability of modular structure via Jacobian self-expression, we must understand the statistical and geometric properties of decoder gradients. In this section, we formalize these conditions by placing mild distributional and smoothness assumptions on the latent variables  $\mathbf{Z}$  and decoder  $f$ . We model  $\mathbf{Z} \in \mathbb{R}^{d_z}$  as sub-Gaussian random vectors. This assumption helps derive concentration inequalities and underpins our stability analyses, provided the decoder  $f$  is smooth in the following sense:

Assumption Asm5.3 [Smoothness of Decoder]
<p>A decoder <math>f</math> with coordinates</p> $f = (f_1, \dots, f_{d_x})^\top$ <p>is said to be <math>L</math>-smooth with <math>L &gt; 0</math> if</p> $f \in \mathcal{C}^2(\mathbb{R}^{d_z}; \mathbb{R}^{d_x})$

and there exists  $L > 0$  such that, for each  $i \in \llbracket 1, d_x \rrbracket$ , the Hessian of the output coordinate  $f_i$  satisfies

$$\sup_{\mathbf{z} \in \mathbb{R}^{d_z}} \|D^2 f_i(\mathbf{z})\|_{\text{op}} \leq L.$$

The Jacobian  $Df(\mathbf{z}) \in \mathbb{R}^{d_x \times d_z}$  captures the local linear structure of the decoder around each latent point  $\mathbf{z}$ . We model  $Df(\mathbf{z})$  as a random matrix whose columns lie on the unit sphere  $\mathbb{S}^{d_z-1}$ , allowing for anisotropy through statistical dependence between columns (cf. Definition Def5.2). Normalizing gradients is not a restrictive condition, it can be enforced during training and is widely used in practice to stabilize optimization, notably via gradient clipping (Zhang et al., 2020a).

Building on the assumption that the Jacobian columns are unit-norm and anisotropic, we now introduce a structured prior that captures modularity in the decoder: the *union of subspaces* model. In particular, we model the columns of the Jacobian  $Df(\mathbf{z})$  as lying in a union of low-dimensional subspaces:

**Assumption Asm5.4 [Union of Subspaces Assumption]**

There exist  $M$  deterministic linear subspaces  $\{\mathcal{S}_m\}_{m=1}^M$ , where each  $\mathcal{S}_m \in \text{Gr}(d_m, d_z)$ . Accordingly, there is a partition of output indices

$$\{1, 2, \dots, d_x\} = \bigsqcup_{m=1}^M I_m, \quad |I_m| = n_m, \quad \sum_{m=1}^M n_m = d_x.$$

We then define the block-wise mapping

$$f^{(m)} : \mathbb{R}^{d_z} \longrightarrow \mathbb{R}^{n_m}, \quad f^{(m)}(\mathbf{z}) := (f_j(\mathbf{z}))_{j \in I_m}.$$

We assume the Jacobian of each block  $f^{(m)}$  has its columns in  $\mathcal{S}_m$ :

$$Df^{(m)}(\mathbf{z}) = [\nabla_{\mathbf{z}} f_j(\mathbf{z})]_{j \in I_m} \in \mathbb{R}^{d_z \times n_m}, \quad \text{cols}(Df^{(m)}(\mathbf{z})) \subseteq \mathcal{S}_m, \quad \forall \mathbf{z} \in \mathbb{R}^{d_z}.$$

As a result, each gradient lies in one of the  $M$  subspaces, that is,  $\nabla_{\mathbf{z}} f_j(\mathbf{z}) \in \cup_{m=1}^M \mathcal{S}_m$ .

Figure 5.2 illustrates Assumption Asm5.4: for an arbitrary realization  $\mathbf{z}$ , the gradients  $\nabla_{\mathbf{z}} f_1(\mathbf{z})$ ,  $\nabla_{\mathbf{z}} f_2(\mathbf{z})$ ,  $\nabla_{\mathbf{z}} f_3(\mathbf{z})$  are assumed to lie on the space  $\mathcal{S}_1$  at the intersection with the unit sphere  $\mathbb{S}^{d_z-1}$  (red contour). Similarly, gradients  $\nabla_{\mathbf{z}} f_4(\mathbf{z})$ ,  $\nabla_{\mathbf{z}} f_5(\mathbf{z})$ ,  $\nabla_{\mathbf{z}} f_6(\mathbf{z})$  lie in the subspace  $\mathcal{S}_2$ , precisely on the dashed blue contour. Assumption Asm5.4 also implies that for another arbitrary  $\mathbf{z}'$ , the gradients  $\nabla_{\mathbf{z}} f_1(\mathbf{z}')$ ,  $\nabla_{\mathbf{z}} f_2(\mathbf{z}')$ ,  $\nabla_{\mathbf{z}} f_3(\mathbf{z}')$  would change position along the red contour but still lie within  $\mathcal{S}_1$ .

Let  $\mathcal{P}(Df(\mathbf{Z}), C_{:,j})$  denote the *column-wise sparse self-expression problem* for the Jacobian column



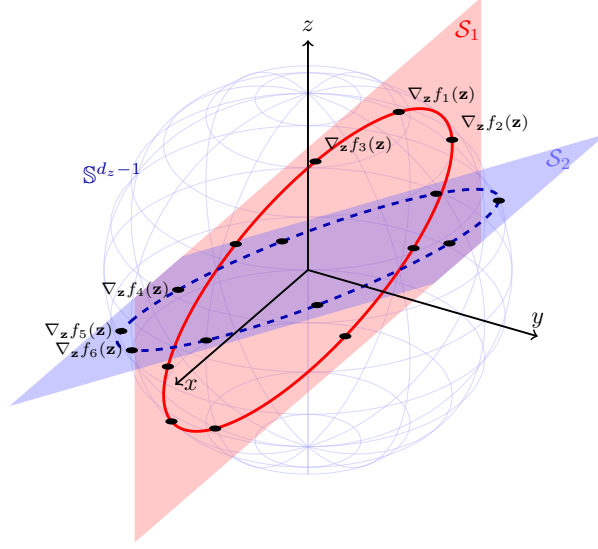


Figure 5.2: A geometric illustration of the assumption of subspaces union (Asm5.4) that underlies subspace clustering. Two planes are presented as subspaces of the Jacobian span ( $\mathcal{S}_1, \mathcal{S}_2$ ), within which gradients are drawn.

$\nabla_{\mathbf{z}} f_j$ , defined by

$$\begin{aligned} \min_{C_{:,j} \in \mathbb{R}^{d_x}} \quad & \|C_{:,j}\|_1, \\ \text{subject to} \quad & \nabla_{\mathbf{z}} f_j(\mathbf{Z}) = Df(\mathbf{Z}) C_{:,j} \quad \text{a.s.}, \\ & C_{j,j} = 0. \end{aligned} \tag{5.8}$$

Alternatively, we define a matrix-level formulation with a quadratic penalty in expectation, referred to as the *expected global self-expression problem*, denoted  $\mathcal{P}_\lambda(Df)$ :

$$\min_{\substack{C \in \mathbb{R}^{d_x \times d_x} \\ \text{diag}(C) = \mathbf{0}}} \|C\|_1 + \lambda \mathbb{E}_{\mathbf{Z}} [\|Df(\mathbf{Z}) - Df(\mathbf{Z}) C\|_F^2]. \tag{5.9}$$

The second formulation is often more convenient in practice, especially during training, since  $f$  is typically implemented as a neural network. However, both formulations are central to our theoretical analysis: the first is used to study the recovery of disjoint clusters (Theorem Thm5.2, Proposition Prop5.1), while the second provides the foundation for analyzing overlapping clusters and establishing stability guarantees (Theorems Thm5.3 and Thm5.4, Proposition Prop5.3).

### Equivalence of $\mathcal{P}(Df(\mathbf{Z}), C_{:,j})$ and $\mathcal{P}_\lambda(Df)$

We now analyze under which conditions one can assert that the series of problems  $\mathcal{P}(Df(\mathbf{Z}), C_{:,j})$  is identical to solving the global and penalized problem  $\mathcal{P}_\lambda(Df)$ .

We first observe that

$$\mathbb{E}_{\mathbf{Z}} [\|Df(\mathbf{Z}) - Df(\mathbf{Z}) C\|_F^2] = \sum_{j=1}^{d_x} \mathbb{E}_{\mathbf{Z}} [\|\nabla_{\mathbf{z}} f_j(\mathbf{Z}) - Df(\mathbf{Z}) C_{:,j}\|_2^2],$$

and likewise

$$\|C\|_1 = \sum_{j=1}^{d_x} \|C_{:,j}\|_1.$$

Thus, the global objective

$$\mathbb{E}_{\mathbf{Z}} [\|Df(\mathbf{Z}) - Df(\mathbf{Z}) C\|_F^2] + \lambda \|C\|_1$$

decouples into  $d_x$  independent column-wise expected-risk Lasso subproblems  $\mathcal{P}_\lambda(Df(\mathbf{Z}), C_{:,j})$  given by

$$\min_{C_{:,j} \in \mathbb{R}^{d_x}} \|C_{:,j}\|_1 + \lambda \mathbb{E}_{\mathbf{Z}} [\|\nabla_{\mathbf{Z}} f_j(\mathbf{Z}) - Df(\mathbf{Z}) C_{:,j}\|_2^2], \quad (5.10)$$

$$\text{subject to } C_{j,j} = 0.$$

In fact, solving the expected global self-expression problem  $\mathcal{P}_\lambda(Df)$  is **equivalent**, i.e., has the same solution set, to solving, **independently** for each  $j = 1, \dots, d_x$  the column-wise expected-risk Lasso subproblem  $\mathcal{P}_\lambda(Df(\mathbf{Z}), C_{:,j})$  by stacking its minimizers  $C_{:,1}^*, \dots, C_{:,d_x}^*$ .

As a result, to show the equivalence of  $\mathcal{P}(Df(\mathbf{Z}), C_{:,j})$  and  $\mathcal{P}_\lambda(Df)$ , it is enough to investigate when the two problems  $\mathcal{P}(Df(\mathbf{Z}), C_{:,j})$  and  $\mathcal{P}_\lambda(Df(\mathbf{Z}), C_{:,j})$  are equivalent for  $j = 1, \dots, d_x$ . In the following, we denote the quadratic penalty as

$$\ell_j(C_{:,j}) = \mathbb{E}_{\mathbf{Z}} [\|\nabla_{\mathbf{Z}} f_j(\mathbf{Z}) - Df(\mathbf{Z}) C_{:,j}\|_2^2]$$

**Remark Rem5.2 [Feasibility and Convexity of  $\mathcal{P}_\lambda(Df(\mathbf{Z}), C_{:,j})$  and  $\mathcal{P}_\lambda(Df)$ ]**

We note that a feasible solution exists to the problem  $\mathcal{P}(Df(\mathbf{Z}), C_{:,j})$  (Equation 5.8) since we assume self-expressiveness (Asm5.2). Moreover, since  $\mathbf{Z}$  is sub-Gaussian ( $\|\mathbf{Z}\|_{\psi_2} < \infty$ ) and  $f$  is smooth as in Assumption Asm5.3, then the second moments are finite, that is,  $\mathbb{E}_{\mathbf{Z}} \|Df(\mathbf{Z})\|_F^2 < \infty$  which is equivalent to saying  $\mathbb{E} \|\nabla f_j(\mathbf{Z})\|_2^2 < \infty$  for  $j \in [1, d_x]$ . Thus, the quadratic penalty in the optimization problem  $\mathcal{P}_\lambda(Df(\mathbf{Z}), C_{:,j})$  (Equation 5.10) is always finite.

Our problem is a convex with affine constraints: the maps

$$C_{:,j} \longrightarrow \|C_{:,j}\|_1, \quad C_{:,j} \longrightarrow \ell_j(C_{:,j})$$

are convex (the Hessian of  $\ell_j$  is  $2 \mathbb{E}_{\mathbf{Z}} [Df(\mathbf{Z})^\top Df(\mathbf{Z})]$  which is positive semi-definite), plus the constraint  $C_{:,j} \longrightarrow \nabla_{\mathbf{Z}} f_j - Df C$  is affine.

Let  $\mathcal{P}_t(Df(\mathbf{Z}), C_{:,j})$  be the *hard-constraint* problem for each column

$$\min_{C_{:,j} \in \mathbb{R}^{d_x}} \|C_{:,j}\|_1 \quad (5.11)$$

$$\text{subject to } \ell_j(C_{:,j}) \leq t, \quad C_{j,j} = 0.$$

**Theorem Thm5.1 [Equivalence of  $\mathcal{P}_t(Df(\mathbf{Z}), C_{:,j})$  and  $\mathcal{P}_\lambda(Df(\mathbf{Z}), C_{:,j})$ ]**

Assume the expected Gram matrix of the Jacobian  $\mathbb{E}_{\mathbf{Z}}[Df(\mathbf{Z})^\top Df(\mathbf{Z})]$  is positive definite, so that the quadratic penalty  $\ell_j$  is strictly convex for each  $j = 1, \dots, d_x$ . Then, for any tolerance  $t \geq 0$ , there is a unique and finite  $\lambda_j(t) \geq 0$  such that the solution set of  $\mathcal{P}_t(Df(\mathbf{Z}), C_{:,j})$  coincides with that of  $\mathcal{P}_\lambda(Df(\mathbf{Z}), C_{:,j})$ .

**Back to the expected global self-expression problem** Because each column  $C_{:,j}$  has its own independent constraint  $C_{j,j} = 0$  and objective term, the optimization problem  $\mathcal{P}_\lambda(Df)$  is solved by combining the  $d_x$  column-wise solutions  $C_{:,j}^*(\lambda)$ . Conversely, solving all column-wise constrained problems with levels  $t_j$  (Theorem Thm5.1) produces the same global minimizer once we pick

$$\bar{\lambda} = \max_{j \in \llbracket 1, d_x \rrbracket} \lambda_j(t_j),$$

by the *exact-penalty theorem* (Di Pillo, 1994; Bertsekas, 2015) and for all  $\lambda \geq \bar{\lambda}$ , the penalized expected-risk subproblem  $\mathcal{P}_\lambda(Df(\mathbf{Z}), C_{:,j})$  recovers the same minimizer  $C_{:,j}^*(\lambda)$  as the hard-constrained version  $\mathcal{P}(Df(\mathbf{Z}), C_{:,j})$ .

## Subspace Geometry and Detection

The goal of solving the sparse self-expression problem is not merely to reconstruct each Jacobian column from others, but to do so in a way that reveals the underlying subspace membership of each feature: we are interested in whether the support of the optimal coefficient vector  $C_{:,j}^*$  includes only indices corresponding to columns that lie in the same subspace as  $\nabla_{\mathbf{z}} f_j$ . This leads to the *subspace detection property* (Soltanolkotabi & Candés, 2012a), which underpins the correctness of subspace clustering:

**Definition Def5.16 [Subspace Detection Property]**

Let  $\{\mathcal{S}_m\}_{m=1}^M \subseteq \mathbb{R}^{d_z}$  be a collection of linear subspaces, and suppose each column  $\nabla_{\mathbf{z}} f_j(\mathbf{Z})$  of the Jacobian  $Df(\mathbf{Z})$  lies in some  $\mathcal{S}_{m_j}$  with  $m_j \in \{1, \dots, M\}$ . We say that the decoder  $f$  satisfies the *subspace detection property* if, for every  $j \in \{1, \dots, d_x\}$ , the minimizer  $C_{:,j}^*$  of  $\mathcal{P}(Df(\mathbf{Z}), C_{:,j})$  obeys

$$C_{k,j}^* \neq 0 \implies \nabla_{\mathbf{z}} f_k(\mathbf{Z}), \nabla_{\mathbf{z}} f_j(\mathbf{Z}) \in \mathcal{S}_{m_j} \text{ almost surely.} \quad (5.12)$$

In other words, nonzero entries in  $C_{:,j}^*$  occur only at indices  $k$  whose gradients lie in the same subspace as  $\nabla_{\mathbf{z}} f_j$ .

From Figure 5.2, if we assume  $\nabla_{\mathbf{z}} f_1(\mathbf{Z})$  is self-expressed by  $\nabla_{\mathbf{z}} f_2(\mathbf{Z})$  and  $\nabla_{\mathbf{z}} f_3(\mathbf{Z})$ , then

$$C_{1,2}^*, C_{1,3}^* \neq 0,$$

and the subspace detection property of Def5.16 holds because

$$\nabla_{\mathbf{z}} f_1(\mathbf{Z}), \nabla_{\mathbf{z}} f_2(\mathbf{Z}), \nabla_{\mathbf{z}} f_3(\mathbf{Z}) \in \mathcal{S}_1,$$

as assumed in Figure 5.2. However, this does not imply that  $\nabla_{\mathbf{z}} f_1(\mathbf{Z}), \nabla_{\mathbf{z}} f_2(\mathbf{Z}), \nabla_{\mathbf{z}} f_3(\mathbf{Z})$  are the only gradients lying in  $\mathcal{S}_1$ ; other gradients  $\nabla_{\mathbf{z}} f_j(\mathbf{Z})$  may also lie in  $\mathcal{S}_1$  (represented by black dots on the red contour in Figure 5.2), but with  $C_{1,j}^* = 0$ .

This is precisely the goal of SSC: to represent each gradient sparsely using only other gradients from the same subspace. Since membership in the same subspace is only a necessary condition for subspace detection, when it is violated, for example,  $\nabla_{\mathbf{z}} f_1(\mathbf{Z}) \in \mathcal{S}_1$  but  $\nabla_{\mathbf{z}} f_4(\mathbf{Z}) \in \mathcal{S}_2$ , the contrapositive of Equation 5.12 gives  $C_{1,4}^* = 0$ .

**Geometry of linear subspaces** A central challenge in subspace clustering is to determine when sparse self-expression can correctly recover the subspace membership of each feature. This requires a quantitative notion of the geometric separation between subspaces. Following the line of geometric arguments of Soltanolkotabi & Candés (2012b), a classical tool is the system of *principal angles* (Def5.17), which generalizes the notion of angle between vectors to the setting of linear subspaces. From these, one can define a scalar measure of closeness known as the *subspace affinity* (Def5.18), which plays a role in the theoretical analysis of clustering algorithms. Intuitively, the smaller the affinity between subspaces, the more they are distinguishable and the more likely the subspace detection property is to hold. In the following, we give a formal definition of both principal angles and affinity for subspaces, and then present our main theorem stating the maximum permissible affinity between subspaces for the subspace detection property to hold w.h.p.

**Definition Def5.17 [Principal Angles Between Subspaces]**

Let  $\mathcal{S}_m \in \text{Gr}(d_m, d_z)$  and  $\mathcal{S}_{m'} \in \text{Gr}(d_{m'}, d_z)$  be linear subspaces of dimensions  $d_m$  and  $d_{m'}$ , respectively, and set  $d = \min\{d_m, d_{m'}\}$ . The *principal angles*  $\theta_{m,m'}^{(1)}, \dots, \theta_{m,m'}^{(d)}$  between  $\mathcal{S}_m$  and  $\mathcal{S}_{m'}$  are defined recursively by

$$\cos(\theta_{m,m'}^{(i)}) := \max_{\substack{\mathbf{y} \in \mathcal{S}_m \\ \|\mathbf{y}\|=1}} \max_{\substack{\mathbf{z} \in \mathcal{S}_{m'} \\ \|\mathbf{z}\|=1}} \mathbf{y}^\top \mathbf{z},$$

subject to the orthogonality constraints

$$\mathbf{y}^\top \mathbf{y}_j = 0, \quad \mathbf{z}^\top \mathbf{z}_j = 0, \quad j = 1, \dots, i-1,$$

where  $\{\mathbf{y}_j\}$  and  $\{\mathbf{z}_j\}$  are the previously selected maximizers.

**Interpretation** The first principal angle  $\theta^{(1)}$  measures the smallest angle between any pair of unit vectors, one from each subspace (cf. Figure 5.3). Subsequent angles capture progressively less aligned

directions, orthogonal to those already considered. Together, these angles quantify the degree of alignment between two subspaces: large angles indicate strong separation, while small angles suggest potential overlap and confusion.

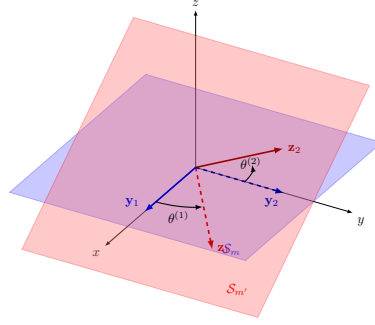


Figure 5.3: An illustration of the two principal angles between two subspaces  $\mathcal{S}_m, \mathcal{S}_{m'}$ .

Although the full sequence of principal angles provides a rich geometric comparison, it is often convenient to compress this information into a single scalar.

**Definition Def5.18 [Subspace Affinity]**

The *affinity* between subspaces  $\mathcal{S}_m$  and  $\mathcal{S}_{m'}$  is defined as

$$\text{aff}(\mathcal{S}_m, \mathcal{S}_{m'}) := \sqrt{\sum_{i=1}^d \cos^2(\theta_{m,m'}^{(i)})},$$

where  $d = \min(d_m, d_{m'})$ .

**Geometric Significance** The affinity captures a cumulative alignment: a zero value indicates orthogonal subspaces, while higher values reflect greater overlap. In the context of sparse self-expression, lower affinities reduce the risk of selecting elements from incorrect subspaces, thereby increasing the likelihood of correct clustering. Thus, subspace affinity is a key factor governing the success of subspace recovery.

We now present our main theoretical result, which provides conditions under which the sparse self-expression problem correctly detects subspace structure w.h.p.

**Theorem Thm5.2 [Subspace Detection via Sparse Self-Expression]**

Let  $\mathbf{Z} \in \mathbb{R}^{d_z}$  be a sub-Gaussian random vector with  $\|\mathbf{Z}\|_{\psi_2} \leq K$ , and let  $f$  be  $L$ -smooth as in Assumption Asm5.3. Suppose the columns of the Jacobian  $Df$  follow the union-of-subspaces model (Assumption Asm5.4), i.e., they lie in a union of  $M$  deterministic subspaces  $\{\mathcal{S}_m\}_{m=1}^M \subset \mathbb{R}^{d_z}$ , with  $n_m$  columns in subspace  $\mathcal{S}_m$ .

Then, there exist universal constants  $\Lambda_1, \Lambda_2 > 0$  such that if

$$\max_{k \neq m} \text{aff}(\mathcal{S}_k, \mathcal{S}_m) \sqrt{\log(n_k + 1)} \leq \Lambda_1 K L \sqrt{\log n_m}, \quad \forall m \in \{1, \dots, M\}, \quad (5.13)$$

Table 5.1: Key differences between our analysis and prior SSC theory.

Aspect	Candès & Soltanolkotabi (2012)	This work
Data to be clustered	Random points <i>on</i> the subspaces (semi-random model)	Random Jacobian columns induced by latent variable $\mathbf{Z}$
Regularity control	Purely geometric; no smoothness parameter	Global Hessian bound $L$ on decoder $f$
Probability tools	Geometric inequalities for uniformly random points on the sphere	Vershynin’s matrix deviation bounds for sub-Gaussian design
Noise/robustness	Outliers handled via robust SSC extensions	Latent noise and curvature enter constants $K, L$ in Prop5.3

then  $f$  satisfies the subspace detection property with a probability of at least

$$1 - \sum_{m=1}^M n_m \exp\left(-\frac{\Lambda_2^2 \log n_m}{2 d_m}\right) + \sum_{m=1}^M \frac{2(M-1)}{\sqrt{n_m+1}}.$$

**From point-based SSC to latent-gradient SSC** Before discussing the results of Theorem Thm5.2, it is important to delineate the main differences in both assumptions, nature of the problem tackled, and nature of the results in our work compared to that of Soltanolkotabi & Candès (2012b). First, Soltanolkotabi & Candès (2012b) analyzed SSC on *standard generative models* among which a semi-random one: *static data points* are sampled uniformly at random but lie *exactly* in a union of fixed linear subspaces, possibly mixed with uniform-spherical outliers. Their proof employs a primal–dual witness construction (Wainwright, 2009) together with sphere-cap concentration (Vershynin, 2018) to show that the  $\ell_1$  self-expressive problem enjoys the subspace-detection property w.h.p whenever a minimal gap in affinity between subspaces is satisfied.

**Our setting is far more challenging:** Our setting is analogous in that the tangent subspaces  $\{\mathcal{S}_m\}_{m=1}^M$  are fixed, whereas the Jacobian columns  $\{\nabla_{\mathbf{z}} f_i(\mathbf{Z})\}_{i=1}^{d_x}$  are random; however, the randomness now stems from a *sub-Gaussian* latent code  $\mathbf{Z}$  propagated through a twice-differentiable decoder  $f$ . Consequently, purely geometric arguments are augmented by high-dimensional probability tools and exploit now a global Hessian bound on coordinates output  $\|D^2 f_i(\mathbf{z})\|_{\text{op}}$  (Asm5.3) to control how fast gradients rotate. Thus, while we retain the three-step template proof (dual certificate  $\rightarrow$  support recovery  $\rightarrow$  spectral clustering) of Soltanolkotabi & Candès (2012b), all probabilistic estimates are new and tailored to the Jacobian self-expression problem (see Appendix C.1.3 for formal proofs and Table 5.1).

Theorem Thm5.2 carries several important implications for CRL via Jacobian self-expression:

- (1) **Sample Complexity per Latent Subspace:** Suppose we want to detect all subspaces with an error of at most  $\epsilon > 0$ . If we allocate "the global budget"  $\epsilon$  uniformly across  $\{\mathcal{S}_m\}_{m=1}^M$ , then for each

$m \in \{1, \dots, M\}$ , we require

$$\underbrace{n_m \exp\left(-\frac{\Lambda_2^2 \log n_m}{2 d_m}\right)}_{A_m} + \underbrace{\frac{2(M-1)}{\sqrt{n_m+1}}}_{B_m} \leq \frac{\epsilon}{M}. \quad (5.14)$$

For  $A_m$ , it suffices to have

$$A_m = n_m^{1-\frac{\Lambda_2^2}{2d_m}} \leq \frac{\epsilon}{2M}. \quad (5.15)$$

An interesting observation is that the failure probability does not decrease indefinitely with increasing  $n_m$  if the subspace dimension  $d_m$  satisfies  $d_m \geq \frac{\Lambda_2^2}{2}$ . Otherwise,  $A_m$  could grow with  $n_m$ , even though  $B_m$  decreases.

In the case  $d_m < \frac{\Lambda_2^2}{2}$ , we have

$$A_m \leq \frac{\epsilon}{2M} \iff n_m \geq \left(\frac{2M}{\epsilon}\right)^{\frac{2d_m}{\Lambda_2^2 - 2d_m}}. \quad (5.16)$$

Similarly, for  $B_m$ , we require

$$B_m \leq \frac{\epsilon}{2M} \iff n_m \geq 16 \left(\frac{M(M-1)}{\epsilon}\right)^2 = \Theta\left(\frac{M^4}{\epsilon^2}\right). \quad (5.17)$$

Therefore, each latent-induced subspace  $\mathcal{S}_m$  should have at least

$$n_m = \Omega\left(\left(\frac{2M}{\epsilon}\right)^{\frac{2d_m}{\Lambda_2^2 - 2d_m}} + \frac{M^4}{\epsilon^2}\right) \quad (5.18)$$

columns observed to reliably detect and separate it from the others.

**Geometric intuition:** For small  $d_m$ , low-dimensional subspaces are "thin" enough to remain well-separated in the ambient space, so random Jacobian columns from different factors are unlikely to align. When  $d_m$  grows large, linear subspaces tend to "flatten", and almost any random direction has a large component in several subspaces. SSC may then fail to correctly detect columns. If  $d_m > \frac{\Lambda_2^2}{2}$ , increasing  $n_m$  does not help; the failure term  $A_m$  stops decaying, signaling an inherent identifiability barrier rather than a dimensionality limitation of the observed space.

(2) **Incoherence Requirement:** The condition

$$\max_{k \neq m} \text{aff}(\mathcal{S}_k, \mathcal{S}_m) \cdot \sqrt{\log(n_k + 1)} \lesssim KL \sqrt{\log n_m} \quad (5.19)$$

quantifies how "far apart" any two subspaces must be, accounting for dimensionality and sub-Gaussian variability in  $\mathbf{Z}$  and, intuitively, the lower the affinity between subspaces, the less they are confused. The Hessian bound  $L$  and latent noise  $K$  suggest that stronger Lipschitz regularization or tighter latent priors can reduce the right-hand side and thus relax the incoherence requirement.

- (3) **Effect of Smoothness and Concentration on Identifiability:** The dependence on  $K$  and  $L$  shows that both the stochasticity of latent  $\mathbf{Z}$  and the nonlinearity of  $f$  affect subspace recovery. Making  $f$  smoother (smaller Hessians) or latent priors more concentrated (smaller sub-Gaussian norm) allows the same clustering guarantees to hold under weaker incoherence conditions.

### 5.5.2 From Subspace Detection to Cluster Recovery

Theorem Thm5.2 guarantees that under suitable incoherence conditions, the sparse self-expression solution  $C^*$  is subspace-preserving: each Jacobian column  $\nabla_{\mathbf{z}} f_j$  is reconstructed using only columns from the same subspace. This property is not only crucial for identifiability but also enables the recovery of the modular structure among the observed features. The following proposition formalizes how this subspace structure, when encoded in  $C^*$ , can be translated into feature clusters using spectral methods.

#### Proposition Prop5.1 [Recovery of Feature Clusters via Spectral Clustering]

Let the following conditions hold:

- **$\ell_1$ -self-expression:** For each column  $j$ , let  $C_{:,j}^*$  be the solution to the problem  $\mathcal{P}(Df(\mathbf{Z}), C_{:,j})$  as in Equation 5.8.
- **Affinity matrix:** Assemble  $C^* \in \mathbb{R}^{d_x \times d_x}$ , and define the symmetric matrix

$$A^* := \frac{1}{2} (|C^*| + |C^*|^\top). \quad (5.20)$$

Suppose the subspace incoherence condition of Equation 5.13 is satisfied. Then, with the same high probability as in Theorem Thm5.2, the following holds:

1. **Block-diagonal structure:** Up to a column-wise permutation,  $A^*$  is block-diagonal, with block sizes  $\{n_m\}_{1 \leq m \leq M}$  corresponding to the subspace decomposition.
2. **Correct clustering:** Unnormalized spectral clustering applied to  $A^*$  recovers the ground-truth feature clusters.

**Constructing the Feature Graph** To operationalize the result of Prop5.1, we interpret the absolute entries of  $C^*$  as encoding similarity between decoder gradients:

$$(i, j) \in E \quad \Leftrightarrow \quad C_{ij}^* \neq 0 \quad \text{or} \quad C_{ji}^* \neq 0 \Leftrightarrow A_{i,j}^* \neq 0.$$

The resulting graph has vertex set  $\mathcal{V} = \{\nabla_{\mathbf{z}} f_1, \dots, \nabla_{\mathbf{z}} f_{d_x}\}$ , and the affinity matrix  $A^*$  defines edge weights. Its block-diagonal structure reflects the disjointness of subspaces: gradients in different subspaces exhibit no mutual support under sparse coding (Figure 5.1c).



**Feature-Level Interpretation** The affinity structure in  $A^*$  mirrors latent support overlap among features. This motivates the following graph-theoretic abstraction:

**Definition Def5.19 [Feature Graph via Self-Expression]**

Let each observed feature  $\mathbf{x}_i$  have latent parent set  $\text{Pa}(i) \subseteq \llbracket 1, d_z \rrbracket$ . Define the *feature graph*  $G_F = (\llbracket 1, d_x \rrbracket, E)$ , where

$$(i, j) \in E \iff A_{i,j}^* \neq \emptyset.$$

Under the union-of-subspaces model (Asm5.4), the feature-graph  $G_F$  is naturally block-structured. Proposition Prop5.1 shows that this combinatorial structure is recoverable via optimization and spectral decomposition, completing the link from geometric identifiability to discrete modular recovery (Figure 5.4). In practice, one chooses the number of clusters  $\hat{M}$  in spectral clustering by inspecting the eigenvalue spectrum of the graph Laplacian of  $G_F$ ,

$$\text{Laplacian}(G_F) := D - A^*, \tag{5.21}$$

where  $D = \text{diag}(d_1, \dots, d_{d_x}) \in \mathbb{R}^{d_x \times d_x}$  is the *degree matrix* with

$$d_i := \sum_{j=1}^{d_x} A_{ij}^*.$$

We then apply the so-called *eigengap heuristic* (Von Luxburg, 2007): let

$$\lambda_1 \leq \lambda_2 \leq \dots \leq \lambda_{d_x}$$

be the eigenvalues of  $\text{Laplacian}(G_F)$  in non-decreasing order, and set

$$\hat{M} = \arg \max_{1 \leq i \leq d_x - 1} (\lambda_{i+1} - \lambda_i),$$

i.e. the index at which the consecutive eigenvalue gap is largest.

### Towards Recovery of Overlapping Feature Clusters

The spectral clustering result established in Proposition Prop5.1 relies on a hard partitioning of observed variables into disjoint subspaces following the shared-parent clustering rule of Definition Def5.12. We now focus on the overlapping-parent clustering rule of Definition Def5.13: the children set  $\text{Ch}(\mathbf{z}^j)$  of each latent variable  $\mathbf{z}^j$ . The resulting clustering structure is naturally overlapping: an observed feature  $\mathbf{x}^i$  may have multiple latent parents. The next result provides sufficient conditions under which such overlapping groupings can be recovered from the self-expression matrix  $C^*$ . Importantly, our analysis does not assume disjointness or even separability of the influence of latents over observable features as in the anchor feature (Section5.1). Instead, we work under a set of relaxed structural assumptions on

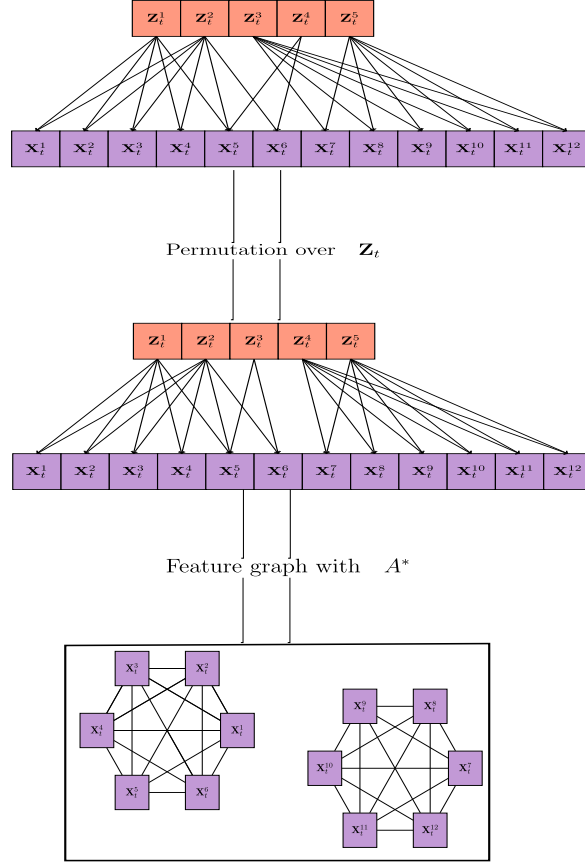


Figure 5.4: Illustration of the modular latent structure from Proposition Prop5.1. Solving the sparse self-expression problem yields an adjacency matrix  $A^*$  (cf. Equation5.4), whose nonzero entries define connected components in the feature graph  $G_F$ . We recover these components via spectral clustering.

the decoder (Assumption Asm5.5). These assumptions ensure that the self-expression affinity matrix  $A^*$  encodes latent parent structure in its edge weights, and that overlapping clustering algorithms, such as SAAC (Panov et al., 2017; Kaufmann et al., 2018) or SymNMF (Kuang et al., 2015; Zhang & Liu, 2022), can recover w.h.p the true groups with bounded misclassification error.

#### Assumption Asm5.5 [Structured Latent–Feature Model]

Let  $\mathbf{Z} \in \mathbb{R}^{d_z}$  be a sub-Gaussian random vector with  $\|\mathbf{Z}\|_{\psi_2} \leq K$ , and let  $f$  be  $L$ -smooth as in Assumption Asm5.3. Recall the parental and children sets

$$\text{Pa}(i) = \{j : \partial f_i / \partial z^j \neq 0\}, \quad \text{Ch}(j) = \{i : j \in \text{Pa}(i)\}.$$

Assume:

(A1) **Sparsity:** Each coordinate  $f_i$  depends on at most  $s \ll d_z$  latents, i.e.

$$\max_{1 \leq i \leq d_x} |\text{Pa}(i)| \leq s.$$

(A2) **Incoherence:** For each  $j \in \llbracket 1, d_z \rrbracket$ , let

$$\partial_j f(\mathbf{Z}) := \left[ \frac{\partial f_1}{\partial z_j}, \dots, \frac{\partial f_{d_x}}{\partial z_j} \right](\mathbf{Z}),$$

and define

$$m_j := \mathbb{E}_{\mathbf{Z}} \|\partial_j f(\mathbf{Z})\|^2, \quad \Sigma_{jk} := \mathbb{E}_{\mathbf{Z}} \langle \partial_j f(\mathbf{Z}), \partial_k f(\mathbf{Z}) \rangle.$$

We assume that  $|\Sigma_{jk}| \leq \mu \sqrt{m_j m_k}$  for all  $j \neq k$ , with  $\mu < 1$ .

(A3) **Dominance:** For each  $i$ , there exists  $j_i \in \text{Pa}(i)$  such that

$$\mathbb{E}_{\mathbf{Z}} [|\partial f_i / \partial z_{j_i}|] \geq (1 - \delta) \sqrt{\mathbb{E}_{\mathbf{Z}} \|\nabla_z f_i(\mathbf{Z})\|^2}, \quad \delta \ll 1.$$

(A4) **Group Size:** There exists  $\gamma = \Omega(\log d_x)$  such that

$$\min_{1 \leq j \leq d_z} |\text{Ch}(j)| \geq \gamma.$$

(A5) **Restricted Eigenvalue:** There exists  $\kappa > 0$  such that for all  $\mathbf{v} \in \mathbb{R}^{d_z}$  with  $\|\mathbf{v}\|_0 \leq s$ ,

$$\mathbf{v}^\top \mathbb{E}_{\mathbf{Z}} [Df(\mathbf{Z}) Df(\mathbf{Z})^\top] \mathbf{v} \geq \kappa \|\mathbf{v}\|_2^2.$$

**Intuition** We explain the role of each assumption in clustering recovery:

- (A1): Restricting  $|\text{Pa}(i)| \leq s$  ensures each feature  $f_i$  depends only on  $s$  latent coordinates, preventing overparameterization in the Lasso regression;
- (A2): Mutual incoherence  $|\Sigma_{jk}| \leq \mu \sqrt{m_j m_k}$  with  $\mu < 1$  controls correlations between gradient directions. It is in principle analogous to the *irrepresentable condition* for Lasso support recovery (Zhao & Yu, 2006; Wainwright, 2009; Meinshausen & Yu, 2009): it guarantees no unused latent direction can enter as a linear combination of the true ones. In our case, the conditions bear the following geometric intuition: if we associate to each latent dimension a stochastic direction vector  $\partial_j f(\mathbf{Z})$  in the observational ambient space  $\mathbb{R}^{d_x}$ , then the condition implies that the expected correlation coefficient between two different direction vectors  $\partial_j f(\mathbf{Z}), \partial_k f(\mathbf{Z})$  is bounded by  $\mu$ . Thus, if one considers the one-dimensional subspaces spanned respectively by  $\partial_j f(\mathbf{Z})$  and  $\partial_k f(\mathbf{Z})$ , then the principal angle  $\theta_{jk}$  (Def5.17) between them verifies in expectation  $\theta_{jk} \geq \arccos \mu$ . We therefore prevent "near-parallelism" in Jacobian rows, which is important in cluster recovery because it helps bound between-cluster affinities;
- (A3): Requiring that a partial derivative  $\frac{\partial f_i}{\partial z_j}$  dominates guarantees that each output coordinate  $i$  is most strongly coupled to a latent variable without being decoded with only one latent as in

the single-parent decoding assumption and without requiring having exact "pure children" as in the anchor features assumption;

- (A4): Having  $|Ch(j)| \geq \gamma = \Omega(\log d_x)$  ensures sufficient "samples" (here observed feature) for concentration inequalities to hold; and
- (A5): Strong convexity (Restricted Eigenvalue condition) is essential for the uniqueness of the Lasso minimizer and for support recovery proofs.

**Theorem Thm5.3 [Self-Expression and Overlapping Cluster Recovery]**

Assume assumptions Asm5.5 hold. Let  $C^*$  be the unique solution to the population-level self-expression problem  $\mathcal{P}_\lambda(Df)$  (Equation 5.9), and let  $A^*$  be the resulting symmetric affinity matrix. Choose

$$\lambda \geq c_1 \mu + c_2 K L \sqrt{d_x \log(d_x^2/\varepsilon)},$$

for constants  $c_1 > 1$ ,  $c_2 \geq 2$ , and confidence parameter  $\varepsilon \in (0, 1)$ . Then, with probability at least  $1 - \varepsilon$ , for each latent group  $Ch(j)$  the following hold:

- **Intra-cluster affinities:** For all  $i, i' \in Ch(j)$ ,

$$A_{ii'}^* \geq (1 - \delta - \mu) m_j - C_3 K L \sqrt{d_x \log(d_x^2/\varepsilon)}.$$

- **Inter-cluster affinities:** For all  $i \in Ch(j)$ ,  $i' \in Ch(k)$ ,  $k \neq j$ ,

$$A_{ii'}^* \leq \mu \sqrt{m_j m_k} + C_3 K L \sqrt{d_x \log(d_x^2/\varepsilon)},$$

where  $C_3 = 2 c_2$ . Moreover, if

$$\min_{1 \leq j \leq d_z} m_j - \mu \max_{k \neq j} \sqrt{m_j m_k} \gg K L \sqrt{d_x \log(d_x^2/\varepsilon)},$$

then overlap-aware clustering methods such as SAAC (Panov et al., 2017; Kaufmann et al., 2018) or SymNMF (Kuang et al., 2015; Zhang & Liu, 2022) recover clusters  $\hat{G}_j$  satisfying

$$\min_{1 \leq j \leq d_z} \frac{|\hat{G}_j \triangle Ch(j)|}{|Ch(j)|} = \mathcal{O}\left(\delta + \frac{\mu}{\gamma} + \frac{K L \sqrt{d_x \log(d_x^2/\varepsilon)}}{\min_{1 \leq j \leq d_z} m_j}\right). \quad (5.22)$$

**Interpretation** At a high level, both SAAC and SymNMF succeed because they first convert the overlapping-community problem into a geometric grouping task in a low-dimensional spectral embedding, then recover the clusters. The misclassification bound in Equation 5.22 splits into three intuitive contributions: 1. *Dominance error*  $\delta$ , reflecting that each feature's strongest latent parent only *almost* dominates its gradient (Assumption (A3)). 2. *Incoherence-rounding error*  $\mu/\gamma$ , arising because residual

cross-group correlations of size  $\mu$  must be averaged out over clusters of minimum size  $\gamma$ . 3. *Embedding-noise error*

$$\frac{K L \sqrt{d_x \log(d_x^2/\varepsilon)}}{\min_{1 \leq j \leq d_z} m_j},$$

which quantifies how sub-Gaussian fluctuations ( $K$ ), Hessian smoothness ( $L$ ), Frobenius norm over the Jacobian ( $\sqrt{d_x}$ ) degrade the ideal block affinities. Again similar to discussion of Theorem Thm5.2, tighter latent priors (smaller  $K$ ), smoother decoder (smaller  $L$ ) tighten the embedding noise term, improving overlap-clustering accuracy. Dependence on  $d_x$  highlights the intuition that the more the input space is higher dimensional, the more an overlapping variables clustering is prone to error.

### 5.5.3 Generalization and Stability of the Self-Expression Objective

We now address the gap between theory and practice in modeling the self-expression loss. The previous results guarantee identifiability under idealized assumptions about the decoder and its Jacobian structure. However, practical training operates on finite data and noisy gradients, often approximated via samples from the latent posterior. This raises three key questions: 1. **Bias:** *How much does the mismatch between the prior and the aggregated posterior distort the self-expression loss?* 2. **Generalization:** *Given a known decoder, how well does the empirical self-expression loss approximate its population counterpart?* 3. **Stability:** *How sensitive is the self-expression loss to perturbations or noise in the Jacobian?*

**Bias from Aggregated Posterior** In practice, variational autoencoders sample latent variables  $\mathbf{z}$  not from the prior  $p(\mathbf{z})$  but from the approximate posterior  $q_\phi(\mathbf{z} \mid \mathbf{x})$ . Consequently, expectations such as those over the self-expression loss

$$\ell(C, \mathbf{z}) = \|Df(\mathbf{z}) - Df(\mathbf{z})C\|_F^2$$

are taken under the *aggregated posterior*

$$q_\phi(\mathbf{z}) := \mathbb{E}_{\mathbf{X} \sim p_{\text{data}}} [q_\phi(\mathbf{z} \mid \mathbf{X})],$$

rather than the prior. This distributional mismatch introduces an *aggregation bias*, which can be quantified in terms of the Kullback–Leibler divergence  $D_{\text{KL}}(q_\phi \parallel p)$ , exactly the term that appears as the ELBO gap in VAE training. The argument relies on bounding the expectation gap via total variation distance:

$$\|q - p\|_{\text{TV}} := \frac{1}{2} \int |q(\mathbf{z}) - p(\mathbf{z})| d\mathbf{z}.$$

#### Lemma Lem5.1 [Bias via Total Variation]

Let  $q$  and  $p$  be probability densities on  $\mathbb{R}^{d_z}$ , and let  $\ell : \mathbb{R}^{d_z} \rightarrow \mathbb{R}$  be measurable with  $\|\ell\|_\infty < \infty$ .

Then

$$|\mathbb{E}_{\mathbf{Z} \sim q}[\ell(C, \mathbf{Z})] - \mathbb{E}_{\mathbf{Z} \sim p}[\ell(C, \mathbf{Z})]| \leq \|\ell\|_\infty \cdot \|q - p\|_{\text{TV}}.$$

**Lemma Lem5.2 [Pinsker’s Inequality (Gibbs & Su, 2002)]**

For any distributions  $q, p$ ,

$$\|q - p\|_{\text{TV}} \leq \sqrt{\frac{1}{2} D_{\text{KL}}(q \| p)}.$$

Combining Lemmas Lem5.1 and Lem5.2, and assuming unit-norm gradients, we obtain:

**Proposition Prop5.2 [Bias Bound via ELBO Gap]**

$$|\mathbb{E}_{\mathbf{Z} \sim q_\phi}[\ell(C, \mathbf{Z})] - \mathbb{E}_{\mathbf{Z} \sim p}[\ell(C, \mathbf{Z})]| \leq \sqrt{d_x}(1 + \|C\|_{\text{op}}) \cdot \sqrt{\frac{1}{2} D_{\text{KL}}(q_\phi \| p)}.$$

This bound reveals a trade-off between model structure and posterior mismatch. The larger the spectral norm  $\|C\|_{\text{op}}$ , the more sensitive the loss becomes to deviations from the prior. Thus, better variational approximations not only improve reconstruction, but also yield more faithful estimates of latent-space geometry.

**Generalization from Finite Data** We now consider generalization from empirical estimates to population risk. Let  $\bar{J}_f(\mathbf{x}; q_\phi) := \mathbb{E}_{\mathbf{Z} \sim q_\phi(\cdot | \mathbf{x})}[Df(\mathbf{Z})]$  denote the expected Jacobian under the posterior. Define the self-expression loss:

$$\bar{\ell}(C, f; \mathbf{x}) := \|\bar{J}_f(\mathbf{x}; q_\phi) - C\bar{J}_f(\mathbf{x}; q_\phi)\|_F^2,$$

and consider the hypothesis class  $\mathcal{C}_\lambda := \{C \in \mathbb{R}^{d_x \times d_x} : \|C\|_1 \leq \lambda, \text{diag}(C) = \mathbf{0}\}$ .

**Theorem Thm5.4 [Generalization of Self-Expression Loss]**

Let  $M_\phi := \sup_{\mathbf{x}} \|\bar{J}_f(\mathbf{x}; q_\phi)\|_F$ . Then with probability at least  $1 - \delta$  over  $N$  i.i.d. samples  $\{\mathbf{X}_i\}_{i=1}^N$ , we have:

$$\sup_{C \in \mathcal{C}_\lambda} \left| \mathbb{E}_{\mathbf{X} \sim p_{\text{data}}}[\bar{\ell}(C, f; \mathbf{X})] - \frac{1}{N} \sum_{i=1}^N \bar{\ell}(C, f; \mathbf{X}_i) \right| \leq 8\lambda M_\phi^2 \sqrt{\frac{2d_z \log d_x}{N}} + \frac{M_\phi^2}{2} \sqrt{\frac{\log(1/\delta)}{N}}.$$

Since gradients are unit-norm by assumption, Jensen’s inequality implies  $M_\phi^2 \leq d_x$ . Thus, empirical minimization of the self-expression loss generalizes well under mild conditions on the decoder and sparsity constraint  $\lambda$ . The logarithmic dependence on  $d_x$  ensures scalability in high-dimensional regimes.

**Stability under Jacobian Perturbation** Finally, we analyze the stability of the self-expression loss under stochastic perturbations of the Jacobian, which may arise from encoder sampling or numerical noise.

**Proposition Prop5.3 [Stability of Self-Expression Loss under Jacobian Noise]**

Suppose

$$Df(\mathbf{Z}) = \widetilde{Df}(\mathbf{Z}) + E(\mathbf{Z}),$$

where  $\widetilde{Df}(\mathbf{Z}) \in \mathbb{R}^{d_x \times d_z}$  is the true Jacobian and each column of  $E$  is an independent, zero-mean sub-Gaussian vector:  $E_{:,j}(\mathbf{Z}) \in \text{subG}_{d_x}(\varepsilon)$ . Let  $C^* \in \mathbb{R}^{d_x \times d_x}$  satisfy  $\text{diag}(C^*) = \mathbf{0}$ . Define the self-expression loss deviation as

$$\Delta(\mathbf{Z}) := \|Df(\mathbf{Z}) - Df(\mathbf{Z})C^*\|_F^2 - \|\widetilde{Df}(\mathbf{Z}) - \widetilde{Df}(\mathbf{Z})C^*\|_F^2.$$

Then, for any  $\delta \in (0, 1)$ , with probability at least  $1 - \delta$ ,

$$|\Delta(\mathbf{Z})| \leq (1 + \|C^*\|_{\text{op}}) (2d_x B(\delta)\varepsilon + (1 + \|C^*\|_{\text{op}})B(\delta)^2\varepsilon^2),$$

where

$$B(\delta) := \Lambda\sqrt{d_z d_x} + \sqrt{2d_z \log(2d_x/\delta)},$$

and  $\Lambda > 0$  is a universal constant.

**Interpretation** A key implication of Proposition Prop5.3 is a stability bound that establishes a principled connection between sparsity, low-rank structure, and robustness of the self-expression loss under perturbations:

- **Perturbation Scaling and Deviation Bound:** Proposition Prop5.3 shows that when the true Jacobian  $\widetilde{Df}$  is corrupted by sub-Gaussian noise of magnitude  $\varepsilon$ , the self-expression loss deviation  $\Delta(\mathbf{Z})$  is controlled by two terms scaling as  $\mathcal{O}(d_x B(\delta)\varepsilon)$  and  $\mathcal{O}(d_x B(\delta)^2\varepsilon^2)$ . The leading absolute deviation is

$$|\Delta(\mathbf{Z})| = \mathcal{O}((1 + \|C^*\|_{\text{op}}) d_x B(\delta)\varepsilon), \quad (5.23)$$

and remains small whenever

$$2d_x B(\delta)\varepsilon \ll \frac{1}{1 + \|C^*\|_{\text{op}}}.$$

- **Role of sparsity:** Sparsity improves stability since

$$\|C^*\|_{\text{op}} \leq \|C^*\|_{1 \rightarrow 1}, \quad \text{where} \quad \|C^*\|_{1 \rightarrow 1} := \max_{1 \leq j \leq d_x} \sum_{i=1}^{d_x} |C_{ij}^*|,$$

and thus sparser coefficients imply lower operator norms and better robustness by Equation 5.23.

- **Influence of Low Rank:** For fixed Frobenius norm, lower-rank solutions are more stable because the lower the rank of  $C^*$ , the smaller the spectral norm, as justified by the matrix-norm inequality (Horn & Johnson, 2012a):

$$\|C^*\|_{\text{op}} \leq \sqrt{\text{rank}(C^*)} \|C^*\|_F,$$

highlighting the beneficial trade-off between sparsity, rank, and noise sensitivity in subspace modeling.

#### 5.5.4 Computational efficiency: Calculating the Penalty $\bar{\ell}(C, f; \mathbf{x})$

Suppose we wish to compute the penalty  $\bar{\ell}(C, f; \mathbf{x})$  by first forming the *full* expected Jacobian  $\bar{J}_f(\mathbf{x}; q_\phi) \in \mathbb{R}^{d_z \times d_x}$ . This poses a computational challenge: in practice,  $\bar{J}_f(\mathbf{x}; q_\phi)$  is approximated using samples  $\mathbf{z}_1, \dots, \mathbf{z}_{S'} \sim q_\phi(\cdot | \mathbf{x})$ ,

$$\bar{J}_f(\mathbf{x}; q_\phi) \approx \frac{1}{S'} \sum_{j=1}^{S'} Df(\mathbf{z}_j).$$

By "backpropagating" once per input dimension, obtaining every row vector  $\nabla_{\mathbf{z}} f_i(\mathbf{z}_j)$  requires one backward pass per output, for a total of  $\mathcal{O}(d_x)$  gradient evaluations, each itself requiring  $\mathcal{O}(T_f)$ , the cost of one forward+backward through the network. Hence, explicitly assembling  $\bar{J}_f(\mathbf{x}; q_\phi) \in \mathbb{R}^{d_z \times d_x}$  takes

$$\mathcal{O}(S' d_x T_f),$$

which grows linearly with  $d_x$  and is thus computationally demanding. The following theorem provides a better computation strategy.

#### Theorem Thm5.5 [Efficient Approximation of the Self-Expression Penalty]

The self-expressiveness penalty

$$\bar{\ell}(C, f; \mathbf{x}) = \|\bar{J}_f(\mathbf{x}; q_\phi) - C \bar{J}_f(\mathbf{x}; q_\phi)\|_F^2$$

can be efficiently approximated via Hutchinson-style trace estimation (Hutchinson, 1989):

$$\bar{\ell}(C, f; \mathbf{x}) \approx \sum_{i=1}^S \|\eta(\epsilon_i, f; \mathbf{x})\|_2^2,$$

where  $\epsilon_1, \dots, \epsilon_S \sim \mathcal{N}(0, I_{d_x})$  are independent Gaussian probe vectors, and

$$\begin{aligned} \eta(\epsilon, f; \mathbf{x}) &= \bar{J}_f(\mathbf{x}; q_\phi) \left( \epsilon - \sum_{j=1}^{d_x} \langle \epsilon, C_{:,j} \rangle \mathbf{e}_j \right) \\ &= \bar{J}_f(\mathbf{x}; q_\phi) (\epsilon - C^\top \epsilon). \end{aligned}$$

where  $C_{:,j}$  is the  $j$ -th column of  $C$ . In practice,  $\bar{J}_f(\mathbf{x}; q_\phi)$  is approximated using samples  $\mathbf{z}_1, \dots, \mathbf{z}_{S'} \sim$



$q_\phi(\cdot \mid \mathbf{x})$ :

$$\bar{J}_f(\mathbf{x}; q_\phi) \approx \frac{1}{S'} \sum_{j=1}^{S'} Df(\mathbf{z}_j),$$

so the full approximation becomes:

$$\bar{\ell}(C, f; \mathbf{x}) \approx \sum_{i=1}^S \left\| \left( \frac{1}{S'} \sum_{j=1}^{S'} Df(\mathbf{z}_j) \right) (\epsilon_i - C^\top \epsilon_i) \right\|_2^2.$$

Theorem Thm5.5 leverages Hutchinson’s trace estimator, which states that:

$$\text{tr}(AA^T) = \mathbb{E}_{\epsilon \sim \mathcal{N}(0, I_{d_x})} [\|\epsilon^T A\|_2^2]$$

to approximate the self-expressiveness penalty in  $\mathcal{O}((S + S') \times T_f)$  Jacobian–vector products, rather than the  $\mathcal{O}(S' \times d_x \times T_f)$  full Jacobian computation required by naive methods. By sampling  $S \ll d_x$  Gaussian probes, one obtains an unbiased estimate of the Frobenius-norm residual with constant per-sample complexity. This reduces both computation by a factor of  $\frac{S'}{S+S'} d_x$ , enabling the incorporation of the self-expression penalty into training loops in PyTorch with only a few extra backpropagations per batch. In experiments,  $S' = 1, S = 4$  and for purchase data  $d_x = 2521$ , so the speed factor is  $\frac{d_x}{5} \approx 504$  compared to using the standard PyTorch’s `"autograd.functional.jacobian"` (Paszke et al., 2019).

### 5.5.5 Applying Static Self-Expression Theory in a CRL in Time-Series Setting

In our temporal model

$$\mathbf{X}_t = f(\mathbf{Z}_t),$$

the decoder  $f : \mathbb{R}^{d_z} \rightarrow \mathbb{R}^{d_x}$  in Equation 5.1 is *memoryless*: it depends only on the current latent  $\mathbf{z}_t$ , which evolves by a fixed structural law, but we assume that it remains marginally  $\text{subG}_{d_z}(K)$  at each  $t$ . Consequently, under the smoothness over  $f$  (Asm5.3), the exact same concentration and subspace-detection guarantees developed in Section 5.5.1 (e.g., Theorem Thm5.2 and Proposition Prop5.3) apply verbatim to each time slice  $\mathbf{z}_t$ . In particular:

- For every  $t$ ,  $\mathbf{z}_t \sim \text{subG}_{d_z}(K)$  and  $f$  is  $L$ -smooth, so all static-Jacobian concentration bounds hold at time  $t$ .
- Solving  $\min_C \mathbb{E}_{\mathbf{Z}_t} \|Df(\mathbf{Z}_t) - Df(\mathbf{Z}_t) C\|_F^2 + \lambda \|C\|_1$  and clustering via  $(|C| + |C|^\top)/2$  recovers feature groups exactly as in the static case.
- No "augmented" input or multi-lag decoder is required: since  $f$  never sees  $\mathbf{z}_{t-\rho}$  for  $\rho > 0$ , our proofs carry over unchanged.

Thus, under the stationarity assumption on the latent process, one can import our entire static CRL framework into a time-series context without modification.

## 5.6 Experiments

**Evaluation** We conceptually associate each scalar observed feature  $\mathbf{x}_t^i$  with a vector given by its gradient  $\nabla_{\mathbf{z}} f_i$ . Clustering the nodes represented by these gradients leads to a *stationary* grouping of features in the observed space. Evaluating such clustering is challenging because internal validation techniques (e.g., Silhouette score, Davies-Bouldin index (Schubert, 2023)) are not easily applicable, the data points being clustered are scalar and vary over time. Instead, we rely on *external validation*, assuming the existence of labels that define semantically coherent and temporally stable groups of variables. For instance, in purchase data,  $\mathbf{x}_t^i$  may represent the quantity of product  $i$  purchased at time  $t$ , but it is well established that products are typically organized into stable categories and subcategories. We, therefore, assess the coherence of our clusters with respect to these predefined labels. Some datasets, like purchase logs, contain multiple layers of labeling (e.g., subcategories and categories), forming a nested structure where subcategories are embedded within broader categories. This hierarchy allows for a more rigorous evaluation of our inferred groupings by measuring their alignment with known label structures.

**Metrics** As an external validation, we adopt the standard suite proposed in (Rosenberg & Hirschberg, 2007): 1. *Homogeneity (H)*: A clustering is homogeneous if each cluster contains only data points from a single class. 2. *Completeness (C)*: A clustering is complete if all members of a class are assigned to the same cluster. 3. *Normalized Mutual Information (NMI)*: Also known as the *V-measure*, it balances homogeneity and completeness to quantify clustering quality.

**Benchmark** We compare the CRL model Leap (Yao et al., 2022) to a baseline that consists of "pseudo"-random generation of labels, where labels are randomly assigned to each feature while following the true categorical distribution of labels across observed features. If multiple labels are available for each feature, then the "pseudo"-random approach will be evaluated for labeling. H, C, and Normalized Mutual Information (NMI) are reported for each configuration.

### 5.6.1 Synthetic data

**Synthetic Data Generation** In our experiments, we generate synthetic data by simulating three main components: 1. the causal process in the latent space, 2. the decoding function mapping latent variables to observed features, and 3. the sparsity structure of the decoding process.

We define a latent process  $\{\mathbf{z}_t \in \mathbb{R}^{d_z}\}_{t=1}^T$  governed by a structured non-linear and non-Gaussian autoregressive process of lag order  $L$ . Specifically, the latent dynamics incorporate nonlinear transformations of lagged components modulated through a set of transition matrices  $\{B^{(\ell)}\}_{\ell=1}^L$ . The latent update equation is

$$\mathbf{z}_t = \text{LeakyReLU} \left( \sum_{\ell=1}^L \sin(\mathbf{z}_{t-\ell} B^{(\ell)}) + \epsilon_t \right), \quad \epsilon_t \sim \text{Laplace}(0, 1).$$

**Decoder Network and Observed Data Generation** Each latent vector  $\mathbf{z}_t$  is decoded to generate an observed vector  $\mathbf{x}_t \in \mathbb{R}^{d_x}$  using a sparse linear transformation followed by a nonlinear probabilistic

decoder. First, a sparse adjacency matrix  $A \in \{0, 1\}^{d_x \times d_z}$  is generated using Algorithm 8, encoding which latent factors influence which observed features.

A weight matrix  $W$  is formed by element-wise multiplication  $W = A \odot B$ , where  $B$  contains continuous values sampled from a uniform distribution  $[0.1, 1]$ . Then, for each time step  $t$ , the observed data is generated as follows (see Algorithm 7):

$$\begin{aligned}\mathbf{u}_t &= \mathbf{z}_t W^\top, \\ \boldsymbol{\mu}_t &= \mu_\theta(\mathbf{u}_t), \\ \boldsymbol{\sigma}_t &= \sigma_\theta(\mathbf{u}_t), \\ \mathbf{x}_t &\sim \mathcal{N}(\boldsymbol{\mu}_t, \text{diag}(\boldsymbol{\sigma}_t^2)).\end{aligned}$$

The decoder networks  $\mu_\theta$  and  $\sigma_\theta$  are randomly initialized 2-layer fully connected networks with LeakyReLU activations and Softplus at the output of  $\sigma_\theta$  to ensure positivity.

---

**Algorithm 7** Nonlinear Non-Gaussian Data Generation

---

**Require:** Lag order  $H$ , Layers  $K$ , Sequence length  $T$ , Negative slope  $\alpha$ , Latent dimension  $d_z$ , Observed dimension  $d_x$ , Batch size  $N$ , Noise scale  $\sigma$ , Structural matrix  $\Gamma \in \{0, 1\}^{d_x \times d_z}$ , Transition matrices  $\{B_h\}_{h=1}^H$ , Decoder functions  $f_\mu, f_\sigma$

**Ensure:** Observed data  $\mathbf{X} \in \mathbb{R}^{N \times (H+T) \times d_x}$ , Latent data  $\mathbf{Z} \in \mathbb{R}^{N \times (H+T) \times d_z}$

```

1: Initialize  $\mathbf{Z}_{\text{lags}} \sim \mathcal{N}(0, 1)$  of shape  $(N, H, d_z)$ 
2: Normalize  $\mathbf{Z}_{\text{lags}}$  along the batch axis
3: Initialize empty sequences:  $\mathbf{Z} \leftarrow []$ ,  $\mathbf{X} \leftarrow []$ 
4: for  $i = 1$  to  $H$  do
5:   Append  $\mathbf{Z}_{\text{lags}}[:, i, :]$  to  $\mathbf{Z}$ 
6: end for
7:  $\mathbf{M} \leftarrow \mathbf{Z}_{\text{lags}}$ 
8:  $\mathbf{D} \leftarrow \mathbf{M} \cdot \Gamma$ 
9:  $\boldsymbol{\mu} \leftarrow f_\mu(\mathbf{D})$ ,  $\boldsymbol{\sigma} \leftarrow f_\sigma(\mathbf{D})$ 
10:  $\mathbf{M}' \sim \mathcal{N}(\boldsymbol{\mu}, \boldsymbol{\sigma})$ 
11:  $\mathbf{X}_{\text{lags}} \leftarrow \mathbf{M}'$ 
12: for  $i = 1$  to  $H$  do
13:   Append  $\mathbf{X}_{\text{lags}}[:, i, :]$  to  $\mathbf{X}$ 
14: end for
15: for  $t = 1$  to  $T$  do
16:   Sample  $\mathbf{z}_t \sim \text{Laplace}(0, \sigma)$  of shape  $(N, d_z)$ 
17:   for  $h = 1$  to  $H$  do
18:      $\mathbf{z}_t \leftarrow \mathbf{z}_t + \sin(\mathbf{Z}_{\text{lags}}[:, h, :] \cdot B_h)$ 
19:   end for
20:    $\mathbf{z}_t \leftarrow \text{LeakyReLU}(\mathbf{z}_t, \alpha)$ 
21:   Append  $\mathbf{z}_t$  to  $\mathbf{Z}$ 
22:    $\mathbf{D} \leftarrow \mathbf{z}_t \cdot \Gamma$ 
23:    $\boldsymbol{\mu} \leftarrow f_\mu(\mathbf{D})$ ,  $\boldsymbol{\sigma} \leftarrow f_\sigma(\mathbf{D})$ 
24:    $\mathbf{x}_t \sim \mathcal{N}(\boldsymbol{\mu}, \boldsymbol{\sigma})$ 
25:   Append  $\mathbf{x}_t$  to  $\mathbf{X}$ 
26:   Update  $\mathbf{Z}_{\text{lags}}$ : append  $\mathbf{z}_t$ , remove oldest lag
27: end for
28: Stack  $\mathbf{Z}$  and  $\mathbf{X}$  along the time axis to shape  $(N, H + T, d_z)$  and  $(N, H + T, d_x)$ 
29: return  $\mathbf{X}, \mathbf{Z}, \Gamma$ 
```

---

**Experimental results: Non-Overlapping clusters** From Table 5.2, Leap achieves  $H \approx 0.85$ ,  $C \approx 0.84$ , and  $NMI \approx 0.84$  on average, compared to  $H \approx 0.25$ ,  $C \approx 0.28$ , and  $NMI \approx 0.26$  for random

---

**Algorithm 8** Generate Sparse Structural Matrix  $\Gamma \in \{0, 1\}^{d_x \times d_z}$ 

---

**Require:** Number of observed features  $d_x$ , number of latent subspaces  $M$ , random seed  $s$

**Ensure:** Structural matrix  $\Gamma \in \{0, 1\}^{d_x \times d_z}$ , subspace sizes  $\mathbf{n} \in \mathbb{N}^M$

```
1: Set min_per_subspace  $\leftarrow 2$ 
2: Set leftover  $\leftarrow d_x - M \times \text{min\_per\_subspace}$ 
3: Initialize random number generator with seed  $s$ 
4: Draw raw  $\sim \text{Dirichlet}(\mathbf{1}_M)$ 
5:  $\mathbf{n} \leftarrow \lfloor \text{raw} \times \text{leftover} \rfloor$  {Initial subspace sizes}
6: diff  $\leftarrow \text{leftover} - \sum_{j=1}^M n_j$ 
7: for  $i = 1$  to diff do
8:    $n_{(i \bmod M)+1} \leftarrow n_{(i \bmod M)+1} + 1$ 
9: end for
10: for  $j = 1$  to  $M$  do
11:    $n_j \leftarrow n_j + \text{min\_per\_subspace}$ 
12: end for
13: Initialize  $\Gamma \leftarrow 0_{d_x \times d_z}$ 
14:  $i \leftarrow 0$ 
15: for  $m = 1$  to  $M$  do
16:   for  $k = 1$  to  $n_m$  do
17:      $\Gamma[i, m] \leftarrow 1$ 
18:      $i \leftarrow i + 1$ 
19:   end for
20: end for
21: Draw a random permutation  $\pi$  of  $\{0, 1, \dots, d_x - 1\}$ 
22: Permute the rows of  $\Gamma$  according to  $\pi$ 
23: return  $\Gamma, \mathbf{n}$ 
```

---

labeling. This gap demonstrates that our inferred clusters capture fine-grained product groupings with more than three times better homogeneity and completeness than chance. Notably, high homogeneity indicates that clusters seldom mix subcategories, while strong completeness shows that most items within a given subcategory are clustered together.

Table 5.2: Clustering coherence on simulated data, true labels are simulated.

Model	H	C	NMI
<b>Leap + SSC</b>	<b>0.85<math>\pm</math>0.02</b>	<b>0.84<math>\pm</math>0.04</b>	<b>0.84<math>\pm</math>0.03</b>
<b>Random clustering</b>	0.25 $\pm$ 0.08	0.28 $\pm$ 0.07	0.26 $\pm$ 0.07

**Experimental results: Overlapping clusters** We evaluate two overlapping-community algorithms, SymNMF and SAAC, on features grouping generated by simulation data (Algorithms 8 and 7), and varying Dirichlet concentration  $\alpha \in \{0.2, 0.5, 1.0\}$  to control overlap. We assess recovery quality using three standard metrics:

1. **Overlapping Normalized Mutual Information (oNMI)**, which generalizes NMI to soft or overlapping labels (McDaid et al., 2011).
2. **F1-score**, averaged over true and estimated memberships, measuring the harmonic mean of precision and recall for node-community assignments (Lancichinetti et al., 2009).
3. **Omega Index**, a chance-corrected measure of agreement for overlapping partitions (Collins & and, 1988).

We report performances in Table 5.3. Both methods substantially outperform a random-assignment

Table 5.3: Performance metrics under overlapping features for synthetic data with varying overlap levels  $\alpha$ .

$\alpha$	Method	oNMI	F1-score	Omega
0.2	<b>SymNMF</b>	<b><math>0.72 \pm 0.04</math></b>	<b><math>0.75 \pm 0.03</math></b>	<b><math>0.68 \pm 0.05</math></b>
	<b>SAAC</b>	$0.68 \pm 0.05$	$0.70 \pm 0.04$	$0.64 \pm 0.06$
	<b>Random clustering</b>	$0.12 \pm 0.03$	$0.11 \pm 0.04$	$0.01 \pm 0.06$
0.5	<b>SymNMF</b>	<b><math>0.65 \pm 0.03</math></b>	<b><math>0.67 \pm 0.04</math></b>	<b><math>0.60 \pm 0.05</math></b>
	<b>SAAC</b>	$0.62 \pm 0.04$	$0.64 \pm 0.05$	$0.57 \pm 0.06$
	<b>Random clustering</b>	$0.13 \pm 0.04$	$0.12 \pm 0.04$	$0.01 \pm 0.03$
1.0	<b>SymNMF</b>	<b><math>0.58 \pm 0.05</math></b>	<b><math>0.60 \pm 0.06</math></b>	<b><math>0.52 \pm 0.07</math></b>
	<b>SAAC</b>	$0.55 \pm 0.06$	$0.57 \pm 0.07$	$0.49 \pm 0.08$
	<b>Random clustering</b>	$0.14 \pm 0.04$	$0.14 \pm 0.03$	$0.01 \pm 0.05$

baseline, demonstrating overlap recovery. As overlap increases ( $\alpha \uparrow$ ), performance degrades slowly, e.g., SymNMF ’s oNMI drops from 0.72 to 0.58, reflecting higher ambiguity in dense overlaps.

## 5.6.2 Real data

**Saint-Gobain Transaction Data** This dataset contains transaction histories, where each client is uniquely identified. Transactions are timestamped and associated with products that can be grouped into bundles or categories. Sequential purchases, such as buying plasterboards, followed by screws and glue for a renovation project, suggest underlying causal structures. Yet, inferring these structures is difficult, especially when many products are similar. For example, two distinct items might simply be plasterboards that differ only in size or brand. In such cases, it is more meaningful to examine whether causal representation learning can be transparently aligned with coherent product groupings in the observational space. Products can be represented at varying levels of granularity (Figure 5.5). The purchase vector might encode the quantity bought per product, per subcategory, or according to broader groupings such as product families or specialties.

### Example Ex5.1 [Product Labeling Hierarchy]

1. **Product:** Walk-in shower enclosure
2. **Sub-family:** Shower cabin and screen
3. **Family:** Bathtub, Shower, Toilet
4. **Product line/specialty:** Sanitary Ware

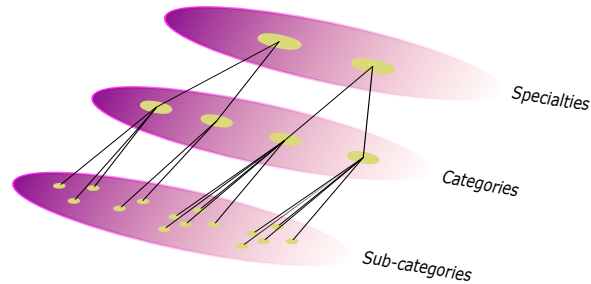


Figure 5.5: Hierarchical relationships in the Saint-Gobain transaction data. Subcategories form product categories, which in turn are grouped into broader product specialties.

We construct the purchase vector  $\mathbf{x}_t$  (Equation 5.24) at the subcategory level: each entry counts the number of distinct products bought within that subcategory in a given week.

$$\mathbf{x}_t = \begin{bmatrix} 3 & 0 & 0 & 5 & \cdots & 0 \end{bmatrix} \quad (5.24)$$

Product 1                  Product 2                  Product 3                  Product 4                   $\cdots$                   Product  $d_x$

purchased 3 times    not purchased    not purchased    purchased 5 times     $\cdots$     not purchased

**Experimental results: Non-Overlapping clusters** As shown in Table 5.4, CRL combined with Sparse Subspace Clustering (SSC) consistently outperforms random clustering across all three labeling levels. The highest coherence is observed at the sub-category level, where the model achieves  $NMI = 0.65$ , suggesting that the learned latent space preserves fine-grained semantic structure in the observational features. This performance decreases slightly at higher levels of abstraction, yet remains significantly above random, indicating that meaningful grouping is retained even at coarser resolutions.

Table 5.4: Clustering coherence of Saint-Gobain data with different true label levels

True Labels	Model	Homogeneity (H)	C	NMI
Sub-categories	<b>CRL + SSC</b>	<b>0.64±0.02</b>	<b>0.68±0.04</b>	<b>0.65±0.03</b>
	<b>Random clustering</b>	0.31±0.10	0.33±0.08	0.32±0.06
Categories	<b>CRL + SSC</b>	<b>0.55±0.03</b>	<b>0.46±0.02</b>	<b>0.39±0.03</b>
	<b>Random clustering</b>	0.22±0.05	0.24±0.06	0.22±0.06
Specialties	<b>CRL + SSC</b>	<b>0.40±0.03</b>	<b>0.42±0.02</b>	<b>0.41±0.03</b>
	<b>Random clustering</b>	0.12±0.04	0.13±0.03	0.12±0.04

## 5.7 Discussion

**Summary and Contributions** This work introduced a geometric framework for interpreting CRL models through the lens of the decoder Jacobian. By imposing a sparse self-expressiveness prior, we show that the column space of the Jacobian decomposes into modular subspaces, each corresponding to latent-induced clusters of observed variables. We provided the first formal recovery guarantees for both disjoint and overlapping feature clusters in CRL, establishing high-probability identifiability under subspace incoherence and structured sparsity assumptions. Our analysis bridges latent-space identifiability and observable-level interpretability: it enables the recovery of semantically meaningful groupings that reflect the causal structure of the data-generating process. Importantly, our method is model-agnostic, complements existing CRL architectures, and requires no assumptions of anchor variables or single-parent decoding.

**Beyond Linearity: Adaptive Self-Expression** In this work, we used a *linear self-expression* model

$$\nabla_{\mathbf{z}} f_j = \sum_{k \neq j} C_{kj} \nabla_{\mathbf{z}} f_k.$$

implying a fixed coefficient matrix  $C$  learned once for all inputs. However, in many settings, the optimal self-expression matrix may *depend on the latent context*  $\mathbf{z}$ . This motivates an *adaptive self-expression* formulation:

$$\nabla_{\mathbf{z}} f_j(\mathbf{z}) = \sum_{k \neq j} C_{kj}(\mathbf{z}) \nabla_{\mathbf{z}} f_k(\mathbf{z}).$$

where  $\mathbf{z} \rightarrow C(\mathbf{z})$  varies smoothly with the latent code  $\mathbf{z}$ . In statistics, *varying-coefficient* models (Fan et al., 2003) formalize this idea and show that allowing coefficients to depend on covariates can improve predictive fit in nonstationary settings. In CRL, letting  $C$  adapt to  $\mathbf{z}$  could capture nonlinear, context-dependent feature interactions, but at the cost of additional model complexity and identifiability challenges.

**Causal Sufficiency and Unobserved Confounding** Leap model and related CRL architectures assume *causal sufficiency*: the latent space  $\mathbf{Z}$  contains all common causes of observed features (Peters et al., 2017). In practice, however, *unobserved confounders* are ubiquitous and may corrupt the learned representations. Extending CRL transparency to the *latent confounding* regime is an open challenge.

**Dynamic Structure in Longitudinal Data** Standard clustering approaches assume a static partitioning of features. Yet in real-world longitudinal settings, such as retail transactions, feature associations often shift over time due to seasonality, external interventions, or latent regime changes (Gama et al., 2014). For example, summer products may co-occur only seasonally, leading to transient clusters that defy static modeling. To draw an analogy, similar phenomena arise in video data, where objects enter and exit dynamically. To accommodate such variability, one could integrate dynamic subspace clustering techniques that track temporal changes in the affinity matrix  $C_t$  via smoothness penalties or online updates (Kriegel et al., 2010; Hashemi & Vikalo, 2018). However, probabilistic guarantees, as we presented in Section 5.5, are yet to be developed in the dynamic case.

**Challenges of Validation in Tabular Domains** Evaluating learned feature clusters in tabular settings presents unique challenges. Unlike vision tasks, which often come with ground-truth segmentations, tabular datasets lack canonical groupings aligned with causal abstractions. Existing labels (e.g., product categories) are typically designed for administrative or marketing purposes, not necessarily for capturing statistical dependencies (Jain & Dubes, 1988). As a result, there may be no external reference that aligns cleanly with the structure uncovered by CRL. Moreover, even domain experts may disagree on what constitutes a coherent feature group. These challenges call for hybrid validation strategies that combine *quantitative metrics* (e.g., NMI, V-measure) with *expert assessments* and *task-driven evaluations*, such as improvements in downstream causal inference or predictive tasks (Vinh et al., 2010).

# Chapter 6

## Epilogue

Science is the topography of ignorance.

---

Oliver Wendell Holmes Sr

This final chapter serves as an epilogue to the thesis. Having concluded each chapter with its own discussion, we now take a broader perspective, highlighting unifying themes, reflecting on limitations, and outlining promising directions for future work.

### 6.1 Towards a causal representation of confounders for causal inference

As we conclude this thesis, it is worth reflecting on how the tools developed in Chapters 3 and 4—which employed RNN and Transformers to learn non-causal summaries of the history  $\mathbf{H}_t$ —can be augmented to deliver even greater robustness and interpretability. A natural next step is to apply CRL (cf. Chapter 5) to the entire history  $\{\mathbf{H}_s\}_{s \leq t}$ , thereby uncovering a latent causal process  $\{\mathbf{Z}_s\}_{s \leq t}$  that admits an explicit graphical structure rather than a flat vector embedding as considered in Chapters 3 and 4. Building on this causal graph, one then leverages the relational inductive bias of Graph Neural Networks (GNNs)—extended to directed edges via methods such as MagNet (Zhang et al., 2021b) and edge-enhanced GNNs (Rossi et al., 2024)—to produce rich node-level embeddings. By propagating messages along the learned causal edges, this two-stage pipeline merges the strengths of CRL for structure discovery with GNNs for efficient, permutation-invariant representation learning.

**Advantages** Leveraging a latent causal graph over the process history, followed by a GNNs and a causal inference layer (e.g., Causal CPC or CDVAE decoders), promises several key benefits: first, it introduces a structural inductive bias (Battaglia et al., 2018) grounded in the learned causal relations, which goes beyond the purely temporal-dependency of sequence models. Second, GNNs are permutation-invariant, producing node embeddings that depend only on graph connectivity rather than on any arbitrary ordering of nodes. Finally, by explicitly encoding causal structure, a graph-based pipeline followed by causal inference promises more reliable adjustment for time-varying confounders.



## 6.2 Invariance of the generative maps and representation identifiability

In Chapter 3, we established that

1. when the adjustment  $\mathbf{U}$  is observed, ACATE is identifiable, and
2. when  $\mathbf{Z} \sim \text{CMM}(p)$  is latent, ACATE remains identifiable under mild regularity conditions (Corollary Cor3.1).

A remaining question is:

*Under what conditions do the CATE augmented with  $\mathbf{Z}$  and that with  $\mathbf{U}$  coincide; that is, when does*

$$\tau_t(\mathbf{h}_t, \mathbf{Z}) = \tau_t(\mathbf{h}_t, \mathbf{U}) ?$$

*Here*

$$\tau_t(\mathbf{h}_t, \mathbf{Z}) = \mathbb{E}[Y_t \mid \mathbf{H}_t = \mathbf{h}_t, \mathbf{Z}, W_t = 1] - \mathbb{E}[Y_t \mid \mathbf{H}_t = \mathbf{h}_t, \mathbf{Z}, W_t = 0],$$

*and*

$$\tau_t(\mathbf{h}_t, \mathbf{U}) = \mathbb{E}[Y_t \mid \mathbf{H}_t = \mathbf{h}_t, \mathbf{U}, W_t = 1] - \mathbb{E}[Y_t \mid \mathbf{H}_t = \mathbf{h}_t, \mathbf{U}, W_t = 0].$$

**Equivalence via Conditional-Density Equality** This equality requires the conditional responses under each treatment arm ( $\omega = 0, 1$ ), augmented with either  $\mathbf{Z}$  or  $\mathbf{U}$ , to be identical. Formally, we need:

$$\mathbb{E}_{Y_t \mid \mathbf{H}_t, W_t, \mathbf{Z}}(Y_t \mid \mathbf{H}_t = \mathbf{h}_t, \mathbf{Z} = \mathbf{z}, W_t = \omega) = \mathbb{E}_{Y_t \mid \mathbf{H}_t, W_t, \mathbf{U}}(Y_t \mid \mathbf{H}_t = \mathbf{h}_t, \mathbf{U} = \mathbf{u}, W_t = \omega).$$

For this equality to hold, it is sufficient to have

$$p(Y_t \mid \mathbf{H}_t, \mathbf{Z}, W_t) = p(Y_t \mid \mathbf{H}_t, \mathbf{U}, W_t).$$

Now, assume the following model for  $Y_t$ :

$$Y_t = f^{\mathbf{u}}(\mathbf{H}_t, \mathbf{U}, W_t) + \epsilon_t^{\mathbf{u}} \quad \text{and} \quad Y_t = f^{\mathbf{z}}(\mathbf{H}_t, \mathbf{Z}, W_t) + \epsilon_t^{\mathbf{z}},$$

where  $\epsilon_t^{\mathbf{u}} \sim \mathcal{N}(0, \Sigma_{\epsilon_t^{\mathbf{u}}})$  and  $\epsilon_t^{\mathbf{z}} \sim \mathcal{N}(0, \Sigma_{\epsilon_t^{\mathbf{z}}})$ . The equality  $p(Y_t \mid \mathbf{H}_t, \mathbf{Z}, W_t) = p(Y_t \mid \mathbf{H}_t, \mathbf{U}, W_t)$  holds if and only if  $f^{\mathbf{u}}(\mathbf{H}_t, \mathbf{U}, W_t) = f^{\mathbf{z}}(\mathbf{H}_t, \mathbf{Z}, W_t)$  almost surely and  $\Sigma_{\epsilon_t^{\mathbf{z}}} = \Sigma_{\epsilon_t^{\mathbf{u}}}$ . This indicates that we can represent the shared function by  $f = f^{\mathbf{u}} = f^{\mathbf{z}}$ , provided that  $\mathbf{U}$  and  $\mathbf{Z}$  have the same support.

**Partial Injectivity: A very restrictive assumption** Let's assume that the noise distribution is fully known, that is,  $\Sigma := \Sigma_{\epsilon_t^{\mathbf{z}}} = \Sigma_{\epsilon_t^{\mathbf{u}}}$  is predefined. Establishing equality in conditional distributions now reduces to demonstrating *partial invariance* in  $f$ .

To illustrate, if  $f$  is partially injective, meaning that for any  $(\mathbf{h}_t, \omega)$ , the map  $\mathbf{z} \rightarrow f(\mathbf{h}_t, \mathbf{z}, \omega)$  is injective, then  $\mathbf{Z} = \mathbf{U}$  almost surely. However, designing a function class that satisfies such partial injectivity would be highly restrictive and impractical, especially when aiming to approximate  $f$  using neural networks. Moreover, learning the exact unobserved adjustment variables  $\mathbf{U}$  is often unrealistic due to the unknown dimensionality of  $\mathbf{U}$ , which is implicitly assumed when considering support equality between  $\mathbf{Z}$  and  $\mathbf{U}$ .

**Group-Equivariance as a Practical Alternative** A more practical assumption involves allowing the identification of generative factors from observed distributions up to trivial ambiguities, such as rotations, permutations, scaling, or sign flips. For example, if  $\mathbf{Z}$  and  $\mathbf{U}$  induce the same observed conditional distribution over response sequences, that is,  $p(Y_{\leq T} \mid \mathbf{H}_{\leq T}, W_{\leq T})$ , then, under mild conditions,  $\mathbf{Z}$  and  $\mathbf{U}$  should be related by a rotation plus translation. Therefore, a form of partial invariance in  $f$  is to verify whether, for any  $(\mathbf{h}_t, \omega)$  and  $\mathbf{z}, \mathbf{z}'$  such that  $\mathbf{z}' = A\mathbf{z} + b$  with  $A$  being a rotation matrix,  $f(\mathbf{h}_t, \mathbf{z}, \omega) = f(\mathbf{h}_t, \mathbf{z}', \omega)$ . This assumption is significantly less restrictive than partial injectivity, as it permits equality in responses for equivalence classes of latent variables connected through simple transformations.

Since  $f$  is often approximated by neural networks, ensuring that the network is invariant to certain transformations of the input connects to existing work on *invariant and equivariant neural networks* (Cohen & Welling, 2016; Zaheer et al., 2017; Kondor & Trivedi, 2018; Xu et al., 2020; Yarotsky, 2022; Immer et al., 2022). Although these methods have been applied in simpler settings, they offer inspiration for future work on designing generative models that leverage such invariances when representations are assumed to be identifiable.

**Research Gap** To our knowledge, this form of consistency has been largely overlooked in the literature of identifiable representations and of CRL (Khemakhem et al., 2020; Klindt et al., 2021; Yao et al., 2021; Mita et al., 2021; Lachapelle et al., 2022a; Wu & Fukumizu, 2022; Xu et al., 2024; Xie et al., 2024; Li et al., 2024). In these works, the objective is the identifiability of the latent space up to equivalence classes induced by trivial ambiguities, yet the generative model is seldom designed to be invariant or equivariant to these transformations.

## 6.3 Uncertainty and Sensitivity in Causal Inference for Longitudinal Data

In causal inference, we are faced with different sources of "ignorance," which may confer uncertainty over the estimated treatment effect. Causality literature discusses three main sources: (1) **data finiteness**: As discussed by Jesson et al. (2021; 2020) in the static setting, which we extrapolate to our longitudinal case, if some individuals at time  $t$  with historical context  $\mathbf{h}_t$  and  $W_t = 1$  are underrepresented in the observed data in such a way that there are no individuals in the control group  $W_t = 0$  with similar historical context, then this will provide uncertainty over treatment effect estimation (Chapter 3). Such uncertainty

comes inherently from the data finiteness, which is a source of epistemic uncertainty. This source is even more critical in the longitudinal case when considering time-varying treatments, as in the Causal CPC model (Chapter 4), due to the exponential explosion of treatment regimes  $\omega_{t+1:t+\rho}$ . (2) **violations of overlap (Assumption Asm2.7)** is another important source of epistemic uncertainty. For example, if there exists a level in the historical context  $\mathbf{h}_t$  where all observed individuals are in  $W_t = 1$ , then we cannot reliably estimate conditional responses when  $W_t = 0$ . Again, when we target longitudinal data and time-varying treatment, the longer the treatment sequence, the more difficult it is for overlap to hold. Adding to this, the fact that the historical context is both high-dimensional and time-varying can lead to overlap violations. (3) **violation of ignorability** (Assumption Asm2.5) leads to the presence of unobserved confounding and any estimation of CATE, ACATE (Chapter 3), or the conditional potential outcome (Chapter 4) will be biased.

**Existing Literature** To date, uncertainty-quantification methods in causal inference have mainly focused on *static* settings and do not readily apply to longitudinal, multi-horizon forecasts as in Chapter 4. We organize these static-setting approaches by the ignorability assumptions they make:

**1. Assuming strong ignorability** Several methods have been proposed under the assumption of *strong ignorability*. Lei & Candès (2021) introduced a conformal inference-based approach to estimate intervals for counterfactuals and ITE under the PO framework. This method accounts for two sources of variability: (1) the variability of the response around the regression function and (2) the variability of CATE estimators due to finite samples. Controlling both sources requires a sufficiently rich set of covariates to explain outcome variability while providing accurate CATE estimates for all covariate values. Building on this, Wang & Qiao (2025) applied conformal prediction to the *conditional density* of the outcome given the covariates, rather than using the conditional expectation, resulting in shorter prediction intervals compared to Lei & Candès (2021).

**2. Assuming hidden confounding** When ignorability is violated, several approaches have been proposed for interval estimation under partial identification. Marmarelis et al. (2024) construct prediction intervals for partially identifiable outcomes via a causal sensitivity model combined with deep ensembles. Kallus et al. (2019) introduced a functional interval estimator for bounding individual treatment effects using adversarially weighted kernel regression, with weights governed by a marginal sensitivity model (Tan, 2006). Normalizing flows have been applied to model the distribution of ITE (Vanderschueren et al., 2023; Papamakarios et al., 2021), while collaborative networks have been extended to estimate full potential outcome distributions in static settings (Zhou et al., 2022; 2021). Kallus (2022) derived sharp bounds on the fraction of negatively affected individuals from observational data. The region of ignorance framework by Jesson et al. (2021) yields CATE intervals that expand under poor overlap, insufficient similarity, or confounding, combining Bayesian deep models with marginal sensitivity analysis (Kallus et al., 2019). Finally, Oprescu et al. (2023) achieved quasi-oracle CATE bounds via meta-learners augmented with marginal sensitivity models.

**Research Gap** Ideally, we would like to have interval estimation around the causal quantity, where the width *simultaneously* changes depending on data finiteness, violation of overlap, and of ignorability. Despite significant advances in uncertainty quantification in this line of work, most existing methods are designed for static settings and do not readily extend to longitudinal data. This creates a critical gap in addressing the challenges posed by temporal dependencies, time-varying treatments, and evolving confounding. In particular, multi-horizon forecasting of causal outcomes introduces an additional challenge: the autoregressive structure causes prediction errors to compound over time, adding a fourth source of randomness beyond data finiteness, overlap violations, and unobserved confounding.

## 6.4 Uncertainty in Causal Representation Learning

While Bayesian causal discovery quantifies uncertainty over observed-variable graphs, far less is known about uncertainty in CRL (Chapter 5). Bayesian Causal Discovery (Chickering et al., 1997; Heckerman et al., 2006; Friedman & Koller, 2003; Mamaghan et al., 2024) defines a posterior distribution over the graph and the parameters of the SCM, thereby quantifying the epistemic uncertainty of the causal model. Accurately estimating this uncertainty is crucial for downstream tasks such as causal effect estimation (Toth et al., 2022; Emezue et al., 2023) and experimental design (Agrawal et al., 2019; Tigas et al., 2023). While recent Bayesian causal discovery methods have effectively provided uncertainty quantification in the static setting (Lorch et al., 2021; Wang et al., 2022a; Deleu et al., 2022; Annadani et al., 2021; 2023; Dhir et al., 2025) and in the time-varying setting (Debeire et al., 2024; Zhao & Bonilla, 2024; Jin et al., 2025), they typically operate on observed variables assumed to be causal.

**Research Gap** Little work has been done on assessing uncertainty in the CRL framework (Chapter 5). The only notable work in this direction is that of Subramanian et al. (2022), where they introduced a Bayesian latent variable decoder model for causal discovery, relaxing the need for direct observation of causal variables. However, their approach remains constrained by linearity and isotropic Gaussian assumptions, significantly limiting the expressiveness of latent structures that can be captured. Thus, existing approaches have not explored uncertainty quantification in latent causal representations within nonlinear or time-varying contexts. A substantial open research direction remains: developing Bayesian causal discovery methods capable of quantifying uncertainty over latent causal representations, particularly in nonlinear settings and/or temporally evolving structures.

# Appendix A

## Appendix: Chapter 3

### A.1 Proofs

#### A.1.1 Identifiability: Treatment Effects and Unobserved Adjustment Variables

**CATE Identifiability.** Assuming the consistency, overlap, and ignorability assumptions (Asm2.6, Asm2.7, Asm2.5), we demonstrate that the Conditional Average Treatment Effect (CATE), as defined in Eq. 3.1, is identifiable from the observed data distribution:

$$\tau_t = \mathbb{E}(Y_t | \mathbf{H}_t = \mathbf{h}_t, W_t = 1) - \mathbb{E}(Y_t | \mathbf{H}_t = \mathbf{h}_t, W_t = 0). \quad (\text{A.1})$$

Establishing the identifiability of CATE requires showing that the two potential outcome expectations are identifiable. By the ignorability assumption (Asm2.5), the potential outcome under treatment can be expressed as:

$$m_t^1(\mathbf{h}_t) = \mathbb{E}_{Y_t(1) | \mathbf{H}_t}(Y_t(1) | \mathbf{H}_t = \mathbf{h}_t) = \mathbb{E}_{Y_t(1) | \mathbf{H}_t, W_t}(Y_t(1) | \mathbf{H}_t = \mathbf{h}_t, W_t = 1).$$

Using the consistency assumption (Asm2.6), the observed response can identify  $Y_t(1)$  when conditioned on  $W_t = 1$ :

$$m_t^1(\mathbf{h}_t) = \mathbb{E}_{Y_t | \mathbf{H}_t, W_t}(Y_t | \mathbf{H}_t = \mathbf{h}_t, W_t = 1).$$

Similarly, we identify the expected potential outcome under no treatment:

$$m_t^0(\mathbf{h}_t) = \mathbb{E}_{Y_t | \mathbf{H}_t, W_t}(Y_t | \mathbf{H}_t = \mathbf{h}_t, W_t = 0).$$

The existence of these expectations is guaranteed by the overlap assumption. □

**Augmented CATE Identifiability.** Assuming that the adjustment variables  $\mathbf{U}$  are observed, we demon-

strate the identifiability of the Augmented CATE:

$$\tau_t(\mathbf{h}_t, \mathbf{u}) = \mathbb{E}(Y_t | \mathbf{H}_t = \mathbf{h}_t, \mathbf{U} = \mathbf{u}, W_t = 1) - \mathbb{E}(Y_t | \mathbf{H}_t = \mathbf{h}_t, \mathbf{U} = \mathbf{u}, W_t = 0).$$

The assumptions of consistency, overlap, and ignorability ensure that CATE is identifiable. Since  $\mathbf{U}$  does not affect the treatment, the overlap assumption (Asm2.7) remains valid. Further,  $\mathbf{U}$  being independent of the treatment implies that the ignorability assumption holds when conditioning on  $\mathbf{U}$ :

$$Y_{it}(\omega) \perp\!\!\!\perp W_t | \mathbf{H}_t = \mathbf{h}_t \implies Y_{it}(\omega) \perp\!\!\!\perp W_t | \mathbf{H}_t = \mathbf{h}_t, \mathbf{U} = \mathbf{u} \quad \forall (\omega, \mathbf{h}_t, \mathbf{u}).$$

The remainder of the proof follows the CATE identifiability argument.  $\square$

**Theorem Thm3.2.** Let  $\mathbf{Z}$  be a latent variable such that  $\mathbf{Z} \sim CMM(p)$ . Any static adjustment variables affecting all response series in the panel must be measurable with respect to  $(\mathbf{Z}, \mathbf{H}_T)$ . We assume weak regularity conditions on treatment and response domains.

**Assumption AsmA.1 [Regularity]**

The response domain  $\mathcal{Y}$  is a Borel subset of a compact interval.

The treatment domain  $\mathcal{W} = \{0, 1\}$  is a Borel subset of  $[0, 1]$ . To prove the theorem, we need the following lemma:

**Lemma LemA.1 [Kernels and Randomization (Kallenberg, 2021)]**

Let  $\mu$  be a probability kernel from a measurable space  $S_1$  to a Borel space  $S_2$ . There exists a measurable function  $f : S_1 \times [0, 1] \rightarrow S_2$  such that if  $\vartheta$  is uniform on  $[0, 1]$ , then  $f(s_1, \vartheta)$  is distributed as  $\mu(s_1, \cdot)$ .

Suppose by contradiction the existence of  $\mathbf{Z}'$  that is not measurable with respect to  $(\mathbf{Z}, \mathbf{H}_T)$  and such that:

$$Y_{it}(\omega) \not\perp\!\!\!\perp \mathbf{Z}'_{it} | \mathbf{H}_{it}, \mathbf{Z}_i \quad \forall \omega, t$$

Let  $t$  be an arbitrary time step in the panel data. By lemma LemA.1, there exists a measurable function  $f_t : \mathcal{H}_t \times \mathcal{W} \times \mathcal{Z} \times [0, 1] \rightarrow \mathcal{Y}$  such that:

$$Y_{it} = f_t(\mathbf{H}_{it}, W_{it}, \mathbf{Z}_i, \gamma_{it}), \quad \gamma_{it} \perp\!\!\!\perp (\mathbf{H}_{it}, W_{it}, \mathbf{Z}_i).$$

The conditional Markov property implies the independence of the following conditional distributions:

$$(Y_{it} | \mathbf{H}_{it}, \mathbf{Z}_i, W_{it} = \omega) \perp\!\!\!\perp (Y_{it'}, | \mathbf{H}_{it'}, \mathbf{Z}_i, W_{it'} = \omega').$$

Such that  $t'$  verifies  $|t - t'| > p$ . We can thus conclude that:

$$(Y_{it}(\omega) \mid \mathbf{H}_{it}, \mathbf{Z}_i) \perp\!\!\!\perp (Y_{it'}(\omega') \mid \mathbf{H}_{it'}, \mathbf{Z}_i).$$

Because :

$$\begin{aligned} (Y_{it}(\omega) \mid \mathbf{H}_{it}, \mathbf{Z}_i) &= (Y_{it}(\omega) \mid \mathbf{H}_{it}, \mathbf{Z}_i, W_{it} = \omega) \\ &= (Y_{it} \mid \mathbf{H}_{it}, \mathbf{Z}_i, W_{it} = \omega). \end{aligned}$$

The first equality follows from the sequential ignorability of the theorem Thm3.1, and the second equality follows the consistency assumption. On the other hand, we also have from the CMM(p) that:

$$\gamma_{it'} \perp\!\!\!\perp Y_{it} \mid \mathbf{H}_{it}, \mathbf{Z}_i.$$

From which it follows using the fact that  $\gamma_{it} \perp\!\!\!\perp (\mathbf{H}_{it}, W_{it}, \mathbf{Z}_i)$  and  $Y_{it}(\omega) \mid \mathbf{H}_{it}, \mathbf{Z}_i = Y_{it} \mid \mathbf{H}_{it}, \mathbf{Z}_i, W_{it} = \omega$ :

$$\gamma_{it'} \perp\!\!\!\perp Y_{it}(\omega) \mid \mathbf{H}_{it}, \mathbf{Z}_i$$

By using twice the lemma LemA.1, we write:

$$\gamma_{it'} = h_t(\mathbf{Z}'_i, \eta_{it'}), \quad \eta_{it'} \perp\!\!\!\perp \mathbf{Z}'_i \tag{A.2}$$

And:

$$Y_{it}(\omega) = g_t(\mathbf{Z}'_i, \epsilon_{it}), \quad \epsilon_{it} \perp\!\!\!\perp \mathbf{Z}'_i. \tag{A.3}$$

Since  $\mathbf{Z}'_i$  is not measurable with respect to  $(\mathbf{Z}_i, \mathbf{H}_{it})$ , then by (A.2) and (A.3):

$$\gamma_{it'} \not\perp\!\!\!\perp Y_{it} \mid \mathbf{H}_{it}, \mathbf{Z}_i$$

We have thus a contradiction. □

### A.1.2 Derivation of CDVAE Loss

**ELBO.** We provide proof that the bound in Eq. (3.13) is indeed the Evidence Lower Bound (ELBO) for the weighted conditional log-likelihood.

By the concavity of the logarithm, for every  $t \in \{1, 2, \dots, T\}$ , we have:

$$\log p_\theta(y_t \mid \mathbf{h}_t, \omega_t) \geq \underbrace{\mathbb{E}_{\mathbf{Z}, C \sim q_\phi(\cdot, \cdot \mid \mathcal{D}_T)} \left[ \log \frac{p_\theta(y_t, \mathbf{Z}, C \mid \mathbf{h}_t, \omega_t)}{q_\phi(\mathbf{Z}, C \mid \mathcal{D}_T)} \right]}_{(*)} \tag{A.4}$$

We use the identity

$$p_\theta(y_t, \mathbf{z}, c \mid \mathbf{h}_t, \omega_t) = p_\theta(y_t \mid \mathbf{z}, \mathbf{h}_t, \omega_t) p(\mathbf{z}, c),$$

and the factorization of the approximate posterior

$$q_\phi(\mathbf{z}, c \mid \mathcal{D}_T) = q_{\phi_z}(\mathbf{z} \mid \mathcal{D}_T) q_{\phi_c}(c \mid \mathcal{D}_T),$$

to write

$$\begin{aligned} (*) &= \mathbb{E}_{\mathbf{Z}, C \sim q_\phi(\cdot, \cdot \mid \mathcal{D}_T)} \left[ \log \frac{p_\theta(y_t \mid \mathbf{Z}, \mathbf{h}_t, \omega_t) p(C \mid \mathbf{Z}) p(\mathbf{Z})}{q_{\phi_z}(\mathbf{Z} \mid \mathcal{D}_T) q_{\phi_c}(C \mid \mathcal{D}_T)} \right] \\ &= \mathbb{E}_{\mathbf{Z}, C \sim q_\phi(\cdot, \cdot \mid \mathcal{D}_T)} \left[ \log p_\theta(y_t \mid \mathbf{Z}, \mathbf{h}_t, \omega_t) \right] \\ &\quad - \underbrace{D_{KL}(q_{\phi_z}(\mathbf{Z} \mid \mathcal{D}_T) q_{\phi_c}(C \mid \mathcal{D}_T) \parallel p(C \mid \mathbf{Z}) p(\mathbf{Z}))}_{(**)}. \end{aligned}$$

The KL divergence term  $(**)$  between the joint approximate posterior and prior decomposes as

$$\begin{aligned} (**) &= \sum_{c=1}^K \mathbb{E}_{\mathbf{Z} \sim q_\phi(\cdot, c \mid \mathcal{D}_T)} \log \left( \frac{p(c \mid \mathbf{Z}) p(\mathbf{Z})}{q_{\phi_z}(\mathbf{Z} \mid \mathcal{D}_T) q_{\phi_c}(c \mid \mathcal{D}_T)} \right) \\ &= \sum_{c=1}^K \mathbb{E}_{\mathbf{Z} \sim q_\phi(\cdot, c \mid \mathcal{D}_T)} \log \left( \frac{p(\mathbf{Z})}{q_{\phi_z}(\mathbf{Z} \mid \mathcal{D}_T)} \right) \\ &\quad + \sum_{c=1}^K \mathbb{E}_{\mathbf{Z} \sim q_\phi(\cdot, c \mid \mathcal{D}_T)} \log \left( \frac{p(c \mid \mathbf{Z})}{q_{\phi_c}(c \mid \mathcal{D}_T)} \right) \\ &= D_{KL}(q_{\phi_z}(\mathbf{z} \mid \mathcal{D}_T) \parallel p(\mathbf{z})) \\ &\quad + \mathbb{E}_{\mathbf{Z} \sim q_{\phi_z}(\cdot \mid \mathcal{D}_T)} D_{KL}(q_{\phi_c}(c \mid \mathcal{D}_T) \parallel p(c \mid \mathbf{Z})). \end{aligned}$$

We define the individual ELBO by performing a weighted sum over log-likelihood terms and marginalizing over  $\mathcal{D}_T$ :

$$L = \sum_{t=1}^T \mathbb{E}_{\mathcal{D}_T} [\alpha(\mathbf{H}_t, W_t) \log p_\theta(Y_t \mid \mathbf{H}_t, W_t)] \geq \underbrace{\mathbb{E}_{\mathcal{D}_T} \sum_{t=1}^T \mathbb{E}_{\mathbf{Z}, C \sim q_\phi(\cdot, \cdot \mid \mathcal{D}_T)} \left[ \alpha(\mathbf{h}_t, \omega_t) \log \frac{p_\theta(y_t, \mathbf{Z}, C \mid \mathbf{h}_t, \omega_t)}{q_\phi(\mathbf{Z}, C \mid \mathcal{D}_T)} \right]}_{\text{ELBO}_0(\mathcal{D}_T; \theta, \phi)}.$$

Finally,  $\text{ELBO}_0(\mathcal{D}_T; \theta, \phi)$  expands to

$$\begin{aligned} \text{ELBO}_0(\mathcal{D}_T; \theta, \phi) &= \sum_{t=1}^T \mathbb{E}_{\mathbf{Z} \sim q_{\phi_z}(\cdot \mid \mathcal{D}_T)} [\alpha(\mathbf{h}_t, \omega_t) \log p_\theta(y_t \mid \mathbf{h}_t, \omega_t, \mathbf{Z})] \\ &\quad - \left( \sum_{t=1}^T \alpha(\mathbf{h}_t, \omega_t) \right) \left\{ D_{KL}(q_{\phi_z}(\mathbf{z} \mid \mathcal{D}_T) \parallel p(\mathbf{z})) \right. \\ &\quad \left. + \mathbb{E}_{\mathbf{Z} \sim q_{\phi_z}(\cdot \mid \mathcal{D}_T)} D_{KL}(q_{\phi_c}(c \mid \mathcal{D}_T) \parallel p(c \mid \mathbf{Z})) \right\}. \end{aligned}$$

The gap in our variational approximation is defined as the difference between the true weighted log-likelihood and the ELBO:

$$\mathbb{E}_{\mathcal{D}_T} \Delta_0(\mathcal{D}_T; \theta, \phi) := L - \mathbb{E}_{\mathcal{D}_T} \text{ELBO}_0(\mathcal{D}_T; \theta, \phi)$$



The per-time-step gap in Eq. (A.4) can be rewritten as:

$$\begin{aligned}
\log p_\theta(y_t \mid \mathbf{h}_t, \omega_t) - (*) &= \mathbb{E}_{\mathbf{Z}, C \sim q_\phi(\cdot, \cdot \mid \mathcal{D}_T)} \left[ \log \frac{p_\theta(y_t \mid \mathbf{h}_t, \omega_t) q_\phi(\mathbf{Z}, C \mid \mathcal{D}_T)}{p_\theta(y_t, \mathbf{Z}, C \mid \mathbf{h}_t, \omega_t)} \right] \\
&= \mathbb{E}_{\mathbf{Z}, C \sim q_\phi(\cdot, \cdot \mid \mathcal{D}_T)} \left[ \log \frac{q_\phi(\mathbf{Z}, C \mid \mathcal{D}_T)}{p_\theta(\mathbf{Z}, C \mid \mathcal{D}_T)} \right] \\
&= D_{KL}(q_\phi(\mathbf{Z}, C \mid \mathcal{D}_T) \parallel p_\theta(\mathbf{Z}, C \mid \mathcal{D}_T))
\end{aligned}$$

This last equation holds because

$$p_\theta(y_t, \mathbf{Z}, C \mid \mathbf{h}_t, \omega_t) = p_\theta(\mathbf{Z}, C \mid y_t, \mathbf{h}_t, \omega_t) p_\theta(y_t \mid \mathbf{h}_t, \omega_t),$$

and  $\{y_t, \mathbf{h}_t, \omega_t\} = \{y_{\leq t}, \mathbf{x}_{\leq t}, \omega_{\leq t}\} = \mathcal{D}_t$ . The individual gap is thus:

$$\Delta_0(\mathcal{D}_T; \theta, \phi) = \sum_{t=1}^T \alpha(\mathbf{h}_t, \omega_t) D_{KL}(q_\phi(\mathbf{Z}, C \mid \mathcal{D}_T) \parallel p_\theta(\mathbf{Z}, C \mid \mathcal{D}_t))$$

□

### A.1.3 Transfer of Ignorability under Invertible Maps

#### Proposition PropA.1

Let  $\Phi$  be an invertible representation function. Then,  $Y_t(\omega) \perp\!\!\!\perp W_t \mid \Phi(\mathbf{H}_t)$  holds if and only if  $Y_t(\omega) \perp\!\!\!\perp W_t \mid \mathbf{H}_t$ . Moreover,  $p(W_t = \omega \mid \Phi(\mathbf{h}_t)) > 0$  holds if and only if  $p(W_t = \omega \mid \mathbf{h}_t) > 0$ .

*Proof.* Assume  $Y_t(\omega) \perp\!\!\!\perp W_t \mid \mathbf{H}_t$ . For a non-invertible  $\Phi$ , let  $\Phi^{-1}(\mathbf{r}) = \{\mathbf{h}_t : \Phi(\mathbf{h}_t) = \mathbf{r}\}$ . Then

$$\begin{aligned}
p(Y_t(\omega) \mid \omega_t, \mathbf{r}) &= \frac{\int_{\mathbf{h}_t \in \Phi^{-1}(\mathbf{r})} p(Y_t(\omega) \mid \omega_t, \mathbf{h}_t) p(\mathbf{h}_t \mid \omega_t) d\mathbf{h}_t}{\int_{\mathbf{h}_t \in \Phi^{-1}(\mathbf{r})} p(\mathbf{h}_t \mid \omega_t) d\mathbf{h}_t} \\
&= \frac{\int_{\mathbf{h}_t \in \Phi^{-1}(\mathbf{r})} p(Y_t(\omega) \mid \mathbf{h}_t) p(\mathbf{h}_t \mid \omega_t) d\mathbf{h}_t}{\int_{\mathbf{h}_t \in \Phi^{-1}(\mathbf{r})} p(\mathbf{h}_t \mid \omega_t) d\mathbf{h}_t},
\end{aligned}$$

where ignorability implies that for general  $\Phi$ ,

$$p(Y_t(\omega) \mid \omega_t, \mathbf{r}) \neq p(Y_t(\omega) \mid \mathbf{r}).$$

For an invertible  $\Phi$ , however,

$$p(Y_t(\omega) \mid \omega_t, \Phi(\mathbf{h}_t)) = p(Y_t(\omega) \mid \Phi(\mathbf{h}_t)),$$

and similarly,

$$p(W_t = \omega \mid \Phi(\mathbf{h}_t)) = p(W_t = \omega \mid \mathbf{h}_t).$$

□

#### A.1.4 CDVAE in the Near-Deterministic Regime

*Theorem Thm3.4. Part 1:*  $\lim_{s \rightarrow +\infty} p_{\theta_s}(y_{\leq T} \mid \mathbf{x}_{\leq T}, \omega_{\leq T}) = p(y_{\leq T} \mid \mathbf{x}_{\leq T}, \omega_{\leq T})$ .

Define the conditional cumulative distribution function (CDF) of the response given covariates, for each  $t$  as:

$$F_t(y_t \mid \mathbf{h}_t, \omega_t) = \int_{-\infty}^{y_t} p(y'_t \mid \mathbf{h}_t, \omega_t) dy'_t.$$

Define the mapping  $F : \mathcal{Y}^T \rightarrow [0, 1]^T$  as:

$$F(y_1, \dots, y_T \mid \mathbf{x}_{\leq T}, \omega_{\leq T}) := [F_1(y_1 \mid \mathbf{h}_1, \omega_1), \dots, F_T(y_T \mid \mathbf{h}_T, \omega_T)].$$

The differential of the mapping is given by:

$$dF(y_1, \dots, y_T \mid \mathbf{x}_{\leq T}, \omega_{\leq T}) = p(y_{\leq T} \mid \mathbf{x}_{\leq T}, \omega_{\leq T}) dy_{\leq T}.$$

Now, define the following mapping for the latent variables using the Darmois construction (Hyvärinen & Pajunen, 1999):

$$G_i(z_i \mid z_1, \dots, z_{i-1}) = \int_{-\infty}^{z_i} p(z'_i \mid z_1, \dots, z_{i-1}) dz'_i.$$

We then define the mapping  $G : \mathbb{R}^{d_{\mathbf{z}}} \rightarrow [0, 1]^T$  such that:

$$G(\mathbf{z}) := [G_1(z_1), G_2(z_2 \mid z_1), \dots, G_i(z_i \mid z_1, \dots, z_{d_{\mathbf{z}}-1})].$$

Since  $d_{\mathbf{z}} \leq T$  by assumption, we can trivially augment the mapping  $G$  to  $\tilde{G}$  so that its image lies in  $[0, 1]^T$ .

That is,

$$\tilde{G} : \mathbb{R}^{d_{\mathbf{z}}} \rightarrow [0, 1]^T, \quad \tilde{G}(\mathbf{z}) := [G(\mathbf{z}), \underbrace{0, \dots, 0}_{T-d_{\mathbf{z}}}].$$

The differential is then given by

$$d\tilde{G}(\mathbf{z}) = p(\mathbf{z}) d\mathbf{z}.$$

We now define the mean and variance of the encoder as follows:

$$f_t(\mathbf{h}_t, \omega_t, \mathbf{z}; \theta_s^*) := [F^{-1}(\tilde{G}(\mathbf{z}) \mid \mathbf{x}_{\leq T}, \omega_{\leq T})]_t, \quad \sigma_s^* = \frac{1}{\sqrt{s}}.$$

There is a consistency issue to address with this definition. First, observe that the function  $f_t(\cdot; \theta_s^*)$  takes as input only data up to time step  $t$ , but the inverse of the cumulative CDF is defined given *the whole sequence* of  $(\mathbf{x}_{\leq T}, \omega_{\leq T})$ . We therefore need to verify the following lemma which holds for our definition of

$f_t(\cdot; \theta_s^*)$ .

**Lemma LemA.2**

Let  $(y_{\leq T}, \mathbf{x}_{\leq T}, \omega_{\leq T})$  and  $(y'_{\leq T}, \mathbf{x}'_{\leq T}, \omega'_{\leq T})$  be two distinct realizations of repeated measurements such that there exists  $t_0$  for which

$$\mathbf{x}_{\leq t_0} = \mathbf{x}'_{\leq t_0}, \quad \omega_{\leq t_0} = \omega'_{\leq t_0}.$$

Then, for every  $t \leq t_0$ ,

$$[F^{-1}(\tilde{G}(\mathbf{z}) \mid \mathbf{x}_{\leq t}, \omega_{\leq t})]_t = [F^{-1}(\tilde{G}(\mathbf{z}) \mid \mathbf{x}'_{\leq t}, \omega'_{\leq t})]_t.$$

Now, we decompose the marginal probabilistic model:

$$\begin{aligned} p_{\theta_s}(y_{\leq T} \mid \mathbf{x}_{\leq T}, \omega_{\leq T}) &= \int_{\mathbb{R}^{d_{\mathbf{z}}}} p_{\theta_s}(y_{\leq T}, \mathbf{z} \mid \mathbf{x}_{\leq T}, \omega_{\leq T}) d\mathbf{z} \\ &= \int_{\mathbb{R}^{d_{\mathbf{z}}}} \prod_{t=1}^T p_{\theta_s}(y_t, \mathbf{z} \mid y_{< t}, \mathbf{x}_{\leq t}, \omega_{\leq t}) p(\mathbf{z}) d\mathbf{z} \\ &= \int_{\mathbb{R}^{d_{\mathbf{z}}}} \prod_{t=1}^T \mathcal{N}(y_t \mid [F^{-1}(\tilde{G}(\mathbf{z}) \mid \mathbf{x}_{\leq T}, \omega_{\leq T})]_t, (\sigma_s^*)^2) p(\mathbf{z}) d\mathbf{z} \\ &= \int_{[0,1]^T} \prod_{t=1}^T \mathcal{N}(y_t \mid [F^{-1}(\xi \mid \mathbf{x}_{\leq T}, \omega_{\leq T})]_t, (\sigma_s^*)^2) d\xi \\ &= \int_{\mathcal{Y}^T} \prod_{t=1}^T \mathcal{N}(y_t \mid [y'_{\leq T}]_t, (\sigma_s^*)^2) p(y'_{\leq T} \mid \mathbf{x}'_{\leq T}, \omega'_{\leq T}) dy'_{\leq T}. \end{aligned}$$

Finally, we have

$$\begin{aligned} \lim_{s \rightarrow +\infty} \int_{\mathcal{Y}^T} \prod_{t=1}^T \mathcal{N}(y_t \mid [y'_{\leq T}]_t, (\sigma_s^*)^2) p(y'_{\leq T} \mid \mathbf{x}'_{\leq T}, \omega'_{\leq T}) dy'_{\leq T} \\ = \int_{\mathcal{Y}^T} \prod_{t=1}^T \delta(y_t - y'_t) p(y'_{\leq T} \mid \mathbf{x}'_{\leq T}, \omega'_{\leq T}) dy'_{\leq T} \\ = p(y_{\leq T} \mid \mathbf{x}_{\leq T}, \omega_{\leq T}). \end{aligned}$$

**Part 2:** Proof of  $\lim_{s \rightarrow +\infty} \Delta(\mathcal{D}_T; \theta_s, \phi_s) = 0$ .

First, we give an explicit writing of the modified individual gap:

$$\begin{aligned} \Delta(\mathcal{D}_T; \theta_s, \phi_s) &= L(\mathcal{D}_T; \theta_s, \phi_s) - \text{ELBO}_0(\mathcal{D}_T; \theta_s, \phi_s) + \text{ELBO}_0(\mathcal{D}_T; \theta_s, \phi_s) - \text{ELBO}(\mathcal{D}_T; \theta_s, \phi_s) \\ &= \Delta_0(\mathcal{D}_T; \theta_s, \phi_s) + \text{ELBO}_0(\mathcal{D}_T; \theta_s, \phi_s) - \text{ELBO}(\mathcal{D}_T; \theta_s, \phi_s) \\ &\quad - \left[ \sum_{t=1}^T \alpha(\mathbf{h}_t, \omega_t) \right] \mathbb{E}_{\mathbf{Z} \sim q_{\phi_s}(\cdot \mid \mathcal{D}_T)} D_{KL}(q_{\phi_s}(c \mid \mathcal{D}_T) \parallel p(c \mid \mathbf{Z})) \\ &\quad - \left[ \sum_{t=1}^T \alpha_s(\mathbf{h}_t, \omega_t) \right] \log Z(q_{\phi_s}(\cdot \mid \mathcal{D}_T)) \\ &= \sum_{t=1}^T \alpha(\mathbf{h}_t, \omega_t) D_{KL}(q_{\phi_s}(\mathbf{z}, c \mid \mathcal{D}_T) \parallel p_{\theta_s}(\mathbf{z}, c \mid \mathcal{D}_t)). \end{aligned}$$

The last equality holds because we assume  $q_{\phi_s}(c \mid \mathcal{D}_T) = \pi_{\phi_s}(c \mid \mathcal{D}_T)$  and  $\pi_{\phi_s}(c \mid \mathcal{D}_T)$  is a minimizer of

$$\min_{q_{\phi_s}(c \mid \mathcal{D}_T)} \mathbb{E}_{\mathbf{Z} \sim q_{\phi_s}(\cdot \mid \mathcal{D}_T)} D_{KL}(q_{\phi_s}(c \mid \mathcal{D}_T) \parallel p(c \mid \mathbf{Z})) = -\log Z(q_{\phi_s}(\cdot \mid \mathcal{D}_T)).$$

To show that  $\lim_{s \rightarrow +\infty} \Delta(\mathcal{D}_T; \theta_s, \phi_s) = 0$ , we will define  $\phi_s$  such that for every  $c \in \{1, \dots, K\}$  and  $t \in \{1, \dots, T\}$ :

$$\lim_{s \rightarrow +\infty} D_{KL}(q_{\phi_s}(\mathbf{z}, c \mid \mathcal{D}_T) \parallel p_{\theta_s}(\mathbf{z}, c \mid \mathcal{D}_t)) = 0.$$

Let us define  $q_{\phi_s}(\mathbf{z} \mid \mathcal{D}_T)$  such that

$$f_{\mu_{\mathbf{z}}}(\mathcal{D}_T, \phi_s) = G^{-1}(F(y_1, \dots, y_{d_{\mathbf{z}}}) \mid \mathbf{x}_{\leq T}, \omega_{\leq T}))$$

and

$$f_{S_{\mathbf{z}}}(\mathcal{D}_T, \phi) = \sigma_s \sqrt{\tilde{\Sigma}_{\mathbf{z}}(\mathcal{D}_T, \phi)},$$

with  $\tilde{\Sigma}_{\mathbf{z}}(\mathcal{D}_T, \phi)$  being the inverse of:

$$\text{Jac}(F^{-1}(\cdot \mid \mathbf{x}_{\leq T}, \omega_{\leq T}) \circ \tilde{G}(\mathbf{z})) \text{Jac}(F^{-1}(\cdot \mid \mathbf{x}_{\leq T}, \omega_{\leq T}) \circ \tilde{G}(\mathbf{z}))^\top.$$

Using Bayes' rule, the true posterior can be written as

$$p_{\theta_s}(\mathbf{z}, c \mid \mathcal{D}_t) = \frac{p_{\theta_s}(y_{\leq T}, \mathbf{z}, c \mid \mathbf{x}_{\leq t}, \omega_{\leq t})}{p_{\theta_s}(y_{\leq t} \mid \mathbf{x}_{\leq t}, \omega_{\leq t})}.$$

Expanding the numerator, we obtain

$$p_{\theta_s}(\mathbf{z}, c \mid \mathcal{D}_t) = \frac{\prod_{l=1}^t \mathcal{N}(y_l \mid [F^{-1}(\tilde{G}(\mathbf{z}) \mid \mathbf{x}_{\leq T}, \omega_{\leq T})]_l, \sigma_s^2) p(\mathbf{z} \mid c) p(c)}{p_{\theta_s}(y_{\leq t} \mid \mathbf{x}_{\leq t}, \omega_{\leq t})}.$$

By the GMM assumption over the prior, we have

$$p(\mathbf{z} \mid c) = \mathcal{N}(\mathbf{z} \mid \mu_c, \Sigma_c).$$

The approximate posterior is of the form

$$\begin{aligned} q_{\phi_s}(\mathbf{z}, c \mid \mathcal{D}_T) &= q_{\phi_s}(\mathbf{z} \mid \mathcal{D}_T) \pi_{\phi_s}(c \mid \mathcal{D}_T) \\ &= \mathcal{N}(\mathbf{z} \mid f_{\mu_{\mathbf{z}}}(\mathcal{D}_T, \phi_s), \sigma_s^2 \tilde{\Sigma}_{\mathbf{z}}(\mathcal{D}_T, \phi)) \pi_{\phi_s}(c \mid \mathcal{D}_T). \end{aligned}$$

We now show convergence by performing a change of variables. Define  $\mathbf{z}' = \sigma_s^{-\frac{t}{d_{\mathbf{z}}}} (\mathbf{z} - \mathbf{z}^*)$ . We analyze the behavior of the distributions  $p'_{\theta_s}(\mathbf{z}', c \mid \mathcal{D}_t)$  and  $q'_{\phi_s}(\mathbf{z}', c \mid \mathcal{D}_T)$ .

We prove that

$$\frac{p'_{\theta_s}(\mathbf{z}', c \mid \mathcal{D}_t)}{q'_{\phi_s}(\mathbf{z}', c \mid \mathcal{D}_T)}$$

converges to a constant independent of  $\mathbf{z}'$  as  $s \rightarrow \infty$ . Since both  $q'_{\phi_s}(\mathbf{z}', c \mid \mathcal{D}_T)$  and  $p'_{\theta_s}(\mathbf{z}', c \mid \mathcal{D}_t)$  are probability distributions, the constant must be 1. Therefore, the KL divergence between them converges to 0 as  $s \rightarrow \infty$ .

We have

$$\frac{p'_{\theta_s}(\mathbf{z}', c \mid \mathcal{D}_t)}{q'_{\phi_s}(\mathbf{z}', c \mid \mathcal{D}_T)} = \frac{\mathcal{N}(\mathbf{z}^* + \sigma_s^{t/d_z} \mathbf{z}' \mid \mathbf{z}^*, \sigma_s^2 \tilde{\Sigma}_{\mathbf{z}}(\mathcal{D}_T, \phi)) \pi_{\phi_s}(c \mid \mathcal{D}_T) p_{\theta_s}(y_{\leq t} \mid \mathbf{x}_{\leq t}, \omega_{\leq T})}{\prod_{l=1}^t \mathcal{N}(y_l \mid f_l(\mathbf{h}_l, \omega_l, \mathbf{z}^* + \sigma_s^{t/d_z} \mathbf{z}'; \theta_s), \sigma_s^2) \mathcal{N}(\mathbf{z}^* + \sigma_s^{t/d_z} \mathbf{z}' \mid \mu_c, \Sigma_c) p(c)}.$$

Now let  $A_t$  be a matrix whose Moore–Penrose inverse  $A^+$  satisfies

$$f_{\leq t}(\mathbf{h}_{\leq t}, \omega_{\leq t}, \mathbf{z}^* + \sigma_s^{t/d_z} \mathbf{z}'; \theta_s) = A^+ f_{\leq T}(\mathbf{h}_{\leq T}, \omega_{\leq T}, \mathbf{z}^* + \sigma_s^{t/d_z} \mathbf{z}'; \theta_s),$$

$$y_{\leq t} = A^+ y_{\leq T}.$$

That is, projecting onto  $A^+$  selects the first  $t$  responses. The matrices  $A^+$  and  $A$  have the forms

$$A^+ = \begin{bmatrix} I_t & 0_{t \times (T-t)} \end{bmatrix}, \quad A = \begin{bmatrix} I_t \\ 0_{(T-t) \times t} \end{bmatrix}.$$

By noticing that  $[A^\top (\sigma_s^2 I_T)^{-1} A]^{-1} = \sigma_s^2 I_t$  We can therefore apply the mean rearranging formula (Petersen et al., 2008):

$$\begin{aligned} & \mathcal{N}\left(A^+ y_{\leq T} \mid A^+ f_{\leq T}(\mathbf{h}_{\leq t}, \omega_{\leq t}, \mathbf{z}^* + \sigma_s^{t/d_z} \mathbf{z}'; \theta_s), [A^\top (\sigma_s^2 I_T) A]^{-1}\right) \\ &= \frac{\sqrt{\det(2\pi \sigma_s^2 I_T)}}{\sqrt{\det(2\pi \sigma_s^2 I_t)}} \mathcal{N}\left(y_{\leq T} \mid f_{\leq T}(\mathbf{h}_{\leq T}, \omega_{\leq T}, \mathbf{z}^* + \sigma_s^{t/d_z} \mathbf{z}'; \theta_s), \sigma_s^2 I_T\right) \end{aligned}$$

$$\begin{aligned} \frac{p'_{\theta_s}(\mathbf{z}', c \mid \mathcal{D}_t)}{q'_{\phi_s}(\mathbf{z}', c \mid \mathcal{D}_T)} &= \frac{\mathcal{N}(\mathbf{z}^* + \sigma_s^{t/d_z} \mathbf{z}' \mid \mathbf{z}^*, \sigma_s^2 \tilde{\Sigma}_{\mathbf{z}}(\mathcal{D}_T, \phi)) \pi_{\phi_s}(c \mid \mathcal{D}_T) p_{\theta_s}(y_{\leq t} \mid \mathbf{x}_{\leq t}, \omega_{\leq T})}{\frac{\sqrt{\det(2\pi \sigma_s^2 I_T)}}{\sqrt{\det(2\pi \sigma_s^2 I_t)}} \mathcal{N}(y_{\leq T} \mid f_{\leq T}(\mathbf{h}_{\leq T}, \omega_{\leq T}, \mathbf{z}^* + \sigma_s^{t/d_z} \mathbf{z}'; \theta_s), \sigma_s^2 I_T) \mathcal{N}(\mathbf{z}^* + \sigma_s^{t/d_z} \mathbf{z}' \mid \mu_c, \Sigma_c) p(c)} \\ &= (2\pi)^{\frac{t-d}{2}} \frac{\det(\tilde{\Sigma}_{\mathbf{z}})^{-1/2}}{\det(\Sigma_c)^{-1/2}} \exp \left\{ -\frac{1}{2} \sigma_s^{2(t/d_z-1)} \mathbf{z}'^\top \tilde{\Sigma}_{\mathbf{z}}^{-1} \mathbf{z}' \right. \\ &\quad \left. + \frac{1}{2\sigma_s^2} \sum_{l=1}^T (y_l - f_l(\mathbf{h}_l, \omega_l, \mathbf{z}^* + \sigma_s^{t/d_z} \mathbf{z}'; \theta_s))^2 \right. \\ &\quad \left. + \frac{1}{2} (\mathbf{z}^* + \sigma_s^{t/d_z} \mathbf{z}' - \mu_c)^\top \Sigma_c^{-1} (\mathbf{z}^* + \sigma_s^{t/d_z} \mathbf{z}' - \mu_c) \right\} \\ &\quad \times \frac{\pi_{\phi_s}(c \mid \mathcal{D}_T) p_{\theta_s}(y_{\leq T} \mid \mathbf{x}_{\leq t}, \omega_{\leq t})}{p(c)}. \end{aligned}$$

By noticing that

$$\sum_{l=1}^T (y_l - f_l(\mathbf{h}_l, \omega_l, \mathbf{z}^* + \sigma_s^{t/d_z} \mathbf{z}'; \theta_s))^2 = \|y_{\leq T} - F^{-1}(\tilde{G}(\mathbf{z}^* + \sigma_s^{t/d_z} \mathbf{z}') \mid \mathbf{x}_{\leq T}, \omega_{\leq T})\|_2^2.$$

We apply a first-order Taylor expansion:

$$y_{\leq T} - F^{-1}(\tilde{G}(\mathbf{z}^* + \sigma_s^{t/d_z} \mathbf{z}') \mid \mathbf{x}_{\leq T}, \omega_{\leq T}) \underset{s \rightarrow \infty}{\approx} -Jac(F^{-1}\tilde{G})(\mathbf{z}^*)(\sigma_s^{t/d_z} \mathbf{z}'),$$

which implies by norm continuity

$$\begin{aligned} \sum_{l=1}^T (y_l - f_l(\mathbf{h}_l, \omega_l, \mathbf{z}^* + \sigma_s^{t/d_z} \mathbf{z}'; \theta_s))^2 &\underset{s \rightarrow \infty}{\approx} \|Jac(F^{-1}\tilde{G})(\mathbf{z}^*)(\sigma_s^{t/d_z} \mathbf{z}')\|_2^2 \\ &\underset{s \rightarrow \infty}{=} \sigma_s^{2t/d_z} \mathbf{z}'^\top \tilde{\Sigma}_{\mathbf{z}}^{-1} \mathbf{z}'. \end{aligned}$$

Define the constant  $\mathcal{Cst}(\mathcal{D}_t; \sigma_s, \theta_s, \phi_s)$  w.r.t.  $\mathbf{z}'$  as

$$\mathcal{Cst}(\mathcal{D}_t; \sigma_s, \theta_s, \phi_s) = (2\pi)^{(t-d_z)/2} \sqrt{\frac{\det(\Sigma_c)}{\det(\tilde{\Sigma}_{\mathbf{z}})}} \frac{\pi_{\phi_s}(c \mid \mathcal{D}_T) p_{\theta_s}(y_{\leq t} \mid \mathbf{x}_{\leq t}, \omega_{\leq t})}{p(c)}.$$

Thus,

$$\begin{aligned} \frac{p'_{\theta_s}(\mathbf{z}', c \mid \mathcal{D}_T)}{q'_{\phi_s}(\mathbf{z}', c \mid \mathcal{D}_T)} &\underset{s \rightarrow \infty}{\approx} \frac{1}{2} (\mathbf{z}^* - \mu_c)^\top \Sigma_c^{-1} (\mathbf{z}^* - \mu_c) \mathcal{Cst}(\mathcal{D}_t; \sigma_s, \theta_s, \phi_s) \\ &\times \exp \left\{ -\frac{1}{2} \sigma_s^{2(t/d_z-1)} \mathbf{z}'^\top \tilde{\Sigma}_{\mathbf{z}}^{-1} \mathbf{z}' + \frac{1}{2} \sigma_s^{2(t/d_z-1)} \mathbf{z}'^\top \mathbf{z}' \right\}. \end{aligned}$$

Finally,

$$\frac{p'_{\theta_s}(\mathbf{z}', c \mid \mathcal{D}_T)}{q'_{\phi_s}(\mathbf{z}', c \mid \mathcal{D}_T)} \underset{s \rightarrow \infty}{\approx} \frac{1}{2} (\mathbf{z}^* - \mu_c)^\top \Sigma_c^{-1} (\mathbf{z}^* - \mu_c) \mathcal{Cst}(\mathcal{D}_t; \sigma_s, \theta_s, \phi_s).$$

To conclude the proof, we still need to show that  $\lim_{s \rightarrow +\infty} \mathcal{Cst}(\mathcal{D}_t; \sigma_s, \theta_s, \phi_s)$  exists and is finite because the model parameters still depend on the chosen variance. This was the main misapprehension of Dai & Wipf (2019) for a VAE in the static setting with an unimodal prior over the continuous latents  $\mathbf{Z}$ .

We have already shown that

$$\lim_{\sigma \rightarrow 0^+} p_{\theta_\sigma}(y_{\leq T} \mid \mathbf{x}_{\leq T}, \omega_{\leq T}) = p(y_{\leq T} \mid \mathbf{x}_{\leq T}, \omega_{\leq T}),$$

and therefore:

$$\begin{aligned} \lim_{s \rightarrow +\infty} \mathcal{Cst}(\mathcal{D}_t; \sigma_s, \theta_s, \phi_s) &= (2\pi)^{(t-d_z)/2} \sqrt{\frac{\det(\Sigma_c)}{\det(\tilde{\Sigma}_{\mathbf{z}})}} \\ &\times \frac{p(y_{\leq T} \mid \mathbf{x}_{\leq T}, \omega_{\leq T})}{p(c)} \cdot \lim_{s \rightarrow +\infty} \pi_{\phi_s}(c \mid \mathcal{D}_T). \end{aligned}$$

We verify that  $\lim_{s \rightarrow +\infty} \pi_{\phi_s}(c \mid \mathcal{D}_T)$  exists and is finite and not zero for all  $c \in \{1, \dots, K\}$ :

$$\begin{aligned}
\pi_{\phi_s}(c \mid \mathcal{D}_T) &= \frac{\exp(\mathbb{E}_{\mathbf{Z} \sim q_{\phi_s}(\cdot \mid \mathcal{D}_T)} \log p(c \mid \mathbf{Z}))}{\sum_{c=1}^K \exp(\mathbb{E}_{\mathbf{Z} \sim q_{\phi_s}(\cdot \mid \mathcal{D}_T)} \log p(c \mid \mathbf{Z}))} \\
&= \frac{\exp(\int_{\mathcal{Z}} \log p(c \mid \mathbf{z}) \mathcal{N}(\mathbf{z} \mid \mathbf{z}^*, \sigma_s^2 \tilde{\Sigma}_{\mathbf{z}}(\mathcal{D}_T, \phi)) d\mathbf{z})}{\sum_{c=1}^K \exp(\int_{\mathcal{Z}} \log p(c \mid \mathbf{z}) \mathcal{N}(\mathbf{z} \mid \mathbf{z}^*, \sigma_s^2 \tilde{\Sigma}_{\mathbf{z}}(\mathcal{D}_T, \phi)) d\mathbf{z})} \\
&\xrightarrow{s \rightarrow \infty} \frac{\exp(\int_{\mathcal{Z}} \log p(c \mid \mathbf{z}) \delta(\mathbf{z} - \mathbf{z}^*) d\mathbf{z})}{\sum_{c=1}^K \exp(\int_{\mathcal{Z}} \log p(c \mid \mathbf{z}) \delta(\mathbf{z} - \mathbf{z}^*) d\mathbf{z})} \\
&= \frac{p(c \mid \mathbf{z}^*)}{\sum_{c=1}^K p(c \mid \mathbf{z}^*)}
\end{aligned}$$

We have therefore proved that the ratio  $\frac{p'_{\theta_s}(\mathbf{z}', c \mid \mathcal{D}_T)}{q'_{\phi_s}(\mathbf{z}', c \mid \mathcal{D}_T)}$  converges into a nonzero constant which finishes the proof of the theorem.  $\square$

**Proof of theorem Thm3.5.** We start by considering the ELBO:

$$\begin{aligned}
\mathcal{L}(\mathcal{D}_T; \theta, \phi) &= - \sum_{t=1}^T \mathbb{E}_{\mathbf{Z} \sim q_{\phi}(\cdot \mid \mathcal{D}_T)} [\alpha(\mathbf{h}_t, \omega_t) \log p_{\theta}(y_t \mid \mathbf{H}_t, W_t, \mathbf{Z})] \\
&\quad + \left[ \sum_{t=1}^T \alpha(\mathbf{h}_t, \omega_t) \right] D_{KL}(q_{\phi}(\mathbf{z} \mid \mathcal{D}_T) \parallel p(\mathbf{z})) \\
&\quad - \left[ \sum_{t=1}^T \alpha(\mathbf{h}_t, \omega_t) \right] \log Z(q_{\phi}(\cdot \mid \mathcal{D}_T)).
\end{aligned}$$

By the positivity of the KL divergence and using the fact that  $-\log Z(q_{\phi}(\cdot \mid \mathcal{D}_T))$  minimizes a positive functional (as explained in Eq. (3.17)), we obtain:

$$\begin{aligned}
\mathcal{L}(\mathcal{D}_T; \theta_{\sigma}^*, \phi_{\sigma}^*) &\geq - \sum_{t=1}^T \mathbb{E}_{\mathbf{Z} \sim q_{\phi}(\cdot \mid \mathcal{D}_T)} [\alpha(\mathbf{h}_t, \omega_t) \log (p_{\theta}(y_t \mid \mathbf{H}_t, W_t, \mathbf{Z}))] \\
&= \sum_{t=1}^T \alpha(\mathbf{h}_t, \omega_t) \mathbb{E}_{\mathbf{Z} \sim q_{\phi}(\cdot \mid \mathcal{D}_T)} \left[ \frac{1}{2} \log(2\pi\sigma^2) + \frac{1}{2\sigma^2} (y_t - f(\mathbf{H}_t, \mathbf{Z}, W_t))^2 \right] \\
&= \frac{1}{2\sigma^2} \left[ \left( \sum_{t=1}^T \alpha(\mathbf{h}_t, \omega_t) \right) \sigma^2 \log(2\pi\sigma^2) + \sum_{t=1}^T \alpha(\mathbf{h}_t, \omega_t) \underbrace{\mathbb{E}_{\mathbf{Z} \sim q_{\phi}(\cdot \mid \mathcal{D}_T)} (y_t - f(\mathbf{H}_t, \mathbf{Z}, W_t))^2}_{\delta_{\sigma}(t)} \right].
\end{aligned}$$

Suppose there exists  $t_0 \in \{1, 2, \dots, T\}$  such that  $\lim_{\sigma \rightarrow 0^+} \delta_{\sigma}(t_0) > 0$ . Then we have  $\lim_{\sigma \rightarrow 0^+} \mathcal{L}(\mathcal{D}_T; \theta_{\sigma}^*, \phi_{\sigma}^*) = +\infty$ , which is impossible since we assume  $\mathcal{L}(\mathcal{D}_T; \theta_{\sigma}^*, \phi_{\sigma}^*)$  to be minimized. Therefore, we conclude that for all  $t \in \{1, 2, \dots, T\}$ ,  $\lim_{\sigma \rightarrow 0^+} \delta_{\sigma}(t) = 0$ .

Consequently, we have

$$\lim_{\sigma \rightarrow 0^+} \mathbb{E}_{\epsilon \sim \mathcal{N}(0, I)} (y_t - f(\mathbf{H}_t, W_t, f_{\mu_{\mathbf{z}}}(\mathcal{D}_T; \phi_{\sigma}^*) + f_{S_{\mathbf{z}}}(\mathcal{D}_T; \theta_{\sigma}^*)\epsilon))^2 = 0,$$

which implies that

$$\lim_{\sigma \rightarrow 0^+} f(\mathbf{H}_t, W_t, f_{\mu_{\mathbf{z}}}(\mathcal{D}_T; \phi_{\sigma}^*) + f_{S_{\mathbf{z}}}(\mathcal{D}_T; \theta_{\sigma}^*)\epsilon) = y_t, \quad \text{almost surely.}$$

In particular, we also have

$$\lim_{\sigma \rightarrow 0^+} f(\mathbf{H}_t, W_t, f_{\mu_{\mathbf{z}}}(\mathcal{D}_T; \phi_\sigma^*)) = y_t.$$

### A.1.5 Upper bound on weighted PEHE

**theorem** *Thm3.6.* To prove the theorem, we rely on the following key lemma, but first, we need to define further mathematical objects. We define the weighted population risk over the whole population as

$$R_{t,g}(f, \Phi) := \mathbb{E}_{\mathbf{H}_t, W_t} [\alpha(\mathbf{H}_t, W_t) \ell_{f, \Phi}(\mathbf{H}_t, W_t)],$$

and the weighted population counterfactual risk as

$$R_{t,g}(f, \Phi)_{CF} := \mathbb{E}_{\mathbf{H}_t, 1-W_t} [\alpha(\mathbf{H}_t, 1-W_t) \ell_{f, \Phi}(\mathbf{H}_t, W_t)].$$

#### Lemma LemA.3

$$R_{t,g}(f, \Phi) + R_{t,g}(f, \Phi)_{CF} \leq R_{t,g}^1(f, \Phi) + R_{t,g}^0(f, \Phi) + B_\Phi \text{IPM}_G(g_\Phi(\cdot | W_t = 1), g_\Phi(\cdot | W_t = 0))$$

The proof immediately follows from Lemma 1 in Shalit et al. (2017).

Next, to complete the proof, we define the expected potential outcome at time  $t$ , given the context history  $\mathbf{H}_t = \mathbf{h}_t$  and latent  $\mathbf{z}$  as

$$m_t^\omega(\mathbf{h}_t, \mathbf{z}) := \mathbb{E}_{Y_t(\omega) | \mathbf{H}_t, \mathbf{Z}}(Y_t(\omega) | \mathbf{H}_t = \mathbf{h}_t, \mathbf{Z} = \mathbf{z}) \quad \omega \in \mathcal{W},$$

and we show the following lemma:

#### Lemma LemA.4

Denote  $\hat{p}_\phi(\mathbf{h}_t, w, \mathbf{z}) := p(\mathbf{h}_t, w) q_\phi(\mathbf{z} | \mathcal{D}_{\leq t-1})$ . We can decompose  $R_{t,g}(f, \Phi)$  and  $R_{t,g}(f, \Phi)_{CF}$  under our distributional assumptions as:

$$\begin{aligned} & \mathbb{E}_{\hat{p}_\phi(\mathbf{h}_t, w, \mathbf{z})} [\alpha(\mathbf{h}_t, w) (f(\mathbf{h}_t, w, \mathbf{z}) - m_t^w(\mathbf{h}_t, \mathbf{z}))] \\ &= 2\sigma^2 (R_{t,g}(f, \Phi) - \tfrac{1}{2} \log(2\pi\sigma^2)) - \sum_{\omega \in \{0,1\}} \text{Var}_{\hat{p}_\phi}(Y_t), \end{aligned}$$

and

$$\begin{aligned} & \mathbb{E}_{\hat{p}_\phi(\mathbf{h}_t, w, \mathbf{z})} [\alpha(\mathbf{h}_t, 1-w) (f(\mathbf{h}_t, 1-w, \mathbf{z}) - m_t^{1-w}(\mathbf{h}_t, \mathbf{z}))] \\ &= 2\sigma^2 (R_{t,g}(f, \Phi)_{CF} - \tfrac{1}{2} \log(2\pi\sigma^2)) - \sum_{\omega \in \{0,1\}} \text{Var}_{\hat{p}_\phi}(Y_t | 1-w). \end{aligned}$$



*Proof.* We have:

$$\begin{aligned}
R_{t,g}(f, \Phi) &= \mathbb{E}_{\mathbf{H}_t, W_t} [\alpha(\mathbf{H}_t, W_t) \ell_{f, \Phi}(\mathbf{H}_t, W_t)] \\
&= \sum_{\omega \in \{0,1\}} \int_{\mathcal{H}_t} \int_{\mathcal{Z}} \int_{\mathcal{Y}} -\alpha(\mathbf{h}_t, \omega) \log p_{\theta}(y_t | \mathbf{h}_t, \omega, \mathbf{z}) \\
&\quad \times p(y_t | \mathbf{h}_t, \omega, \mathbf{z}) p(\mathbf{h}_t, \omega) q_{\phi}(\mathbf{z} | \mathcal{D}_{\leq t-1}) dy_t d\mathbf{z} d\mathbf{h}_t \\
&= \sum_{\omega \in \{0,1\}} \int_{\mathcal{H}_t} \int_{\mathcal{Z}} \int_{\mathcal{Y}} \alpha(\mathbf{h}_t, \omega) \left\{ \frac{1}{2} \log(2\pi\sigma^2) + \frac{(y_t - f(\mathbf{h}_t, \omega, \mathbf{z}))^2}{2\sigma^2} \right\} \\
&\quad \times p(y_t | \mathbf{h}_t, \omega, \mathbf{z}) p(\mathbf{h}_t, \omega) q_{\phi}(\mathbf{z} | \mathcal{D}_{\leq t-1}) dy_t d\mathbf{z} d\mathbf{h}_t \\
&= \frac{1}{2} \log(2\pi\sigma^2) + \frac{1}{2\sigma^2} \sum_{\omega \in \{0,1\}} \text{Var}_{\hat{p}_{\phi}(\mathbf{h}_t, \omega, \mathbf{z})}(Y_t) \\
&\quad + \int_{\mathcal{H}_t} \int_{\mathcal{Z}} \alpha(\mathbf{h}_t, \omega) (f(\mathbf{h}_t, \omega, \mathbf{z}) - m_t^{\omega}(\mathbf{h}_t, \mathbf{z}))^2 \\
&\quad \times p(\mathbf{h}_t, \omega) q_{\phi}(\mathbf{z} | \mathcal{D}_{\leq t-1}) d\mathbf{z} d\mathbf{h}_t.
\end{aligned}$$

In a similar way, we can show the decomposition related to  $R_{t,g}(f, \Phi)_{CF}$ .  $\square$

The remainder idea of the proof is to decompose the PEHE in such a way we can upper bound it with an expression including  $R_{t,g}(f, \Phi)$  and  $R_{t,g}(f, \Phi)_{CF}$  and then use lemma LemA.3. We actually have:

$$\begin{aligned}
\epsilon_{\text{PEHE}_{t,g}} &= \mathbb{E}_{\mathbf{H}_t \sim g} \mathbb{E}_{\mathbf{Z} \sim q_{\phi}(\mathbf{Z} | \mathcal{D}_{\leq t-1})} \left[ \left( \tau(\mathbf{H}_t, \mathbf{Z}) - \hat{\tau}_{f, \Phi}(\mathbf{H}_t, \mathbf{Z}) \right)^2 \right] \\
&= \mathbb{E}_{\mathbf{H}_t \sim g} \mathbb{E}_{\mathbf{Z} \sim q_{\phi}(\mathbf{Z} | \mathcal{D}_{\leq t-1})} \left[ \left( m_t^1(\mathbf{h}_t, \mathbf{z}) - m_t^0(\mathbf{h}_t, \mathbf{z}) - f(\mathbf{h}_t, 1, \mathbf{z}) + f(\mathbf{h}_t, 0, \mathbf{z}) \right)^2 \right] \\
&\stackrel{(1)}{\leq} 2 \mathbb{E}_{\mathbf{H}_t \sim g} \mathbb{E}_{\mathbf{Z} \sim q_{\phi}(\mathbf{Z} | \mathcal{D}_{\leq t-1})} \left[ (f(\mathbf{h}_t, 1, \mathbf{z}) - m_t^1(\mathbf{h}_t, \mathbf{z}))^2 \right] \\
&\quad + 2 \mathbb{E}_{\mathbf{H}_t \sim g} \mathbb{E}_{\mathbf{Z} \sim q_{\phi}(\mathbf{Z} | \mathcal{D}_{\leq t-1})} \left[ (f(\mathbf{h}_t, 0, \mathbf{z}) - m_t^0(\mathbf{h}_t, \mathbf{z}))^2 \right] \\
&= \mathbb{E}_{\mathbf{H}_t | W_t=1} \mathbb{E}_{\mathbf{Z}} [\alpha(\mathbf{h}_t, 1) (f(\mathbf{h}_t, 1, \mathbf{z}) - m_t^1(\mathbf{h}_t, \mathbf{z}))^2] \\
&\quad + \mathbb{E}_{\mathbf{H}_t | W_t=0} \mathbb{E}_{\mathbf{Z}} [\alpha(\mathbf{h}_t, 0) (f(\mathbf{h}_t, 1, \mathbf{z}) - m_t^1(\mathbf{h}_t, \mathbf{z}))^2] \\
&\quad + \mathbb{E}_{\mathbf{H}_t | W_t=0} \mathbb{E}_{\mathbf{Z}} [\alpha(\mathbf{h}_t, 0) (f(\mathbf{h}_t, 0, \mathbf{z}) - m_t^0(\mathbf{h}_t, \mathbf{z}))^2] \\
&\quad + \mathbb{E}_{\mathbf{H}_t | W_t=1} \mathbb{E}_{\mathbf{Z}} [\alpha(\mathbf{h}_t, 1) (f(\mathbf{h}_t, 0, \mathbf{z}) - m_t^0(\mathbf{h}_t, \mathbf{z}))^2] \\
&= \mathbb{E}_{\mathbf{H}_t, W_t} \mathbb{E}_{\mathbf{Z}} [\alpha(\mathbf{H}_t, W_t) (f(\mathbf{H}_t, W_t, \mathbf{Z}) - m_t^{W_t}(\mathbf{H}_t, \mathbf{Z}))^2] \\
&\quad + \mathbb{E}_{\mathbf{H}_t, 1-W_t} \mathbb{E}_{\mathbf{Z}} [\alpha(\mathbf{H}_t, 1-W_t) (f(\mathbf{H}_t, W_t, \mathbf{Z}) - m_t^{W_t}(\mathbf{H}_t, \mathbf{Z}))^2] \\
&\stackrel{(2)}{=} 2\sigma^2 (R_{t,g}(f, \Phi) + R_{t,g}(f, \Phi)_{CF} - \log(2\pi\sigma^2)) \\
&\quad - \sum_{\omega \in \{0,1\}} (\text{Var}_{\hat{p}_{\phi}(\mathbf{h}_t, 1-\omega, \mathbf{z})}(Y_t) + \text{Var}_{\hat{p}_{\phi}(\mathbf{h}_t, \omega, \mathbf{z})}(Y_t)) \\
&\stackrel{(3)}{\leq} 2\sigma^2 (R_{t,g}(f, \Phi) + R_{t,g}(f, \Phi)_{CF} - \log(2\pi\sigma^2)) \\
&\stackrel{(4)}{\leq} 2\sigma^2 \left( R_{t,g}^1(f, \Phi) + R_{t,g}^0(f, \Phi) + B_{\Phi} \text{IPM}_G(g_{\Phi}(\cdot | W_t=1), g_{\Phi}(\cdot | W_t=0)) - \log(2\pi\sigma^2) \right).
\end{aligned}$$

The inequality  $\stackrel{(1)}{\leq}$  follows from the property  $(a-b)^2 \leq 2a^2 + 2b^2$ . The equation  $\stackrel{(2)}{=}$  follows from plugging in the equations from Lemma LemA.4, the inequality  $\stackrel{(3)}{\leq}$  follows from the positivity of the variance terms, and  $\stackrel{(4)}{\leq}$  follows from Lemma LemA.3.  $\square$

## A.1.6 Proof of Proposition Prop3.2

Using a Monte Carlo approximation, we can express the approximate factual risk as:

$$R_{t,g}^\omega(f, \Phi) \approx \frac{1}{n_\omega^{(t)}} \sum_{i \in \mathcal{B}, W_{it}=\omega} \mathbb{E}_{\mathbf{Z} \sim q_\phi(\mathbf{Z} | \mathcal{D}_{i, \leq t-1})} [\alpha(\mathbf{h}_{it}, \omega) \log \mathcal{N}(y_{it}; f(\Phi(\mathbf{h}_{it}), \mathbf{Z}, \omega), \sigma^2)].$$

By the stationarity assumption, for  $t \geq t_0$ , this approximation holds:

$$R_{t,g}^\omega(f, \Phi) \approx \frac{1}{n_\omega^{(t)}} \sum_{i \in \mathcal{B}, W_{it}=\omega} \mathbb{E}_{\mathbf{Z} \sim q_\phi(\mathbf{Z} | \mathcal{D}_{iT})} [\alpha(\mathbf{h}_{it}, \omega) \log \mathcal{N}(y_{it}; f(\Phi(\mathbf{h}_{it}), \mathbf{Z}, \omega), \sigma^2)].$$

On the other hand, the reconstruction term in the ELBO can be written as:

$$\begin{aligned} & \sum_{t=t_0}^T \mathbb{E}_{\mathbf{Z} \sim q_\phi(\cdot | \mathcal{D}_T)} [\alpha(\mathbf{H}_t, W_t) \log p_\theta(Y_t | \mathbf{H}_t, W_t, \mathbf{Z})] \\ & \approx \sum_{t=t_0}^T \frac{1}{|\mathcal{B}|} \sum_{i \in \mathcal{B}} \mathbb{E}_{\mathbf{Z} \sim q_\phi(\mathbf{Z} | \mathcal{D}_{iT})} \left[ \alpha(\mathbf{h}_{it}, \omega) \log \mathcal{N}(y_{it}; f(\Phi(\mathbf{h}_{it}), \mathbf{Z}, \omega), \sigma^2) \right] \\ & \approx \frac{1}{|\mathcal{B}|} \sum_{t=t_0}^T \sum_{\omega \in \mathcal{W}} \sum_{i \in \mathcal{B}, W_{it}=\omega} \mathbb{E}_{\mathbf{Z} \sim q_\phi(\mathbf{Z} | \mathcal{D}_{iT})} \left[ \alpha(\mathbf{h}_{it}, \omega) \log \mathcal{N}(y_{it}; f(\Phi(\mathbf{h}_{it}), \mathbf{Z}, \omega), \sigma^2) \right] \\ & \approx \frac{1}{|\mathcal{B}|} \sum_{t=t_0}^T \left\{ -n_1^{(t)} R_t^1(f, \Phi) - n_0^{(t)} R_t^0(f, \Phi) \right\}. \end{aligned}$$

## A.2 Experiments on synthetic data: Details

### A.2.1 Additional results

**Results of baselines on the synthetic datasets** The following Table A.1 provides the detailed results responsible for Figures 3.4 related to baselines with the three different approaches across levels of  $\gamma_{(1)}^{YU}$ .

Table A.1: Results on the synthetic data reported by PEHE. Smaller is better.

Model	$\gamma_{(1)}^{YU} = 0$	$\gamma_{(1)}^{YU} = 0.25$	$\gamma_{(1)}^{YU} = 0.5$	$\gamma_{(1)}^{YU} = 0.75$	$\gamma_{(1)}^{YU} = 1$	$\gamma_{(1)}^{YU} = 1.25$	$\gamma_{(1)}^{YU} = 1.5$	$\gamma_{(1)}^{YU} = 1.75$	$\gamma_{(1)}^{YU} = 2$	$\gamma_{(1)}^{YU} = 2.25$	$\gamma_{(1)}^{YU} = 2.5$
<b>CDVAE (ours)</b>	<b>0.43±0.02</b>	<b>0.50±0.03</b>	<b>0.96±0.09</b>	<b>1.57±0.08</b>	<b>1.90±0.10</b>	<b>2.35±0.18</b>	<b>3.57±0.17</b>	<b>4.80±0.20</b>	<b>6.84±0.20</b>	<b>7.64±0.48</b>	<b>9.03±0.50</b>
Causal CPC	0.43±0.01	0.50±0.03	1.08±0.08	2.49±0.14	2.98±0.09	4.98±0.21	5.91±0.29	10.15±0.38	12.25±0.49	15.65±0.56	19.39±0.59
Causal CPC (with substitute)	0.46±0.02	0.49±0.01	1.02±0.05	2.38±0.08	2.83±0.09	4.81±0.13	5.38±0.22	8.13±0.39	10.11±0.41	12.01±0.54	14.03±0.64
Causal CPC (oracle)	0.45±0.02	0.43±0.03	0.96±0.04	1.59±0.06	2.14±0.08	4.41±0.10	5.08±0.30	6.93±0.25	8.70±0.17	10.15±0.47	12.91±0.51
Causal Transformer	0.46±0.02	0.68±0.04	1.50±0.06	2.55±0.18	3.65±0.20	5.55±0.50	8.15±0.72	12.35±0.25	15.48±1.02	24.77±2.21	43.84±2.58
Causal Transformer (with substitute)	0.46±0.02	0.67±0.02	1.46±0.03	2.48±0.08	3.53±0.09	5.23±0.11	7.72±0.18	11.86±0.17	15.22±0.17	20.12±0.35	33.58±0.45
Causal Transformer (oracle)	0.46±0.02	0.60±0.03	1.48±0.03	2.35±0.06	3.30±0.07	5.11±0.09	7.34±0.13	11.55±0.25	16.98±0.29	18.64±0.31	28.45±0.33
G-Net	0.62±0.05	0.80±0.05	4.90±0.03	5.56±0.05	4.82±0.15	5.79±0.12	10.36±0.23	15.17±0.25	23.89±0.54	32.75±1.20	49.35±2.35
G-Net (with substitute)	0.56±0.04	0.75±0.01	3.61±0.02	4.99±0.20	4.27±0.18	5.50±0.15	8.34±0.64	13.55±0.97	17.97±1.83	19.25±2.04	40.21±2.10
G-Net (oracle)	0.48±0.02	0.69±0.03	3.10±0.05	4.36±0.08	4.45±0.12	5.28±0.17	8.28±0.23	13.10±0.50	17.47±0.65	16.22±0.95	35.35±1.77
CRN	0.53±0.02	0.68±0.03	1.63±0.04	2.94±0.11	5.14±0.17	6.66±0.19	9.08±0.25	11.93±0.37	16.54±0.65	18.68±0.67	29.66±1.12
CRN (with substitute)	0.48±0.01	0.65±0.01	1.51±0.02	2.56±0.18	3.98±0.21	6.05±0.35	6.81±0.65	8.50±1.16	13.81±0.76	16.23±0.73	26.11±1.41
CRN (oracle)	0.53±0.01	0.60±0.01	1.69±0.02	2.87±0.09	3.75±0.13	5.69±0.17	8.92±0.22	9.65±0.31	13.49±0.54	15.64±0.61	25.98±0.97
RMSN	0.57±0.02	0.67±0.02	1.60±0.03	2.67±0.05	4.31±0.15	5.58±0.17	7.40±0.32	11.25±0.57	15.01±0.89	19.41±1.13	25.07±0.97
RMSN (with substitute)	0.45±0.01	0.67±0.02	1.51±0.04	2.31±0.03	3.61±0.20	4.61±0.20	6.14±0.50	7.58±0.82	10.63±1.31	18.53±1.50	21.08±1.60
RMSN (oracle)	0.48±0.01	0.62±0.01	1.43±0.03	1.97±0.03	3.42±0.13	4.43±0.15	6.00±0.27	7.31±0.34	9.20±0.48	17.06±0.83	19.32±1.26

**Robustness to Number of Prior Components** The Table A.2 gives detailed results summarized in Figure 3.7a that assess the sensitivity of CDVAE to the variation of the prior cluster numbers  $K$ .

Table A.2: Results of CDVAE when varying the number of components  $K$  of the prior. The study is conducted on the synthetic data and is reported by PEHE. Smaller is better.

Model	$\gamma_{(1)}^{YU} = 0$	$\gamma_{(1)}^{YU} = 0.25$	$\gamma_{(1)}^{YU} = 0.5$	$\gamma_{(1)}^{YU} = 0.75$	$\gamma_{(1)}^{YU} = 1$	$\gamma_{(1)}^{YU} = 1.25$	$\gamma_{(1)}^{YU} = 1.5$	$\gamma_{(1)}^{YU} = 1.75$	$\gamma_{(1)}^{YU} = 2$	$\gamma_{(1)}^{YU} = 2.25$	$\gamma_{(1)}^{YU} = 2.5$
<b>CDVAE (ours)</b>	<b>0.43±0.02</b>	<b>0.50±0.03</b>	<b>0.96±0.09</b>	<b>1.57±0.08</b>	<b>1.90±0.10</b>	<b>2.35±0.18</b>	<b>3.57±0.17</b>	<b>4.80±0.20</b>	<b>6.84±0.20</b>	<b>7.64±0.48</b>	<b>9.03±0.50</b>
CDVAE ( $K = 2$ )	0.43±0.01	0.50±0.01	0.96±0.03	1.52±0.04	2.07±0.07	2.51±0.14	4.10±0.41	4.44±0.43	6.98±0.38	7.90±0.33	8.88±0.45
CDVAE ( $K = 5$ )	0.42±0.01	0.48±0.02	0.93±0.02	1.41±0.11	2.02±0.03	2.52±0.06	3.27±0.22	4.25±0.45	6.32±0.25	7.97±0.31	8.12±0.48
CDVAE ( $K = 8$ )	0.40±0.01	0.46±0.01	0.96±0.06	1.57±0.03	2.13±0.04	2.59±0.07	3.20±0.26	4.15±0.45	6.63±0.48	6.93±0.25	8.91±0.19
CDVAE ( $K = 11$ )	0.42±0.02	0.47±0.01	0.94±0.03	1.40±0.05	2.09±0.07	2.47±0.22	3.76±0.28	5.09±0.52	6.48±0.14	7.73±1.232	9.02±1.22

## A.3 Experiments on MIMIC-III data

### A.3.1 Additional results

**Results of baselines on the semi-synthetic MIMIC III** The following Table A.3 provides the detailed results responsible for Figures 3.5 related to baselines with the three different approaches.

Table A.3: Results on the MIMIC III data reported by PEHE. Smaller is better.

Model	PEHE
<b>CDVAE (ours)</b>	<b>17.63±0.25</b>
Causal CPC	19.27±0.25
Causal CPC (with substitute)	18.45±0.26
Causal CPC (oracle)	17.98±0.21
Causal Transformer	19.68±0.20 ±
Causal Transformer (with substitute)	18.58± 0.21
Causal Transformer (oracle)	17.91 ± 0.20
G-Net	19.75±0.21
G-Net (with substitute)	18.60±0.25
G-Net (oracle)	17.95± 0.23
CRN	19.80±0.23
CRN (with substitute)	18.58±0.22
CRN (oracle)	17.91± 0.21
RMSN	19.85±0.25
RMSN (with substitute)	18.66±0.23
RMSN (oracle)	18.01± 0.19

## A.4 Models hyperparameters Details

We report in the following tables the search space of hyperparameters for all baselines.

## A.5 The Neural Architecture of CDVAE

The extended neural architecture of CDVAE comprises multiple components which we did not explicit in Section 3.6. We first begin by detailing neural network functions related to the generative model. The Table A.11 outlines the architecture for the Representation Learner  $\Phi$  which encodes the context history, Table A.10 presents the identical architecture for both  $f_{\theta_y^1}$  and  $f_{\theta_y^0}$  responsible for generating the two potential outcomes. Meanwhile, Table A.12 illustrates the design of propensity network  $e_{\theta_\omega}(\cdot)$  built on the top of the shared representation. Lastly, Tables A.13 depict the architecture used to learn both the mean and covariance matrix for the approximate posterior assumed to be Gaussian.

Table A.4: Hyper-parameters search range for RMSN

Model	Sub-model	Hyperparameter	Synthetic data	MIMIC III
RMSNs	Propensity Treatment Network	LSTM layers	1	1
		Learning rate	0.01, 0.005, 0.001, 0.0001	0.01, 0.005, 0.001, 0.0001
		Batch size	32, 64, 128	32, 64, 128
		LSTM hidden units	6, 8, ..., 12, 14	4, 6, ..., 20
		LSTM dropout rate	-	-
		Max gradient norm	0.5, 1, 2	0.5, 1, 2
		Early Stopping (min delta)	0.001	0.001
	Propensity History Network	Early Stopping (patience)	10	30
		LSTM layers	1	1
		Learning rate	0.01, 0.005, 0.001, 0.0001	0.01, 0.005, 0.001, 0.0001
		Batch size	32, 64, 128	64, 128, 256
		LSTM hidden units	6, 8, ..., 12, 14	4, 6, ..., 30
		LSTM dropout rate	-	-
		Early Stopping (min delta)	0.001	0.0001
	Encoder	Early Stopping (patience)	10	30
		LSTM layers	1	1
		Learning rate	0.01, 0.005, 0.001, 0.0001	0.01, 0.005, 0.001, 0.0001
		Batch size	32, 64, 128, 256	32, 64, 128
		LSTM hidden units	6, 8, ..., 18, 20	6, 8, ..., 18, 20
		LSTM dropout rate	-	-
		Early Stopping (min delta)	0.001	0.001
	Decoder	Early Stopping (patience)	10	30
		LSTM layers	1	1
		Learning rate	0.01, 0.005, 0.001, 0.0001	0.01, 0.005, 0.001, 0.0001
		Batch size	32, 64, 128, 256	128, 512, 1024
		LSTM hidden units	6, 8, ..., 18, 20	6, 8, ..., 18, 20
		LSTM dropout rate	-	-
		Max gradient norm	0.5, 1, 2	0.5, 1, 2
		Early Stopping (min delta)	0.001	0.0001
		Early Stopping (patience)	10	30

Table A.5: Hyper-parameters search range for CRN

Model	Sub-model	Hyperparameter	Synthetic data	MIMIC III
CRN	Encoder	LSTM layers	1	1
		Learning rate	0.01, 0.005, 0.001, 0.0001	0.01, 0.005, 0.001, 0.0001
		Batch size	32, 64, 128, 256	32, 64, 128
		LSTM hidden units	6, 8, ..., 18, 20	6, 8, ..., 18, 20
		LSTM dropout rate	-	-
		BR size	6, 8, ..., 18, 20	6, 8, ..., 18, 20
		Early Stopping (min delta)	0.001	0.001
	Decoder	Early Stopping (patience)	10	30
		LSTM layers	1	1
		Learning rate	0.01, 0.005, 0.001, 0.0001	0.01, 0.005, 0.001, 0.0001
		Batch size	128, 256, 512	256, 512, 1024
		LSTM hidden units	6, 8, ..., 18, 20	6, 8, ..., 18, 20
		LSTM dropout rate	-	-
		BR size	6, 8, ..., 18, 20	6, 8, ..., 18, 20
		Early Stopping (min delta)	0.001	0.001
		Early Stopping (patience)	10	30

Table A.6: Hyper-parameters search range for G-Net

Hyperparameter	Cancer simulation	MIMIC III (SS)
LSTM layers	1	1
Learning rate	0.01, 0.005, 0.001, 0.0001	0.01, 0.005, 0.001, 0.0001
Batch size	32, 64, 128	32, 64, 128
LSTM hidden units	6, 8, ..., 18, 20	6, 8, ..., 18, 20
FC hidden units	6, 8, ..., 18, 20	6, 8, ..., 18, 20
LSTM dropout rate	-	-
R size	6, 8, ..., 18, 20	4, 6, ..., 30
MC samples	50	50
Early Stopping (min delta)	0.001	0.001
Early Stopping (patience)	10	30

Table A.7: Hyper-parameters search range for Causal Transformer

Hyperparameter	Cancer simulation	MIMIC III (SS)
Transformer blocks	1	1
Learning rate	0.01, 0.005, 0.001, 0.0001	0.01, 0.005, 0.001, 0.0001
Batch size	32, 64, 128	32, 64, 128
Attention heads	2	2
Transformer units	4, 6, ..., 20	4, 6, ..., 20
LSTM dropout rate	-	-
BR size	6, 8, ..., 18, 20	4, 6, ..., 20
FC hidden units	6, 8, ..., 18, 20	4, 6, ..., 20
Sequential dropout rate	0.1, 0.2, 0.3	0.1, 0.2, 0.3
Max positional encoding	15	20
Early Stopping (min delta)	0.001	0.001
Early Stopping (patience)	10	30

Table A.8: Hyper-parameters search range for Causal CPC

Model	Sub-model	Hyperparameter	Cancer simulation	MIMIC III (SS)
Causal CPC	Encoder	GRU layers	1	1
		Learning rate	0.01, 0.005, 0.001, 0.0001	0.01, 0.005, 0.001, 0.0001
		Batch size	32, 64, 128	64, 128, 256
		GRU hidden units	6, 8, ..., 18, 20	6, 8, ..., 18, 20
		GRU dropout rate	-	-
		Local features (LF) size	6, 8, ..., 18, 20	4, 6, ..., 20
		Context Representation (CR) size	6, 8, ..., 18, 20	4, 6, ..., 20
		Early Stopping (min delta)	0.001	0.001
		Early Stopping (patience)	10	30
	Decoder	GRU layers	1	1
		Learning rate (decoder w/o treatment sub-network)	0.01, 0.005, 0.001, 0.0001	0.01, 0.005, 0.001, 0.0001
		Learning rate (encoder fine-tuning)	0.001, 0.0005, 0.0001, 0.00005	0.001, 0.0005, 0.0001, 0.00005
		Learning rate (treatment sub-network)	0.05, 0.01, 0.005, 0.0001	0.05, 0.01, 0.005, 0.0001
		Batch size	32, 64, 128	32, 64, 128
		GRU hidden units	CR size	CR size
		GRU dropout rate	-	-
		BR size	CR size	CR size
		GRU layers (Treat Encoder)	1	1
		GRU hidden units (Treat Encoder)	6	6
		FC hidden units	6, 8, ..., 18, 20	4, 6, ..., 20
		Random time indices (m)	10%	10%
		Early Stopping (min delta)	0.001	0.001
		Early Stopping (patience)	10	30

Table A.9: Hyper-parameters search range for CDVAE

Model	Sub-model	Hyperparameter	Synthetic data	MIMIC III
CDVAE	Inference Network	GRU layers	1	1
		GRU hidden units	6, 8, ..., 12, 14	4, 6, ..., 20
		GRU dropout rate	-	-
		Latent dim of $\mathbf{z}$	0.001	0.001
	Propensity Network	FC hidden units	6, 8, ..., 12, 14	4, 6, ..., 30
	Representation Learner	LSTM layers	1	1
		GRU hidden units	6, 8, ..., 18, 20	6, 8, ..., 18, 20
		GRU dropout rate	-	-
		Dimension of representation	6, 8, ..., 18, 20	4, 6, ..., 20
	Decoder	FC hidden units	$(\dim(\mathbf{z}) + \dim(\Phi(\mathbf{H}_t)))/2$	$(\dim(\mathbf{z}) + \dim(\Phi(\mathbf{H}_t)))/2$
	Global	Learning rate (w/o propensity network)	0.01, 0.005, 0.001, 0.0001	0.01, 0.005, 0.001, 0.0001
		Learning rate (propensity network)	0.01, 0.005, 0.001, 0.0001	0.01, 0.005, 0.001, 0.0001
		Batch size	32, 64, 128, 256	128, 512, 1024
		Max gradient norm	0.5, 1, 2	0.5, 1, 2
		Number of components in Prior	2, 4, ..., 18, 20	2, 4, ..., 20

Inputs: $\{\Phi(\mathbf{h}_t)\}_{1 \leq t \leq T}, \mathbf{z}$
Concatenate: $[\Phi(\mathbf{h}_t), \mathbf{z}]_{1 \leq t \leq T}$
Linear Layer
Weight Normalization
ELU
Linear Layer
Weight Normalization
Linear Layer
Output: $\{\hat{Y}_{t+1}(\omega)\}_{1 \leq t \leq T-1}$

Table A.10: Architecture of the outcome model prediction, i.e., the decoder.

Inputs: $\{y_t, \mathbf{x}_t, \omega_t\}_{1 \leq t \leq T}$
Concat: $[y_t, \mathbf{x}_t, \omega_t]_{1 \leq t \leq T}$
GRU layer
Linear Layer
Tanh
Outputs: $\{\Phi(\mathbf{h}_t)\}_{1 \leq t \leq T}$

Table A.11: Architecture: representation learner  $\phi$  of CDVAE

Inputs: $\{\Phi(\mathbf{h}_t)\}_{1 \leq t \leq T}$
Linear Layer
ELU
Sigmoid
Output: $\{\hat{W}_{t+1}(\omega)\}_{1 \leq t \leq T-1}$

Table A.12: Architecture: propensity network  $e_{\theta_\omega}(\cdot)$ .

Inputs: $\{y_t, \mathbf{x}_t, \omega_t\}_{1 \leq t \leq T}$
Concat: $[y_t, \mathbf{x}_t, \omega_t]_{1 \leq t \leq T}$
GRU layer
Linear Layer
$\Sigma_{\phi_3}(\mathbf{g}_T)$
Linear Layer
$\mu_{\phi_2}(\mathbf{g}_T)$

Table A.13: Inference network  $q_\phi(\mathbf{z} \mid y_{\leq T}, \mathbf{x}_{\leq T}, \omega_{\leq T})$

# Appendix B

## Appendix: Chapter 4

### B.1 Experiments on semi-synthetic data: Details

#### B.1.1 Additional results

##### Comparison to benchmark models: standard train/test split

We also tested Causal CPC on MIMIC III semi-synthetic data using the same experimental protocol as Melnychuk et al. (2022), namely by using the split of patients into train/validation/test as 800/200/200. As a result, baseline performances in Table B.1 are exactly the same as in Melnychuk et al. (2022).

Table B.1: Results over the MIMIC III semi-synthetic data set (same experimental protocol as in Melnychuk et al. (2022)): mean±standard deviation of Rooted Mean Squared Errors (RMSEs). The best value for each metric is given in bold: smaller is better.

Model	$\rho = 1$	$\rho = 2$	$\rho = 3$	$\rho = 4$	$\rho = 5$	$\rho = 6$	$\rho = 7$	$\rho = 8$	$\rho = 9$	$\rho = 10$
Causal CPC (ours)	$0.25 \pm 0.03$	<b><math>0.37 \pm 0.02</math></b>	<b><math>0.40 \pm 0.01</math></b>	<b><math>0.45 \pm 0.01</math></b>	<b><math>0.49 \pm 0.02</math></b>	<b><math>0.52 \pm 0.02</math></b>	<b><math>0.55 \pm 0.03</math></b>	<b><math>0.56 \pm 0.03</math></b>	<b><math>0.58 \pm 0.04</math></b>	<b><math>0.60 \pm 0.03</math></b>
Causal Transformer	<b><math>0.20 \pm 0.01</math></b>	$0.38 \pm 0.01$	$0.45 \pm 0.01$	$0.49 \pm 0.01$	$0.52 \pm 0.02$	$0.53 \pm 0.02$	$0.55 \pm 0.02$	<b><math>0.56 \pm 0.02</math></b>	<b><math>0.58 \pm 0.02</math></b>	<b><math>0.59 \pm 0.02</math></b>
G-Net	$0.34 \pm 0.01$	$0.67 \pm 0.03$	$0.83 \pm 0.04$	$0.94 \pm 0.04$	$1.03 \pm 0.05$	$1.10 \pm 0.05$	$1.16 \pm 0.05$	$1.21 \pm 0.06$	$1.25 \pm 0.06$	$1.29 \pm 0.06$
CRN	$0.30 \pm 0.01$	$0.48 \pm 0.02$	$0.59 \pm 0.02$	$0.65 \pm 0.02$	$0.68 \pm 0.02$	$0.71 \pm 0.01$	$0.72 \pm 0.01$	$0.74 \pm 0.01$	$0.76 \pm 0.01$	$0.78 \pm 0.02$
RMSN	$0.24 \pm 0.01$	$0.47 \pm 0.01$	$0.60 \pm 0.01$	$0.70 \pm 0.02$	$0.78 \pm 0.04$	$0.84 \pm 0.05$	$0.89 \pm 0.06$	$0.94 \pm 0.08$	$0.97 \pm 0.09$	$1.00 \pm 0.11$
MSM	$0.37 \pm 0.01$	$0.57 \pm 0.03$	$0.74 \pm 0.06$	$0.88 \pm 0.03$	$1.14 \pm 0.10$	$1.95 \pm 1.48$	$3.44 \pm 4.57$	$> 10.0$	$> 10.0$	$> 10.0$

### B.2 Proofs of theoretical results

#### B.2.1 Relation between InfoNCE loss and mutual information

##### Proposition PropB.1

$$I(\mathbf{F}_{t+j}, \mathbf{C}_t) \geq \log(|\mathcal{B}|) - \mathcal{L}_j^{(InfoNCE)}$$

*Proof.* In the following, we draw inspiration from the proof of Oord et al. (2018). The InfoNCE loss can be interpreted as the categorical cross-entropy of correctly classifying the positive sample  $\mathbf{F}_{t+j}$  given the

context  $\mathbf{C}_t^{\text{enc}}$ . This is done with probability

$$\frac{\exp(T_j(\mathbf{F}_{t+j}, \mathbf{C}_t))}{\sum_{l=1}^{|\mathcal{B}|} \exp(T_j(\mathbf{F}_{l,t+j}, \mathbf{C}_t))},$$

where  $\mathbf{F}_{t+j}$  is treated as the positive sample within the batch  $\mathcal{B}$ , and the remaining elements serve as negative samples. Let  $\text{pos} \in \{1, \dots, |\mathcal{B}|\}$  be the indicator of the positive sample  $\mathbf{F}_{t+j}$ . The optimal probability is

$$\begin{aligned} p(\text{Index} = \text{pos} \mid \mathcal{B}, \mathbf{C}_t^{\text{enc}}) &= \frac{p(\mathbf{f}_{\text{pos},t+j} \mid \mathbf{C}_t^{\text{enc}}) \prod_{l \neq \text{pos}}^{\mathcal{B}} p(\mathbf{f}_{l,t+j})}{\sum_{j=1}^{\mathcal{B}} \left[ p(\mathbf{f}_{j,t+j} \mid \mathbf{C}_t^{\text{enc}}) \prod_{l \neq j}^{\mathcal{B}} p(\mathbf{f}_{l,t+j}) \right]} \\ &= \frac{\frac{p(\mathbf{f}_{\text{pos},t+j} \mid \mathbf{C}_t^{\text{enc}})}{p(\mathbf{f}_{\text{pos},t+j})}}{\sum_{j=1}^{\mathcal{B}} \frac{p(\mathbf{f}_{j,t+j} \mid \mathbf{C}_t^{\text{enc}})}{p(\mathbf{f}_{j,t+j})}}. \end{aligned}$$

Now, for the score  $\exp(T_j(\mathbf{F}_{t+j}, \mathbf{C}_t))$  to be optimal, it should be proportional to  $\frac{p(\mathbf{f}_{\text{pos},t+j} \mid \mathbf{C}_t^{\text{enc}})}{p(\mathbf{f}_{\text{pos},t+j})}$ . The MI lower bound comes from the fact that  $\exp(T_j(\mathbf{F}_{t+j}, \mathbf{C}_t))$  estimates the density ratio  $\frac{p(\mathbf{f}_{\text{pos},t+j} \mid \mathbf{C}_t^{\text{enc}})}{p(\mathbf{f}_{\text{pos},t+j})}$ .

$$\begin{aligned} \mathcal{L}_j^{(\text{InfoNCE})} &= -\mathbb{E}_{\mathcal{B}} \log \left[ \frac{\frac{p(\mathbf{f}_{t+j} \mid \mathbf{C}_t^{\text{enc}})}{p(\mathbf{f}_{t+j})}}{\frac{p(\mathbf{f}_{t+j} \mid \mathbf{C}_t^{\text{enc}})}{p(\mathbf{f}_{t+j})} + \sum_{\mathbf{f}_{l,t+j} \in \mathcal{B}_{\text{neg}}} \frac{p(\mathbf{f}_{l,t+j} \mid \mathbf{C}_t^{\text{enc}})}{p(\mathbf{f}_{l,t+j})}} \right] \\ &= \mathbb{E}_{\mathcal{B}} \log \left[ 1 + \frac{p(\mathbf{f}_{t+j})}{p(\mathbf{f}_{t+j} \mid \mathbf{C}_t^{\text{enc}})} \sum_{\mathbf{f}_{l,t+j} \in \mathcal{B}_{\text{neg}}} \frac{p(\mathbf{f}_{l,t+j} \mid \mathbf{C}_t^{\text{enc}})}{p(\mathbf{f}_{l,t+j})} \right] \\ &\approx \mathbb{E}_{\mathcal{B}} \log \left[ 1 + \frac{p(\mathbf{f}_{t+j})}{p(\mathbf{f}_{l,t+j} \mid \mathbf{C}_t^{\text{enc}})} (|\mathcal{B}| - 1) \mathbb{E}_{\mathbf{F}_{t+j}} \frac{p(\mathbf{f}_{l,t+j} \mid \mathbf{C}_t^{\text{enc}})}{p(\mathbf{f}_{l,t+j})} \right] \quad (\text{B.1}) \\ &= \mathbb{E}_{\mathcal{B}} \log \left[ 1 + \frac{p(\mathbf{f}_{t+j})}{p(\mathbf{f}_{t+j} \mid \mathbf{C}_t^{\text{enc}})} (|\mathcal{B}| - 1) \right] \\ &\geq \mathbb{E}_{\mathcal{B}} \log \left[ \frac{p(\mathbf{f}_{t+j})}{p(\mathbf{f}_{t+j} \mid \mathbf{C}_t^{\text{enc}})} |\mathcal{B}| \right] \\ &= -I(\mathbf{f}_{t+j}, \mathbf{C}_t^{\text{enc}}) + \log(|\mathcal{B}|), \end{aligned}$$

The approximation in the third equation, Eq. (B.1), becomes more precise as the batch size increases.  $\square$

### B.2.2 Relation between InfoMax and input reconstruction

We now prove the proposition Prop4.1 stating that :  $I(\mathbf{C}_t^{\text{enc},h}, \mathbf{C}_t^{\text{enc},f}) \leq I(\mathbf{H}_t, (\mathbf{C}_t^{\text{enc},h}, \mathbf{C}_t^{\text{enc},f}))$

*Proof.* This is followed by two applications of the data processing inequality Cover (1999), which states that for random variables  $A$ ,  $B$ , and  $C$  satisfying the Markov relation  $A \rightarrow B \rightarrow C$ , we have

$$I(A; C) \leq I(A; B).$$

First, note that

$$\mathbf{C}_t^{\text{enc},h} = \Phi_{\theta_1, \theta_2}(\mathbf{H}_t^h), \quad \mathbf{C}_t^{\text{enc},f} = \Phi_{\theta_1, \theta_2}(\mathbf{H}_t^f),$$

where  $\mathbf{H}_t^h = \text{trunc}_f(\mathbf{H}_t)$  and  $\mathbf{H}_t^f = \text{trunc}_h(\mathbf{H}_t)$ . Here,  $\text{trunc}_f$  and  $\text{trunc}_h$  truncate the future and history



processes, respectively, relative to a splitting time  $t_0$ .

We now observe the Markov relation

$$\mathbf{C}_t^{\text{enc},h} \xleftarrow{\Phi_{\theta_1,\theta_2} \circ \text{trunc}_f} \mathbf{H}_t \xrightarrow{\Phi_{\theta_1,\theta_2} \circ \text{trunc}_h} \mathbf{C}_t^{\text{enc},f},$$

which is Markov equivalent to

$$\mathbf{C}_t^{\text{enc},h} \xrightarrow{\Phi_{\theta_1,\theta_2} \circ \text{trunc}_f} \mathbf{H}_t \xrightarrow{\Phi_{\theta_1,\theta_2} \circ \text{trunc}_h} \mathbf{C}_t^{\text{enc},f}.$$

By the data processing inequality, this gives

$$I(\mathbf{C}_t^{\text{enc},h}; \mathbf{C}_t^{\text{enc},f}) \leq I(\mathbf{H}_t; \mathbf{C}_t^{\text{enc},h}).$$

On the other hand, we trivially have the Markov relation

$$\mathbf{H}_t \rightarrow (\mathbf{C}_t^{\text{enc},h}, \mathbf{C}_t^{\text{enc},f}) \rightarrow \mathbf{C}_t^{\text{enc},h},$$

which yields

$$I(\mathbf{H}_t; \mathbf{C}_t^{\text{enc},h}) \leq I(\mathbf{H}_t; (\mathbf{C}_t^{\text{enc},h}, \mathbf{C}_t^{\text{enc},f})).$$

Combining the two inequalities proves the proposition.  $\square$

### B.2.3 Proof of Theorem Thm4.1

To begin, we split the process history into two non-overlapping views (Figure 4.2):  $\mathbf{H}_t^h := \mathbf{F}_{1:t_0}$  and  $\mathbf{H}_t^f := \mathbf{F}_{t_0+1:t}$ , representing a historical subsequence and a future subsequence within the process history  $\mathbf{H}_t$ , respectively. We then computed representations of these two views denoted  $\mathbf{C}_t^{\text{enc},h}$  and  $\mathbf{C}_t^{\text{enc},f}$ , respectively. This naturally gives rise to the Markov chain, as in showed in the proof of proposition Prop4.1:

$$\mathbf{C}_t^{\text{enc},h} \leftarrow \mathbf{H}_t \rightarrow \mathbf{C}_t^{\text{enc},f}$$

which is Markov equivalent to:

$$\mathbf{C}_t^{\text{enc},h} \rightarrow \mathbf{H}_t \rightarrow \mathbf{C}_t^{\text{enc},f}$$

Following this Markov chain, we can show that Shwartz Ziv & LeCun (2024):

$$I(\mathbf{C}_t^{\text{enc},f}, \mathbf{C}_t^{\text{enc},h}) = I(\mathbf{H}_t; \mathbf{C}_t^{\text{enc},h}) - \mathbb{E}_{\mathbf{h}_t \sim \mathbb{P}_{\mathbf{H}_t}} \mathbb{E}_{\mathbf{c}_t^f \sim \mathbb{P}_{\mathbf{C}_t^f | \mathbf{h}_t}} \left[ D_{KL}[\mathbb{P}_{\mathbf{C}_t^h | \mathbf{h}_t} \| \mathbb{P}_{\mathbf{C}_t^h | \mathbf{c}_t^f}] \right]$$

On the other hand, by applying the chain rule of the mutual information to  $I(\mathbf{H}_t; (\mathbf{C}_t^{\text{enc},h}, \mathbf{C}_t^{\text{enc},f}))$  we get:

$$I(\mathbf{H}_t; (\mathbf{C}_t^{\text{enc},f}, \mathbf{C}_t^{\text{enc},h})) = I(\mathbf{H}_t; \mathbf{C}_t^{\text{enc},h}) + I(\mathbf{H}_t; \mathbf{C}_t^{\text{enc},f} | \mathbf{C}_t^{\text{enc},h})$$

Combining these equations, the tightness of our bounds can be written as:

$$\begin{aligned}
I(\mathbf{H}_t; (\mathbf{C}_t^{\text{enc},f}, \mathbf{C}_t^{\text{enc},h})) &= I(\mathbf{C}_t^{\text{enc},f}, \mathbf{C}_t^{\text{enc},h}) \\
&= I(\mathbf{H}_t; \mathbf{C}_t^{\text{enc},f} \mid \mathbf{C}_t^{\text{enc},h}) \\
&\quad + \mathbb{E}_{\mathbf{h}_t \sim \mathbb{P}_{\mathbf{H}_t}} \mathbb{E}_{\mathbf{c}_t^f \sim \mathbb{P}_{\mathbf{C}_t^f | \mathbf{h}_t}} \left[ D_{\text{KL}}(\mathbb{P}_{\mathbf{C}_t^h | \mathbf{h}_t} \parallel \mathbb{P}_{\mathbf{C}_t^h | \mathbf{c}_t^f}) \right].
\end{aligned} \tag{B.2}$$

#### B.2.4 On the relation between conditional entropy and reconstruction

We now prove the statement in the core paper, saying that the conditional entropy  $H(\mathbf{H}_t \mid (\mathbf{C}_t^{\text{enc},h}, \mathbf{C}_t^{\text{enc},f})) \geq 0$  is minimized if  $\mathbf{H}_t$  is a function of  $(\mathbf{C}_t^{\text{enc},h}, \mathbf{C}_t^{\text{enc},f})$  almost surely.

##### Proposition PropB.2

$H(\mathbf{A} \mid \mathbf{B}) = 0$  implies that  $\mathbf{A} = f(\mathbf{B})$  almost surely.

*Proof.* For simplicity, suppose  $\mathbf{A}$  and  $\mathbf{B}$  are discrete. Assume, by contradiction, that there exists  $\mathbf{b}_0$  and two distinct values  $\mathbf{a}_1$  and  $\mathbf{a}_2$  such that  $p(\mathbf{a}_1 \mid \mathbf{b}_0), p(\mathbf{a}_2 \mid \mathbf{b}_0) > 0$ . Then the conditional entropy is given by:

$$H(\mathbf{A} \mid \mathbf{B}) = - \sum_{\mathbf{b}} p(\mathbf{b}) \sum_{\mathbf{a}} p(\mathbf{a} \mid \mathbf{b}) \log p(\mathbf{a} \mid \mathbf{b}).$$

In particular, we have:

$$H(\mathbf{A} \mid \mathbf{B}) \geq p(\mathbf{b}_0) \left( -p(\mathbf{a}_1 \mid \mathbf{b}_0) \log p(\mathbf{a}_1 \mid \mathbf{b}_0) - p(\mathbf{a}_2 \mid \mathbf{b}_0) \log p(\mathbf{a}_2 \mid \mathbf{b}_0) \right) > 0,$$

where we used the fact that  $-t \log t \geq 0$  for  $0 \leq t \leq 1$ , with strict inequality for  $t \notin \{0, 1\}$ .

Therefore,  $H(\mathbf{A} \mid \mathbf{B}) = 0$  if and only if  $\mathbf{A}$  is a function of  $\mathbf{B}$  almost surely.  $\square$

#### B.2.5 Proof of theorem Thm4.3

To prove the Theorem Thm4.3, we first prove the following lemma and proposition.

##### Lemma LemB.1

Let  $\Phi$  be a fixed representation function. Given that  $q(W_{t+1} \mid \Phi(\mathbf{H}_t))$  is the conditional likelihood of observing the treatment  $W_{t+1}$ , denote the probability of observing each treatment value as  $q^j = q(\Phi(\mathbf{H}_t)) := q(W_{t+1} = j \mid \Phi(\mathbf{H}_t))$  for  $j \in \{0, 1, \dots, K-1\}$ . Then, the optimal treatment prediction function is such that

$$q^{j,*}(\Phi(\mathbf{H}_t)) = \frac{p(\Phi(\mathbf{H}_t) \mid W_{t+1} = j)}{\sum_{l=0}^{K-1} p(\Phi(\mathbf{H}_t) \mid W_{t+1} = l) p(W_{t+1} = l)} \tag{B.3}$$

*Proof.* For a fixed representation  $\Phi$ , finding the optimal treatment probabilities reduces to solving the following constrained optimization problem:

$$\begin{aligned} \max_q \quad & \mathbb{E}_{\mathbb{P}(\Phi(\mathbf{H}_t), W_{t+1})} [\log q(W_{t+1} \mid \Phi(\mathbf{H}_t))] \\ \text{subject to} \quad & \sum_{l=0}^{K-1} q^l(\Phi(\mathbf{H}_t)) = 1. \end{aligned} \quad (\text{B.4})$$

First, we write the likelihood  $q(W_{t+1} \mid \Phi(\mathbf{H}_t))$  using the conditional probabilities  $q^j(\Phi(\mathbf{H}_t))$ .

$$q(W_{t+1} \mid \Phi(\mathbf{H}_t)) = \prod_{j=0}^{K-1} q^j(\Phi(\mathbf{H}_t))^{\mathbb{I}_{\{W_{t+1}=j\}}}$$

Then, the treatment likelihood can be written as

$$\begin{aligned} \mathbb{E}_{\mathbb{P}(\Phi(\mathbf{H}_t), W_{t+1})} [\log q(W_{t+1} \mid \Phi(\mathbf{H}_t))] &= \mathbb{E}_{\mathbb{P}(\Phi(\mathbf{H}_t), W_{t+1})} \left[ \sum_{l=0}^{K-1} \log(q^l(\Phi(\mathbf{H}_t))) \mathbb{I}_{\{W_{t+1}=l\}} \right] \\ &= \sum_{l=0}^{K-1} \int \log(q^l(\Phi(\mathbf{H}_t))) \mathbb{I}_{\{W_{t+1}=l\}} p(W_{t+1} \mid \Phi(\mathbf{H}_t)) p(\Phi(\mathbf{H}_t)) dW_{t+1} d\Phi(\mathbf{H}_t) \\ &= \sum_{l=0}^{K-1} \int \log(q^l(\Phi(\mathbf{H}_t))) p(W_{t+1} = l \mid \Phi(\mathbf{H}_t)) p(\Phi(\mathbf{H}_t)) d\Phi(\mathbf{H}_t) \\ &= \sum_{l=0}^{K-1} \int \log(q^l(\Phi(\mathbf{H}_t))) p(\Phi(\mathbf{H}_t) \mid W_{t+1} = l) p(W_{t+1} = l) d\Phi(\mathbf{H}_t) \end{aligned}$$

Let's denote  $\alpha_l = p(W_{t+1} = l)$ , the marginal probability of observing the  $l$ -th treatment regime, and  $p_l^\Phi(\mathbf{H}_t) = p(\Phi(\mathbf{H}_t) \mid W_{t+1} = l)$  with a corresponding probability distribution  $\mathbb{P}_l^\Phi$ . We intend to maximize point-wise the objective in Eq. (B.4). Plugging the latter formulation of the conditional likelihood in Eq. (B.4) and writing the Lagrangian function, we get

$$\max_q \sum_{l=0}^{K-1} \log(q^l(\Phi(\mathbf{H}_t))) p_j^\Phi(\mathbf{H}_t) \alpha_l + \lambda \left( \sum_{l=0}^{K-1} q^l(\Phi(\mathbf{H}_t)) - 1 \right) \quad (\text{B.5})$$

Computing the gradient w.r.t  $q^l(\Phi(\mathbf{H}_t))$  for  $l \in \{0, 1, \dots, K-1\}$  and setting to zero, we have

$$q^{l,*}(\Phi(\mathbf{H}_t)) = -\frac{\alpha_l p_j^\Phi(\mathbf{H}_t)}{\lambda} \quad (\text{B.6})$$

Then, by the equality constraint, we find that  $\lambda = -\sum_{l=0}^{K-1} \alpha_l p_j^\Phi(\mathbf{H}_t)$ . □

### Proposition PropB.3

Let  $\Phi$  be a fixed representation function. The  $I_{CLUB}$  objective when the treatment prediction function is optimal (i.e.  $q = q^*$ ) has the following form:

$$I_{CLUB} = \sum_{j=0}^{K-1} \alpha_l D_{KL}(\mathbb{P}_j^\Phi \parallel \sum_{l=0}^{K-1} \alpha_l \mathbb{P}_l^\Phi) + \mathbb{E}_{\mathbb{P}_{\Phi(\mathbf{H}_t)}} [D_{KL}(\mathbb{P}_{W_{t+1}} \parallel \mathbb{P}_{W_{t+1} \mid \Phi(\mathbf{H}_t)})] \quad (\text{B.7})$$

*Proof.* First, recall that

$$I_{\text{CLUB}}(\Phi(\mathbf{H}_t), W_{t+1}; q^*) = \mathbb{E}_{\mathbb{P}_{(\Phi(\mathbf{H}_{t+1}), W_{t+1})}} [\log q^*(W_{t+1} \mid \Phi(\mathbf{H}_{t+1}))] \\ - \mathbb{E}_{\mathbb{P}_{\Phi(\mathbf{H}_{t+1})}} \mathbb{E}_{\mathbb{P}_{W_{t+1}}} [\log q^*(W_{t+1} \mid \Phi(\mathbf{H}_{t+1}))].$$

$$I_{\text{CLUB}}(\Phi(\mathbf{H}_t), W_{t+1}; q^*) = A - B$$

Let's detail  $A$  and  $B$  separately,

$$\begin{aligned} A &= \sum_{j=0}^{K-1} \int \alpha_j \log(q^{j,*}(\Phi(\mathbf{H}_t))) p_j^\Phi(\mathbf{H}_t) d\Phi(\mathbf{H}_t) \\ &= \sum_{j=0}^{K-1} \int \alpha_j \log\left(\frac{\alpha_j p_j^\Phi(\mathbf{H}_t)}{\sum_{l=0}^{K-1} p_l^\Phi(\mathbf{H}_t) \alpha_l}\right) p_j^\Phi(\mathbf{H}_t) d\Phi(\mathbf{H}_t) \\ &= \sum_{j=0}^{K-1} \int \alpha_j \log\left(\frac{p_j^\Phi(\mathbf{H}_t)}{\sum_{l=0}^{K-1} p_l^\Phi(\mathbf{H}_t) \alpha_l}\right) p_j^\Phi(\mathbf{H}_t) d\Phi(\mathbf{H}_t) + \log(\alpha_j) \alpha_j \\ &= \sum_{j=0}^{K-1} \alpha_j D_{KL}(\mathbb{P}_j^\Phi \parallel \sum_{l=0}^{K-1} \alpha_l \mathbb{P}_l^\Phi) + \sum_{j=0}^{K-1} \log(\alpha_j) \alpha_j \end{aligned}$$

Finally, we can write

$$A = \sum_{j=0}^{K-1} \alpha_j D_{KL}(\mathbb{P}_j^\Phi \parallel \sum_{l=0}^{K-1} \alpha_l \mathbb{P}_l^\Phi) - H(W_{t+1}) \quad (\text{B.8})$$

For the remaining term  $B$ , we have

$$\begin{aligned} B &= \mathbb{E}_{\mathbb{P}_{\Phi(\mathbf{H}_t)}} \mathbb{E}_{\mathbb{P}_{W_{t+1}}} (\log q^*(W_{t+1} \mid \Phi(\mathbf{H}_{t+1}))) \\ &= \sum_{j=0}^{K-1} \mathbb{E}_{\mathbb{P}_{\Phi(\mathbf{H}_t)}} \mathbb{E}_{\mathbb{P}_{W_{t+1}}} [\log(q^j(\Phi(\mathbf{H}_t))) \mathbb{1}_{\{W_{t+1}=j\}}] \\ &= \sum_{j=0}^{K-1} \mathbb{E}_{\mathbb{P}_{\Phi(\mathbf{H}_t)}} [\alpha_j \log(q^j(\Phi(\mathbf{H}_t)))] \\ &= \sum_{j=0}^{K-1} \alpha_j \int \log \left[ \frac{\alpha_j p_j^\Phi(\mathbf{H}_t)}{\sum_{l=0}^{K-1} p_l^\Phi(\mathbf{H}_t) \alpha_l} \right] p(\Phi(\mathbf{H}_t)) d\Phi(\mathbf{H}_t) \\ &= \sum_{j=0}^{K-1} \alpha_j \int \log \left[ \frac{p(\Phi(\mathbf{H}_t))}{\sum_{l=0}^{K-1} p_l^\Phi(\mathbf{H}_t) \alpha_l} \frac{p(W_{t+1}=j \mid \Phi(\mathbf{H}_t))}{p(W_{t+1}=j)} \right] p(\Phi(\mathbf{H}_t)) d\Phi(\mathbf{H}_t) \\ &\quad - H(W_{t+1}) \\ &= \sum_{j=0}^{K-1} \alpha_j \int \underbrace{\log \left[ \frac{p(\Phi(\mathbf{H}_t))}{\sum_{l=0}^{K-1} p_l^\Phi(\mathbf{H}_t) \alpha_l} \right]}_{=0} p(\Phi(\mathbf{H}_t)) d\Phi(\mathbf{H}_t) \\ &\quad + \sum_{j=0}^{K-1} \alpha_j \int \log \left[ \frac{p(W_{t+1}=j \mid \Phi(\mathbf{H}_t))}{p(W_{t+1}=j)} \right] p(\Phi(\mathbf{H}_t)) d\Phi(\mathbf{H}_t) - H(W_{t+1}) \end{aligned}$$

The final form of  $B$  is therefore

$$B = - \int D_{KL}(\mathbb{P}_{W_{t+1}} \parallel \mathbb{P}_{W_{t+1} \mid \Phi(\mathbf{H}_t)}) p(\Phi(\mathbf{H}_t)) d\Phi(\mathbf{H}_t) - H(W_{t+1}) \quad (\text{B.9})$$

The proposition follows immediately from Equations (B.8) and (B.9).  $\square$

*Proof.* (Theorem Thm4.3) Since by lemma LemB.1, the  $I_{CLUB}$  formulation in proposition PropB.3 holds, then to prove that the representation is balanced, it is enough to see that by the positivity of  $D_{KL}$

$$I_{CLUB} \geq \mathbb{E}_{\mathbb{P}_{\Phi(\mathbf{H}_t)}} [D_{KL}(\mathbb{P}_{W_{t+1}} || \mathbb{P}_{W_{t+1}|\Phi(\mathbf{H}_t)})] \geq 0 \quad (\text{B.10})$$

$I_{CLUB}$  is minimal when  $I_{CLUB} = 0$ , which happens if and only if for  $j \in \{0, 1, \dots, K-1\}$   $p(W_{t+1} = j) = p(W_{t+1} = j | \Phi(\mathbf{H}_t))$  almost surely which, by Bayes rule is equivalent to say  $p(\Phi(\mathbf{H}_t)) = p(\Phi(\mathbf{H}_t) | W_{t+1} = j)$ .

□

### B.3 Causal CPC: Architecture details

<b>Inputs:</b> $[\mathbf{X}_t, W_{t-1}, Y_{t-1}]$
Linear Layer
WeightNorm
SELU
Linear Layer
WeightNorm
<b>Outputs:</b> $\mathbf{Z}_t = \Phi_{\theta_1}([\mathbf{X}_t, W_{t-1}, Y_{t-1}])$

Table B.2: Architecture for learning local features  $\mathbf{Z}_t$

<b>Inputs:</b> $\mathbf{Z}_{\leq t}$
GRU (1 layer)
<b>Outputs:</b> Hidden state $\mathbf{C}_t^{\text{enc}} = \Phi_{\theta_2}^{ar}(\mathbf{Z}_{\leq t})$

Table B.3: Architecture for learning context representation  $\mathbf{C}_t^{\text{enc}}$

<b>Inputs:</b> $[\Phi_t, W_t]$
Linear Layer
WeightNorm
SELU
Linear Layer
WeightNorm
<b>Outputs:</b> $\hat{Y}_t$

Table B.4: Architecture for outcome prediction

<b>Inputs:</b> $\Phi_t$
Linear Layer
SpectralNorm
SELU
Linear Layer
SpectralNorm
<b>Outputs:</b> $\hat{W}_t$

Table B.5: Architecture for treatment prediction

## B.4 Models hyperparameters

In this section, we report the range of all hyperparameters to be fine-tuned, as well as fixed hyperparameters for all models and across the different datasets used in experiments. Best hyperparameter values are reported in the configuration files in the code repository.

Table B.6: Hyper-parameters search range for RMSN

Model	Sub-model	Hyperparameter	Cancer simulation	MIMIC III (SS)
RMSNs	Propensity Treatment Network	LSTM layers	1	1
		Learning rate	0.01, 0.005, 0.001, 0.0001	0.01, 0.005, 0.001, 0.0001
		Batch size	32, 64, 128	32, 64, 128
		LSTM hidden units	4, 6, ..., 12	4, 6, ..., 30
		LSTM dropout rate	-	-
		Max gradient norm	0.5, 1, 2	0.5, 1, 2
		Early Stopping (min delta)	0.0001	0.0001
		Early Stopping (patience)	30	30
Propensity History Network		LSTM layers	1	1
		Learning rate	0.01, 0.005, 0.001, 0.0001	0.01, 0.005, 0.001, 0.0001
		Batch size	32, 64, 128	64, 128, 256
		LSTM hidden units	4, 6, ..., 20	4, 6, ..., 30
		LSTM dropout rate	-	-
		Early Stopping (min delta)	0.0001	0.0001
		Early Stopping (patience)	30	30
Encoder		LSTM layers	1	1
		Learning rate	0.01, 0.005, 0.001, 0.0001	0.01, 0.005, 0.001, 0.0001
		Batch size	32, 64, 128	32, 64, 128
		LSTM hidden units	4, 6, ..., 20	4, 6, ..., 30
		LSTM dropout rate	-	-
		Early Stopping (min delta)	0.0001	0.0001
		Early Stopping (patience)	30	30
Decoder		LSTM layers	1	1
		Learning rate	0.01, 0.005, 0.001, 0.0001	0.01, 0.005, 0.001, 0.0001
		Batch size	32, 64, 128	128, 512, 1024
		LSTM hidden units	4, 6, ..., 20	4, 6, ..., 30
		LSTM dropout rate	-	-
		Max gradient norm	0.5, 1, 2	0.5, 1, 2
		Early Stopping (min delta)	0.0001	0.0001
		Early Stopping (patience)	30	30

Table B.7: Hyper-parameters search range for CRN

Model	Sub-model	Hyperparameter	Cancer simulation	MIMIC III (SS)
CRN	Encoder	LSTM layers	1	1
		Learning rate	0.01, 0.005, 0.001, 0.0001	0.01, 0.005, 0.001, 0.0001
		Batch size	32, 64, 128	32, 64, 128
		LSTM hidden units	4, 6, ..., 30	4, 6, ..., 30
		LSTM dropout rate	-	-
		BR size	4, 6, ..., 20	4, 6, ..., 30
		Early Stopping (min delta)	0.0001	0.0001
		Early Stopping (patience)	30	30
Decoder		LSTM layers	1	1
		Learning rate	0.01, 0.005, 0.001, 0.0001	0.01, 0.005, 0.001, 0.0001
		Batch size	128, 256, 512	256, 512, 1024
		LSTM hidden units	4, 6, ..., 30	4, 6, ..., 30
		LSTM dropout rate	-	-
		BR size	4, 6, ..., 20	4, 6, ..., 30
		Early Stopping (min delta)	0.0001	0.0001
		Early Stopping (patience)	30	30

Table B.8: Hyper-parameters search range for G-Net

Hyperparameter	Cancer simulation	MIMIC III (SS)
LSTM layers	1	1
Learning rate	0.01, 0.005, 0.001, 0.0001	0.01, 0.005, 0.001, 0.0001
Batch size	32, 64, 128	32, 64, 128
LSTM hidden units	4, 6, ..., 30	4, 6, ..., 30
FC hidden units	4, 6, ..., 30	4, 6, ..., 30
LSTM dropout rate	-	-
R size	4, 6, ..., 20	4, 6, ..., 30
MC samples	10	10
Early Stopping (min delta)	0.0001	0.0001
Early Stopping (patience)	30	30

Table B.9: Hyper-parameters search range for Causal Transformer

Hyperparameter	Cancer simulation	MIMIC III (SS)
Transformer blocks	1	1
Learning rate	0.01, 0.005, 0.001, 0.0001	0.01, 0.005, 0.001, 0.0001
Batch size	32, 64, 128	32, 64, 128
Attention heads	2	2
Transformer units	4, 6, ..., 20	4, 6, ..., 20
LSTM dropout rate	-	-
BR size	4, 6, ..., 20	4, 6, ..., 20
FC hidden units	4, 6, ..., 20	4, 6, ..., 20
Sequential dropout rate	0.1, 0.2, 0.3	0.1, 0.2, 0.3
Max positional encoding	15	15
Early Stopping (min delta)	0.0001	0.0001
Early Stopping (patience)	30	30

Table B.10: Hyper-parameters search range for Causal CPC

Model	Sub-model	Hyperparameter	Cancer simulation	MIMIC III (SS)
Causal CPC	Encoder	GRU layers	1	1
		Learning rate	0.01, 0.005, 0.001, 0.0001	0.01, 0.005, 0.001, 0.0001
		Batch size	32, 64, 128	64, 128, 256
		GRU hidden units	4, 6, ..., 30	4, 6, ..., 30
		GRU dropout rate	-	-
		Local features (LF) size	4, 6, ..., 20	4, 6, ..., 20
		Context Representation (CR) size	4, 6, ..., 20	4, 6, ..., 20
		Early Stopping (min delta)	0.001	0.001
		Early Stopping (patience)	100	100
		GRU layers	1	1
Decoder		Learning rate (decoder w/o treatment sub-network)	0.01, 0.005, 0.001, 0.0001	0.01, 0.005, 0.001, 0.0001
		Learning rate (encoder fine-tuning)	0.001, 0.0005, 0.0001, 0.00005	0.001, 0.0005, 0.0001, 0.00005
		Learning rate (treatment sub-network)	0.05, 0.01, 0.005, 0.0001	0.05, 0.01, 0.005, 0.0001
		Batch size	32, 64, 128	32, 64, 128
		GRU hidden units	CR size	CR size
		GRU dropout rate	-	-
		BR size	CR size	CR size
		GRU layers (Treat Encoder)	1	1
		GRU hidden units (Treat Encoder)	6	6
		FC hidden units	4, 6, ..., 20	4, 6, ..., 20
		Random time indices (m)	10%	10%
		Early Stopping (min delta)	0.001	0.001
		Early Stopping (patience)	50	50

# Appendix C

## Appendix: Chapter 5

### C.1 Proofs

#### C.1.1 Background: Subspace detection in a deterministic model

**Standard SSC problem** In the setting of Elhamifar & Vidal (2013); Soltanolkotabi & Candés (2012b), we consider data points  $\mathbf{X} = [\mathbf{x}_1, \dots, \mathbf{x}_N] \in \mathbb{R}^{n \times N}$  and we define the SSC as

$$\min_{\mathbf{c} \in \mathbb{R}^N} \|\mathbf{c}\|_1 \quad \text{subject to} \quad \mathbf{X}\mathbf{c} = \mathbf{x}_i \quad \text{and} \quad \mathbf{c}_i = 0. \quad (\text{C.1})$$

Let  $\mathbf{X}^{(m)} \in \mathbb{R}^{n \times N_m}$  be the matrix whose columns are the  $N_m$  points on subspace  $\mathcal{S}_m$ . For each  $m = 1, \dots, M$  and  $i = 1, \dots, N_m$ , we define

$$\mathbf{X}_{-i}^{(m)} = [\mathbf{x}_1^{(m)}, \dots, \mathbf{x}_{i-1}^{(m)}, \mathbf{x}_{i+1}^{(m)}, \dots, \mathbf{x}_{N_m}^{(m)}]$$

which is the matrix obtained by removing the  $i$ -th column from  $\mathbf{X}^{(m)}$ . We can therefore "absorb" the constrating equality  $\mathbf{c}_i = 0$  of Euation C.1 in  $\mathbf{X}_{-i}$  and write

$$\min_{\mathbf{c} \in \mathbb{R}^N} \|\mathbf{c}\|_1 \quad \text{subject to} \quad \mathbf{X}_{-i} \mathbf{c} = \mathbf{x}_i \quad (\text{C.2})$$

To understand when a solution of the optimization problem in C.2, we turn to the dual problem:

$$\max_{\boldsymbol{\lambda} \in \mathbb{R}^n} \langle \boldsymbol{\lambda}, \mathbf{x}_i \rangle \quad \text{subject to} \quad \|\mathbf{X}_{-i}^\top \boldsymbol{\lambda}\|_\infty \leq 1 \quad (\text{C.3})$$

Here,  $\boldsymbol{\lambda} \in \mathbb{R}^n$  is a vector in the ambient space whose purpose is to witness/certify the optimality and support of the primal solution. This lead us to the definition of a dual point:

<b>Definition DefC.1 [Dual point]</b>



Consider a point  $\mathbf{x}_i \in \mathbb{R}^n$ , and let  $\mathcal{C}^*(\mathbf{x}_i, \mathbf{X}_{-i})$  be the set of optimal solutions to C.3. The *dual point*  $\boldsymbol{\lambda}(\mathbf{x}_i, \mathbf{X}_{-i})$  is defined as the element of  $\mathcal{C}^*(\mathbf{x}_i, \mathbf{X}_{-i})$  with the minimum Euclidean norm.

$\boldsymbol{\lambda}(\mathbf{x}_i, \mathbf{X}_{-i})$  represents the dual certificate for the sparsest code representing  $\mathbf{x}_i$  using atoms in  $\mathbf{X}_{-i}$ .

Next, let  $\mathbf{U}^{(m)} \in \mathbb{R}^{n \times d_m}$  be any orthonormal basis of  $\mathcal{S}_m$ . In this basis, we write

$$\mathbf{X}^{(m)} = \mathbf{U}^{(m)} \mathbf{A}^{(m)},$$

where

$$\mathbf{A}^{(m)} = [\mathbf{a}_1^{(m)}, \dots, \mathbf{a}_{N_m}^{(m)}] \in \mathbb{R}^{d_m \times N_m}$$

has unit-norm columns  $\mathbf{a}_i^{(m)}$ . The columns of  $\mathbf{A}^{(m)}$  are precisely the coordinates of each point in the orthonormal basis  $\mathbf{U}^{(m)}$ .

#### Definition DefC.2 [Dual directions]

For each subspace index  $m$  and data-point index  $i$ , define the *dual direction*  $\mathbf{v}_i^{(m)} \in \mathbb{R}^n$ , arranged as columns of the matrix

$$\mathbf{V}^{(m)} = [\mathbf{v}_1^{(m)}, \mathbf{v}_2^{(m)}, \dots, \mathbf{v}_{N_m}^{(m)}].$$

These vectors correspond to the dual points

$$\boldsymbol{\lambda}_i^{(m)} = \boldsymbol{\lambda}(\mathbf{a}_i^{(m)}, \mathbf{A}_{-i}^{(m)})$$

via

$$\mathbf{v}_i^{(m)} = \mathbf{U}^{(m)} \frac{\boldsymbol{\lambda}_i^{(m)}}{\|\boldsymbol{\lambda}_i^{(m)}\|}.$$

The dual direction is nothing but a unit-norm projection of the dual point into the subspace of  $\mathbf{x}_i$  when  $\boldsymbol{\lambda}_i^{(m)}$  is the dual point's latent coordinates. Intuitively, it is direction in space that best aligns with  $x_i$ , maximizing the inner product  $\langle \boldsymbol{\lambda}, x_i \rangle$ , while still respecting the dual constraint  $\|\mathbf{X}_{-i}^\top \boldsymbol{\lambda}\|_\infty \leq 1$ .

One of the utilities of dual directions is that it allows us to describe the **worst-case alignment** between any point from another subspace (i.e., not in  $\mathcal{S}_m$ ) and the dual directions  $\mathbf{V}^{(m)}$  of that subspace.

#### Definition DefC.3 [Subspace incoherence]

Let  $\mathcal{X} = \bigcup_{m=1}^M \mathcal{X}_m$  be a union of point sets, and let  $\mathbf{V}^{(m)}$  be the matrix of dual directions for  $\mathcal{X}_m$  as in Definition DefC.2. The *subspace incoherence* of  $\mathcal{X}_m$  with respect to the other points is

$$\mu(\mathcal{X}_m) = \max_{\mathbf{x} \in \mathcal{X} \setminus \mathcal{X}_m} \|\mathbf{V}^{(m)T} \mathbf{x}\|_{\ell_\infty}.$$

Subspace incoherence quantifies how "confusable" or "close" the directions of external points are to those characterizing the subspace. If  $\mu(\mathcal{X}_m)$  is small then no out-of-subspace point aligns strongly with any dual direction of  $\mathcal{S}^{(m)}$ . This helps prevent such points from leaking into the sparse representation of points from  $\mathcal{S}^{(m)}$ .

Subspace incoherence plays a central role in theoretical guarantees in SSC and support recovery, as shown in the following theorem of Soltanolkotabi & Candés (2012b): let's define

$$\mathcal{P}(\mathbf{X}) := \text{conv}\{\pm \mathbf{x}_1, \pm \mathbf{x}_2, \dots, \pm \mathbf{x}_N\},$$

where  $\text{conv}(S)$  denotes the convex hull of a set  $S \subseteq \mathbb{R}^n$ , i.e. the smallest convex set containing  $S$ , and  $\{\pm \mathbf{x}_i\} = \{\mathbf{x}_i, -\mathbf{x}_i\}$ . Then subspace detection property (5.12) is guaranteed under a bounding of the maximum subspace incoherence:

**Theorem ThmC.1 [Soltanolkotabi & Candés (2012b)]**

Suppose that for each  $m = 1, \dots, M$ ,

$$\mu(\mathcal{X}_m) < \min_{i: \mathbf{x}_i \in \mathcal{X}_m} r(\mathcal{P}_{-i}^m). \quad (\text{C.4})$$

Then the subspace-detection property holds. Moreover, if C.4 is satisfied for a fixed  $m$ , then the *local* subspace-detection property holds in the following sense: for every  $\mathbf{x}_i \in \mathcal{X}_m$ , the solution to C.2 can have nonzero entries only at columns of  $\mathbf{X}$  that lie in the same subspace  $\mathcal{X}_m$ .

### C.1.2 Proof of Theorem Thm5.1

Define Lagrangian for the problem  $\mathcal{P}_t(Df(\mathbf{Z}), C_{:,j})$ :

$$\mathcal{L}_t(C_{:,j}, \lambda, \nu) = \|C_{:,j}\|_1 + \lambda(\ell_j(C_{:,j}) - t) + \nu C_{j,j}, \quad \lambda \geq 0, \nu \in \mathbb{R},$$

where  $\lambda$  and  $\nu$  are the multipliers for the constraints  $\ell_j(C_{:,j}) \leq t$  and  $c_j = 0$ , respectively.

Since

- $\ell_j(\cdot)$  is continuous and convex (indeed strictly convex quadratic if  $\mathbb{E}_{\mathbf{Z}}[Df(\mathbf{Z})^\top Df(\mathbf{Z})]$  is positive definite),
- $\|\cdot\|_1$  is convex,
- there exists a feasible solution  $C_{:,j}^*$  to  $\mathcal{P}_t(Df(\mathbf{Z}), C_{:,j})$ , that is, with  $\ell_j(C_{:,j}^*) < t$  and  $C_{j,j}^* = 0$  (e.g.  $C_{:,j}^* = \mathbf{0}$  if  $t > \ell_j(\mathbf{0})$ ),

Slater's condition holds (one inequality plus one equality), so strong duality applies.

Let  $C_{:,j}^{\text{LS}} = \arg \min_{C_{:,j} \in \mathbb{R}^{d_x}} \ell_j(C_{:,j})$ , the solutions exists and is unique by strict convexity of  $\ell_j(\cdot)$ .

### KKT system

A triple  $(C_{:,j}^*, \lambda^*, \nu^*)$  solves  $\mathcal{P}_t(Df(\mathbf{Z}), C_{:,j})$  if and only if it satisfies the following KKT conditions:

$$\text{Primal feasibility:} \quad \ell_j(C_{:,j}^*) \leq t, \quad C_{j,j}^* = 0, \quad (K1)$$

$$\text{Dual feasibility:} \quad \lambda^* \geq 0, \quad (K2)$$

$$\text{Complementary slackness:} \quad \lambda^* (\ell_j(C_{:,j}^*) - t) = 0, \quad (K3)$$

$$\text{Stationarity:} \quad 0 \in \partial \|C_{:,j}^*\|_1 + \lambda^* \nabla \ell_j(C_{:,j}^*) + \nu^* \mathbf{e}_j, \quad (K4)$$

Here  $\mathbf{e}_j$  denotes the  $j$ -th standard basis vector in  $\mathbb{R}^{d_x}$ .

Because  $\ell_j$  it is strictly convex and there is only a single equality constraint  $C_{j,j} = 0$ , the stationarity condition (K4) uniquely determines  $(C_{:,j}^*, \nu^*)$  it once  $\lambda^*$  is fixed. Moreover, complementary slackness (K3) forces  $\lambda^* > 0$  whenever  $\ell_j(C_{:,j}^*) < t$  is impossible—i.e. for all  $t > \ell_j(C_{:,j}^{\text{LS}})$ .

Consider now the penalized problem  $\mathcal{P}_\lambda(Df(\mathbf{Z}), C_{:,j})$ , whose Lagrangian is

$$\mathcal{L}_\lambda(C_{:,j}, \nu) = \ell_j(C_{:,j}) + \lambda \|C_{:,j}\|_1 + \nu C_{j,j}, \quad \nu \in \mathbb{R}. \quad (C.5)$$

Its first-order optimality (stationarity) condition reads

$$\mathbf{0} \in \nabla \ell_j(C_{:,j}^*) + \lambda \partial \|C_{:,j}^*\|_1 + \nu^* \mathbf{e}_j. \quad (C.6)$$

Comparing (C.6) with (K4) shows that any  $(C_{:,j}^*, \lambda^*, \nu^*)$  satisfying the KKT system for  $\mathcal{P}_t(Df(\mathbf{Z}), C_{:,j})$  also satisfies (C.6) with  $\lambda = \lambda^*$ . Together with the common constraint  $c_j^* = 0$ , we obtain: If  $c^*$  solves  $\mathcal{P}_t(Df(\mathbf{Z}), C_{:,j})$  with multipliers  $(\lambda^*, \nu^*)$ , then  $C_{:,j}^*$  also solves  $\mathcal{P}_\lambda(Df(\mathbf{Z}), C_{:,j})$  under the constraint  $C_{j,j} = 0$ .

**Bijection between  $\lambda$  and  $t$**  Define the penalized-solution path (respecting  $c_j = 0$ ):

$$C_{:,j}^*(\lambda) := \arg \min_{\substack{C_{:,j} \in \mathbb{R}^{d_x} \\ C_{j,j} = 0}} \{ \ell_j(C_{:,j}) + \lambda \|C_{:,j}\|_1 \}. \quad (C.7)$$

By strict convexity of  $\ell_j$ , convexity of  $\|\cdot\|_1$ , and the affine constraint  $C_{j,j} = 0$ , the minimiser  $C_{:,j}^*(\lambda)$  is unique. Now set

$$t_j(\lambda) := \ell_j(C_{:,j}^*(\lambda)).$$

$\lambda \longrightarrow t_j(\lambda)$  is continuous and piecewise linear (Proposition 1 (Rosset & Zhu, 2007)) and strictly decreasing; its limit values are the following

As  $\lambda \rightarrow 0^+$ , the penalty vanishes and  $C_{:,j}^*(\lambda) \rightarrow C_{:,j}^{\text{LS}}$ . Thus

$$\lim_{\lambda \rightarrow 0^+} t_j(\lambda) = \ell_j(C_{:,j}^{\text{LS}}).$$

As  $\lambda \rightarrow \infty$ , the  $\lambda \|C_{:,j}\|_1$  term dominates in Equation C.7, forcing  $C_{:,j}^*(\lambda) \rightarrow \mathbf{0}$ ; hence

$$\lim_{\lambda \rightarrow \infty} t_j(\lambda) = \ell_j(\mathbf{0}).$$

Therefore

$$t: (0, \infty) \longrightarrow [\ell_j(C_{:,j}^{\text{LS}}), \ell_j(\mathbf{0})]$$

is a continuous bijection. Note that since we assume self-expressiveness Asm5.2  $\ell_j(C_{:,j}^{\text{LS}}) = 0$

Given any

$$t_j^* \in [\ell_j(C_{:,j}^{\text{LS}}), \ell_j(\mathbf{0})],$$

continuity and bijectivity of  $t_j(\cdot)$  guarantee a unique  $\lambda_j \geq 0$  such that

$$t_j(\lambda_j) = t_j^*.$$

At that  $\lambda_j$ , the solution  $C_{:,j}^*(\lambda_j)$  of  $\mathcal{P}_\lambda(Df(\mathbf{Z}), C_{:,j})$  satisfies

$$\ell_j(C_{:,j}^*(\lambda_j)) = t_j^* \quad \text{and} \quad \mathbf{0} \in \nabla \ell_j(C_{:,j}^*(\lambda_j)) + \lambda_j \partial \|C_{:,j}^*(\lambda_j)\|_1 + \nu^* \mathbf{e}_j,$$

which matches the stationarity KKT condition (K4) for  $\mathcal{P}_t(Df(\mathbf{Z}), C_{:,j})$ . Hence  $C_{:,j}^*(\lambda_j)$  is also the minimizer of  $\mathcal{P}_t(Df(\mathbf{Z}), C_{:,j})$ . This establishes a one-to-one correspondence  $\lambda$  and  $t$ .

### C.1.3 High-Probability Guarantee for Subspace Detection

We provide in this section the proof of Theorem Thm5.2. We recall that  $\mathbf{Z} \in \text{subG}_{d_z}(K)$  (Definition Def5.8) and the smoothness assumption (Asm5.3) over  $f$ : the decoder  $f \in \mathcal{C}^2(\mathbb{R}^{d_z}; \mathbb{R}^{d_x})$  is twice continuously differentiable, with uniformly bounded curvature. That is, for each output coordinate  $f_i$ , the Hessian satisfies

$$\sup_{\mathbf{z} \in \mathbb{R}^{d_z}} \|D^2 f_i(\mathbf{z})\|_{\text{op}} \leq L, \quad \text{for all } i \in \llbracket 1, d_x \rrbracket.$$

Define the gradient vectors:

$$P_i(\mathbf{Z}) := \nabla f_i(\mathbf{Z}) \in \mathbb{R}^{d_z}, \quad i = 1, \dots, d_x,$$

and let the symmetric convex polytope  $\mathcal{K}(\mathbf{Z}) \subset \mathbb{R}^{d_z}$  be given by:

$$\mathcal{K}(\mathbf{Z}) := \text{conv}(\pm P_1(\mathbf{Z}), \dots, \pm P_{d_x}(\mathbf{Z})).$$

Let the in-radius of  $\mathcal{K}(\mathbf{Z})$  be defined by:

$$r(\mathbf{Z}) := r(\mathcal{K}(\mathbf{Z})) = \min_{\mathbf{u} \in \mathbb{S}^{d_z-1}} \max_{1 \leq i \leq d_x} |\langle P_i(\mathbf{Z}), \mathbf{u} \rangle|.$$

**Lemma LemC.1 [Concentration of the in-radius of the Gradient Polytope]**

The in-radius of  $\mathcal{K}(\mathbf{Z})$  has the concentration inequality:

$$\mathbb{P}(|r(\mathbf{Z}) - \mathbb{E}r(\mathbf{Z})| \geq t) \leq 2 \exp\left(-\frac{t^2}{2K^2L^2}\right).$$

Moreover, the expected in-radius is bounded by:

$$\mathbb{E}r(\mathbf{Z}) \leq \Lambda_1 K L \sqrt{\frac{\log(d_x/d_z)}{d_z}},$$

for a universal constant  $\Lambda_1 > 0$ . In particular, we have the one-sided, lower tail bound over the in-radius:

$$\mathbb{P}\left\{r(\mathbf{Z}) < \Lambda_1 K L \sqrt{\frac{\log d_x}{d_z}}\right\} \leq \exp\left(-\frac{\Lambda_1^2 \log(d_x)}{2d_z}\right). \quad (\text{C.8})$$

*Proof. In-radius Concentration* Since  $\|D^2 f_i(\mathbf{z})\|_{\text{op}} \leq L$  for all  $i \in [d_x]$  and  $\mathbf{z} \in \mathbb{R}^{d_z}$ , the gradient map  $z \mapsto P_i(\mathbf{z}) = \nabla f_i(\mathbf{z}) \in \mathbb{R}^{d_z}$  is  $L$ -Lipschitz for each  $i$ , i.e.,

$$\|P_i(\mathbf{z}) - P_i(\mathbf{z}')\| \leq L\|\mathbf{z} - \mathbf{z}'\|.$$

For any fixed unit vector  $\mathbf{u} \in \mathbb{S}^{d_z-1}$ , define the support function:

$$\phi_{\mathbf{u}}(\mathbf{Z}) := \max_{1 \leq i \leq d_x} |\langle P_i(\mathbf{Z}), \mathbf{u} \rangle|.$$

Since each  $P_i$  is  $L$ -Lipschitz, it follows that  $\phi_{\mathbf{u}}(\mathbf{Z})$  is also  $L$ -Lipschitz. Moreover, the in-radius

$$r(\mathbf{Z}) := \inf_{\mathbf{u} \in \mathbb{S}^{d_z-1}} \phi_{\mathbf{u}}(\mathbf{Z})$$

is also  $L$ -Lipschitz as an infimum over a uniformly Lipschitz family. Therefore,

$$|r(\mathbf{Z}) - r(\mathbf{Z}')| \leq L\|\mathbf{Z} - \mathbf{Z}'\| \quad \text{for all } \mathbf{Z}, \mathbf{Z}' \in \mathbb{R}^{d_z}.$$

Since  $\mathbf{Z}$  is sub-Gaussian with constant  $K$ , applying standard concentration for Lipschitz functions of sub-Gaussian variables (Vershynin, 2018) gives:

$$\mathbb{P}(|r(\mathbf{Z}) - \mathbb{E}r(\mathbf{Z})| \geq t) \leq 2 \exp\left(-\frac{t^2}{2K^2L^2}\right),$$

which proves the first part.

**Bound on the Expected in-radius.** We now estimate the mean value  $\mathbb{E}r(\mathbf{Z})$ . Since

$$r(\mathbf{Z}) = \inf_{\mathbf{u} \in \mathbb{S}^{d_z-1}} \max_{1 \leq i \leq d_x} |\langle P_i(\mathbf{Z}), \mathbf{u} \rangle| = \inf_{\mathbf{u} \in \mathbb{S}^{d_z-1}} \max_{1 \leq i \leq d_x} X_{i,\mathbf{u}}(\mathbf{Z}),$$

we define the stochastic process:

$$X_{i,\mathbf{u}}(\mathbf{Z}) := |\langle P_i(\mathbf{Z}), \mathbf{u} \rangle|.$$

Each map  $\mathbf{Z} \mapsto X_{i,\mathbf{u}}(\mathbf{Z})$  is  $L$ -Lipschitz and hence sub-Gaussian with norm at most  $KL$ . Furthermore, for any pairs  $(i, \mathbf{u}), (j, \mathbf{v}) \in \llbracket 1, d_x \rrbracket \times \mathbb{S}^{d_z-1}$ ,

$$|X_{i,\mathbf{u}}(\mathbf{Z}) - X_{j,\mathbf{v}}(\mathbf{Z}')| \leq L\|\mathbf{Z} - \mathbf{Z}'\|(1 + \|\mathbf{u} - \mathbf{v}\|),$$

implying the variance proxy:

$$\rho((i, \mathbf{u}), (j, \mathbf{v})) := KL(\mathbf{1}_{i \neq j} + \|\mathbf{u} - \mathbf{v}\|).$$

Hence, the collection  $\{X_{i,\mathbf{u}}(\mathbf{Z})\}$  is a  $\rho$ -sub-Gaussian process over the index set  $T = \llbracket 1, d_x \rrbracket \times \mathbb{S}^{d_z-1}$ .

By Dudley's entropy integral bound for sub-Gaussian processes:

$$\mathbb{E} \sup_{(i,\mathbf{u}) \in T} X_{i,\mathbf{u}}(\mathbf{Z}) \leq C \int_0^{\text{diam}(T)} \sqrt{\log N(T, \rho; \varepsilon)} d\varepsilon,$$

where  $N(T, \rho; \varepsilon)$  is the  $\varepsilon$ -covering number of  $T$  under  $\rho$ , and  $\text{diam}(T) \leq KL(2 + \pi)$ .

To bound the covering number: The discrete index set  $\llbracket 1, d_x \rrbracket$  contributes a factor of  $d_x$ . The unit sphere  $\mathbb{S}^{d_z-1}$  has  $\varepsilon$ -covering number at most  $(3/\delta)^{d_z}$  in Euclidean norm, where  $\delta = \varepsilon/(KL)$ . Thus,

$$N(T, \rho; \varepsilon) \leq d_x \left( \frac{3KL}{\varepsilon} \right)^{d_z}.$$

Plugging into Dudley's integral gives:

$$\mathbb{E} \sup_{(i,\mathbf{u})} X_{i,\mathbf{u}}(\mathbf{Z}) \leq \Lambda_1 KL \int_0^{2KL} \sqrt{\log d_x + d_z \log(3KL/\varepsilon)} d\varepsilon \lesssim KL \sqrt{\frac{\log d_x}{d_z}},$$

where the last step follows from standard integral splitting and evaluation (Ledoux, 2001).

Since  $r(\mathbf{Z}) = \inf_{\mathbf{u} \in \mathbb{S}^{d_z-1}} \max_{1 \leq i \leq d_x} X_{i,\mathbf{u}}(\mathbf{Z}) \leq \sup_{(i,\mathbf{u})} X_{i,\mathbf{u}}(\mathbf{Z})$ , it follows that:

$$\mathbb{E}r(\mathbf{Z}) \leq \mathbb{E} \sup_{(i,\mathbf{u})} X_{i,\mathbf{u}}(\mathbf{Z}) \lesssim KL \sqrt{\frac{\log d_x}{d_z}}.$$

**In-radius lower tail bound** Since for each  $t > 0$

$$\mathbb{P}(|r(\mathbf{Z}) - \mathbb{E}r(\mathbf{Z})| \geq t) \leq 2 \exp \left( -\frac{t^2}{2K^2L^2} \right),$$

and given  $\mathbb{E}[r(\mathbf{Z})] \leq \Lambda_1 K L \sqrt{\frac{\log(d_x)}{d_z}}$ , then setting  $t = \frac{1}{2} \mathbb{E}[r(\mathbf{Z})]$  yields

$$\mathbb{P}\left\{r(\mathbf{Z}) < \frac{1}{2} \Lambda_1 K L \sqrt{\frac{\log d_x}{d_z}}\right\} \leq 2 \exp\left(-\frac{\Lambda_1^2 \log(d_x)}{8 d_z}\right),$$

or equivalently

$$\mathbb{P}\left\{r(\mathbf{Z}) < \Lambda_1 K L \sqrt{\frac{\log d_x}{d_z}}\right\} \leq \exp\left(-\frac{\Lambda_1^2 \log(d_x)}{2 d_z}\right).$$

□

**Lemma LemC.2 [Frobenius-Norm Tail and Expectation Bounds]**

Let

$$\mathbf{A} = [\mathbf{a}_1, \dots, \mathbf{a}_{N_1}] \in \mathbb{R}^{d_1 \times N_1}, \quad \mathbf{a}_i \stackrel{\text{iid}}{\sim} \text{Unif}(\mathbb{S}^{d_1-1}),$$

and let  $\Sigma \in \mathbb{R}^{d_1 \times d_2}$  be deterministic, and  $\lambda \stackrel{\text{iid}}{\sim} \text{Unif}(\mathbb{S}^{d_2-1})$  independent of  $\mathbf{A}$ . Define

$$X_i := \langle \mathbf{a}_i, \Sigma \lambda \rangle, \quad \sigma_i^2 := \text{Var}(X_i \mid \mathbf{a}_i) = \frac{\|\Sigma^\top \mathbf{a}_i\|_2^2}{d_2}, \quad \sigma_{\max} := \max_{1 \leq i \leq N_1} \sigma_i.$$

Then there exist universal constants  $\Lambda_2 > 0$  such that, for all  $t > 0$ ,

(i) *High-Probability Tail Bound.*

$$\mathbb{P}\left\{\max_{1 \leq i \leq N_1} |X_i| > \mathbb{E}\left[\max_i |X_i|\right] + t\right\} \leq 2 \exp\left(-\frac{d_2 t^2}{2 \|\Sigma\|_F^2}\right).$$

(ii) *Expectation Bound.*

$$\mathbb{E}\left[\max_{1 \leq i \leq N_1} |X_i|\right] \leq \Lambda_2 \frac{\|\Sigma\|_F}{\sqrt{d_2}} \sqrt{\log(N_1 + 1)}.$$

In particular, we have the one-sided tail bound:

$$\mathbb{P}\left\{\max_{1 \leq i \leq N_1} |X_i| \leq (1 + \Lambda_2) \frac{\|\Sigma\|_F}{\sqrt{d_2}} \sqrt{\log(N_1 + 1)}\right\} \geq 1 - \frac{2}{\sqrt{N_1 + 1}}. \quad (\text{C.9})$$

*Proof. Step 1: Concentration of individual terms.* For each fixed  $\mathbf{a}_i$ , the function  $\lambda \mapsto X_i(\lambda) = \langle \mathbf{a}_i, \Sigma \lambda \rangle$  is  $\|\Sigma^\top \mathbf{a}_i\|_2$ -Lipschitz on the sphere  $\mathbb{S}^{d_2-1}$ . By Lévy's lemma on the sphere (see Ledoux (2001); Vershynin (2018)), for all  $\epsilon > 0$ ,

$$\mathbb{P}\{|X_i - \mathbb{E}[X_i \mid \mathbf{a}_i]| \geq \epsilon \mid \mathbf{a}_i\} \leq 2 \exp\left(-\frac{d_2 \epsilon^2}{2 \|\Sigma^\top \mathbf{a}_i\|_2^2}\right).$$

Since  $\mathbb{E}[X_i \mid \mathbf{a}_i] = 0$ , we conclude  $X_i \mid \mathbf{a}_i$  is sub-Gaussian with proxy  $\sigma_i = \|\Sigma^\top \mathbf{a}_i\|_2 / \sqrt{d_2}$ .

**Step 2: Concentration of the maximum.** Define

$$F(\lambda) := \max_{1 \leq i \leq N_1} |X_i(\lambda)|.$$

Conditioned on  $\mathbf{A}$ , each  $X_i$  is fixed and  $F(\lambda)$  is  $\sigma_{\max}$ -Lipschitz over  $\mathbb{S}^{d_2-1}$ . Applying Lévy's lemma (Milman & Schechtman, 1986) gives

$$\mathbb{P}\{F(\lambda) - \mathbb{E}[F(\lambda) \mid \mathbf{A}] > t \mid \mathbf{A}\} \leq 2 \exp\left(-c \frac{d_2 t^2}{\sigma_{\max}^2}\right) \leq 2 \exp\left(-c \frac{d_2 t^2}{\|\Sigma\|_F^2}\right),$$

where the final inequality uses  $\sigma_{\max} \leq \frac{\|\Sigma\|_F}{\sqrt{d_2}}$ . Averaging over  $\mathbf{A}$  completes the proof of part (i).

**Step 3: Expectation via Dudley's entropy integral.** Conditioned on  $\mathbf{A}$ , the collection  $\{X_i\}_{i=1}^{N_1}$  forms a finite sub-Gaussian process indexed by  $\{1, \dots, N_1\}$ . Dudley's theorem implies (Talagrand, 2005)

$$\mathbb{E}[F(\lambda) \mid \mathbf{A}] \leq \Lambda_2 \int_0^{\sigma_{\max}} \sqrt{\log N_1} d\varepsilon = \Lambda_2 \sigma_{\max} \sqrt{\log N_1}.$$

Since  $\sigma_{\max} \leq \frac{\|\Sigma\|_F}{\sqrt{d_2}}$ , we conclude

$$\mathbb{E}\left[\max_{1 \leq i \leq N_1} |X_i|\right] = \mathbb{E}[F(\lambda)] \leq \Lambda_2 \frac{\|\Sigma\|_F}{\sqrt{d_2}} \sqrt{\log(N_1 + 1)},$$

completing part (ii).

**Step 4: One-sided tail bound.** Since

$$\mathbb{P}\left\{\max_{1 \leq i \leq N_1} |X_i| > \mathbb{E}\left[\max_i |X_i|\right] + t\right\} \leq 2 \exp\left(-\frac{d_2 t^2}{2\|\Sigma\|_F^2}\right),$$

and given the expectation bound

$$\mathbb{E}\left[\max_{1 \leq i \leq N_1} |X_i|\right] \leq \Lambda_2 \frac{\|\Sigma\|_F}{\sqrt{d_2}} \sqrt{\log(N_1 + 1)},$$

then choosing  $t = \frac{\|\Sigma\|_F}{\sqrt{d_2}} \sqrt{\log(N_1 + 1)}$  yield

$$\mathbb{P}\left\{\max_{1 \leq i \leq N_1} |X_i| \leq (1 + \Lambda_2) \frac{\|\Sigma\|_F}{\sqrt{d_2}} \sqrt{\log(N_1 + 1)}\right\} \geq 1 - 2 \exp\left(-\frac{1}{2} \log(N_1 + 1)\right) = 1 - \frac{2}{\sqrt{N_1 + 1}}.$$

□

Let  $\mathcal{P}_{-i}^m := \mathcal{P}(\mathbf{X}_{-i}^m)$ , then application of Lemma LemC.1 yields

$$\mathbb{P}\left\{\Lambda_1 K L \sqrt{\frac{\log n_m}{d_m}} \leq r(\mathcal{P}_{-i}^m) \text{ for all pairs } (m, i)\right\} \geq 1 - \sum_{m=1}^M n_m \exp\left(-\frac{\Lambda_1^2 \log(n_m)}{2 d_m}\right). \quad (\text{C.10})$$

On the other hand, by noticing that

$$\begin{aligned} \left\|\mathbf{X}^{(k)\top} \mathbf{V}^{(\ell)}\right\|_{\ell_\infty} &= \max_{i=1, \dots, N_\ell} \left\|\mathbf{X}^{(k)\top} \mathbf{v}_i^{(\ell)}\right\|_{\ell_\infty} \\ &= \max_{i=1, \dots, N_\ell} \left\|\mathbf{A}^{(k)\top} \mathbf{U}^{(k)\top} \mathbf{U}^{(\ell)} \frac{\boldsymbol{\lambda}_i^{(\ell)}}{\|\boldsymbol{\lambda}_i^{(\ell)}\|_2}\right\|_{\ell_\infty}, \end{aligned} \quad (\text{C.11})$$

and that  $\text{aff}(\mathcal{S}_k, \mathcal{S}_m) = \|\mathbf{U}^{(k)\top} \mathbf{U}^{(m)}\|_F$  (Soltanolkotabi & Candés, 2012b), an application of LemC.2



to Equation C.11 yields

$$\mathbb{P} \left\{ \left\| \mathbf{X}^{(k)\top} \mathbf{V}^{(m)} \right\|_{\ell_\infty} \leq (1 + \Lambda_2) \frac{\text{aff}(\mathcal{S}_k, \mathcal{S}_m)}{\sqrt{d_2}} \sqrt{\log(n_m + 1)} \right\} \geq 1 - \frac{2}{\sqrt{n_m + 1}}.$$

and therefore

$$\begin{aligned} \mathbb{P} \left\{ \left\| \mathbf{X}^{(k)\top} \mathbf{V}^{(m)} \right\|_{\ell_\infty} \leq (1 + \Lambda_2) \frac{\text{aff}(\mathcal{S}_k, \mathcal{S}_m)}{\sqrt{d_2}} \sqrt{\log(n_m + 1)} \right. \\ \left. \text{for all } (m, k) \text{ with } m \neq k \right\} &\geq 1 - \sum_{1 \leq k \neq m \leq M} \frac{2}{\sqrt{n_m + 1}} \\ &= 1 - \sum_{m=1}^M \frac{2(M-1)}{\sqrt{n_m + 1}}. \end{aligned} \quad (\text{C.12})$$

As a consequence of Equations C.12 and C.10, if we impose the condition

$$\max_{k \neq m} \Lambda'_2 \text{aff}(\mathcal{S}_k, \mathcal{S}_m) \frac{\sqrt{\log(n_k + 1)}}{\sqrt{d_m}} \leq \Lambda_1 K L \sqrt{\frac{\log n_m}{d_m}},$$

which is equivalent to saying

$$\max_{k \neq m} \text{aff}(\mathcal{S}_k, \mathcal{S}_m) \sqrt{\log(n_k + 1)} \leq \Lambda K L \sqrt{\log n_m}, \quad \text{with } \Lambda = \frac{\Lambda_1}{\Lambda'_2}, \quad (\text{C.13})$$

then the subspace detection property holds with probability

$$1 - \sum_{m=1}^M n_m \exp\left(-\frac{\Lambda_1^2 \log(n_m)}{2d_m}\right) - \frac{2(M-1)}{\sqrt{n_m + 1}}.$$

The condition of Equation C.13 is exactly that of Theorem Thm5.2.

#### C.1.4 Recovery of Feature Clusters via Spectral Clustering

We now prove Proposition Prop5.1. We show that spectral clustering on the affinity matrix

$$A = |C^*| + |C^*|^\top$$

recovers with high probability the connected components of the feature graph  $G_F$  under standard SSC assumptions. Since we assume the incoherence gap of Theorem Thm5.2 holds, then by the same theorem, the subspace detection property holds, and therefore classical results on subspace clustering apply with high probability. In the following, we detail the arguments for cluster recovery with spectral clustering; we omit the expression "with high probability" for better readability.

**Union-of-Subspaces from Latent Structure** Let feature  $i$  have latent-parent set  $\text{Pa}(i) \subseteq [d_z]$ . Then the Jacobian row can be written as

$$Df_{i,:}(\mathbf{Z}) = \nabla_{\mathbf{z}} f_i(\mathbf{Z})^\top = \sum_{j \in \text{Pa}(i)} \alpha_{i,j}(\mathbf{Z}) \mathbf{e}_j^\top,$$

so each  $Df_{i,:}(\mathbf{Z})$  lies in a union of low-dimensional subspaces spanned by subsets of  $\{\mathbf{e}_j\}$ . This corresponds to a union-of-subspaces model (Soltanolkotabi & Candés, 2012b).

**SSC Self-Expression Recovers Graph Structure** We solve the population Lasso problem:

$$\mathbf{C}^* = \arg \min_{\substack{\mathbf{C} \in \mathbb{R}^{d_x \times d_x} \\ \text{diag}(\mathbf{C})=0}} \mathbb{E}_{\mathbf{Z}} [\|\mathbf{D}f(\mathbf{Z}) - \mathbf{C}\mathbf{D}f(\mathbf{Z})\|_F^2] + \lambda \|\mathbf{C}\|_1.$$

Under standard SSC conditions, such as subspace incoherence and low-noise (Elhamifar & Vidal, 2013), we have:

$$\mathbf{C}_{ii'}^* \neq 0 \quad \Leftrightarrow \quad \text{Pa}(i) \cap \text{Pa}(i') \neq \emptyset.$$

Define the affinity matrix  $\mathbf{A} = |\mathbf{C}^*| + |\mathbf{C}^*|^\top$ . Then the support of  $\mathbf{A}$  corresponds exactly to the edge set of the feature graph  $G_F$ .

**Connected Components from Laplacian Nullspace** Let  $\mathbf{D} = \text{diag}(\mathbf{A}\mathbf{1})$  and form the symmetric normalized Laplacian

$$\mathbf{L}_{\text{sym}} = \mathbf{I} - \mathbf{D}^{-1/2} \mathbf{A} \mathbf{D}^{-1/2}.$$

It is well known (Von Luxburg, 2007) that the multiplicity of the zero eigenvalue of  $\mathbf{L}_{\text{sym}}$  equals the number of connected components in  $G_F$ , and its nullspace is spanned by indicator vectors of those components.

**Recovery via Spectral Clustering** Spectral clustering (e.g., Ng–Jordan–Weiss variant) computes the first  $k$  eigenvectors of  $\mathbf{L}_{\text{sym}}$ , stacks them into a matrix  $\mathbf{U} \in \mathbb{R}^{d_x \times k}$ , and applies  $k$ -means to its rows. In the exact block-diagonal case, these rows are standard basis vectors corresponding to the true partition, so clustering achieves zero error (Ng et al., 2001).

### C.1.5 Guarantees of features grouping via clustering techniques

We now prove Theorem Thm5.3. We break the argument into six main steps:

1. **Concentration of Gram entries (Step 1)** we show that with high probability

$$\|\hat{\Sigma} - \Sigma\|_\infty$$

is of order  $O(KL\sqrt{d_x \log(d_x^2/\varepsilon)})$ .

2. **Restricted strong convexity (Step 2)** we prove that the population and empirical Lasso risks are strongly convex on  $s$ -sparse rows, guaranteeing a unique minimizer.
3. **Support recovery via primal–dual witness (Step 3 & 4)** uses mutual incoherence and dominance to show that all off-support coefficients vanish and that in-group coefficients are large.
4. **Affinity block bounds (Step 5)** translates the coefficient bounds into lower and upper bounds on the entries of the affinity matrix  $\mathbf{A}^*$ .

**5. Spectral perturbation and rounding (Step 6)** we control the eigenspace deviation  $O(\|E\|_2/\Delta)$  and show that both SAAC and SymNMF recover the true (possibly overlapping) clusters up to the stated error rate.

## Step 1: Concentration of Inner-Product Entries

We begin by controlling the entries of the empirical Gram matrix  $\widehat{\Sigma}$ , whose  $(i, i')$ -th entry is

$$g_{ii'}(\mathbf{Z}) = \langle \partial_i f(\mathbf{Z}), \partial_{i'} f(\mathbf{Z}) \rangle.$$

This uniform control is essential for later bounding the population Lasso risk.

First, the vector mean-value theorem tells us that for any  $\mathbf{z}, \mathbf{z}' \in \mathbb{R}^{d_z}$ ,

$$\nabla f_i(\mathbf{z}) - \nabla f_i(\mathbf{z}') = \int_0^1 D^2 f_i(\mathbf{z} + t(\mathbf{z}' - \mathbf{z})) (\mathbf{z}' - \mathbf{z}) dt.$$

Since  $\|D^2 f_i\|_{\text{op}} \leq L$  by Assumption Asm5.3, it follows immediately that

$$\|\nabla f_i(\mathbf{z}) - \nabla f_i(\mathbf{z}')\| \leq L \|\mathbf{z}' - \mathbf{z}\|,$$

so each coordinate gradient  $\partial_i f(\mathbf{z})$  is  $L$ -Lipschitz in  $\mathbf{z}$ .

Turning next to the inner-product function itself, differentiation yields

$$\nabla g_{ii'}(\mathbf{z}) = \sum_{\ell \in \{i, i'\}} D^2 f_\ell(\mathbf{z}) \partial_{\ell'} f(\mathbf{z}).$$

Again, using  $\|D^2 f_\ell\|_{\text{op}} \leq L$  together with the bounded-Jacobian condition  $\sup_{\mathbf{z}} \|Df(\mathbf{z})\|_F = \sqrt{d_x}$ , we deduce

$$\|\nabla g_{ii'}(\mathbf{z})\| \leq 2L \sqrt{d_x},$$

so  $g_{ii'}$  is  $2L\sqrt{d_x}$ -Lipschitz.

Because  $\mathbf{Z}$  is  $K$ -sub-Gaussian, the Borell–Tsirelson–Ibragimov–Sudakov inequality (Sudakov & Tsirel'son, 1978) applies to any  $2L\sqrt{d_x}$ -Lipschitz function of  $\mathbf{Z}$ . In particular, for each pair  $(i, i')$  and any  $t > 0$ ,

$$\Pr(|g_{ii'}(\mathbf{Z}) - \mathbb{E}_{\mathbf{Z}} g_{ii'}(\mathbf{Z})| \geq t) \leq 2 \exp\left(-\frac{t^2}{2K^2 L^2 d_x}\right).$$

A union bound over the  $\binom{d_x}{2}$  entries then shows that for any  $\varepsilon \in (0, 1)$ , with probability at least  $1 - \varepsilon/3$ ,

$$\|\widehat{\Sigma} - \Sigma\|_\infty = \max_{i, i'} |g_{ii'}(\mathbf{Z}) - \mathbb{E}_{\mathbf{Z}} g_{ii'}(\mathbf{Z})| \leq c_2 K L \sqrt{d_x \log(d_x^2/\varepsilon)},$$

where  $c_2 > 0$  is an absolute constant. We denote this event by  $E_1$ . Establishing  $E_1$  completes our concentration argument for the inner-product entries and sets the stage for analyzing the population Lasso estimator.

## Step 2: Primal–Dual Witness for the Population Lasso

Building on the Gram-matrix control from the previous section, we now analyze the population-level Lasso problem. Recall the population Gram

$$\mathbf{\Sigma} = \mathbb{E}_{\mathbf{Z}} [Df(\mathbf{Z}) Df(\mathbf{Z})^\top],$$

and consider the estimator

$$\min_{C \in \mathbb{R}^{d_x \times d_x}} \mathbb{E}_{\mathbf{Z}} \|Df(\mathbf{Z}) - C Df(\mathbf{Z})\|_F^2 + \lambda \|C\|_1.$$

*Restricted strong convexity.* By Assumption (A5), the population Gram satisfies

$$\mathbf{v}^\top \mathbf{\Sigma} \mathbf{v} \geq \kappa \|\mathbf{v}\|_2^2 \quad \text{whenever } \|\mathbf{v}\|_0 \leq s. \quad (3.1a)$$

Hence, the smooth part of the objective has the Hessian

$$D^2 Q(C)[\Delta C, \Delta C] = 2 \sum_i (\Delta C)_{i,:} \mathbf{\Sigma} (\Delta C)_{i,:}^\top \geq 2\kappa \|\Delta C\|_F^2,$$

so  $Q(C)$  is  $2\kappa$ -strongly convex on all row-wise  $s$ -sparse directions, implying a unique minimizer  $C^*$ .

*Sample curvature.* In practice, we replace  $\mathbf{\Sigma}$  by its sample version  $\hat{\mathbf{\Sigma}} = \frac{1}{N} \sum_t Df(Z^{(t)}) Df(Z^{(t)})^\top$ . Raskutti et al. (2010) shows that if  $N \gtrsim s \log d_z$ , then with probability greater than  $1 - \varepsilon/3$ ,

$$\mathbf{v}^\top \hat{\mathbf{\Sigma}} \mathbf{v} \geq (\kappa/2) \|\mathbf{v}\|_2^2 \quad \forall \|\mathbf{v}\|_0 \leq s. \quad (3.1b)$$

Thus, the empirical risk is also strongly convex with high probability, again guaranteeing a unique minimizer over  $s$ -sparse rows.

*Dual feasibility and setting  $\lambda$ .* Let  $S$  denote the true support of  $C^*$ . The KKT conditions on the complement  $S^c$  read

$$\nabla_{S^c} \mathbb{E} \|Df - C Df\|_F^2 \big|_{C=C^*} + \lambda U_{S^c} = 0,$$

with  $U_{S^c} \in [-1, 1]^{|S^c|}$ . Enforcing the primal–dual witness  $C_{S^c}^* = 0$  yields

$$2 \mathbf{\Sigma}_{S^c, S} C_S^* + \lambda U_{S^c} = 0 \implies \|\mathbf{\Sigma}_{S^c, S} C_S^*\|_\infty < \lambda.$$

By mutual incoherence,  $\|\mathbf{\Sigma}_{S^c, S} \mathbf{\Sigma}_{S, S}^{-1}\|_\infty \leq 1 - \gamma$ , and dominance ensures  $\|\mathbf{\Sigma}_{S, S} C_S^*\|_\infty \approx m_{\max}$ , so deterministically  $\|\mathbf{\Sigma}_{S^c, S} C_S^*\|_\infty \leq (1 - \gamma) m_{\max}$ . Meanwhile, the high-probability event  $E_1$  controls random fluctuations by  $\delta_{\text{rand}} = c_2 K L \sqrt{d_x \log(d_x^2/\varepsilon)}$ . Thus, choosing

$$\lambda = \left(1 - \frac{\gamma}{2}\right) m_{\max} + c_2 K L \sqrt{d_x \log(d_x^2/\varepsilon)}$$

strictly exceeds  $(1 - \gamma)m_{\max} + \delta_{\text{rand}}$ , forcing  $C_{S^c}^* = 0$ .

At this point, we have shown that under  $E_1$  and the RE event, the population Lasso solution  $C^*$  recovers the correct support with high probability. In the next section, we translate these coefficient bounds into affinity-matrix guarantees and, ultimately, into clustering accuracy.

### Step 3: Sign Consistency & In-Group Recovery

Next, we show that any two features  $i, i', i \neq i'$ , in the same latent group  $G_j$  obtain a large positive self-expression coefficient

$$C_{ii'}^* = \arg \min_{c \in \mathbb{R}} \mathbb{E}_{\mathbf{Z}} \|\partial_i f(\mathbf{Z}) - c \partial_{i'} f(\mathbf{Z})\|_2^2,$$

and in particular

$$C_{ii'}^* \geq 1 - (\delta + \mu) - \frac{c_2 K L \sqrt{d_x} \log(d_x^2/\varepsilon)}{m_j}.$$

To see this, note first that on the true one-dimensional support  $S = \{(i, i')\}$ , the  $\ell_1$  penalty drops out and  $C_{ii'}^*$  solves the simple least-squares problem

$$\min_{c \in \mathbb{R}} \mathbb{E}_{\mathbf{Z}} \|\partial_i f(\mathbf{Z}) - c \partial_{i'} f(\mathbf{Z})\|_2^2.$$

Differentiating under the expectation and setting to zero gives the closed-form

$$C_{ii'}^* = \frac{\mathbb{E}_{\mathbf{Z}} \langle \partial_i f(\mathbf{Z}), \partial_{i'} f(\mathbf{Z}) \rangle}{\mathbb{E}_{\mathbf{Z}} \|\partial_{i'} f(\mathbf{Z})\|_2^2}.$$

We now bound the numerator and denominator in turn. By Dominance (A3), the key partial  $\partial f_i / \partial z_j$  satisfies

$$\mathbb{E}_{\mathbf{Z}} \left| \frac{\partial f_i}{\partial z_j}(\mathbf{Z}) \right| \geq (1 - \delta) \sqrt{\mathbb{E}_{\mathbf{Z}} \|\nabla_{\mathbf{z}} f_i(\mathbf{Z})\|^2} = (1 - \delta) \sqrt{m_j}.$$

Moreover, Mutual Incoherence ensures that cross-terms contribute at most  $\mu \sqrt{m_j^2}$ , so altogether

$$\mathbb{E}_{\mathbf{Z}} \langle \partial_i f(\mathbf{Z}), \partial_{i'} f(\mathbf{Z}) \rangle \geq (1 - \delta - \mu) m_j.$$

On the other hand, from the uniform deviation event  $E_1$  we know each entry of the empirical Gram deviates by at most  $\Delta := c_2 K L \sqrt{d_x \log(d_x^2/\varepsilon)}$ . In particular,

$$|\|\partial_{i'} f(\mathbf{Z})\|_2^2 - \mathbb{E} \|\partial_{i'} f(\mathbf{Z})\|_2^2| \leq \Delta,$$

and since  $\mathbb{E}_{\mathbf{Z}} \|\partial_{i'} f(\mathbf{Z})\|_2^2 = m_j$ , we have

$$\mathbb{E}_{\mathbf{Z}} \|\partial_{i'} f(\mathbf{Z})\|_2^2 \leq m_j + \Delta.$$

Putting these together,

$$C_{ii'}^* = \frac{\mathbb{E}_{\mathbf{Z}} \langle \partial_i f(\mathbf{Z}), \partial_{i'} f(\mathbf{Z}) \rangle}{\mathbb{E}_{\mathbf{Z}} \|\partial_{i'} f(\mathbf{Z})\|_2^2} \geq \frac{(1 - \delta - \mu) m_j}{m_j + \Delta} \geq 1 - (\delta + \mu) - \frac{\Delta}{m_j},$$

which is the stated bound

$$C_{ii'}^* \geq 1 - (\delta + \mu) - \frac{c_2 K L \sqrt{d_x} \log(d_x^2/\varepsilon)}{m_j}.$$

## Step 4: Affinity Matrix & Block Bounds

With the support recovery and coefficient bounds in place, define the induced affinity

$$A_{ii'}^* = |C_{ii'}^*| + |C_{i'i}^*|.$$

On the intersection of our two high-probability events  $E_1$  (uniform deviation of  $\widehat{\Sigma}$ ) and  $E_2$  (empirical RE), we obtain sharp “block” estimates separating in-group from cross-group affinities.

*Intra-cluster bound.* If  $i, i' \in Ch(j)$ , then by the sign-consistency argument, each of  $C_{ii'}^*$  and  $C_{i'i}^*$  obeys

$$C_{\bullet\bullet}^* \geq 1 - (\delta + \mu) - \frac{c_2 K L \sqrt{d_x} \log(d_x^2/\varepsilon)}{m_j},$$

so summing yields

$$A_{ii'}^* \geq 2 \left( 1 - (\delta + \mu) \right) - \frac{2 c_2 K L \sqrt{d_x} \log(d_x^2/\varepsilon)}{m_j}.$$

Absorbing constants into  $C_3 = 2c_2$  and re-scaling by  $m_j$  gives the clean form

$$A_{ii'}^* \geq (1 - \delta - \mu) m_j - C_3 K L \sqrt{d_x} \log\left(\frac{d_x^2}{\varepsilon}\right).$$

*Inter-cluster bound.* If  $i \in Ch(j)$  and  $i' \in Ch(k)$  with  $k \neq j$ , then dual-feasibility forces  $C_{ii'}^* = 0$  on the population level, and concentration adds at most  $c_2 K L \sqrt{d_x} \log(d_x^2/\varepsilon)$  to each coefficient. Hence

$$A_{ii'}^* \leq \left| \mathbb{E}_{\mathbf{Z}} \langle \partial_i f(\mathbf{Z}), \partial_{i'} f(\mathbf{Z}) \rangle \right| + C_3 K L \sqrt{d_x} \log\left(\frac{d_x^2}{\varepsilon}\right) \leq \mu \sqrt{m_j m_k} + C_3 K L \sqrt{d_x} \log\left(\frac{d_x^2}{\varepsilon}\right),$$

which in the symmetric-affinity form becomes

$$A_{ii'}^* \leq \mu m_j m_k + C_3 K L \sqrt{d_x} \log\left(\frac{d_x^2}{\varepsilon}\right).$$

These two inequalities reveal a gap between “strong” in-group affinities and “weak” cross-group affinities—precisely the structure needed for the subsequent spectral perturbation and clustering steps.

## Step 5: Spectral Perturbation & Eigenspace Deviation

To transition from coefficient bounds to clustering, we compare the observed affinity  $A^*$  with the ideal block matrix

$$H = \sum_j m_j 1_{G_j} 1_{G_j}^\top,$$

and let the perturbation be

$$E = A^* - H.$$

Our goal is to show that  $E$  is small in operator norm and thus the leading eigenspaces of  $A^*$  and  $H$  remain close.

Gershgorin’s circle (Horn & Johnson, 2012b) theorem first controls the size of  $E$ . Since each row of  $E$  has at most  $d_x$  nonzero entries, each is bounded in magnitude by

$$C_3 K L \sqrt{d_x \log(d_x^2/\varepsilon)},$$

we obtain

$$\|E\|_2 \leq \|E\|_{1,\infty} \leq d_x C_3 K L \sqrt{d_x \log(d_x^2/\varepsilon)}.$$

Next, Weyl’s inequality for symmetric matrices (Horn & Johnson, 2012b) implies that every eigenvalue of  $A^*$  deviates from its counterpart in  $H$  by at most  $\|E\|_2$ :

$$|\lambda_i(A^*) - \lambda_i(H)| \leq \|E\|_2 \quad \forall i.$$

We then define the critical eigengap

$$\Delta = \min_j m_j - \mu \max_{k \neq j} \sqrt{m_j m_k} - 2\|E\|_2.$$

Whenever  $\Delta > 0$ , the Davis–Kahan sin  $\Theta$  theorem (Davis & Kahan, 1970) guarantees that the distance between the top- $d_z$  eigenspaces of  $H$  and  $A^*$  is controlled by

$$\|\sin \Theta(\widehat{U}, U)\|_2 \leq \frac{\|E\|_2}{\Delta},$$

and in particular, each eigenvector satisfies

$$\|\widehat{u}_i - u_i\|_2 \leq \frac{\|E\|_2}{\Delta}.$$

Thus, under the gap condition  $\Delta > 0$ , the spectral embeddings produced by  $A^*$  remain within a small radius of the ideal block-model embeddings—paving the way for accurate rounding in the clustering step.

## Step 6.1: SAAC Rounding

After forming the affinity matrix  $A^*$ , SAAC (Panov et al., 2017) extracts its top  $d_z$  eigenvectors

$$\widehat{U} = [\hat{u}^1, \dots, \hat{u}^{d_z}] \in \mathbb{R}^{d_x \times d_z},$$

and then fits a binary membership matrix  $Z \in \{0, 1\}^{d_x \times d_z}$  alongside a prototype matrix  $X \in \mathbb{R}^{d_x \times d_z}$  by minimizing

$$\|\widehat{U} - Z X\|_F^2 \quad \text{subject to } Z_{i,\cdot} \neq 0 \ \forall i,$$

so that each feature  $i$  is assigned to at least one cluster and  $\widehat{U} \approx Z X$ .

In practice, SAAC alternates between

$$X = \arg \min_X \|\widehat{U} - Z X\|_F^2 = (Z^\top Z)^{-1} Z^\top \widehat{U}$$

and, for each  $i$ ,

$$Z_i = \arg \min_{z \in \{0, 1\}^{d_z} \setminus \{0\}} \|\widehat{U}_i - z X\|_2^2 = \begin{cases} 1 & \text{at } j = \arg \min_k \|\widehat{U}_i - X_k\|_2, \\ 0 & \text{otherwise,} \end{cases}$$

i.e. each feature picks the single prototype  $X_j$  closest in Euclidean distance to its embedding  $\widehat{U}_i$ . These two updates are repeated until convergence.

The success of this *nearest-neighbor rounding* follows from our perturbation bounds: with probability  $\geq 1 - \varepsilon$ ,

$$\|\widehat{U}_i - U_i\|_2 \leq \frac{\|E\|_2}{\Delta},$$

where  $U_i$  is the ideal block-model embedding and  $\Delta$  the eigengap. In the noiseless block model  $H = \sum_j m_j 1_{G_j} 1_{G_j}^\top$ , the normalized indicator eigenvectors  $\{u_j\}$  satisfy

$$\|u_j - u_{j'}\|_2 \geq 2, \quad j \neq j'.$$

Hence if

$$\frac{\|E\|_2}{\Delta} < \frac{1}{2},$$

then each  $\widehat{U}_i$  lies within  $1/2$  of its true  $U_i$  and farther from any other  $u_{j'}$ . Nearest-neighbor rounding therefore selects the correct cluster(s), and when overlaps occur, features lie near intersections of the relevant  $\{u_j\}$ , still recovered as long as the intersection angles exceed the noise radius. Combining these facts yields the misclassification rate

$$\max_{1 \leq j \leq d_z} \frac{|\widehat{G}_j \triangle G_j|}{|G_j|} = \mathcal{O}\left(\delta + \frac{\mu}{\gamma} + \frac{K L \sqrt{d_x \log(d_x^2/\varepsilon)}}{\min_{1 \leq j \leq d_z} m_j}\right).$$



as claimed in the Theorem Thm5.3.

## Step 6.2: SymNMF Rounding

SymNMF (Kuang et al., 2015) replaces the binary assignment of SAAC with a nonnegative factorization.

We fit

$$\min_{Y \geq 0} F(Y) = \|A^* - Y Y^\top\|_F^2,$$

where each row  $Y_i$  encodes soft memberships of feature  $i$ . The classic multiplicative update of Kuang et al. (2015),

$$Y_{ij} \leftarrow Y_{ij} \times \frac{[A^* Y]_{ij}}{[Y Y^\top Y]_{ij}},$$

preserves nonnegativity and drives  $F(Y)$  downward until a stationary point  $Y^*$  is reached.

Once converged, we normalize each row,

$$T_i = Y_i^* / \|Y_i^*\|_1 \in \Delta^{d_z-1},$$

and then “round” by hard-thresholding:

$$Z_{i,j} = \begin{cases} 1, & j = \arg \max_k T_{i,k}, \\ 0, & \text{otherwise.} \end{cases}$$

In practice, when several entries tie within a small tolerance, all corresponding clusters may be assigned to  $i$ , capturing overlaps.

Under the same eigenspace perturbation bound  $\|\widehat{U} - U\|_{2 \rightarrow \infty} \leq \|E\|_2 / \Delta$ , the ideal block-model solution  $Y = U \Lambda^{1/2}$  (with rows proportional to the indicator eigenvectors) is perturbed only slightly. A perturbation smaller than half the gap between the top two coordinates of each ideal row cannot change the index of the largest entry, so hard-thresholding recovers the exact cluster memberships. Allowing ties yields overlap-aware assignments. Hence, SymNMF achieves the same misclassification rate,

$$\max_j \frac{|\widehat{G}_j \Delta G_j|}{|G_j|} = O\left(\delta + \frac{\mu}{\gamma} + \frac{KL\sqrt{d_x \log(d_x^2/\varepsilon)}}{\min_j m_j}\right),$$

completing the proof of the theorem Thm5.3.

## C.1.6 Generalization and Stability Under the Self-Expression Problem

**Proof of Theorem Thm5.4** We aim to control the uniform generalization gap:

$$\Delta := \sup_{C \in \mathcal{C}_\lambda} \left| \mathbb{E}_{\mathbf{x} \sim p_{data}} [\bar{\ell}(C, f; \mathbf{x})] - \frac{1}{N} \sum_{i=1}^N \bar{\ell}(C, f; \mathbf{x}) \right|, \quad \text{where} \quad \bar{\ell}(C, f; \mathbf{x}) = \|(I - C) \bar{J}_f(\mathbf{x}; q_\phi)\|_F^2.$$

**Step 1: Symmetrization.** By the standard symmetrization inequality (see (Bartlett & Mendelson, 2002, Theorem 3.1)), we have:

$$\mathbb{E}_{\mathbf{x}_{1:N}}[\Delta] \leq 2 \mathbb{E}_{\mathbf{x}_{1:N}, \sigma_{1:N}} \left[ \sup_{C \in \mathcal{C}_\lambda} \frac{1}{N} \sum_{i=1}^N \sigma_i \ell(C; \mathbf{x}_i) \right],$$

where  $\sigma_i \in \{\pm 1\}$  are Rademacher variables which are independent.

**Step 2: Contraction via Ledoux–Talagrand.** Fix  $\mathbf{x} \in \mathcal{X} \subset \mathbb{R}^{d_x}$ . Since  $\|\bar{J}_f(\mathbf{x}; q_\phi)\|_F \leq M_\phi$ , applying the contraction inequality (Ledoux, 2001) gives:

$$\mathbb{E}_\sigma \left[ \sup_{C \in \mathcal{C}_\lambda} \frac{1}{N} \sum_{i=1}^N \sigma_i \|\bar{\ell}(C, f; \mathbf{x}_i)\|_F^2 \right] \leq 4M \cdot \mathbb{E}_\sigma \left[ \sup_{C \in \mathcal{C}_\lambda} \frac{1}{N} \sum_{i=1}^N \sigma_i \langle \bar{\ell}(C, f; \mathbf{x}_i), E \rangle_F \right],$$

where  $E \in \mathbb{R}^{n \times d}$  is an auxiliary matrix (a “ghost sample”) used in the contraction argument.

**Step 3: Reduction to linear class.** Since

$$\langle \bar{\ell}(C, f; \mathbf{x}_i), E \rangle_F = \langle \bar{J}_f(\mathbf{x}_i; q_\phi), E \rangle_F - \langle C \bar{J}_f(\mathbf{x}_i; q_\phi), E \rangle_F,$$

and the first term is independent of  $C$ , we reduce to bounding:

$$\mathbb{E}_\sigma \left[ \sup_{C \in \mathcal{C}_\lambda} \frac{1}{N} \sum_{i=1}^N \langle C \bar{J}_f(\mathbf{x}_i; q_\phi), \sigma_i \rangle_F \right].$$

**Step 4: Bounding the Rademacher complexity.** Define the class of self-expressive tangent maps:

$$\mathcal{H}_{\lambda, f} := \{ \mathbf{x} \mapsto C \bar{J}_f(\mathbf{x}; q_\phi) \mid C \in \mathbb{R}^{d_x \times d_x}, \text{diag}(C) = 0, \|C\|_1 \leq \lambda \}.$$

Using the duality  $\sup_{\|C\|_1 \leq \lambda} \langle C, A \rangle = \lambda \|A\|_\infty$ , the Rademacher complexity  $\mathfrak{R}_N(\mathcal{H}_{\lambda, f})$  of  $\mathcal{H}_{\lambda, f}$  is bounded:

$$\mathfrak{R}_N(\mathcal{H}_{\lambda, f}) \leq \frac{\lambda}{N} \mathbb{E}_\sigma \left\| \sum_{i=1}^N \sigma_i \bar{J}_f(\mathbf{x}_i; q_\phi)^\top \right\|_\infty.$$

Since  $\|\bar{J}_f(\mathbf{x}_i; q_\phi)\|_F \leq M_\phi$  implies  $\|\bar{J}_f(\mathbf{x}_i; q_\phi)\|_{\text{op}} \leq M_\phi$ , classical matrix concentration (Tropp, 2012) gives:

$$\mathbb{E}_\sigma \left\| \sum_{i=1}^N \sigma_i \bar{J}_f(\mathbf{x}_i; q_\phi)^\top \right\|_\infty \leq M_\phi \sqrt{2N \log d_x},$$

thus:

$$\mathfrak{R}_N(\mathcal{H}_{\lambda, f}) \leq \lambda M_\phi \sqrt{\frac{2 \log d_x}{N}}.$$

**Step 5: Final bound via McDiarmid’s inequality.** Combining the above gives:

$$\mathbb{E}_{\mathbf{x}_{1:N}}[\Delta] \leq 8\lambda M_\phi^2 \sqrt{\frac{2 \log d_x}{N}}.$$

To lift this to a high-probability bound, we apply McDiarmid's inequality (Shalev-Shwartz & Ben-David, 2014): with probability at least  $1 - \delta$  we finally obtain

$$\Delta \leq 8\lambda M_\phi^2 \sqrt{\frac{2 \log d_x}{N}} + M_\phi^2 \sqrt{\frac{2 \log(1/\delta)}{N}}.$$

**Proof of Proposition Prop5.3** Write  $A = \tilde{D}f(\mathbf{Z})$ ,  $E = E(\mathbf{Z})$ , and  $\Delta = I - C^*$ . Then:

$$\|Df(\mathbf{Z}) - Df(\mathbf{Z})C^*\|_F^2 = \|(\tilde{D}f(\mathbf{Z}) + E(\mathbf{Z}))\Delta\|_F^2 = \|\tilde{D}f(\mathbf{Z})\Delta\|_F^2 + 2\langle \tilde{D}f(\mathbf{Z})\Delta, E(\mathbf{Z})\Delta \rangle_F + \|E(\mathbf{Z})\Delta\|_F^2.$$

Thus, the deviation satisfies:

$$\left| \|Df(\mathbf{Z}) - Df(\mathbf{Z})C^*\|_F^2 - \|\tilde{D}f(\mathbf{Z}) - \tilde{D}f(\mathbf{Z})C^*\|_F^2 \right| = \left| 2\langle \tilde{D}f(\mathbf{Z})\Delta, E(\mathbf{Z})\Delta \rangle_F + \|E(\mathbf{Z})\Delta\|_F^2 \right|.$$

**Step 1: Bounding  $\|E(\mathbf{Z})\Delta\|_F$ .** We have  $\|E(\mathbf{Z})\Delta\|_F \leq \|E(\mathbf{Z})\|_F \|\Delta\|_{\text{op}}$ . Since  $E$  has  $d_x$  independent sub-Gaussian columns, by vector concentration (Vershynin, 2018, Proposition 3.3.7), there exists  $\Lambda_1 > 0$  such that for any  $\delta \in (0, 1)$ ,

$$\mathbb{P} \left\{ \|E(\mathbf{Z})\|_F > \Lambda_1 \varepsilon \sqrt{d_z d_x} + \varepsilon \sqrt{2d_z \ln(2d_x/\delta)} \right\} \leq \delta.$$

Thus, with probability at least  $1 - \delta$ ,

$$\|E(\mathbf{Z})\Delta\|_F \leq \|\Delta\|_{\text{op}} \left( \Lambda_1 \varepsilon \sqrt{d_z d_x} + \varepsilon \sqrt{2d_z \ln \frac{2d_x}{\delta}} \right).$$

**Step 2: Bounding the cross term.** By Cauchy-Schwarz inequality:

$$\left| \langle \tilde{D}f(\mathbf{Z})\Delta, E(\mathbf{Z})\Delta \rangle_F \right| \leq \|\tilde{D}f(\mathbf{Z})\Delta\|_F \|E(\mathbf{Z})\Delta\|_F \leq \|\tilde{D}f(\mathbf{Z})\|_F \|\Delta\|_{\text{op}} \|E(\mathbf{Z})\Delta\|_F.$$

Since  $\|\tilde{D}f(\mathbf{Z})\|_F = \sqrt{d_x}$ , we have:

$$\left| \langle \tilde{D}f(\mathbf{Z})\Delta, E(\mathbf{Z})\Delta \rangle_F \right| \leq \sqrt{d_x} \|\Delta\|_{\text{op}} \left( \Lambda_1 \varepsilon \sqrt{d_z d_x} + \varepsilon \sqrt{2d_z \ln \frac{2d_x}{\delta}} \right).$$

**Step 3: Final combination.** Thus, with probability at least  $1 - \delta$ ,

$$\begin{aligned} \left| \|Df(\mathbf{Z}) - Df(\mathbf{Z})C^*\|_F^2 - \|\tilde{D}f(\mathbf{Z}) - \tilde{D}f(\mathbf{Z})C^*\|_F^2 \right| &\leq 2\sqrt{d_x} \|\Delta\|_{\text{op}} \left( \Lambda_1 \varepsilon \sqrt{d_z d_x} + \varepsilon \sqrt{2d_z \ln \frac{2d_x}{\delta}} \right) \\ &\quad + \|\Delta\|_{\text{op}}^2 \left( \Lambda_1 \varepsilon \sqrt{d_z d_x} + \varepsilon \sqrt{2d_z \ln \frac{2d_x}{\delta}} \right)^2. \end{aligned}$$

Recalling  $\|\Delta\|_{\text{op}} = \|I - C^*\|_{\text{op}} \leq 1 + \|C^*\|_{\text{op}}$  and setting

$$B(\delta) := \Lambda_1 \sqrt{d_z d_x} + \sqrt{2d_z \ln \frac{2d_x}{\delta}},$$

the bound simplifies to:

$$\left| \|Df(\mathbf{Z}) - Df(\mathbf{Z})C^*\|_F^2 - \|\tilde{D}f(\mathbf{Z}) - \tilde{D}f(\mathbf{Z})C^*\|_F^2 \right| \leq (1 + \|C^*\|_{\text{op}}) \left( 2\sqrt{d_x}B(\delta)\varepsilon + (1 + \|C^*\|_{\text{op}})B(\delta)^2\varepsilon^2 \right).$$

# Bibliography

- Alberto Abadie. Semiparametric difference-in-differences estimators. *The review of economic studies*, 72(1):1–19, 2005.
- Alberto Abadie and Guido W Imbens. Large sample properties of matching estimators for average treatment effects. *econometrica*, 74(1):235–267, 2006.
- Alberto Abadie, David M. Drukker, Jane Leber Herr, and Guido Imbens. Implementing matching estimators for average treatment effects in stata. *The Stata Journal*, 4:290 – 311, 2004.
- Alberto Abadie, Alexis Diamond, and Jens Hainmueller. Synthetic control methods for comparative case studies: Estimating the effect of california’s tobacco control program. *Journal of the American statistical Association*, 105(490):493–505, 2010.
- Mahdi Abavisani and Vishal M Patel. Deep multimodal subspace clustering networks. *IEEE Journal of Selected Topics in Signal Processing*, 12(6):1601–1614, 2018.
- Maryam Abdolali and Nicolas Gillis. Beyond linear subspace clustering: A comparative study of nonlinear manifold clustering algorithms. *Computer Science Review*, 42:100435, 2021.
- Jeffrey Adams and Niels Richard Hansen. Substitute adjustment via recovery of latent variables. *arXiv preprint arXiv:2403.00202*, 2024.
- Julius Adebayo, Justin Gilmer, Michael Muelly, Ian Goodfellow, Moritz Hardt, and Been Kim. Sanity checks for saliency maps. *Advances in neural information processing systems*, 31, 2018.
- Raj Agrawal, Chandler Squires, Karren Yang, Karthikeyan Shanmugam, and Caroline Uhler. Abcd-strategy: Budgeted experimental design for targeted causal structure discovery. In *The 22nd International Conference on Artificial Intelligence and Statistics*, pp. 3400–3409. PMLR, 2019.
- Ahmed Alaa and Mihaela Van Der Schaar. Validating causal inference models via influence functions. In *International Conference on Machine Learning*, pp. 191–201. PMLR, 2019.
- David Alvarez Melis and Tommi Jaakkola. Towards robust interpretability with self-explaining neural networks. *Advances in neural information processing systems*, 31, 2018.
- Joshua D. Angrist and Jörn-Steffen Pischke. *Mostly Harmless Econometrics: An Empiricist’s Companion*. Princeton University Press, 2009. ISBN 9780691120348. URL <http://www.jstor.org/stable/j.ctvc4j72>.

- Joshua D Angrist, Guido W Imbens, and Donald B Rubin. Identification of causal effects using instrumental variables. *Journal of the American statistical Association*, 91(434):444–455, 1996.
- Yashas Annadani, Jonas Rothfuss, Alexandre Lacoste, Nino Scherrer, Anirudh Goyal, Yoshua Bengio, and Stefan Bauer. Variational causal networks: Approximate bayesian inference over causal structures. *CoRR*, abs/2106.07635, 2021. URL <https://arxiv.org/abs/2106.07635>.
- Yashas Annadani, Nick Pawlowski, Joel Jennings, Stefan Bauer, Cheng Zhang, and Wenbo Gong. Bayesdag: Gradient-based posterior inference for causal discovery. *Advances in Neural Information Processing Systems*, 36:1738–1763, 2023.
- Dmitry Arkhangelsky and Guido W Imbens. Double-robust identification for causal panel data models. Technical report, National Bureau of Economic Research, 2021.
- Dmitry Arkhangelsky, Susan Athey, David A Hirshberg, Guido W Imbens, and Stefan Wager. Synthetic difference in differences. Technical report, National Bureau of Economic Research, 2019.
- Sanjeev Arora, Rong Ge, Yonatan Halpern, David Mimno, Ankur Moitra, David Sontag, Yichen Wu, and Michael Zhu. A practical algorithm for topic modeling with provable guarantees. In *International conference on machine learning*, pp. 280–288. PMLR, 2013a.
- Sanjeev Arora, Rong Ge, Yonatan Halpern, David Mimno, Ankur Moitra, David Sontag, Yichen Wu, and Michael Zhu. A practical algorithm for topic modeling with provable guarantees. In *International conference on machine learning*, pp. 280–288. PMLR, 2013b.
- Sanjeev Arora, Rong Ge, Yoni Halpern, David Mimno, Ankur Moitra, David Sontag, Yichen Wu, and Michael Zhu. Learning topic models—provably and efficiently. *Communications of the ACM*, 61(4): 85–93, 2018.
- Serge Assaad, Shuxi Zeng, Chenyang Tao, Shounak Datta, Nikhil Mehta, Ricardo Henao, Fan Li, and Lawrence Carin. Counterfactual representation learning with balancing weights. In *International Conference on Artificial Intelligence and Statistics*, pp. 1972–1980. PMLR, 2021.
- Onur Atan, James Jordon, and Mihaela Van der Schaar. Deep-treat: Learning optimal personalized treatments from observational data using neural networks. In *Proceedings of the AAAI Conference on Artificial Intelligence*, volume 32, 2018.
- Susan Athey and Guido W Imbens. The state of applied econometrics: Causality and policy evaluation. *Journal of Economic perspectives*, 31(2):3–32, 2017.
- Susan Athey, Julie Tibshirani, and Stefan Wager. Generalized random forests. *The Annals of Statistics*, 2019.
- Peter C. Austin. An introduction to propensity score methods for reducing the effects of confounding in observational studies. *Multivariate Behavioral Research*, 46:399 – 424, 2011a.

- Peter C Austin. An introduction to propensity score methods for reducing the effects of confounding in observational studies. *Multivariate behavioral research*, 46(3):399–424, 2011b.
- Sergul Aydore, Bertrand Thirion, and Gaël Varoquaux. Feature grouping as a stochastic regularizer for high-dimensional structured data. In *International Conference on Machine Learning*, pp. 385–394. PMLR, 2019.
- Francis Bach, Rodolphe Jenatton, Julien Mairal, and Guillaume Obozinski. Structured Sparsity through Convex Optimization. *Statistical Science*, 27(4):450 – 468, 2012. doi: 10.1214/12-STS394. URL <https://doi.org/10.1214/12-STS394>.
- Philip Bachman, R Devon Hjelm, and William Buchwalter. Learning representations by maximizing mutual information across views. *Advances in neural information processing systems*, 32, 2019.
- Junwen Bai, Weiran Wang, and Carla P Gomes. Contrastively disentangled sequential variational autoencoder. *Advances in Neural Information Processing Systems*, 34:10105–10118, 2021a.
- Jushan Bai. Panel data models with interactive fixed effects. *Econometrica*, 77(4):1229–1279, 2009.
- Ray Bai, Veronika Ročková, and Edward I George. Spike-and-slab meets lasso: A review of the spike-and-slab lasso. *Handbook of Bayesian variable selection*, pp. 81–108, 2021b.
- Heejung Bang and James M Robins. Doubly robust estimation in missing data and causal inference models. *Biometrics*, 61(4):962–973, 2005.
- Peter L Bartlett and Shahar Mendelson. Rademacher and gaussian complexities: Risk bounds and structural results. *Journal of machine learning research*, 3(Nov):463–482, 2002.
- Peter W Battaglia, Jessica B Hamrick, Victor Bapst, Alvaro Sanchez-Gonzalez, Vinicius Zambaldi, Mateusz Malinowski, Andrea Tacchetti, David Raposo, Adam Santoro, Ryan Faulkner, et al. Relational inductive biases, deep learning, and graph networks. *arXiv preprint arXiv:1806.01261*, 2018.
- Justin Bayer and Christian Osendorfer. Learning stochastic recurrent networks. *ArXiv*, abs/1411.7610, 2014.
- Nathaniel Beck. Time-series–cross-section data: What have we learned in the past few years? *Annual review of political science*, 4(1):271–293, 2001.
- Sander Beckers and Joseph Y Halpern. Abstracting causal models. In *Proceedings of the aaai conference on artificial intelligence*, volume 33, pp. 2678–2685, 2019.
- Sander Beckers, Frederick Eberhardt, and Joseph Y Halpern. Approximate causal abstractions. In *Uncertainty in artificial intelligence*, pp. 606–615. PMLR, 2020.
- Mohamed Ishmael Belghazi, Aristide Baratin, Sai Rajeshwar, Sherjil Ozair, Yoshua Bengio, Aaron Courville, and Devon Hjelm. Mutual information neural estimation. In *International conference on machine learning*, pp. 531–540. PMLR, 2018.

- Andrew Bell and Kelvyn Jones. Explaining fixed effects: Random effects modeling of time-series cross-sectional and panel data. *Political Science Research and Methods*, 3(1):133–153, 2015.
- Anthony J Bell and Terrence J Sejnowski. An information-maximization approach to blind separation and blind deconvolution. *Neural computation*, 7(6):1129–1159, 1995.
- Eli Ben-Michael, Avi Feller, and Jesse Rothstein. The augmented synthetic control method. *Journal of the American Statistical Association*, 116(536):1789–1803, 2021.
- Thomas Bendokat, Ralf Zimmermann, and P-A Absil. A grassmann manifold handbook: Basic geometry and computational aspects. *Advances in Computational Mathematics*, 50(1):6, 2024.
- Yoshua Bengio, Aaron Courville, and Pascal Vincent. Representation learning: A review and new perspectives. *IEEE transactions on pattern analysis and machine intelligence*, 35(8):1798–1828, 2013.
- Jeroen Berrevoets, Alicia Curth, Ioana Bica, Eoin McKinney, and Mihaela van der Schaar. Disentangled counterfactual recurrent networks for treatment effect inference over time. *arXiv preprint arXiv:2112.03811*, 2021.
- Jeroen Berrevoets, Krzysztof Kacprzyk, Zhaozhi Qian, Mihaela van der Schaar, et al. Causal deep learning: encouraging impact on real-world problems through causality. *Foundations and Trends® in Signal Processing*, 18(3):200–309, 2024.
- Dimitri Bertsekas. *Convex optimization algorithms*. Athena Scientific, 2015.
- Ioana Bica, Ahmed M Alaa, James Jordon, and Mihaela van der Schaar. Estimating counterfactual treatment outcomes over time through adversarially balanced representations. In *International Conference on Learning Representations*, 2020a. URL <https://openreview.net/forum?id=BJg866NFvB>.
- Ioana Bica, Ahmed M. Alaa, and Mihaela van der Schaar. Time series deconfounder: Estimating treatment effects over time in the presence of hidden confounders. In *International Conference on Machine Learning*, 2020b.
- Patrick Billingsley. *Probability and measure*. John Wiley & Sons, 2017.
- Xin Bing, Florentina Bunea, Yang Ning, and Marten Wegkamp. Adaptive estimation in structured factor models with applications to overlapping clustering. *The Annals of Statistics*, 48(4):2055 – 2081, 2020. doi: 10.1214/19-AOS1877. URL <https://doi.org/10.1214/19-AOS1877>.
- Xin Bing, Florentina Bunea, and Marten Wegkamp. Inference in latent factor regression with clusterable features. *Bernoulli*, 28(2):997–1020, 2022.
- Matthew Blackwell and Adam N Glynn. How to make causal inferences with time-series cross-sectional data under selection on observables. *American Political Science Review*, 112(4):1067–1082, 2018.
- Stéphane Bonhomme and Elena Manresa. Grouped patterns of heterogeneity in panel data. *Econometrica*, 83(3):1147–1184, 2015.



- Mouad El Bouchattaoui, Myriam Tami, Benoit Lepetit, and Paul-Henry Cournède. Causal dynamic variational autoencoder for counterfactual regression in longitudinal data. *arXiv preprint arXiv:2310.10559*, 2023.
- Mouad El Bouchattaoui, Myriam Tami, BENOIT LEPETIT, and Paul-Henry Cournède. Causal contrastive learning for counterfactual regression over time. In *The Thirty-eighth Annual Conference on Neural Information Processing Systems*, 2024. URL <https://openreview.net/forum?id=bK0ZYBJE4Z>.
- Julien Boussard, Chandni Nagda, Julia Kaltenborn, Charlotte Emilie Elektra Lange, Philippe Brouillard, Yaniv Gurwicz, Peer Nowack, and David Rolnick. Towards causal representations of climate model data. *arXiv preprint arXiv:2312.02858*, 2023.
- Samuel R Bowman, Luke Vilnis, Oriol Vinyals, Andrew M Dai, Rafal Jozefowicz, and Samy Bengio. Generating sentences from a continuous space. *arXiv preprint arXiv:1511.06349*, 2015.
- Philemon Brakel and Yoshua Bengio. Learning independent features with adversarial nets for non-linear ica. *arXiv preprint arXiv:1710.05050*, 2017.
- NW Bray, TJ Doherty, and Manuel Montero-Odasso. The effect of high dose vitamin d3 on physical performance in frail older adults. a feasibility study. *The Journal of Frailty & Aging*, 7:155–161, 2018.
- L. Breiman. Random forests. *Machine Learning*, 45:5–32, 2001.
- Philippe Brouillard, Sebastien Lachapelle, Julia Kaltenborn, Yaniv Gurwicz, Dhanya Sridhar, Alexandre Drouin, Peer Nowack, Jakob Runge, and David Rolnick. Causal representation learning in temporal data via single-parent decoding, 2024. URL <https://openreview.net/forum?id=e2jDr8NdJm>.
- Yurun Cai, Amal A Wanigatunga, Christine M Mitchell, Jacek K Urbanek, Edgar R Miller, Stephen P Juraschek, Erin D Michos, Rita R Kalyani, David L Roth, Lawrence J Appel, et al. The effects of vitamin d supplementation on frailty in older adults at risk for falls. *BMC geriatrics*, 22(1):1–9, 2022.
- Brantly Callaway and Pedro HC Sant’Anna. Difference-in-differences with multiple time periods. *Journal of econometrics*, 225(2):200–230, 2021.
- Defu Cao, James Enouen, and Yan Liu. Estimating treatment effects in continuous time with hidden confounders. *arXiv preprint arXiv:2302.09446*, 2023.
- Gianluca Carloni, Andrea Berti, and Sara Colantonio. The role of causality in explainable artificial intelligence. *Wiley Interdisciplinary Reviews: Data Mining and Knowledge Discovery*, 15(2):e70015, 2025.
- Marie Chavent, Robin Genuer, and Jerome Saracco. Combining clustering of variables and feature selection using random forests. *Communications in Statistics-Simulation and Computation*, 50(2):426–445, 2021.
- Guangyi Chen, Yifan Shen, Zhenhao Chen, Xiangchen Song, Yuewen Sun, Weiran Yao, Xiao Liu, and Kun Zhang. Caring: learning temporal causal representation under non-invertible generation process. In *Proceedings of the 41st International Conference on Machine Learning, ICML’24*. JMLR.org, 2024.

- Xi Chen, Yan Duan, Rein Houthooft, John Schulman, Ilya Sutskever, and Pieter Abbeel. Infogan: Interpretable representation learning by information maximizing generative adversarial nets. *Advances in neural information processing systems*, 29, 2016.
- Yehu Chen, Annamaria Prati, Jacob Montgomery, and Roman Garnett. A multi-task gaussian process model for inferring time-varying treatment effects in panel data. In *International Conference on Artificial Intelligence and Statistics*, pp. 4068–4088. PMLR, 2023.
- Yunxiao Chen, Xiaoou Li, and Siliang Zhang. Structured latent factor analysis for large-scale data: Identifiability, estimability, and their implications. *Journal of the American Statistical Association*, 115 (532):1756–1770, 2020. doi: 10.1080/01621459.2019.1635485. URL <https://www.tandfonline.com/doi/abs/10.1080/01621459.2019.1635485>.
- Zhengming Chen, Feng Xie, Jie Qiao, Zhifeng Hao, Kun Zhang, and Ruichu Cai. Identification of linear latent variable model with arbitrary distribution. In *Proceedings of the AAAI Conference on Artificial Intelligence*, volume 36, pp. 6350–6357, 2022.
- Debo Cheng, Ziqi Xu, Jiuyong Li, Lin Liu, Jixue Liu, and Thuc Duy Le. Causal inference with conditional instruments using deep generative models. In *Proceedings of the AAAI Conference on Artificial Intelligence*, volume 37, pp. 7122–7130, 2023.
- Lu Cheng, Ruocheng Guo, and Huan Liu. Causal mediation analysis with hidden confounders. *Proceedings of the Fifteenth ACM International Conference on Web Search and Data Mining*, null:null, 2021. doi: 10.1145/3488560.3498407. URL <https://www.semanticscholar.org/paper/81209a11b05b4bd3ca254d6b0519a274d1f79723>.
- Pengyu Cheng, Weituo Hao, Shuyang Dai, Jiachang Liu, Zhe Gan, and Lawrence Carin. Club: A contrastive log-ratio upper bound of mutual information. In *International conference on machine learning*, pp. 1779–1788. PMLR, 2020.
- Victor Chernozhukov, Matt Goldman, Vira Semenova, and Matt Taddy. Orthogonal machine learning for demand estimation: High dimensional causal inference in dynamic panels. *arXiv*, pp. arXiv-1712, 2017.
- Victor Chernozhukov, Denis Chetverikov, Mert Demirer, Esther Duflo, Christian Hansen, Whitney Newey, and James Robins. Double/debiased machine learning for treatment and structural parameters, 2018.
- Victor Chernozhukov, Christian Bailey Hansen, Yuan Liao, and Yinchu Zhu. Inference for heterogeneous effects using low-rank estimations. Technical report, CEMMAP working paper, 2019.
- David Maxwell Chickering, David Heckerman, and Christopher Meek. A bayesian approach to learning bayesian networks with local structure. In *Proceedings of the Thirteenth Conference on Uncertainty in Artificial Intelligence (UAI 1997)*, UAI’97, pp. 80–89, San Francisco, CA, USA, 1997. Morgan Kaufmann Publishers Inc. ISBN 1558604855.

- Kyunghyun Cho, Bart Van Merriënboer, Caglar Gulcehre, Dzmitry Bahdanau, Fethi Bougares, Holger Schwenk, and Yoshua Bengio. Learning phrase representations using rnn encoder-decoder for statistical machine translation. *arXiv preprint arXiv:1406.1078*, 2014.
- Edward Choi, Mohammad Taha Bahadori, Jimeng Sun, Joshua Kulas, Andy Schuetz, and Walter Stewart. Retain: An interpretable predictive model for healthcare using reverse time attention mechanism. *Advances in neural information processing systems*, 29, 2016.
- Zhixuan Chu, Stephen L Rathbun, and Sheng Li. Learning infomax and domain-independent representations for causal effect inference with real-world data. In *Proceedings of the 2022 SIAM International Conference on Data Mining (SDM)*, pp. 433–441. SIAM, 2022.
- Carlos Cinelli and Chad Hazlett. Making sense of sensitivity: Extending omitted variable bias. *Journal of the Royal Statistical Society Series B: Statistical Methodology*, 82(1):39–67, 2020.
- Tom S Clark and Drew A Linzer. Should i use fixed or random effects? *Political science research and methods*, 3(2):399–408, 2015.
- William G Cochran. Some consequences when the assumptions for the analysis of variance are not satisfied. *Biometrics*, 3(1):22–38, 1947.
- Taco Cohen and Max Welling. Group equivariant convolutional networks. In *International conference on machine learning*, pp. 2990–2999. PMLR, 2016.
- Francis S Collins and Harold Varmus. A new initiative on precision medicine. *New England journal of medicine*, 372(9):793–795, 2015.
- Linda M. Collins and Clyde W. Dent and. Omega: A general formulation of the rand index of cluster recovery suitable for non-disjoint solutions. *Multivariate Behavioral Research*, 23(2):231–242, 1988. doi: 10.1207/s15327906mbr2302\\_6. URL [https://doi.org/10.1207/s15327906mbr2302\\_6](https://doi.org/10.1207/s15327906mbr2302_6). PMID: 26764947.
- Joao Paulo Costeira and Takeo Kanade. A multibody factorization method for independently moving objects. *International Journal of Computer Vision*, 29:159–179, 1998.
- Thomas M Cover. *Elements of information theory*. John Wiley & Sons, 1999.
- Daniel Csillag, Claudio Jose Struchiner, and Guilherme Tegoni Goedert. Generalization bounds for causal regression: Insights, guarantees and sensitivity analysis. In *Forty-first International Conference on Machine Learning*, 2024. URL <https://openreview.net/forum?id=TejqrQBv11>.
- Marco Cuturi and Arnaud Doucet. Fast computation of wasserstein barycenters. In *International conference on machine learning*, pp. 685–693. PMLR, 2014.
- Ralph B. D’Agostino. Propensity score methods for bias reduction in the comparison of a treatment to a non-randomized control group. *Statistics in Medicine*, 17:2265–2281, 1998.

- Bin Dai and David Wipf. Diagnosing and enhancing VAE models. In *International Conference on Learning Representations*, 2019. URL <https://openreview.net/forum?id=B1e0X3C9tQ>.
- Imant Daunhawer, Alice Bizeul, Emanuele Palumbo, Alexander Marx, and Julia E Vogt. Identifiability results for multimodal contrastive learning. *arXiv preprint arXiv:2303.09166*, 2023.
- Chandler Davis and W. M. Kahan. The rotation of eigenvectors by a perturbation. iii. *SIAM Journal on Numerical Analysis*, 7(1):1–46, 1970. doi: 10.1137/0707001. URL <https://doi.org/10.1137/0707001>.
- Edward De Brouwer, Javier Gonzalez, and Stephanie Hyland. Predicting the impact of treatments over time with uncertainty aware neural differential equations. In *International Conference on Artificial Intelligence and Statistics*, pp. 4705–4722. PMLR, 2022.
- Clément De Chaisemartin and Xavier d’Haultfoeuille. Two-way fixed effects estimators with heterogeneous treatment effects. *American economic review*, 110(9):2964–2996, 2020.
- Kevin Debeire, Andreas Gerhardus, Jakob Runge, and Veronika Eyring. Bootstrap aggregation and confidence measures to improve time series causal discovery. In *Causal Learning and Reasoning*, pp. 979–1007. PMLR, 2024.
- Tristan Deleu, António Góis, Chris Emezue, Mansi Rankawat, Simon Lacoste-Julien, Stefan Bauer, and Yoshua Bengio. Bayesian structure learning with generative flow networks. In *Uncertainty in Artificial Intelligence*, pp. 518–528. PMLR, 2022.
- Eugene Demidenko. *Mixed models: theory and applications with R*. John Wiley & Sons, 2013.
- Zizhen Deng, Xiaolong Zheng, Hu Tian, and Daniel Dajun Zeng. Deep causal learning: representation, discovery and inference. *arXiv preprint arXiv:2211.03374*, 2022.
- Shachi Deshpande, Kaiwen Wang, Dhruv Sreenivas, Zheng Li, and Volodymyr Kuleshov. Deep multi-modal structural equations for causal effect estimation with unstructured proxies. *Advances in Neural Information Processing Systems*, 35:10931–10944, 2022.
- Anish Dhir, Matthew Ashman, James Requeima, and Mark van der Wilk. A meta-learning approach to bayesian causal discovery. In *The Thirteenth International Conference on Learning Representations*, 2025. URL <https://openreview.net/forum?id=eeJz7eDWK0>.
- Gianni Di Pillo. Exact penalty methods. In *Algorithms for continuous optimization: the state of the art*, pp. 209–253. Springer, 1994.
- Reinhard Diestel. *Graph theory*, volume 173. Springer Nature, 2025.
- Peng Ding and Fan Li. Causal inference: A generalized missing data approach. *Statistical Science*, 33(2): 214–237, 2018.
- Kien Do and Truyen Tran. Theory and evaluation metrics for learning disentangled representations. In *International Conference on Learning Representations*, 2020. URL <https://openreview.net/forum?id=HJgK0h4Ywr>.

- Yinpeng Dong, Hang Su, Jun Zhu, and Bo Zhang. Improving interpretability of deep neural networks with semantic information. In *Proceedings of the IEEE Conference on Computer Vision and Pattern Recognition (CVPR)*, July 2017.
- Monroe D Donsker and SR Srinivasa Varadhan. Asymptotic evaluation of certain markov process expectations for large time. iv. *Communications on pure and applied mathematics*, 36(2):183–212, 1983.
- Alexander D’Amour. On multi-cause approaches to causal inference with unobserved counfounding: Two cautionary failure cases and a promising alternative. In *The 22nd International Conference on Artificial Intelligence and Statistics*, pp. 3478–3486. PMLR, 2019a.
- Alexander D’Amour. Comment: Reflections on the deconfounder. *Journal of the American Statistical Association*, 114(528):1597–1601, 2019b.
- Alexander D’Amour, Peng Ding, Avi Feller, Lihua Lei, and Jasjeet Sekhon. Overlap in observational studies with high-dimensional covariates. *Journal of Econometrics*, 221(2):644–654, 2021.
- Ehsan Elhamifar and René Vidal. Clustering disjoint subspaces via sparse representation. In *2010 IEEE International Conference on Acoustics, Speech and Signal Processing*, pp. 1926–1929. IEEE, 2010.
- Ehsan Elhamifar and René Vidal. Sparse subspace clustering: Algorithm, theory, and applications. *IEEE transactions on pattern analysis and machine intelligence*, 35(11):2765–2781, 2013.
- Chris Chinenye Emezue, Alexandre Drouin, Tristan Deleu, Stefan Bauer, and Yoshua Bengio. Benchmarking bayesian causal discovery methods for downstream treatment effect estimation. In *ICML 2023 Workshop on Structured Probabilistic Inference & Generative Modeling*, 2023. URL <https://openreview.net/forum?id=9aDnWNPyeC>.
- Fabian Falck, Haoting Zhang, Matthew Willetts, George Nicholson, Christopher Yau, and Chris C Holmes. Multi-facet clustering variational autoencoders. *Advances in Neural Information Processing Systems*, 34:8676–8690, 2021.
- William Falcon and The PyTorch Lightning team. Pytorch lightning. <https://github.com/PyTorchLightning/pytorch-lightning>, 2019. Version 1.0.
- Jianqing Fan, Qiwei Yao, and Zongwu Cai. Adaptive varying-coefficient linear models. *Journal of the Royal Statistical Society. Series B (Statistical Methodology)*, 65(1):57–80, 2003. ISSN 13697412, 14679868. URL <http://www.jstor.org/stable/3088826>.
- Junpeng Fang, Qing Cui, Gongduo Zhang, Caizhi Tang, Lihong Gu, Longfei Li, Jinjie Gu, Jun Zhou, and Fei Wu. Alleviating matching bias in marketing recommendations. In *Proceedings of the 46th International ACM SIGIR Conference on Research and Development in Information Retrieval*, pp. 3359–3363, 2023.
- Carlos Fernández-Loría and Foster Provost. Causal classification: Treatment effect estimation vs. outcome prediction. *The Journal of Machine Learning Research*, 23(1):2573–2607, 2022.

- Garrett M Fitzmaurice, Nan M Laird, and James H Ware. *Applied longitudinal analysis*, volume 998. John Wiley & Sons, 2012.
- Dylan J. Foster and Vasilis Syrgkanis. Orthogonal statistical learning. *The Annals of Statistics*, 51(3):879 – 908, 2023. doi: 10.1214/23-AOS2258. URL <https://doi.org/10.1214/23-AOS2258>.
- Constantine Frangakis and Donald B. Rubin. Principal stratification in causal inference. *Biometrics*, 58, 2002.
- Dennis Frauen, Tobias Hatt, Valentyn Melnychuk, and Stefan Feuerriegel. Estimating average causal effects from patient trajectories. In *Proceedings of the AAAI Conference on Artificial Intelligence*, volume 37, pp. 7586–7594, 2023.
- Simon Freyaldenhoven, Shikun Ke, Dingyi Li, and José Luis Montiel Olea. On the testability of the anchor-words assumption in topic models, March 2025. Available at SSRN: <https://ssrn.com/abstract=5220497> or <http://dx.doi.org/10.21799/frbp.wp.2025.14>.
- Nir Friedman and Daphne Koller. Being bayesian about network structure. a bayesian approach to structure discovery in bayesian networks. *Machine learning*, 50:95–125, 2003.
- Hao Fu, Chunyuan Li, Xiaodong Liu, Jianfeng Gao, Asli Celikyilmaz, and Lawrence Carin. Cyclical annealing schedule: A simple approach to mitigating kl vanishing. *arXiv preprint arXiv:1903.10145*, 2019.
- João Gama, Indrė Žliobaitė, Albert Bifet, Mykola Pechenizkiy, and Abdelhamid Bouchachia. A survey on concept drift adaptation. *ACM computing surveys (CSUR)*, 46(4):1–37, 2014.
- Yaroslav Ganin, Evgeniya Ustinova, Hana Ajakan, Pascal Germain, Hugo Larochelle, François Laviolette, Mario Marchand, and Victor Lempitsky. Domain-adversarial training of neural networks. *The journal of machine learning research*, 17(1):2096–2030, 2016.
- Élisabeth Gassiat, Alice Cleynen, and Stephane Robin. Inference in finite state space non parametric hidden markov models and applications. *Statistics and Computing*, 26:61–71, 2016.
- Andrew Gelman, John B Carlin, Hal S Stern, and Donald B Rubin. *Bayesian data analysis*. Chapman and Hall/CRC, 1995.
- Changran Geng, Harald Paganetti, and Clemens Grassberger. Prediction of treatment response for combined chemo-and radiation therapy for non-small cell lung cancer patients using a bio-mathematical model. *Scientific reports*, 7(1):1–12, 2017.
- Amirata Ghorbani, James Wexler, James Y Zou, and Been Kim. Towards automatic concept-based explanations. *Advances in neural information processing systems*, 32, 2019.
- Alison L. Gibbs and Francis Edward Su. On choosing and bounding probability metrics. *International Statistical Review / Revue Internationale de Statistique*, 70(3):419–435, 2002. ISSN 03067734, 17515823. URL <http://www.jstor.org/stable/1403865>.

- Nicolas Gillis. *Nonnegative Matrix Factorization*. Data Science. Society for Industrial and Applied Mathematics, Philadelphia, PA, 2020. ISBN 978-1-61197-640-3. doi: 10.1137/1.9781611976410. URL <https://epubs.siam.org/doi/book/10.1137/1.9781611976410>.
- Laurent Girin, Simon Leglaive, Xiaoyu Bie, Julien Diard, Thomas Hueber, and Xavier Alameda-Pineda. Dynamical variational autoencoders: A comprehensive review. *ArXiv*, abs/2008.12595, 2021.
- Alvina Goh and René Vidal. Segmenting motions of different types by unsupervised manifold clustering. In *2007 IEEE Conference on Computer Vision and Pattern Recognition*, pp. 1–6. IEEE, 2007.
- Andrew Goodman-Bacon. Difference-in-differences with variation in treatment timing. *Journal of econometrics*, 225(2):254–277, 2021.
- Ali Grami. Chapter 9 - relations. In Ali Grami (ed.), *Discrete Mathematics*, pp. 155–176. Academic Press, 2023. ISBN 978-0-12-820656-0. doi: <https://doi.org/10.1016/B978-0-12-820656-0.00009-5>. URL <https://www.sciencedirect.com/science/article/pii/B9780128206560000095>.
- Arthur Gretton, Karsten M Borgwardt, Malte J Rasch, Bernhard Schölkopf, and Alexander Smola. A kernel two-sample test. *The Journal of Machine Learning Research*, 13(1):723–773, 2012.
- Michael Gutmann and Aapo Hyvärinen. Noise-contrastive estimation: A new estimation principle for unnormalized statistical models. In *Proceedings of the thirteenth international conference on artificial intelligence and statistics*, pp. 297–304. JMLR Workshop and Conference Proceedings, 2010.
- Michael U Gutmann and Aapo Hyvärinen. Noise-contrastive estimation of unnormalized statistical models, with applications to natural image statistics. *Journal of machine learning research*, 13(2), 2012.
- Joseph F Hair Jr and Marko Sarstedt. Data, measurement, and causal inferences in machine learning: opportunities and challenges for marketing. *Journal of Marketing Theory and Practice*, 29(1):65–77, 2021.
- Hermanni Hälvä and Aapo Hyvärinen. Hidden markov nonlinear ica: Unsupervised learning from nonstationary time series. In *Conference on Uncertainty in Artificial Intelligence*, 2020. URL <https://api.semanticscholar.org/CorpusID:219965657>.
- Hermanni Hälvä, Sylvain Le Corff, Luc Lehéricy, Jonathan So, Yongjie Zhu, Elisabeth Gassiat, and Aapo Hyvarinen. Disentangling identifiable features from noisy data with structured nonlinear ica. *Advances in Neural Information Processing Systems*, 34:1624–1633, 2021.
- Jun Han, Martin Renqiang Min, Ligong Han, Li Erran Li, and Xuan Zhang. Disentangled recurrent wasserstein autoencoder. In *International Conference on Learning Representations*, 2021. URL <https://openreview.net/forum?id=07ms4LFdsX>.
- Jason Hartford, Greg Lewis, Kevin Leyton-Brown, and Matt Taddy. Deep iv: A flexible approach for counterfactual prediction. In *International Conference on Machine Learning*, pp. 1414–1423. PMLR, 2017.

- Uzma Hasan, Emam Hossain, and Md Osman Gani. A survey on causal discovery methods for i.i.d. and time series data. *Transactions on Machine Learning Research*, 2023. ISSN 2835-8856. URL <https://openreview.net/forum?id=YdMrdhGx9y>. Survey Certification.
- Abolfazl Hashemi and Haris Vikalo. Evolutionary self-expressive models for subspace clustering. *IEEE Journal of Selected Topics in Signal Processing*, 12(6):1534–1546, 2018.
- Negar Hassanpour and Russell Greiner. Learning disentangled representations for counterfactual regression. In *International Conference on Learning Representations*, 2019a.
- Negar Hassanpour and Russell Greiner. Counterfactual regression with importance sampling weights. In *IJCAI*, pp. 5880–5887, 2019b.
- Trevor Hastie, Robert Tibshirani, Jerome H Friedman, and Jerome H Friedman. *The elements of statistical learning: data mining, inference, and prediction*, volume 2. Springer, 2009.
- Tobias Hatt and Stefan Feuerriegel. Sequential deconfounding for causal inference with unobserved confounders. *arXiv preprint arXiv:2104.09323*, 2021.
- Tobias Hatt and Stefan Feuerriegel. Sequential deconfounding for causal inference with unobserved confounders. In Francesco Locatello and Vanessa Didelez (eds.), *Proceedings of the Third Conference on Causal Learning and Reasoning*, volume 236 of *Proceedings of Machine Learning Research*, pp. 934–956. PMLR, 01–03 Apr 2024. URL <https://proceedings.mlr.press/v236/hatt24a.html>.
- David Heckerman, Christopher Meek, and Gregory Cooper. A bayesian approach to causal discovery. *Innovations in Machine Learning: Theory and Applications*, pp. 1–28, 2006.
- Olivier Henaff. Data-efficient image recognition with contrastive predictive coding. In *International conference on machine learning*, pp. 4182–4192. PMLR, 2020.
- Miguel A Hernán and James M Robins. Instruments for causal inference: an epidemiologist’s dream? *Epidemiology*, 17(4):360–372, 2006.
- Miguel A. Hernán and James M. Robins. *Causal Inference: What If*. Chapman & Hall/CRC, 2020. URL <https://www.hsph.harvard.edu/miguel-hernan/causal-inference-book/>.
- Robins JM Hernán MA. *Causal Inference: What If*. Boca Raton: Chapman & Hall/CRC, 2020.
- Tom Heskes, Evi Sijben, Ioan Gabriel Bucur, and Tom Claassen. Causal shapley values: Exploiting causal knowledge to explain individual predictions of complex models. *Advances in neural information processing systems*, 33:4778–4789, 2020.
- Irina Higgins, Loic Matthey, Arka Pal, Christopher P Burgess, Xavier Glorot, Matthew M Botvinick, Shakir Mohamed, and Alexander Lerchner. beta-vae: Learning basic visual concepts with a constrained variational framework. *ICLR (Poster)*, 3, 2017.



- Jennifer L Hill. Bayesian nonparametric modeling for causal inference. *Journal of Computational and Graphical Statistics*, 20(1):217–240, 2011.
- Keisuke Hirano and Guido W Imbens. Estimation of causal effects using propensity score weighting: An application to data on right heart catheterization. *Health Services and Outcomes research methodology*, 2:259–278, 2001.
- Çağlar Hızlı, ST John, Anne Tuulikki Juuti, Tuure Tapani Saarinen, Kirsi Hannele Pietiläinen, and Pekka Marttinen. Causal modeling of policy interventions from treatment-outcome sequences. In *International Conference on Machine Learning*, pp. 13050–13084. PMLR, 2023.
- R Devon Hjelm, Alex Fedorov, Samuel Lavoie-Marchildon, Karan Grewal, Phil Bachman, Adam Trischler, and Yoshua Bengio. Learning deep representations by mutual information estimation and maximization. In *International Conference on Learning Representations*, 2019. URL <https://openreview.net/forum?id=Bklr3j0cKX>.
- Paul W Holland. Statistics and causal inference. *Journal of the American statistical Association*, 81(396):945–960, 1986.
- Roger A Horn and Charles R Johnson. *Matrix analysis*. Cambridge university press, 2012a.
- Roger A Horn and Charles R Johnson. *Matrix analysis*. Cambridge university press, 2012b.
- Cheng Hsiao. Panel data analysis—advantages and challenges. *Test*, 16(1):1–22, 2007.
- Kejun Huang, Xiao Fu, and Nicholas D. Sidiropoulos. Anchor-free correlated topic modeling: Identifiability and algorithm. In *Advances in Neural Information Processing Systems*, volume 29, pp. 1786–1794, 2016. URL <https://papers.nips.cc/paper/6308-anchor-free-correlated-topic-modeling-identifiability-and-algorithm.pdf>.
- Zenan Huang, Haobo Wang, Junbo Zhao, and Nenggan Zheng. Latent processes identification from multi-view time series. In Edith Elkind (ed.), *Proceedings of the Thirty-Second International Joint Conference on Artificial Intelligence, IJCAI-23*, pp. 3848–3856. International Joint Conferences on Artificial Intelligence Organization, 8 2023. doi: 10.24963/ijcai.2023/428. URL <https://doi.org/10.24963/ijcai.2023/428>. Main Track.
- Iris AM Huijben, Wouter Kool, Max B Paulus, and Ruud JG Van Sloun. A review of the gumbel-max trick and its extensions for discrete stochasticity in machine learning. *IEEE transactions on pattern analysis and machine intelligence*, 45(2):1353–1371, 2022.
- Michael F Hutchinson. A stochastic estimator of the trace of the influence matrix for laplacian smoothing splines. *Communications in Statistics-Simulation and Computation*, 18(3):1059–1076, 1989.
- Noorie Hyun, Abisola E Idu, Andrea J Cook, and Jennifer F Bobb. Increased risk of type i errors for detecting heterogeneity of treatment effects in cluster-randomized trials using mixed-effect models. *arXiv preprint arXiv:2407.06466*, 2024.

- Aapo Hyvarinen and Hiroshi Morioka. Unsupervised feature extraction by time-contrastive learning and nonlinear ica. *Advances in neural information processing systems*, 29, 2016.
- Aapo Hyvarinen and Hiroshi Morioka. Nonlinear ica of temporally dependent stationary sources. In *Artificial Intelligence and Statistics*, pp. 460–469. PMLR, 2017.
- Aapo Hyvärinen and Petteri Pajunen. Nonlinear independent component analysis: Existence and uniqueness results. *Neural networks*, 12(3):429–439, 1999.
- Aapo Hyvarinen, Hiroaki Sasaki, and Richard Turner. Nonlinear ica using auxiliary variables and generalized contrastive learning. In *The 22nd international conference on artificial intelligence and statistics*, pp. 859–868. PMLR, 2019a.
- Aapo Hyvarinen, Hiroaki Sasaki, and Richard Turner. Nonlinear ica using auxiliary variables and generalized contrastive learning. In *The 22nd International Conference on Artificial Intelligence and Statistics*, pp. 859–868. PMLR, 2019b.
- Duligur Ibeling and Thomas Icard. Comparing causal frameworks: Potential outcomes, structural models, graphs, and abstractions. In *Thirty-seventh Conference on Neural Information Processing Systems*, 2023. URL <https://openreview.net/forum?id=1zKRwh5Rl2>.
- Kosuke Imai and Zhichao Jiang. Comment: The challenges of multiple causes. *Journal of the American Statistical Association*, 114(528):1605–1610, 2019.
- Kosuke Imai and In Song Kim. When should we use unit fixed effects regression models for causal inference with longitudinal data? *American Journal of Political Science*, 63(2):467–490, 2019.
- Guido Imbens. Instrumental variables: An econometrician’s perspective. Technical report, National Bureau of Economic Research, 2014.
- Guido W Imbens. Causal inference in the social sciences. *Annual Review of Statistics and Its Application*, 11, 2024.
- Guido W Imbens and Donald B Rubin. *Causal inference in statistics, social, and biomedical sciences*. Cambridge University Press, 2015.
- Alexander Immer, Tycho van der Ouderaa, Gunnar Rätsch, Vincent Fortuin, and Mark van der Wilk. Invariance learning in deep neural networks with differentiable laplace approximations. *Advances in Neural Information Processing Systems*, 35:12449–12463, 2022.
- Laurent Jacob, Guillaume Obozinski, and Jean-Philippe Vert. Group lasso with overlap and graph lasso. In *Proceedings of the 26th annual international conference on machine learning*, pp. 433–440, 2009.
- Anil K Jain and Richard C Dubes. *Algorithms for clustering data*. Prentice-Hall, Inc., 1988.
- Eric Jang, Shixiang Gu, and Ben Poole. Categorical reparameterization with gumbel-softmax. In *International Conference on Learning Representations*, 2017. URL <https://openreview.net/forum?id=rkE3y85ee>.

- Andrew Jesson, Sören Mindermann, Uri Shalit, and Yarin Gal. Identifying causal-effect inference failure with uncertainty-aware models. *Advances in Neural Information Processing Systems*, 33:11637–11649, 2020.
- Andrew Jesson, Sören Mindermann, Yarin Gal, and Uri Shalit. Quantifying ignorance in individual-level causal-effect estimates under hidden confounding. In *International Conference on Machine Learning*, pp. 4829–4838. PMLR, 2021.
- Pan Ji, Tong Zhang, Hongdong Li, Mathieu Salzmann, and Ian Reid. Deep subspace clustering networks. *Advances in neural information processing systems*, 30, 2017.
- Song Jiang, Zijie Huang, Xiao Luo, and Yizhou Sun. Cf-gode: Continuous-time causal inference for multi-agent dynamical systems. In *Proceedings of the 29th ACM SIGKDD Conference on Knowledge Discovery and Data Mining, KDD '23*, pp. 997–1009, New York, NY, USA, 2023. Association for Computing Machinery. ISBN 9798400701030. doi: 10.1145/3580305.3599272. URL <https://doi.org/10.1145/3580305.3599272>.
- Zhuxi Jiang, Yin Zheng, Huachun Tan, Bangsheng Tang, and Hanning Zhou. Variational deep embedding: an unsupervised and generative approach to clustering. In *Proceedings of the 26th International Joint Conference on Artificial Intelligence, IJCAI'17*, pp. 1965–1972. AAAI Press, 2017. ISBN 9780999241103.
- Wei Jin, Yang Ni, Amanda B Spence, Leah H Rubin, and Yanxun Xu. Directed cyclic graphs for simultaneous discovery of time-lagged and instantaneous causality from longitudinal data using instrumental variables. *Journal of Machine Learning Research*, 26(22):1–62, 2025.
- Fredrik Johansson, Uri Shalit, and David Sontag. Learning representations for counterfactual inference. In *International conference on machine learning*, pp. 3020–3029. PMLR, 2016.
- Fredrik D Johansson, Nathan Kallus, Uri Shalit, and David Sontag. Learning weighted representations for generalization across designs. *arXiv preprint arXiv:1802.08598*, 2018.
- Fredrik D Johansson, David Sontag, and Rajesh Ranganath. Support and invertibility in domain-invariant representations. In *The 22nd International Conference on Artificial Intelligence and Statistics*, pp. 527–536. PMLR, 2019.
- Fredrik D Johansson, Uri Shalit, Nathan Kallus, and David Sontag. Generalization bounds and representation learning for estimation of potential outcomes and causal effects. *The Journal of Machine Learning Research*, 23(1):7489–7538, 2022.
- Alistair EW Johnson, Tom J Pollard, Lu Shen, Li-wei H Lehman, Mengling Feng, Mohammad Ghassemi, Benjamin Moody, Peter Szolovits, Leo Anthony Celi, and Roger G Mark. Mimic-iii, a freely accessible critical care database. *Scientific data*, 3(1):1–9, 2016.
- Michael I Jordan and Tom M Mitchell. Machine learning: Trends, perspectives, and prospects. *Science*, 349(6245):255–260, 2015.

- Yonghan Jung, Jin Tian, and Elias Bareinboim. Learning causal effects via weighted empirical risk minimization. *Advances in neural information processing systems*, 33:12697–12709, 2020.
- Olav Kallenberg. Foundations of modern probability. *Probability Theory and Stochastic Modelling*, 2021.
- Nathan Kallus. Balanced policy evaluation and learning. *Advances in neural information processing systems*, 31, 2018.
- Nathan Kallus. Deepmatch: Balancing deep covariate representations for causal inference using adversarial training. In *International Conference on Machine Learning*, pp. 5067–5077. PMLR, 2020.
- Nathan Kallus. What’s the harm? sharp bounds on the fraction negatively affected by treatment. *Advances in Neural Information Processing Systems*, 35:15996–16009, 2022.
- Nathan Kallus, Xiaojie Mao, and Angela Zhou. Interval estimation of individual-level causal effects under unobserved confounding. In *The 22nd international conference on artificial intelligence and statistics*, pp. 2281–2290. PMLR, 2019.
- Ken-ichi Kanatani. Motion segmentation by subspace separation and model selection. In *Proceedings Eighth IEEE International Conference on computer Vision. ICCV 2001*, volume 2, pp. 586–591. IEEE, 2001.
- Emilie Kaufmann, Thomas Bonald, and Marc Lelarge. A spectral algorithm with additive clustering for the recovery of overlapping communities in networks. *Theoretical Computer Science*, 742:3–26, 2018.
- Ilyes Khemakhem, Diederik Kingma, Ricardo Monti, and Aapo Hyvarinen. Variational autoencoders and nonlinear ica: A unifying framework. In *International conference on artificial intelligence and statistics*, pp. 2207–2217. PMLR, 2020.
- Diederik P Kingma and Jimmy Ba. Adam: A method for stochastic optimization. *arXiv preprint arXiv:1412.6980*, 2014.
- Günter Klambauer, Thomas Unterthiner, Andreas Mayr, and Sepp Hochreiter. Self-normalizing neural networks. *Advances in neural information processing systems*, 30, 2017.
- David A. Klindt, Lukas Schott, Yash Sharma, Ivan Ustyuzhaninov, Wieland Brendel, Matthias Bethge, and Dylan Paiton. Towards nonlinear disentanglement in natural data with temporal sparse coding. In *International Conference on Learning Representations*, 2021. URL <https://openreview.net/forum?id=EbIDjBynYJ8>.
- Pang Wei Koh, Thao Nguyen, Yew Siang Tang, Stephen Mussmann, Emma Pierson, Been Kim, and Percy Liang. Concept bottleneck models. In *International conference on machine learning*, pp. 5338–5348. PMLR, 2020.
- Daphane Koller. Probabilistic graphical models: Principles and techniques, 2009.

- Aneesh Komanduri, Yongkai Wu, Feng Chen, and Xintao Wu. Learning causally disentangled representations via the principle of independent causal mechanisms. *arXiv preprint arXiv:2306.01213*, 2023.
- Risi Kondor and Shubhendu Trivedi. On the generalization of equivariance and convolution in neural networks to the action of compact groups. In *International conference on machine learning*, pp. 2747–2755. PMLR, 2018.
- Hans-Peter Kriegel, Peer Kröger, Irene Ntoutsi, and Arthur Zimek. Towards subspace clustering on dynamic data: an incremental version of predecon. In *Proceedings of the First International Workshop on Novel Data Stream Pattern Mining Techniques*, StreamKDD '10, pp. 31–38, New York, NY, USA, 2010. Association for Computing Machinery. ISBN 9781450302265. doi: 10.1145/1833280.1833285. URL <https://doi.org/10.1145/1833280.1833285>.
- Rahul G Krishnan, Uri Shalit, and David Sontag. Deep kalman filters. *arXiv preprint arXiv:1511.05121*, 2015.
- Da Kuang, Chris Ding, and Haesun Park. Symmetric nonnegative matrix factorization for graph clustering. In *Proceedings of the 2012 SIAM International Conference on Data Mining (SDM)*, pp. 106–117, 2012. doi: 10.1137/1.9781611972825.10. URL <https://epubs.siam.org/doi/10.1137/1.9781611972825.10>.
- Da Kuang, Sangwoon Yun, and Haesun Park. Symnmf: nonnegative low-rank approximation of a similarity matrix for graph clustering. *J. of Global Optimization*, 62(3):545–574, July 2015. ISSN 0925-5001. doi: 10.1007/s10898-014-0247-2. URL <https://doi.org/10.1007/s10898-014-0247-2>.
- Abhishek Kumar, Prasanna Sattigeri, and Avinash Balakrishnan. VARIATIONAL INFERENCE OF DISENTANGLED LATENT CONCEPTS FROM UNLABELED OBSERVATIONS. In *International Conference on Learning Representations*, 2018. URL <https://openreview.net/forum?id=H1kG7GZAW>.
- Manabu Kuroki and J. Pearl. Measurement bias and effect restoration in causal inference. *Biometrika*, 101: 423–437, 2014. doi: 10.1093/BIOMET/AST066. URL <https://www.semanticscholar.org/paper/19dabe9fdb82d74a584f5ece882f5825e4effdb>.
- Milan Kuzmanovic, Tobias Hatt, and Stefan Feuerriegel. Deconfounding temporal autoencoder: estimating treatment effects over time using noisy proxies. In *Machine Learning for Health*, pp. 143–155. PMLR, 2021.
- Sébastien Lachapelle, Pau Rodriguez, Yash Sharma, Katie E Everett, Rémi Le Priol, Alexandre Lacoste, and Simon Lacoste-Julien. Disentanglement via mechanism sparsity regularization: A new principle for nonlinear ica. In *Conference on Causal Learning and Reasoning*, pp. 428–484. PMLR, 2022a.
- Sébastien Lachapelle, Pau Rodriguez, Yash Sharma, Katie E Everett, Rémi Le Priol, Alexandre Lacoste, and Simon Lacoste-Julien. Disentanglement via mechanism sparsity regularization: A new principle for nonlinear ica. In *Conference on Causal Learning and Reasoning*, pp. 428–484. PMLR, 2022b.

- Nan M Laird and Christoph Lange. *The fundamentals of modern statistical genetics*. Springer, 2011.
- Andrea Lancichinetti, Santo Fortunato, and János Kertész. Detecting the overlapping and hierarchical community structure in complex networks. *New Journal of Physics*, 11(3):033015, mar 2009. doi: 10.1088/1367-2630/11/3/033015. URL <https://dx.doi.org/10.1088/1367-2630/11/3/033015>.
- S. L. Lauritzen, A. P. Dawid, B. N. Larsen, and H.-G. Leimer. Independence properties of directed markov fields. *Networks*, 20(5):491–505, 1990. doi: <https://doi.org/10.1002/net.3230200503>. URL <https://onlinelibrary.wiley.com/doi/abs/10.1002/net.3230200503>.
- Steffen L Lauritzen. *Graphical models*, volume 17. Clarendon Press, 1996.
- Yann LeCun, Yoshua Bengio, and Geoffrey Hinton. Deep learning. *nature*, 521(7553):436–444, 2015.
- Michel Ledoux. *The concentration of measure phenomenon*. Number 89. American Mathematical Soc., 2001.
- Lihua Lei and Emmanuel J Candès. Conformal inference of counterfactuals and individual treatment effects. *Journal of the Royal Statistical Society Series B: Statistical Methodology*, 83(5):911–938, 2021.
- Greg Lewis and Vasilis Syrgkanis. Double/debiased machine learning for dynamic treatment effects. In A. Beygelzimer, Y. Dauphin, P. Liang, and J. Wortman Vaughan (eds.), *Advances in Neural Information Processing Systems*, 2021. URL <https://openreview.net/forum?id=StKuQ0-dltN>.
- Fan Li, Kari Lock Morgan, and Alan M Zaslavsky. Balancing covariates via propensity score weighting. *Journal of the American Statistical Association*, 113(521):390–400, 2018a.
- Rui Li, Stephanie Hu, Mingyu Lu, Yuria Utsumi, Prithwish Chakraborty, Daby M. Sow, Piyush Madan, Jun Li, Mohamed F. Ghalwash, Zach Shahn, and Li wei H. Lehman. G-net: a recurrent network approach to g-computation for counterfactual prediction under a dynamic treatment regime. In *ML4H@NeurIPS*, 2021.
- Ya Li, Xinmei Tian, Mingming Gong, Yajing Liu, Tongliang Liu, Kun Zhang, and Dacheng Tao. Deep domain generalization via conditional invariant adversarial networks. In *Proceedings of the European Conference on Computer Vision (ECCV)*, pp. 624–639, 2018b.
- Yingzhen Li and Stephan Mandt. Disentangled sequential autoencoder. In *International Conference on Machine Learning*, 2018.
- Zijian Li, Ruichu Cai, Zhenhui Yang, Haiqin Huang, Guangyi Chen, Yifan Shen, Zhengming Chen, Xiangchen Song, Zhifeng Hao, and Kun Zhang. When and how: Learning identifiable latent states for nonstationary time series forecasting. *arXiv preprint arXiv:2402.12767*, 2024.
- Paul Pu Liang, Zihao Deng, Martin Ma, James Zou, Louis-Philippe Morency, and Ruslan Salakhutdinov. Factorized contrastive learning: Going beyond multi-view redundancy. In *Advances in Neural Information Processing Systems*, 2023.

- Bryan Lim. Forecasting treatment responses over time using recurrent marginal structural networks. *advances in neural information processing systems*, 31, 2018a.
- Bryan Lim. Forecasting treatment responses over time using recurrent marginal structural networks. *advances in neural information processing systems*, 31, 2018b.
- Pantelis Linardatos, Vasilis Papastefanopoulos, and Sotiris Kotsiantis. Explainable ai: A review of machine learning interpretability methods. *Entropy*, 23(1), 2021. ISSN 1099-4300. doi: 10.3390/e23010018. URL <https://www.mdpi.com/1099-4300/23/1/18>.
- Ralph Linsker. Self-organization in a perceptual network. *Computer*, 21(3):105–117, 1988.
- Guangcan Liu, Zhouchen Lin, Shuicheng Yan, Ju Sun, Yong Yu, and Yi Ma. Robust recovery of subspace structures by low-rank representation. *IEEE transactions on pattern analysis and machine intelligence*, 35(1):171–184, 2012.
- Yuhang Liu, Zhen Zhang, Dong Gong, Biwei Huang, Mingming Gong, Anton van den Hengel, Kun Zhang, and Javen Qinfeng Shi. Revealing multimodal contrastive representation learning through latent partial causal models. *arXiv preprint arXiv:2402.06223*, 2024.
- Francesco Locatello, Stefan Bauer, Mario Lucic, Gunnar Raetsch, Sylvain Gelly, Bernhard Schölkopf, and Olivier Bachem. Challenging common assumptions in the unsupervised learning of disentangled representations. In *international conference on machine learning*, pp. 4114–4124. PMLR, 2019.
- Marian Longa and João F Henriques. Interpretable representation learning from videos using nonlinear priors. *arXiv preprint arXiv:2410.18539*, 2024.
- Michael J Lopez and Roee Gutman. Estimation of causal effects with multiple treatments: a review and new ideas. *Statistical Science*, pp. 432–454, 2017.
- Lars Lorch, Jonas Rothfuss, Bernhard Schölkopf, and Andreas Krause. Dibs: Differentiable bayesian structure learning. *Advances in Neural Information Processing Systems*, 34:24111–24123, 2021.
- Ilya Loshchilov and Frank Hutter. Decoupled weight decay regularization. *arXiv preprint arXiv:1711.05101*, 2017.
- Christos Louizos, Uri Shalit, Joris M Mooij, David Sontag, Richard Zemel, and Max Welling. Causal effect inference with deep latent-variable models. *Advances in neural information processing systems*, 30, 2017.
- Can-Yi Lu, Hai Min, Zhong-Qiu Zhao, Lin Zhu, De-Shuang Huang, and Shuicheng Yan. Robust and efficient subspace segmentation via least squares regression. In *Computer Vision–ECCV 2012: 12th European Conference on Computer Vision, Florence, Italy, October 7-13, 2012, Proceedings, Part VII 12*, pp. 347–360. Springer, 2012.

- Danni Lu, Chenyang Tao, Junya Chen, Fan Li, Feng Guo, and Lawrence Carin. Reconsidering generative objectives for counterfactual reasoning. *Advances in Neural Information Processing Systems*, 33: 21539–21553, 2020.
- James Lucas, George Tucker, Roger B Grosse, and Mohammad Norouzi. Don’t blame the elbo! a linear vae perspective on posterior collapse. *Advances in Neural Information Processing Systems*, 32, 2019.
- Amir Mohammad Karimi Mamaghan, Panagiotis Tigas, Karl Henrik Johansson, Yarin Gal, Yashas Annadani, and Stefan Bauer. Challenges and considerations in the evaluation of bayesian causal discovery. In *Forty-first International Conference on Machine Learning*, 2024. URL <https://openreview.net/forum?id=bqgkBDkNs>.
- Myrl G Marmarelis, Greg Ver Steeg, Aram Galstyan, and Fred Morstatter. Ensembled prediction intervals for causal outcomes under hidden confounding. In *Causal Learning and Reasoning*, pp. 18–40. PMLR, 2024.
- Stefan Matthes, Zhiwei Han, and Hao Shen. Towards a unified framework of contrastive learning for disentangled representations. *Advances in Neural Information Processing Systems*, 36:67459–67470, 2023.
- P. McCullagh and J.A. Nelder. *Generalized Linear Models, Second Edition*. Chapman and Hall/CRC Monographs on Statistics and Applied Probability Series. Chapman & Hall, 1989. ISBN 9780412317606. URL [http://books.google.com/books?id=h9kFH2\\_FfBkC](http://books.google.com/books?id=h9kFH2_FfBkC).
- Charles E McCulloch and Shayle R Searle. *Generalized, linear, and mixed models*. John Wiley & Sons, 2004.
- Aaron F McDaid, Derek Greene, and Neil Hurley. Normalized mutual information to evaluate overlapping community finding algorithms. *arXiv preprint arXiv:1110.2515*, 2011.
- Nicolai Meinshausen and Bin Yu. Lasso-type recovery of sparse representations for high-dimensional data. *The Annals of Statistics*, 37(1):246 – 270, 2009. doi: 10.1214/07-AOS582. URL <https://doi.org/10.1214/07-AOS582>.
- Valentyn Melnychuk, Dennis Frauen, and Stefan Feuerriegel. Causal transformer for estimating counterfactual outcomes. In *International Conference on Machine Learning*, pp. 15293–15329. PMLR, 2022.
- Xiao-Li Meng. Posterior predictive  $p$ -values. *The annals of statistics*, 22(3):1142–1160, 1994.
- W. Miao, Z. Geng, and E. T. Tchetgen Tchetgen. Identifying causal effects with proxy variables of an unmeasured confounder. *Biometrika*, 105 4:987–993, 2016. doi: 10.1093/BIOMET/ASY038. URL <https://www.semanticscholar.org/paper/09341c95b87b2ab7c9a8a063b786f2c396687a10>.



- Haben Michael, Yifan Cui, Scott A Lorch, and Eric J Tchetgen Tchetgen. Instrumental variable estimation of marginal structural mean models for time-varying treatment. *Journal of the American Statistical Association*, 119(546):1240–1251, 2024.
- Vitali D Milman and Gideon Schechtman. *Asymptotic theory of finite dimensional normed spaces: Isoperimetric inequalities in riemannian manifolds*, volume 1200. Springer Science & Business Media, 1986.
- Graziano Mita, Maurizio Filippone, and Pietro Michiardi. An identifiable double vae for disentangled representations. In *International Conference on Machine Learning*, pp. 7769–7779. PMLR, 2021.
- Gemma E Moran, Dhanya Sridhar, Yixin Wang, and David M Blei. Identifiable deep generative models via sparse decoding. *arXiv preprint arXiv:2110.10804*, 2021.
- Stephen L Morgan. *Handbook of causal analysis for social research*. Springer, 2013.
- Hiroshi Morioka, Hermanni Hälvä, and Aapo Hyvarinen. Independent innovation analysis for nonlinear vector autoregressive process. In *International conference on artificial intelligence and statistics*, pp. 1549–1557. PMLR, 2021.
- Scott Mueller and Judea Pearl. Personalized decision making—a conceptual introduction. *Journal of Causal Inference*, 11(1):20220050, 2023.
- Alfred Müller. Integral probability metrics and their generating classes of functions. *Advances in applied probability*, 29(2):429–443, 1997.
- Susan A Murphy. Optimal dynamic treatment regimes. *Journal of the Royal Statistical Society Series B: Statistical Methodology*, 65(2):331–355, 2003.
- Andrew Ng, Michael Jordan, and Yair Weiss. On spectral clustering: Analysis and an algorithm. *Advances in neural information processing systems*, 14, 2001.
- XuanLong Nguyen, Martin J Wainwright, and Michael I Jordan. Estimating divergence functionals and the likelihood ratio by convex risk minimization. *IEEE Transactions on Information Theory*, 56(11):5847–5861, 2010.
- Xinkun Nie and Stefan Wager. Quasi-oracle estimation of heterogeneous treatment effects. *Biometrika*, 108(2):299–319, 2021.
- Yang Ning, Peng Sida, and Kosuke Imai. Robust estimation of causal effects via a high-dimensional covariate balancing propensity score. *Biometrika*, 107(3):533–554, 2020.
- Sebastian Nowozin, Botond Cseke, and Ryota Tomioka. f-gan: Training generative neural samplers using variational divergence minimization. *Advances in neural information processing systems*, 29, 2016.
- Eun Jeong Oh, Min Qian, and Ying Kuen Cheung. Generalization error bounds of dynamic treatment regimes in penalized regression-based learning. *The Annals of Statistics*, 50(4):2047–2071, 2022.

- Aaron van den Oord, Yazhe Li, and Oriol Vinyals. Representation learning with contrastive predictive coding. *arXiv preprint arXiv:1807.03748*, 2018.
- Miruna Oprescu, Jacob Dorn, Marah Ghoummaid, Andrew Jesson, Nathan Kallus, and Uri Shalit. B-learner: Quasi-oracle bounds on heterogeneous causal effects under hidden confounding. In *International Conference on Machine Learning*, pp. 26599–26618. PMLR, 2023.
- Maxim Panov, Konstantin Slavnov, and Roman Ushakov. Consistent estimation of mixed memberships with successive projections. *COMPLEX NETWORKS 2017*, 2017. URL <https://arxiv.org/abs/1707.01350>.
- George Papamakarios, Eric Nalisnick, Danilo Jimenez Rezende, Shakir Mohamed, and Balaji Lakshminarayanan. Normalizing flows for probabilistic modeling and inference. *The Journal of Machine Learning Research*, 22(1):2617–2680, 2021.
- Adam Paszke, Sam Gross, Francisco Massa, Adam Lerer, James Bradbury, Gregory Chanan, Trevor Killeen, Zeming Lin, Natalia Gimelshein, Luca Antiga, Alban Desmaison, Andreas Köpf, Edward Yang, Zach DeVito, Martin Raison, Alykhan Tejani, Sasank Chilamkurthy, Benoit Steiner, Lu Fang, Junjie Bai, and Soumith Chintala. Pytorch: An imperative style, high-performance deep learning library. In *Neural Information Processing Systems*, 2019.
- Vishal M Patel, Hien Van Nguyen, and René Vidal. Latent space sparse subspace clustering. In *Proceedings of the IEEE international conference on computer vision*, pp. 225–232, 2013.
- Judea Pearl. Causal inference in statistics: An overview. *Statistics Surveys*, 3:96–146, 2009a. doi: 10.1214/09-SS057. URL <https://projecteuclid.org/journals/statistics-surveys/volume-3/issue-none/Causal-inference-in-statistics-An-overview/10.1214/09-SS057.full>.
- Judea Pearl. *Causality*. Cambridge university press, 2009b.
- Xi Peng, Jiashi Feng, Joey Tianyi Zhou, Yingjie Lei, and Shuicheng Yan. Deep subspace clustering. *IEEE transactions on neural networks and learning systems*, 31(12):5509–5521, 2020.
- Benjamin M Peter, Desislava Petkova, and John Novembre. Genetic landscapes reveal how human genetic diversity aligns with geography. *Molecular biology and evolution*, 37(4):943–951, 2020.
- Jonas Peters, Dominik Janzing, and Bernhard Schölkopf. *Elements of causal inference: foundations and learning algorithms*. The MIT Press, 2017.
- Kaare Brandt Petersen, Michael Syskind Pedersen, et al. The matrix cookbook. *Technical University of Denmark*, 7(15):510, 2008.
- Trang Pham, Truyen Tran, Dinh Phung, and Svetha Venkatesh. Predicting healthcare trajectories from medical records: A deep learning approach. *Journal of biomedical informatics*, 69:218–229, 2017.
- Robert W Platt, Enrique F Schisterman, and Stephen R Cole. Time-modified confounding. *American journal of epidemiology*, 170(6):687–694, 2009.

- Ben Poole, Sherjil Ozair, Aaron Van Den Oord, Alex Alemi, and George Tucker. On variational bounds of mutual information. In *International Conference on Machine Learning*, pp. 5171–5180. PMLR, 2019a.
- Ben Poole, Sherjil Ozair, Aaron Van Den Oord, Alex Alemi, and George Tucker. On variational bounds of mutual information. In *International Conference on Machine Learning*, pp. 5171–5180. PMLR, 2019b.
- Zhaozhi Qian, Yao Zhang, Ioana Bica, Angela Wood, and Mihaela van der Schaar. Synctwin: Treatment effect estimation with longitudinal outcomes. *Advances in Neural Information Processing Systems*, 34: 3178–3190, 2021.
- Liu Qidong, Tian Feng, Ji Weihua, and Zheng Qinghua. A new representation learning method for individual treatment effect estimation: Split covariate representation network. In *Asian conference on machine learning*, pp. 811–822. PMLR, 2020.
- Wentao Qu, Xianchao Xiu, Huangyue Chen, and Lingchen Kong. A survey on high-dimensional subspace clustering. *Mathematics*, 11(2):436, 2023.
- Tom Rainforth, Adam Kosior, Tuan Anh Le, Chris Maddison, Maximilian Igl, Frank Wood, and Yee Whye Teh. Tighter variational bounds are not necessarily better. In *International Conference on Machine Learning*, pp. 4277–4285. PMLR, 2018.
- Rajesh Ranganath and Adler Perotte. Multiple causal inference with latent confounding. *arXiv preprint arXiv:1805.08273*, 2018.
- Garvesh Raskutti, Martin J. Wainwright, and Bin Yu. Restricted eigenvalue properties for correlated gaussian designs. *Journal of Machine Learning Research*, 11(78):2241–2259, 2010. URL <http://jmlr.org/papers/v11/raskutti10a.html>.
- James Robins. A new approach to causal inference in mortality studies with a sustained exposure period—application to control of the healthy worker survivor effect. *Mathematical Modelling*, 7(9):1393–1512, 1986. ISSN 0270-0255. doi: [https://doi.org/10.1016/0270-0255\(86\)90088-6](https://doi.org/10.1016/0270-0255(86)90088-6). URL <https://www.sciencedirect.com/science/article/pii/0270025586900886>.
- James M Robins. Causal inference from complex longitudinal data. In *Latent variable modeling and applications to causality*, pp. 69–117. Springer, 1997.
- James M. Robins. Association, causation, and marginal structural models. *Synthese*, 121(1/2):151–179, 1999a. ISSN 00397857, 15730964. URL <http://www.jstor.org/stable/20118224>.
- James M Robins. Association, causation, and marginal structural models. *Synthese*, 121(1/2):151–179, 1999b.
- James M Robins. Optimal structural nested models for optimal sequential decisions. In *Proceedings of the Second Seattle Symposium in Biostatistics: analysis of correlated data*, pp. 189–326. Springer, 2004.
- James M Robins and Miguel A Hernán. Estimation of the causal effects of time-varying exposures. *Longitudinal data analysis*, 553:599, 2009a.

- James M Robins and Miguel A Hernán. Estimation of the causal effects of time-varying exposures. *Longitudinal data analysis*, 553:599, 2009b.
- James M Robins and Andrea Rotnitzky. Semiparametric efficiency in multivariate regression models with missing data. *Journal of the American Statistical Association*, 90(429):122–129, 1995.
- James M Robins, Sander Greenland, and Fu-Chang Hu. Estimation of the causal effect of a time-varying exposure on the marginal mean of a repeated binary outcome. *Journal of the American Statistical Association*, 94(447):687–700, 1999.
- James M Robins, Miguel Angel Hernan, and Babette Brumback. Marginal structural models and causal inference in epidemiology, 2000.
- Paul R Rosenbaum. The consequences of adjustment for a concomitant variable that has been affected by the treatment. *Journal of the Royal Statistical Society Series A: Statistics in Society*, 147(5):656–666, 1984.
- Paul R. Rosenbaum and Donald B. Rubin. The central role of the propensity score in observational studies for causal effects. *Biometrika*, 70:41–55, 1983.
- Andrew Rosenberg and Julia Hirschberg. V-measure: A conditional entropy-based external cluster evaluation measure. In *Proceedings of the 2007 joint conference on empirical methods in natural language processing and computational natural language learning (EMNLP-CoNLL)*, pp. 410–420, 2007.
- Saharon Rosset and Ji Zhu. Piecewise linear regularized solution paths. *The Annals of Statistics*, pp. 1012–1030, 2007.
- Emanuele Rossi, Bertrand Charpentier, Francesco Di Giovanni, Fabrizio Frasca, Stephan Günnemann, and Michael M Bronstein. Edge directionality improves learning on heterophilic graphs. In *Learning on graphs conference*, pp. 25–1. PMLR, 2024.
- Donald B Rubin. Matching to remove bias in observational studies. *Biometrics*, pp. 159–183, 1973a.
- Donald B Rubin. The use of matched sampling and regression adjustment to remove bias in observational studies. *Biometrics*, pp. 185–203, 1973b.
- Donald B Rubin. Estimating causal effects of treatments in randomized and nonrandomized studies. *Journal of educational Psychology*, 66(5):688, 1974.
- Donald B Rubin. Randomization analysis of experimental data: The fisher randomization test comment. *Journal of the American statistical association*, 75(371):591–593, 1980.
- Donald B. Rubin. Bayesianly Justifiable and Relevant Frequency Calculations for the Applied Statistician. *The Annals of Statistics*, 12(4):1151 – 1172, 1984. doi: 10.1214/aos/1176346785. URL <https://doi.org/10.1214/aos/1176346785>.

- Donald B Rubin. Causal inference using potential outcomes: Design, modeling, decisions. *Journal of the American Statistical Association*, 100(469):322–331, 2005.
- Michal Sadowski, Mike Thompson, Joel Mefford, Tanushree Haldar, Akinyemi Oni-Orisan, Richard Border, Ali Pazokitoroudi, Julien Ayroles, Sriram Sankararaman, Andy Dahl, et al. Characterizing the genetic architecture of drug response using gene-context interaction methods. *medRxiv*, pp. 2024–03, 2024.
- Pedro Sanchez, Jeremy P. Voisey, Tian Xia, Hannah I. Watson, Alison Q. O’Neil, and Sotirios A. Tsaftaris. Causal machine learning for healthcare and precision medicine. *Royal Society Open Science*, 9(8):220638, August 2022. doi: 10.1098/rsos.220638. URL <https://doi.org/10.1098/rsos.220638>.
- Pedro HC Sant’Anna and Jun Zhao. Doubly robust difference-in-differences estimators. *Journal of econometrics*, 219(1):101–122, 2020.
- Enrique F Schisterman, Stephen R Cole, and Robert W Platt. Overadjustment bias and unnecessary adjustment in epidemiologic studies. *Epidemiology (Cambridge, Mass.)*, 20(4):488, 2009.
- Peter Z Schochet. Design-based rct estimators and central limit theorems for baseline subgroup and related analyses. *Journal of Causal Inference*, 12(1):20230056, 2024.
- Alice Schoenauer-Sebag, Louise Heinrich, Marc Schoenauer, Michele Sebag, Lani F Wu, and Steve J Altschuler. Multi-domain adversarial learning. *arXiv preprint arXiv:1903.09239*, 2019.
- Bernhard Schölkopf and Julius von Kügelgen. From statistical to causal learning. In *Proceedings of the International Congress of Mathematicians*, pp. 1, 2022.
- Bernhard Schölkopf, Francesco Locatello, Stefan Bauer, Nan Rosemary Ke, Nal Kalchbrenner, Anirudh Goyal, and Yoshua Bengio. Toward causal representation learning. *Proceedings of the IEEE*, 109(5): 612–634, 2021.
- Rianne M. Schouten. On the role of prognostic factors and effect modifiers in structural causal models. In *NeurIPS 2024 Causal Representation Learning Workshop*, 2024. URL <https://openreview.net/forum?id=SR0G5JLi2N>.
- Erich Schubert. Stop using the elbow criterion for k-means and how to choose the number of clusters instead. *ACM SIGKDD Explorations Newsletter*, 25(1):36–42, 2023.
- Peter Schulam and Suchi Saria. Reliable decision support using counterfactual models. *Advances in neural information processing systems*, 30, 2017.
- Alejandro Schuler, Michael Baiocchi, Robert Tibshirani, and Nigam Shah. A comparison of methods for model selection when estimating individual treatment effects. *arXiv preprint arXiv:1804.05146*, 2018.
- Phillip J Schulte, Anastasios A Tsiatis, Eric B Laber, and Marie Davidian. Q-and a-learning methods for estimating optimal dynamic treatment regimes. *Statistical science: a review journal of the Institute of Mathematical Statistics*, 29(4):640, 2014.

- Patrick Schwab, Lorenz Linhardt, and Walter Karlen. Perfect match: A simple method for learning representations for counterfactual inference with neural networks. *CoRR*, abs/1810.00656, 2018. URL <http://arxiv.org/abs/1810.00656>.
- Nabeel Seedat, Fergus Imrie, Alexis Bellot, Zhaozhi Qian, and Mihaela van der Schaar. Continuous-time modeling of counterfactual outcomes using neural controlled differential equations. *arXiv preprint arXiv:2206.08311*, 2022.
- Shai Shalev-Shwartz and Shai Ben-David. *Understanding Machine Learning: From Theory to Algorithms*. Cambridge University Press, 2014.
- Uri Shalit. Can we learn individual-level treatment policies from clinical data? *Biostatistics*, 21(2): 359–362, 2020.
- Uri Shalit, Fredrik D Johansson, and David Sontag. Estimating individual treatment effect: generalization bounds and algorithms. In *International Conference on Machine Learning*, pp. 3076–3085. PMLR, 2017.
- Claudia Shi, David Blei, and Victor Veitch. Adapting neural networks for the estimation of treatment effects. *Advances in neural information processing systems*, 32, 2019.
- Hidetoshi Shimodaira. Improving predictive inference under covariate shift by weighting the log-likelihood function. *Journal of statistical planning and inference*, 90(2):227–244, 2000.
- HyunJung Shin and Sungzoon Cho. Response modeling with support vector machines. *Expert Systems with applications*, 30(4):746–760, 2006.
- Ravid Shwartz Ziv and Yann LeCun. To compress or not to compress—self-supervised learning and information theory: A review. *Entropy*, 26(3):252, 2024.
- Richard Sinkhorn. Diagonal equivalence to matrices with prescribed row and column sums. *The American Mathematical Monthly*, 74(4):402–405, 1967.
- Hossein Soleimani, James Hensman, and Suchi Saria. Scalable joint models for reliable uncertainty-aware event prediction. *IEEE transactions on pattern analysis and machine intelligence*, 40(8):1948–1963, 2017a.
- Hossein Soleimani, Adarsh Subbaswamy, and Suchi Saria. Treatment-response models for counterfactual reasoning with continuous-time, continuous-valued interventions. *ArXiv*, abs/1704.02038, 2017b.
- Mahdi Soltanolkotabi and Emmanuel J. Candès. A geometric analysis of subspace clustering with outliers. *The Annals of Statistics*, 40(4):2195 – 2238, 2012a. doi: 10.1214/12-AOS1034. URL <https://doi.org/10.1214/12-AOS1034>.
- Mahdi Soltanolkotabi and Emmanuel J. Candès. A geometric analysis of subspace clustering with outliers. *The Annals of Statistics*, 40(4):2195 – 2238, 2012b. doi: 10.1214/12-AOS1034. URL <https://doi.org/10.1214/12-AOS1034>.

- Shriyank Somvanshi, Subasish Das, Syed Aaqib Javed, Gian Antariksa, and Ahmed Hossain. A survey on deep tabular learning. *arXiv preprint arXiv:2410.12034*, 2024.
- Casper Kaae Sønderby, Tapani Raiko, Lars Maaløe, Søren Kaae Sønderby, and Ole Winther. Ladder variational autoencoders. *Advances in neural information processing systems*, 29, 2016.
- Jiaming Song and Stefano Ermon. Understanding the limitations of variational mutual information estimators. In *International Conference on Learning Representations*, 2020. URL <https://openreview.net/forum?id=B1x62TNtDS>.
- Xiangchen Song, Weiran Yao, Yewen Fan, Xinshuai Dong, Guangyi Chen, Juan Carlos Niebles, Eric Xing, and Kun Zhang. Temporally disentangled representation learning under unknown nonstationarity. In *Thirty-seventh Conference on Neural Information Processing Systems*, 2023. URL <https://openreview.net/forum?id=V8GHCGYLkf>.
- Peter Spirtes. Introduction to causal inference. *Journal of Machine Learning Research*, 11(5), 2010a.
- Peter Spirtes. Introduction to causal inference. *Journal of Machine Learning Research*, 11(5), 2010b.
- Peter Spirtes, Clark Glymour, and Richard Scheines. *Causation, prediction, and search*. MIT press, 2001.
- Jerzy Splawa-Neyman, D. M. Dabrowska, and T. P. Speed. On the Application of Probability Theory to Agricultural Experiments. Essay on Principles. Section 9. *Statistical Science*, 5(4):465 – 472, 1990. doi: 10.1214/ss/1177012031. URL <https://doi.org/10.1214/ss/1177012031>.
- Bharath K Sriperumbudur, Kenji Fukumizu, Arthur Gretton, Bernhard Schölkopf, and Gert RG Lanckriet. On integral probability metrics,  $\phi$ -divergences and binary classification. *arXiv preprint arXiv:0901.2698*, 2009.
- Elizabeth A Stuart. Matching methods for causal inference: A review and a look forward. *Statistical science: a review journal of the Institute of Mathematical Statistics*, 25(1):1, 2010.
- Liangjun Su, Zhentao Shi, and Peter CB Phillips. Identifying latent structures in panel data. *Econometrica*, 84(6):2215–2264, 2016.
- Jithendaraa Subramanian, Yashas Annadani, Ivaxi Sheth, Stefan Bauer, Derek Nowrouzezahrai, and Samira Ebrahimi Kahou. Latent variable models for bayesian causal discovery. In *ICML 2022: Workshop on Spurious Correlations, Invariance and Stability*, 2022. URL <https://openreview.net/forum?id=Au60kZskzgH>.
- V. N. Sudakov and B. S. Tsirel’son. Extremal properties of half-spaces for spherically invariant measures. *Journal of Soviet Mathematics*, 9(1):9–18, 1978. doi: 10.1007/BF01693783.
- BaoLuo Sun, Lan Liu, Wang Miao, Kathleen Wirth, James Robins, and Eric J Tchetgen Tchetgen. Semiparametric estimation with data missing not at random using an instrumental variable. *Statistica Sinica*, 28(4):1965, 2018.

- Ilya Sutskever, James Martens, George Dahl, and Geoffrey Hinton. On the importance of initialization and momentum in deep learning. In *International conference on machine learning*, pp. 1139–1147. PMLR, 2013.
- Vasilis Syrgkanis, Victor Lei, Miruna Oprescu, Maggie Hei, Keith Battocchi, and Greg Lewis. Machine learning estimation of heterogeneous treatment effects with instruments. *Advances in Neural Information Processing Systems*, 32, 2019.
- Yuhta Takida, Wei-Hsiang Liao, Chieh-Hsin Lai, Toshimitsu Uesaka, Shusuke Takahashi, and Yuki Mitsufuji. Preventing oversmoothing in vae via generalized variance parameterization. *Neurocomputing*, 509:137–156, 2022.
- Michel Talagrand. *The Generic Chaining: Upper and Lower Bounds of Stochastic Processes*. Springer Monographs in Mathematics. Springer, 2005. ISBN 978-3-540-27499-5. URL <https://link.springer.com/book/10.1007/3-540-27499-5>.
- Zhiqiang Tan. A distributional approach for causal inference using propensity scores. *Journal of the American Statistical Association*, 101(476):1619–1637, 2006.
- Eric J Tchetgen Tchetgen, Andrew Ying, Yifan Cui, Xu Shi, and Wang Miao. An introduction to proximal causal learning. *arXiv preprint arXiv:2009.10982*, 2020.
- Anbupalam Thalamuthu, Indranil Mukhopadhyay, Xiaojing Zheng, and George C Tseng. Evaluation and comparison of gene clustering methods in microarray analysis. *Bioinformatics*, 22(19):2405–2412, 2006.
- Yonglong Tian, Dilip Krishnan, and Phillip Isola. Contrastive multiview coding. In *Computer Vision—ECCV 2020: 16th European Conference, Glasgow, UK, August 23–28, 2020, Proceedings, Part XI 16*, pp. 776–794. Springer, 2020.
- Panagiotis Tigas, Yashas Annadani, Desi R Ivanova, Andrew Jesson, Yarin Gal, Adam Foster, and Stefan Bauer. Differentiable multi-target causal bayesian experimental design. In *International Conference on Machine Learning*, pp. 34263–34279. PMLR, 2023.
- Michael E Tipping and Christopher M Bishop. Mixtures of probabilistic principal component analyzers. *Neural computation*, 11(2):443–482, 1999.
- Christian Toth, Lars Lorch, Christian Knoll, Andreas Krause, Franz Pernkopf, Robert Peharz, and Julius Von Kügelgen. Active bayesian causal inference. *Advances in Neural Information Processing Systems*, 35:16261–16275, 2022.
- Dustin Tran and David M. Blei. Implicit causal models for genome-wide association studies. In *International Conference on Learning Representations*, 2018. URL <https://openreview.net/forum?id=SyELrEeAb>.
- Joel A. Tropp. User-friendly tail bounds for sums of random matrices. *Foundations of Computational Mathematics*, 12(4):389–434, 2012. doi: 10.1007/s10208-011-9099-z. URL <https://doi.org/10.1007/s10208-011-9099-z>.



- Michael Tschannen, Josip Djolonga, Paul K. Rubenstein, Sylvain Gelly, and Mario Lucic. On mutual information maximization for representation learning. In *International Conference on Learning Representations*, 2020. URL <https://openreview.net/forum?id=rkxoh24FPH>.
- Paul Tseng. Nearest q-flat to m points. *Journal of Optimization Theory and Applications*, 105:249–252, 2000.
- George Tucker, Andriy Mnih, Chris J Maddison, John Lawson, and Jascha Sohl-Dickstein. Rebar: Low-variance, unbiased gradient estimates for discrete latent variable models. *Advances in Neural Information Processing Systems*, 30, 2017.
- Mark J. van der Laan and Maya L Petersen. Causal effect models for realistic individualized treatment and intention to treat rules. *The International Journal of Biostatistics*, 3(1), 2007. doi: 10.2202/1557-4679.1022. URL <https://doi.org/10.2202/1557-4679.1022>.
- Mark J Van Der Laan and Daniel Rubin. Targeted maximum likelihood learning. *The international journal of biostatistics*, 2(1), 2006.
- Toon Vanderschueren, Jeroen Berrevoets, and Wouter Verbeke. Noflite: Learning to predict individual treatment effect distributions. *Transactions on Machine Learning Research*, 2023.
- Tyler J VanderWeele. Confounding and effect modification: distribution and measure. *Epidemiologic methods*, 1(1):55–82, 2012.
- Tyler J. VanderWeele and James M. Robins. Four types of effect modification: A classification based on directed acyclic graphs. *Epidemiology*, 18:561–568, 2007.
- Leena Chennuru Vankadara, Philipp Michael Faller, Michaela Hardt, Lenon Minorics, Debarghya Ghosh-dastidar, and Dominik Janzing. Causal forecasting: generalization bounds for autoregressive models. In *Uncertainty in Artificial Intelligence*, pp. 2002–2012. PMLR, 2022.
- Stijn Vansteelandt and Marshall Joffe. Structural Nested Models and G-estimation: The Partially Realized Promise. *Statistical Science*, 29(4):707 – 731, 2014. doi: 10.1214/14-STS493. URL <https://doi.org/10.1214/14-STS493>.
- Vladimir N. Vapnik. *Statistical Learning Theory*. Wiley, 1998.
- Victor Veitch, Dhanya Sridhar, and David Blei. Adapting text embeddings for causal inference. In *Conference on Uncertainty in Artificial Intelligence*, pp. 919–928. PMLR, 2020.
- Roman Vershynin. *High-Dimensional Probability: An Introduction with Applications in Data Science*. Cambridge Series in Statistical and Probabilistic Mathematics. Cambridge University Press, 2018. ISBN 978-1-108-41519-4. URL <https://www.cambridge.org/core/books/highdimensional-probability/797C466DA29743D2C8213493BD2D2102>.
- Ehsan Elhamifar René Vidal et al. Sparse subspace clustering. In *2009 IEEE conference on computer vision and pattern recognition (CVPR)*, volume 6, pp. 2790–2797, 2009.

- Nguyen Xuan Vinh, Julien Epps, and James Bailey. Information theoretic measures for clusterings comparison: Variants, properties, normalization and correction for chance. *Journal of Machine Learning Research*, 11(95):2837–2854, 2010. URL <http://jmlr.org/papers/v11/vinh10a.html>.
- Ulrike Von Luxburg. A tutorial on spectral clustering. *Statistics and computing*, 17:395–416, 2007.
- Stefan Wager and Susan Athey. Estimation and inference of heterogeneous treatment effects using random forests. *Journal of the American Statistical Association*, 113:1228 – 1242, 2018.
- Martin J Wainwright. Sharp thresholds for high-dimensional and noisy sparsity recovery using  $\ell_1$ -constrained quadratic programming (lasso). *IEEE transactions on information theory*, 55(5):2183–2202, 2009.
- Martin J Wainwright. *High-dimensional statistics: A non-asymptotic viewpoint*, volume 48. Cambridge university press, 2019.
- Martin J Wainwright, Michael I Jordan, et al. Graphical models, exponential families, and variational inference. *Foundations and Trends® in Machine Learning*, 1(1–2):1–305, 2008.
- Baozhen Wang and Xingye Qiao. Conformal inference of individual treatment effects using conditional density estimates. *arXiv preprint arXiv:2501.14933*, 2025.
- Benjie Wang, Clare Lyle, and Marta Kwiatkowska. Provable guarantees on the robustness of decision rules to causal interventions. In Zhi-Hua Zhou (ed.), *Proceedings of the Thirtieth International Joint Conference on Artificial Intelligence, IJCAI-21*, pp. 4258–4265. International Joint Conferences on Artificial Intelligence Organization, August 2021a. doi: 10.24963/ijcai.2021/585. URL <https://doi.org/10.24963/ijcai.2021/585>. Main Track.
- Benjie Wang, Matthew R Wicker, and Marta Kwiatkowska. Tractable uncertainty for structure learning. In *International Conference on Machine Learning*, pp. 23131–23150. PMLR, 2022a.
- Haotian Wang, Wenjing Yang, Longqi Yang, Anpeng Wu, Liyang Xu, Jing Ren, Fei Wu, and Kun Kuang. Estimating individualized causal effect with confounded instruments. In *Proceedings of the 28th ACM SIGKDD Conference on Knowledge Discovery and Data Mining*, pp. 1857–1867, 2022b.
- Xin Wang, Hong Chen, Zihao Wu, Wenwu Zhu, et al. Disentangled representation learning. *IEEE Transactions on Pattern Analysis and Machine Intelligence*, 2024.
- Yixin Wang and David M Blei. The blessings of multiple causes. *Journal of the American Statistical Association*, 114(528):1574–1596, 2019a.
- Yixin Wang and David M Blei. The blessings of multiple causes: A reply to ogburn et al.(2019). *arXiv preprint arXiv:1910.07320*, 2019b.
- Yixin Wang, Dawen Liang, Laurent Charlin, and David M. Blei. The deconfounded recommender: A causal inference approach to recommendation. *CoRR*, abs/1808.06581, 2018. URL <http://arxiv.org/abs/1808.06581>.

- Yixin Wang, David Blei, and John P Cunningham. Posterior collapse and latent variable non-identifiability. *Advances in neural information processing systems*, 34:5443–5455, 2021b.
- Zhao Wang, Kai Shu, and Aron Culotta. Enhancing model robustness and fairness with causality: A regularization approach. In Amir Feder, Katherine Keith, Emaad Manzoor, Reid Pryzant, Dhanya Sridhar, Zach Wood-Doughty, Jacob Eisenstein, Justin Grimmer, Roi Reichart, Molly Roberts, Uri Shalit, Brandon Stewart, Victor Veitch, and Diyi Yang (eds.), *Proceedings of the First Workshop on Causal Inference and NLP*, pp. 33–43, Punta Cana, Dominican Republic, November 2021c. Association for Computational Linguistics. doi: 10.18653/v1/2021.cinlp-1.3. URL <https://aclanthology.org/2021.cinlp-1.3/>.
- Ronald J Williams and David Zipser. A learning algorithm for continually running fully recurrent neural networks. *Neural computation*, 1(2):270–280, 1989.
- Sven E Wilson and Daniel M Butler. A lot more to do: The sensitivity of time-series cross-section analyses to simple alternative specifications. *Political analysis*, 15(2):101–123, 2007.
- Jeffrey M Wooldridge. *Econometric analysis of cross section and panel data*. MIT press, 2010.
- Chuhan Wu, Fangzhao Wu, and Yongfeng Huang. Rethinking infonce: How many negative samples do you need? In Lud De Raedt (ed.), *Proceedings of the Thirty-First International Joint Conference on Artificial Intelligence, IJCAI-22*, pp. 2509–2515. International Joint Conferences on Artificial Intelligence Organization, 7 2022. doi: 10.24963/ijcai.2022/348. URL <https://doi.org/10.24963/ijcai.2022/348>. Main Track.
- Pengzhou Abel Wu and Kenji Fukumizu.  $\beta$ -intact-VAE: Identifying and estimating causal effects under limited overlap. In *International Conference on Learning Representations*, 2022. URL <https://openreview.net/forum?id=q7n2Rngw0M>.
- Shenghao Wu, Wenbin Zhou, Minshuo Chen, and Shixiang Zhu. Counterfactual generative models for time-varying treatments. *arXiv preprint arXiv:2305.15742*, 2023.
- Kevin Xia and Elias Bareinboim. Neural causal abstractions. In *Proceedings of the AAAI Conference on Artificial Intelligence*, volume 38, pp. 20585–20595, 2024.
- Yang Xie, Ziqi Xu, Debo Cheng, Jiuyong Li, Lin Liu, Yinghao Zhang, and Zaiwen Feng. Causal effect estimation using identifiable variational autoencoder with latent confounders and post-treatment variables. *arXiv preprint arXiv:2408.07219*, 2024.
- Yuan Xie, Jinyan Liu, Yanyun Qu, Dacheng Tao, Wensheng Zhang, Longquan Dai, and Lizhuang Ma. Robust kernelized multiview self-representation for subspace clustering. *IEEE transactions on neural networks and learning systems*, 32(2):868–881, 2020.
- Wenju Xu, Guanghui Wang, Alan Sullivan, and Ziming Zhang. Towards learning affine-invariant representations via data-efficient cnns. In *Proceedings of the IEEE/CVF Winter Conference on Applications of Computer Vision*, pp. 904–913, 2020.

- Yiqing Xu. Generalized synthetic control method: Causal inference with interactive fixed effects models. *Political Analysis*, 25(1):57–76, 2017.
- Ziqi Xu, Debo Cheng, Jiuyong Li, Jixue Liu, Lin Liu, and Kui Yu. Causal inference with conditional front-door adjustment and identifiable variational autoencoder. In *The Twelfth International Conference on Learning Representations*, 2024. URL <https://openreview.net/forum?id=wFf9m4v7oC>.
- Jingyu Yan and Marc Pollefeys. A general framework for motion segmentation: Independent, articulated, rigid, non-rigid, degenerate and non-degenerate. In *Computer Vision–ECCV 2006: 9th European Conference on Computer Vision, Graz, Austria, May 7-13, 2006, Proceedings, Part IV 9*, pp. 94–106. Springer, 2006.
- Shuai Yang, Wenqi Zhu, and Yuesheng Zhu. Residual encoder-decoder network for deep subspace clustering. In *2020 IEEE International Conference on Image Processing (ICIP)*, pp. 2895–2899. IEEE, 2020.
- Yingzhen Yang, Jiashi Feng, Nebojsa Jojic, Jianchao Yang, and Thomas S Huang.  $\ell_0$ -sparse subspace clustering. In *European Conference on Computer Vision*, pp. 731–747. Springer, 2016.
- Yingzhen Yang, Jiashi Feng, Nebojsa Jojic, Jianchao Yang, and Thomas S Huang. Subspace learning by  $\ell_0$ -induced sparsity. *International Journal of Computer Vision*, 126(10):1138–1156, 2018.
- Weiran Yao, Yuewen Sun, Alex Ho, Changyin Sun, and Kun Zhang. Learning temporally causal latent processes from general temporal data. *ArXiv*, abs/2110.05428, 2021. URL <https://api.semanticscholar.org/CorpusID:238583013>.
- Weiran Yao, Yuewen Sun, Alex Ho, Changyin Sun, and Kun Zhang. Learning temporally causal latent processes from general temporal data. In *International Conference on Learning Representations*, 2022. URL <https://openreview.net/forum?id=RD1LMjLJXdq>.
- Dmitry Yarotsky. Universal approximations of invariant maps by neural networks. *Constructive Approximation*, 55(1):407–474, 2022.
- Yasin Yazıcı, Chuan-Sheng Foo, Stefan Winkler, Kim-Hui Yap, Georgios Piliouras, and Vijay Chandrasekhar. The unusual effectiveness of averaging in GAN training. In *International Conference on Learning Representations*, 2019. URL [https://openreview.net/forum?id=SJgw\\_sRqFQ](https://openreview.net/forum?id=SJgw_sRqFQ).
- Mingzhang Yin, Claudia Shi, Yixin Wang, and David M Blei. Conformal sensitivity analysis for individual treatment effects. *Journal of the American Statistical Association*, 119(545):122–135, 2024.
- Andrew Ying, Yifan Cui, and Eric J Tchetgen Tchetgen. Proximal causal inference for marginal counterfactual survival curves. *arXiv preprint arXiv:2204.13144*, 2022.
- Andrew Ying, Wang Miao, Xu Shi, and Eric J Tchetgen Tchetgen. Proximal causal inference for complex longitudinal studies. *Journal of the Royal Statistical Society Series B: Statistical Methodology*, 85(3):684–704, 2023.

- Jinsung Yoon, James Jordon, and Mihaela van der Schaar. GANITE: Estimation of individualized treatment effects using generative adversarial nets. In *International Conference on Learning Representations*, 2018. URL <https://openreview.net/forum?id=ByKWUeWA->.
- Chong You, Chun-Guang Li, Daniel P Robinson, and René Vidal. Oracle based active set algorithm for scalable elastic net subspace clustering. In *Proceedings of the IEEE conference on computer vision and pattern recognition*, pp. 3928–3937, 2016.
- Manzil Zaheer, Satwik Kottur, Siamak Ravanbakhsh, Barnabas Poczos, Russ R Salakhutdinov, and Alexander J Smola. Deep sets. *Advances in neural information processing systems*, 30, 2017.
- Jeffrey Zhang and Eric Tchetgen Tchetgen. On identification of dynamic treatment regimes with proxies of hidden confounders. *arXiv preprint arXiv:2402.14942*, 2024.
- Jingzhao Zhang, Tianxing He, Suvrit Sra, and Ali Jadbabaie. Why gradient clipping accelerates training: A theoretical justification for adaptivity. In *International Conference on Learning Representations*, 2020a. URL <https://openreview.net/forum?id=BJgnXpVYwS>.
- Linying Zhang, Yixin Wang, Anna Ostropolets, Jami J Mulgrave, David M Blei, and George Hripcsak. The medical deconfounder: assessing treatment effects with electronic health records. In *Machine Learning for Healthcare Conference*, pp. 490–512. PMLR, 2019.
- Mengyuan Zhang and Kai Liu. Rethinking symmetric matrix factorization: A more general and better clustering perspective. In *2022 IEEE International Conference on Data Mining (ICDM)*, pp. 695–702. IEEE, 2022.
- Teng Zhang, Arthur Szlam, and Gilad Lerman. Median k-flats for hybrid linear modeling with many outliers. In *2009 IEEE 12th International Conference on Computer Vision Workshops, ICCV Workshops*, pp. 234–241. IEEE, 2009.
- Weijia Zhang, Lin Liu, and Jiuyong Li. Treatment effect estimation with disentangled latent factors. In *Proceedings of the AAAI Conference on Artificial Intelligence*, volume 35, pp. 10923–10930, 2021a.
- Xitong Zhang, Yixuan He, Nathan Brugnone, Michael Perlmuter, and Matthew Hirn. Magnet: A neural network for directed graphs. *Advances in neural information processing systems*, 34:27003–27015, 2021b.
- Yao Zhang, Alexis Bellot, and Mihaela Schaar. Learning overlapping representations for the estimation of individualized treatment effects. In *International Conference on Artificial Intelligence and Statistics*, pp. 1005–1014. PMLR, 2020b.
- He Zhao and Edwin V. Bonilla. Bayesian factorised granger-causal graphs for multivariate time-series data. *CoRR*, abs/2402.03614, 2024. doi: 10.48550/ARXIV.2402.03614. URL <https://doi.org/10.48550/arXiv.2402.03614>.
- Nanxuan Zhao, Zhirong Wu, Rynson WH Lau, and Stephen Lin. What makes instance discrimination good for transfer learning? *arXiv preprint arXiv:2006.06606*, 2020.

- Peng Zhao and Bin Yu. On model selection consistency of lasso. *The Journal of Machine Learning Research*, 7:2541–2563, 2006.
- Xiangyu Zheng, Guogang Tian, Sen Wang, and Zhixiang Huang. Adr: An adversarial approach to learn decomposed representations for causal inference. In *Joint European Conference on Machine Learning and Knowledge Discovery in Databases*, pp. 268–284. Springer, 2024.
- Yujia Zheng and Kun Zhang. Generalizing nonlinear ica beyond structural sparsity. *Advances in Neural Information Processing Systems*, 36:13326–13355, 2023.
- Yujia Zheng, Ignavier Ng, and Kun Zhang. On the identifiability of nonlinear ica: Sparsity and beyond. *Advances in Neural Information Processing Systems*, 35:16411–16422, 2022.
- Lei Zhou, Bai Xiao, Xianglong Liu, Jun Zhou, Edwin R Hancock, et al. Latent distribution preserving deep subspace clustering. In *28th International joint conference on artificial intelligence*, 2019.
- Tianhui Zhou, Yitong Li, Yuan Wu, and David Carlson. Estimating uncertainty intervals from collaborating networks. *Journal of Machine Learning Research*, 22(257):1–47, 2021.
- Tianhui Zhou, William E Carson IV, and David Carlson. Estimating potential outcome distributions with collaborating causal networks. *Transactions on machine learning research*, 2022, 2022.
- Roland S Zimmermann, Yash Sharma, Steffen Schneider, Matthias Bethge, and Wieland Brendel. Contrastive learning inverts the data generating process. In *International Conference on Machine Learning*, pp. 12979–12990. PMLR, 2021.
- José R Zubizarreta. Stable weights that balance covariates for estimation with incomplete outcome data. *Journal of the American Statistical Association*, 110(511):910–922, 2015.